

IAEA-TECDOC-1299

# ***Technical and economic limits to fuel burnup extension***

*Proceedings of a Technical Committee meeting  
held in San Carlos de Bariloche, Argentina, 15–19 November 1999*



INTERNATIONAL ATOMIC ENERGY AGENCY

IAEA

July 2002

The originating Section of this publication in the IAEA was:  
Nuclear Fuel Cycle and Materials Section  
International Atomic Energy Agency  
Wagramer Strasse 5  
P.O. Box 100  
A-1400 Vienna, Austria

TECHNICAL AND ECONOMIC LIMITS TO FUEL BURNUP EXTENSION  
IAEA, VIENNA, 2002  
IAEA-TECDOC-1299  
ISBN-92-0-112802-9  
ISSN 1011-4289

© IAEA, 2002

Printed by the IAEA in Austria  
July 2002

## FOREWORD

For many years, the increase of efficiency in the production of nuclear electricity has been an economic challenge in many countries which have developed this kind of energy. The increase of fuel burnup leads to a reduction in the volume of spent fuel discharged to longer fuel cycles in the reactor, which means bigger availability and capacity factors.

After having increased the authorized burnup in plants, developing new alloys capable of resisting high burnup, and having accumulated data on fuel evolution with burnup, it has become necessary to establish the limitations which could be imposed by the physical evolution of the fuel, influencing fuel management, neutron properties, reprocessing or, more generally, the management of waste and irradiated fuels. It is also necessary to verify whether the benefits of lower electricity costs would not be offset by an increase in fuel management costs. The main questions are: Are technical and economic limits to the increasing of fuel burnup in parallel? Can we envisage nowadays the hardest limitation in some of these areas? Which are the main points to be solved from the technical point of view? Is this effort worthwhile considering the economy of the cycle? To which extent?

For these reasons, the IAEA, following a recommendation by the International Working Group on Fuel Performance and Technology, held a Technical Committee Meeting on Technical and Economic Limits to Fuel Burnup Extension. This meeting, hosted by the Atomic Energy Commission of Argentina, took place in San Carlos de Bariloche, Argentina, from 15 to 19 November 1999.

The purpose of this meeting was to provide an international forum to review the evolution of fuel properties at increased burnup in order to estimate the limitations both from a physical and an economic point of view. The meeting was therefore divided into two parts. The first part, focusing on technical limits, was devoted to the improvement of the fuel element, such as fission gas release (FGR), RIM effect, cladding, etc. and the fabrication, core management, spent fuel and reprocessing. Eighteen related papers were presented which covered new developments and presented a state of art on the subject.

The second part, relating to economic limits, was devoted to safety improvements and the economic impact of the increasing burnup. Six papers described different methods and criteria.

The meeting was attended by 37 participants from 14 countries and one international organization. The IAEA officers responsible for this publication were P. Menut and F. Sokolov of the Division of Nuclear Fuel Cycle and Waste Technology.

## *EDITORIAL NOTE*

*This publication has been prepared from the original material as submitted by the authors. The views expressed do not necessarily reflect those of the IAEA, the governments of the nominating Member States or the nominating organizations.*

*The use of particular designations of countries or territories does not imply any judgement by the publisher, the IAEA, as to the legal status of such countries or territories, of their authorities and institutions or of the delimitation of their boundaries.*

*The mention of names of specific companies or products (whether or not indicated as registered) does not imply any intention to infringe proprietary rights, nor should it be construed as an endorsement or recommendation on the part of the IAEA.*

*The authors are responsible for having obtained the necessary permission for the IAEA to reproduce, translate or use material from sources already protected by copyrights.*

## CONTENTS

Summary .....	1
TECHNICAL LIMITS (Session I)	
Fission gas release and temperature data from instrumented high burnup LWR fuel .....	7
<i>T. Tverberg, W. Wiesenack</i>	
Modelling isothermal fission gas release .....	17
<i>P. van Uffelen</i>	
Influence of rounds sub-grains in high burnup UO <sub>2</sub> fuel.....	32
<i>N. Lozano, L. Desgranges, D. Aymes, J.C. Niepce</i>	
Does rim microstructure formation degrade the fuel rod performance? .....	41
<i>D. Baron, J. Spino</i>	
Recent studies on the formation of the rim structure and on polygonization in LWR fuel.....	50
<i>Hj. Matzke</i>	
Fuel and fuel cycles with high burnup for WWER reactors.....	94
<i>V. Chernushev, F. Sokolov</i>	
Technological and licensing challenges for high burnup fuel.....	101
<i>H. Gross, P. Urban, C. Fenzlein</i>	
Development of advanced cladding material for burnup extension.....	112
<i>K. Kiuchi, I. Ioka, M. Takizawa, S. Wada</i>	
High burnup fuel R&D activities in Japan .....	126
<i>M. Ichikawa</i>	
Management of the fuel cycles and fuel performance analyses in the Kozloduy NPP WWER-440 reactors .....	136
<i>T. Haralampieva, V. Spassova, N. Georgieva, A. Antov, I. Stojanova, S. Stefanova, G. Passage, M. Drenska, K. Lassmann</i>	
Core analysis of the first cycle of Chashma nuclear power plant.....	160
<i>Subhan Gul, M. Khan, Waseem Azhar, M. Kamran, Abid Hussain</i>	
Overview of the SEU project for extended burnup at the Atucha-I NPP. Four years of operating experience .....	170
<i>J.M. Fink, M. Higa, R. Pérez, J. Piñeyro, J. Sidelnik, J.A. Casario, L. Alvarez</i>	
Extended burnup with SEU fuel in Atucha-1 NPP .....	181
<i>L. Alvarez, J. Casario, J. Fink, R. Pérez, M. Higa</i>	
Technologies for manufacturing UO <sub>2</sub> sintered pellets to fuel burnup extension .....	193
<i>D. Ohai</i>	
Technological problems and counter-measures on equipment materials for reprocessing of high burnup fuels.....	210
<i>K. Kiuchi, T. Kato, H. Motooka, S. Hamada</i>	
CARA design criteria for HWR fuel burnup extension .....	216
<i>P.C. Florido, R.O. Cirimello, J.E. Bergallo, A.C. Marino, D.F. Delmastro D.O. Brasnarof, J.H. Gonzalez, L.A. Juanicó</i>	
Experimental programmes related to high burnup fuel.....	228
<i>P.R. Vasudeva Rao, R. Vidhya, K. Ananthasivan, T.G. Srinivasan, K. Nagarajan</i>	
ECONOMIC LIMITS (Session II)	
Fuel with burnable absorber for RBMK-1500 .....	246
<i>G. Krivosein</i>	

The adequacy of methods used for the approval of high burnup core loading.....	256
<i>H.G. Sonnenburg</i>	
Probabilistic safety criteria on high burnup HWR fuels .....	263
<i>A.C. Marino</i>	
Fuel burnup extension effect on the fuel utilization and economical impact for a typical PWR plant.....	279
<i>S.E. Gomez, T. Yoshizu, Y. Komano, T. Kanagawa, K. Goto</i>	
The commercial impact of burnup increase .....	293
<i>C. Fenzlein, W. Schricker</i>	
Fuel cycle economical improvement by reaching high fuel burnup.....	304
<i>A. Afanasyev, G. Raspopin</i>	
List of Participants.....	323

## SUMMARY

### 1. SESSION I: TECHNICAL LIMITS

#### 1.1. Improvement of the fuel element

For both WWERs and PWRs, the strategy proposed in terms of core management and fuel design evolution is done to approach a burn up of about 60 MWd/kg.

In Norway, experimental studies on the fission gas behaviour are conducted in the HALDEN Research Reactor up to 59 MWd/kg using re-instrumented fuel elements. Studies on simulated fuel (SIMFUEL Program in IUT) behaviour is also used to help the understanding of the high burn up fuel behaviour.

Theoretical studies are conducted to model the fission gas behaviour according to the observed changes in the fuel structure for this burn up:

- Simulation of the fission gas atoms' behaviour along the grain boundaries,
- Description of different models of the subgrain formation in the RIM region which is developed with the burnup,
- Discussions about the influence of the microstructure formation and the degradation of the performances of the fuel based on the changes in porosity.

Much research also is being done regarding the examination of the structure and composition of the fuel. Efforts are directed at improving the cladding materials for high burnup fuels and also for higher neutron flux used with MOX fuel.

A consensus emerged from the overall presentations and discussions about the technical feasibility of the 60 MWd/kgUO<sub>2</sub> fuel management in LWR and VVER plants, thanks mainly to the new zirconium alloys developed in the last decade. A confirmation of the good behaviour of the actual design up to 70 MWd/kgUO<sub>2</sub> in the industrial power plants is expected for LWR plants in the next three years. There are certainly still some reserves concerning the MOX fuel for which the fission gas release limit at present the performances. More research is envisaged for particular fuels.

Concerning the fuel rod thermo-mechanical behaviour modelling, the large amount of experimental data provided in the 80s and 90s in the national and international programmes has allowed a real improvement in the understanding of the chemical and physical evolution of the fuel properties at high burnup. More mechanistic modelling has been developed or is still in development, allowing an easier extrapolation of the simulations. As a consequence, the nuclear fuel design codes are already able to simulate properly the fuel rod behaviour up to 70 MWd/kgUO<sub>2</sub>.

Nevertheless, further research is required to elucidate the basic mechanisms. For the future, prospective programmes are already in place to define the limits of the actual fuel assembly design and the alternative solutions to achieve higher burnups (100 to 120 MWd/kgUO<sub>2</sub>). This concerns mainly the fuel and cladding materials, but also the assembly design. Regarding cladding materials, alternative alloys like modified stainless steel could be considered as one of the candidates.

## 1.2. Fabrication, core management, spent fuel and reprocessing

There is considerable experience from a number of countries concerning both technical and economic aspects of extended burnup fuel. Fuel fabrication, fuel chemistry, fuel management, extended burnup fuel experience in both power reactors and research reactors, reprocessing issues, were all discussed.

Bulgaria, Pakistan and Argentina showed that there has been very good experience in the area of core management and evaluation of core characteristics for different kinds of reactors.

In-core fuel management in WWER Kozloduy (Bulgaria) and in PWR Chasma NPP (Pakistan) was reported to support the fuel burnup extension.

New developments in fuel design were considered for ATUCHA reactor (Argentina), and the reduced PCI failure for higher fuel performance was explained.

The fabrication cost was discussed regarding the reprocessing cost in Japan and the fuel element design improvement.

In Japan, reprocessing has been improved by developing new alloys with low corrosion. This is done in order to decrease the cost of the reprocessing as a limiting factor for the fuel burnup extension. Progress in fuel fabrication was reported in Romania where large-grain pellets were noted as a means of enhancing fuel performance at extended burnup. In ATUCHA, the new CARA bundle used with natural uranium and slightly enriched uranium was designed to facilitate the achievement of higher burnup through reducing the fuel temperatures and the fission gas release.

In India, an important experimental program for high burnup fuels, including also some improvement on the reprocessing, was reported.

The recommendations drawn from the panel discussion are therefore the following:

- taking into account the variety of core designs (PWR, BWR, WWER, PHWR), the qualification of high burnup fuel management must be conducted for each of these separately. However, cross comparisons are necessary to enlarge the qualification database supporting the core and mechanistic fuel design codes;
- it is still necessary to improve the fuel chemistry modelling at high burnup ( $\text{UO}_2$ , MOX, Uranium carbides or others) as the fuel chemistry controls the local fuel properties evolution;
- an improvement is needed on the evaluation of the local hydrostatic pressure in the fuel pellet as far as it appears to be a key parameter in the fission gases modelling;
- efforts must be continued towards an understanding of the rim formation mechanisms, on its fission gas retention capability and on the respective role of the rim material and the “under rim” material in the pellet expansion during RIA experiments;
- in order to prepare for the future (2010-2020) with increasing burnups, research is needed on alternative materials for the fuel and the cladding or on alternative assembly design (skeleton modifications for example);
- in addition, more investigations are required in order to elucidate basic mechanisms thereby enabling the extension of the validity domain of the existing models or the development of more mechanistic models. Furthermore, it has been identified that cross calculations between LWR fuel designers and CANDU fuel designers should be

beneficial as the operating conditions of these two fuels are widely different, although similar basic mechanisms are involved.

## 2. SESSION II: ECONOMIC LIMITS

### 2.1. Safety improvements

Through the presentation of Lithuania on RBMKs, participants agreed on the demonstration that a well-conceived modification of fuel material may improve the economic utilization of nuclear fuel and at the same time improve the safety of reactor operation.

Participants agreed upon the necessity to update the codes applied in the licensing process in order to account the recent developments in fuel rod fabrication and burnup levels. This is the case in Germany where studies on the limitations of models describing fuel and cladding under burnup values above 50 MWd/kgU was done with the TESPAC code and in Argentina where a probabilistic safety criteria on high burnup HWR fuels was done using probabilistic analysis as a technique for sensitivity analysis applied to the Argentine developed BACO code.

### 2.2. Economical impact of the increasing of burnup

From the experience of WWER-1000 fuel operation, an economical improvement is reached through the increase of fuel burnup by using some FA of 3-fuel cycles design in 4-th fuel loading cycle. It leads to a reduction of the fuel cycle costs by 10%. Fuel reliability is satisfactory. The operation experience shows that the increase of Ukrainian WWER-1000 fuel burnup has not worsened fuel reliability and FA bow situation.

The results of the investigation of the irradiated fuel in hot cells shows that the state of fuel pins of all tested assemblies is satisfactory (elongation about 15mm, diameter decrease about 0.08, fuel cladding gap between 3 to 43 mm and FGR between 0.19 to 2.50 %). All controlled parameters (elongation and diameter change, corrosion state of the claddings, their mechanical properties, gas fission fragments' release and pressure inside the pins, ballooning of the fuel, etc.) comply with the requirements in accordance with the design for the WWER-1000 fuel pins. The principal results of the irradiated FAs examination allow approving a possibility of further fuel burnup increase.

For further increasing fuel burnup and for continuous improvements of WWER-1000 fuel utilization, it is necessary to implement advanced uranium- gadolinium ( $\text{UO}_2\text{-Gd}_2\text{O}_3$  fuel). Advanced fuel implementation allows to reduce the initial enrichment of fuel by 5 -7 % in comparison with the existing value and at the same time to increase fuel burnup by 5 - 7 %.

The economic availability of the further LWR and HWWR fuel cycle development was determined by:

- the required enrichment of  $^{235}\text{U}$  or fissile Pu contents to achieve higher burnup. The lower initial contents of fissile materials in the HWWR are required to reach the same PWR fuel burnup but it depends on the burnup that was achieved during the previous irradiation in the PWR;
- the MOX fuel fabrication cost (spent fuel regeneration + MOX FA fabrication), spent fuel storage and disposal cost and the cost of natural uranium. The achieved burnup in PWR or initial enrichment of the PWR uranium fuel in the case of DUPIC technology.

The present enrichment limitation plays an important role in the achievable fuel burnup but the fuel burnup increase from the present values to those achievable with the 5 wt %  $^{235}\text{U}$  enrichment still has an economic incentive. The fuel burnup increase has also a very important effect on the reduction of the volume of the spent fuel assemblies.

In the near future, even with the present enrichment limit (5 wt %), fuel burnup could be extended up to 70 MWd/kgUO<sub>2</sub> without technical obstacles for licensing. The saving on the electricity cost by extending the fuel burnup could be achievable in most of the countries, but there are some exceptions for countries with backend costs related to the electricity generation and not to the waste volume. In such countries, the burnup increase is not a clear incentive because the backend costs became independent from the volume. The reduction of the electricity cost depends strongly on the countries where they are analyzed.

In the future, the relaxation of the 5 wt % limitation could allow extra savings in electricity cost and spent fuel volume, but it will require the solution of the technological problems as well as a licensing process.

TECHNICAL LIMITS  
(Session I)



# Fission gas release and temperature data from instrumented high burnup LWR fuel

**T. Tverberg, W. Wiesenack**  
Institutt for Energiteknikk,  
OECD Halden Reactor Project,  
Norway

**Abstract.** The in-pile performance of light water reactor fuels with high burnup is being assessed as part of the experimental programme of the Halden Reactor Project. To this end, fuel segments pre-irradiated in commercial LWRs are instrumented with fuel centre thermocouples and pressure transducers in order to obtain data on two key performance parameters, namely fuel temperature and rod pressure or fission gas release. The paper describes the results of a re-irradiation of fuel with burnup 59 MWd/kgUO<sub>2</sub> as related to the initial re-irradiation startup and power cycle in the Halden reactor. With emphasis on fission gas release behaviour, one can determine from the observations: the point of onset of fission gas release; restricted axial gas transport in high burnup, bonded fuel which is a characteristic feature of such fuel; the release of trapped fission gas to the plenum volume during power reduction; the response of the fuel temperatures to a degraded gap conductance as the released fission gases mix with the fill gas. The fission gas release data indicate that the onset of release is lower than extrapolated from medium burnup experience. During operation, when the fuel-cladding gap is tightly closed, only minor amounts of released gas reach the plenum. Fuel temperatures remain unaffected in this case. Even during power reduction, when gap conduction is changed, the fuel temperatures are not significantly affected by fission gas release due to a small gap. In total, the data provide valuable insight into the in-pile performance of high burnup fuel and extend the basis for model development and verification.

## 1. Introduction

The experimental programme of the Halden Reactor Project (HRP) has for several years focused on high burnup effects. The objectives of the test programme include

- extending the data base of UO<sub>2</sub> fuel performance,
- assessing the influence of fuel microstructure on pellet-cladding mechanical interaction (PCMI) and fission gas release in medium and high burnup fuel,
- investigating integral fuel rod behaviour at high burnup,
- investigating rim effects.

The work in the areas mentioned above is mainly performed through re-instrumentation of pre-irradiated LWR fuel segments, taken from PWRs as well as BWRs, for irradiation in the Halden Boiling Water Reactor (HBWR) and then collecting on-line data of measured parameters for subsequent storing in the Halden Test Fuel Data Bank (TFDB) system. The instrumentation that has been used by the Halden Project over the years in this respect include:

- fuel thermocouples (TF) for investigation of thermal behaviour of the fuel,
- cladding extensometers (EC) for studies of PCMI,
- pressure transducers (PF) for internal rod pressure measurements,
- fuel stack extensometers (EF) for densification and swelling assessment,
- diameter gauges for in-pile measurements of fuel rod diameter changes.

This paper will address one such experiment containing a fuel segment previously irradiated in a commercial LWR and re-instrumented with a TF and a PF. The discussion and analysis will mainly focus on the determination of point of onset of fission gas release and comparing with known relations and the influence of fission gas release on the thermal behaviour of high burnup fuel.

## 2. Description of experiment

The irradiation rig contained two fuel segments from a  $8 \times 8$  BWR rod. When discharged from the BWR, the segments had achieved a burnup of  $\sim 59$  MWd/kgUO<sub>2</sub>. Towards the end of the commercial irradiation, the segments were running at a very low power:  $\sim 12$  kW/m.

Non-destructive post irradiation examination (PIE) was performed before shipment to Halden. Of the main results from this examination it is worth to mention about 3.3% fission gas release and an outer oxide layer of ca. 43  $\mu\text{m}$ . Cold gap measurements were also performed and an average cold gap (diametral) of ca. 30  $\mu\text{m}$  was found. This corresponds to a closed gap at around 11 kW/m. These and further data on the rods are summarized in Table I.

Table I. Properties of the fuel segment

Base power (commercial irradiation) [kW/m]	12
Burnup after commercial irradiation [MWd/kgUO <sub>2</sub> ]	59
Outer oxide layer after comm. irr.[ $\mu\text{m}$ ]	43
Enrichment at BOL [w/o <sup>235</sup> U]	3.35
Density [% of T.D.]	95.7
Active length [mm]	327.5
TF centre hole diam.[mm]	2.5
Pellet outer diam. [mm]	10.44
Clad. inner diam. [mm]	12.25
Clad. thickness [mm]	0.8
Diametral gap at BOL [ $\mu\text{m}$ ]	210
Diametral gap before HBWR irradiation (from PIE) [ $\mu\text{m}$ ]	30
Filler gas/Pressure [bar]	He/5.0
Free volume at start of HBWR irradiation [cc]	5
Fuel weight [kg]	0.287

Before loading in the HBWR, both rods were re-instrumented with a TF and a PF, hence allowing monitoring both temperature and pressure data. Figure 1 shows a schematic of the rig that was used for the irradiation. The TF is situated at the top of the rod in a ~35 mm deep centre hole, 2.5 mm in diameter. The remaining fuel pellets are solid. The instrumentation in the rig include 5 vanadium neutron detectors (ND) for power monitoring. The NDs are positioned at different axial and radial positions hence allowing for calculating a power distribution. In addition, the rig is equipped with inlet and outlet thermocouples and flow turbines which together with the calibration valve at the inlet is used for the calorimetric power calibration which was performed at an initial stage in the HBWR irradiation.

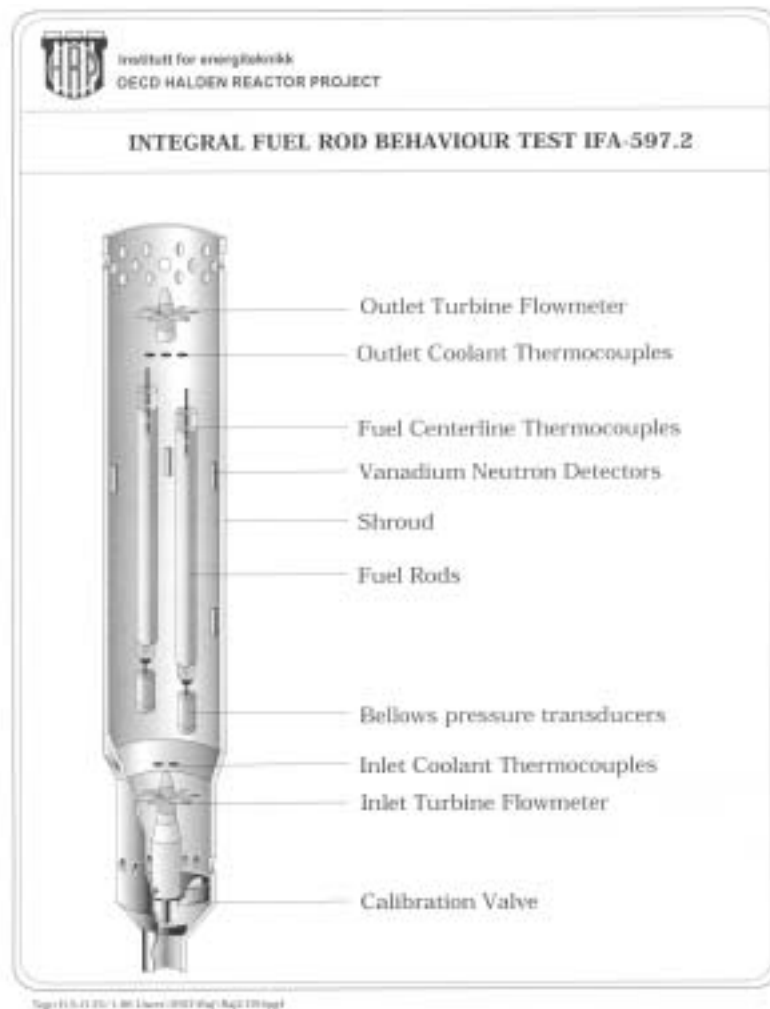


FIG. 1. Schematic of the rig.

### 3. Operation in the HBWR

Figure 2 shows the operation history of the rod during the irradiation in the HBWR. We note the power cycles during the first 3 to 7 days, which are due to power calibration of this and other rigs during the start of the irradiation cycle. Three such short cycles can be seen during the early stages of irradiation and the average linear heat rate (ALHR) of the rod reaches ~20.5 kW/m, 18.5 kW/m and 18 kW/m respectively as a maximum during these three ramps before being reduced to zero. The corresponding fuel centre temperatures, as measured by the thermocouples, are 830°C, 780°C and 760°C. The internal rod pressure follows the rod power during these cycles. Little or no indication of fission gas release can be seen.

Following this initial 'conditioning' phase, after a ~4 day power shutdown the power is again increased to about 25 kW/m where it is kept for a period of ca. 10 days, before the final shutdown cycle. During this shutdown, there is an intermediate power increase (from 11 to 17 kW/m) before the final shutdown after a total of 21 days of irradiation. It is seen that while the fuel temperature essentially remains constant throughout the steady-state phase of the cycle, the rod internal pressure increases significantly during the shutdown. This development will be discussed in more detail below.

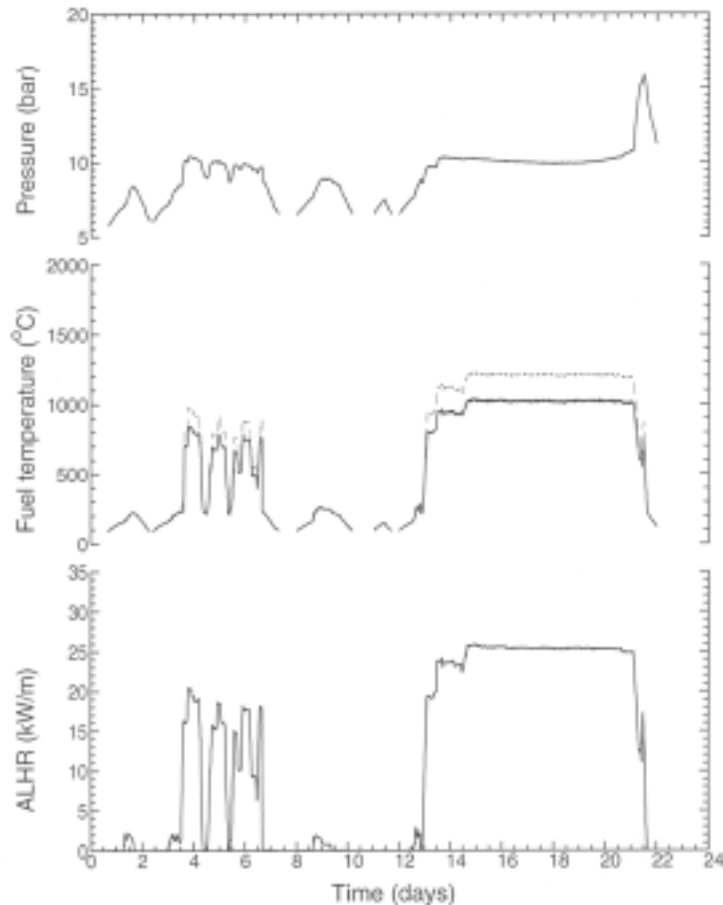


FIG. 2. Irradiation history. The dotted temperature curve shows the calculated peak temperature. Note the pressure increase coinciding with the power shutdown at around 21 days.

#### 4. Pressure data

Figure 3 (pressure versus power for the first power cycle) shows that there is little fission gas release. The pressure change indicates a release of about 0.5%. No further release is registered for the next two cycles which went to powers slightly below those of the initial cycle. For the last cycle, this changes however, as was seen in Fig. 2. The pressure increases slightly during the last few days at power, and then increases rapidly when the power is reduced during the shutdown.

In Figure 4, the same period is shown in the pressure power domain. Initially at zero power, the pressure is at 9 bar and at the peak power of ~26 kW/m the pressure is ~10.2 bar. During the steady state period with about 25 kW/m, the pressure increases only little by about 0.5 bar. The pressure continues to increase to ~15 bar as the power is reduced further to ~12 kW/m. When the power is kept at this intermediate power level for a short period, the pressure still

increases (~0.5 bar). Finally the power is again increased to about 18 kW/m before the final shutdown occurs and the power is reduced to zero upon which the pressure is ~ 14.8 bar. The total increase in pressure at zero power is thus ~5.8 bar during the period. This behaviour is typical of what is often referred to as delayed measured fission gas release which is seen for high burnup fuel rods. In this case the gap will be tightly closed at power, thus leaving little room for the gas to diffuse into the plenum and hence to the pressure detector. Only when the power is reduced and the gap opens, can the released gas be detected by the transducer. The pressure increase at 20°C is 4.1 bar between the initial startup and the final shutdown.

Using a burnup of 59 MWd/kgUO<sub>2</sub> and a value for produced fission gas of 31 cc per MWd together with the values for fuel mass and initial free volume from Table I, we obtain a fission gas release of 3.9%. It can be inferred that the onset of fission gas release occurs at an average linear heat rate somewhere between 18 and 25 kW/m, corresponding to calculated maximum fuel temperatures in the solid pellets of ~880 and 1170 °C, respectively.

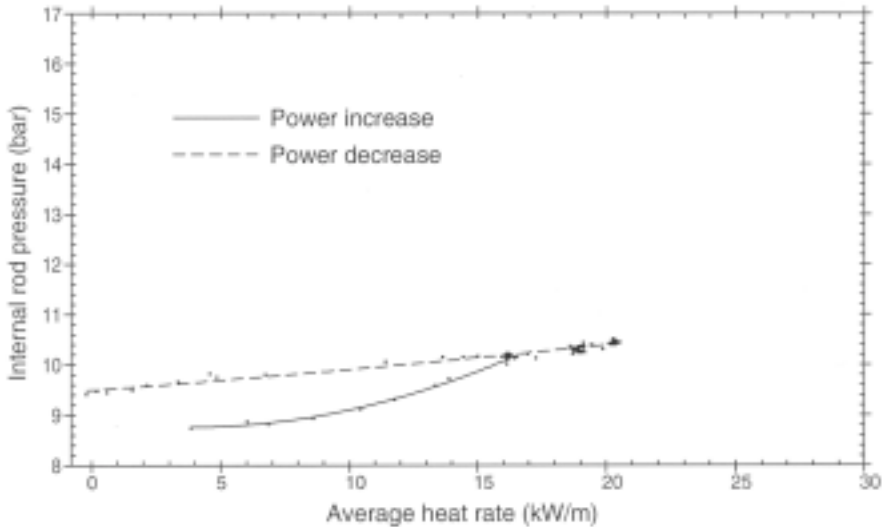


FIG. 3. Pressure versus rod power during first cycle.

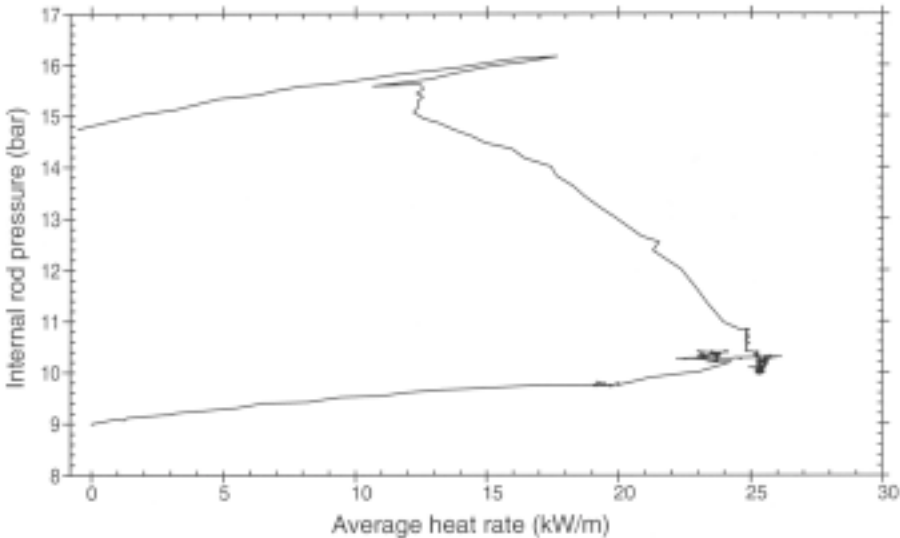


FIG. 4. Pressure versus rod power during the last operation cycle.

The two release fractions which can be deduced from this fuel rod, together with the result from a sibling rod are shown in Fig. 5. The interpolation curve indicates that the temperature of 1 % release is below the Halden 1 % fission gas release threshold curve defined as [1]

$$T = \frac{9800}{\ln\left(1000 \cdot \frac{BU}{5}\right)} \quad [^{\circ}\text{C}] \quad (1)$$

where T is the fuel centreline temperature for 1% fission gas release and BU is the burnup in MWd/kgUO<sub>2</sub>. Eq. (1) predicts a threshold temperature of 1050°C for fuel with a burnup of 59 MWd/kgUO<sub>2</sub>.

## 5. Temperature data

Figure 7 shows the temperature-power relation for the whole of the last power cycle seen in Fig. 2. It is seen that the release of fission gas during the last cycle induces only a small effect of thermal feedback on the temperatures between the startup and the shutdown. Included in the figure are lines of 2nd order least squares fit through the startup and shutdown data, respectively. At 15 kW/m, the temperature at the thermocouple position is ca. 25 K higher for the down-ramp compared to the same power of the up-ramp.

In analysing the measured fuel temperatures, it is important to have a good estimate of the fuel-to-clad gap. As mentioned above, PIE was performed on these segments after unloading from the BWR and a cold (diametral) gap of 30 µm was found. Gap closure can also be confirmed by looking at clad elongation measurements on a sibling rod that was irradiated in a different loading of the same IFA. This is shown in Fig. 6, where clad elongation data and gap prediction are plotted versus rod average linear heat rate for the first 3 power ramps above the power level the rod saw at its final stage of commercial irradiation. For the first ramp, the cladding elongation curve starts to deviate from the calculated curve of cladding free thermal expansion indicating onset of PCMI for powers > 10 kW/m.

LWRFTEMP, a modified version of the HRP's FTEMP2 steady state fuel modelling code, was used with this input for analysing the measured fuel temperatures. LWRFTEMP is specially tuned to properly handle the radial burnup and plutonium distribution in rods pre-irradiated in a LWR to burn-ups beyond where rim structure formation occurs. The code uses the TUBRNP model [2] for radial distribution of plutonium and burnup in high burnup UO<sub>2</sub> fuel, and the conductivity degradation model derived from other Halden data [3].

Figure 8 shows the LWRFTEMP calculations for the last power cycle. For the final shutdown sequence a Xenon content of 45% is assumed, as derived from the pressure data. Complete mixing of the gas is assumed. Good agreement between measured and calculated temperatures is achieved. It should be noted that the small difference between the case with pure helium and the case with considerable admixture of fission gas can only be obtained if the roughness of fuel and cladding is not increased as is the case in some gap conductance models.

In the upper curve, the calculated diametral fuel-clad gap is shown. The predicted power for gap closure is about 11 kW/m, which is about the same power at which the rod was running during the end of commercial irradiation.

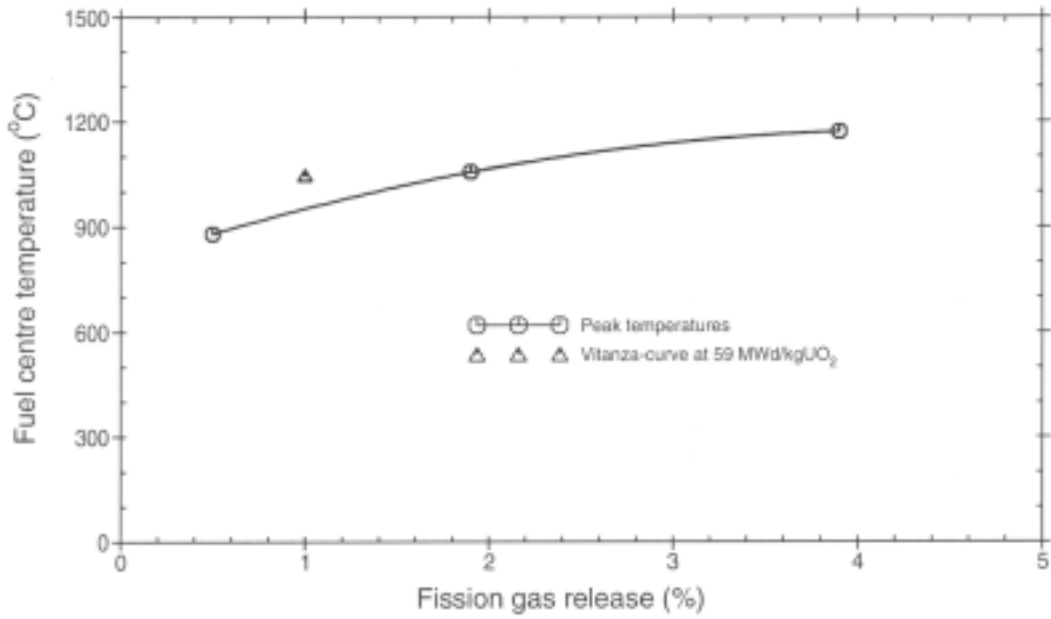


FIG. 5. Comparison of measured fission gas release data with the release threshold curve at 59Wd/kgUO<sub>2</sub>.

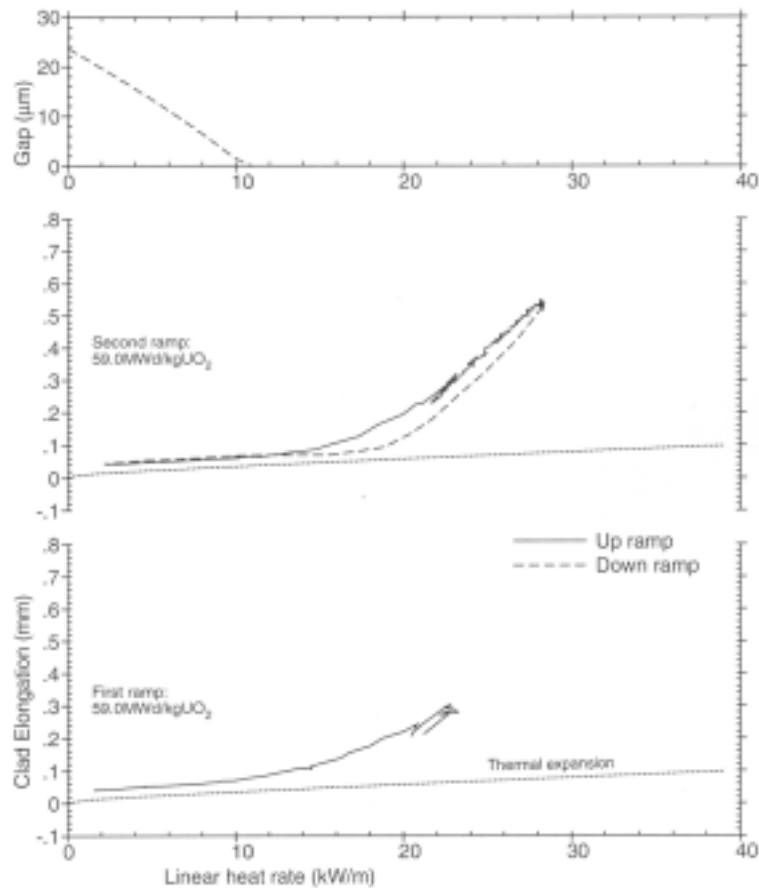


FIG. 6. Cladding elongation versus average rod power for sibling rod in later loading. The elongation curve starts to deviate from the calculated curve of free thermal expansion, indicating PCMI, at about the same power as L WRFTEMP predicts gap closure.

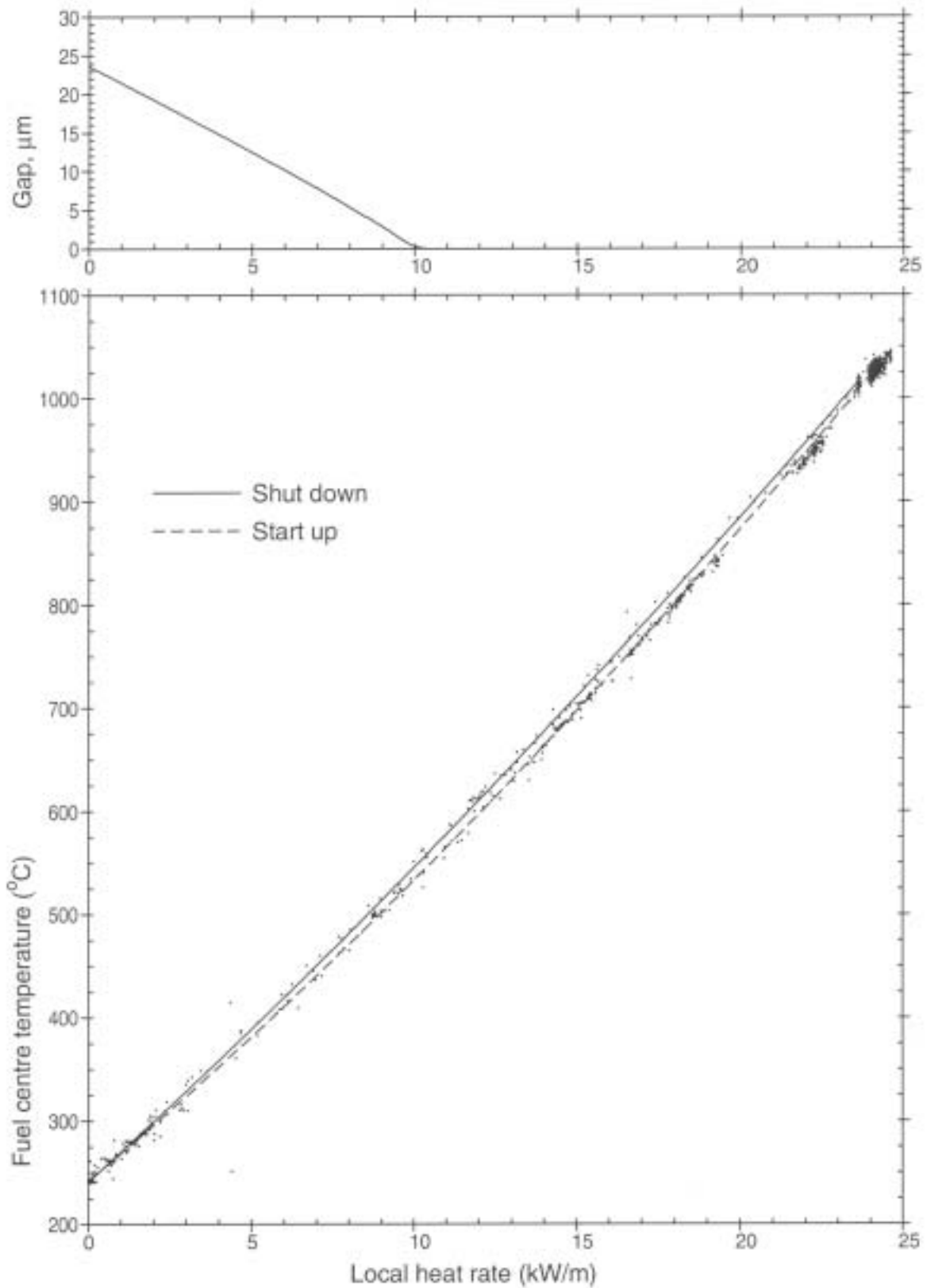


FIG. 7. Measured fuel centre temperatures versus local power during the last operating cycle. The curves are second order least squares fits for the startup and shutdown sequences as indicated in the figure. Because of the poisoned gap, temperatures during the shutdown sequence are higher than during the startup: -15  $^{\circ}\text{C}$  at a linear heat rate of 15 kW/m.

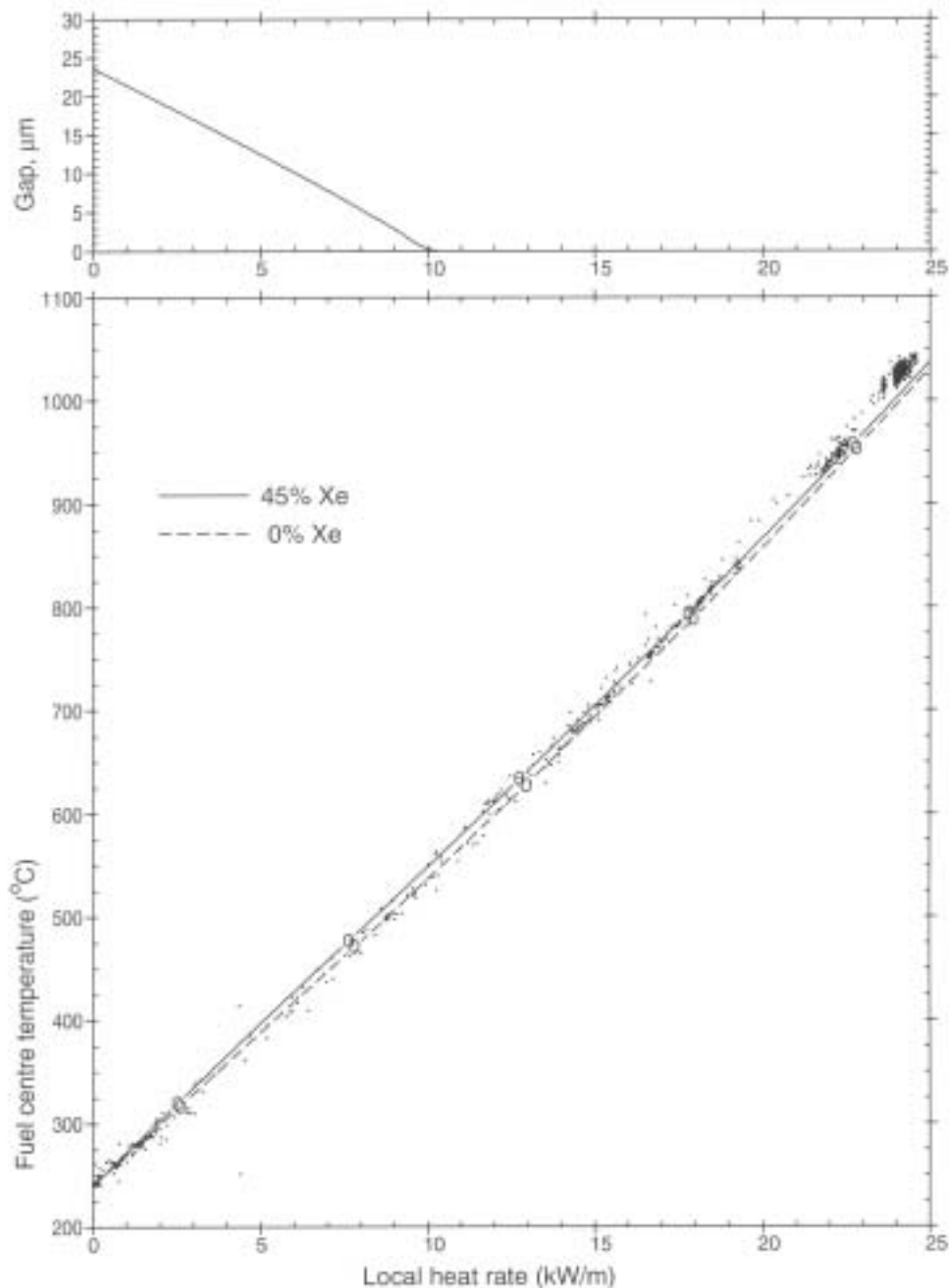


FIG. 8. Fuel centre temperature calculated and measured at thermocouple position versus local power during the last operating cycle.

## SUMMARY AND CONCLUSIONS

- For the first period of operation, a small amount of FGR is observed;
- At high power, the fission gas is trapped inside the fuel rod, with no communication to the plenum and hence the pressure transducer;
- A significant release can only be detected when the power is reduced and the pellet-cladding gap opens;

Because of the tightly closed gap at power, an almost 50% fission gas mix has only a small effect on the fuel centre temperature.

## REFERENCES

- [1] VITANZA C., KOLSTAD E., GRAZIANI U., "Fission gas release from UO<sub>2</sub> fuel at high burnup", ANS topical meeting on light water reactor fuel performance, Portland 1979.
- [2] LASSMANN K., OVARROLL C., van de LAAR J., WALKER C. T., "The radial distribution of plutonium in high burnup UO<sub>2</sub> fuels", Journal of Nuclear Materials, 208 (1994), 223-231.
- [3] WIESENACK, W., "Assessment of UO<sub>2</sub> conductivity degradation based on in-pile temperature data", International Topical Meeting on Light Water Reactor Fuel Performance, Portland, March 1997.

# Modelling isothermal fission gas release

P. van Uffelen

SCK•CEN,  
Mol, Belgium

**Abstract.** The present paper presents a new fission gas release model consisting of two coupled modules. The first module treats the behaviour of the fission gas atoms in spherical grains with a distribution of grain sizes. This module considers single atom diffusion, trapping and fission induced re-resolution of gas atoms associated with intragranular bubbles, and re-resolution from the grain boundary into a few layers adjacent to the grain face. The second module considers the transport of the fission gas atoms along the grain boundaries. Four mechanisms are incorporated: diffusion controlled precipitation of gas atoms into bubbles, grain boundary bubble sweeping, re-resolution of gas atoms into the adjacent grains and gas flow through open porosity when grain boundary bubbles are interconnected. The interconnection of the intergranular bubbles is affected both by the fraction of the grain face occupied by the cavities and by the balance between the bubble internal pressure and the hydrostatic pressure surrounding the bubbles. The model is under validation. In a first step, some numerical routines have been tested by means of analytic solutions. In a second step, the fission gas release model has been coupled with the FTEMP2 code of the Halden Reactor Project for the temperature distribution in the pellets. A parametric study of some steady-state irradiations and one power ramp have been simulated successfully. In particular, the Halden threshold for fission gas release and two simplified FUMEX cases have been computed and are summarised.

## 1. INTRODUCTION

Economics and prudent utilisation of natural resources have provided strong incentives for extending the average discharge burnup levels of light water reactor (LWR) fuel in commercial power plants. This might have implications for fuel integrity and, accordingly, this could be in conflict with safety requirements. One of the issues of primary interest in high burnup fuel is the behaviour of the fission gas atoms. In addition to the build-up of the rod internal pressure, the release of volatile and inert gas atoms could impede the heat transfer between the cladding and the pellets. On the other hand, gas atoms remaining in the pellets engender swelling which in turn can boost the mechanical interaction between the pellets and the cladding at high burnup. It is therefore essential to be able to predict the amount of gas produced and released during operation, especially at high burnup where the release is expected to increase [[1], [2]].

From the FUMEX exercise [3], it appeared that difficulties still remain with modelling fission gas release. It has been recognised that being a highly non-linear process, strongly influenced by temperature and feedback effects, accurate modelling is difficult over the whole range of release values from 0 to 100%. In particular, the region around 1% is extremely difficult to predict accurately and this just happens to be the most important region above which gas release and rod internal pressure can run away. Although there is available the empirical Halden criterion relating fuel central temperature to burnup at which 1% release can be exceeded, there is a need for elucidating the underlying mechanisms in order to refine the kinetics of release in this region. This constitutes the driving force for our attempt at developing an improved mechanistic model for fission gas release (FGR) in LWR fuel.

In a first step towards modelling FGR, the different mechanisms have been recapitulated in an internal document [4]. In a second step, an overview was made of the relevant models from which a first proposal was made in order to reconcile two contradictory approaches to the

behaviour of fission gases at the grain boundaries [5]: some people favour the grain boundary diffusion mechanism [6][7][8], while others advocate that fission products only accumulate in the grain boundary bubbles until saturation occurs, entailing the opening of the tunnel network along grain edges and the venting of the bubbles [9][10][11][12][13][14][15]. Both points of view could be reconciled as follows: grain boundary diffusion in presence of grain boundary traps is operative at low burnup values while there is a switch to nucleation and growth of grain boundary bubbles in controlling intergranular fission gas atom motion under certain conditions. In order to assess this switch, we assessed the mean distance travelled by a gas atom at the grain boundary before being swallowed up by an intergranular trap [16]. It was concluded that the contribution of grain boundary diffusion to fission gas release on the pellet scale is strongly inhibited as soon as the aerial coverage of the grain boundary traps is about 1% and the trap density exceeds  $0.1 \mu\text{m}^{-2}$ . Consequently we have proposed a simplified or alternative model for the intergranular behaviour of fission products.

In the following section, we describe the resulting mechanistic model for FGR and the concomitant gaseous swelling in LWR fuel. The model is related to the model of Kogai [17], in which we have implemented several modifications, among which a new description of fission product precipitation in grain boundaries [18] and fission induced resolution effects.

The model is under validation. In a first step, some numerical routines have been tested by means of analytic solutions. In the second step of the validation, the fission gas release model has been coupled with the FTEMP2 code [19] of the Halden Reactor Project for the temperature distribution in the pellets, as summarised in the third section of the present paper. A parametric study of some steady-state irradiations and one power ramp have been simulated successfully. In particular, the Halden threshold for fission gas release and two simplified FUMEX [3] cases have been computed and are presented in the fourth section. Finally, in the last section we draw the conclusions of the present computations and sketch the future work on the model for fission gas release.

## 2. MODEL DESCRIPTION

The model treats the migration of the fission gas atoms in two coupled phases.

### 2.1. Intragranular Module

The first phase of the FGR model deals with the transport of the fission products in spherical grains with a distribution of grain sizes [20] in order to avoid overprediction of the released fraction [6]. Three mechanisms are incorporated in this part: single atom diffusion in the bulk of the fuel matrix, trapping and resolution associated with intragranular bubbles, and resolution of fission products from grain boundary bubbles into a resolution layer adjacent to the grain face:

$$\frac{\partial C_v(r,t)}{\partial t} = D_{eff} \Delta C_v(r,t) + S_v(r,t) \quad (1)$$

where

$$D_{eff} = \frac{b}{b+g} D_v \quad (2)$$

The single atom diffusion coefficient ( $D_v$ ) given by Kogai [17] has been applied. The trapping ( $g$ ) and resolution ( $b$ ) associated with the intragranular bubbles [21][22] are taken into account by means of an effective diffusion coefficient ( $D_{eff}$ ) [23], which is only valid when the bubbles are considered to be saturated [24].

The resolution of fission products accumulated at the grain boundary [25][26], introduces a supplementary source term ( $S_{res}$ ) into a few layers adjacent to the grain face:

$$S_v(r,t) = \begin{cases} Y_{FP} \dot{F} & 0 \leq r \leq R_{grain} - 2\delta_R \\ Y_{FP} \dot{F} + S_{res} & R_{grain} - 2\delta_R \leq r \leq R_{grain} \end{cases} \quad (3)$$

The supplementary source term has been incorporated by means of the smeared model [27]:

$$S_{res} = B_{gb} \frac{3R_{grain}^3 \delta_{gb}}{2\delta_R (3R_{grain}^2 - 3R_{grain} \delta_R + \delta_R^2)} (C_{gbv} + C_{gbb}) \quad (4)$$

where the grain boundary concentrations ( $C_{gbv}$  and  $C_{gbb}$ ) are determined by the intergranular module of the FGR model.

## 2.2. Intergranular Module

In the second phase of the model, we consider the transport of the fission gas atoms along the grain boundaries in presence of secondary phases and grain face bubbles [16]. The gas atoms are considered to exist in two phases at the grain boundary: one fraction is dissolved in the grain boundary volume ( $C_{gbv}$ ) whereas the other part is accumulated in bubbles ( $C_{gbb}$ ). Four mechanisms are incorporated: diffusion controlled precipitation of gas atoms into bubbles [18], grain boundary bubble sweeping associated to bubble growth, re-resolution of gas atoms into the adjacent grains and gas flow through open porosity when grain boundary bubbles are interconnected [17]. This results in a coupled system of 3 ordinary differential equations:

$$\begin{cases} \frac{\partial \rho_{bl}}{\partial t} = \frac{\delta_{gb} D_m^v \Omega}{4 f(\theta) \rho_{bl}^2 k T} \left( P_{bl} - P_h - \frac{2\gamma}{\rho_{bl}} \right) k \\ \frac{\partial \hat{C}_{gbv}}{\partial t} = (1 - \phi) J_1 - J_2' - J_2'' - J_3' \\ \frac{\partial \hat{C}_{gbb}}{\partial t} = \phi J_1 + J_2' + J_2'' - J_3'' - J_4 \end{cases} \quad (5)$$

where the aerial fraction occupied by the grain boundary bubbles ( $\phi$ ) is given by

$$\phi = \begin{cases} \pi R_{bl}^2 C_{bl}^0 & R_{bl} < R_{bl}^* \\ \frac{\pi}{4} & R_{bl} \geq R_{bl}^* \end{cases} \quad (6)$$

The radius at which grain boundary bubble interconnect ( $R_{bl}^*$ ) is determined by the initial grain boundary bubble density:

$$R_{bl}^* = \frac{1}{2\sqrt{C_{bl}^0}} \quad (7)$$

The grain boundary concentrations  $C_{gbv}$  and  $C_{gbb}$  per unit of volume of the grain boundary are converted to the quantities  $\hat{C}_{gbv}$  and  $\hat{C}_{gbb}$  respectively, in order to express them per unit volume of the macroscopic solid:

$$\begin{aligned} \hat{C}_{gbv} &= C_{gbv} \delta_{gb} S_{gb} \\ \hat{C}_{gbb} &= C_{gbb} \delta_{gb} S_{gb} \end{aligned} \quad (8)$$

In the following sections we will formulate the different terms in (5) explicitly.

### 2.2.1. The intergranular source term

$J_1$  represents the average outcoming flux of a distribution of grains and is coupled to the intragranular module of the FGR model:

$$J_1 = \sum_{k,l} N_{klm} \cdot 2 \left[ - \frac{4\pi R_{klm}^2}{2} D_{v,klm} \frac{\partial (C_{v,klm})}{\partial r} \Big|_{r=R_{klm}} \right] \quad (9)$$

where the term between brackets represents the outcoming flux of fission products from a grain with indices  $k,l,m$ . The factor 2 in front of the brackets in the right hand side of (9) accounts for the fact that fission products flow to or from both sides of a grain boundary.

### 2.2.2. Diffusion controlled precipitation of fission gas atoms

The flux  $J'_2$  represents the flow of gas atoms dissolved in the grain boundary volume to the intergranular bubbles by diffusive capture [18]:

$$J'_2 = \left[ \frac{8D_{gb}\phi(1-\phi)^2}{(1-\phi)(\phi-3) - 2\ln(\phi)} \right] \frac{\hat{C}_{gbv}}{R_{bl}^2} \quad (10)$$

### 2.2.3. Grain boundary bubble sweeping

In deriving the expression for the capture rate constant for the flux of gas atoms precipitating in intergranular bubbles, we have neglected bubble growth. In order to account for the growth of the grain boundary bubbles, we introduce a supplementary flux term ( $J''_2$ ) of fission gas atoms dissolved in the grain boundary to the intergranular bubbles by bubble sweeping:

$$J''_2 = \begin{cases} 2\pi \frac{\phi}{\rho_{bl}} \frac{d\rho_{bl}}{dt} \hat{C}_{gbv} & \frac{d\rho_{bl}}{dt} > 0 \\ 0 & \frac{d\rho_{bl}}{dt} \leq 0 \end{cases} \quad (11)$$

#### 2.2.4. Fission induced re-resolution at grain boundaries

The fission spikes can redissolve a fraction of the fission gas atoms accumulated in the grain boundary into the adjacent grains. The rate at which this occurs is determined by the re-resolution rate coefficient ( $B_{gb}$ ) which in turn is dependent on the fission rate density ( $\dot{F}$ ). The resulting flux of gas atoms leaving the grain boundary (thereby opposing the outgoing diffusive flux  $J_I$ ) reads:

$$J_3 = J'_3 + J''_3 = B_{gb} (\hat{C}_{gbv} + \hat{C}_{gbb}) \quad (12)$$

where

$$B_{gb} = B_{gb}^* \frac{\dot{F}}{\dot{F}^{ref}} \quad (13)$$

and the reference fission rate density ( $\dot{F}^{ref}$ ) is taken at a linear heat rate of 20kW/m.

#### 2.2.5. Gas flow through the interconnected tunnel network

When the grain boundary bubbles reach a critical size ( $R_{bl}^*$ ), they interconnect and vent their content to the free volume of the rod. This release by gaseous flow through the tunnel network of interconnected grain boundary bubbles, cracks and open porosity is incorporated in  $J_4$ . The additional flux term is derived from the equation of Poiseuille in a capillary tube [17][28]:

$$J_4 = \frac{V_t P_{bl}^2 N_{bl} S_{gb}}{\eta k T} \quad (14)$$

where

$$\eta = \frac{1}{\pi \zeta^2 N_A} \sqrt{\frac{MRT}{\pi}} \cong 26.69 \frac{\sqrt{MT}}{\zeta^2} \quad (15)$$

$$V_t = V_i^0 f(\phi) g(\sigma_e) \quad (16)$$

$$V_i^0 = \frac{\pi a^4}{8L} \quad (17)$$

$$\sigma_e = \frac{P_h + \phi P_{bl}}{1 - \phi} \quad (18)$$

$$f(\phi) = 1 - \exp \left[ 1 - \left( \frac{\phi}{\phi^*} \right)^{10} \right] \quad (19)$$

$$g(\sigma_e) = 1 - \exp \left[ 1 - \left( \frac{\sigma_e}{\sigma_e^*} \right)^{10} \right] \quad (20)$$

The interconnection of the intergranular bubbles is thus affected both by the fraction of the grain face occupied by the cavities ( $\phi$ ) and by the balance between the bubble internal pressure ( $P_{bl}$ ) and the hydrostatic pressure surrounding the bubbles ( $P_h$ ).

### 2.2.6. Grain boundary bubble growth

Once the grain boundary bubbles are nucleated, they can growth (or shrink) by means of a vacancy flow along the grain boundary. The balance between the bubble internal pressure, the hydrostatic pressure and the surface tension constitutes the driving force for the growth or shrinkage of the bubbles [29]. The expression for the growth of the lenticular intergranular bubbles is based on the model for void growth on grain boundaries presented by Speight et al. [30]. Yang et al. [31] have verified this model by means of small angle neutron scattering. Matthews et al. [32] and Hayns et al. [33] have extended the idea of Speight et al. by considering gas filled bubbles rather than voids. To include the presence of gas within the cavity, they simply included the gas pressure ( $P_{bl}$ ) into the chemical potential of the cavity:

$$\frac{\partial \rho_{bl}}{\partial t} = \frac{\delta_{gb} D_m^v \Omega}{4 f(\theta) \rho_{bl}^2 kT} \left( P_{bl} - P_h - \frac{2\gamma}{\rho_{bl}} \right) k(\phi) \quad (21)$$

where

$$k(\phi) = \frac{8(1-\phi)}{(\phi-1)(3-\phi) - 2\ln(\phi)} \quad (22)$$

Matthews et al. have compared their results on swelling in nuclear fuel successfully with the experimental data of Zimmermann [34]. Kashibe et al. [29] confirmed these findings more recently.

## 3. MODEL APPLICATION

Proper testing of a fission gas release model requires coupling with a general fuel performance code in view of the interrelationship with other phenomena. In a first step, we used the FTEMP2 code [19] from the Halden Reactor Project to assess the radial temperature distribution in the pellets. More precisely, we assume a parabolic temperature distribution in the pellet:

$$T(r) = T_s + (T_c - T_s) \left[ 1 - \left( \frac{r}{R_{pellet}} \right)^2 \right] \quad (23)$$

where the central temperature ( $T_c$ ) and the surface temperature ( $T_s$ ) are provided by FTEMP2. A further simplification in the analysis comes from the normalised fission rate distribution in the pellets ( $\dot{f}$ ) which was taken to be independent of burnup:

$$\dot{f}(x) = \frac{F_1(x)}{\int_0^1 F_1(x) dx} = \frac{\dot{F}(x)}{\dot{F}_{avg}} \quad (24)$$

where

$$F_1(x) = 1 + 0.4x^4 \quad (25)$$

$$x = \frac{r}{R_{\text{pellet}}} \quad (26)$$

and  $\dot{F}_{\text{avg}}$  corresponds to the pellet averaged fission rate density.

### 3.1. Simulation of the Threshold For Fission Gas Release

#### 3.1.1. Test procedure

We simulate the (Halden) threshold for the onset of fission gas release, that is we determine the central temperature in the rod and the average burnup in the pellet when the fraction of the released gases reaches 1% during an irradiation at constant linear heat rate (25 kW/m, 30 kW/m, 35 kW/m, and 38 kW/m). We assess the effect of the average grain size ( $5 \mu\text{m} \leq R_{\text{grain}} \leq 11.25 \mu\text{m}$ ), the resolution rate constant for fission gas atoms at the grain boundaries at 20kW/m ( $10^{-5} \text{ s}^{-1} \leq B^*_{\text{gb}} \leq 10^{-6} \text{ s}^{-1}$  [21][23][27]), the effect of the hydrostatic pressure ( $P_h$ ) and the grain boundary surface energy ( $0.7 \text{ J/m}^2 \leq \gamma \leq 1 \text{ J/m}^2$  [17][21]) on the fission gas release.

#### 3.1.2. Results and discussion

The effects of the parameters under consideration are summarised in Fig. 1, 2, 3 and 4. In the discussion we should bear in mind that the Halden threshold corresponds to a correlation between small and large gas releases -- taken to be 0.5% to 2% -- with the peak fuel centre temperature. This should be kept in mind when comparing our results for a single pellet (i.e. we consider a uniform axial power profile) with that of a whole fuel rod. In view of this our results are very satisfactory and reflect the decline of the release threshold at high burnup [35][36][37].

FIG. 1 reveals the substantial role played by the hydrostatic pressure. According to our model, increasing the hydrostatic pressure leads to a shift of the onset for fission gas release to a higher burnup. These results are in accordance with several observations, both from in-pile and out-of-pile experiments [12][13][29][34][38][39]. Precise knowledge of the hydrostatic stress in the pellet therefore appears to be a prerequisite for the calibration of a fission gas release model.

The effect of the surface energy of the grain face bubbles is very small as expected (FIG. 2). The effect of the grain size on the fission gas release has two different aspects. First, the onset of fission gas release is unaffected by the grain size. This stems from the increase of the specific surface of the grains which is inversely proportional to the grain size alike the amount of gas reaching the grain boundaries by diffusion. The onset of fission gas release corresponds to a certain concentration of the grain boundaries at which saturation occurs with the subsequent venting of the bubbles through an interconnected tunnel network of bubbles. In the present calculations, this saturation concentration is in the order of  $2 \times 10^{15} \text{ atoms/cm}^2$  which corresponds quite well with other data in the literature [9][40]. According to the results in FIG. 3, there is a slight shift of the burnup where 1% of the fission gases are vented. This can be understood from FIG. 5, where the released fraction is shown as a function of the burnup at a constant linear heat rate of 38 kW/m for three different grain radii. FIG. 5 reveals that the onset of fission gas release, which starts in the pellet centre, is not dependent on the grain size. However, the release after the opening of the tunnel network is diffusion controlled hence it is

increasing with decreasing grain size. The incubation period after which 1% average fission gas release in the pellet is reached, therefore depends slightly on the grain size.

The effect of the resolution rate constant ( $B^*_{gb}$ ) is significant in the present model, as illustrated in FIG. 4. The effect of the rate constant becomes more perceptible at higher burnups. The results indicate that a value for  $B^*_{gb}$  in the order of  $10^{-5} \text{ s}^{-1}$  provides a good fit. This is in good agreement with  $1.55 \text{ s}^{-1}$  used by Denis et al [23].

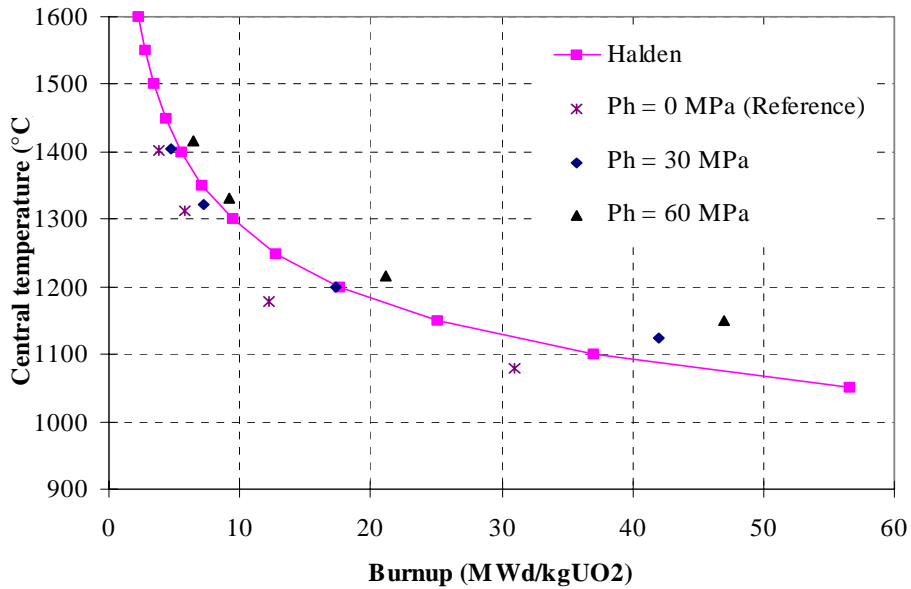


FIG. 1: The effect of the hydrostatic pressure on the central temperature for 1% average fission gas release versus burnup during irradiation at constant linear heat rate.

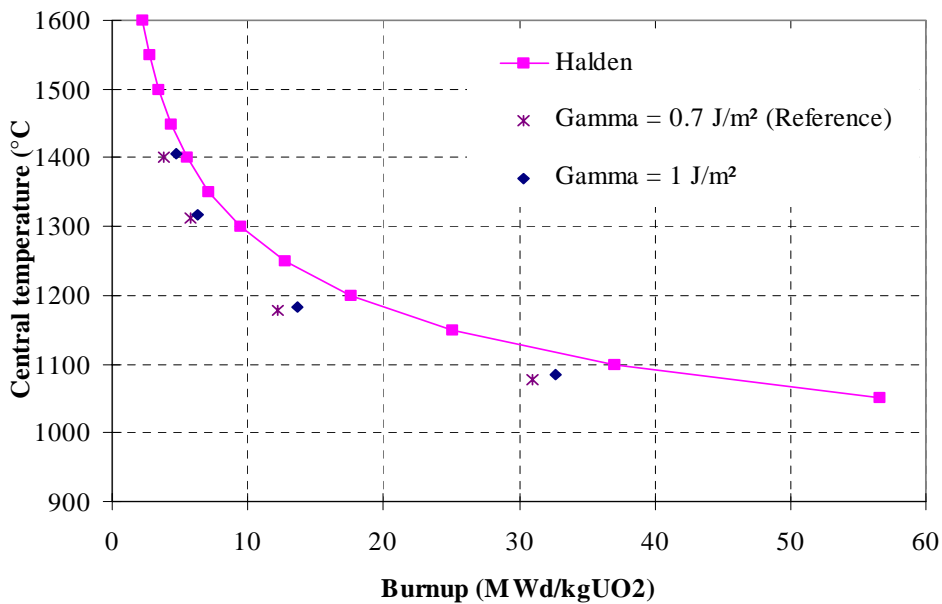


FIG. 2: The effect of the surface energy of intergranular bubbles ( $\gamma$ ) on the central temperature for 1% average fission gas release versus burnup during irradiation at constant linear heat rate.

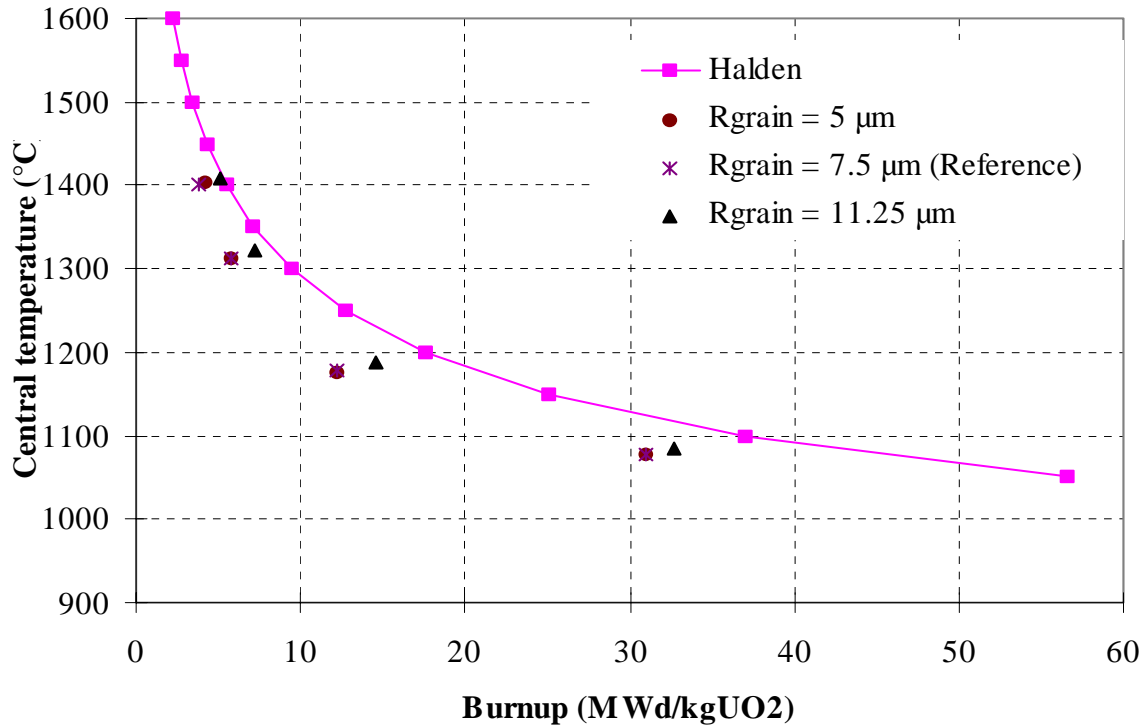


FIG. 3: The effect of the average grain radius on the central temperature for 1% average fission gas release versus burnup during irradiation at constant linear heat rate.

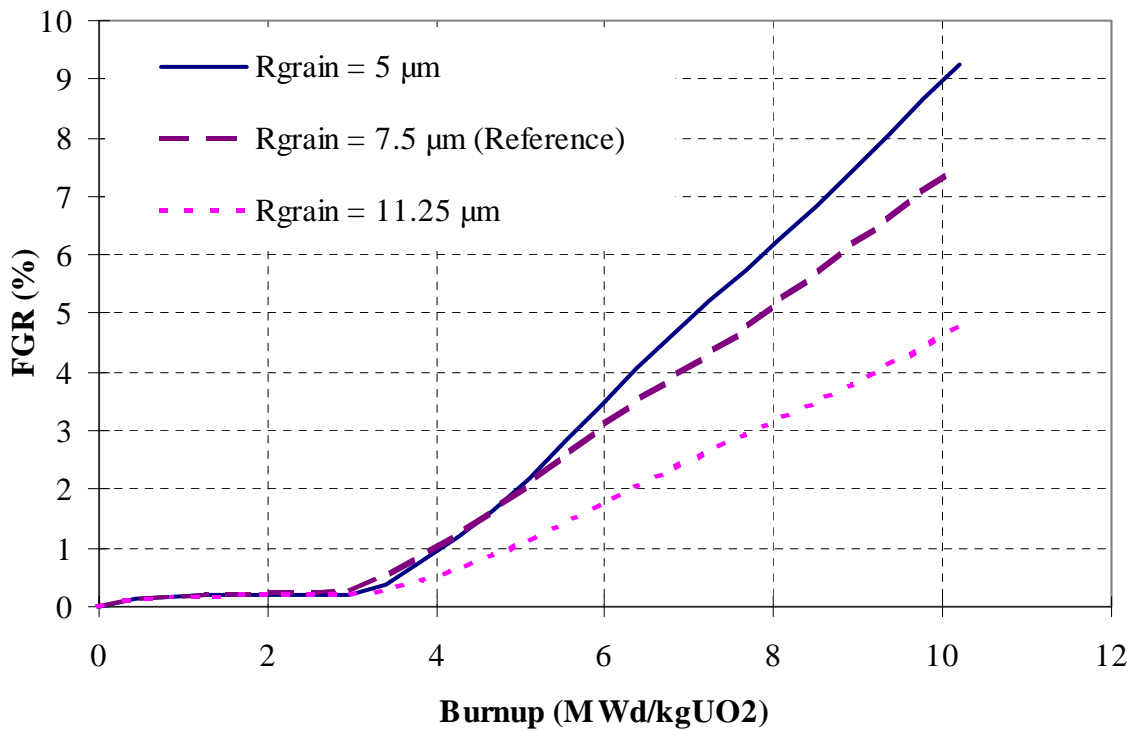


FIG. 4: The fission gas release rate at 38 kW/m as a function of the average burnup for three different average grain radii.

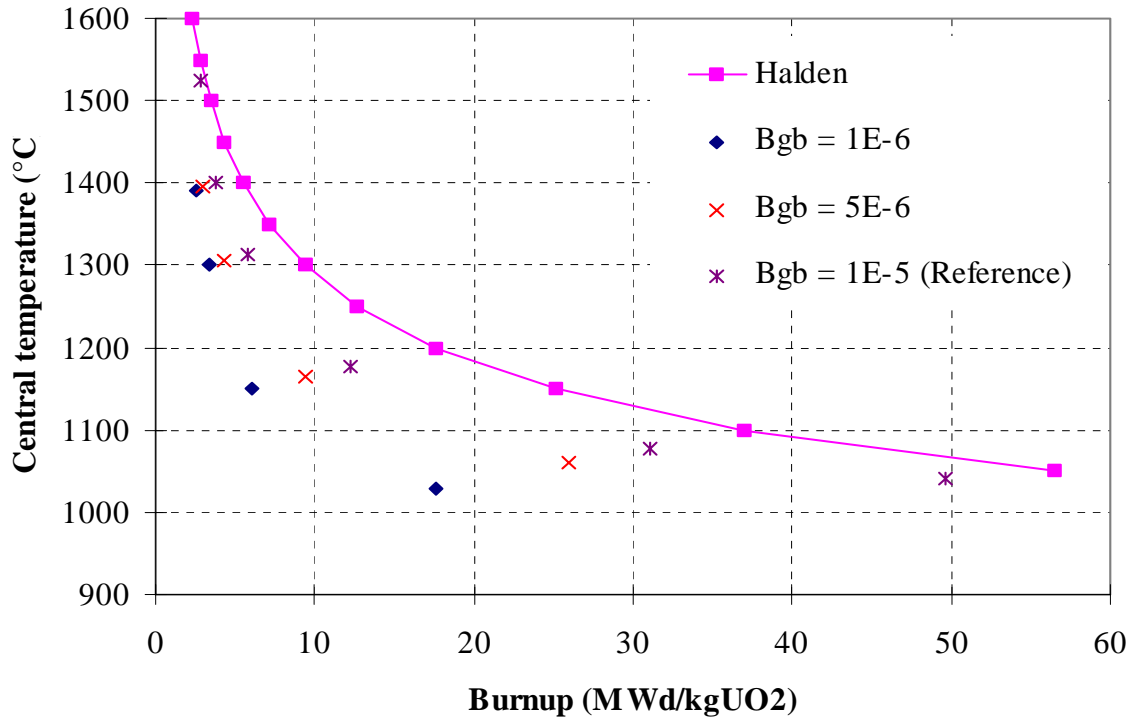


FIG. 5: The effect of resolution rate constant at the grain boundary for 20 kW/m ( $B_{gb}^{ref}$ ) on the central temperature for 1% average fission gas release versus burnup during irradiation at constant linear heat rate.

### 3.2. Simulation of the Simplified Fumex Cases

#### 3.2.1. Test procedure

In a second step of testing the model we have simulated the two simplified FUMEX cases [3]. Given the absence of any experimental data, the two cases enable an intercomparison with other model predictions along with testing the sensitivity to changes in experimental variables as well as the stability of the calculation. Case 1 consisted of a fuel rod running at a constant power of 20 kW/m to a final burnup of 50 MWd/kgUO<sub>2</sub>. In the second case, the power was held constant at 20 kW/m to a burnup of 30 MWd/kgUO<sub>2</sub> when there was a ramp to 40 kW/m in half an hour. This high power was held to an end-of-life (EOL) burnup of 50 MWd/kgUO<sub>2</sub>. In both cases, we have considered an uncertainty of 5% on the linear heat generating rate of the fuel rods. The general fuel rod characteristics used in the calculations are summarised in Table .

#### 3.2.2. Results and discussion

The results for the first simplified FUMEX case are summarised in T. At end-of-life the mean central temperature prediction of the codes in the FUMEX exercise was 980.4 °C with a standard deviation of  $\pm 110.5$  °C. The fission gas release predictions at the end-of-life were typically less than 3%, with many codes predicting a release of less than 1%, that is below the

Halden empirical threshold. Our code also predicts a low fraction of released fission gases, which is in accordance with the relatively low central temperature. The results in T also highlight the rather limited sensitivity to the linear heat rate as well as the good convergence of the program.

The results for the second simplified FUMEX case are summarised in Table 3. . The mean and standard deviation of the predicted temperatures by the codes in the FUMEX exercise were  $911\text{ °C} \pm 78\text{ °C}$  before ramp,  $1620\text{ °C} \pm 73\text{ °C}$  after ramp, and  $1845\text{ °C} \pm 193\text{ °C}$  at end-of-life. The temperatures obtained by means of the FTEMP2 code (cf. Table 3. ) were slightly lower but still within the error margins.

Table 1. Main parameters for the simplified FUMEX case calculations

Parameter	value	unit
pellet inside diameter	0	mm
pellet outside diameter	10.67	mm
cladding inside diameter	10.90	mm
cladding outside diameter	12.78	mm
dishing	-	-
plenum volume	2.5	cm <sup>3</sup>
fuel column length	20	cm
fuel density	95	% TD
grain size	15	µm
enrichment U <sup>235</sup>	10	%
fuel surface roughness	3	µm
clad surface roughness	1	µm
fill gas	He	-
fill gas pressure	5	bar

Table 2. Main results from the simulation of the first simplified FUMEX case

Case 1	T <sub>c,EOL</sub> (°C)	FGR <sub>EOL</sub> (%)
nominal	900	0.42
+5% LHR	944	0.45
-5% LHR	859	0.40

Table 3. Main results from the simulation of the second simplified FUMEX case

Case 2	T <sub>c,1</sub> (°C)	FGR <sub>1</sub> (%)	T <sub>c,2</sub> (°C)	FGR <sub>2</sub> (%)	T <sub>c,3</sub> (°C)	FGR <sub>3</sub> (%)
nominal	850	0.36	1535	12.69	1693	30.95
+ 5% LHR	886	0.39	1619	14.89	1802	35.25
- 5% LHR	815	0.33	1455	9.89	1584	25.74

1: before ramp  
2: after ramp  
3: at end-of-life

The majority of the codes predict a low release  $\leq 1\%$  before the ramp, an increase to  $\approx 20\%$  at 31 MWd/kgUO<sub>2</sub> following the ramp and a mean end-of-life FGR of 35 % with a standard deviation of  $\pm 8.2\%$  (Three code results have been omitted in view of their unexplained extreme values). Our results are thus in good accordance with the mean values. In addition, they indicate that the fission gas release is diffusion-controlled during the high power irradiation. However, shortly after the ramp we predict slightly lower values for the fission gas release (10-15%) in comparison with the other codes (20%). There are a few factors which could affect the release kinetics during a ramp and which have to be investigated more thoroughly before drawing definite conclusions: the tube conductivity ( $V_t^0$ ), the sigmoidal functions  $f(\phi)$  and  $g(\sigma_e)$ , the hydrostatic pressure, the intragranular bubble behaviour which affects the effective volume diffusion coefficient, the resolution rate at the grain boundary bubbles, etc. However, these values can only be fine-tuned when the model for fission gas release will be coupled with an integral fuel performance code (e.g. COMETHE developed by BELGONUCLEAIRE), which is the next step of our validation process. Another contributing factor to the underprediction of the release during the ramp could also stem from the slightly lower central temperature predictions (Table 3. ) and from the fact that fuel restructuring (e.g. grain growth) is disregarded in the present FGR model.

#### 4. CONCLUSIONS AND FUTURE WORK

We have developed a new mechanistic model for fission gas release in LWR fuel. The model embodies a large number of the underlying basic mechanisms of fission gas release and it couples the kinetics of the intra- and intergranular behaviour of the gas atoms.

In a first step of the validation we have simulated the empirical Halden criterion, relating fuel central temperature to burnup at which 1% release can be exceeded, which is extremely difficult to predict accurately [3]. The general tendency of the fission gas release model is very satisfactory, more precisely it predicts the decrease of the incubation period with burnup under stationary conditions quite well. In addition, the predicted concentration of the grain boundaries at which saturation occurs is in the order of  $2 \times 10^{15}$  atoms/cm<sup>2</sup> which corresponds with other data in the literature [9][40].

The parametric simulation of the empirical threshold for fission gas release revealed the most important parameters for further calibration of the FGR model, namely the resolution rate at grain boundary bubbles ( $B_{gb}$ ) and the hydrostatic pressure in the fuel pellet ( $P_h$ ). The average grain size on the other hand does not affect the release threshold. It does however affect the release rate after interlinkage of the grain boundary bubbles occurred.

The simulation of the two simplified cases in the FUMEX round robin exercise were also satisfactory, if it wasn't for the slightly underpredicted release kinetics during the ramp in the second case. Nevertheless, before drawing definite conclusions, it is necessary to include a few improvements:

- (a) obtain the fission rate, the temperature and the burnup distribution in a pellet from an integral fuel performance code (e.g. COMETHE);
- (b) the hydrostatic pressure should also be accounted for since it appears to play an important role, both in the threshold for release as in the release kinetics after interlinkage occurred;

- (c) we should analyse the interconnection of grain boundary bubbles by means of percolation theory in order to justify the sigmoidal curves  $f(\phi)$  and  $g(\sigma_e)$  provided by Kogai [17];
- (d) we should reduce the calculation time in order to be able to incorporate the model in a general fuel performance code.

## ACKNOWLEDGEMENTS

The author wishes to express his gratitude Dr. M. Lippens (S.A. BELGONUCLEAIRE) and Dr. M. Verwerft (SCK•CEN) for the valuable discussions and their interest in the work.

## Nomenclature

$\delta_{gb}$	=	grain boundary thickness (= 0.5 nm)
$D_m^v$	=	vacancy diffusion coefficient on grain boundary
$\Omega$	=	atomic volume (= $4.09 \cdot 10^{-29} \text{ m}^3$ )
$P_h$	=	hydrostatic pressure around the bubble
$\gamma$	=	surface tension of the intergranular bubble
$\theta$	=	dihedral angle between the intergranular bubble and the grain boundary (= $50^\circ$ )
$\rho_{bl}$	=	grain boundary bubble radius of curvature
$R_{bl}$	=	grain boundary bubble radius in the grain face ( $R_{bl} = \rho_{bl} \sin \theta$ )
$C_{bl}^0$	=	initial concentration of intergranular bubbles (= $10^{12}/\text{m}^2$ )
$C_{bl}$	=	concentration of intergranular bubbles
$S_{gb}$	=	specific surface of the grain boundaries
$k$	=	index corresponding to the origin of the grain (e.g. $\text{UO}_2$ or $\text{PuO}_2$ grain)
$l$	=	index corresponding to the grain size
$m$	=	index corresponding to the macroscopic annulus in which the grain is embedded
$N_{klm}$	=	number of grains of type $k, l, m$ per unit of volume
$R_{klm}$	=	radius of the grains of type $k, l, m$
$D_{klm}$	=	volume diffusion coefficient of the fission product in the grain of type $k, l, m$
$\zeta^2$	=	hard sphere diameter of the gas (= $4.047 \cdot 10^{-10} \text{ m}$ )
$a$	=	tube radius of interconnected grain boundary bubbles
$L$	=	tube length of interconnected grain boundary bubbles
$b$	=	resolution rate at intragranular bubbles
$g$	=	capture rate at intragranular bubbles
$B_{gb}$	=	resolution rate at intergranular bubbles
$\delta_R$	=	half width of the zone adjacent to the grain faces where gas atoms are re-dissolved from grain boundary bubbles (= 22nm)
$R$	=	gas constant (= 8.314 J/mole/K)
$N_A$	=	number of Avogadro (= $6.02310^{23} /\text{mole}$ )
$\sigma_e$	=	the sum of the hydrostatic pressure (compressive) imposed on the pellet $\sigma$ and the bubble pressure $P_{bl}$ (tensile)
$Y_{FP}$	=	cumulative yield of fission gas atoms Xe and Kr (= 0.25)
$\phi^*$	=	0.78 ( $\approx \pi/4$ )
$\sigma_e^*$	=	10 MPa
$V_t^0$	=	$(2/3) \cdot 10^{-12} \mu\text{m}^3$

## REFERENCES

- [1] K. UNE, S. KASHIBE, "Fission gas release during post irradiation annealing of BWR fuels", *J. Nucl. Sci. and Techn.* 27 (11) (1990) 1002.
- [2] C. FORAT, P. BLANPAIN, B. KAPUSTA, P. GUEDENEY, P. PERMEZEL, "Fission gas release enhancement at extended burnup: experimental evidence from French PWR irradiation", IAEA-TECDOC-697, 68–75, 1992.
- [3] INTERNATIONAL ATOMIC ENERGY AGENCY, "Fuel modelling at extended burnup", IAEA-TECDOC-998, 1998.
- [4] P. VAN UFFELEN, "An overview of fission product release mechanisms", SCK•CEN Report R-3144, 1997.
- [5] P. VAN UFFELEN, "Developments of a new fission gas release and fuel swelling model", Enlarged Halden Programme Group meeting, Lillehammer (Norway), 1998, HPR-349.
- [6] U.M. EL-SAIED, D.R. OLANDER, "Fission gas release during grain growth", *J. Nucl. Mat.* 207 (1993) 313–326.
- [7] D.R. OLANDER, "Combined grain-boundary and lattice diffusion in fine-grained ceramics", *Advances in Ceramics*, Vol. 17 (1986) 271–293.
- [8] M.V. SPEIGHT, J.A. TURNBULL, "Enhanced fission product release by grain boundary diffusion", *J. Nucl. Mat.* 68 (1977) 244–249.
- [9] K. UNE, S. KASHIBE, "Fission gas release during post irradiation annealing of BWR fuels", *J. Nucl. Sci. Techn.* 27 (11), (1990) 1002–1016.
- [10] R.J. WHITE, M.O. TUCKER, "A new fission gas release model", *J. Nucl. Mat.* 118 (1983) 1–38.
- [11] R.J. WHITE, "A new mechanistic model for the calculation of fission gas release", Proceedings ANS Top. Meet. on LWR Fuel Performance, West Palm Beach, Florida (USA), April 17–21, (1994).
- [12] M. MOGENSEN, C. BAGGER, C.T. WALKER, "An experimental study of the distribution of retained xenon in transient-tested UO<sub>2</sub> fuel", *J. Nucl. Mat.* 199 (1993) 85–101.
- [13] C.T. WALKER, P. KNAPPIK, M. MOGENSEN, "Concerning the development of grain face bubbles and fission gas release in UO<sub>2</sub> fuel", *J. Nucl. Mat.* 160 (1988) 10–23.
- [14] C.T. WALKER, M. MOGENSEN, "On the rate determining step in fission gas release from high burnup water reactor fuel during power transients", *J. Nucl. Mat.* 149 (1987) 121–131.
- [15] M.O. TUCKER, "Grain boundary porosity and gas release in irradiated UO<sub>2</sub>", *Rad. Eff.* 53 (1980) 251–256.
- [16] P. VAN UFFELEN, "Assessing the contribution of grain boundary diffusion to fission gas release in nuclear fuel", Enlarged Halden Programme Group meeting, Loen (Norway), 1999.
- [17] T. KOGAI, "Modelling fission gas release and gaseous swelling of light water reactor fuels" *J. Nucl. Mat.* 244 (1997) 131–140.
- [18] P. VAN UFFELEN, "Modelling precipitation of fission products at grain boundaries in nuclear fuel" submitted to *J. Nucl. Mat.*, 1999.
- [19] T.J. BJORLO, E. KOLSTAD, C. VITANZA, "FUEL-TEMP-2 computer programme for analysis of the steady state thermal behaviour of oxide fuel rods", HPR-211, March 1977.

- [20] HILLERT, "On the theory of normal and abnormal grain growth", *Acta Metallurgica*, 13 (1965) 227.
- [21] C. RONCHI, P.T. ELTON, "Radiation re-resolution of fission gas in uranium dioxide and carbide", *J. Nucl. Mat.* 140 (1986) 228–244.
- [22] D.R. OLANDER, "Fundamental aspects of nuclear reactor fuel elements", TID-26711-P1 (1976).
- [23] A. DENIS, R. PIOTRKOWSKI, "Simulation of isothermal fission gas release", *J. Nucl. Mat.* 229 (1996) 149–154.
- [24] M.V. SPEIGHT, "A calculation on the migration of fission gas in material exhibiting precipitation and re-resolution of gas atoms under irradiation", *Nucl. Sci. Eng.* 37 (1969) 180–185.
- [25] J.A. TURNBULL, "A review of irradiation induced re-resolution in oxide fuels", *Rad. Eff.* 83 (1980) 243–250.
- [26] R. HARGREAVES, D.A. COLLINS "A quantitative model for fission gas release and swelling in irradiated uranium dioxide", *J. BR. Nucl. Energy Soc.*, Vol 15. No. 4 (1976) 311–318.
- [27] D.M. DOWLING, R.J. WHITE, M.O. TUCKER, "The effect of irradiation-induced re-resolution on fission gas release", *J. Nucl. Mat.* 110 (1982) 37–46.
- [28] L. LANDAU, E. LIFCHITZ, "Physique Théorique. Mécanique des fluides", Chap. 2, MIR, 1971.
- [29] S. KASHIBE, K. UNE, "Effect of external restraint on bubble swelling in UO<sub>2</sub> fuels", Enlarged Halden Programme Group meeting, Lillehammer (Norway), 1998, HPR-349.
- [30] M.V. SPEIGHT, W. BEERE, "Vacancy potential and void growth on grain boundaries", *Metal Science* 9 (1975) 190–191.
- [31] M.S. YANG, J.R. WEERTMAN, "A test of grain boundary void growth theories by small angle neutron scattering", *Scripta Metallurgica* 18 (1984) 543–548.
- [32] J.R. MATTHEWS, M.H. WOOD, "A simple operational gas release and swelling model II. Grain boundary gas", *J. Nucl. Mat.* 91 (1980) 241–256.
- [33] M.R. HAYNS, M.W. FINNIS, "The response of grain boundary cavities to stress and temperature changes under conditions of continuous gas generation", *Nucl. Sc. Techn.* 1 (1979) 255–260.
- [34] H. ZIMMERMANN, "Investigations on swelling and fission gas behaviour in uranium dioxide", *J. Nucl. Mat.* 75 (1978) 154–161.
- [35] P. KNUDSEN, C. BAGGER, M. MOGENSEN, H. TOFTEGAARD, "Fission gas release and fuel temperature during power transients in water reactor fuel at extended burnup", IAEA-TECDOC-697, 1993, 25–31.
- [36] M. MOGENSEN, C. BAGGER, H. TOFTEGAARD, P. KNUDSEN, "Fission gas release below 20 kW/m in transient tested water reactor fuel at extended burnup", IAEA-TECDOC-697, 1993, 32–37.
- [37] R. MANZEL, R.P. BODMER, G. BART, "Fission gas release in high burnup fuel", IAEA-TECDOC-697, 1993, 63–67.
- [38] T. KOGAI, K. ITO, Y. IWANO, "The effect of cladding restraint on fission gas release behaviour", *J. Nucl. Mat.* 158 (1988) 64–70.
- [39] NAKAMURA, M. SUZUKI, H. UETSUKA, "Re-irradiation tests of LWR spent fuel at JMTR", Enlarged Halden Programme Group meeting, Loen (Norway), 1999.
- [40] J.A. TURNBULL, "An assessment of fission gas release and the effect of microstructure at high burnup", Halden Work Report HWR-604, 1999.

# **Influence of rounds sub-grains in high burnup UO<sub>2</sub> fuel**

**N. Lozano, L. Desgranges**

CEA/DRN/DEC/SECI/LECMI,  
Centre de Cadarache, Saint Paul lez Durance

**D. Aymes, J.C. Niepce**

Université de Bourgogne,  
LRRS Dijon

France

## **Abstract**

In a recent paper, it has been shown that the so called “rim structure” in high burnup UO<sub>2</sub> fuel contains in fact two types of sub-grains: polyhedral and round ones. Polyhedral sub-grains have an average size of approximately 0.5 μm, and have been observed for more than ten years. The faceted porosity associated to these polyhedral sub-grains is characteristic of the rim effect. Round sub-grains have an average size of approximately 0.2 μm and are found to be formed on the free surface of initial grains or of polyhedral sub-grains. Round sub-grains can be observed in the rim area and also continuously from the periphery to the mid-pellet. This suggests that round sub-grains do not depend on rim effect, but are more likely to derive from a surface effect. In this contribution SEM photographs showing the evolution of the round sub-grains morphology will support a proposed mechanism for round sub-grains formation. This mechanism involves a surface modification due to stresses applied on a free surface using the Greenfel'd formalism. These stresses could be due to segregation of fission products on some grain faces. This supposition is supported by EPMA experiments which show the segregation of some fission products on surfaces where round sub-grains are observed, while other surfaces with no round sub-grains have the same concentration in fission products as the bulk of the grains. Segregation of fission products on surface has also been observed in CANDU fuel by XPS. This specific behaviour of fission products gives a new insight in the chemistry of irradiated fuel and asks the question of the influence of round sub-grains formations on the release of fission products.

## **1. INTRODUCTION**

In the seek of high burnup for LWR fuels, one important aspect is the occurrence of the so called “rim” structure. The rim effect is now known for years and has been extensively studied by optical ceramography and Electron Micro Probe Analysis (EMPA): it is characterised by an increase of porosity [1], a decrease of the concentration of xenon as seen by EMPA [2] and a subdivision of the initial grain (whose size is about 10 μm) into much smaller sub-grains (whose size is about 0.5 μm) [3].

Recently, however, a study using high magnification SEM [4] gave a new insight of the rim phenomenon, showing that two types of sub-grains should be considered and not only one as previously thought. This examination indeed evidenced the coexistence of already observed polyhedral sub-grains (0.5-0.8 μm) and round sub-grains (0.1μm) which were identified for the first time. Rounds sub-grains were shown to appear on open surfaces, especially inside

pores [4]. In this paper, new experimental material on round sub-grains is presented, and their formation mechanism is discussed in more details.

## 2. EXPERIMENTAL

The UO<sub>2</sub> samples, with nominal enrichment of 4.5% of <sup>235</sup>U, were taken from two PWR fuel rods, J07 and J12, with zircaloy cladding, irradiated simultaneously in a EDF power reactor for five and four cycles respectively. Table 1 gives the values of the mean linear power density for each cycles for J07. Pellets of 8.19 mm diameter, and 13.7 mm long exhibit a 10.45 density with a total porosity of 4.4 %. Grain size varies from 12.2 μm at the pellet edge to 10.2 μm at the pellet centre.

Sampling was made at 800 mm from the bottom of the fissile column for J07, and 2870 mm from the bottom of the fissile column for J12. The average local burnup was calculated to be 61 and 49.7 GWd/tU for J07 and J12 respectively. The two slices obtained were polished up to a surface roughness of about 1 μm. The samples were embedded in metallic alloy with low melting point, as required for Electron Probe Micro Analysis. A part of J07 polished cross section was damaged giving an area that can be considered as a fresh fractured one. Thus, it was possible to observe and compare fuel structure both with a polished surface and a fractured surface.

SEM characterisations were performed with a shielded SEM Philips XL30 on J07 sample.

Electron Probe Micro-Analysis (EPMA) was performed with a shielded CAMEBAX on J12 sample to study fission products concentration on open surface in the inside of pores. This measure is difficult because the analysed surface is not perpendicular to the electron beam. The sample surface is indeed perpendicular to the electron beam, but the grain surface inside a pore is not. Therefore the usual quantitative method to measure the concentration of an element cannot be applied. So the concentration of an element was measured using uranium as a reference. Uranium is supposed to keep constant in the area where the measure in a pore was performed, and its real concentration is measured on a flat surface outside of the pore. This measure depends on the orientation of the detector towards the analysed surface. On a flat surface perpendicular to the electron beam, the four spectrometers of our CAMEBAX give an equivalent signal, but it is not the case if the surface is no more perpendicular to the beam. So only elements which are measured on the spectrometer used uranium can give a quantitative measurement. This implies that no reliable data could be obtained on Caesium and neodymium. The results presented in this paper were all obtained with the presented method.

## 3. RESULTS

SEM study was devoted to the characterisation of round sub-grains as a function of their location on the pellet. The examination of grain surface was performed inside fabrication pores revealed by polishing, all along a pellet radius. A specific evolution of surface morphology is illustrated on Photo 1 to 3.

Photo 1a illustrates the three types of surface morphology that can be observed from pellet centre to 500 μm from pellet edge. In pellet centre, grain surfaces are plane, dotted with 0.1 to 0.3 μm pores. Grains can also exhibit surfaces with stairs 0.7 μm thick, that can be viewed as a succession of hills and valleys along one direction. The third surface morphology consists in a two dimensional array of hills and valleys defining 0.3 to 0.6 μm rectangular sub-grains. The

arrangement of the sub-grains follows a very regular pattern, as shown in Photo 1b which is a detail of Photo 1a.

Only two dimension ordered surfaces are observed while getting close to the pellet edge as shown on Photo 2. On this photo the influence of the crystallographic orientation of the grain face is evidenced. In the centre of the Photo 2, a grain face exhibits square-shaped sub-grains, aligned along row making right angles between each other. On the hexagon-shaped face on the right of the Photo 2, sub-grains look like ellipsoids with their greatest direction aligned. On the face in the bottom of Photo 2, sub-grains are more or less round and aligned along some specific directions. These patterns reflect the crystallographic orientation of the face. They do not appear at the same radius as it is clearly demonstrated by the comparison between Photo 1 and 2.

At 200  $\mu\text{m}$  from the pellet edge, (Photo 3) sub-grain shape becomes more spherical. Inside rim area (Photo 4), at 150  $\mu\text{m}$  from the cladding, it becomes clear that the ordered pattern disappears leaving room for a random distribution of round sub-grains. From the previous photo, the size of the round sub-grains decreases when approaching the pellet outer surface, as summarised in Table 2. In fact the size evolution of round sub-grains is not continuous. It seems that once a sub-grain is created, it is cut in smaller sub-grains. This is clearly seen on Photo 3, where sub-grains with approximately 0.7 $\mu\text{m}$  size are still visible, while new sub-grains of 0.2-0.3  $\mu\text{m}$  appear inside the former ones.

EMPA measurements were performed in a fabrication pore located at 90  $\mu\text{m}$  from the pellet edge. The positions, where measurements were performed, are given on photo 5 and labelled by a number. Points 1 and 2 are located in the bulk of a grain. Points 3 and 4 are located on the edge of the grain. Points 5 and 6 are located on grain faces where round sub-grains are observed. Usually EPMA measurements are performed in the bulk of the grains.

The quantitative results, normalised to the intensity of uranium (see experimental), are plotted on Figure 1 for xenon, molybdenum and ruthenium. Uranium, zirconium, oxygen, plutonium and palladium were also measured. These last fission products have a constant concentration except palladium which behaves like molybdenum and ruthenium. Xenon concentration decreases from grain bulk to round sub-grains. For ruthenium and molybdenum, on the contrary it increases. Caesium and neodymium could not be measured in suitable conditions because their signal cannot be detected on the same detector as uranium.

The concentration of the metallic fission products is given by the fission yield in the grain bulk. This means that a segregation of metallic fission products occurs on the grain face with round sub-grains with a greater concentration than the one given by the fission yield.

At 90  $\mu\text{m}$  from the edge of the pellet, EPMA in standard conditions already reveals a lack of xenon compared to the fission yield. This means that the concentration measured in the bulk of the grain should be lower than the one given by the fission yield. The decrease on the grain face with round sub-grains should be interpreted as a depletion of fission gas on this surface.

#### 4. DISCUSSION

These new EPMA results enlighten a specific chemical effect on the surface where sub-grains appear. It is of importance since no chemical evolution at the grain scale of French LWR has been observed before except the formation of small metallic clusters in the rim. In the

following an interpretation of this chemical evolution is proposed, and then a mechanism for the formation of the round sub-grains is described as a consequence of this chemical evolution.

#### **4.1. Chemical Evolution**

Rare gases and metallic fission products are known to be non-soluble in  $\text{UO}_2$  and  $(\text{UPu})\text{O}_2$  fuel. TEM observation on  $\text{UO}_2$  fuel evidenced nano-bubbles of rare gases associated with nano-clusters of metallic precipitate (Mo, Ru, Tc, Rh) [5]. In the vicinity of a grain boundary, these elements are more likely to segregate, which induces an enrichment of the grain boundary. This enrichment is not uniform because some faces are enriched and others are not.

This can be related to the crystallographic orientation of the grain face. As an example of the influence of the grain orientation, recent calculations [6] determined the most stable grain faces of a  $\text{UO}_2$  crystal. The behaviour of fission products may then be different as a function of the crystallographic orientation of the grain face. This has been recently demonstrated for the formation of gas bubbles in irradiated fuel heated to temperatures over  $1400\text{ }^\circ\text{C}$  [7]. In our case the enrichment of some grain faces can be interpreted by different diffusion coefficient, the faces with the lowest diffusion coefficient act as sink for mobile fission products.

Thus a phenomenon of grain face enrichment should be taken in consideration. It depends on burnup which determine the amount of fission products and also on the temperature (who is linked to linear power of the rod) which influences the diffusion coefficient. Its dependence on crystallographic orientation could become less sensitive when burnup is high enough to segregate fission products on all faces. This would be consistent with Photo 4 which shows the whole inside of pore covered with round sub-grains.

Surface segregation has already been observed on CANDU fuel by X-ray Photo-electron Spectroscopy (XPS) [8]. A fractured surface of the order of  $1\text{ mm}^2$  was analysed. So it was not possible to distinguish between grain boundaries and grain free surfaces, and also not possible to isolate the contribution of face with round sub-grains, although they were clearly observed. CANDU fuel routinely exhibited segregation of Caesium, Ruthenium, tellurium and barium on the surface of the sample. Our results also show a segregation of ruthenium, but unfortunately all the fission products can not be compared between the two experiments because of the detection limits of the two methods and because of our specific procedure (see experimental). Apparently, despite the differences between the two fuels and their irradiation histories, it seems that the same phenomenon of surface segregation occurs on surfaces with round sub-grains, according to our results.

#### **4.2 Morphological Evolution**

Segregation of fission products has been evidenced previously. This segregation has not only a chemical but also a mechanical influence. The size of the  $\text{UO}_2$  unit cell indeed varies with the concentration of doping elements. The difference in concentration of fission products between the face and the bulk of a grain then implies a difference of cell parameter, which means a stress between the face and the bulk of the grain. The behaviour of a stressed surface can be described in the frame of the Greenfel'd mechanism.

Asaro and Tiller [9] and Greenfel'd showed that a stressed surface (in their case a thin film on a semiconductor) is unstable, and that a wavy surface is formed with a given wavelength  $\lambda_p$ .

Grihlé [10] calculated the energy of this system as a balance of an increase of energy due to the increased surface and a decrease of energy due to the stresses relaxed in the bent areas of the surface. Considering that the shape of the surface is a sinusoid,  $\lambda_p$  can be calculated [10], and is equal to

$$\lambda = \frac{4\pi\mu\gamma}{(1-\nu)\cdot\sigma_0^2} \quad (1)$$

with  $\mu$  the elastic modulus,  $\gamma$  the surface energy,  $\nu$  the Poisson coefficient and  $\sigma_0$  the stress applied on the surface.

When increasing the stress, the surface can become more complex than a sinusoid, and Grihlé proposed a mechanism leading to the formation of round oscillations as illustrated on Figure 2 [10]. However the formation of round sub-grains needs bulk diffusion processes to be active.

The conditions needed for Greenfel'd effect are operating on a grain face in the inside of the pore, i.e. a stressed surface and surface diffusion. And the observed round sub-grains are consistent with the predicted evolution of the surface with Greenfel'd mechanism.

The segregation of fission product on a surface are supposed to create a stress on the grain face. It is known that the burnup increases when reaching the edge of high burnup LWR pellet [11]. When increasing burnup, the concentration of fission products increases and the segregation of some fission products on the grains faces should also increase. As a consequence, the induced stress should increase and, using equation (1), the size of the round sub-grains should decrease. This is consistent with our observations where the size of the round sub-grains is evidenced to decrease when approaching the pellet edge (see table 2). Our observations also show that smaller sub-grains are formed by slicing former ones. This is consistent with a Greenfel'd effect in the case of an increasing surface stress. After first round sub-grains are formed, with increasing burnup a stress is created on their surface by the newly formed fission products. Because of this new stress the surface of the round sub-grains becomes wavy, however this wavy surface is not infinite and has the bounding condition that the stresses are released on the sub-grains edges. As a consequence the wavelength is a multiple of the sub-grain size which is observed.

Greenfel'd effect is defined for a free surface. This is consistent with our results, showing that round sub-grains are only obtained on the grain faces in the inside of a pore. Greenfel'd effect also needs diffusion. In the case of irradiated  $UO_2$ , bulk diffusion is expected to be very low at the operating temperature where round sub-grains are observed. However surface diffusion is much higher than bulk diffusion, and a thermal diffusion due to fission recoils must not be neglected.

### 4.3 . Xenon Behaviour

Among all the fission products measured with EPMA, xenon has a specific behaviour. Its concentration decreases on surfaces where round sub-grains appear. This is consistent with the hypothesis of surface diffusion. Xenon is indeed non-soluble in  $UO_2$  and is likely to leave the  $UO_2$  matrix if it can diffuse to a free surface.

Thus a new type of gas release is evidenced. Its influence on the total gas release can be estimated by taking into account the free surface of the fuel and the depth out of which the gas

can escape. This can be of importance in the case of the rim. Taking a rim with 10% of porosity and with spherical pores of 1  $\mu\text{m}$  diameter, the gas release in the pores associated to round sub-grains formation could be as high as 30 % of the total inventory of gas of the rim, if it is assumed that all the gas has escaped from a layer of 1 $\mu\text{m}$  depth opposite to the pores. It would be 6% if a layer of only 0.2 $\mu\text{m}$  depth is considered. Round sub-grains formation could then significantly contribute to the gas release in the rim.

This hypothesis is supported by the measured concentration of remaining xenon. It is indeed approximately the same in the rim [2] and on the grain faces with round sub-grains, equal to 0.2-0.3 % in mass.

## 5. CONCLUSION

Newly evidenced round sub-grains were studied by SEM and EPMA. Results emphasise a segregation of some fission products on the grains faces where round sub-grains appear. An interpretation is proposed assuming the modification of the grain face due to the stresses created by the segregation of fission products. From the obtained results it can be concluded that round sub-grains formation may have an important play on:

- Surface reactivity of the  $\text{UO}_2$  fuel because of the segregation of fission products on the free surface of the fuel.
- Fission gas release in the rim because of its high density of pores covered with round sub-grains.

## ACKNOWLEDGEMENTS

The authors want to thank B. Pasquet and V. Cuisset who perform the EPMA experiment, and J. Noirot for fruitful discussions.

## REFERENCES

- [1] J. SPINO, K. VENNIX, M. COQUERELLE, J. Nucl Mater vol 231 (1996) 179–190.
- [2] C.T.WALKER, J. Nucl Mater vol 275 (1999) 56–62.
- [3] HJ. MATZKE J. Nucl Mater vol 189 (1992) 141–148.
- [4] N.LOZANO, L.DESGRANGES, D.AYMES, J.C.NIEPCE J. Nucl Mater vol 257 (1998) 78–87.
- [5] K. NOGITA, K. UNE, Y. KOREI Nucl. Instr. and Meth. in Phys. Res. B116 (1996) 521–526.
- [6] M.ABRAMOWSKI, R.W.GRIMES, S.OWENS J. Nucl Mater vol275 (1999) 12–18.
- [7] Ph.D thesis, S.Vallin Université de Grenoble 1999.
- [8] W.H.HOCKING, A.M.DUCLOS, L.H.JOHNSON J. Nucl Mater vol 209 51994° 1–26.
- [9] R.J. ASARO, W.A. TILLER Metall. Trans. Vol 3 (1972) 1789.
- [10] J. GRILHE. Europhys. Lett. vol 23 (2) (1993) 141–146.
- [11] H.J. MATZKE, A. TUROS J. Nucl Mater vol 188 (1992) 210–215.

Table 1: Linear Power values for each irradiation cycle for J07

<b>Cycle</b>	1	2	3	4	5
<b>Linear Power W.cm-1</b>	220	270	230	190	170

Table 2: Grain open surface observation on fabrication pores

<b>Distance from the pellet edge in <math>\mu\text{m}</math></b>	0 to 50	150	200	500 to 2000
<b>Rolls or subgrain size in <math>\mu\text{m}</math></b>	0,1	0,2-0,5	0,3-0,7	0,7
<b>Observations</b>	Disordered Round subgrains	Disordered Round subgrains	Ordered Round subgrains	Ordered rolls

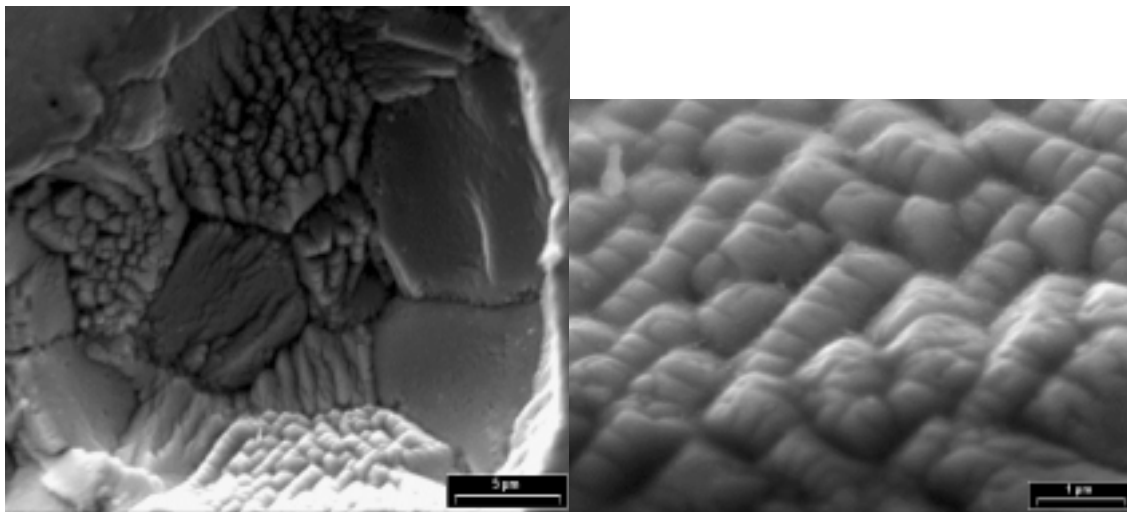


Photo 1a : inside of a pore located at 500  $\mu\text{m}$  from the pellet edge, where sub-grains appear on some faces and not on other ones.

Photo 1b : detail of Photo 1a showing the 2 dimension ordered pattern formed by round sub-grains.

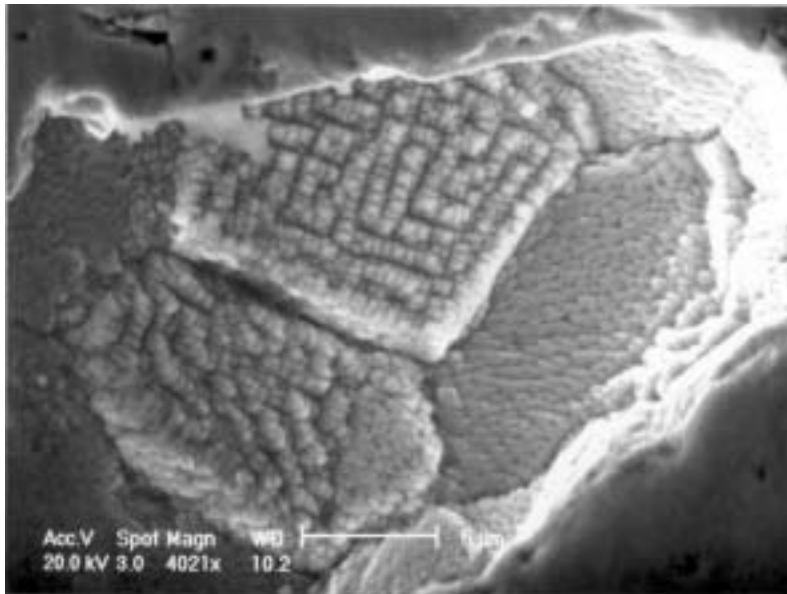


Photo 2 : inside of a pore showing different patterns of ordered sub-grains.

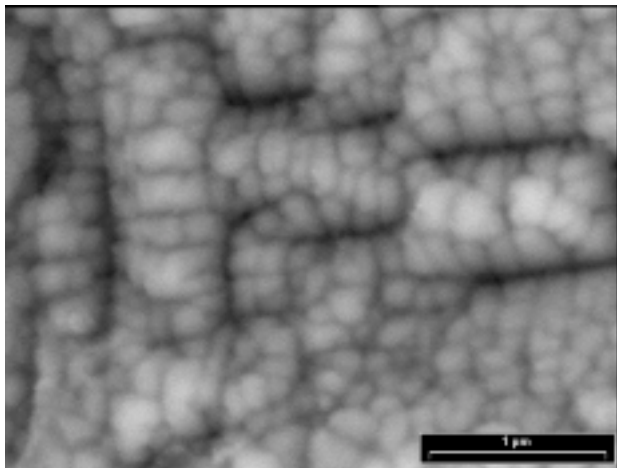


Photo 3 : At 200  $\mu\text{m}$  from the pellet edge on a fabrication pore, grains face subdivision on rolls, which are subdivided on ordered round sub-grains.

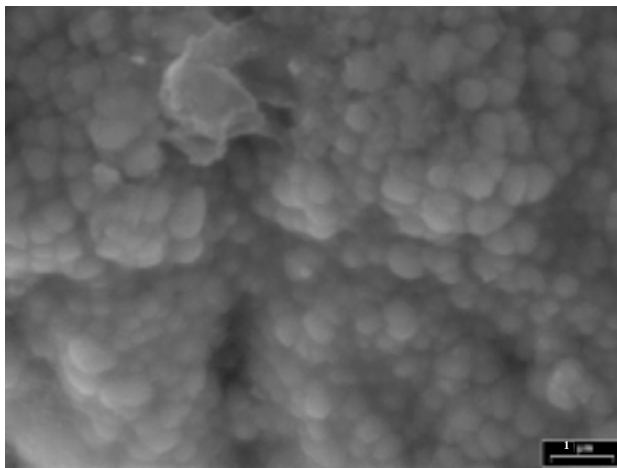


Photo 4 : at 150  $\mu\text{m}$  from the pellet edge, disordered round sub-grains on a fabrication pore.

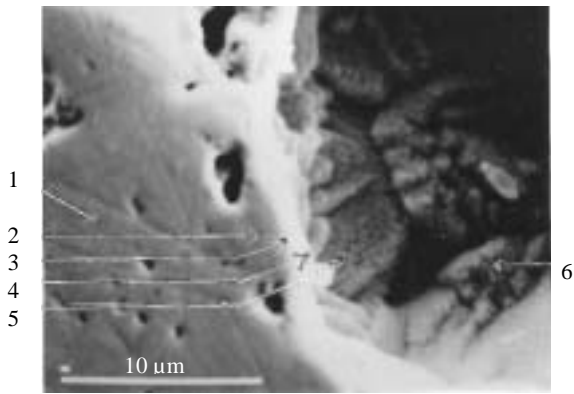


Photo 5: points where EPMA measurements were performed in a pore located at 90 μm from the pellet edge.

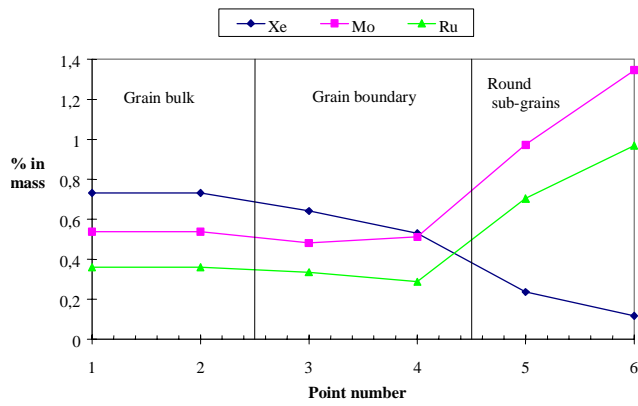


FIG. 1: mass percentage of xenon, molybdenum and ruthenium measured on photo 5.

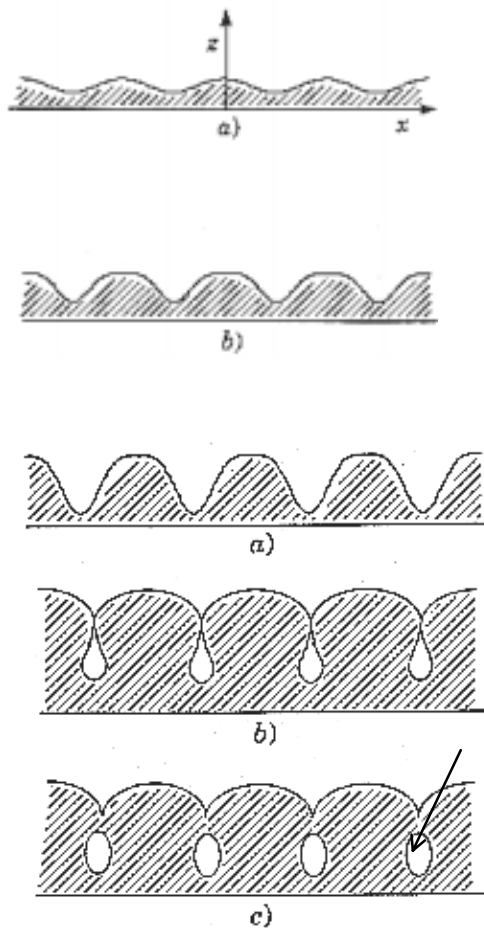


FIG. 2: evolution a free surface under increasing stress according [10].

# Does rim microstructure formation degrade the fuel rod performance?

**D. Baron**

EDF Etudes et Recherches, Moret-sur-loing, France

**J. Spino**

CEC Joint Research Centre, ITU, Karlsruhe, Germany

**Abstract.** High burnup extension of LWR fuel is progressing to reduce the total process flow and eventually the costs of the nuclear fuel cycle. A particular fuel restructuring at high burnups, commonly observed at the periphery of LWR fuel pellets (rim structure), but also in FBR fuels to some extent and in the Plutonium rich clusters of the MOX Fuels, was considered a priori as a limitation for burnup extension. Since more than ten years this rim effect have been deeply investigated. Its causes and consequences are however not yet totally elucidated. The three steps actually identified of this phenomenon are first a progressive disappearing of the intra-granular Xenon, the outset of numerous 0.5 to 1  $\mu\text{m}$  pores and finally a grain subdivision around the pores. Penalty of the porosity increase on the thermal conductivity is obvious. One expect the fission gases to remain trapped in the rim porosity up to a 75 MWd/kgUO<sub>2</sub> local burnup. Above this threshold, 15 to 20 % of the fission gases seem to be quickly released. Microindentation tests conducted at ITU have shown the rim structure to resist fracture extension under punching. It is still open whether this implies certain ductility and viscosity of the material, or if it corresponds to stress relaxation by microcracking. Whatever the case be, it is suggested that the rim material would be able to decrease the interaction stresses and to equalise the cladding strains during a power ramp. Moreover, in the RIA tests, it was concluded so far that the grain de-cohesion caused by gas expansion at the grain boundaries was responsible for the cladding strain and failure. However, not the rim zone was affected by grain de-cohesion but the region adjacent to it. Therefore, in front of the question whether the rim structure degrades the fuel rod behaviour, we continue to argue on its benefit for fuel burnup extension.

## 1. INTRODUCTION

High burnup extension of LWR fuel is progressing to reduce the total process flow and eventually the costs of the nuclear fuel cycle. A particular fuel restructuring at high burnups, commonly observed at the periphery of LWR fuel pellets (rim structure), but also in FBR fuels to some extent and in the Plutonium rich clusters of the MOX fuels, was considered a priori as a limitation for burnup extension.

Since more than ten years this rim effect has been deeply investigated. Albeit, controversies are still existing on the rim formation process and its consequences on the LWR fuel management with increasing burnups. Even if the rim affect only, as in most of the cases, a thin peripheral zone around the fuel pellet, it plays a primordial role in the pellet to cladding mechanical interaction, in the gap-thermal conductance and, directly or indirectly, in the fission gas release at high burnups. However, from all the data available today, it can be said that the rim formation is more a benefit than a disadvantage for the global fuel rod thermo-mechanical behaviour. Arguments for this statement are given in the following sections.

## 2. CHARACTERISATION OF A HIGH BURNUP FUEL PELLETS

In most of the cases four radial zones can be distinguished on the ceramographic picture of a high burnup irradiated fuel pellet cross section (figure 1); each zone is characterised by a different evolution of the porosity feature due to different local temperatures and cumulated burnups. A description of these zones can be done as follows:

- The central part which has operated at temperatures higher than 1150°C, where a large part of the fission gases has been released. The longer the temperature has been over 1150°C, the higher the fraction of gases that will be released. Then most of the gases move towards the grain boundaries and progressively diffuse along the grain surfaces, leaving large pores at the triple boundaries locations and smaller pores along the grain surfaces. The grains themselves are often free of porosity.
- The so called intermediate fission gas release zone which has operated at temperatures between 1000 and 1150°C and exhibits a dark appearance on the ceramography. This dark aspect is due to a very dense intra- and inter-granular thin porosity, < 1 µm diameter, that is mainly revealed on etching. On EPMA analysis, this zone corresponds to the transition between the central high release fraction zone and the outer part of the pellet with a low release fraction.
- The third zone, often called the “under-rim” zone, where the initial large porosity is still observable intact. The thin “as-fabricated” porosity has disappeared due to fission activated densification during the first irradiation cycles.
- Finally, the outermost 200 to 500 µm-thick region called the “rim zone”, which exhibits a dense intra- and inter-granular thin porosity similar to the second zone about 1 µm diameter, as soon as the local burnup exceeds 55 MWd/kgUO<sub>2</sub>. Origin of this zone is the neutron self shielding effect of the Uranium 238, that makes the burnup profiles to become very steep in the outer zone (200 µm), leading to a local pellet edge burnup more than twice the average pellet burnup (e.g., in standard LWR fuels with an Uranium 235 enrichment in the range 3.5 to 4 %). Generally a grain subdivision is observed, turning progressively to a kind of cauliflower structure (figure 2). For power reactor fuels, this phenomenon has been identified in the eighties first within a Franco-American high burnup program named PWS1.72 (Framatome-Westinghouse-EDF-CEA) and then confirmed within the HBEP international program [1].

## 3. RIM FORMATION STEPS OBSERVATIONS

Since 1985, many works have been conducted for a better understanding of the rim structure formation. Controversies still exist in the interpretation of the formation kinetic or formation steps. The main discussion concerns the mechanisms driving the grain subdivision. In a previous paper [2] we brought an argumentation on the chronology of the rim formation, having the conviction that all the phenomena involved do not start simultaneously at a unique burnup and that the grain subdivision may be not necessarily achieved, depending on the irradiation conditions. Thus, we argued that three or four steps may be observable in the rim formation, in the following sequence:

Step 1 — decrease in the matrix-Xenon concentration as detected by EPMA for burnups around and above 55 MWd/kgUO<sub>2</sub>.

Step 2 — The onset and growth of micrometer sized pores starting not necessarily on the original grain boundaries.

Step 3 — Local grain subdivision around the pores with equiaxed-sharp shaped subgrains in a size range 100 to 500 nanometers,

Step 4 — Propagation or not of the grain subdivision in regions between the pores, depending on the particular irradiation conditions and fuel characteristics (e.g. higher  $^{235}\text{U}$ -enrichment and larger  $\text{UO}_2$ -grain size seem to delay this propagation step).

#### 4. POSSIBLE RIM FORMATION MECHANISM

TEM on 55 MWd/kg $\text{UO}_2$  uniformly burned samples has shown that during the above described step 1, an onset of nanometers sized bubbles is observed inside the grains, often distributed along dislocation lines (figure 3). The rim zone is operating at temperatures too low for defect recovering ( $< 750^\circ\text{C}$ ). Thus, the lattice energy is continuously increasing due to the numerous accumulated defects, i.e. Frenkel pairs in the Oxygen sub-lattice, Schottky neutral defects (vacancies trios: i.e. one U and two O-vacancies), and also other defects as fission elements occupying interstitial positions. Xenon has a high yield rate, about 30 atoms for 100 fissions. Usually, Xenon is accommodated by Schottky defects, whose number increases with the fission density. However, if one can evaluate that at 60 MWd/kg $\text{UO}_2$ , nearly 2 % of the atoms other than Oxygen are Xenon or Krypton, it is certain that the Schottky sites may become saturated at a certain burnup. When the number of Xenon atoms overpasses the number of sites available they can precipitate into small bubbles, join the nearest porosity or enter in an interstitial position. Added to the other fission products in interstitial positions, these atoms can progressively distort the lattice, increasing the lattice strain (lattice parameter) so far that the system becomes unstable.

This instability would result in an increase of the mobility of the vacancies, group of vacancies or interstitials. In other terms, one would observe that the apparent diffusion coefficient of the vacancies and of the Xenon increases when this instability is reached. (We have evaluated in a previous publication [3] that the Xenon diffusion coefficient would be increased by a factor 100 in the rim zone.) However, the diffusion distance is small accounting for the numerous group of defects able to trap the vacancies and the Xenon (group of vacancies, dislocation lines, dislocation clusters, grain boundaries), so that trapping of vacancies would lead in a **first step** to the formation of nano-pores, as those observed by TEM along the dislocation lines.

These tiny pores are certainly still able to move or to be destroyed by fission spikes, thanks to their small size. Some pores are more bonded than others. These bonded pores should then be able to grow, provided the inflow of surrounding mobile vacancies. This assumption should then lead to the **second step**, which exhibits micro-meter pores uniformly distributed with a distance between pores of the order of the average free path of the defects. The pore trapping results in a vacancies depletion in its neighbourhood, and then to a local excess of interstitials not able to recombine. The Xenon next to these pores has then a high probability to be trapped.

The high density of fission spikes induces a perpetual exchange of Xenon between the pore and the surrounding matrix (about 100 nm). This is the resolution process. This exchange between the pores and the fuel could lead to a grain subdivision around the pore by a surface diffusion mechanism (figure 4). However, this kind of grain subdivision would appear on any

type free surface (as-fabricated pores, cracks, etc), also in hotter parts of the fuel [4]. Differently to that, the characteristic grain subdivision of the rim-zone (**third step** of the above section), with formation of 200 to 500 nm sized polyhedral subgrains around micrometer pores, may be explained by the formation of dislocation walls and the rotation of the lattice fragments to relax stresses. UNE and NOGITA [5] have observed this disorientation between the sub-grains.

However, referring to the **forth step** of section 3 and to our work reported in reference [2], this grain subdivision have not been observed to propagate beyond the pores in the examined N118 fuel rod, irradiated up to 67 MWd/kgUO<sub>2</sub> in the BR3 reactor with a pellet edge burnup about 110 MWd/kgUO<sub>2</sub> (figure 5). How can it be explained? We give here a possible interpretation.

Most of authors presume that rim pores become over-pressurised, inducing a compressive stress field in their neighbourhood. This stress field can then act as a driving force for point defect mobility, aiding the feeding of the dislocation loops and the reorganisation of the fuel lattice (i.e. sub-grain formation). However, these micro-stress fields may be eventually balanced by the average hydrostatic pressure (i.e. the macro-stress field), induced by fuel “solid” swelling with subsequent PCMI (Pellet/cladding mechanical Interaction).

The particular N118 fuel rod mentioned in reference [2] had a recrystallised Zircaloy-4 type cladding (CEA standard with a final heat treatment at 575°C). Furthermore, this rod has been irradiated most of the time in the periphery of the BR3 reactor, where the high energy neutron flux was two times lower than in a commercial PWR. Therefore, during irradiation, the cladding creep rate has been more than four times lower than in a standard fuel rod. This has led to a PCMI stress on the cladding four times higher than normal, estimated to be around 160 to 180 MPa instead of the usual 40 MPa in standard EDF PWR fuel rods. Then, it is possible that the increased hydrostatic stress has slowed down the stress controlled point defect mobility in the rim-zone and therefore delayed the grain subdivision.

On the other hand, non-constrained samples irradiated within the HBRP project [6], have achieved a total grain subdivision for burnups as low as 80 MWd/kgUO<sub>2</sub>.

## 5. TEMPERATURE AND BURNUP THRESHOLD FOR RIM FORMATION

From lattice parameter and thermal diffusivity measurements, one can assume that the thermal recovery of the lattice defects starts between 750 and 800 °C. That allows to say that the lattice damage, if that being the main responsible of the rim formation, is sufficiently reduced above this temperature threshold so as to avoid rim formation. Speaking of the burnup threshold, we have already given the value of 55 MWd/kgUO<sub>2</sub> for the initiation of the rim processes.

However, on account of results of the HBRP project, managed by CRIEPI and in which EDF is involved, and whose main address is to better define these two thresholds [6] [7] [8] [9], it seems that the temperature threshold has not been confirmed, as grain subdivision has been observed on samples which have operated at temperature higher than 1000 °C.

But there, the criterion for rim formation had been the grain subdivision. Other criteria can be used, however, to define the rim width on a pellet cross section: i.e. Xenon depletion on EPMA profiles, radial pore buildup onset, decrease of the hardness properties. Depending on the criteria, the rim width evaluation would be not always the same. The question is then, whether the grain subdivision can be considered specific to the rim.

## 6. GRAIN SUBDIVISION AND RIM

We have reported here above that the identification of the rim can be based on several criteria: the partial disappearance of fission gas atoms on EPMA, the onset of numerous intra- and inter-granular micrometers pores and the grain subdivision with a cauliflower like structure, etc.

Disappearance of gas atoms can also be observed in the central part of the fuel. The only difference is that in the rim the Xenon mobility is not due to thermal activation. On the other side, onset of numerous intra- and inter-granular micrometers pores are also observable in the fission gas release transition zone (1050°C–1150°C), where the main phenomenon involved concerning the gas mobility is the thermally activated Xenon diffusion.

Also, the grain subdivision has been reported in hotter parts of the fuel, but always associated with high density thin pores similar to the rim zone [4]. On the other hand, we have also observed that grain subdivision is not always achieved in the rim, even at a local burnup of 110 MWd/kgUO<sub>2</sub>[2].

Then, compared to the rest of the fuel pellet, the main characteristic of the rim seems to be not the grain subdivision but the athermally induced matrix Xe-depletion (or Xe-mobility or diffusion). In section 4, it was suggested that the enhanced Xenon-mobility in the cold fuel periphery may be related to the saturation of the preferential trapping sites for Xe (e.g. Schottky trios), together with the continued production of irradiation lattice defects, at temperatures where no thermal recovery is to be expected. The threshold temperature for point defect recovering is estimated around 750 °C.

The grain subdivision effect can then be considered as a consequence of the local stress field gradients induced by the highly pressurised pores to their surrounding matrix, whatever be the origin of the pore feature and its pressurization, i.e. athermally or thermally activated phenomena. This could explain why cauliflower like structures have been observed on HBRP discs having operated at temperatures in the range 1000–1150°C, as well as in Plutonium rich particles in MOX fuel operated at similar temperatures.

## 7. RIM AND FISSION GAS RELEASE

What is the participation of the rim on the average pellet fission gas release? Mogensen and Walker [10] have recently reanalysed the data provided within the High Burnup Effect Program (1979–1988) [11]. Comparing the EPMA Xenon profiles, representative of the Xenon distribution in the fuel matrix (about 1µm penetration), and the X ray fluorescence profiles performed in the RISOE laboratories (about 60µm penetration), the gas trapped and released can be estimated [10]. This analysis shows that most of the gases are still retained in the fuel up to a local burnup of 75 MWd/kgUO<sub>2</sub>. Nevertheless, above this threshold, the information provided in the HBEP programme and the further analysis by Mogensen and Walker, show a sudden release of 20 % (figure 6).

This observation could be recently confirmed by more recent works performed within the HBRP Project. Using the KNUDSEN cell technique on high burnup fuel disks samples, a 20 % fission gas release has been determined on the highest burnup samples. Nevertheless, this confirms that most of the fuel rim porosity remained not interconnected, even at very high local burnups, since on the contrary higher release fractions would have been measured.

## 8. RIM MECHANICAL PROPERTIES

The high burnup fuel mechanical properties has been investigated in ITU by SPINO et. al, using a micro-hardness device [12,13]. Works are under way to put in operation in hot cells more sophisticated investigation devices using micro-indentation and micro-acoustic methodologies, to determine creep and elastic properties [14,15]. From SPINO's data, the material hardness is decreasing quickly in the rim region (figures 10 and 11), exhibiting a higher toughness. The explanation of these observations is not completely elucidated, but the mechanical properties evolution seems more related to the pore formation (and the Xenon redistribution) than to the grain subdivision itself. The hardness level measured versus burnup is indeed similar between two samples of similar burnups, although one having complete grain subdivision in its periphery (rim normally constrained) and the other showing a few grain subdivision (rim region highly constrained).

The increase of the material toughness can be explained by the presence in the rim of the dense thin porosity, deviating microcracks in there surrounding in order to dissipate the indentation test energy (crack-arrest). However, the works performed by ITU and EDF several years ago [16] on Caesium Uranates properties had led to the following conclusions :

- High hydrostatic pressure favour  $\text{Cs}_2\text{UO}_4$  formation
- $\text{Cs}_2\text{UO}_4$  remains stable up to 800 °C and then decomposes
- $\text{Cs}_2\text{UO}_4$  has a thermal expansion coefficient 40 % higher than  $\text{UO}_2$
- $\text{Cs}_2\text{UO}_4$  is highly viscous over 400°C.

Given the quantity of Cs formed in the rim region, one can then assume that this kind of Cs-compound, even formed in very small local amounts, could modify the material overall properties, especially the mechanical behaviour. Thus, for fuel rods irradiated under constrain, it can be assumed that  $\text{Cs}_2\text{UO}_4$ -type compounds could form at grain boundaries, enhancing the material cohesion. This could explain why in the rim zone the fracture toughness increases (less crack propagation), although the increased porosity in the zone would normally impose the material toughness to drop. However, for fuels irradiated under non-constrained conditions, the formation of Cs-compounds and the eventual material cohesion improvement in porous regions would not have to be expected. In the sense of the above, in PWR-fuels under normal operating conditions, the deformation of the chamfer region (figure 7) confirms the better capability of the material to flow axially and therefore accommodate partly the PCMI stress.

## 9. CONSEQUENCES ON THE FUEL ROD BEHAVIOUR

### 9.1 Standard Power Ramps

Since a long time, it has been observed that in the LWR plants the risk of a cladding failure during a power ramp is higher in the burnup range 20–35 GWd /tM than for higher burnup. This burnup corresponds to the phase of the fuel-cladding gap closure (ie OVERRAMP, SUPERRAMP, TRANSRAMP, INTERRAMP programs...).

When the average fuel pellet burnup reaches 50 MWd/kg $\text{UO}_2$ , the rim buildup is initiated, with a rate of formation depending mainly on the fuel initial enrichment in Uranium 235. As

soon as the rim exists, a cross section micro-acoustic image shows a perfect chemical continuity between the fuel and the cladding (figure 8). This means that the pellet hoop strain is uniformly transmitted to the cladding, while at lower burnup, local high stress concentrations are involved, induced by the pellet radial cracks opening. Stress concentration factors between 1.5 to 2.5, can then be estimated.

In fact, several phenomena contribute at high burnups to the uniformisation of the cladding strain applied by the fuel pellet during a power ramp, namely:

- the hoop fuel swelling that is quasi proportional to the local burnup, avoiding the reopening of the fuel radial cracks,
- many tiny radial closed end micro-cracks that are to be observed after a power ramp in the rim region,
- the overall capability of the rim material to dissipate applied mechanical energy like explained in the paragraph 8, here above.

One can then conclude that from the mechanical point of view, the high burnup effects, including the rim formation, constitute a benefit regarding the failure risk during a power ramp. However, what is the validity of such a conclusion for the fast RIA transients ?

## **9.2 Reactivity Initiated Accident Tests**

Many affirmations have been done during the last five years on the negative role of the rim in an adiabatic fast RIA ramp-test. Such a test induces a high energy deposit in the fuel, during a very short transient lasting about 1 minute (pulse about 10 s). Accounting for the fission gas movement kinetics, this duration is not long enough to induce a gas swelling or an important intra-granular gas redistribution. The PIE observations do not exhibit thus the typical gas-bubble precipitation on grain boundaries of slow power ramps, but a cladding expansion (and eventual rupture) accompanied with a strong grain de-cohesion in the intermediate-outer crown of the fuel. This grain de-cohesion can only be explained by the previous presence of gaseous and volatile fission products at grain boundaries or regions very close to them, which suddenly burst during the fast ramp test. This explosive gas thermal expansion is assumed to cause extensive crack propagation along the grain boundaries, with sudden pellet diameter increase as a consequence.

However, the rim region seems not to be responsible of this phenomenon. Examining the post-irradiation ceramography, one can easily observe that the so called “ under rim ” zone is the most affected by grain de-cohesion (figure 9). In fact, the rim region or high burnup agglomerates in MOX fuel as well, exhibits a high stability during the power ramps.

This means that the rim material should not be the main responsible of the high strain applied by the fuel on the cladding during the RIA ramp. Moreover, the extension of the rim zone towards the centre of the pellet should be even beneficial in that case.

## **10. CONCLUSIONS**

Since the first observations of the rim effect in the eighties, many works and programs has been performed providing with a large data base of observations. Many controversies are still existing in the origin and the kinetic of the process.

We have shown that the rim formation appears to be related to various phenomena occurring in four separable phases, i.e. Xe-depletion, pore buildup, grain subdivision and propagation, in this order. These four steps are not starting at the same time (burnup), and even the last phase (i.e. propagation of the grain subdivision), can be eventually delayed, depending upon the increase of the material constraint during irradiation and or the increase of  $^{235}\text{U}$ -enrichment and the initial  $\text{UO}_2$ - grain size. We have also reported that the grain subdivision is not specific of the rim zone and that it can also appear even in hotter parts of the fuel, provided the pre-existence of pressurized micropores. The rim phenomenon is therefore mainly related to the capability of the fission gas and other fission products to move at low temperatures, tentatively below  $750^\circ\text{C}$  which is the temperature threshold to activate the point defects recovering processes.

We have indicated that the fission gas retention in the rim is higher than 80 % and that the rim material remains mechanically stable during power ramps. Moreover, fuel materials under standard operating conditions seem able to deform and then allow the better accommodation of the PCMI stresses with more uniform distribution of the hoop strain on the cladding. Finally, it is to remark that the grain de-cohesion observed in the RIA fast transients doesn't concern the rim zone.

We then conclude from all the data collected that the rim formation is certainly not a handicap to achieve higher burnups.

## ACKNOWLEDGEMENTS

The authors wish to thank Motoyasu KINOSHITA who allowed to provide this document with an SEM and TEM image from the HBRP project, and for the fruitful discussions on the rim interpretation. Thanks also to Hans Joachim MATZKE, Philippe GARCIA and Yannick GUERIN for their useful discussions all along these last past years.

## REFERENCES

- [1] BARNER J.O., CUNNINGHAM M.E., FRESHLEY M.S., LANNING D.D., "High Burnup Effects Program - Final report", DOE/NE/34046-1, HBEP61(3P27), April 1990.
- [2] SPINO J., BARON D., COQUERELLE M., STALIOS A.D., High Burnup Rim Structure: Evidences that Xenon-depletion, Pore formation and Grain Subdivision start at different local Burnups, *Journal of Nuclear Materials* 256 (1998) p189.
- [3] BARON D., HERMITTE B. and PIRON J.P., An attempt to simulate the Porosity Buildup in the Rim at High Burnup, paper 3.7, IAEA TCM on Advances in Pellet Technology for Improved Performance at High Burnup, Tokyo, 28 October–1 November 1996.
- [4] LOZANO N., DESGRANGES L.; High Magnification SEM Observations for Two Types of Granularity in a High Burnup PWR Fuel Rim ; *Journal of Nuclear Materials* 257 (1998) p78.
- [5] UNE K., NOGITA K., KASHIBE S., IMAMURA M., Microstructural Change and its Influence on Fission Gas Release in High Burnup Fuel, 188, (1992) pp 65–72.

- [6] KINOSHITA M., KITAJIMA S., KAMEYAMA T., MATSUMURA T., KOLSTAD E., MATZKE Hj., „High Burnup Rim Project, progress of irradiation and preliminary analysis," ANS Topical meeting on LWR Fuel Performance, Portland, Oregon, March 1997.
- [7] KINOSHITA M., "High Burnup Rim Project, (II) Progress of Irradiation and Preliminary Analysis," Proceedings of Enlarged HPG Meeting, Loen, Norway, 19–24 May 1996. HPR-347, OECD Halden Reactor Project.
- [8] KINOSHITA M., MATSUMURA T., KAMEYAMA T., KITAJIMA S., KOLSTAD E., MATZKE Hj., "High Burnup Rim Project, Irradiation Program to Study Rim Structure Formation, -Outline and Preliminary Analysis -," EHPG meeting, Bolkesjø, Oct. 31–Nov. 4, 1994.
- [9] SONODA T., MATZKE Hj., and KINOSHITA M., “Threshold Burnup of Rim Structure Formation”, Loen, Norway, 24–28 May 1999, OECD Halden Reactor Project.
- [10] MOGENSEN M., PEARCE J.H., WALKER C.T., Behaviour of fission gas in the rim region of high burnup UO<sub>2</sub> fuel pellets with particular reference to results from XRF investigation, JNM 264 (1998) 99–112.
- [11] GUEDENEY P., TROTABAS M., BISCHIERO M., FORAT C., “FRAGEMA Fuel Behaviour Characterization at High Burnup”, ANS/ENS International Topical Meeting on LWR Fuel Performance, Avignon (France), April 21–24, 1991, P 627, Vol 2.
- [12] SPINO J., BARON D., Microstructure and Fracture Toughness Characterisation of Irradiated PWR Fuels in the Burnup Range 40–67 MWd/kgUO<sub>2</sub>, Same IAEA TCM, TOKYO, Japan, 29 October to 1 November 1996.
- [13] SPINO J., VENNIX K., COQUERELLE M., Detailed Characterisation of the Rim Microstructure in PWR Fuels in the Burnup range 40–67 MWd/kgUO<sub>2</sub>, Journal of Nuclear Materials (1996).
- [14] BARON D., LECLERQ S., SPINO J. and TAHERI S., Development of a Microindentation Technique to determine the Fuel Mechanical Behaviour at High Burnup, paper 6.6, IAEA TCM on Advances in Pellet Technology for Improved Performance at High Burnup, Tokyo 28 October–1 November 1996.
- [15] CROS B., BARON D., ROQUE V., Microacoustic Techniques to assess to local Characteristics of irradiated Fuel Materials, 6<sup>th</sup> International Conference on CANDU Fuels, Niagara Falls (Canada), September 26–30, 1999.
- [16] BERTON J.P. and BARON D., Chemical Stability and Physical Properties of Caesium Uranates, paper 6.4, IAEA TCM on Advances in Pellet Technology for Improved Performance at High Burnup, Tokyo 28 Octobre–1er November 1996.

## Recent studies on the formation of the rim structure and on polygonization in LWR fuel

**Hj. Matzke**

European Commission, Joint Research Centre, Institute for Transuranium Elements, Karlsruhe, Germany

**Abstract.** At cross sectional burnups in excess of  $\sim 40$  MWd/kgUO<sub>2</sub>, a grain subdivision process occurs at the outer rim of LWR UO<sub>2</sub> fuel. A similar phenomenon can be observed in the Pu-rich inclusions in MOX fuel. Three phenomena are usually observed in the resulting "Rim zone": formation of small grains of sub- $\mu$ m size, formation of pores of about  $\mu$ m size, and reduction of the signal of fission Xe in EPMA measurements. The mechanisms for rim-structure formation are still not fully understood, and it is not completely obvious, whether the above three processes occur simultaneously or one after the other in sequential steps. Also, two different types of small grains have recently been found at CEA in France. The present state of knowledge on rim structure formation in LWR fuel is reviewed, as well as recent progress in observing and understanding the formation of nanocrystals and of polygonization in other ceramics. Controlled ion irradiation techniques, including fission product ions at fission energy (e.g. 72 MeV iodine ions) have been applied to UO<sub>2</sub> and to simulated high burnup UO<sub>2</sub>, so-called SIMFUEL. The process of polygonization, i.e. the rearrangement of dislocations into dislocation walls forming low energy "sub-boundaries" and rather perfect, but slightly misoriented subgrains, was studied in these experiments. The same experiments confirmed the extreme radiation stability of UO<sub>2</sub> and demonstrated effects of fission spikes: fission-induced bubble formation, re-resolution of fission gases from bubbles and fission-enhanced gas diffusion and release. No temperature dependence was found between room temperature and 500 °C. The combined results are used to discuss possible mechanisms for polygonization and rim structure formation in UO<sub>2</sub>.

*On the following pages, copies of the main viewgraphs shown during the presentation are reproduced.*

**Part I** summarizes results on high burnup fuel.

**Part II** describes single effect studies using ion beams including fission products at fission energy to better understand radiation damage. A text is given to explain the main results.

**Part III**, finally, gives some suggestions on possible reasons and mechanisms for formation of the rim structure. Again, copies of viewgraphs are reproduced.

At the end, a list of references to relevant work performed in ITU and by the author is given.

## Recent Studies on the Formation of the RIM Structure and on Polygonization in LWR Fuel

# CONTENTS OF THE LECTURE

The three phenomena usually observed in the "rim zone"

- grain subdivision
- formation of  $\mu\text{m}$ -sized porosity
- reduction of the signal for Xe in epma

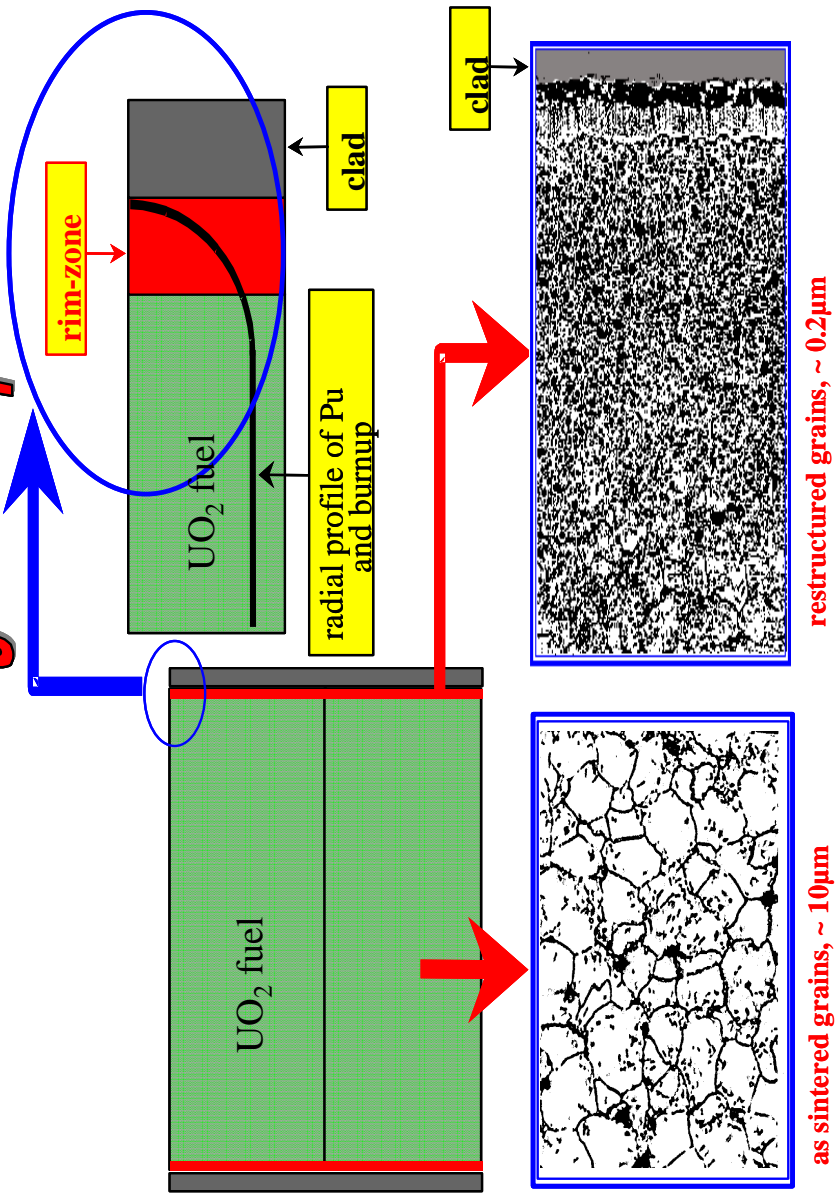
Do these phenomena necessarily occur simultaneously?

Towards understanding the mechanism

- effect of fission spikes (fission-induced bubble formation, re-solution of gas from bubbles, fission-induced gas release, studied by using fission products of fission energy from large accelerators)
- polygonization and formation of nanocrystals in  $\text{UO}_2$  and other ceramics due to ion impact (radiation damage)
- subgrain formation in  $\text{UO}_2$  due to stress
- experimental work on high burnup  $\text{UO}_2$ , e.g. on Kr/Xe ratios

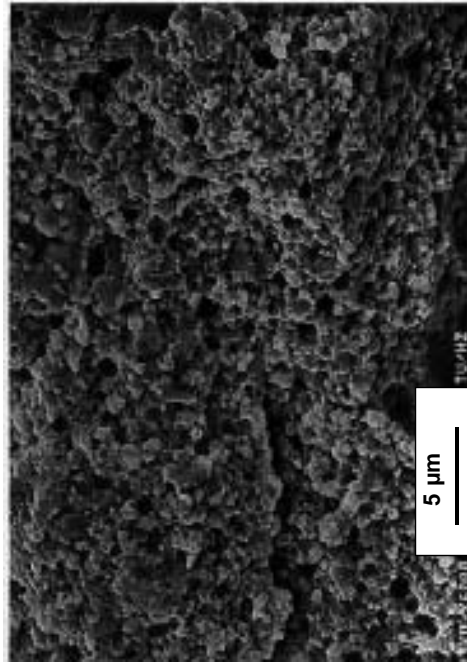
Possible mechanism for polygonization and rim structure formation in  $\text{UO}_2$

# *R'im effect in high burnup LWR fuel*



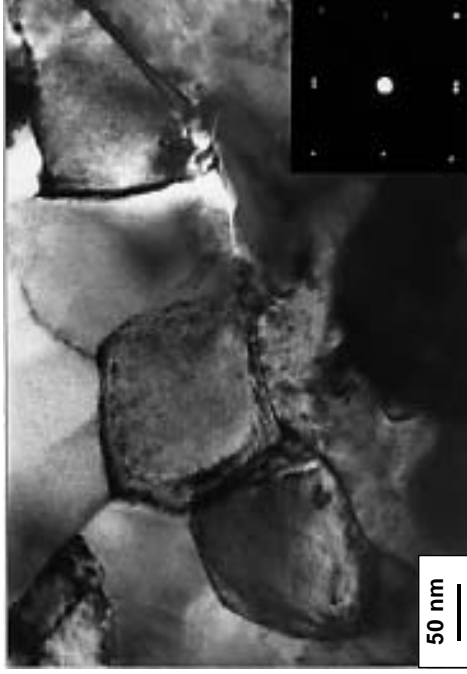
## The RIM Effect

in today's fuel for nuclear power stations,  $\text{UO}_2$   
a very interesting and technologically important phenomenon, still poorly understood.



Scanning

Electron microscopy



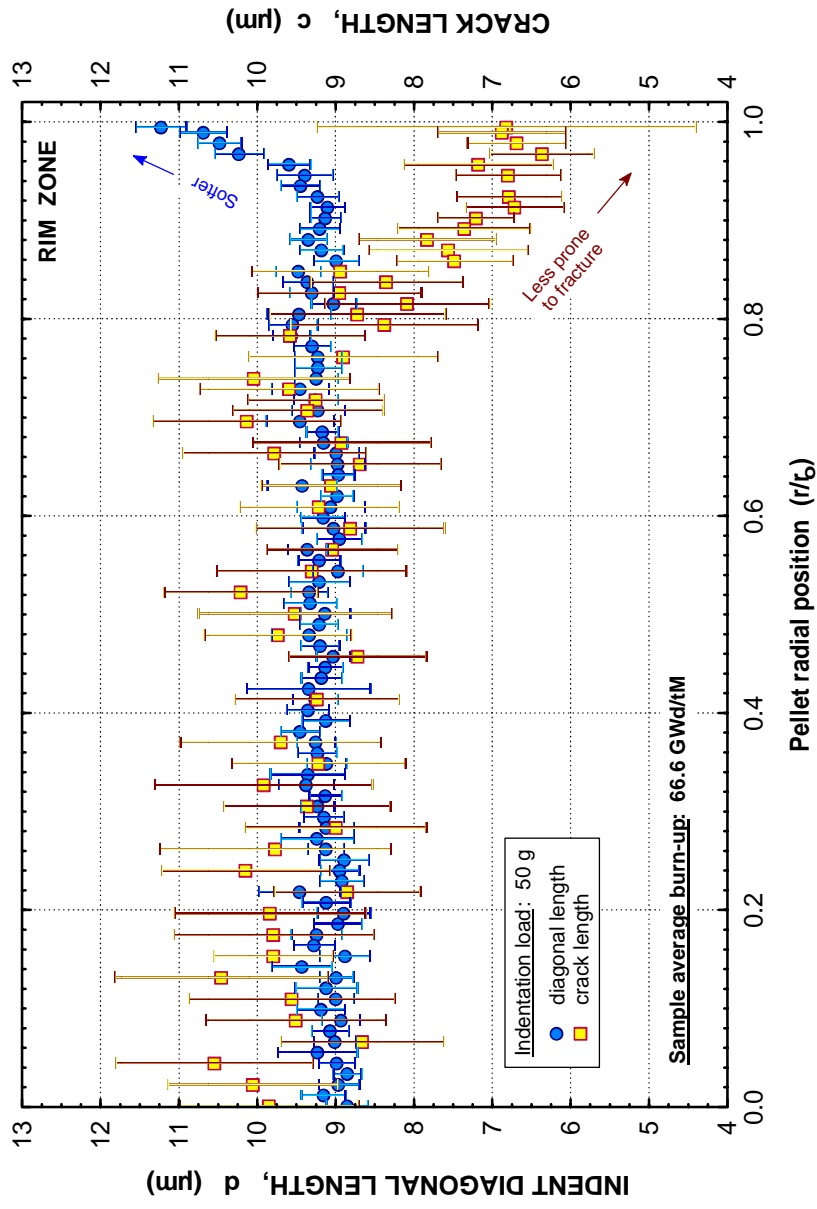
Transmission

The Rim effect is due to a grain-subdivision process. Each original grain is divided into  $10^4$  to  $10^5$  small subgrains. At the same time, porosity is formed. This process occurs first at a local burnup of  $\sim 70$  GWd/tM, average burnup  $\sim 45$  GWd/tM, i.e. after about 3 years operation in a power station.

Hj. Matzke, V. Meyritz, April 98

### INDENTATION BEHAVIOUR OF IRRADIATED PWR FUEL

Application of the Vickers method at room temperature



Hj. Matzke and J. Spino, J. Nucl. Mater. 248(1997) 170

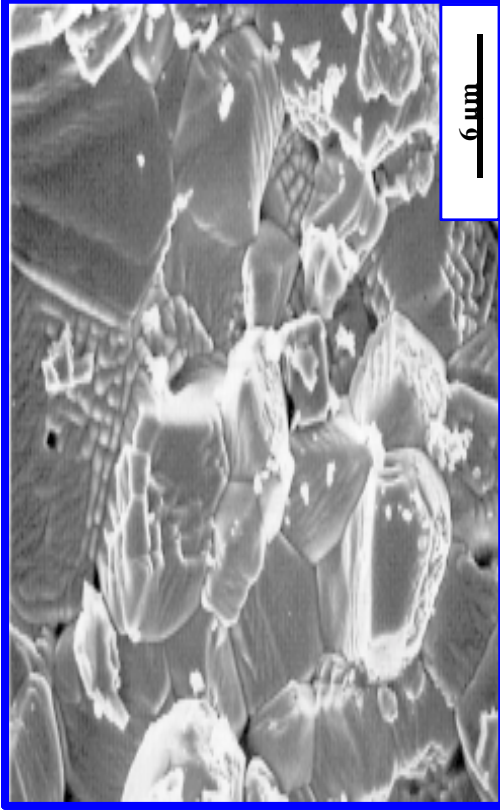
D134

Example of the rim effect and mechanical properties: the hardness decreases and the fracture toughness increases

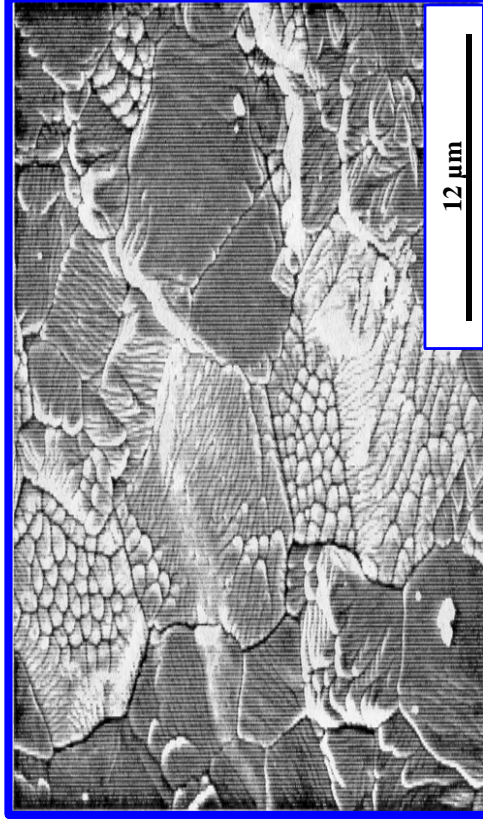
(data of J. Spino et al., see also contribution of D. Baron)

# CANDU fuel $U_{nat}O_2$

13.7 GWd/tU  
intact element

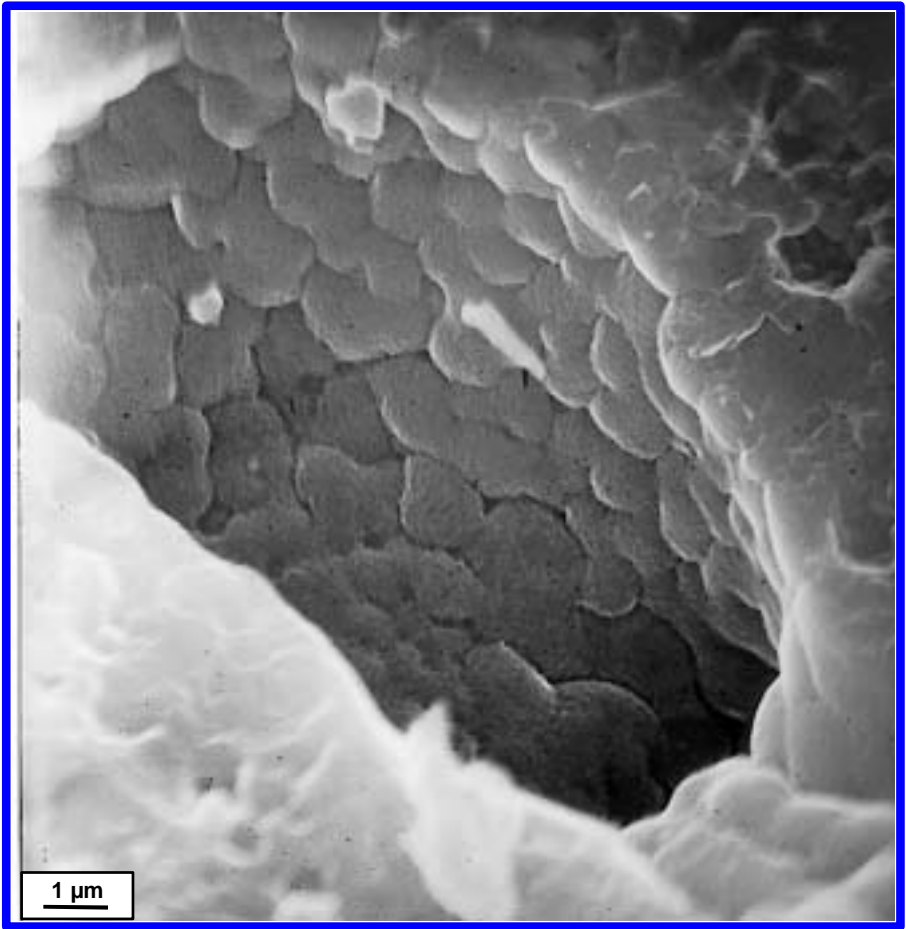


8.5 GWd/tU  
fractured following exposure to  
dry air at 150°C for ~10 years



W. Hocking, Chalk River, AECL, Canada

Rounded subgrains at pores at low burnup

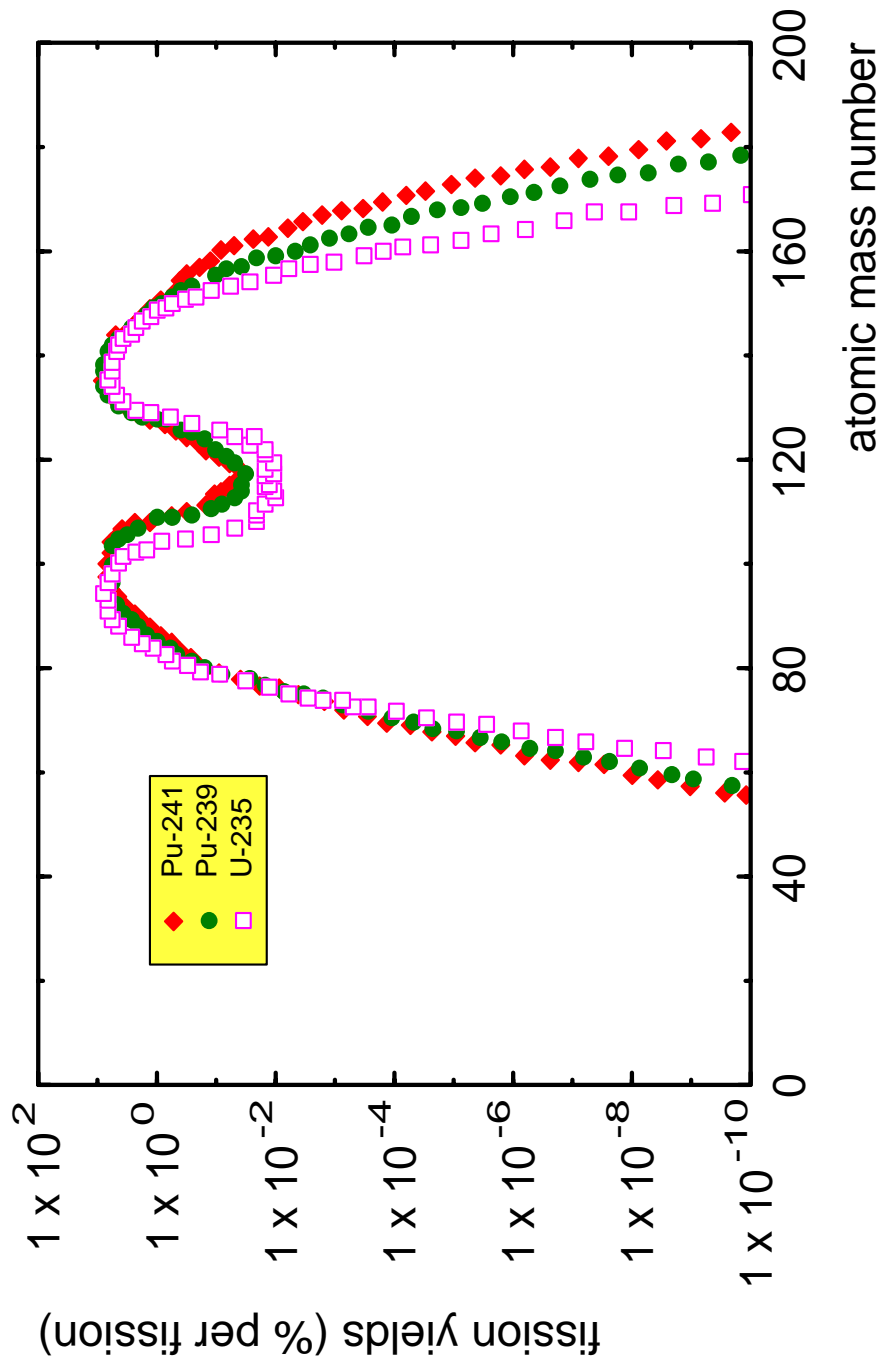


**Scanning Electron Micrograph of a fractured fuel surface showing how the subgrain structure is particularly clearly visible on the inner surface of large pores.**

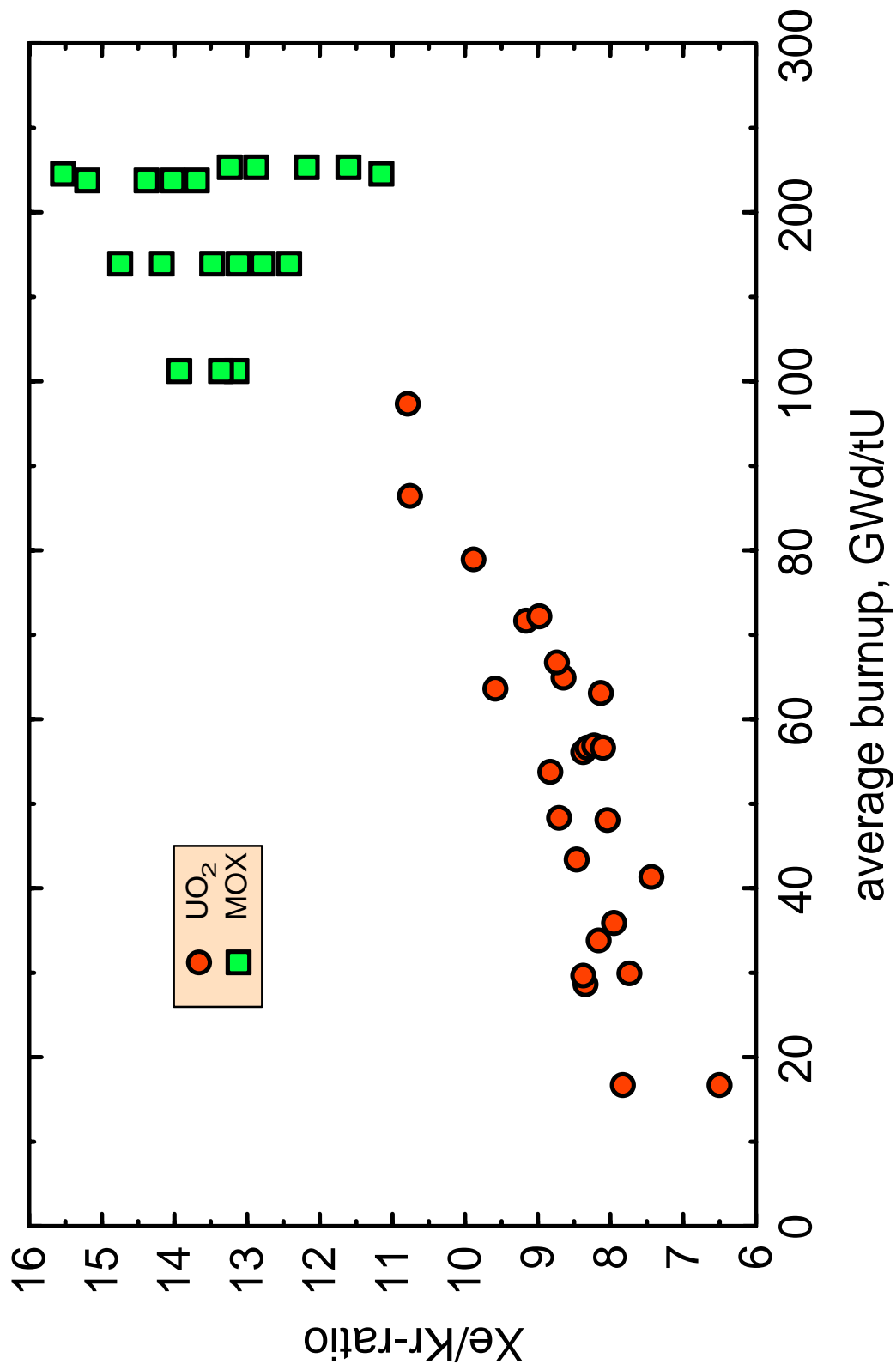
Hj. Matzke, V. Meyritz, April 98

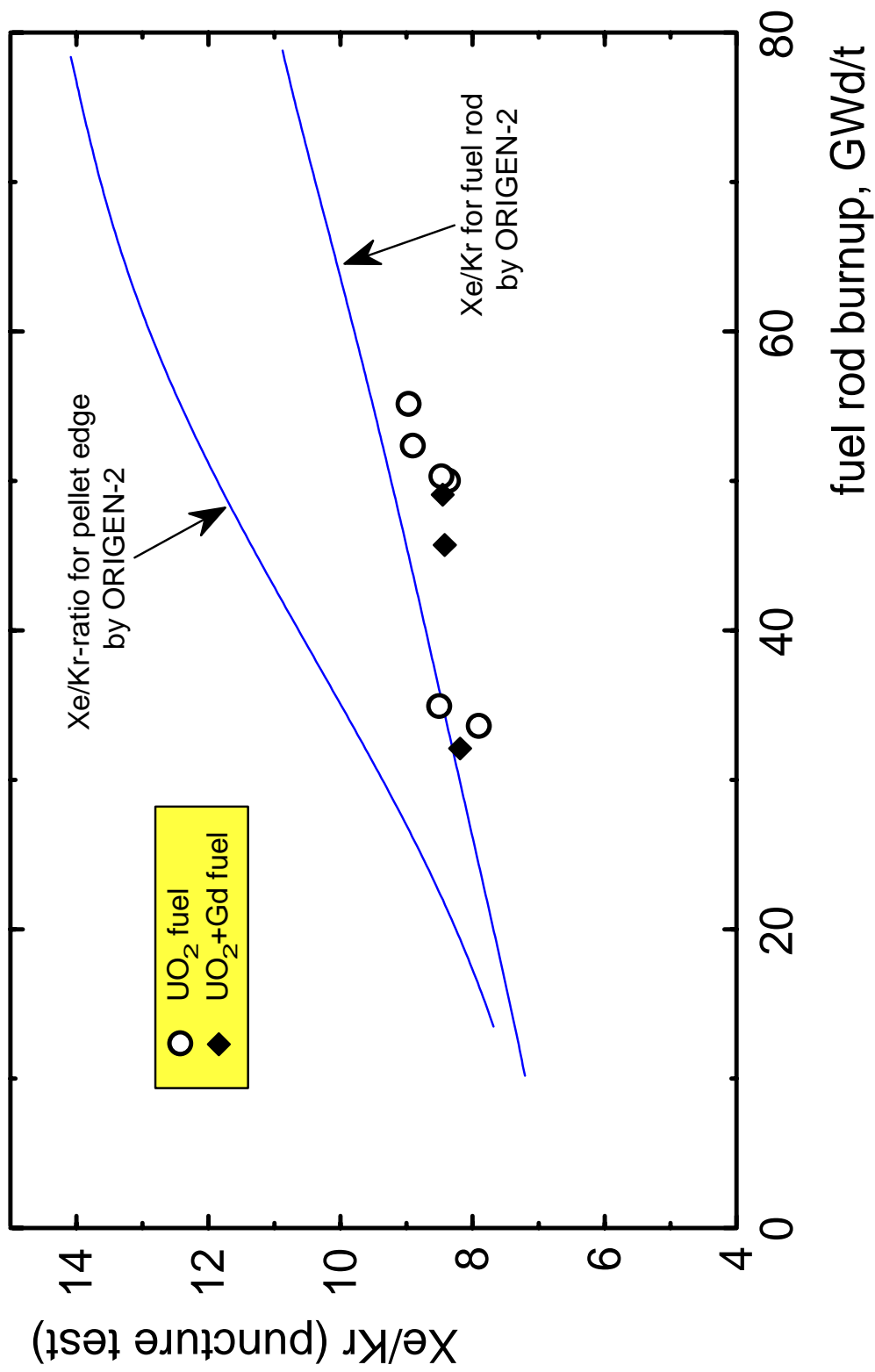
Measurements of the Xe/Kr-ratio with puncture test of high burnup LWR fuel.

**Fission yields (thermal neutrons) for U-235 and fissile Pu isotopes**

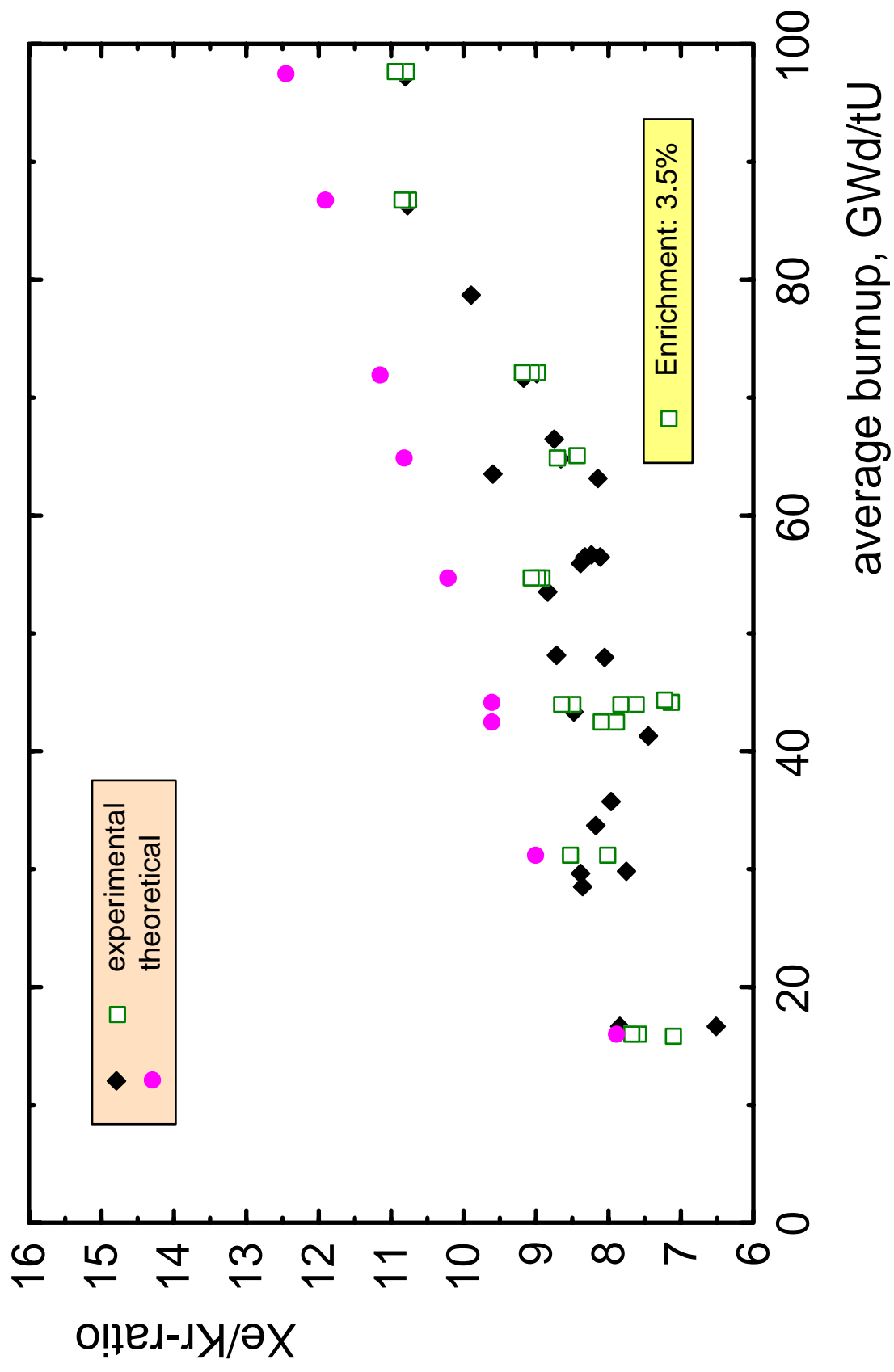


Pu-fission produces less Kr than U-fission





## Xe / Kr-ratio in puncture test of LWR fuel elements



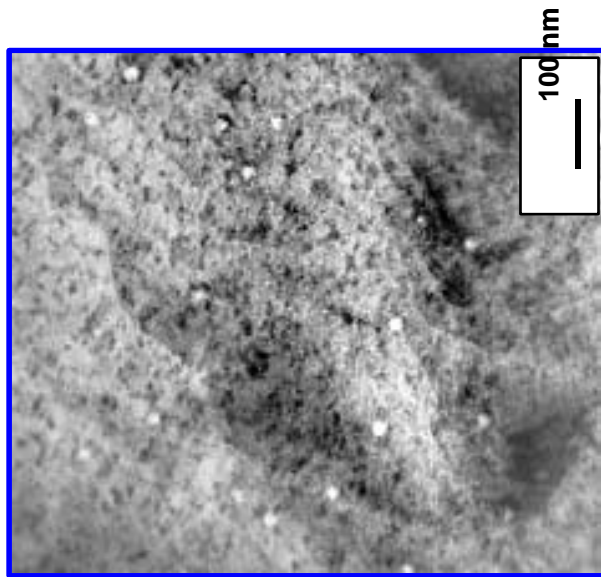


Fig. 1: Tracks in UO<sub>2</sub> irradiated with 1300 MeV U-ions.

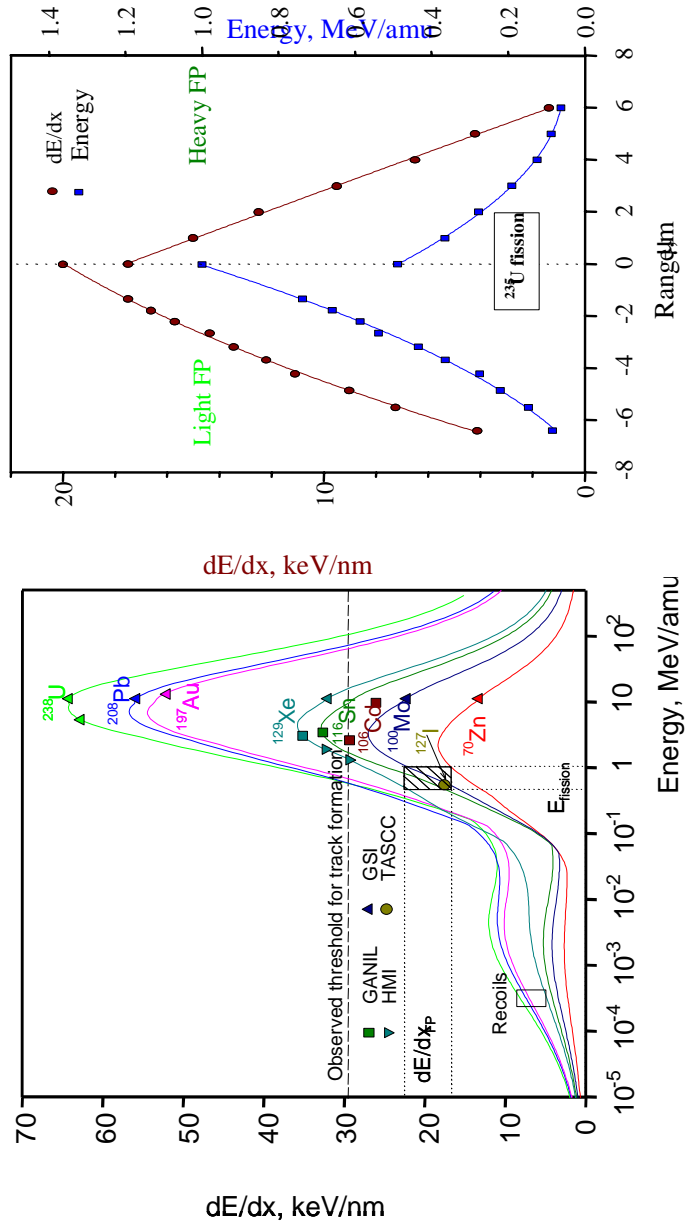


Fig. 2: Conditions for irradiations of UO<sub>2</sub> with swift heavy ions (left) and energy loss of fission products along their range (right).

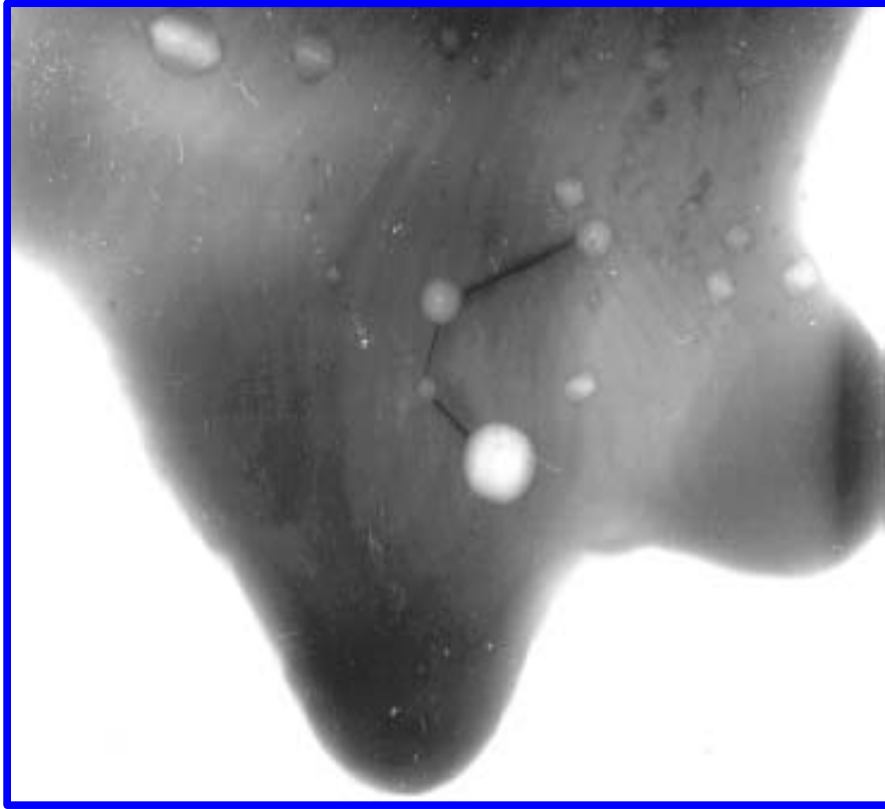
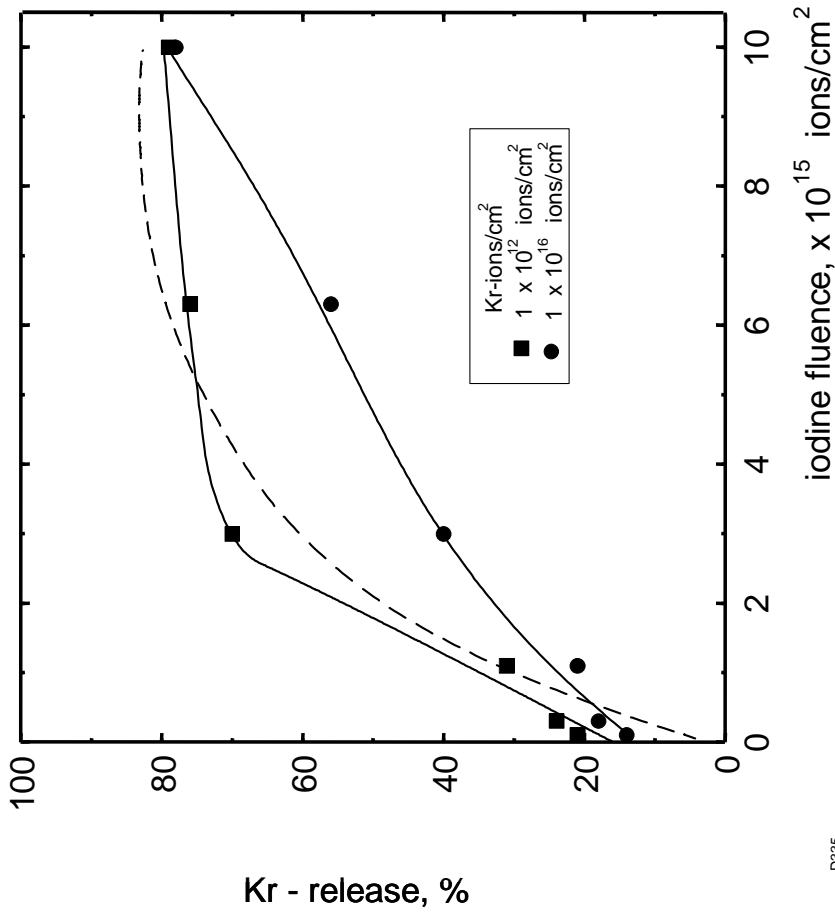


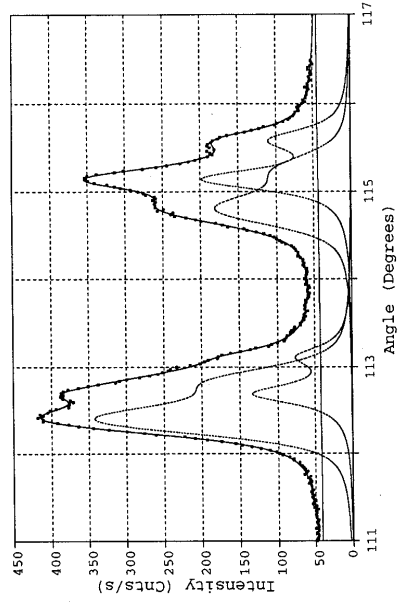
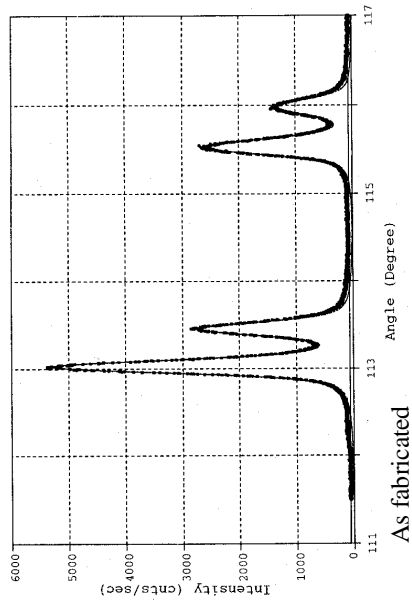
Fig. 3: Kr-bubbles formed by the impact of 72 MeV iodine ions.



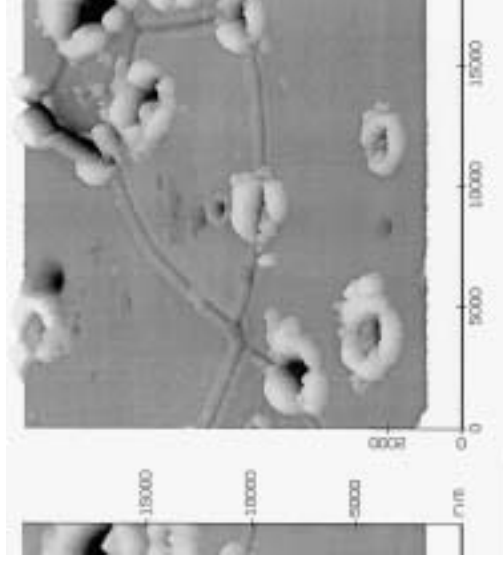
D335

Fig. 4: Release of Kr<sup>85</sup> due to the impact of 72 MeV iodine ions.

### XRD measurements on SIMFUEL



AFM micrograph of UO<sub>2</sub> irradiated with 70 MeV iodine ions



FM 506

Further effects of iodine at fission energy: increase of the lattice parameter, but no amorphisation.  
Surface effects stand at pores and grain boundaries.

## Part 2: SWIFT HEAVY ION AND FISSION DAMAGE EFFECTS IN UO<sub>2</sub>\*

**Abstract.** Irradiations of uranium dioxide, UO<sub>2</sub> with different swift heavy ions were performed using wide ranges of energies and fluences from fission energy (72 MeV) to 2.7 GeV in the range 5.109 to 1017 ions/cm<sup>2</sup>. The ions were Zn, Mo, Cd, Sn, Xe, I, Pb, Au and U. The threshold energy loss for formation of visible tracks in UO<sub>2</sub> could be determined to be in the range 22 - 29 keV/nm. Fission products of fission energy are below this threshold but nevertheless form thermal spikes in UO<sub>2</sub>- Observable fission tracks are only found at the surface. By using 127 I-beams of 72 MeV energy the consequences of fission product impact, i.e. lattice parameter increase, fission gas bubble formation, resolution of fission gas from bubbles and fission-enhanced diffusion were all observed and measured. The swelling of UO<sub>2</sub> was confirmed to be small and the technologically important process of polygonization (grain subdivision or rim-effect) could be simulated.

### INTRODUCTION

The main physical process of heat production in UO<sub>2</sub> fuel is the slowing down of the two fission products, fp, which are produced in the fission event. These fp fall into two families, the "light" ones centered around e.g. Mo and having energies of around 100 MeV, and the "heavy" ones centered around e.g. Ba with about 70 MeV energy. Their nuclear and electronic stopping with  $(dE/dx)_{e,ax} \approx 18$  keV/nm for the heavy and  $\approx 22$  keV/nm for the light fp's produces heat and radiation damage. At end of life, i.e. at about 50 GWd, some 4-6 % of the U atoms have been fissioned, partly via the formation of <sup>239</sup>Pu by neutron capture of <sup>238</sup>U and subsequent  $\beta$ -decay of <sup>239</sup>Np, about 10% fission products have been accumulated and the fuel has seen some 2000 to 3000 displacements-per-atom, dpa. A thorough understanding of these physical and chemical processes is necessary to understand the performance of the fuel and its behavior at long operating times.

The present study deals with the interaction of UO<sub>2</sub> with swift heavy ions of energies up to 2.7 GeV, performed in order to determine the threshold energy loss for formation of visible tracks at ambient temperature. In a second part, the use of beams of a fission product of fission energy, <sup>127</sup>I, of 72 MeV, obtained from the TASC accelerator at AECL Chalk River, Canada, is described with the aim of quantifying in single effect studies fission damage and related effects such as fission-induced diffusion, precipitation of fission rare gas and, indirectly, resolution of precipitated fission gas from bubbles or trapping sites by the interaction with fission spikes. Polygonization of UO<sub>2</sub>, i.e. the subdivision of individual grains of as-sintered UO<sub>2</sub> into  $\approx 10^4$  small subgrains, (rim-effect) is also studied in this type of single effect experiments, in parallel to investigations on UO<sub>2</sub> irradiated in test reactors and UO<sub>2</sub> power reactor fuel.

**Experimental** Different UO<sub>2</sub> Specimens, both single crystals and sinters (96% of theoretical density), were irradiated at different accelerators with a range of ions and with energies between 72 MeV and 2.7 GeV. Table 1 shows the irradiation conditions (type of ion, energy,  $(dE/dx)$ , at initial energy and fluence) and lists the accelerators and the scientists cooperating in this activity. For TEM investigations, 3 mm disks were dimpled, i.e. excavated in the center with a spherical diamond-impregnated drill. For other investigations (e.g. XRD, gas release measurements etc.) slices of about 5x5 mm size, and

1 mm thickness were prepared and the face to be irradiated was polished down to 0.25  $\mu$ m diamond paste. All specimens were annealed at 1400 °C in Ar/H<sub>2</sub> to eliminate the **cutting** and polishing damage and to adjust the oxygen-to-metal (O/Ij)-ratio to the stoichiometric value of 2.0.

In order to further increase the sets of energy, energy loss and velocity of the available ion beams, some samples were covered with polycarbonate or steel foils of different thickness to slow the energetic ions down to different lower effective energies. The TRIM code [1] was used to calculate these effective energies and the  $dE/dx$ -values. Most irradiations were performed at ambient

temperature except for some irradiations with iodine-ions of 72 MeV in the TASCC accelerator at Chalk River, AECL where a heating stage kept the UO<sub>2</sub> at 500 °C during the irradiation. At high beam current in the TASCC and without the heating stage, some limited beam heating increased the sample temperature to ~ 120 °C (only in the irradiations with 127 I since the beam currents were much lower in all other irradiations).

After irradiation, the (dimpled) TEM specimens were ion-milled in order to become transparent to the 200 keV electrons of a Hitachi H 700 electron microscope. Also, in some cases, cross-sectional TEM was performed successfully.

Some of the UO<sub>2</sub> specimens were implanted with 40 keV <sup>15</sup>Kr ions to different fluences in the Chalk River isotope mass separator. High fluences were achieved by implanting inactive <sup>84</sup>Kr at high concentration before labeling the specimens with radioactive <sup>85</sup>Kr. Fission-induced fission gas mobility was investigated by using such specimens as targets for iodine irradiation in the TASCC accelerator and measuring the P-activity of <sup>85</sup>Kr on the implanted surfaces after different irradiation steps (iodine fluences). Radiat ion- induced fission gas bubble formation and resolution was observed on prethinned UO<sub>2</sub> TEM foils implanted with Kr, also at 40 keV energy. These specimens were characterized by TEM before and after the iodine irradiation.

X-ray diffraction using Cu K $\alpha$  radiation was performed on the surfaces irradiated with <sup>127</sup>I, in order to determine irradiation- induced changes in the lattice parameter. Lattice strain  $\epsilon$  was estimated from peak broadening. Finally, laser profilometry, scanning electron and atomic force microscopy were used to observe possible modifications at the surfaces of the specimens irradiated with high iodine fluences in the TASCC accelerator.

## Results and Discussion

*Tracks in UO<sub>2</sub>* Visible tracks were observed in TEM only in the cases when the electronic energy loss (dE/dx), was 29 keV/nm or larger. An example of tracks is shown in Fig. 1. In the area shown, about 15 tracks are expected, based on the known fluence, which corresponds closely to the observation. Some tracks are hexagonal with {111} faces, as is sometimes also the case for fission gas bubbles and pores in UO<sub>2</sub>. The experimental conditions (type of ions, beam energies, dE/dx-values) are shown in Fig. 2 (see also Table 1). The experimentally observed lowest dE/dx of 29 keV/nm for track formation is shown as dashed line, and the dE/dx-E conditions for fission products and for the heavy recoil atoms of the  $\alpha$ -decay of actinides (e.g. <sup>238</sup>U in the decay of <sup>239</sup>Pu) are shown as squares. This diagram shows that the dE/dx-values for fission products (-18 to -22 keV/nm; see above) are near, but below the dashed line.

Fission tracks have never been observed in bulk UO<sub>2</sub>, though they are found at UO<sub>2</sub> surfaces for fission products passing near or parallel to the surface. This is explained as being due to a shock wave mechanism caused by thermal pressure of the hot center of the fission spike [2]. We thus conclude that the threshold for formation of visible tracks in the bulk UO<sub>2</sub> is in the range 22 to 29 keV/nm.

The radii of the observed tracks were measured. They increased with dE/dx from ~1.5  $\mu$ m for 29 keV/nm to 5  $\mu$ m for dE/dx ~60 keV/nm. The nature (e.g. crystalline vs. amorphous) of the tracks could not be defined. However, even in the overlapping region, no amorphization was observed. Rather, with increasing fluence, an increasing loop density was seen. The model of Toulemonde et al. [3, 4] was used to explain track formation. The model assumes that the energetic ions transfer their energy in a first step to the target electrons, and then to the lattice via electron-phonon coupling. Published thermodynamical parameters [5] were used to calculate the radial dependence of the local lattice temperatures along the range of two typical fission fragments (e.g. 70 MeV <sup>133</sup>Ba as a heavy fragment and 95 MeV <sup>95</sup>Zr as a light one). For much of the range, the calculated central temperatures in the spike were above the melting point. This "molten zone" was calculated to have a maximal radial extension of ~ 1.5 - 2  $\mu$ m for irradiation at ambient temperature. The spike

effect is additive to the specimen temperature. The molten zone will be correspondingly larger in operating (i.e. hot) reactor fuel. These high temperatures reached along a fission spike support many effects as described below.

*Structural changes, swelling, lattice parameter changes* X-ray diffraction analysis clearly showed increases in lattice parameter and lattice strain at the irradiated surfaces, hence due to electronic stopping. The results were in good agreement with those of Hyashi et al. [e.g. 6]. As expected, no amorphization occurred, but polygonization was observed, both in Rutherford backscattering/channeling measurements and with SEM if the fluence was increased to  $10^{17}$  ions/cm<sup>2</sup> (see next paragraph).

*Surface modifications due to the impact of 72 MeV iodine ions* The spots irradiated with iodine, about 3  $\mu$ m in diameter, were clearly visible on the polished specimen surfaces. Both laser profilometry and profilometry with a stylus did not reveal any measurable swelling. Any swelling of UO<sub>2</sub> was  $<0.1 \mu$ m, hence  $< 1.5\%$  for fluences up to  $10^{16}$  ions/cm<sup>2</sup>. The main observable effect in UO<sub>2</sub> up to this fluence were limited "expulsions" of matter at sintering pores and at some locations at grain boundaries. At the highest fluence of  $10^{17}$  ions/cm<sup>2</sup>, complete polygonization occurred, causing the formation of  $\mu$ m-size pores, similar to those observed in rim-structured high burnup UO<sub>2</sub> fuel [7]. As with the previous paragraph, a more detailed description of these observations and measurements will be published elsewhere.

*Radiation - induced fission gas bubble formation and resolution* The effects of the passage of the high energy iodine ions through UO<sub>2</sub> on the behavior of fission gases was investigated as described in Section 2. Formation of gas bubbles in Kr-containing UO<sub>2</sub> following irradiation with iodine ions (see Fig. 3) was clearly seen in TEM foils not containing bubbles before irradiation. The bubbles were formed in the electronic stopping region following multiple overlap of fission spikes.

Irradiation with **72 MeV** iodine of UO<sub>2</sub> foils containing thermally formed Kr-bubbles produced gas release similar to the results reported in section 3.2.4. This provides indirect evidence that fission fragments are efficient to cause resolution of gas from bubbles thus enabling gas atoms to diffuse and to be released. Fission fragments can thus produce and destroy small fission gas bubbles.

*Irradiation - induced gas diffusion and release* Fission is known to cause enhanced U-diffusion [8] and creep [9] in operating UO<sub>2</sub> fuel. Uranium (and plutonium) self-diffusion during irradiation was found to be completely athermal, temperature independent below about 1000 °C. The radiation-enhanced diffusion coefficient,  $D^*$ , varied linearly with the fission rate,  $F$ , according to the relation [8]

$$D^* = AF \text{ with } A = 1.2 \times 10^{-9} \text{ cm}^2 \text{ and } F \text{ in fissions/sec} - \text{CM}^3.$$

Enhanced in-pile release of fission gases was also reported before [10].

A larger number of specimens of UO<sub>2</sub> and of UO<sub>2</sub> with simulated burnup (SIMFUEL), preimplanted with 85 Kr to total Kr-fluences of either  $10^{12}$  or  $10^{16}$  ions/cm<sup>2</sup>, were irradiated with increasing doses of 72 MeV iodine ions. A typical set of results is shown in Fig. 4. Due to beam heating, the measured specimen temperature was  $\sim 120$  °C. Very similar results as shown in Fig. 4 were obtained with UO<sub>2</sub> kept at 500 °C during irradiation, showing that the release process is athermal at least up to 500 °C.

The release from the low-dose implanted samples was consistently higher than that from the high-dose implanted samples. As mentioned above, gas bubbles were formed at the high Kr-concentration, due to the impact of the iodine ions. The fact that most gas is released nevertheless, can be taken as an indication for resolution of trapped gas.

The dashed curve in Fig. 4 shows the theoretically expected release (see ref [1]) for details on release kinetics) for a diffusion coefficient  $D=2 \times 10^{-15} \text{ cm}^2 \text{ s}^{-1}$ . Since the beam current was kept constant, the fluence scale can also be taken as a time scale. Converting the ion beam impact into the equivalent fission rate showed that the factor A in equ. (1) is significantly smaller (by about a factor of 10) for Kr than it is for U and Pu. For the latter, the relatively high values of  $D^*$  were explained by a larger than expected separation of uranium Frenkel defects (interstitial and vacancies) due to the large pressure gradients along the hot fission spikes [12]. Uranium interstitials are known to be highly mobile, even at low temperatures. They will therefore be subjected to biased migration towards lower pressure, hence away from the center of the spike, thus increasing the effective  $D^*$ . For fission gases, this additional mixing does not exist due to the absence of such a fast mobility. The *minimum* possible  $D^*$  is given by the atomic mixing in the collision cascades of the fission spikes providing momentum transfer to the atoms in the cascade. This value is estimated to be about  $2 \times 10^{-16} \text{ cm}^2 \text{ s}^{-1}$  for the conditions of Fig. 4. Obviously, the fission-induced diffusion coefficient for krypton is just inbetween this minimum value and the  $D^*$  for uranium self-diffusion.

**Conclusions and Summary** The present study consists of two parts. In the first part, the interaction of  $\text{UO}_2$  with swift heavy ions of nine different elements in the energy range of 72 MeV to 2.7 GeV was studied. Visible tracks were seen in TEM whenever the electronic energy loss was at or above 29 keV/m-n. The electronic energy loss of fission products is below this threshold explaining why no visible tracks are formed due to fission in  $\text{UO}_2$ . However, based on the measured dependence of the

track radii on  $(dE/dx)$ , for the ions of higher energy where tracks were visible and with a thermodynamic model of Toulemonde et al., the temperature conditions for stopping of fission products could be estimated. For much of the range, the calculated local lattice temperatures were above the melting point of  $\text{UO}_2$ . In the second part, technologically interesting consequences of the fission spikes were studied. Besides lattice expansion and subsequently polygonization (grain subdivision of sintered  $\text{UO}_2$  or a phase change single crystal  $\rightarrow$  polycrystal with  $\text{UO}_2$  single crystals, combined with pore formation similar to the rim effect in high burnup  $\text{UO}_2$ , the behavior of the rare gas Kr, due to the impact of a fission product of fission energy (72 MeV iodine ions), was investigated. It could be shown that at high Kr-concentrations, fission gas bubbles form due to impact of the iodine ions. Irradiation-induced athermal gas release existed for both low and high Kr-concentrations. The corresponding enhanced diffusion coefficient was about one order of magnitude smaller than that for U self-diffusion. This was explained to be due to the high mobility of U-interstitials which does not occur for Kr. Indirect evidence of resolution of gas from bubbles and trapping sites was also observed.

## ACKNOWLEDGEMENTS

Thanks are due to the scientists who enabled the swift heavy ion irradiations to be performed and who helped to interpret the results: C. Trautmann and J. Vetter at GSI; M. Toulemonde at GANIL; S. Klaumiinzer at ISL, HMI; R.A. Verrall and H.R. Andrews at the TASCC, AECL. They also gratefully acknowledge the contributions of I. Ray, H. Thiele and W. Huber to obtain good TEM results.

## REFERENCES

- [1] J.F. Ziegler, J.P. Biersack and U. Littmark, the Stopping and Range of Ions in Solids (Pergamon Press, London, 1985)
- [2] C. Ronchi, J. Appl. Phys. 44 (1973) 3573
- [3] M. Toulemonde, J.M. Constantini, C. Dufour, A. Meflah and E. Pournier, Nucl. Instrum. Methods in Phys. Research B 116 (1996) 37
- [4] M. Toulemonde, E. Paumier and C. Dufour, Rad. Effects Sol. 126 (1993) 205

- [5] T. Wiss, Hj. Matzke, C. Trautmann, M. Toulemonde and S. Klaumiinzer, Nucl. Instrum. Methods in Phys. Research B 122 (1997) 593
- [6] K. Hayashi, H. Kikuchi and K. Fukuda, J. Nucl. Mater. 42 (1972) 191
- [7] Hj. Matzke and J. Spino, J. Nucl. Mater. 248 (1997) 170
- [8] Hj. Matzke, Rad. Effects 75 (1983) 317
- [9] D. Brucklacher and W. Dienst, J. Nucl. Mater. 42 (1972) 285
- [10] J.A. Turnbull, C.A. Friskney, J.R. Findlay, F.H. Johnson and A.J. Walter, J. Nucl. Mater. 107 (1982) 168
- [11] Hj. Matzke, Z. Naturforschlig. 22a (1967) 507
- [12] H. Blank and Hj. Matzke, Rad. Effects 17 (1973) 57

## Figure Captions

- Fig. 1 TEM micrograph Of UO<sub>2</sub> irradiated with U-ions of 1300 MeV energy with (dE/dx), = 56 keV/nm. Tracks are seen as white spots.
- Fig. 2 Plot of dE/dx as a function of the energy of different ions (Zn, Mo, Cd, Sri, Xe, I, Au, Pb, and U) expressed in MeV per atomic mass unit, arnu. The squares and triangles show the experimental conditions used. A circle indicates the conditions for 72 MeV ions of 127, . The two big squares show the dE/dx-E conditions for fission products and for the heavy recoil atoms of a-decaying actinides. The inset shows the energy loss and the remaining energy of typical light and heavy fission products along their range of -7 um length.
- Fig. 3 TEM micrograph Of UO<sub>2</sub> implanted with 10<sup>16</sup> Kr-ionS/CM<sup>2</sup> at 40 keV, followed by irradiation with 72 MeV iodine ion. This irradiation causes formation of gas bubbles. Continued irradiation causes release of most Kr.
- Fig. 4 Fission gas release due to the impact of 72 MeV iodine ions from UO<sub>2</sub> preirnpanted with 40 keV Kr-ions at low or high fluence. The dashed curve shows the expected time dependence of release for a diffusion coefficient  $D=R10^{-1}cin^{-s-1}$ .

**Table 1: Irradiation conditions for UO<sub>2</sub> specimens**

Ion	Energy MeV	(dE/dx), keV/nm	Fluence <sup>2</sup> ions/cm	Accelerator
Xe- 129	173	29.1	7x10 <sup>12</sup> to	ISL, HMI
	250	32.3	9x10 <sup>13</sup>	
Xe- 129	1470	32	5x10 <sup>12</sup>	UNILAC, GSI
Mo-100	1140	22.2	5x10 <sup>10</sup>	UNILAC, GSI
Pb-208	2371	55.8	5x10 <sup>12</sup>	UNILAC, GSI
Zn-70	805	13.2	5x10 <sup>11</sup>	UNILAC, GSI
Au-197	2638	52	5x10 <sup>9</sup>	LTNILAC, GSI
U-238	1300	56	5x10 <sup>10</sup>	UNILAC, GSI
	2713	59	5x10 <sup>10</sup>	
I-127	72	17.5	IXIO15 to	TASCC,CRL
			IXIO17	
Sn- 116	403	32.6	5x10 <sup>10</sup> to	GANIL
			3x10 <sup>13</sup>	
Cd- 106	1050	29.3	3x10 <sup>13</sup>	GANIL
ISL, HMI	Ionenstrahllabor of the Hahn-Meitner Institute, Berlin, Germany (S. Klauemper)			
TASCC,CRL	Tandem Accelerator Superconducting Cyclotron, AECL, Chalk River Laboratories, Canada (P.G. Lucuta, R.A. Verrall, H.R. Andrews)			
GANIL	Grand Accélérateur National pour les Ions Lourds, Caen, France (M. Toulemonde)			
UNILAC, GSI	Universal Linear Accelerator, Gesellschaft für Schwerionenforschung, Darmstadt, Germany (C. Trautmann, J. Vetter)			

### List of "rim-related" papers

H. Blank, Hj. Matzke, R. Manzel, M. Coquerelle, I.L.F. Ray, C.T. Walker, K. Lassmann and C. Ronchi:

Jahrestagung Kemtechnik German Atomforum, Bonn (1988) p. 433, (in German)

Hj. Matzke, H. Blank, M. Coquerelle, K. Lassmann, I.L.F. Ray, C. Ronchi and C.T. Walker:  
J. Nucl. Mater. **166, 165** (1989)

Hj. Matzke:

J. Nucl. Mater. 189 (1992) 141

Hj. Matzke, A. Turos and G. Linker:

Proc. Int. ConE Radiation Effects in Insulators, REI-7, Nagoya (1993), Nucl. Instrum. Meth. in Phys. Research B 91 (1994) 294

Hj. Matzke:

J. Nucl. Mater. 208 (1994) 18

I.L.F. Ray, Hj. Matzke, H. Thiele and M. Kinoshita:

J. Nucl. Mater. 245 (1997) 115

M. Kinoshita, S. Kitajima, T. Kameyama, T. Matsurnura, E. Kolstad and Hj. Matzke:

Proc. ANS Topical Meeting on LWR Fuel Performance going beyond Current Burnup Limits, Portland, March 97, (1997) p. 530

Hj. Matzke and J. Spino:

Proc. Int. Workshop on Interfacial Effects in Quantum Energy Systems, IEQES 96, Mito, Japan, August 21-23, 1996, Special issue J. Nucl. Mater. 248 (1997) 170

M. Kinoshita, T. Kameyama, S. Kitajima and Hj. Matzke:

J. Nucl. Mater. 252 (1998) 71

Hj. Matzke and M. Kinoshita:

Proc. 9. Int. Symp. Thermodyn. Nucl. Mater., Osaka, Aug. 25-30, 1996, J. Nucl. Mater. 247 (1997) 108

S. Kitajima, Hj. Matzke and M. Kinoshita: presented at Enlarged Halden Project Meeting, Lillehammer, March 1998, Proceedings Paper F-3.11 (1998)

T. Sonoda, Hj. Matzke and M. Kinoshita:

Enlarged Halden Project Meeting, Loen. May 1999, Proc. Paper F 1. 1

### **Part 3 – On the way to understand the mechanism of formation of the rim structure**

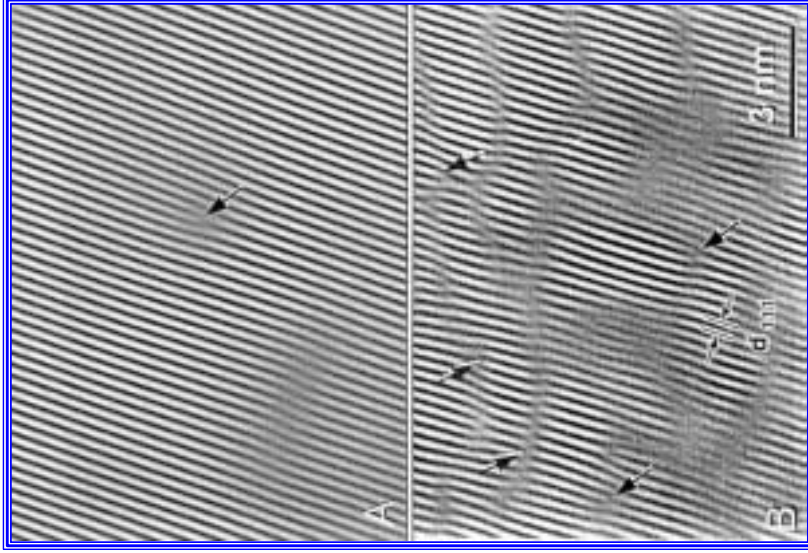
- § What is polygonization?
- § Why is it not recrystallization?
- § Formation of nanocrystals in different ceramics

#### Separate effect studies

- § Effect of impurities Xe, I, Cs, La
- § Effect of stress.

The “acicular” or “needle” structure and the effects of fracture and cleavage

Possible models

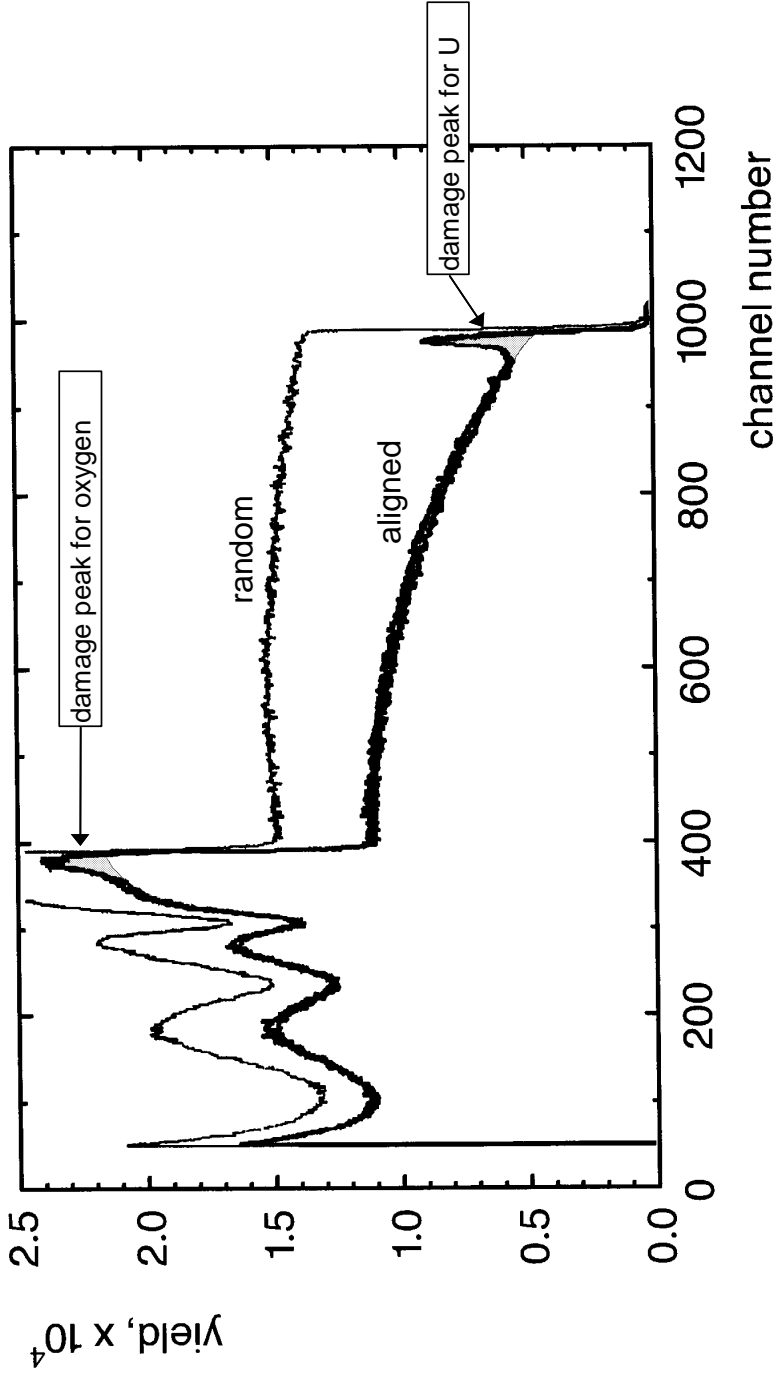


Filtered HRTEM micrographs showing the (111) lattice fringes of a  $\text{UO}_2$ -specimen (A) before and (B) after  $500 \text{ keV Xe}^+$ -irradiation to  $1 \times 10^{20} \text{ ions/cm}^2$  at  $170 \text{ }^\circ\text{C}$ .

The formation of subgrain boundaries is seen in B whereas very rarely single dislocation lines are seen before irradiation (see arrow in A)  
(Hj. Matzke and L.M. Wang, J. Nucl. Mater. **231** (1996) 155)

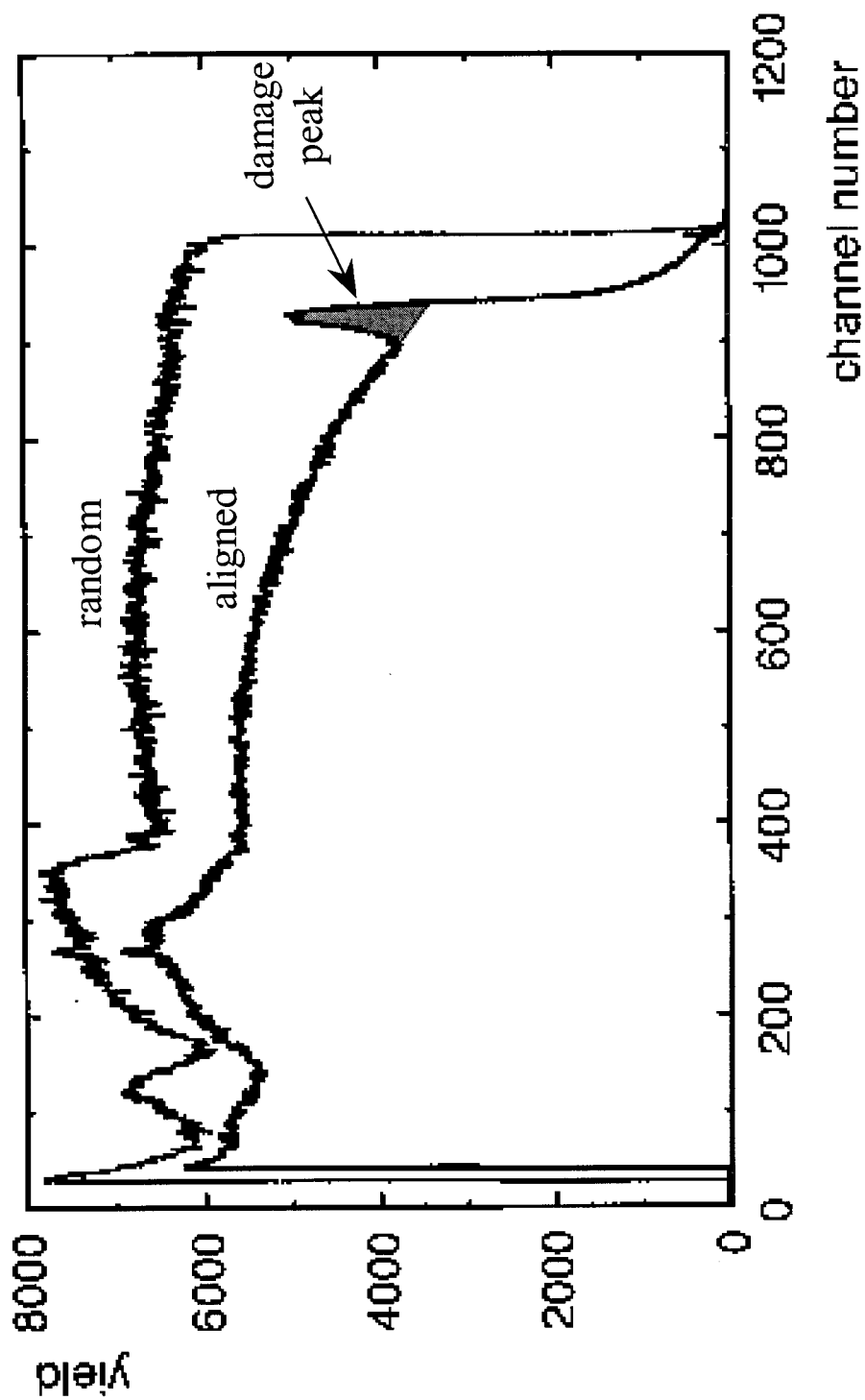
## Damage in $\text{UO}_2$ , 40 keV Kr-implants

measured with 7.57 MeV He-ions



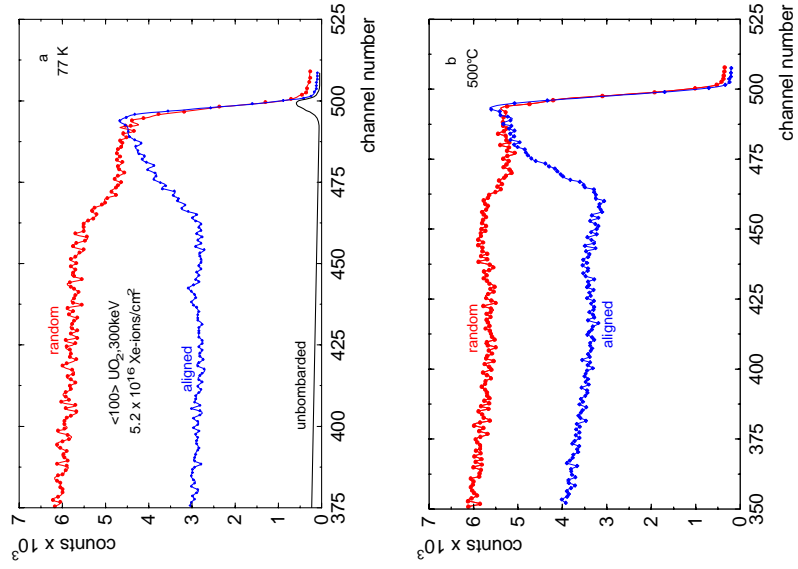
Radiation stability of  $\text{UO}_2$ : Rutherford backscattering/channeling experiments on irradiated  $\text{UO}_2$  show its stability against simulated  $\alpha$ -decay (He-ion and heavy recoil atom)

## Damage in $\text{UO}_2$ , 1 MeV He-implants



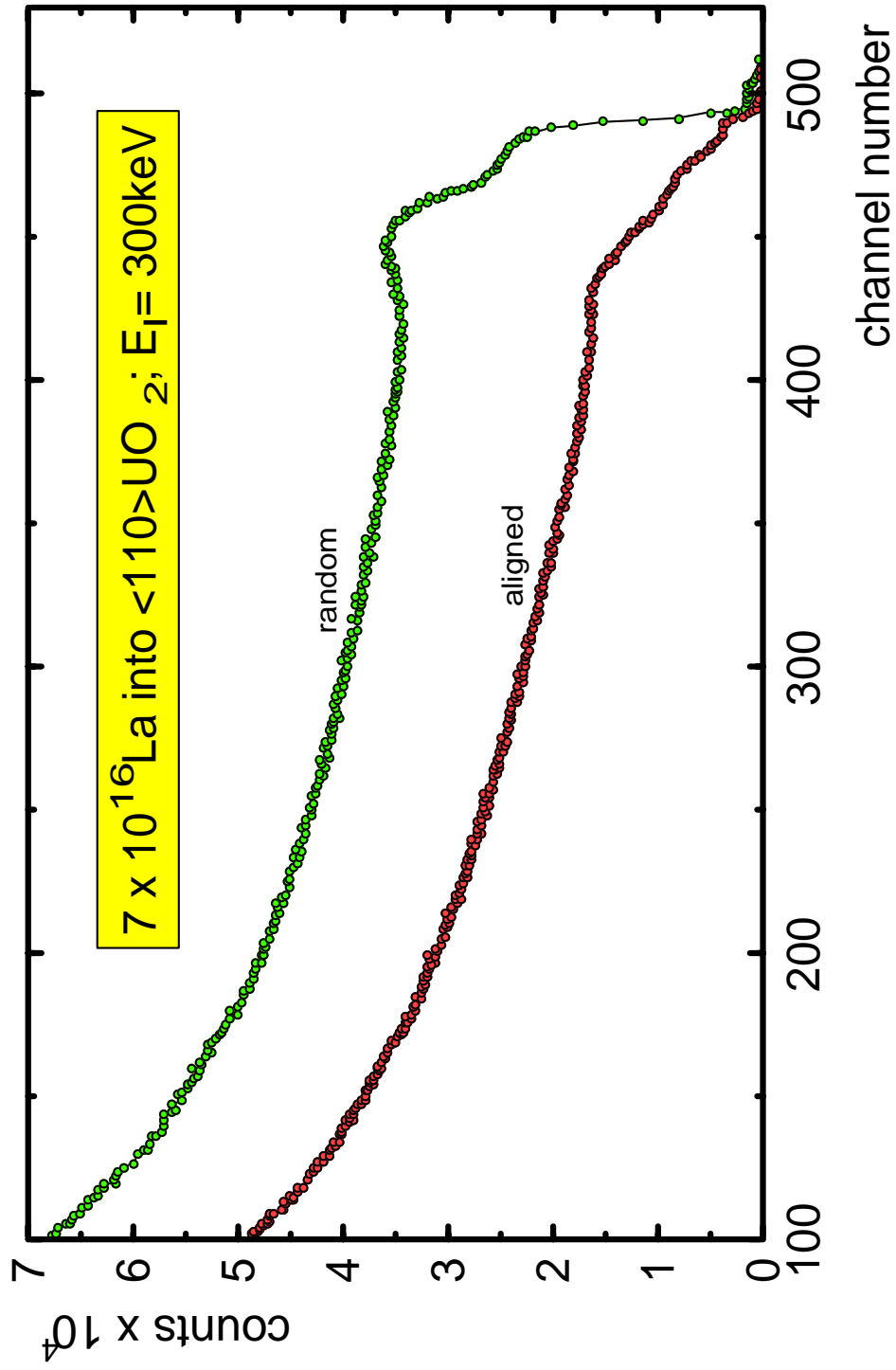
Evaluation of the "damage peak" proves a very pronounced instantaneous defect recovery. For instance, only about 3 of 60 U-defects formed by the He-ion are permanently displaced (Hj. Matzke, J. Nucl. Mater. **270** (1999) 49)

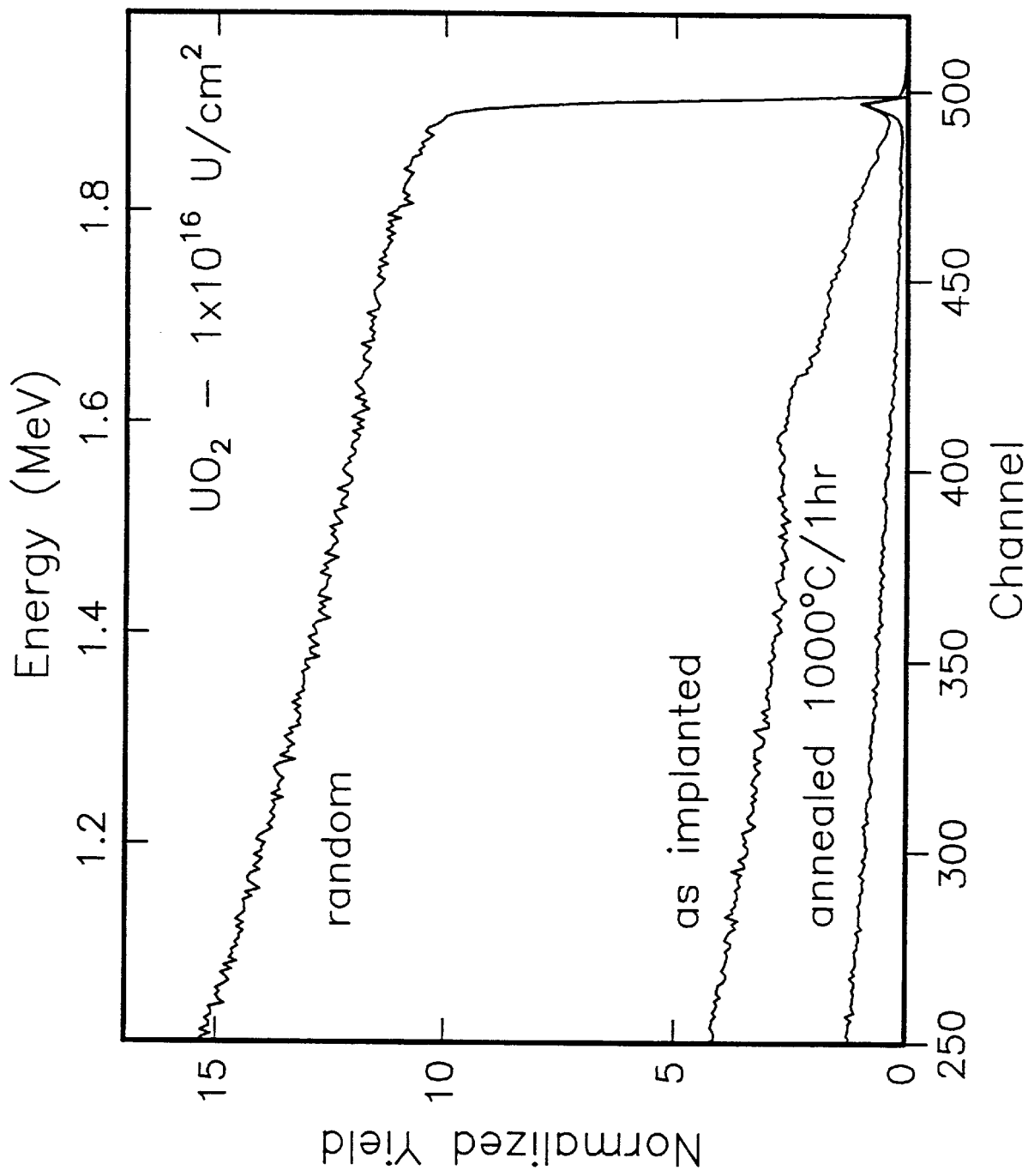
**Rutherford backscattering/channeling spectra showing polygonization due to irradiation with Xe-ions.**



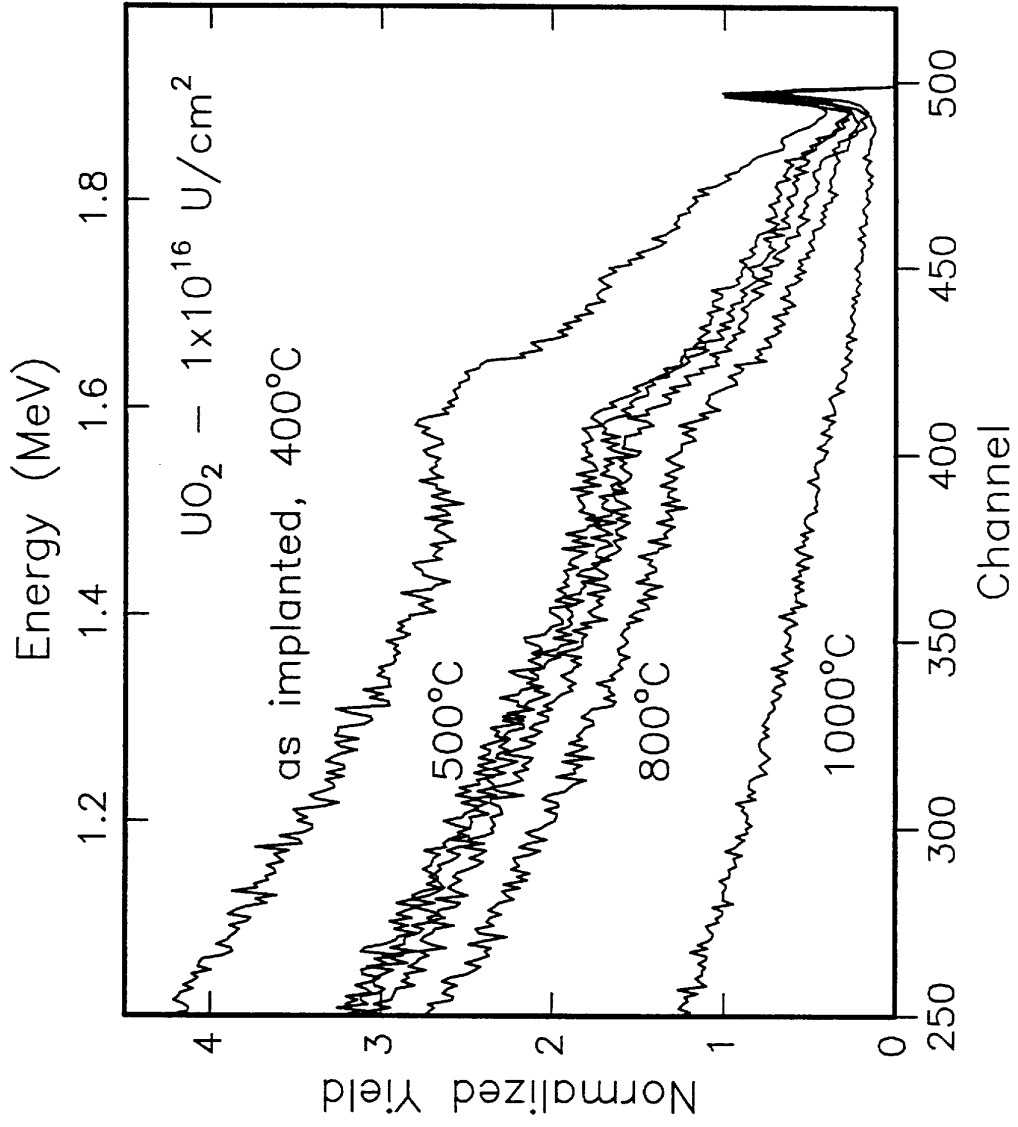
(Hj. Matzke, A. Turos and G. Linker, Nucl. Instrum. Methods in Phys. Research B **91** (1994) 294).  
 The dashed areas, together with X-ray diffraction, show clearly polygonization of  $UO_2$  irradiated with Xe-ions.

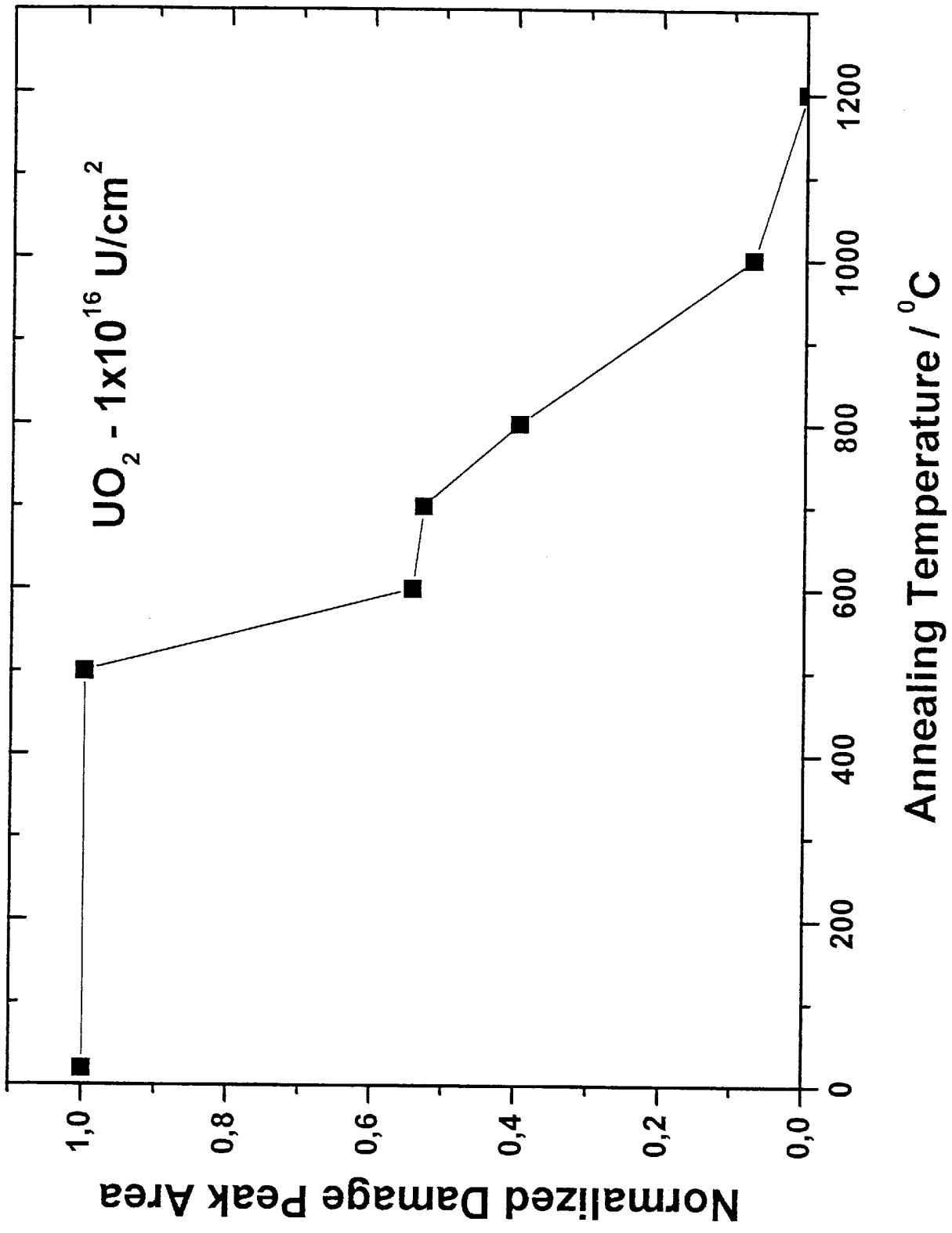
Rutherford backscattering/channeling spectra showing absence of polygonization if the irradiations are performed with soluble La-ions or with U-ions.



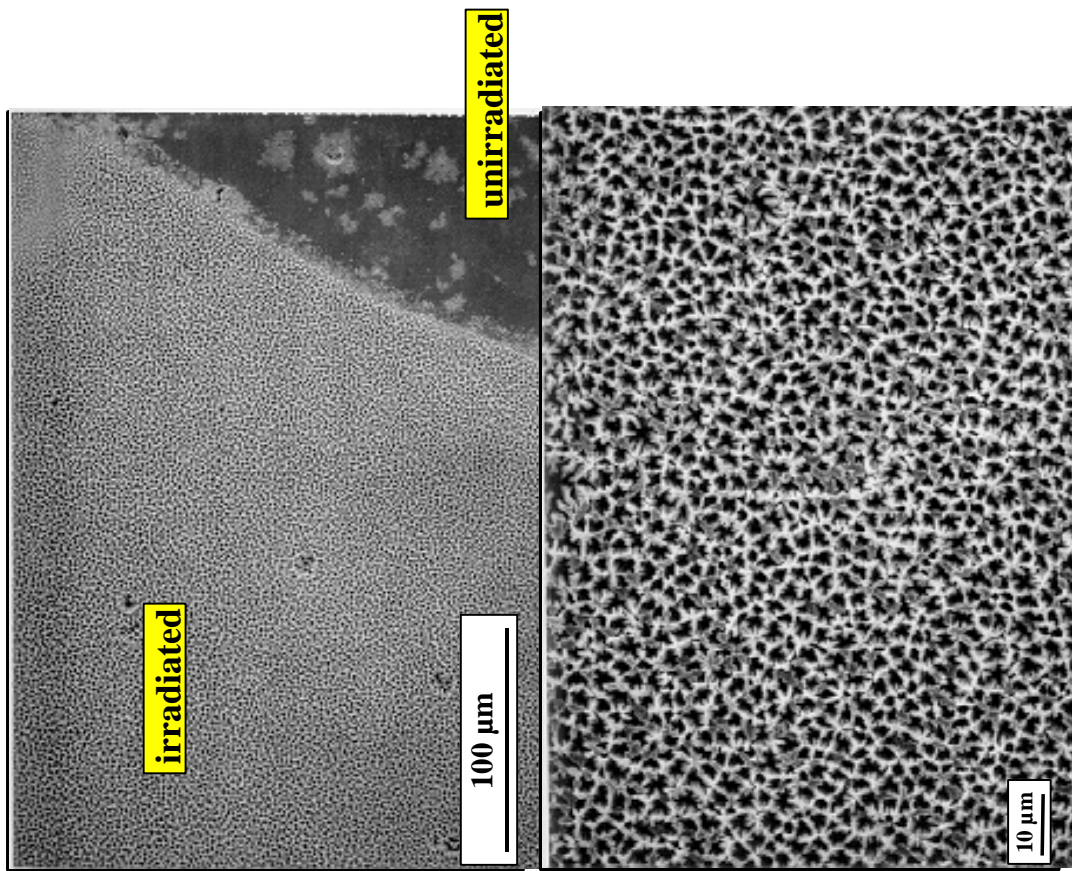


**Defect recovery in "self-irradiated"  $\text{UO}_2$ -  
 $\text{UO}_2$  irradiated with U-ions.**

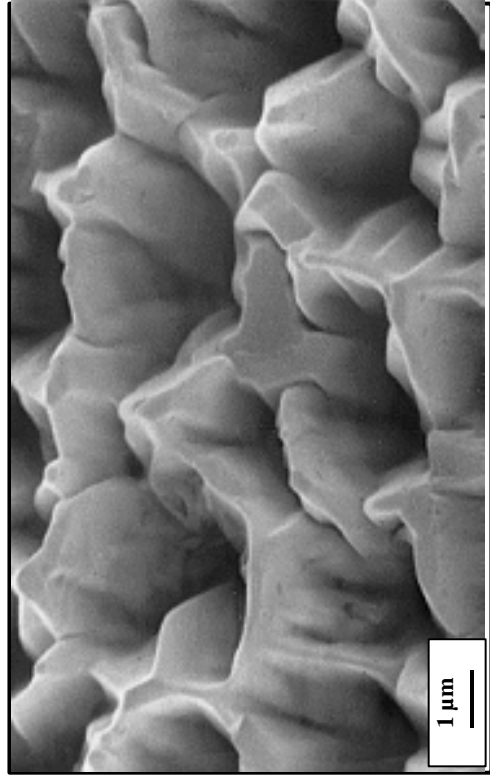
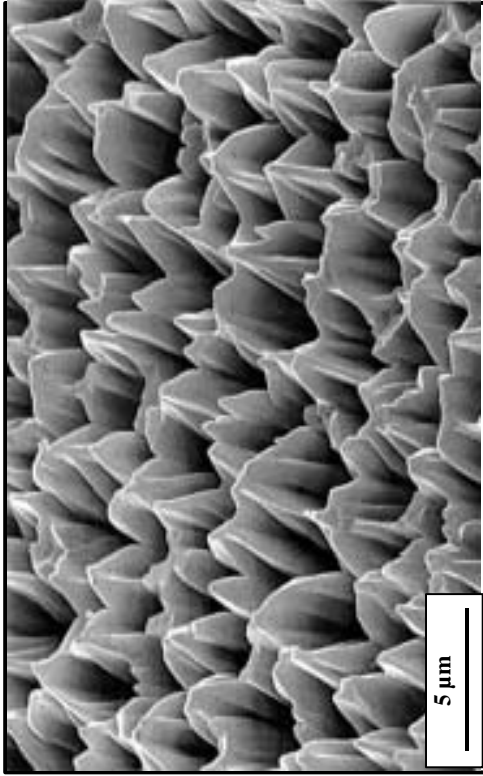




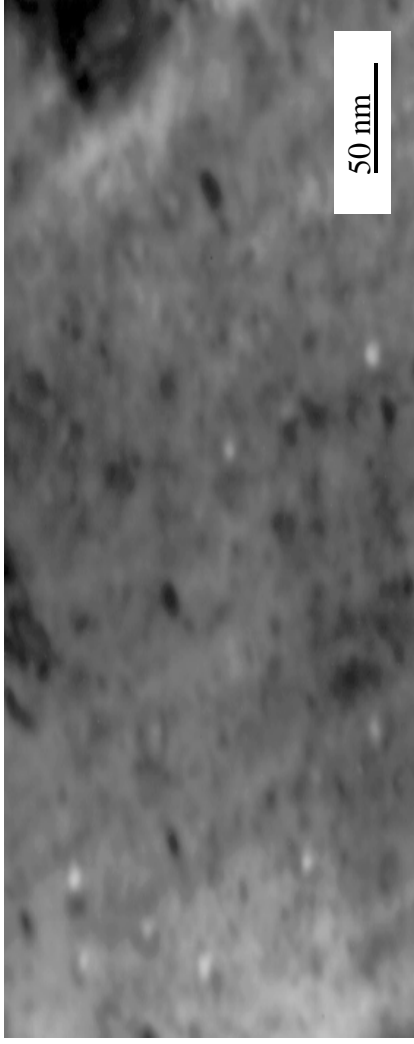
**UO<sub>2</sub> single crystal, cleaved { 111 } face  
irradiated with 10<sup>17</sup> iodine ions of fission energy (72 MeV)**



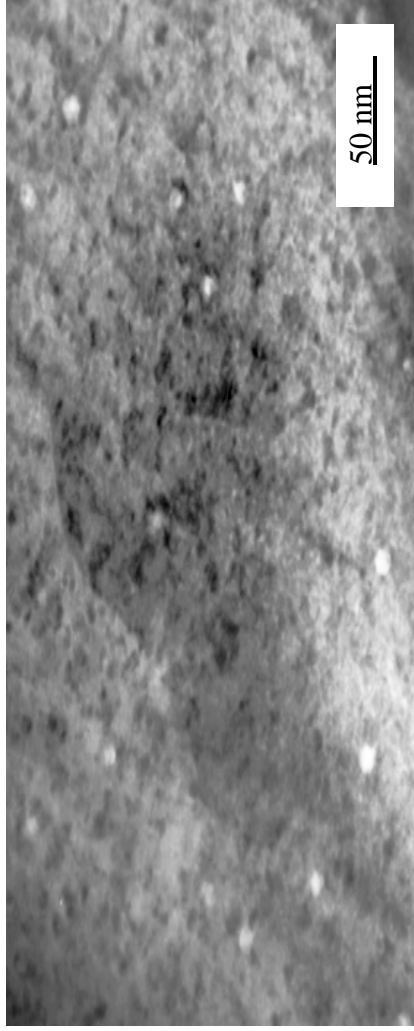
**UO<sub>2</sub> single crystal, cleaved { 111 } face  
irradiated with 10<sup>17</sup> iodine ions of fission energy (72 MeV)**



**TEM view of irradiated UO<sub>2</sub> samples**

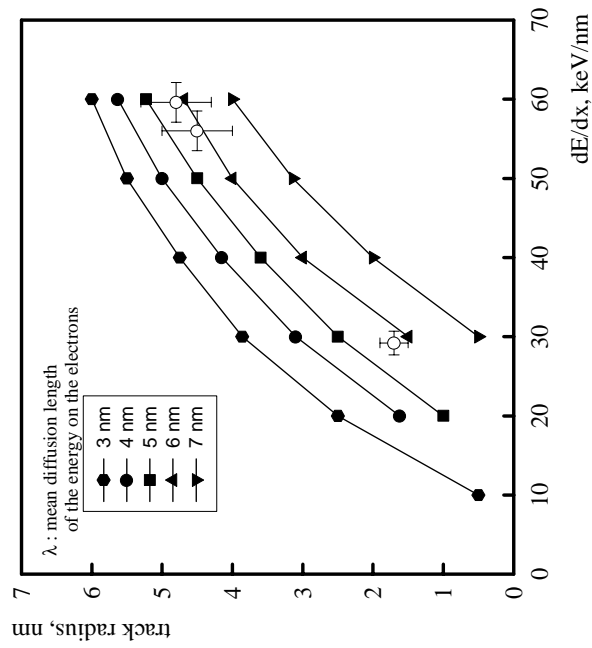


UO<sub>2</sub> covered with a 20µm steel foil irradiated with U ions of 2.6 GeV



Uncovered UO<sub>2</sub> sample irradiated with U ions of 2.6 GeV

**Track radius in  $\text{UO}_2$  vs electronic energy loss for different  $\lambda$  values**



Empty dots with error bars are the experimental points

Evaluation with thermodynamic models shows that  $\text{UO}_2$  is above its melting point along much of the paths of the fission fragments forming (molten) thermal spikes.

## Radiation Enhanced Diffusion in UO<sub>2</sub>

The diffusion of U and Pu in UO<sub>2</sub> and (U,Pu)O<sub>2</sub> was measured under different conditions in the Siloë-Reactor

- varying n-flux
- varying fission rate, F
- different temperatures (150 to 1500 °C)
- different Pu-contents in (U,Pu)O<sub>2</sub>

The enhanced diffusion coefficients D\* for U and Pu were

T-independent between 150 and 1000 °C  
independent of n-flux  
proportional to fission rate F

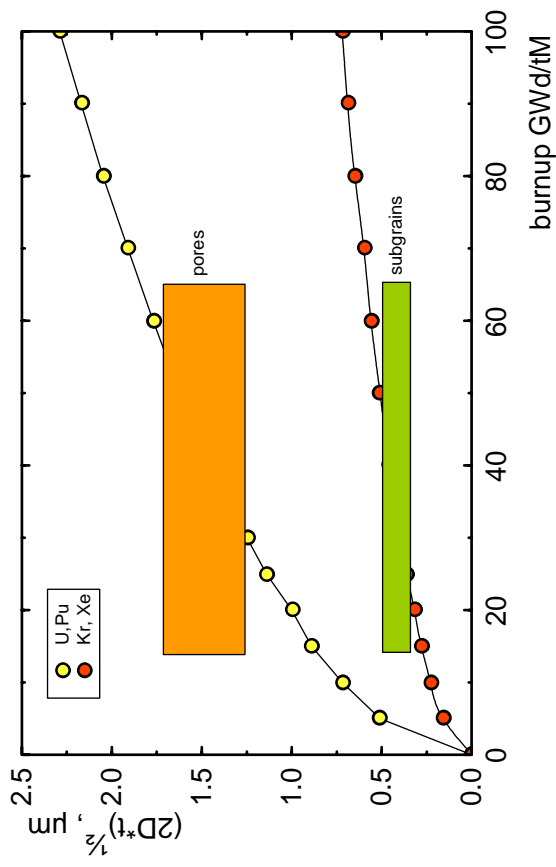
$$D^*(U,Pu) = AF \text{ with } A = 1.2 \times 10^{-29} \text{ cm}^5, F \text{ in fissions/cm}^3\text{s}$$

The T-range covered all recovery stages, hence neither neutrons nor recovery of surviving defects determine D\*, but fission events do.  $\alpha$ -particles were also shown to be ineffective.

For Kr, recent work showed that  $D^*(Kr) \sim 0.1 D^*(U,Pu)$ .

Explanation: U-interstitials being mobile even below RT migrate away from fission track following the pressure gradients around fission tracks, but rare gas atoms do not.

## Mean square displacement of U,Pu and Kr,Xe by fission-enhanced diffusion as a function of burnup (time)



$D^*$  (U,Pu) = AF with  $A = 1.2 \times 10^{-29} \text{ cm}^5$ ,  $F = \text{fissions/cm}^3\text{s}$   
 (Hj. Matzke, Rad. Effects **75** (1983) 317)

$D^*$  (Kr,Xe) = A'F with  $A' \sim 0.1 \text{ A}$   
 (Hj. Matzke, P.G. Lucuta and T. Wiss, Nucl. Instrum. Methods in Physics Research, in press)

Subgrain size  $\sim 0.4$  to  $0.5 \mu\text{m}$   
 (I.L.F. Ray, Hj. Matzke, H.A. Thiele and M. Kinoshita, J. Nucl. Mater **245** (1997) 115)

Pores:  $\sim 16\%$  porosity of  $\sim 1 \mu\text{m}$  sized pores assumed.

# Polygonization in Materials

## Polygonization can have many reasons

1) Related to damage accumulation

UO<sub>2</sub> (no f. p., only damage)

\*intermetallics: Zr<sub>3</sub>Al, U<sub>3</sub>Si

\*ceramics: olivine

(Mg<sub>0.88</sub>Fe<sub>0.12</sub>)<sub>2</sub>SiO<sub>4</sub>,

neptunite Na<sub>2</sub>KLi(Fe,

Mn)<sub>2</sub>Ti<sub>2</sub>(SiO<sub>3</sub>)<sub>8</sub>

\*Zircon ZrSiO<sub>4</sub>, formation of nano crystals

in amorphous matrix

\*breakage by formation of amorphous

regions (damage cascades)

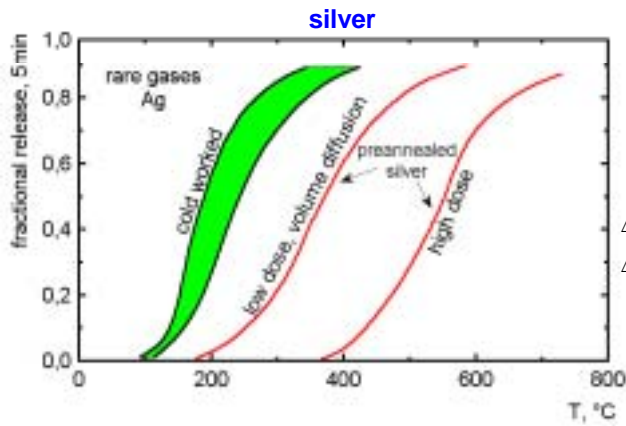
2) Related to damage and impurities

UO<sub>2</sub>, f. p. implantations

fracture between overpressurized bubbles

3) Related to impurities alone, no damage at all

## Release of Inert Gases and Recrystallization of Cold-Worked Metals



Hj. Matzke

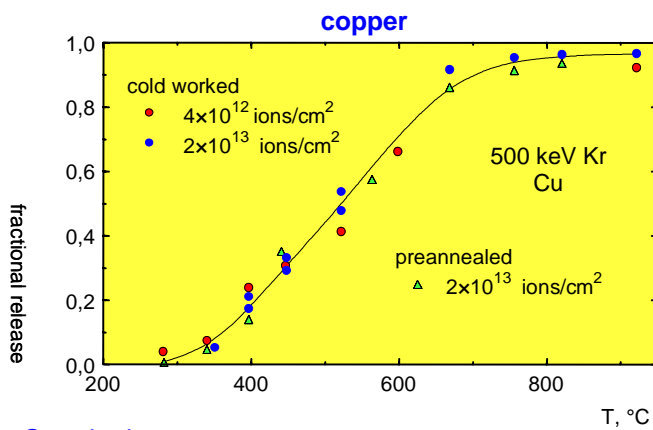
Acta Met. 20(1972)1241

Acta Met. 23(1975)1529

$\Delta H = 1.35\text{eV}$  for gas release

$\Delta H = 1.4\text{ eV}$  for recovery of  $\rho$

T ranges identical



Hj. Matzke

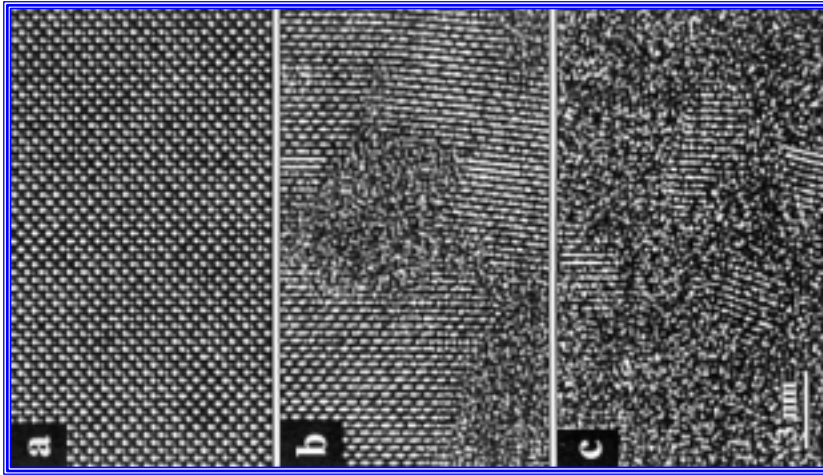
Rad. Effects 29(1976)113

No effect  
of cold-work.

**Conclusion:**

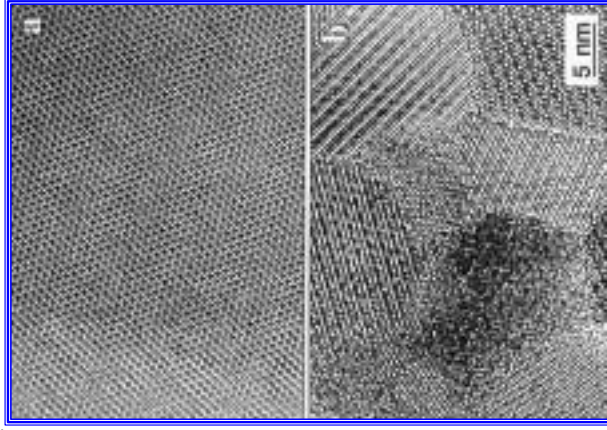
- No instantaneous recrystallization due to gas and damage.
- Increased T needed for recrystallization.
- Recrystallization does not necessarily sweep gases.

Nanocrystals are found in many ceramics due to the impact of heavy ions. The mechanisms are known but are not relevant for  $\text{UO}_2$ .



High resolution transmission electron microscope (HRTEM) images of synthetic zircon  $\text{ZrSiO}_4$  taken a) before and b) after  $1.5 \text{ MeV Kr}^+$ -irradiation to  $1.7$  and c) to  $5.1 \times 10^{17}$  ions/ $\text{m}^2$  at room temperature showing the formation of nanocrystalline zircon in an amorphous matrix.

(L.M. Wang, S.X. Wang, R.C. Ewing, A. Meldrum, R.C. Birtcher, P.P. Newcomer, W.J. Weber and H.J. Matzke, Mater. Sci. Eng., in press)



HRTEM micrograph of a  $\text{Ca}_2\text{La}_8(\text{SiO}_4)_6\text{O}_2$ -specimen a) before and b) after irradiation with  $1.5 \text{ MeV Kr}^+$ -ions to a fluence of  $1 \times 10^{18}$  ions/ $\text{m}^2$  at  $400 \text{ }^\circ\text{C}$ . The thin region of the sample has become nanocrystalline due to the irradiation.

## Models of rim structure formation\*

fall into three classes describing

- I. initiation, threshold
- II. growth after irradiation
- III. fuel performance, property changes

### Proposed models

Rest

- 1) free moving dislocation structure, pairs of fp solute and vacancies move
- 2) based on MD calculations - shock waves, centers of expansion and of compression

Lemekhov

saturation of matrix with fission gas, formation and collapse of capillaries along fission tracks

Kinoshita

spatial instability

Baron

see his presentation (excess matrix energy creates subgrain boundaries)

Une and Chkuaseli, Matzke

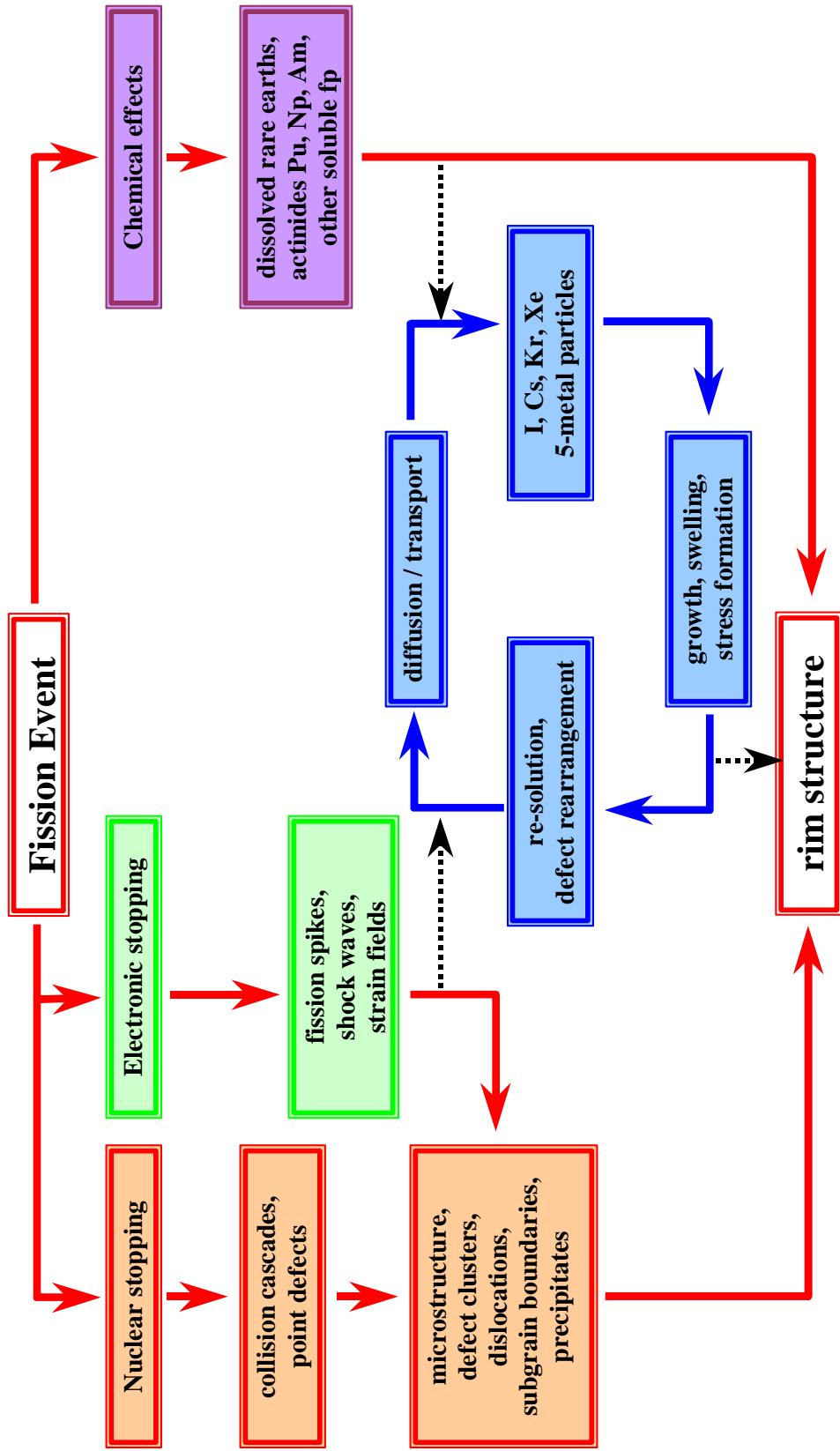
see viewgraphs

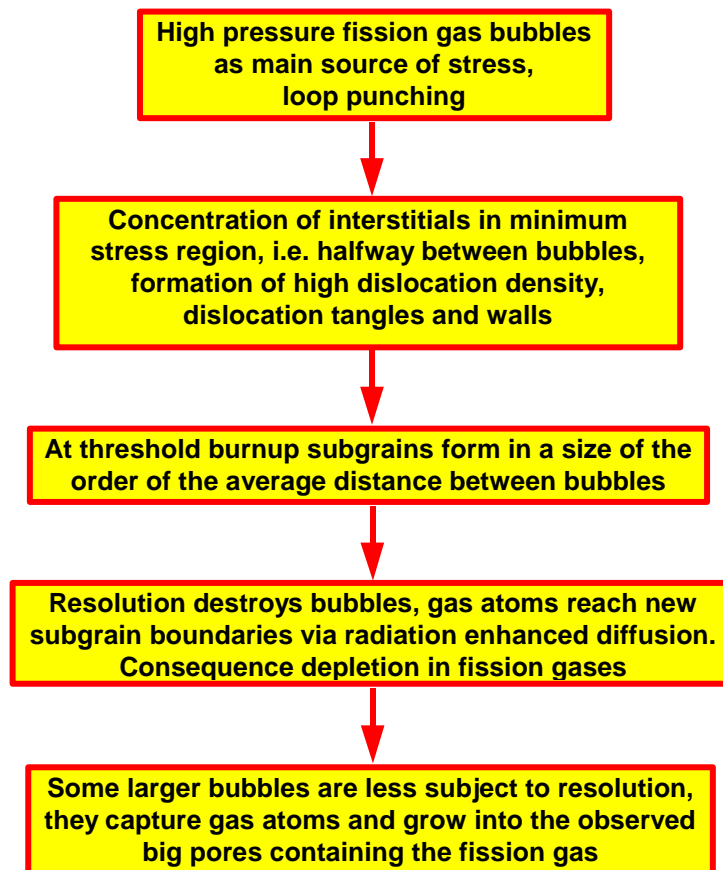
L. Desgranges and N. Lozano

see presentation by L. Desgranges

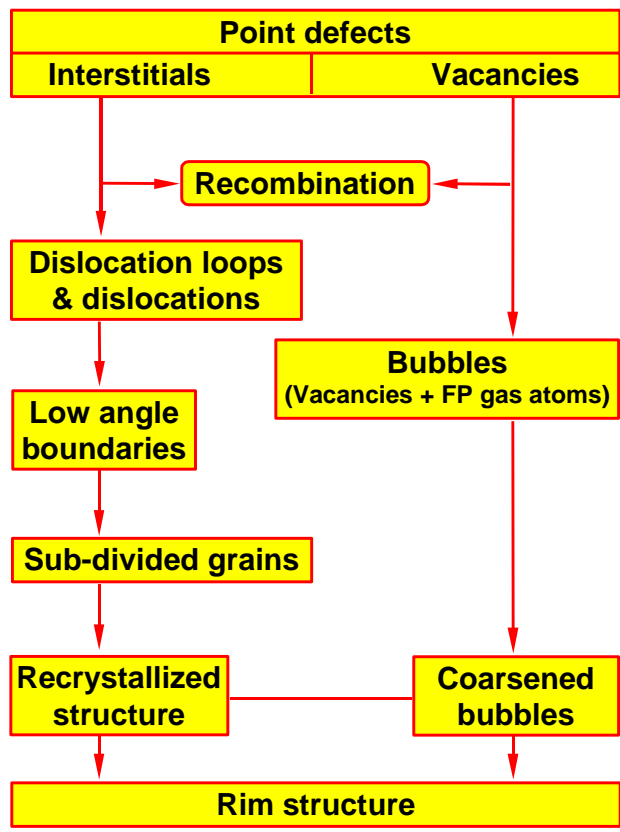
\* see M. Kinoshita and Hj. Matzke, J. Nucl. Mater. **247** (1997) 108 for more details

## Physical and Chemical Processes Involved in the Formation of the Rim Structure





**Possible mechanism of formation of the rim structure as suggested by Matzke and Chkuaseli**



**Mechanism of Formation of the rim structure as suggested by Nogita and Une**

J. Nucl. Mater. 226 (1995) 302

# Fuel and fuel cycles with high burnup for WWER reactors

**V. Chernushev, F. Sokolov**  
Joint Stock Company TVE,  
Moscow, Russian Federation

**Abstract.** The paper discusses the status and trends in development of nuclear fuel and fuel cycles for WWER reactors. Parameters and main stages of implementation of new fuel cycles will be presented. At present, these new fuel cycles are offered to NPPs. Development of new fuel and fuel cycles based on the following principles: profiling fuel enrichment in a cross section of fuel assemblies; increase of average fuel enrichment in fuel assemblies; use of refuelling schemes with lower neutron leakage (“in-in-out”); use of integrated fuel gadolinium-based burnable absorber (for a five-year fuel cycle); increase of fuel burnup in fuel assemblies; improving the neutron balance by using structural materials with low neutron absorption; use of zirconium alloy claddings which are highly resistant to irradiation and corrosion. The paper also presents the results of fuel operation.

## 1. INTRODUCTION

The ways of increasing the technical and economic characteristics of the nuclear fuel for NPPs with WWER-440 and WWER-1000 reactors are rather traditional. First of all, they include the further improvement of the operational reliability and fuel burnup, and the increase of the fuel cycle length. These directions are actively dictated by NPP’s operators.

However, the strict conditions of the nuclear fuel operation result in the reduction of its operational reliability.

The following problems can be mentioned during the NPPs operation with WWER reactors:

- time extension for inserting absorber rods of WWER-1000 control and protection system (CPS) (and sometimes, sticking) because of fuel assembly guide tubes bowing. Besides, fuel assembly bowing might lead to the creation of water gaps beyond the design ones, that in its turn may result in the local growth of power rating;
- the fuel rods failure caused by fretting wear of a cladding due to more intensive conditions of hydrodynamic effect of the coolant flow in previous WWER-440 designs.

The above mentioned as well as other problems under the conditions of the current strategy for reactors operation raise serious questions on the nuclear fuel reliability, the volume of the required R&D activities, and the accumulation of the sufficient operational experience. Also, a substantial scope of the activities in licensing the nuclear fuel with higher burnup and lifetime in normal and emergency modes.

All the abovementioned has required from the Russian nuclear fuel supplier JSC TVEL to make a comprehensive critical analysis of the design, production and operation of the nuclear fuel for NPPs with WWER reactors. As a result, under Minatom of Russia a special complex programme on the nuclear fuel and nuclear cycles improvement with a participation of the leading nuclear scientific centers of Russia was developed. This programme includes a stage-by-stage introduction of the advanced nuclear fuel and fuel cycles with overall calculated experimental and operational testing of reliability and safety.

Table 1. Characteristics of WWER-440 Fuel Cycles

Fuel cycle	Average FA enrichment, %	Core lifetime, effective days	Average burnup, MW·xd/kg U	Natural uranium consumption, kg/MW(heat)·day
Three-year fuel cycle (design)	3.28 (3.6; 2.4; 2.4)	292	28.9	0.247
Four-year fuel cycle, zirconium spacer grids, 3.82 %	3.62 (3.8; 2.4)	325	41.0	0.207
Five-year fuel cycle, zirconium spacer grids, 3.82 %	4.12 (4.21; 3.6)	337	45.0	0.198
Five (Gd)-year fuel cycle, 4.4 %, U Gd fuel assembly	4.28 (4.4; 3.6)	337	49.0	0.198

8 Table 2. Modernization of WWER-440 Fuel Cycles

Fuel cycle	Implementation	
	Implemented at	Introduction Stage
Four-year fuel cycle with fuel 4.4 % (non-profiled)	3 <sup>rd</sup> unit at Kola NPP	Experimental use at Rovno NPP
Zirconium spacer grids	3 <sup>rd</sup> unit at Novovoronezhsk NPP	At the rest of NPPs including experimental use at Loviisa NPP
Five-year fuel cycle with fuel 4.4 % (non-profiled)	3 <sup>rd</sup> unit at Kola NPP	
Modernized four-year fuel cycle with fuel 3.82 % (enrichment profiling, zirconium spacer grids, in-in-out)	4 <sup>th</sup> unit at Novovoronezhsk NPP (from 1995)	Czech NPPs (from 1998), Slovakian NPPs (from 1999)
Modernized four-year fuel cycle with fuel 4.21 % (enrichment profiling, zirconium spacer grids, in-in-out)		1 <sup>st</sup> unit at Rovno NPP (313 fuel assemblies in the core) from 1999
Modernized five-year fuel cycle with fuel 4.21 % (enrichment profiling, zirconium spacer grids, in-in-out)		2 <sup>nd</sup> unit at Rovno NPP (349 fuel assemblies in the core) from 1998
Experimental use of fuel assemblies 4.41 %, zirconium spacer grids, uranium-gadolinium fuel		4 <sup>th</sup> unit at Kola NPP from 1998

## 2. WWER-440

The characteristics of fuel cycles that have been developed for WWER-440 NPPs, as well as main stages in their current implementation are shown in Tables 1 and 2. As seen from Tables 1 and 2, the characteristics of nuclear fuel and fuel cycles stipulate the use of the principles in modern nuclear power engineering:

- profiling fuel enrichment in a cross section of fuel assemblies;
- increase of average fuel enrichment in fuel assemblies;
- use of refuelling schemes with lower neutron leakage (“in-in-out”);
- use of integrated fuel gadolinium-based burnable absorber (for a five-year fuel cycle);
- Increase of fuel burnup in fuel assemblies.

By now, more than 56 000 fuel assemblies (7,000,000 fuel rods) have operated used at 28 NPP units with WWER-440. High operational reliability of WWER-440 nuclear fuel is characterized by the average number of leaking fuel rods about  $\sim 3 \times 10^{-5}$  1/year.

It should be noted that the operational reliability of the previous WWER-440 designs is somewhat lower, and in recent years several cases of leaking fuel rods have been reported. The reason is that the fuel assemblies of the previous designs (of the W-179/230 type) are subjected to a more intense hydrodynamic impact of coolant flow.

The design of such fuel assemblies has been improved based on the results of numerous design and experimental work aimed at increasing the vibration strength of a fuel rod cluster. At present, it is under commercial production.

## 3. WWER-1000

WWER-1000 was developed based on successful operational experience of NPPs with WWER-440 reactors. At present, WWER-1000 is the main nuclear reactor in the Russian nuclear industry. Naturally, the development and production of WWER-1000 nuclear fuel proceeded from the experience with WWER-440.

Nuclear fuel and fuel cycles were updated continually from the beginning of operation of NPPs with WWER-1000 (the first unit with WWER-1000 was started up 1980). Below follow the world wide trends in upgrading nuclear fuel and fuel cycles:

- improving the neutron balance by using structural materials with low neutron absorption;
- use of a integrated fuel burnable absorber;
- use of an improved core layout with low neutron leakage;
- increase of the fuel burnup rate;
- increase of the duration of a fuel cycle;
- use of zirconium alloy claddings which are highly resistant to irradiation and corrosion;
- possible operation of the core under NPP load-follow conditions.

Table 3. Characteristics of WWER-1000 Fuel Cycles

Fuel cycle	Average FA enrichment, %	Core lifetime, effective days	Average burnup, MW <sub>xd</sub> /kg U	Natural uranium consumption, kg/MW(heat)·day
Three-year fuel cycle with a burnable absorber (design)	4.31	291	40.3	0.243
3-to-4-year fuel cycle with U Gd fuel assemblies with zirconium spacer grids and guide channels	3.86	293	42.7	0.205
Four-year fuel cycle with U Gd fuel assemblies with zirconium spacer grids and guide channels	4.17	291	47.7	0.198

includes all the stages of calculation and experimental validation and studies; industrial operation of the experimental batches of fuel assemblies in commercial WWER-1000 reactors at NPPs; as well as detailed post-irradiation examination of spent fuel assemblies at a specialized research institute.

Therefore, a multistage and lengthy procedure for developing and licensing nuclear fuel conducted by JSC “TVEL” ensures a high level of reliability, cost-efficiency and safety of fuel.

The main characteristics of WWER-1000 fuel cycles (including design ones) for steady state refuelling are shown in Table 3. The design fuel cycles shown there differ in terms of progress made in development, licensing and approbation procedures.

It should be noted that experimental and industrial operation of WWER-1000 advanced fuel assemblies with zirconium spacer grids and zirconium guide tubes, and uranium-gadolinium fuel at commercial NPPs in Russia (*Balakovo* and *Novovoronezh* NPPs) and Ukraine (*Zaporozhskaya* and *Rovno* NPPs) has been under way for more than six years. There was not a single case of a leaking fuel rod over four fuel campaigns with a design time of three years (average burnup in a fuel assembly was  $\sim 49$  MWd/ kgU). The successful use of fuel assemblies (totalling 312,000 fuel rods) may give grounds for licensing a project of a four-year fuel cycle based on the advanced fuel assemblies with uranium-gadolinium fuel to start its full-scale introduction at WWER-1000 NPPs somewhere between 2001 and 2002.

In 1997, the development was completed of fuel assemblies with a constantly functioning reinforced skeleton supported by spacer grids and special angels that were not loaded by external forces. This design solution does not allow fuel assemblies to bow in the course of operation and increases the stability of fuel assemblies thermo-mechanical behaviour. In 1998 12 fuel assemblies were loaded at Unit I of Kalinin NPP for experimental and industrial operation.

By now, about 20,000 fuel assemblies ( $6 \times 10^6$  fuel rods) have been irradiated at 20 WWER-1000 reactors. According to the results of fuel assemblies operation, the average number of leaking fuel rods amounts to  $\sim 1.8 \times 10^{-5}$  per a spent fuel cycle (in recent years), which testifies to a rather high operational reliability of the fuel.

Therefore, the characteristics of the updated fuel cycles for NPPs with WWER-440 and WWER-1000 have the following advantages over the design ones:

- decrease in consumption of natural uranium by 12 – 19 %;
- reduction in the total number of fuel assemblies used by 25-30 % (as a result, costs incurred at transportation and storage of spent fuel will be cut, too);
- decrease by 20-25 % in neutron flux per reactor vessel;
- increase in fuel burn-up in fuel assemblies.

Major guidelines for further improvements in WWER nuclear fuel and fuel cycles based on the successful R&D results, that are now under way, are aimed at:

- development of nuclear fuel with a burnup rate of up to 60 MW·day/ kg U;
- creating a five-year WWER-1000 fuel cycle;
- development of fuel cycles with campaign duration ranging from 18 to 24 months;
- development of nuclear fuel and algorithms for reactor management, which ensure NPP's operation under load-follow condition;
- involving reprocessed uranium in the fuel cycle.

# Technological and licensing challenges for high burnup fuel

**H. Gross, P. Urban, C. Fenzlein**

Siemens AG (KWU),

Erlangen, Germany

**Abstract.** Deregulation of electricity markets is driving electricity prices downward as well in the U.S. as in Europe. As a consequence high burnup fuel will be demanded by utilities using either the storage or the reprocessing option. At a minimum, burnups consistent with the current political enrichment limit of 5 w/o will be required for both markets. Significant progress has been achieved in the past by Siemens in meeting the demands of utilities for increased fuel burnup. The technological challenges posed by the increased burnup are mainly related to the corrosion and hydrogen pickup of the clad, the high burnup properties of the fuel and the dimensional changes of the fuel assembly structure. Clad materials with increased corrosion resistance appropriate for high burnup have been developed. The high burnup behaviour of the fuel has been extensively investigated and the decrease of thermal conductivity with burnup, the rim effect of the pellet and the increase of fission gas release with burnup can be described, with good accuracy, in fuel rod computer codes. Advanced statistical design methods have been developed and introduced. Materials with increased corrosion resistance are also helpful controlling the dimensional changes of the fuel assembly structure. In summary, most of the questions about the fuel operational behaviour and reliability in the high burnup range have been solved –some of them are still in the process of verification- or the solutions are visible. This fact is largely acknowledged by regulators too. The main licensing challenges for high burnup fuel are currently seen for accident condition analyses, especially for RIA and LOCA.

## 1. INTRODUCTION

The contribution of fuel assemblies to safe and economic production of electricity in light water reactors is focused in two main directions. The first and most important requirement is the increase of fuel reliability in order to avoid losses in the availability of the power plant as well as directly and indirectly related cost disadvantages. The second requirement is the reduction of fuel cycle cost which is most efficiently achieved by increasing the fuel assembly burnup.

In this contribution at first the present status of discharge burnups will be described and the technical potential and the incentives for further increases will be discussed. In the main part selected technical and licensing challenges are dealt with in detail.

## 2. PRESENTLY ACHIEVED DISCHARGE BURNUPS

The progress in increasing discharge burnup in the past may representatively be demonstrated by a look at the corresponding numbers for Siemens fuel assemblies. The average discharge burnup of all Siemens PWR fuel assemblies plotted versus the year of discharge is shown by the lower curve in Figure 1. The value increased since the beginning of the last decade by about 30 %. It has to be considered, that this average value contains fuel assemblies from power plants where burnup increase has not strongly been pursued due to lacking attractiveness and technical or licensing limitations.

Cases where technically feasible increases have been licensed and realized are represented by the upper curve of Figure 1. It shows the average discharge burnup of the leading complete reload batch which increased by about 50 % in less than two decades. Fuel assemblies which

will be discharged in the coming years are already inserted today or are under detailed planning. Thus the further increase of this curve is easily predictable. The burnup will reach 55 MWd/kgU by the year 2005.

The corresponding diagram for boiling water reactors is shown in Figure 2.

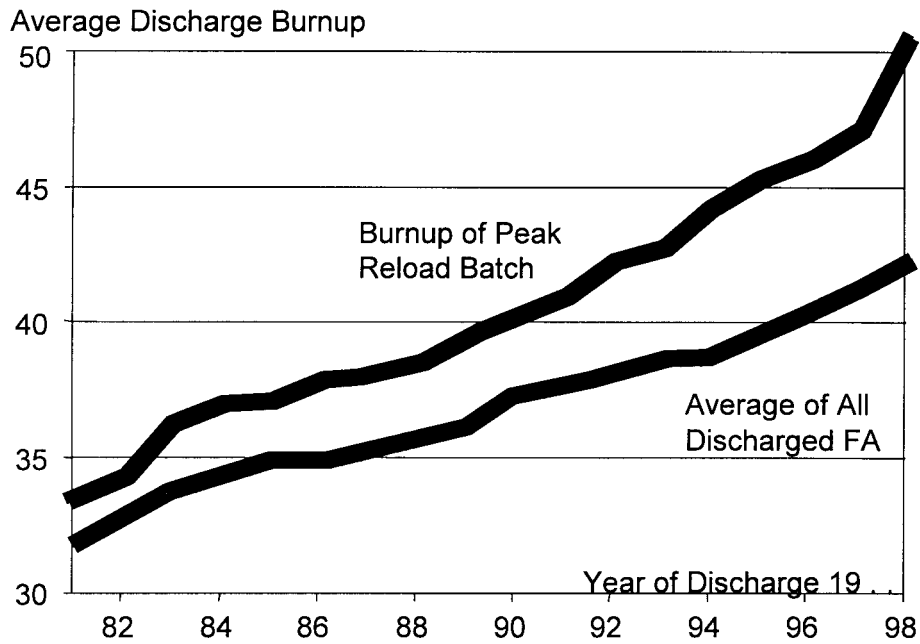


FIG. 1. The average discharge burnup of Siemens fuel assemblies in European PWR increases continuously.

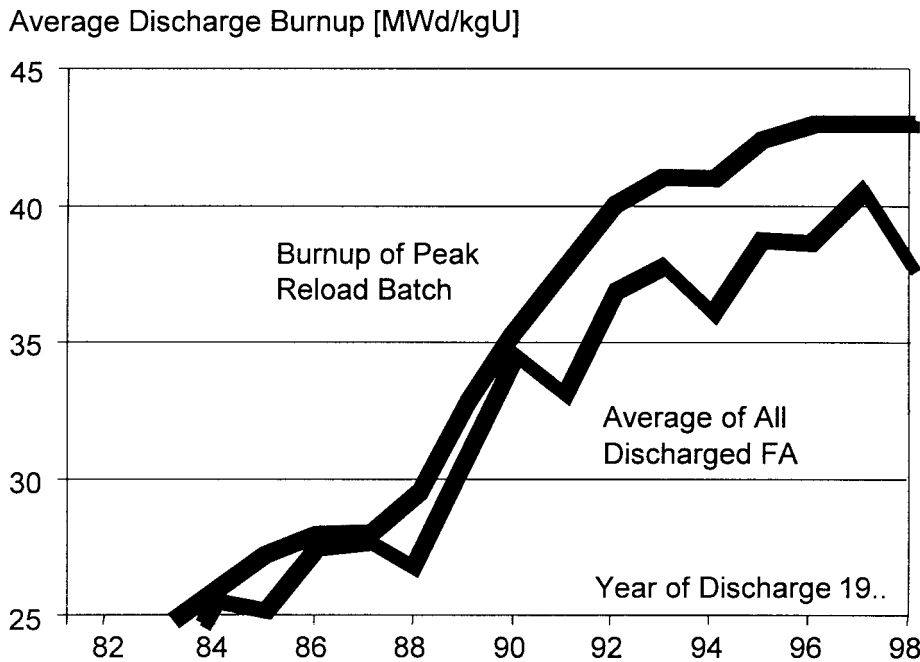


FIG. 2. The average discharge burnup of Siemens fuel assemblies in European BWR has approached values of PWR.

The average burnup was at rather low values around 1980 but increased strongly since then and today almost reached the PWR level. The value of the leading batch, however, is still well behind the corresponding PWR value.

The burnup increases shown in Figure 1 and Figure 2 have reduced the reload batch sizes considerably and have created annual savings for a large PWR or BWR in the order of magnitude of up to 35 million EURO in the corresponding period of time.

### 3. POTENTIAL AND INCENTIVES FOR FURTHER INCREASE OF DISCHARGE BURNUP

Increased discharge burnup results in increased loads and more demanding requirements for the fuel assemblies which in principle could also raise the risk of fuel failures. Considerable research and development expenses have been made to achieve the technical standard of today's fuel assembly designs. A level has been reached where the economic advantages described above can be utilized along with significantly reduced failure rates compared to fuel assemblies of former generations.

Also for the future there seems to be further technical potential to continue the increase of discharge burnup. Advanced fuel assemblies offer sufficient margins to be used with higher enrichments in smaller batch sizes and with increasingly heterogeneous core loading schemes. Cladding and structure materials have been developed and irradiated to burnups far above today's average values.

Though it is not possible to quantify exactly the enrichment and the corresponding burnup which appear to be feasible based on presently available technical solutions, it is very likely, that this limit is above 5 w/o U-235. This enrichment level, on the other hand, represents a world wide established limit for fabrication, transport and storage of nuclear fuel for light water reactors. Considerable effort seems to be necessary to exceed this limit. Therefore, it seems to be reasonable, to assume 5 w/o U-235 as a long term target for further burnup increases.

Depending on detailed conditions, this enrichment is equivalent to about 67 MWd/kgU batch average discharge burnup for a large PWR operated in annual cycles. Operation at increased cycle length of 18 or even 24 months of course results in considerable burnup reduction.

In a BWR, the more heterogeneous distribution of moderator and thermal neutron flux requires a radial and possibly axial distribution of U-235. The maximum average fuel assembly enrichment consistent with the 5 w/o U-235 limit, therefore, results in a value of about 4.6 w/o U235. The corresponding batch average burnup in a large BWR is around 63 MWd/kgU for annual cycles.

The "target burnups" derived under the described assumptions are about 15 to 20 MWd/kgU above the burnups reached to date with full reload batches. Assuming about the same increase of the "leading batch" burnup with time as in the past, it would take another 15 to 20 years until a complete reload batch would be discharged with the "target burnup" mentioned above.

The economic incentive to further increase discharge burnup is demonstrated in Figure 3. Fuel cycle costs are plotted for a 1300 MW PWR as a function of batch average burnup for annual cycles. The savings have been calculated in million EURO per year relative to an average

discharge burnup of 40 MWd/kgU. Disposal cost is used as a parameter. For the upper curve a high value of 2500 DM per kg uranium was used. The curve in the middle was calculated with value of 1250 DM per kg, which might be representative for direct disposal. For the lowermost curve the disposal cost has been assumed independent from uranium mass. In this case there are only small savings with increased burnup resulting from reduced fabrication cost for the reduced number of fuel assemblies.

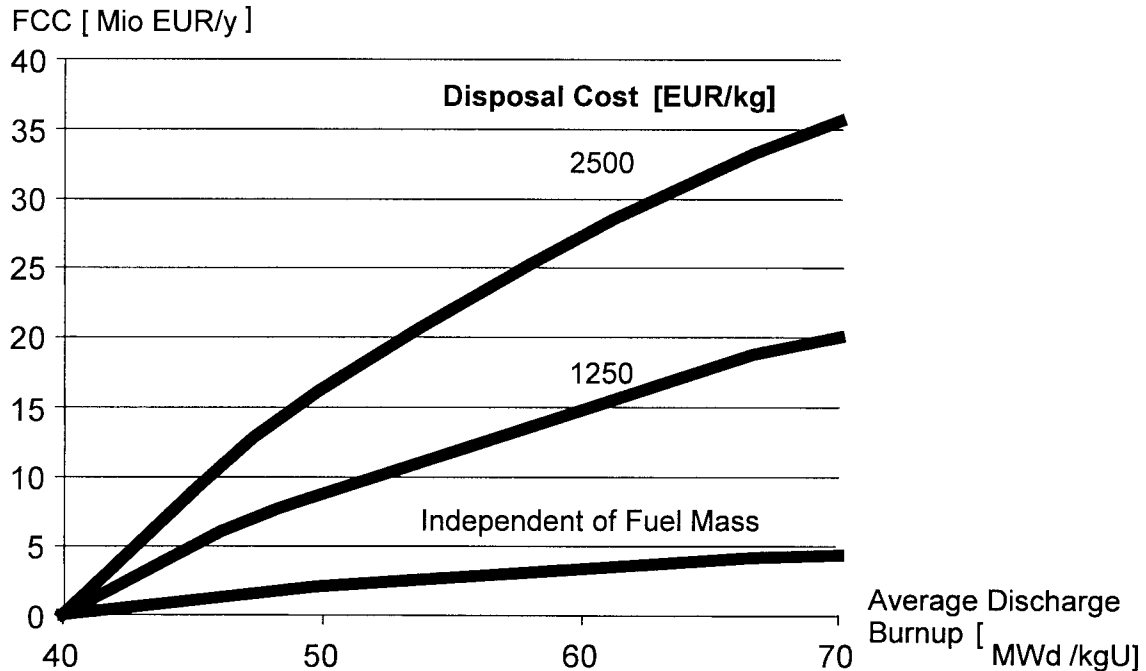


FIG. 3. Savings in fuel cycle cost depend on disposal cost model (1300 MW PWR, annual cycle).

For realistic disposal costs, the diagram shows still considerable savings by comparing to reached burnup levels reached to date with the achievable “target burnup” mentioned above. Depending on the assumptions of disposal costs, these savings might be in the range between 15 and 30 million EUR per year.

For boiling water reactors the span between present burnups and the “target burnup” is about the same as for pressurized water reactors. Consequently the savings are in the same order of magnitude.

#### 4. CORROSION AND HYDROGEN PICKUP

It has been recognized many years ago that the corrosion resistance of standard Zry will be not sufficient for the demands for increased burnup. Zry variants with increased corrosion resistance have been developed as well as other Zr based alternative clad materials. The current Siemens standard PWR clad materials are the Duplex clad and optimized Zry-4 which have been described several times in detail, e. g. [1]. Today, the improved corrosion resistance of these clad materials yields lower corrosion thickness today compared to those observed several years ago although the burnups have significantly increased since this time. By this reason we have seen no need to push the use of alternate clad materials which have been also developed by Siemens. Alternative clad materials have been inserted in lead assemblies in several plants. This will give us sound irradiation experience with various operating

conditions which is the prerequisite for insertion in reload quantities in the future if the further burnup increase should require this.

For high burnup it is also necessary to look carefully on the influence of corrosion and hydrogen pickup on the dimensional behavior of guide tubes and spacers. Precipitated hydrides have about 15 % more volume than Zry. Obviously higher hydrogen contents in a Zry component will contribute to an increase of the outer component dimensions. ZrO<sub>2</sub> has also a higher volume than Zry. It will therefore impose tensile stresses on the Zry metal below the corrosion layer. If the metallic wall thickness is small, the tensile stresses can be high enough to contribute to a macroscopic dimensional changes of the respective component due to irradiation induced stress relaxation. By this reason we are on the way to switch to optimized Zry as material for guide tubes and spacers. Alternative Zr based materials are also tested.

## 5. HIGH BURNUP EFFECTS

Siemens has intensively examined the fuel behavior at high burnup experimentally as well as theoretically and we have participated in a large number of international programs. The experimental examinations are partly based on the insertion of lead fuel rods which have been irradiated to burnups far above the range of commercial operation. The maximum peak pellet burnup achieved by Siemens up to now is 105 MWd/kgU. Hot cell examinations have been completed for fuel rod burnups of 90 MWd/kgU with the peak pellet burnup correspondingly higher. The data base for the validation of our fuel rod code CARO includes currently more than 100 fuel rods with burnups greater 44 MWd/kgU going up to the above mentioned 90 MWd/kgU.

Especially the high burnup effects :

- burnup dependence of the fuel thermal conductivity,
- pellet rim formation and rim structure,
- fission gas release at high burnup,

have been examined in detail. A summary of the examinations on the burnup dependence of the fuel thermal conductivity and of the pellet rim is given below.

- |   |
|---|
| <ul style="list-style-type: none"><li>- Integral measurements to determine fuel thermal conductivity<ul style="list-style-type: none"><li>• Continuous fuel center temperature measurements (in pile) in Halden, RISØ and Mol for burnups from 0 to 100 MWd/kgU</li><li>• Continuous fuel center temperature measurements on fuel re-fabricated from power reactors and instrumented with thermocouples</li></ul></li><li>- Direct measurements of fuel thermal conductivity<ul style="list-style-type: none"><li>• Irradiation of high enriched fuel discs for laser flash measurements (NFIR program)</li><li>• Laser flash measurements on UO<sub>2</sub> and UO<sub>2</sub>/Gd<sub>2</sub>O<sub>3</sub> fuel with simulated burnup up to 90 MWd/kgU (AECL, JAERI)</li><li>• Laser flash measurements on irradiated UO<sub>2</sub> and UO<sub>2</sub>/Gd<sub>2</sub>O<sub>3</sub> fuel with burnup up to 80 MWd/kgU (AEA, JAERI)</li></ul></li></ul> |
|---|

*Examinations for burnup dependence of fuel thermal conductivity*

- Irradiation in power reactors up to > 100MWd/kgU peak pellet burnup
- Irradiation of instrumented fuel rods in test reactors up to 100 MWd/kgU
- Systematic hot cell examinations of fuel rods with high burnup
- Measurement of microscopic properties of high burnup test samples like quantitative optical microscopy, electron probe micro analysis (EPMA) and scanning and transmission electron microscopy (SEM & TEM)

*Examinations for rim formation and rim structure*

Based on the experimental examinations a new fuel thermal conductivity correlation has been developed [2, 3]. The phonon term of the new correlation has the form  $(1/x) \cdot \arctan(x)$ , where  $x$  is a measure of the defect concentration introduced by burnup or Gadolinia addition. For low defect concentrations, this term is identical with the classical form for the phonon term. For higher defect concentrations, the new correlation deviates from the classical formulation and has a distinctly weaker dependence on temperature and defect concentration which fits well to the experimental results. A comparison of the new correlation with the Halden recommendation [4] is given in Fig. 4. Agreement between the new model and the Halden recommendation is very good up to 40 MWd/kgU. At 60 MWd/kgU, the saturation tendency of the new model becomes apparent at low temperature. Experimental results for the rim width as function of burnup are given in Fig. 5.

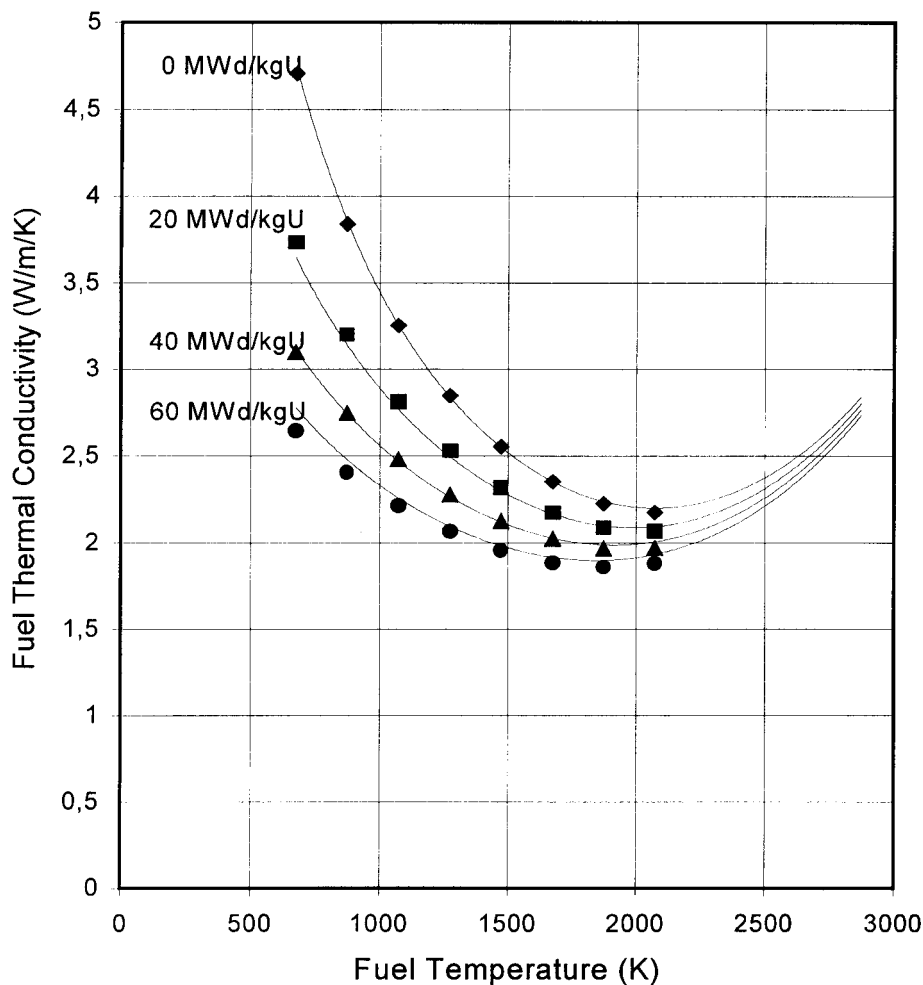


FIG. 4. Fit of new correlation (curves) to halden data (points).

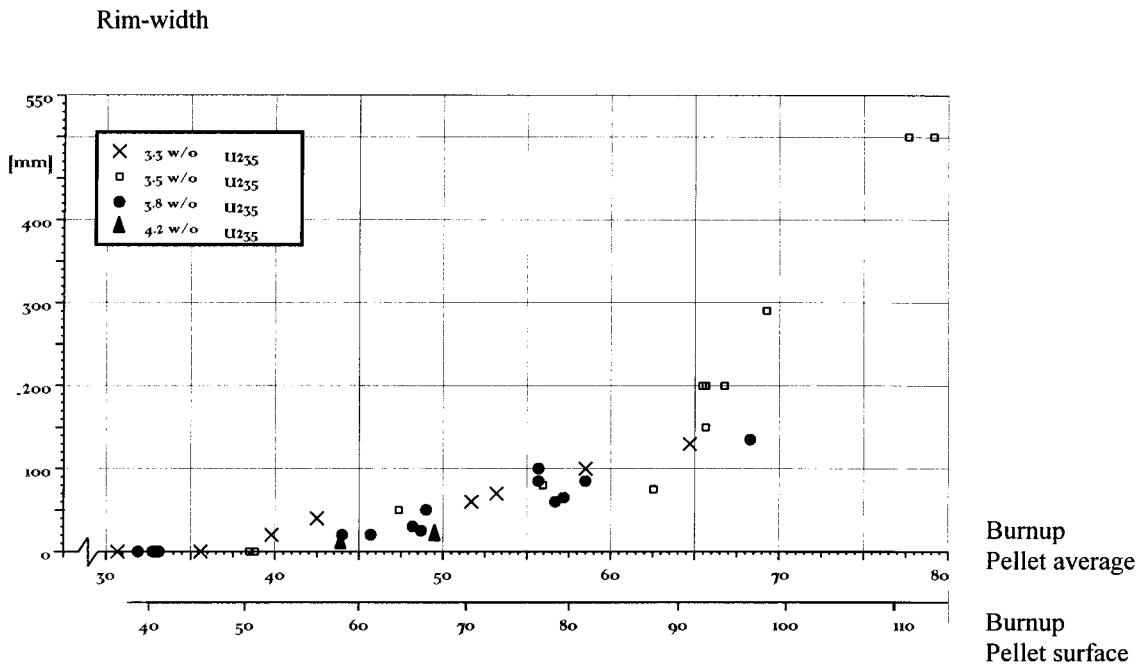


FIG. 5. Rim-width as function of burnup.

A special challenge is the modeling of fission gas release at high burnup. Radial matrix fission gas release profiles of  $UO_2$  fuel measured by electron probe micro analysis usually have the shape of a bowler hat: High release in the fuel central part, low release in the rim and a continuous transition zone in between. This holds for both, fuel irradiated under steady state conditions and ramped fuel. Good fission gas release models based mainly on diffusional processes are capable of describing such radial fission gas release profiles. At high burnup the bowler becomes battered. The formerly smooth transition zone gets pronounced steps and the height of the bowler increases (continued fission gas release in central part) despite decreasing temperatures at high burnup. Additionally, the rim of the bowler swings up at high burnup due to the rim effect which transports gas from the matrix to the rim bubbles. A new generalized model for fission gas release is used in the new version of our fuel rod code CARO. It excellently describes even details of various "battered bowlers" for the radial profile of fission gas release at very high burnup [5]. Examples are shown in Figures 6 and 7.

In summary it can be stated that high burnup effects are modeled very well in the current version of our fuel rod code and this has been also acknowledged in 1998 by the German reactor safety commission when a status report on high burnup was given to the commission by the German utilities. The report was presented by Siemens.

Additionally to the fuel rod code improvements for high burnup, we have also developed an advanced fuel rod design methodology using statistical methods [6]. The scheme of the statistical methodology is shown in Fig. 8. Monte Carlo calculations are performed using the fuel rod code CARO. For each run with CARO, the set of input data is modified: parameters describing the design of the fuel rod (geometrical data, density etc.) and modeling parameters are randomly selected according to their individual distributions. Power histories are varied systematically in a way that each power history of the relevant core management calculation is represented in the Monte Carlo calculations with equal frequency. The frequency distributions of the results as rod internal pressure and cladding strain which are generated by the Monte

Carlo calculations are evaluated and compared with the design criteria. Up to now, this methodology has been applied to licensing calculations for PWRs and BWRs, UO<sub>2</sub> and MOX fuel, for 10 different plants in 3 countries. Especially for the insertion of MOX fuel resulting in power histories with relatively high linear heat generation rates at higher burnup, the statistical methodology is an appropriate approach to demonstrate the compliance of licensing requirements.

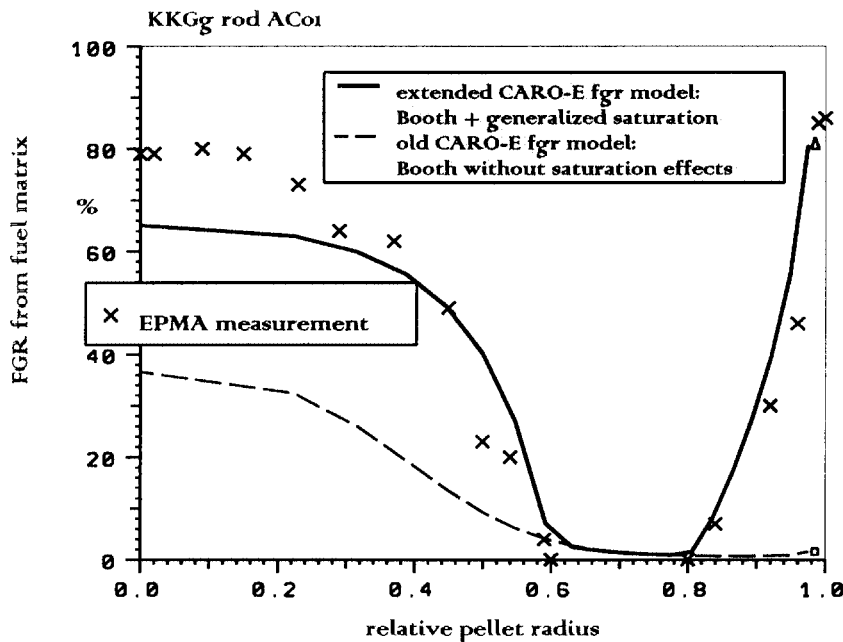
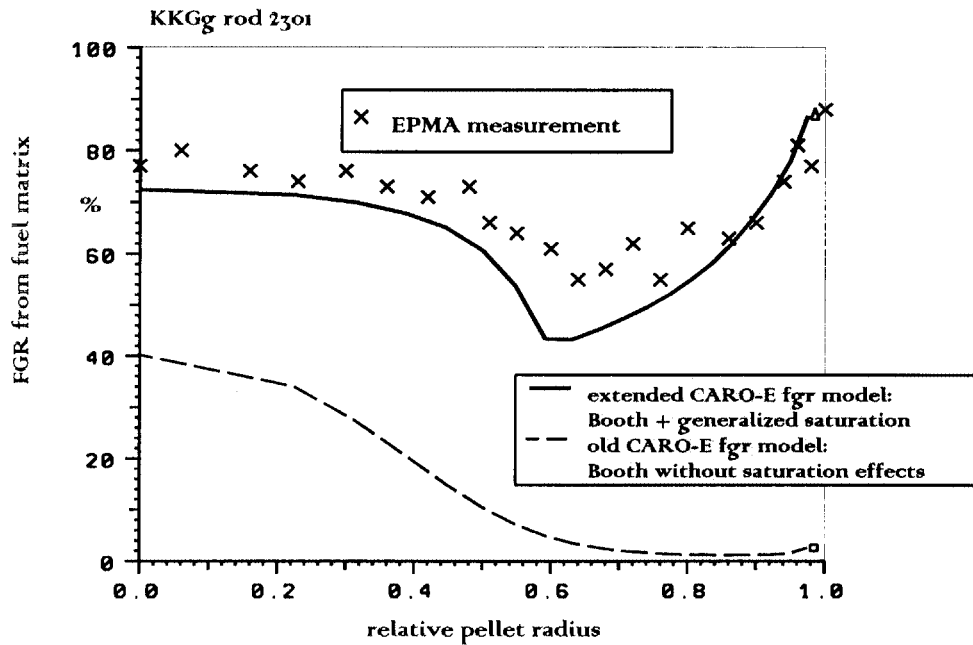


FIG. 6. & 7. Pellet radial Xe release profiles (matrix) calculated with CARO-E for rods with burnup of 69 MWd/kgU and 85 MWd/kgU in comparison to measurements.

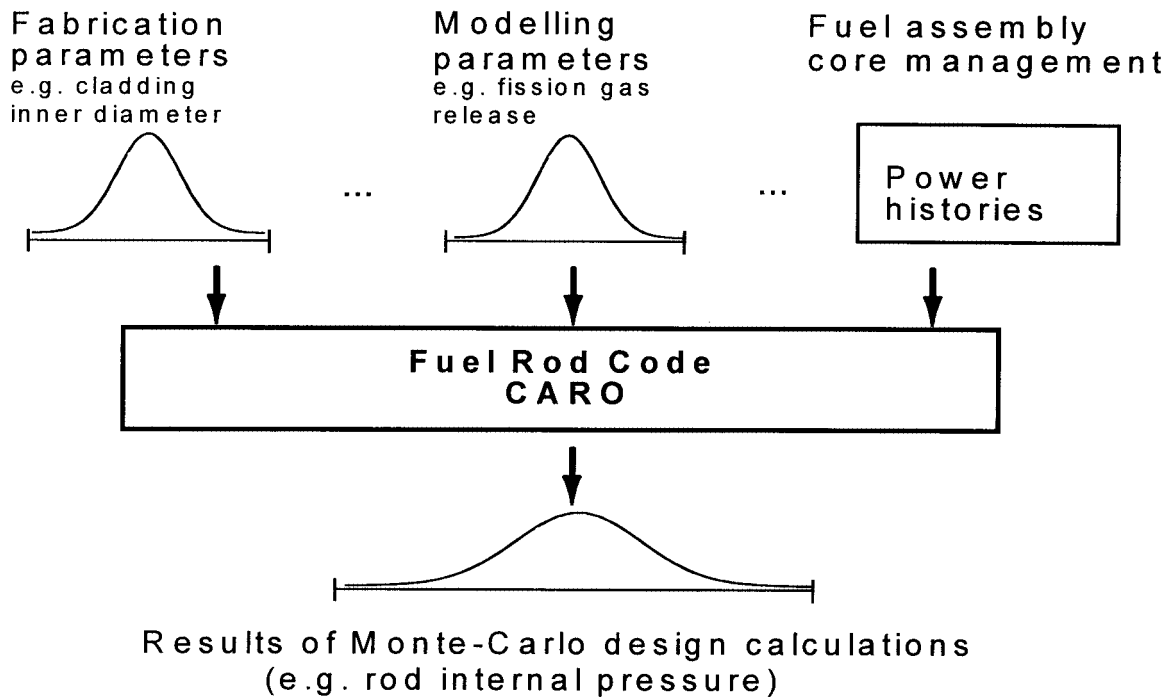


FIG. 8. Scheme of statistical fuel rod design.

The confirmation of the statistical methodology as an appropriate tool for design analysis was given by the fact, that this methodology has been accepted by our customers, see e.g. [6], and successfully applied for licensing. The Swiss Federal Nuclear Safety Inspectorate (HSK) published its positive assessment of our methodology in [7]. Another analysis, using statistical methods, the calculation of core damage extent during a hypothetical loss of coolant accident, is currently being licensed.

The introduction of the new methodology revealed interesting discussions with customers and licensing authorities which led to improvements and further development of the statistical methods.

## 6. RIA AND LOCA

A detailed technical view on high burnup issues related to RIA and LOCA has been given by Siemens in [8]. The main conclusions have not changed until today. The main parameters influencing the outcome of RIA simulation tests are the pulse width of the test and the clad condition. The burnup itself seems to have only a minor influence. The following failure limits for the enthalpy rise  $\Delta H$  can be derived from the CABRI and the NSRR RIA simulation for LWR typical pulse width (60 –100 ms) in the burnup range above 50 MWd/kgU:

$\Delta H \geq 60$  cal/g for fuel rods with oxide spalling and local hydrides,

$\Delta H > 100$  cal/g for fuel rods without oxide spalling and local hydrides.

These conclusions are confirmed by the CABRI test REP Na-10 which has been performed meanwhile (July 1998). The REP Na-10 test was done with same type of fuel rod as Na-1 and Na-8, i.e. high corrosion layer thickness, oxide spalling and local hydrides, but with an

intermediate pulse width of 31 ms. The pulse width of REP Na-1 and REP Na-8 had been 9.5 ms and 75 ms respectively. The pulse width of 31 ms is below the range expected for LWRs, nevertheless the thermal effects are close to those for LWR typical pulse width and significantly different to a pulse width of about 10 ms. The test REP Na-10 failed at an enthalpy level of 79 cal/g [9] which corresponds to  $\Delta H = 64$  cal/g because the initial enthalpy in the CABRI loop is about 15 cal/g. So the test REP Na-10 supports the failure limit  $\Delta H \geq 60$  cal/g given above for fuel rods with oxide spalling and local hydrides for LWR typical pulse width.

Siemens calculations with modern methods have shown enthalpy increases at RIA for high burnup below the above limits with ample margin[8]. Calculations by others support this [10]. Therefore RIA should not be a licensing obstacle for high burnup. This, however, is not the case. Firstly, we have currently no general internationally accepted RIA failure limit at high burnup although the German reactor safety commission (RSK) followed the Siemens conclusions for the failure limit at least for fuel rods without significant spalling. Secondly, the German society for reactor safety (GRS) opposes any extrapolation of the current test results to burnups above the level achieved in the tests up to now, Of course, thus supporting future CABRI tests.

For LOCA we can be very short. We have to wait for the outcome of the NRC test program for high burnup to see whether the established LOCA criteria will change for high burnup or not. Considering French experiments, no or at least no significant change is to be expected.

## 7. CONCLUSION

Significant progress has been achieved in the past by Siemens in meeting the demands of utilities for increased burnup. This has given the utilities considerable reductions of fuel cycle costs. The economic incentive for further burnup increase is still valid taking into account realistic disposal costs.

Clad materials with increased corrosion resistance have been developed which promise to be appropriate for the discussed burnup range. The high burnup behavior of the fuel has been extensively investigated. The decrease of thermal conductivity with burnup, the rim effect of the pellet and the increase of fission gas release with burnup can be described, with good accuracy, by the Siemens fuel rod code up to burnup levels of about 90 MWd/kgU. Advanced statistical methods for fuel rod design calculations have also been developed and successfully used in licensing. Materials with increased corrosion resistance are also helpful controlling the dimensional changes of the fuel assembly structure. In summary, most of the technical questions for the fuel operational behavior and reliability in the discussed burnup range have been solved or the solutions are visible. This is also acknowledged by regulators.

The main licensing challenges for high burnup fuel are currently seen for accident conditions, especially for RIA and LOCA. One major open question is, if and how far experimental results for accident conditions can be extrapolated above the burnups covered by the experiments. This open question might possibly slow down significantly the future rate of burnup increases.

## REFERENCES

- [1] VAN SWAM, L., GARZAROLLI, F., STEINBERG, E., International Topical Meeting on Light Water Reactor Fuel Performance, West Palm Beach, Florida, April 17 –21, 1994.
- [2] SONTHEIMER, F., LANDSKRON, H., BILLAUX, M. R., A fuel thermal conductivity correlation based on the latest experimental results, Seminar Proceedings “Thermal Performance of High Burn-up LWR Fuel”, Cadarache, France, 3 – 6 March 1998.
- [3] SONTHEIMER, F., LANDSKRON, H., BILLAUX, M. R., A uniform thermal conductivity correlation for UO<sub>2</sub> and gadolinia fuel –comparison with Halden data for thermal conductivity and other experimental results, EHPGM Lillehammer, March 1998
- [4] WIESENACK, W., et al., Fuel conductivity degradation assessment based on HBWR data, HWR-469, May 1996
- [5] SONTHEIMER, F., LANDSKRON, H., Puzzling features of EPMA radial fission gas release profiles: The key to realistic modeling of fission gas release up to ultra high burnup, EHPM Loen, 24 – 29 May 1999
- [6] HEINS, L., Fuel rod design by statistical methods for increased demands, to be presented at Topfuel '99, Avignon, 13 – 15 September 1999
- [7] VAN DOESBURG, W., MAEDER, C., WAND, H., Licensing of MOX fuel in Switzerland, Proceedings of the International Topical Meeting on Safety of Operating Reactors, San Francisco, October 11 – 14, 1998
- [8] GROSS, H., KREBS W.-D., Siemens View on Safety Issues on Advanced Fuel, ATW, May 98, pages 318 ff.
- [9] LANGENBUCH, S., et al., Ongoing and future Research on Fuel Rod Behavior under LOCA and RIA, Conditions, GRS/IPSN Seminar, Berlin, Nov. 1998
- [10] ROME, M., et al., Use of 3D Core Kinetic Methods for the Analysis of Reactivity Insertion, Accidents in PWRs, International Conference on the Physics of Nuclear Science and Technology, New York, October 5 – 8, 1998

# Development of advanced cladding material for burnup extension

**K. Kiuchi, I. Ioka**

Japan Atomic Energy Research Institute

**M. Takizawa**

Mitsubishi Research Institute, Inc.

**S. Wada**

The Japan Atomic Power Company

Japan

**Abstract.** The development of new cladding materials is one of the critical issues on burnup extension. The practical life of Zircaloy would be limited by the growth of oxide films and by the ductility loss due to hydride precipitation, oxygen absorption and radiation damage. In the case of high burnup using MOX fuels, the low neutron adsorption cross section of Zircaloy is not a dominant factor for selecting the cladding material, because MOX fuels can be enriched up to 20%Pu. Austenitic stainless steel, titanium alloy, niobium alloy, ferritic steel and nickel base superalloy are considered as candidate materials. The corrosion resistance, mechanical properties and the irradiation resistance of these materials were examined for evaluating the practical possibility as a cladding material. The austenitic stainless steel with high  $\gamma$  phase stability was selected as the primary candidate material. However, it is required to improve the resistance to irradiation associated stress corrosion cracking through the experience in LWR plants. In the JAERI, the austenitic stainless steel with intergranular corrosion resistance has been developed by the adjustment of the chemical composition, the modification of the metallographic structure by thermo-mechanical treatment and the purification by electron beam melting.

## 1. GENERAL SITUATION OF BURNUP EXTENSION

The burnup extension is considered to be an indispensable technology for establishing nuclear power plants as the most promising energy system in Japan with economical and ecological standing points<sup>(1-3)</sup>. The advanced light water reactor using MOX fuels for this purpose would be developed with standing two different viewpoints. One is the ultra-high burnup more than average 100 GWd/t (HB-ABWR, high burnup advanced boiling water reactor). The other is fast neutron spectrum water cooling reactors (HCPWR, high conversion pressurized water reactor, etc.) with the breeding ratio higher than 1<sup>(4-5)</sup>. It is possible to overcome the technological problem on the former by developing alternative fuel cladding materials instead of Zircaloys. On the other hand, it underlying in the latter is to select the appropriate reactor design with the high conversion ratio, by evaluating the safety allowance to nuclear reaction and commercial reality<sup>(3,4)</sup>. It would be required to authorize in time schedule for developing the advanced energy systems in Japan that includes the modified LMFBRs postponed by both the `Monju` accident and economical reason. However, the almost similar technological problems would be laying in the development of cladding materials applied for above water cooling reactors. The new project for the advanced fuel cladding in JAERI started from 1998, by accompanying the collaboration research between JAERI and The Japan Atomic Power Company. Major objectives on this project are mainly two issues, namely, to elucidate the technological limit to use zirconium alloys modified for high burnup and to select advanced cladding materials for HB-ABWR and HC-PWR.

In this report, the major technological problems on developing alternative fuel claddings required for the ultra-high burnup and fast neutron spectrum reactor designed with full MOX

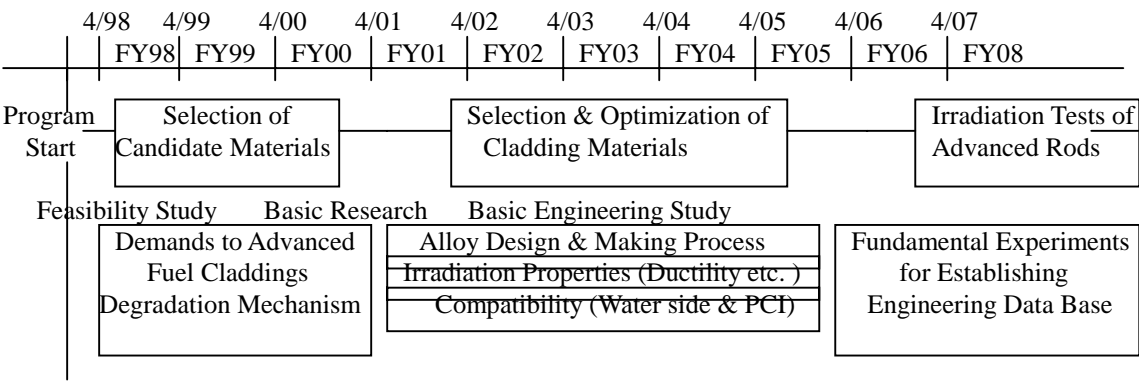
core are discussed, by considering commercial reality. Major points on feasibility study for selecting advanced cladding materials were pre-examined withstanding neutron economy, material properties required for water side corrosion, irradiation resistance, PC (M, C)I at MOX fuel side and the safety allowance to transient operation accidents. Environmental conditions are evaluated with thermal-fluid dynamics by simulating the pin-cell model for representative reactor designs of HB-ABWR and HCPWR<sup>(4,5)</sup>.

2. CLADDING MATERIALS SECTION WITH RESPECT TO NUCLEAR CHARACTERISTICS

2.1. Demands to advanced cladding materials

Zirconium base alloys have been mainly selected with respect to the low neutron absorption cross-section. This requirement is still important factor on selecting cladding materials for high burnup UO<sub>2</sub> fuel, because the enrichment factor is limited within 5%. However, it is not the preferential factor on selecting cladding materials for full MOX reactors, because Pu enrichment factor is possible up to 20% as used in LMFBRs. Therefore, the advanced cladding material required for ultra-high burnup fuels and/or fast neutron spectrum reactor could be selected from representative heat resistant materials with thermal neutron absorption cross-section lower than 10 barn. From the micro-structural change in the performance by heavy neutron irradiation, the resistances against corrosion, ductility loss and creep are considered to be more important than neutron economy.

Table 1. Time schedule on the development of advanced fuel cladding materials program



We are planning to develop advanced cladding materials and to clarify the performance of zirconium alloy as the JAERI project combined with the collaboration research with electric companies as described above and shown in time schedule of Table 1. Fundamental characteristics of candidate materials are summarized in Table 2. Major technological issues expected in the advanced fuel cladding are pictured in Fig.1. On the present study, major requirements for cladding materials were pre-examined in three kinds of candidate alloys with different metallurgical properties, namely, austenitic stainless steels, niobium alloys and Zircaloy-2 as reference materials.

Table 2. Difference in major technological problems and characteristics among candidate alloys

Materials	Water side corrosion	Irradiation properties	Resistance against PCI	Resistance to LOCA
Zirconium alloy	' **	'	liner (Zr)	ÿ
Stainless steel	• *	•	liner (Nb,Ti,Cu)	'
Ni base superalloy	• *	•	liner (Nb,Ti,Cu)	?
Titanium Alloy	' **	'	•	ÿ
Vanadium Alloy	ÿ	•	'	ÿ
Niobium Alloy	'	•	'	'

\*IASCC \*\*Embrittlement by hydrides Good • > ' > ÿ Poor

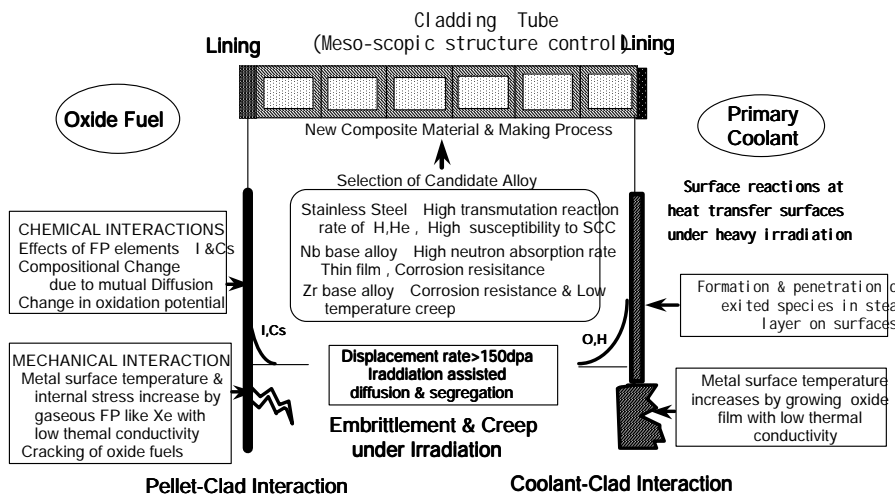


FIG. 1. A schematic view of major important factors on the performance of cladding materials.

## 2.2. Limitations on selecting advanced cladding materials

The nuclear characteristics required to the full MOX fuel cladding were pre-examined with computer simulation method based on reactor design data of HB-ABWR and HCPWR obtained by JAERI research<sup>(4,5)</sup>. Table 3 shows the major results obtained with this calculation using several codes<sup>(6-9)</sup>. Although the cladding thickness for obtaining the same reactivity depends on the neutron cross-section, the nuclear economy depends on the reactor design. Even if HB-ABWR, it is possible to control the excess reactivity at running-in period by nuclear poison contents of Gd<sub>2</sub>O<sub>3</sub> within the adjustable range by control rods. Although the burnup fraction decreases with operation time, the slope is independent on the neutron adsorption cross-section of each candidate material. As shown in Fig, 2, the infinite multiplication factor in HB-ABWR can be kept higher than 1 at 100GWd/t. The difference in maximum specific burnup among three candidates would be within nearly 10%. Accordingly, the total cost benefit originated from the high burnup using alternative cladding materials should be evaluated to minimize the waste management cost and effective use of nuclear resources. On the other hand, as shown in Fig, 3, the infinite multiplication factor on HCPWR is maintained more than 1 by breeding fissile Pu. The difference of neutron economy among above candidates is possible to neglect.

Table 3. Difference in irradiation properties among three candidates for fuel cladding of HB-ABWR and HCPWR evaluated by computer simulation

Materials	Irradiation Effect 100GWd/TU,Enrichment Max.20% PuO <sub>2</sub> ,: Void ratio: 0.40.70 %			Neutron absorption*
	Displacement Rate dpa HB-ABWR (HC-PWR)	Transmutation He, appm HB-ABWR (HC-PWR)	Transmutation H, appm HB-ABWR (HC-PWR)	Relative thickness of cladding, mm HB-ABWR
Zircaloy-2	52.7 (MOX) 81.6 (UO <sub>2</sub> )	1.3 (MOX) 1.5 (UO <sub>2</sub> )	11 (MOX) 13 (UO <sub>2</sub> )	0.7
SUS (15-25Cr- 14-35Ni-2.5Mo)	48 - 50 (107 - 112)	59 - 128 (105 - 228)	593 - 1162 (1045 - 2022)	0.2
Niobium Alloy (0-10%Mo-Nb)	52 - 54 (120 - 123)	1.2 - 1.4 (2.0 - 2.3)	9 - 12 (16 - 19)	<0.1

\* This is calculated without considering the adjustment of initial excess reactivity by adding nuclear poison. This evaluation was done using several calculation codes as follows.

Neutron spectra ( LANL,MCNP), Nuclear reaction (ANL,SPECTER), Thermal-fluid analysis (RELAP5/MOD2)

Irradiation effect; MOX (Uniform burn up rate) < UO<sub>2</sub> (Initial burn up rate; high)

Limitation to neutron absorption; MOX (Pu Enrichment Max.20%) < UO<sub>2</sub> (235U Enrichment Max.5%)

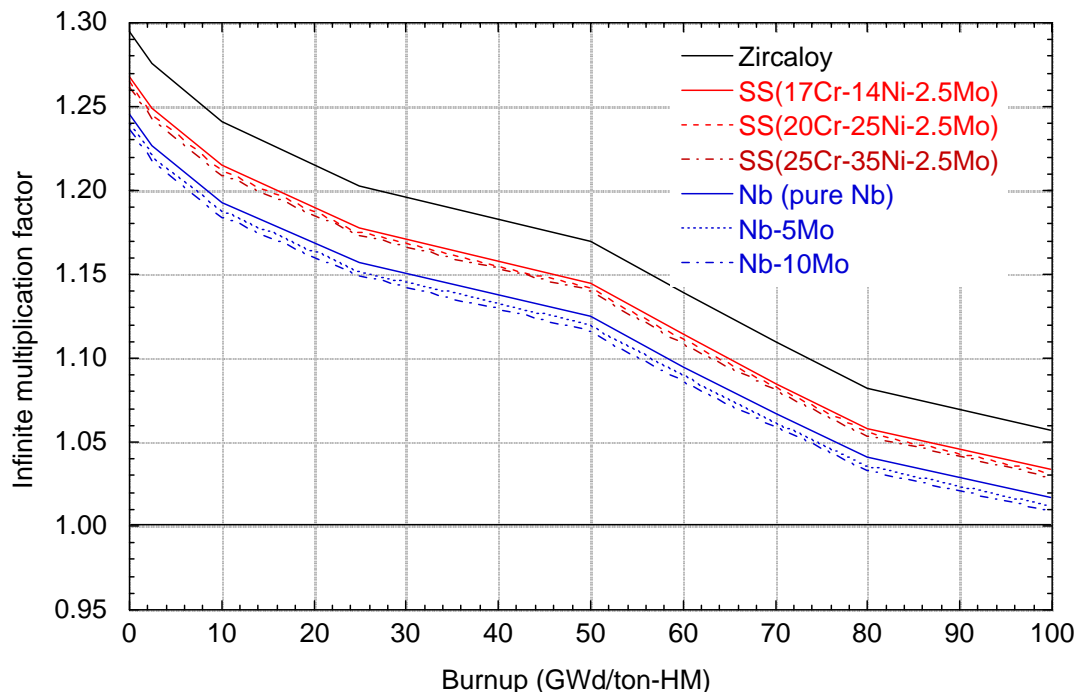


FIG. 2. A relationship of the infinite multiplication factor as a function of the specific burnup evaluated by simulating HB-ABWR with each cladding material.

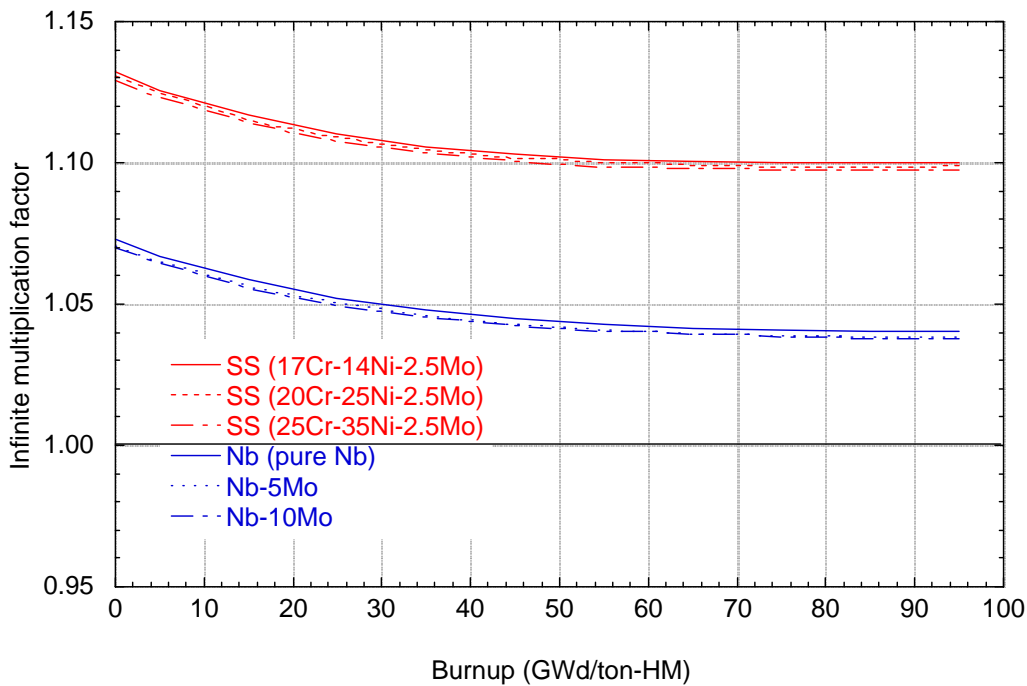


FIG. 3. A relationship between the infinite multiplication factor and the specific burnup (HCPWR).

The major irradiation properties calculated at 100GWd/t are shown in Table 3. Although markedly difference in displacement rate by irradiation damage is not shown, the production rate of hydrogen and helium by transmutation reactions of (n, p) and (n,  $\alpha$ ) respectively are markedly different among candidate alloys. Especially, these rates in stainless steels are enhanced not only the first stage of transmutation reactions, but also the second stage of it by the high reaction cross-section of  $^{58}\text{Ni}$  which is a intermediate transmutation product of  $^{57}\text{Ni}$ . Niobium alloy showed the lowest production rate. of p and  $\alpha$  among candidates.

### 3. TECHNOLOGICAL PROBLEMS ON ZIRCONIUM BASE ALLOYS

#### 3.1. Commercial plant experiences and empirical results of alloy modification

The most important technological problem on zirconium base alloys like Zircaloy-2 and -4 is considered to be the waterside corrosion. Aiming at high burnup, to adjust alloying elements like Sn, Fe, Cr, Ni and Nb and to control the metallographic structure have been made for improving the corrosion resistance by electric companies. Zircaloy-2 used in BWR fuels had been suffered from nodular corrosion. This is markedly improved by adjusting above metallic elements like low Sn and by distributing uniformly fine intermetallic compounds in fine grain matrix through the modified alloy making process. On the other hand, the improvement effect on uniform corrosion is not clear for both BWR and PWR claddings. Corrosion data obtained by experimental heats modified by above elements did not show the systematic results among each testing techniques; namely, laboratory loop, in-pile loop and fuel rod. At least, the obtained results could not be explained by general principles on corrosion control of Zircaloy. This reason is discussed in following session. As the other important information, the mutual correlation between oxide film growth<sup>(10)</sup> and hydrogen picked up was found. The PCI problem on high burnup would be controlled by the formation of rim layer and the FP gas release rate.

### 3.2. Important factors on waterside corrosion of zirconium alloys

The controlling factors on waterside corrosion of zirconium alloy have been discussed with several kinds of surface reactions. As discussed already, it is difficult to explain the oxide growth mechanism of  $ZrO_2$  with based on n-type semiconductor defect model. The oxidation rate of fuel cladding evaluated by ISI is nearly one order of magnitude higher than that expected from the same water temperature by laboratory loop tests. The mechanism of hydrogen pick-up accompanied with oxidation is also difficult to be explained from viewpoint of the thermodynamic equilibrium, because of dry corrosion covered with protective oxide film,. From our fundamental study on the surface reaction at heat transfer surface under heavy irradiation, we turn out following hypothesis and propose the concepts of Fig.4.

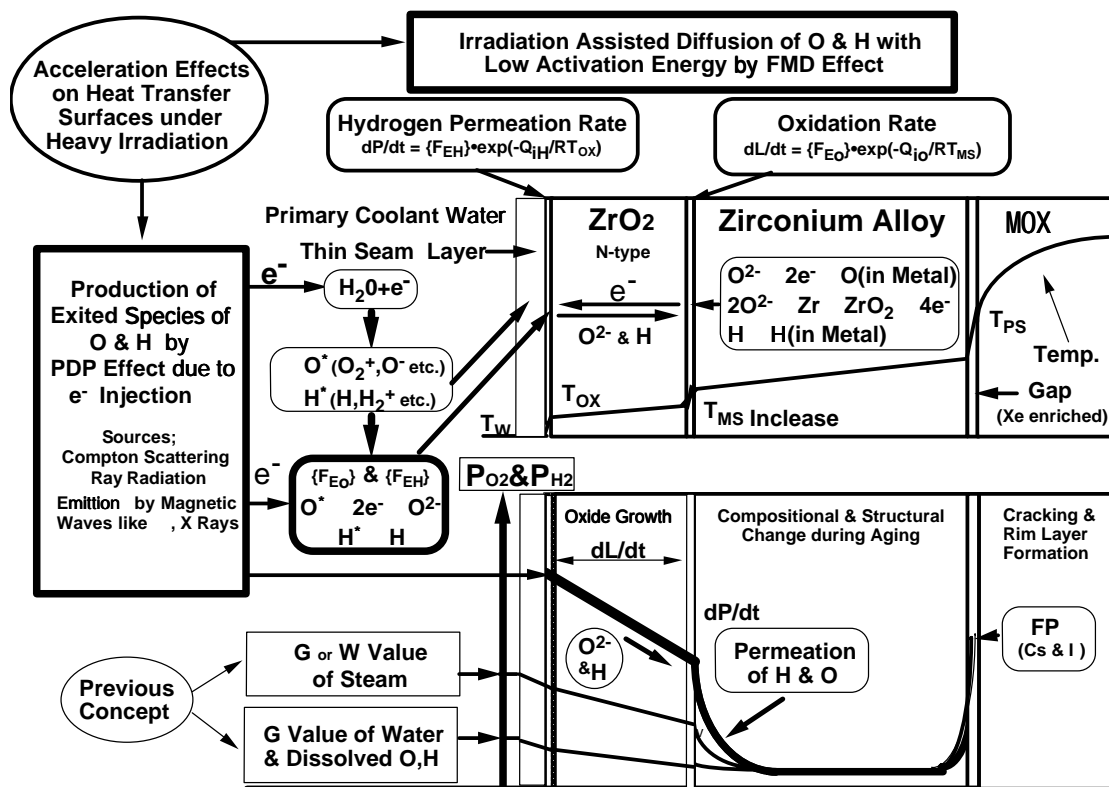


FIG. 4. A schematic model of aging degradation of zirconium alloys due to heavy irradiation effect.

- (1) PDP effect (low energy plasma induced permeation); oxidation and permeation of H and O;
- (2) FMD effect (freely migrating defects); penetration of H and O.

Comparing with G-value in water<sup>(11)</sup> and/or steam layer near material surfaces under heavy irradiation, above PDP model<sup>(12)</sup> takes account of direct reactions with exited species by irradiation assisted decomposition of water. Above reaction is expected in corrosion data obtained in PWR fuel claddings as shown in Fig. 5. The corrosion rate at cladding surfaces under heavy irradiation would be controlled by two steps of acceleration factors, namely above PDP/FMD effect and increasing of the surface temperature due to  $ZrO_2$  film growth with low thermal conductivity<sup>(10)</sup>. The PDP effect is already clarified with hydrogen

permeation data obtained by experiments using low temperature plasma testing devices exited by ECR and RF in vacuum. As shown in Fig. 6 and 7<sup>(12-14)</sup>, PDP effect consists of two kinds of acceleration effects enhanced by incident particles of both exited ions and electrons. The activation energy on such reactions shows the low value. On the other hand, FMD effect corresponds to directly displacement effect by particles with high kinetic energy like n, b and electrons formed by Compton scattering and neutron annihilation. Under irradiation aging, the sensitization of stainless steels was enhanced by accelerated diffusion of Cr as shown in Fig.8. It is possible to diffuse at temperature lower than 100°C. Although there is no quantitative experimental data, interstitial impurities like H and O with small atomic radius are also considered to be able to migrate in metals and oxide films with high diffusion rate under heavy irradiation. The grainboundary segregation of S and P in stainless steels is observed in early stage under heavy irradiation. Therefore, to inhibit the corrosion rate of Zircalloys covered with n-type semiconductor oxide film is considered to be difficult to be modified by adjusting small amount of alloying elements. The performance of Zircalloys expected at high burnup are shown in schematic view of Fig.9, from analysis based on corrosion data of cladding tubes obtained up to date. Moreover, shadow corrosion and the effect of intermetallic compounds can be explained with respect to the emitter effect of electrons.

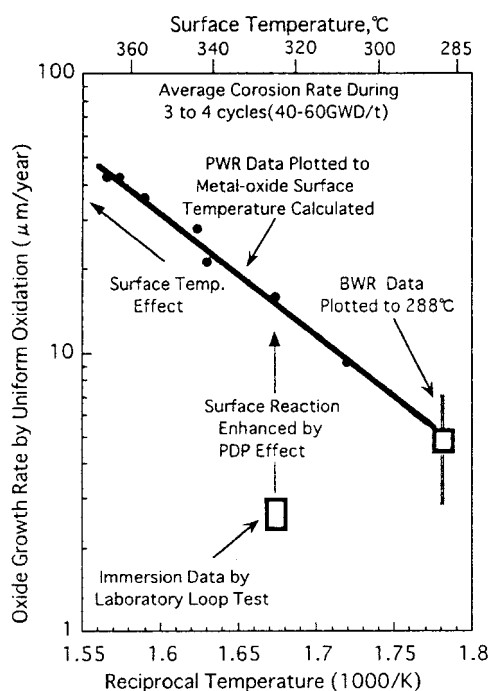


FIG. 5. Arrhenius dependency of the oxide growth rate of zircalloys as a function of the surface temperature evaluated by thermal-fluid dynamics.

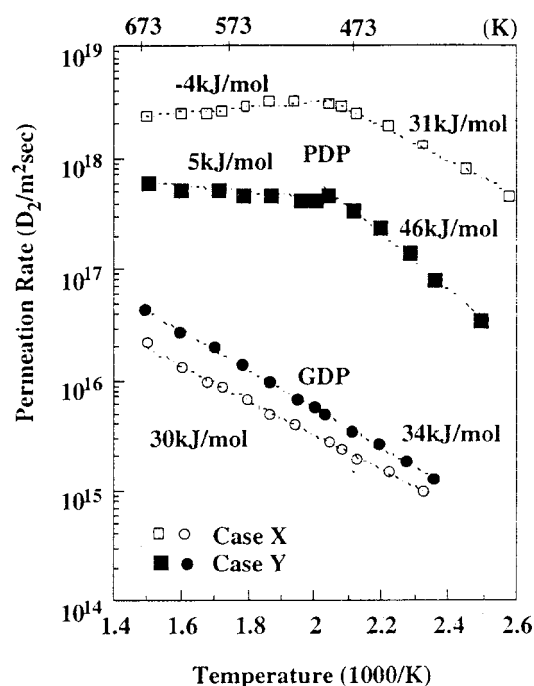


FIG. 6. An example of the PDP effects due to ionised deuterium evaluated with permeation tests of stainless steel by ECR plasma. GDP; Thermal equilibrium. Case X; contaminated with water.

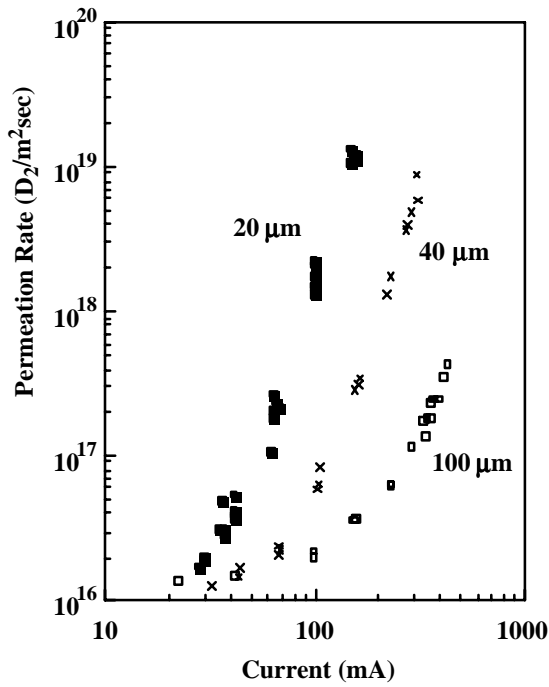


FIG. 7. An example of the PDP effect due to excited electrons evaluated by hydrogen permeation tests of Ni membrane by RF plasma under plus bias.

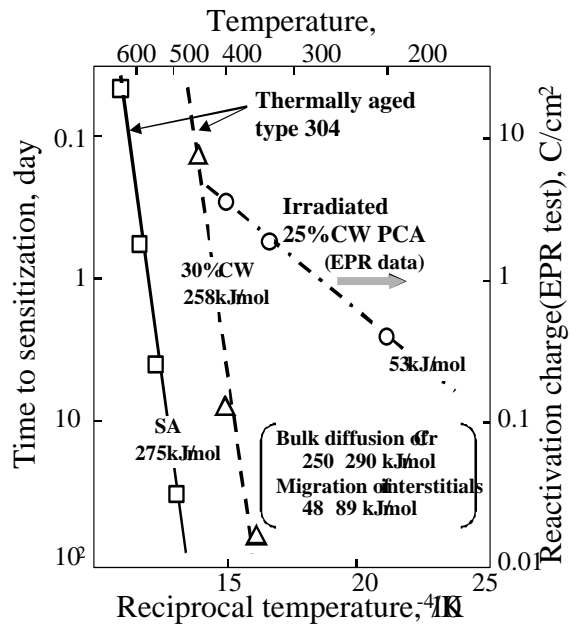


FIG. 8. The effect of irradiation on the low temperature sensitization of stainless steels.

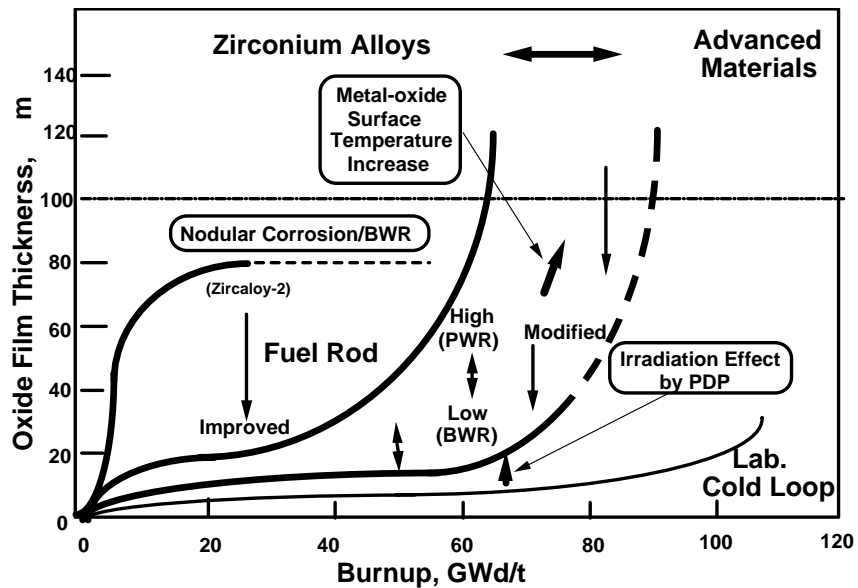


FIG. 9. A schematic view of the corrosion rate of Zircalloys in high temperature water as a function of the specific burnup.

#### 4. TECHNOLOGY PROBLEMS AND FEASIBILITY OF STAINLESS STEELS

Fuel cladding tubes made of austenitic stainless steels such as types 304 and 316 had been used in PWR and BWR plants. However, these tubes had been suffered from environmental cracking along with longitudinal direction after operated a few cycles (40~50GWd/t). It was considered to be due to IASCC (irradiation assisted stress corrosion cracking, mainly IGSCC) at water side and/or tritium degradation produced from oxide fuel side<sup>(15-18)</sup>. However, as shown in Table 3, a large amount of hydrogen is can be produced by the transmutation reaction and/or by the penetration of H due to the irradiation assisted surface reactions at waterside. Accordingly, characteristics of grainboundaries that act as sink sites of impurities and crack propagating path are considered to be important factor on performance of stainless steels for burnup extension.

##### 4.1. Irradiation effect of stainless steels

The phase stability of austenite in Fe-Cr -Ni phase diagram of stainless steels is limited in narrow region at temperatures lower than 500°C as shown in Fig. 10. At practical temperature, major commercial type 300 series steels are situated on meta-stable austenite.<sup>(15)</sup> Therefore, irradiation properties show the different behavior with dependent on this phase stability. At temperature region higher than 500°C, the void swelling rate decreases with increasing the concentration of electron vacancies which is one of the index for evaluating austenite phase stability as following (Fig.11).

$$N_V = 4.66 (\text{Cr} + \text{Mo}) + 3.66\text{Mn} + 2.66\text{Fe} + 1.7\text{Co} + 0.66\text{Ni} \text{ ( element,at\% )}$$

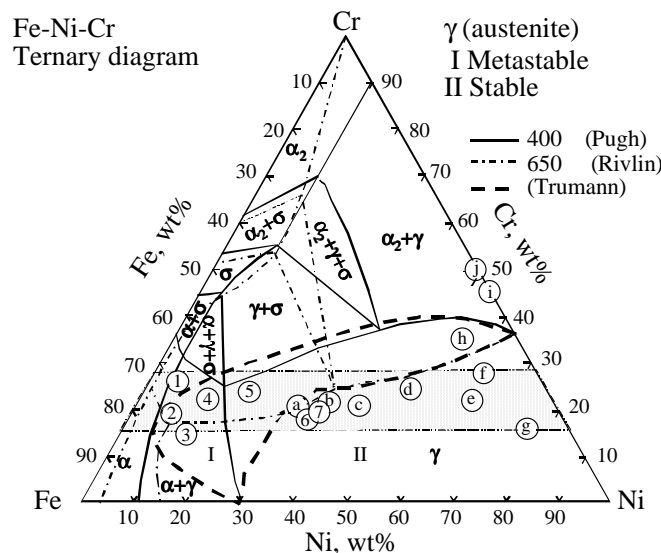


FIG. 10. Austenite phase stable region seen in Fe-Cr-Ni phase diagram at the practical temperature lower than 500C.

On the other hand, at temperature region lower than 500°C, the void swelling rate shows the saddle point to this value, because of meta-stable austenite. <sup>(29)</sup> (Fig.12). On this temperature region, the ductility loss is clearly observed in 300°C to 400°C region (Fig. 13). Moreover, from corrosion results for detecting the degree of sensitization, we found out a new type of the low temperature degradation region (MPC) as shown in an inserted view of Fig. 14. <sup>(15,25)</sup> The corrosion rate of annealed and strain-aged specimens at this temperature region depends on the index of austenite phase stability, namely, sum of  $Ni_{eq}$  and  $Cr_{eq}$ .

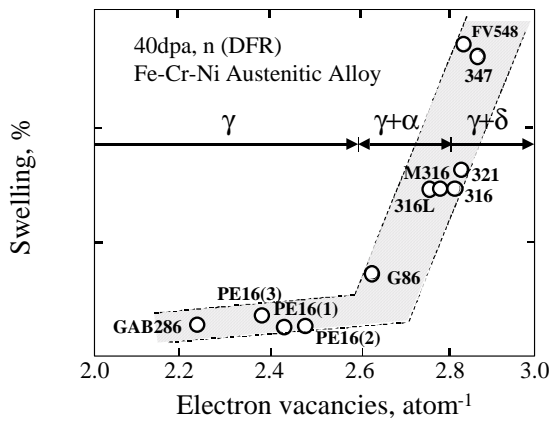


FIG. 11. The void swelling rate as a function of the electron vacancies at temperature region with stable austenite phase matrix.

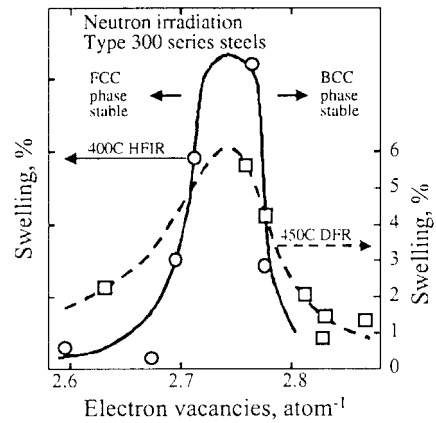


FIG. 12. The void swelling rate as a function of the electron vacancies at temperature region with meta-stable austenite phase matrix.

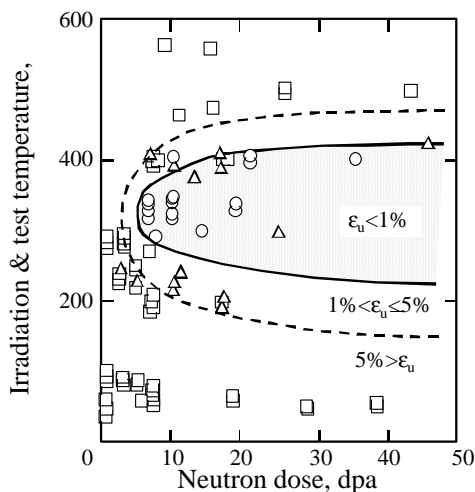


FIG. 13. Ductility loss due to dynamic interactions between solutes and irradiation defects at practical temperature evaluated by tensile tests after irradiation in reactors.

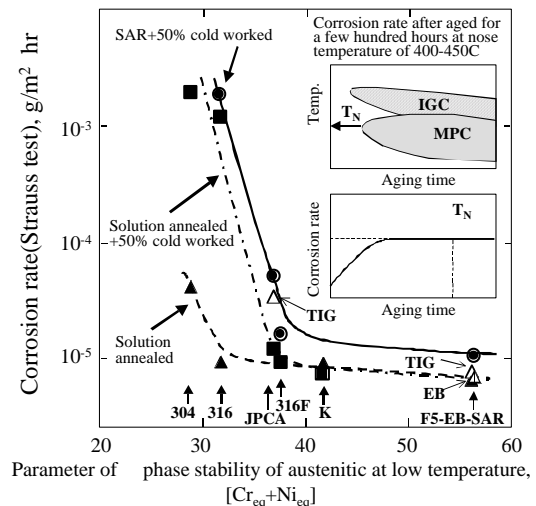


FIG. 14. A relationship between the corrosion resistance and the electron vacancies as denoted of austenite phase stability at low temperature.

## 4. 2. Computer-measure to inhibit low temperature degradation of stainless steels

As stated above, the development of stainless steels applied for cladding materials would be required to maintain the sufficient phase stability of austenite to inhibit IASCC and ductility loss. From pre-examination study pursued in JAERI, following modification techniques were clarified to be effective means for this purpose<sup>(20-24)</sup>. The super-saturated solutes affect to the sensitization and void swelling<sup>(25)</sup>.

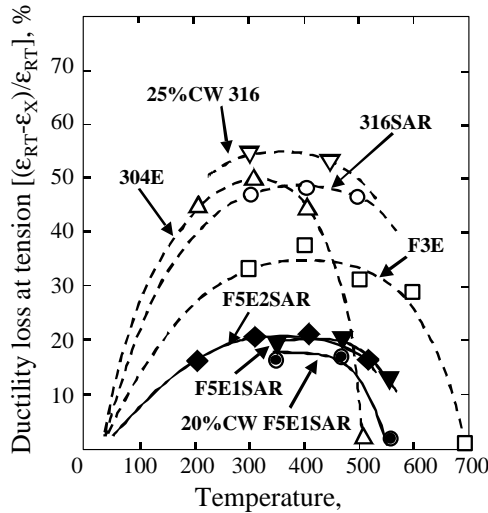


FIG. 15. The effect of austenite phase stability on the ductility loss at practical temperature.

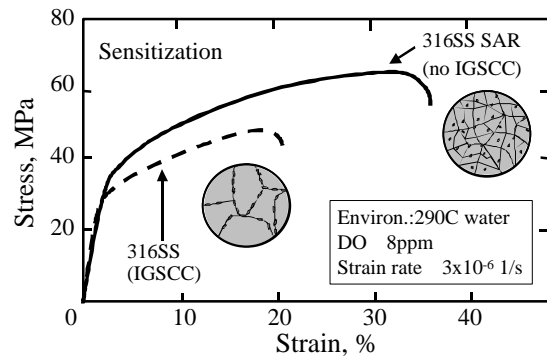


FIG. 16. A schematic view of the EB-SAR treatment and the inhibition effect to IGSCC in SSRT results in high temperature water.

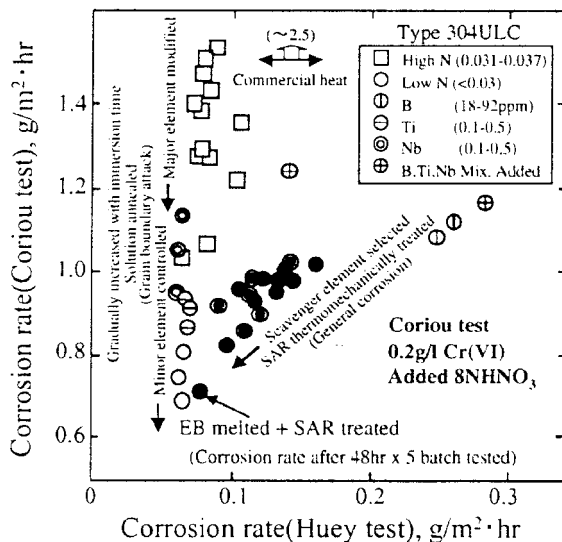


FIG. 17. The effect of scavenger elements and SAR treatment on the corrosion resistance of stainless steel.

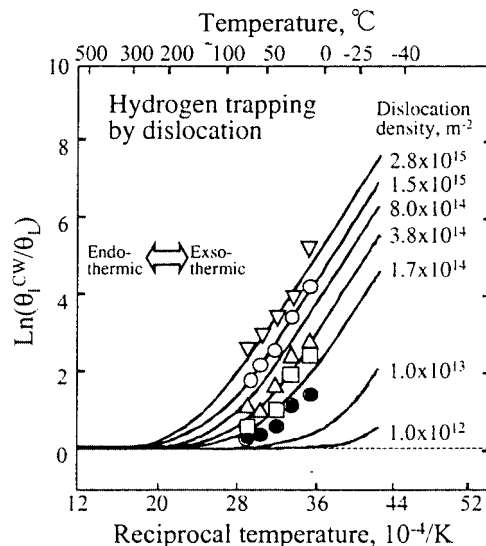


FIG. 18. Effect of the exo-thermic hydrogen defect interactions on hydrogen solubility in deformed iron at practical temperature.

\* Adjustment of major element; Cr and Ni for obtaining the sufficient phase stability of austenite and corrosion resistance at irradiation temperature. Cr and Ni contents would be optimized in 18–25wt%, 25–35wt% respectively and to select the appropriate scavenger elements for SAR (Strained, Aged and recrystallized ) process.

\* Purification of alloy matrix; To make the purified ingot through the combined melting techniques by VAR, EB-CHR and ESR process. Total interstitial impurities is possible to limit less than 100appm.

\* Modification of metallographic structure; To form the fine grain structure with uniformly dispersed precipitates through thermo-mechanical treatment so-called the SAR process which consists of strain-aging and recrystallization at intermediate temperature.

As shown in Fig. 14 and 15 comparing with 300series low carbon steels, F3 (25%Ni) and F5 (35%Ni) shows a good corrosion resistance and low ductility.loss at the degradation nose temperature <sup>(25)</sup>. Even if commercial grade type 304 stainless steels, IGSCC and IGC resistance is markedly improved as seen in SSRT data in high temperature water (Fig.16). The appropriate scavenger element was already selected by examining the corrosion resistance of several experimental heats added Ti,Nb and B (Fig.17). The most excellent improving effect was seen in Ti added heat and low nitrogen. At least, the susceptibility to IGC and IGSCC of EB-SAR treated austenitic stainless steels is completely inhibited <sup>(27,28)</sup>. However, the most important problem on the steel under heavy irradiation is considered to be the high production rates of H and He by (n,p) and (n, a) transmutation reactions. There is no significant irradiation effect of He on mechanical properties <sup>(30)</sup>. On the other hand, H is considered to be affected in the ductility and the corrosion resistance due to hydrogen-dislocation interactions at low temperature <sup>(31)</sup>. As one of these examples, Fig.18 shows increase in hydrogen solubility with increasing this interaction. Hydrogen embrittlement is considered to play an important role on reliability at temperature lower than operation temperature. We are planning to evaluate these effects by irradiation tests using ion accelerators and exposure tests in high temperature water under irradiation of g ray and high energy electron beams.

The resistance against PCI of LMFBR fuel cladding made of stainless steels has been improved by metal lining techniques like Ti. We had already developed Cu lining technique by means of diffusion bonding. The appropriate candidate base metals for lining would be selected from Ti, Nb and Cu, by considering the performance and compatibility with stainless steels and MOX oxides. On the other hand, one of engineering problems of stable austenite stainless steels is to decrease cracking resistance to welding. However, there is no problems in TIG welding of EB-SAR treated stainless steels, because harmful elements are removed by purification process <sup>(32)</sup>. The mechanical strength of this ULC grade steel is maintained by the Hall-Petch strengthening effect., because it has very fine grain structure higher than ASTM No.10 <sup>(21)</sup>.

## 5. CONCLUSIONS

The technological problems and important issues on the development of advanced cladding materials aiming at burnup extension for H\_B-\_ABWR and HCPWR with full MOX fuels were evaluated among three candidate alloys of zirconium, niobium and stainless steel as follows.

\* The low neutron adsorption cross section is not a dominant factor for selecting cladding materials, because it is possible to enrich fissile Pu up to 20% as well as LMFBRs. The difference in the maximum specific burnup among above candidates is within nearly 10%. Comparing with UO<sub>2</sub>, the excess reactivity of MOX fuels is small. It is possible to adjust the initial excess reactivity that can be controlled by adding the nuclear poison of Gd<sub>2</sub>O<sub>3</sub>. The over all economy depends on the endurance limit of cladding materials.

\* The performance of zirconium alloys is limited by thickening of ZrO<sub>2</sub> at steady state and by ductility loss due to the penetration of H and O. The aging degradation is controlled by two kinds of surface reactions at heat transfer surfaces under heavy irradiation. The permeation of H and O into metals are considered to be promoted by PDP and FMD effects. The oxide film growth rate shows Arrhenius dependency to the metal surface temperature by thinning ZrO<sub>2</sub> film with the low heat conductivity. The performance of fuels and resistance against PCI decrease with increasing pellet temperature due to form the low heat conductivity barriers of both FP gas gap like Xe and ZrO<sub>2</sub> film.

\* The development of austenitic stainless steel with the sufficient resistance against IASCC is considered to be the most promising alternative technology for advanced fuel claddings. To adjust alloying elements for obtaining the sufficient  $\gamma$  phase stability and to minimize the grainboundary segregation can be applied for such improvement. The EB-SAR technique developed by JAERI is considered to be an effective means to inhibit IGSCC. To improve the resistance against PCI is possible by means of diffusion bonding liner of Cu and refractory metals like Nb. The effect of high amount of H produced by transmutation is considered to be the most important issue on irradiation aging degradation.

## REFERENCES

- [1] P. E. MACDONARD; High Efficiency Nuclear Fuel Program, DOE/NE-50, INEEL, ANL (1998).
- [2] Y. NAITOU, T. FURUTA, H. ICHIKAWA AND H. TAKANO; JAERI-M 91-026 (1991).
- [3] F. NAGASE et.al.; JAERI-M 93-104 (1993).
- [4] T. SHIRAKAWA, T. OOKUBO AND M. OCHIAI; JAERI-Research 98-047 (1998).
- [5] M. OCHIAI; JAERI-Conf 98-013 (1998) 56.
- [6] J.F. GREENWOOD AND R.K. SMITHER; SPECTOR Code, ANL/FPP/TM-197 (1985).
- [7] J.F. BRIESMEISTER ed.; MCMP-A Code Version 4A, LA-12625-M (1993).
- [8] R. KISNEY; ENDF, BNL-NCS-50496 (ENDF102) 2<sup>nd</sup> Ed. ENDF/B-V (1979).
- [9] ASTM; ASTM Designation E693-86 (1986).
- [10] G.R. KLIP et.al.; Proc. ANS-ENS Int. Topical Meeting on LWR fuel Performance, 2 (1991) 730.
- [11] K. ISHIGURE et.al; Radiat. Phys. Chem. 46 (1995) 557.
- [12] M. TAKIZAWA, K. KIUCHI, M. OKAMOTO AND Y. FUJI; J. of Nuclear Materials, 248 (1997) 15.
- [13] M. TAKIZAWA, K. KIUCHI, H.I SHIZUKA et.al; Fusion Engineering and Design, 39-40 (1998) 923.

- [15] K.KIUCHI, T.ISHIYAMA AND A.HISHINUMA; Proc. of Water Chemistry'91 (1991) 327.
- [16] A. HISHINUMA AND K. KIUCHI; ASTM STP 1046 (1990).
- [17] T. INAZUMI, G.E.C. BELL, E.A. KENIK AND K. KIUCHI; ORNL/TM 12094 (1992).
- [18] T. INAZUMI, G.E.C. BELL, E.A. KENIK AND K. KIUCHI; Corrosion, 46 (199) 786.
- [19] T. INAZUMI, G.E.C.BELL AND K.KIUCHI; 179–181 (1991) 619.
- [20] K. KIUCHI, M.KIKUCHI AND T. KONDO; J. of Nuclear Materials, 179–181 (1991) 481.
- [21] K. KIUCHI AND T. KONDO; J. TETSU-TO-HAGANE 70 (1984) 112.
- [22] K. KIUCHI AND T.KONDO; J. BOSHOKU GIJUTSU 32 (1983) 503.
- [23] K. KIUCHI AND T.KONDO; J. BOSHOKU GIJUTSU 32 (1983) 572.
- [24] T. ISHIYAMA, K. KIUCHI AND A. HISHINUMA; Fusion Technology 1990 (1991) 443.
- [25] K. KIUCHI, M. KIKUCHI, T. ISHIYAMA et.al.; J. of Nuclear Materials, 212–215 (1994) 551.
- [26] K. KIUCHI, H. IDE, K. HIRATSUKA AND A. TOOYAMA; Pro.of Int. Sym. on RECOD'98 (1998) 867.
- [27] K. KIUCHI, T. ISHIYAMA AND A. HISHINUMA; J. of Nuclear Materials, 258–293 (1988) 797.
- [28] K. KIUCHI, IDE AND T. ISHIYAMA; Proc. of Water Chemistry'98 (1998).
- [29] J.P. ROBERTSON, I. IOKA, A.F. ROWCLIFF, M.L.GROSSBECK AND S. JITSUKAWA, STP1325 (1999) 671.
- [30] K. SHIBA, I. IOKA, S. JITSUKAWA, S. HAMADA, A. HISHINUMA AND J.P. ROBERTSON: STP1325 (1999) 659.
- [31] K. KIUCHI AND R.B. MCLELLAN; Acta metall. 31 (1983) 961.
- [32] K. KIUCHI, M. KIKUCHI, H. BOLT, M. ARAKI AND M. SEKI.; J. of Nuclear Materials, 179–181 (1991) 282.

# High burnup fuel R&D activities in Japan

**M. Ichikawa**

The Japan Atomic Power Company,  
Japan

**Abstract.** The general status of R&D activities on high burnup fuel in Japan is described. The verification tests of BWR/PWR fuels have been conducted by NUPEC (Nuclear Power Engineering Corporation) have been continued to lead advanced and high burnup fuels in Japan. The general programs, together with some typical results of cladding waterside corrosion, fission gas release, PCI, are described. The properties change with the advance of burnup, like thermal conductivity degradation, rim structure formation, bonding of pellet cladding significantly affect fuel rod behaviour. Some recent studies in these areas in Japan are presented. Accumulated knowledge and data of high burnup fuel behaviour have been reflected to the fuel modeling activities in Japan. Among them FEMAXI code of JAERI (Japan Atomic Energy Research Institute) has been updated and the general status of the recent version with some verifications is presented. Fuel rod behaviour during transient and accident conditions is important for extension of burnup. Recent RIA simulation tests at NSRR (Nuclear Safety Research Reactor) of JAERI on high burnup BWR/PWR fuel are also described.

## 1. INTRODUCTION

The nuclear power generation in Japan accounted for 44,917 MW provided by 51 nuclear plants in March 1, 1999. The operating water reactors include 28 BWRs (2 ABWRs), 23 PWRs, 1 ATR (Fugen). Nuclear power generation provides about 36.4 % of total electric power generation in 1998. The average availability of plant facilities in fiscal 1998 is 84.2 % which is the highest record ever in Japan [1].

The fuels in BWR and PWR show excellent performance with very low leak rate (order of 10<sup>-6</sup> rod/year and less, respectively) [2].

The use of MOX fuel in some of the BWR/PWR plants will be started in near future and the preliminary irradiation tests have been performed [3].

The burnup of BWR/PWR fuel have been increased step by step from the maximum assembly burnup of 40 GWd/t to 50 GWd/t (48 for PWR) and to 55 GWd/t (reload batches for BWR and LUAs in PWR). The aim of the high burnup of the LWR fuel in Japan is to reduce the number of spent fuel assemblies, to reduce fuel cycle cost, to prepare for the extension of reactor operation period, and to contribute to effective use of uranium resources. The preparation to extend the burnup to 70 GWd/t (discharge average assembly burnup) has been conducted including irradiation studies.

## 2. HIGH BURNUP FUEL DEVELOPMENT

### 2.1. NUPEC Programs

The excellent fuel performance has been confirmed through continuous verification programs of NUPEC. NUPEC has been conducting large scale verification programs under the sponsorship of MITI (Ministry of International Trade and Industries) [4] [5] [6].

NUPEC started the programs since 1976. Generally, following programs have been conducted:

- Proving tests of 1970's BWR/PWR fuel;
- Verification tests of improved fuel for BWR/PWR (BWR high performance fuel (Step 1 fuel): the major improvement is the use of zirconium liner cladding. PWR improved fuel: the major test parameters are solid/ annular pellet, claddings with/without zirconium liner);
- Verification tests of high burnup fuel for BWR/PWR.

The first two programs have been completed and published.

The high burnup programs for BWR fuel consist of the testing of high burnup 8x8 assemblies (Step-11 fuel) and 9x9 (Step-111) LUAs (Lead Use assembly). In the Step 11 fuel, large diameter water rod and round cell-type spacers are used. In the Step 3 fuels, two types of the structures are used: one has two round water rods, and the other has a square water rod in the center. Power ramping tests are included in both programs.

The irradiation of high burnup 8x8 assemblies were conducted at Fukushima 2-2 up to 50 GWd/t and PIEs and analyses are almost finished. LUAs of 9x9 fuel (Step-111) finished 2 cycles of irradiation and will be continued up to 5 cycles.

The high burnup programs for PWR fuel consist of irradiation of the fuel with low tin Zircaloy-4 cladding and reduced pre-pressurization (Step 1 fuel) up to 48 GWd/t and new fuel (Step-11 fuel) aiming at 55 GWd/t. The Step 1 fuel has already commercially used since 1988. The verification test of Step 1 fuel was conducted at Takahama-3 and the PIEs have also been finished.

The features of the PWR Step-11 fuel are the use of higher enrichment (4.5 %, tentative), large grain size pellets to reduce fission gas release, and the use of improved cladding for better corrosion properties and PCI resistance. The irradiation of Step 11 fuel is conducted at Vandellós-2 (Spanish PWR). Fuel segments irradiated at Vandellós-2 were subjected to power ramping at Studsvik R2 reactor to demonstrate the improvement for PCI resistance.

## **2.2. Major Results**

### *2.2.1. Cladding Waterside Corrosion*

In BWR nodular corrosion have been remarkably suppressed after introduction of corrosion resistant Zircaloy-2 with appropriate heat treatments. The high burnup 8x8 fuel after irradiation of 50GWd/t showed uniform corrosion with about 10  $\mu\text{m}$  thick oxide layer. The oxide thickness change with burnup is shown in Fig.1 [4][7]. Microstructure observation of the cladding showed that irradiation induced dissolution of intermetallic precipitates was faster in the improved Zircaloy-2 than that in the conventional cladding because of the smaller precipitate sizes. To improve resistance for corrosion and water chemistry change, new cladding alloys have been developed [8].

In PWR, low tin Zircaloy-4 cladding is currently used and advanced claddings (MDA, NDA) have been developed for further improvements. According to the oxide thickness measurements from high burnup irradiation program at Takahama-3 with low tin cladding

(Step-1 fuel), waterside corrosion has been kept reasonably low [9]. The corrosion of MDA cladding in the irradiation program at Vandellos-2 showed lower than that of low tin cladding [10].

### *2.2.2. Fission Gas Release (FGR)*

In BWR high burnup fuel (Step-11 fuel), helium pre-pressurization is 0.5 MPa (Step-1 fuel: 0.3 MPa), and pellet cladding gap is 0.20 mm (0.24 mm) to keep the pellet temperature low by reducing FGR. The FGR of the high burnup fuel is shown in Fig.2 as a function of burnup together with the published BWR data [11]. When compared with the previous types of fuel rods the FGR of high burnup fuel was less, indicating the effectiveness of the design improvements.

For reduction of FGR at high burnup, the effect of large grain size has been investigated by BWR [12] and PWR groups [13]. Some dopants to increase grain size used by a BWR group result in softening of pellets and are considered to be effective to mitigating PCI, as well as to reducing FGR.

In PWR fuel, FGR data were obtained in high burnup program of Takahama 3 (Step-1 fuel) and Vandellos-2 irradiation (Step-11 fuel) combined with power ramping. The Vandellos-2 irradiation included large grain pellets. FGR during ordinary irradiation was quite low [10].

### *2.2.3. PCI*

In BWR fuel, verification of zirconium liner on PCI resistance has been continued for high burnup program of NUPEC. The results of power ramping tests demonstrated excellent PCI resistance up to about 50 GWd/t [14].

In PWR fuel radial textured cladding has been developed to improve PCI resistance. In this type of cladding, the basal pole (C-axis) of the hexagonal lattice of Zirconium is highly concentrated in the radial direction of the tube [13], as PCI fracture surface tends to occur on basal plane. The power ramping results are shown in Fig.3 confirming the improvements of PCI resistance by the radial textured cladding [10].

## **2.3. High Burnup Pellet Properties**

In the area of pellet properties change at high burnup, significant progress has been noticed in the studies of thermal conductivity degradation, rim effect, and high burnup bonding of pellet/cladding in Japan.

Recently, several measurements of thermal diffusivity of highly irradiated pellets by laser flash method have been conducted in Japan. Nakamura et al., [15] measured pellets irradiated to 63 GWd/t, Hirai et al., [16] and Amaya et al., [17] did with the pellet irradiated to 45 GWd/t, Ohira et al [18] did with 61 GWd/t pellet. More data are needed for UO<sub>2</sub> and MOX fuels at higher burnup. Data of specific heat of highly irradiated fuel are also needed to calculate accurate thermal conductivity from thermal diffusivity.

Formation of rim structure in the pellet at high burnup brings about several potential effects on fuel behaviour: FGR, thermal barrier effect, swelling and so on. Rim structure will also

affect RIA behaviour. International high burnup rim project organized by CRIEPI (Central Research Institute of Electric Power Industries) is progressing [19].

To study the origin of FGR in the pellet, whether from fissions of uranium or plutonium, isotope ratios of Kr and Xe were measured using the fuel irradiated up to about 60 GWd/t. Comparison of the measured ratio and calculated ones is shown in Fig.4 [20]. The ratios indicated that released fission gas was from uranium fissions. This implies that FGR up to about 60 GWd/t is not from rim. A realistic calculation was published concerning the effect of rim on pellet temperature [20]. Taking into account of pore distribution in the rim region and thermal conductivity degradation due to high local burnup together with large porosity, pellet center temperature was calculated. The results show that temperature increase was only about 20' C in a typical case of 300 W/cm at rod burnup of 60 GWd/t.

The effect of large grain size on rim structure formation was studied [21]. The specimen irradiated up to 86 GWd/t at Halden reactor was examined for rim structure formation by EPMA. The standard grain specimen showed low Xe concentration at low temperature region due to the formation of rim structure in comparison with two large grain specimens (undoped large grain, Al-Si-0 added large grain).

At high burnup, pellet and cladding are firmly compressed after closure of gap due to swelling of pellet and creep-down of cladding. A bonding layer which is composed of mixed oxides of uranium and zirconium. The mixed oxide layer was formed by the irradiation induced diffusion under firm contact at high burnup [22]. The bonding layer is believed to affect adversely during PCI.

### 3. FUEL MODELLING FOR HIGH BURNUP

Fuel modelling for design, analyses of fuel behaviour, licensing, reactor operations, have been active in Japan [23]. Among them, FEMAXI code of JAERI has been developed since late 1970s and revisions of the code have been conducted aiming at gaining better capabilities for analyses of fuel rod behaviour [24, 25].

The FEMAXI code consists of thermal analysis part and mechanical one utilizing finite element method. The finite element method enables to analyze local stress/strain accurately for better PCI assessment with the help of exact treatment of contact problem of pellet and cladding, treatment of cracked pellet, use of advanced method for creep calculation, and so on. The latest version FEMAXI-V aims at analyses of high burnup fuel [26]. For this purpose, the code includes :

- Subroutine to calculate radial power distribution change with burnup;
- Fission gas release model (diffusion including irradiation enhanced/induced diffusion, resolution, boundary saturation, etc) with submodel for pellet/cladding restraint force;
- Degradation of thermal conductivity, etc.,

FEMAXI-V has been extensively verified for data from instrumented Halden high burnup fuel rods and other high burnup data. One of the characteristics of FEMAXI-V is the use of cladding and pellet restraint force model for fission gas release as mentioned above. Fig. 5

shows a typical example of the comparison of the rod inner pressure calculation with the measurement [27]. With the use of restraint force model, fission gas release is enhanced during power decrease and calculation agrees quite well with the measurement. The source program of FEMAXI-V code is available from JAERI.

#### 4. SAFETY RESEARCH FOR HIGH BURNUP FUEL

In Japan, safety research program has been authorized as five year plan by the Nuclear Safety Commission. A revised new plan started in 1996. The fuel safety research consists of fuel reliability during normal operating conditions, fuel behaviour during off-normal and accident conditions, and some material studies during postulated severe accident conditions.

The major safety interest of the fuel at high burnup has been directed to the fuel failure in simulated RIA experiments at NSRR and related research at JAERI. High burnup PWR and BWR fuel specimens have been tested at NSRR. The burnup of PWR fuel ranged up to 50 GWd/t and that of BWR fuel ranged up to 56 GWd/t [28, 29].

At high burnup during RIA transient, hydride assisted PCMI (Pellet Clad Mechanical Interaction) was identified as the mechanism of fuel failure. At RIA transient prompt increase of pellet temperature occurs. Pellet thermal expansion and swelling assisted by rapid expansion of accumulated fission gas results in PCMI. Decreased cladding integrity due to radially localized hydride layer causes "hydride assisted PCMI failure".

Therefore, the cracks start from oxide layer of cladding and continue to brittle hydride layer at the periphery to inner surface. This hydride assisted PCMI failure occurs in the early stage of the transient when the cladding temperature remains low. To clarify and evaluate the early phase PCMI process, out of pile experiments which consist of highly rapid burst test are being performed. Unirradiated cladding, with artificially concentrated hydride precipitated in the periphery, is tested under pulse like pressure. As a result, a long axial crack similar to those observed in high burnup PWR rods in NSRR was observed. Metallographic observation revealed similar fracture characteristics as the high burnup rods.

In NSRR experiments, residual strain due to swelling of the pellet of PWR rods ranged to 27 % and fission gas release up to 23 %. The residual strain of BWR rods was less than 2 %. The detailed analyses of FGR and deformation are underway in consideration of rim effect.

The summary of NSRR experiments together with other existing in-pile RIA experiments is shown in Fig. 6. In the figure, failure threshold for safety evaluation is also shown.

#### 5. CONCLUSIONS

Currently, LWR fuel performance in Japan is quite satisfactory. In the future, the further burnup extensions UOX and MOX fuel utilization are planned and some irradiation studies have been performed. On the other hand, more experience and data are needed for fuel performance and for fuel safety studies.

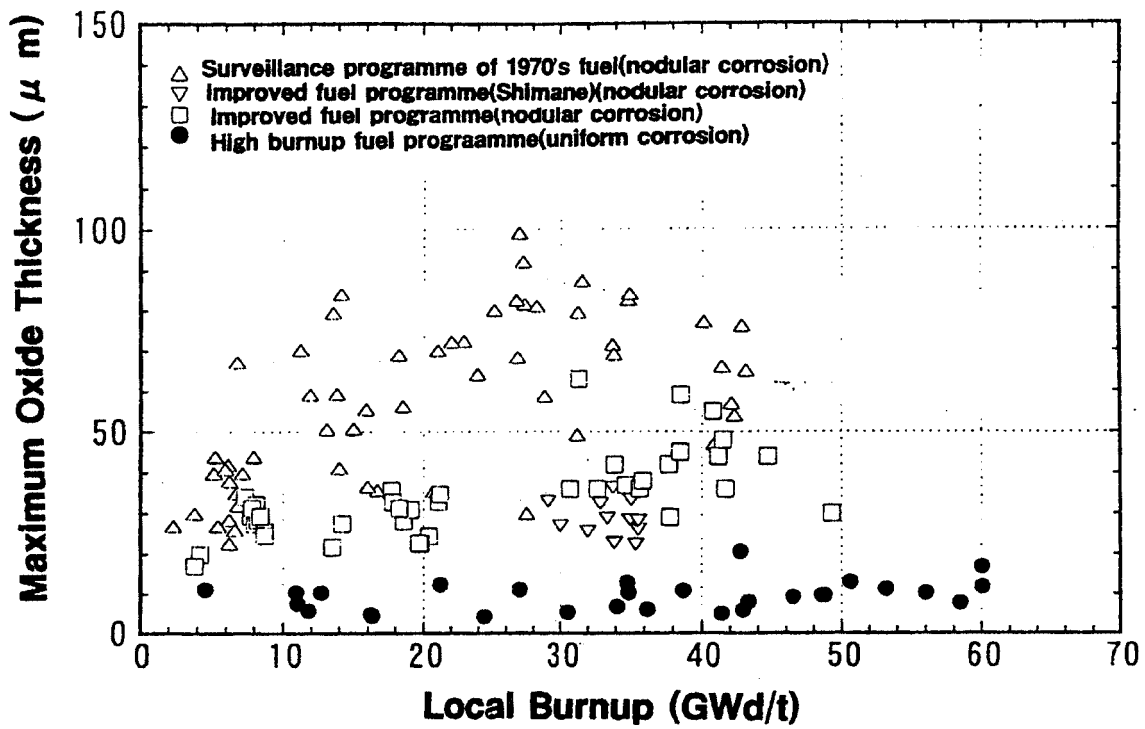


FIG. 1. Burnup dependence of Oxide thickness [4].

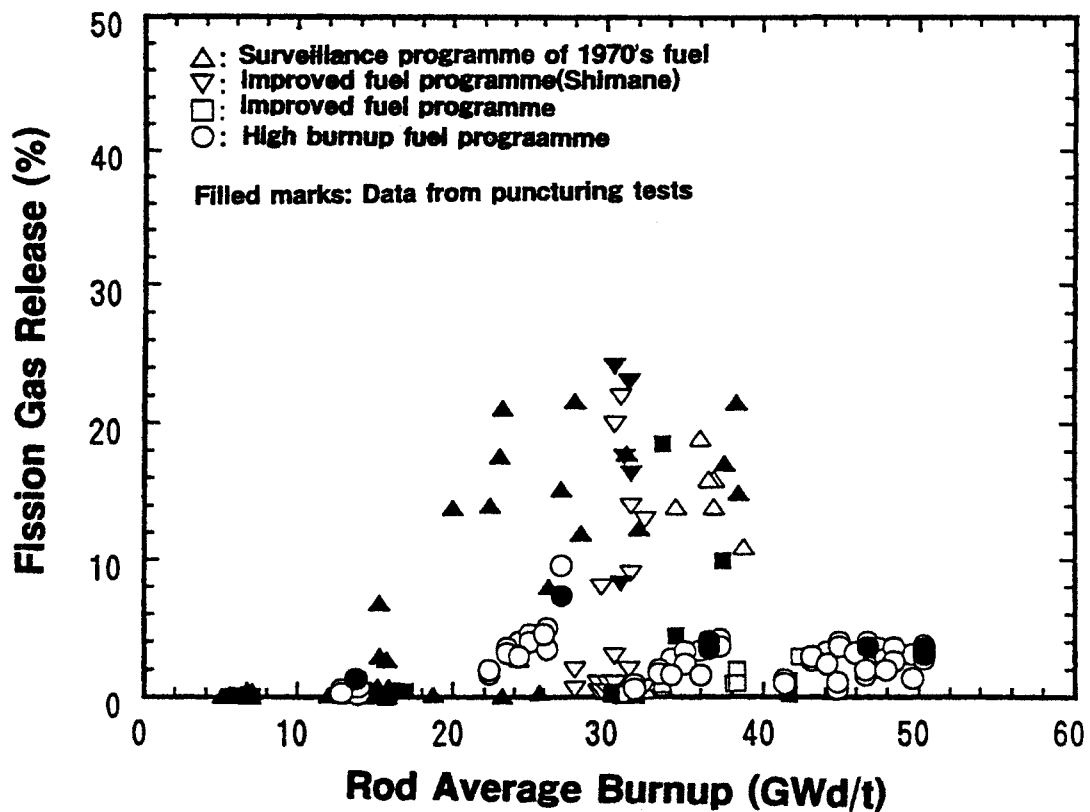


FIG. 2. Burnup dependence of fission gas release [4].

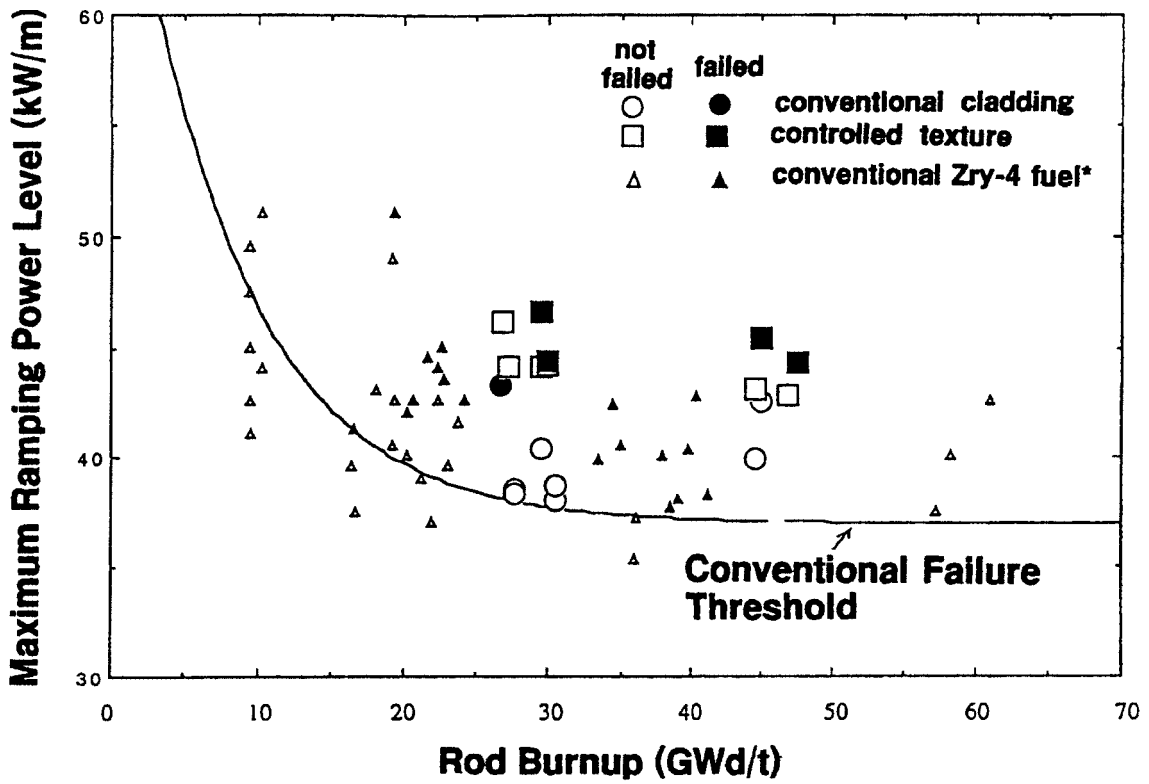


FIG. 3. PCI failure threshold of controlled texture cladding [4].

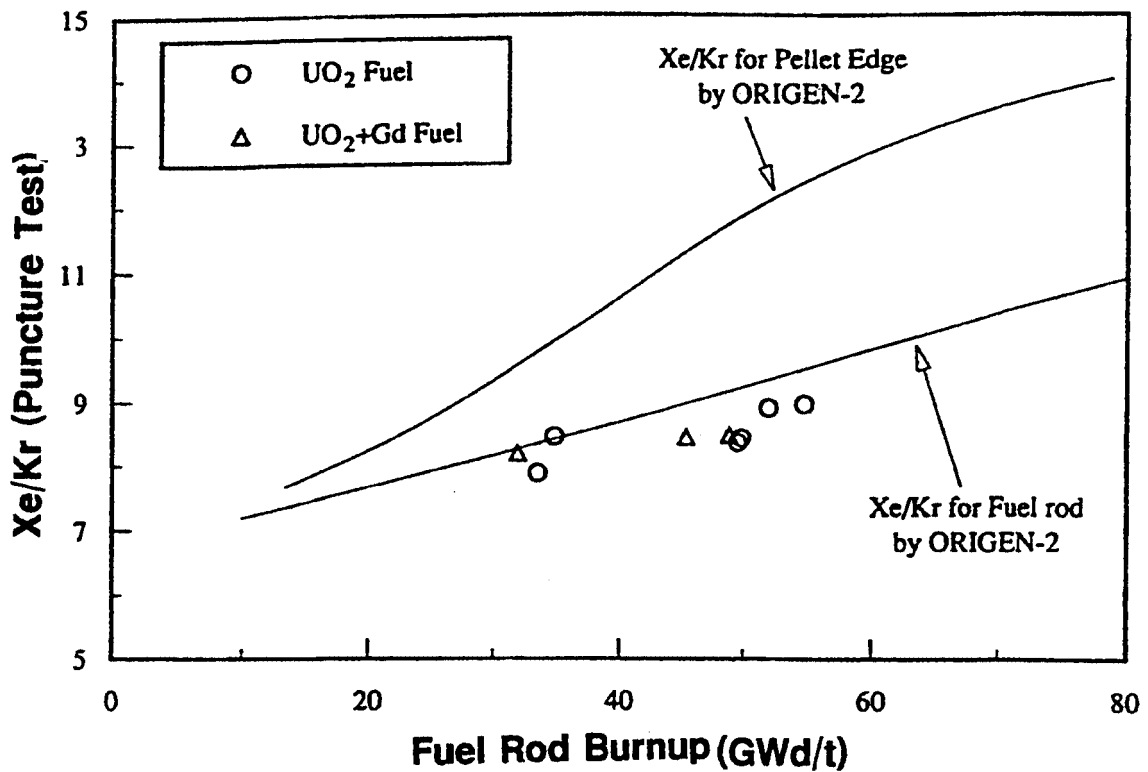


FIG. 4. Comparison of calculated Xe/Kr with measurements [20].

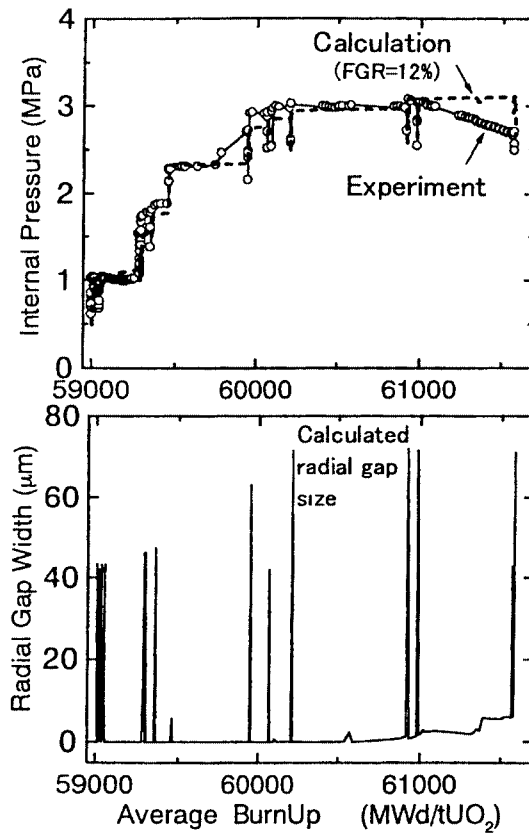


FIG. 5. Comparison of internal pressure calculation by FEMAXI-V with measurement [27].

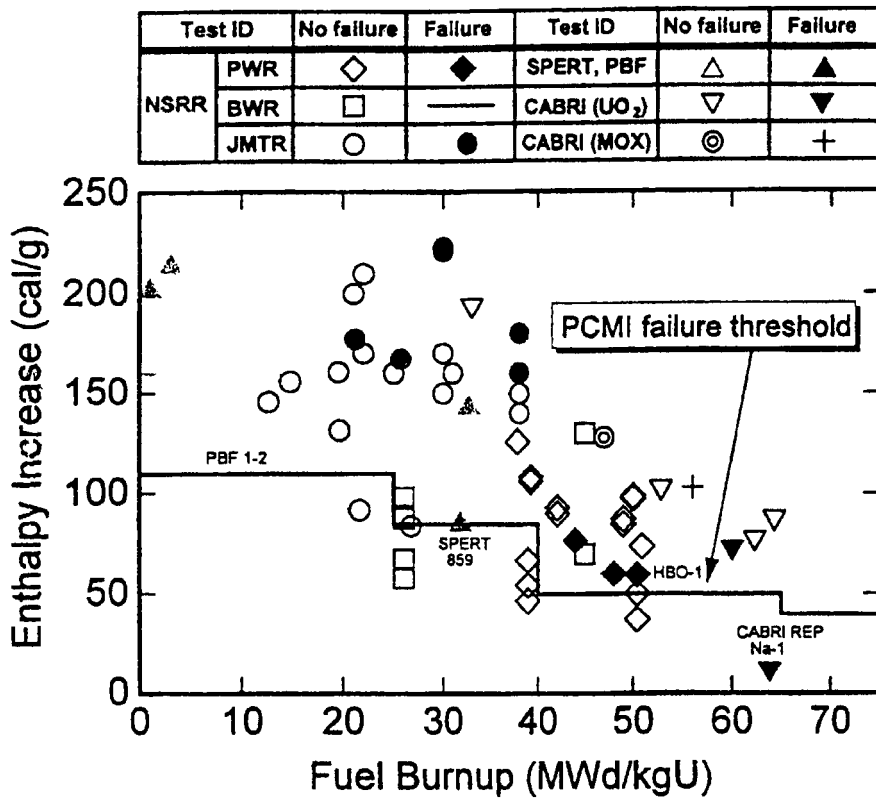


FIG. 6. PCMI failure threshold in RIA transient [28].

## REFERENCES

- [1] Electric Power Industry in Japan 1998/99, Japan Electric Power Information Center (1999).
- [2] M. ICHIKAWA, IAEA-IWGFPT-46(1999).
- [3] M. ICHIKAWA, et al., J. At. Energy Soc. Japan, 39,2 (1997) 93-111 (In Japanese).
- [4] Report for LWR Improvement Technology (High Burnup Fuel) (In Japanese) NUPEC (1999).
- [5] Y. TUKUDA, Proceedings of Achievements of NUPEC, Keldanren-Kaikan (in Japanese) (1999).
- [6] K. KAMIMURA, et al., Japan Atomic Energy Soc. Autumn Meeting, 1-34 (in Japanese), Niigata, (1999).
- [7] Y. TUKUDA, et al., ibid, 1-42 (1999).
- [8] Y. TSUKUDA, et al., ibid, 1-40 (1999).
- [9] Y. ETOH, et al., Proc. Int. Topical Meeting on Light Water Fuel Performance, Portland, March, 1997.
- [10] H. UCHIDA, et al., TOPFUEL'99 (1999).
- [11] Y. TSUKUDA, et al., Japan Atomic Energy Soc. Autumn Meeting, 1-41 (In Japanese), Niigata, (1999).
- [12] M. HIRAI, et al., Proc. Int. Topical Meeting on Light Water Fuel Performance, Portland, March, 1997.
- [13] M. YOKOTE, et al., Proc., 10th Pacific Basin Nuclear conference, Kobe, October 1996, 697.
- [14] R. IWASAKI, et al., Japan Atomic Energy Soc. Autumn Meeting, 1-44 (in Japanese), Niigata, (1999).
- [15] J. NAKAMURA, et al., OECD/NEA-IAEA International Seminar on thermal Performance of high burnup LWR fuel, Cadarache (1998).
- [16] M. HIRAI, et al., IAEA/TCM, Advances in Pellet Tech. Improved Performance at High Burnup, Tokyo, Nov. 1996.
- [17] M. AMAYA, et al., TOPFUEL'97, Manchester (1997).
- [18] K. OHIRA, et al., Proc. Int. Topical Meeting on Light Water Fuel Performance, Portland, March, 1997.
- [19] M. KINOSHITA, et al., Proc. Int. Topical Meeting on Light Water Fuel Performance, Portland, March, 1997.
- [20] N. IKATSU, et al., IAEA/TCM on fuel chemistry and PCI related to high burnup, Nykoping (1998).
- [21] K. UNE, et al., Proc. Japan Atomic Energy Soc. Autumn Meeting 1-46 (in Japanese), Niigata, 1999.
- [22] K. UNE, et al., Proc. Int. Topical Meeting on Light Water Fuel Performance, Portland, March, 1997.
- [23] M. ICHIKAWA, Nuclear Fuel Technology, Chapter 10.2, Japan Atomic Energy Society (1993).
- [24] M. ICHIKAWA, et al., Proceedings of ANS topical Meeting, Williamsburg, USA (1988).
- [25] T. NAKAJIMA, et al., IAEA/TCM on fuel Modelling, Preston, England (1988).
- [26] S. SUZUKI, et al., LWR fuel analysis code FEMAXI-V (Ver. 1), JAERI-Data/Code 99-046 (1999) (in Japanese).
- [27] S. SUZUKI, et al., Proc. Japan Atomic Energy Soc. Spring Meeting 1999, K-13, Hiroshima (in Japanese).

- [28] T. FUKETA, et al., 26 th Water Reactor Safety Information Meeting, Bethesda, Maryland, USA, 1998.
- [29] T. FUKETA, et al., 27 th Water Reactor Safety Information Meeting, Bethesda, Maryland, USA, 1999.

# Management of the fuel cycles and fuel performance analyses in the Kozloduy NPP WWER-440 reactors

**T. Haralampieva, V. Spassova, N. Georgieva,  
A. Antov, I. Stojanova**  
"Kozloduy" NPP, Bulgaria

**S. Stefanova, G. Passage, M. Drenska**  
Institute for Nuclear Research and Nuclear Energy (I NRN E),  
Bulgarian Academy of Sciences, Bulgaria

**K. Lassmann**  
Institute for Transuranium Elements,  
CEC, Karlsruhe, Germany

**Abstract.** The basic characteristics of the previous fuel cycles carried out on Units at the Kozloduy NPP are described in this report. Design optimization methods and safety assessments of specific fuel reloads are presented. The tasks related to the fuel performance efficiency enhancement are reviewed. Advanced fuel implementation possibilities and achieved results in the Kozloduy NPP WWER reactors are discussed. Some basic results obtained by fuel behavior analyses are presented and discussed as well. Computational and experimental investigations of the WWER -440 fuel rod limiting maximal linear power are presented and compared with operational data. On the basis of the present operational experience and the analyses performed, conclusions and proposals for better and more efficient fuel and fuel cycle utilization are made. Up to now the Kozloduy NPP WWER-440 reactors produced totally about 70 fuel cycles.

## 1. CORE RELOAD DESIGN BASIC PRINCIPLES OF THE KOZLODUY NPP WWER - 440 REACTORS

The goals of the core reload design and reshuffling schemes management are:

- to define the optimal amount of fresh fuel for the desired cycle duration,
- to maintain the reactor and fuel parameters in the permissible operational limits, in compliance with the safety criteria.

Following the requirement to reduce the fast neutron exposure and to provide maximal resource of the pressure vessel, 36 dummy assemblies used to be placed at the Units 1, 2 and 3 core periphery, thus the total number of working fuel assemblies (FA) remains 313, including the fuel parts of 37 control assemblies (CA).

In Unit 4 the total number of FA corresponds to the original design, 349 FA, including the fuel parts of 37 CA.

For 14 years the low leakage loading patterns (LLLP) are being successfully applied for all Kozloduy NPP WWER-440 core reloads [15-26].

On 1-3 Units, 24-30 highly burnt-up assemblies are placed together with the dummy assemblies (see Chart I.1) and on Unit 4 - 48 highly burnt assemblies are loaded as well (see Chart I.2). The application of the LLLP schemes using FA with 3.6% U-235 enrichment and CA with 2.4% (in Units 1 and 2) and 3.6% (in Units 3 and 4) enrichment provides cycle duration of 270-330 full power days.



Assembly <sup>1</sup> in 360° sector (313 assemblies)



Dummy assembly

Cycles number and assembly type

24 25 26 27 28 29 30 31 32 33 34 35 36 37 38 39 40 41 42 43 44 45 46 47 48 49 50 51 52 53 54 55 56 57 58 59 60 61 62

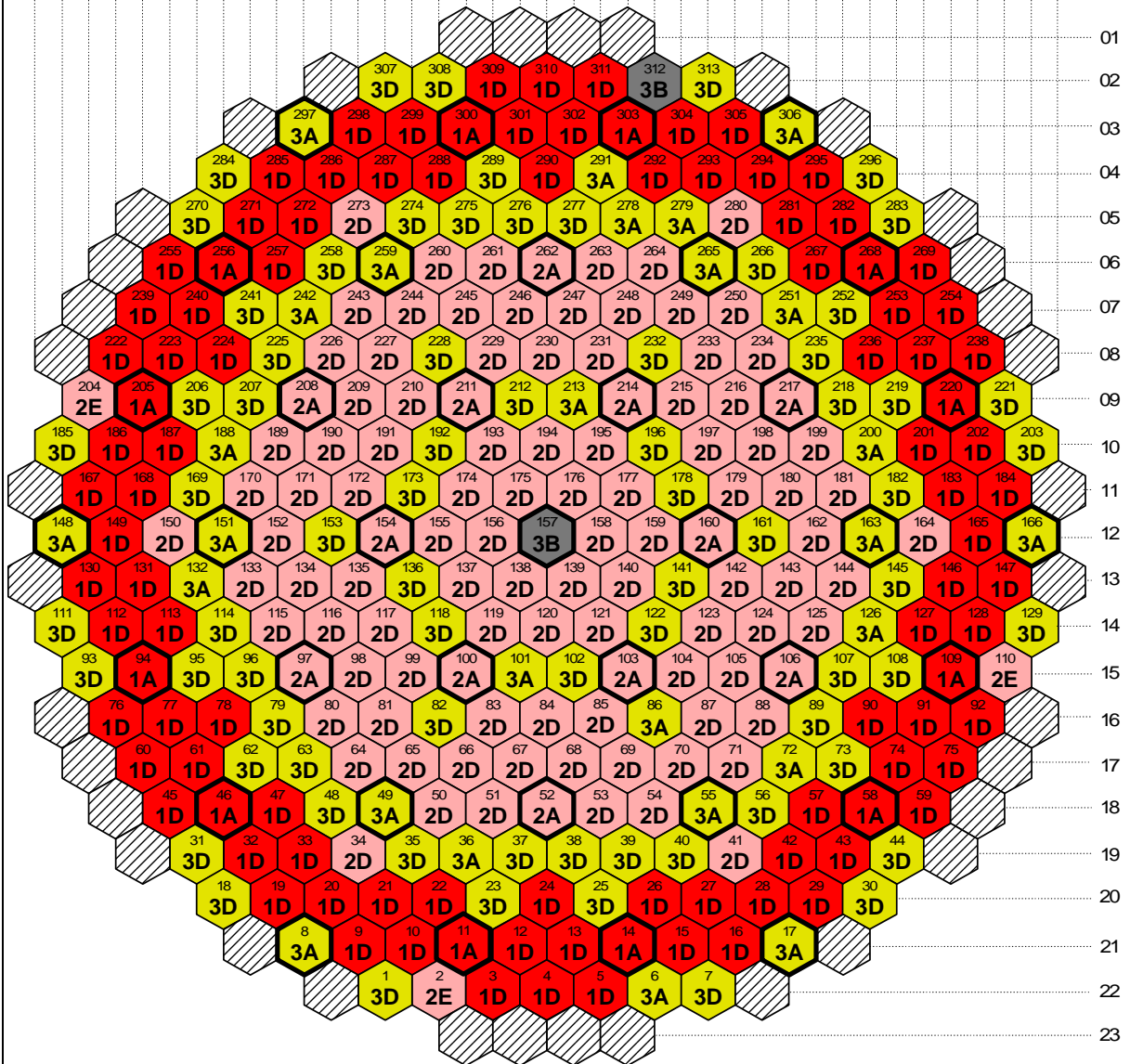


Chart I.1

A - 3.6% wall thickness 2.1mm

Å - 2.4% wall thickness 1.5mm

B - 2.4% wall thickness 2.1mm

D - 3.6% wall thickness 1.5mm

Chart of 14-th core fuel loading of Unit 3



Assembly in 360° sector (349 assemblies)

Cycles number and assemblies type

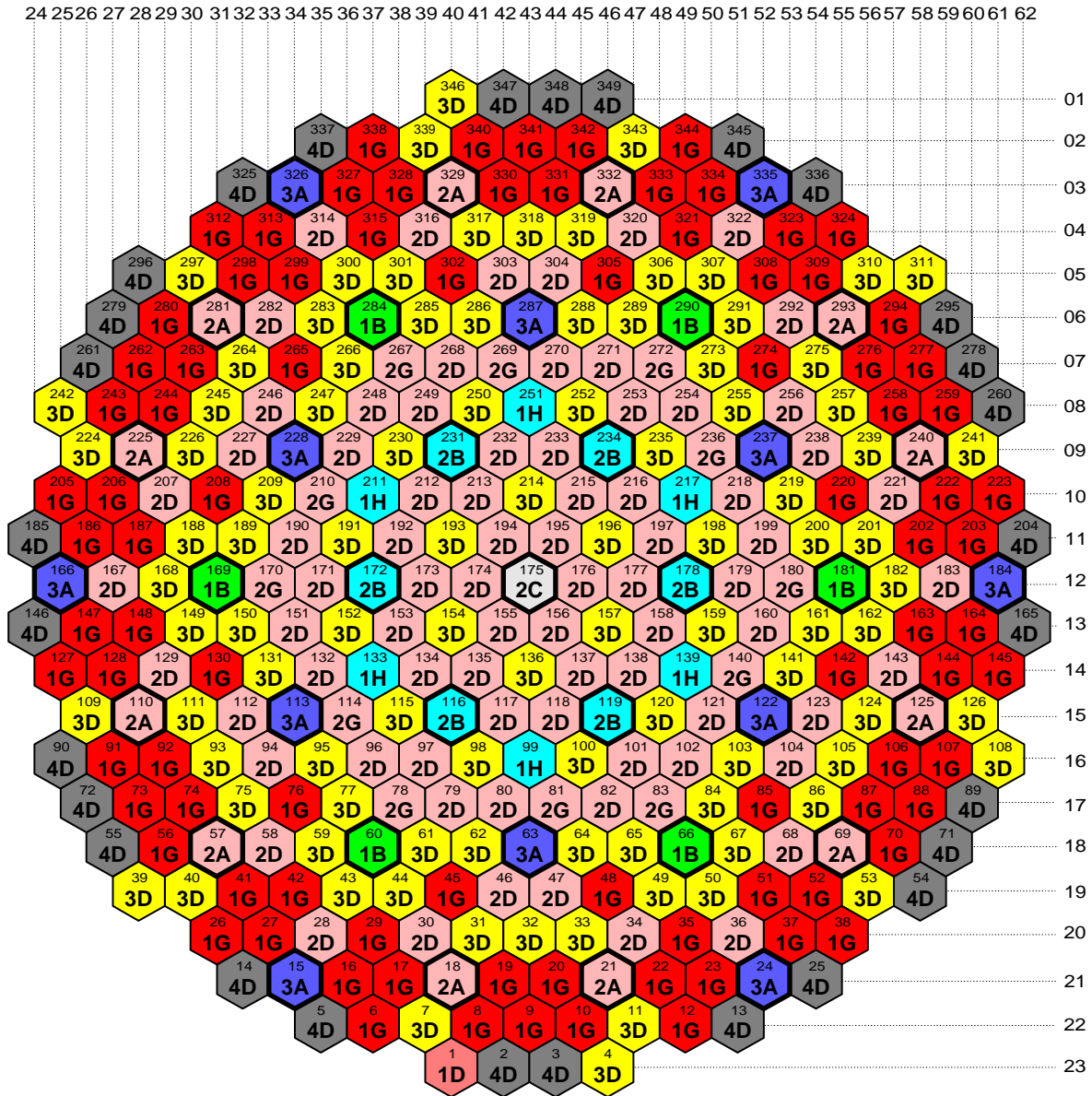


Chart I.2

Å - 3.6% wall thickness 2.1mm

D - 3.6% wall thickness 1.5mm

Ā - 2.4% wall thickness 2.1mm

G - 3.6% wall thickness 1.5mm and  
Zr spacer grids

Ñ - 1.6% wall thickness 2.1mm

Ī - 2.4% wall thickness 1.5mm and  
Zr spacer grids

Chart of 14-core fuel loading , Unit 4

Table I.1. Basic data on the previous 14 fuel cycles carried out on Unit 3

1	Loaded fuel				Cycle life- time  FPD	TPAF %	calc Kq	exp Kq	Core periphery  special features	Average burnup of withdrawn assemblies  [MWd/kgU]		
	CA		WFA							1.6%	2.4%	3.6%
	Year/e nrichm ent	num ber	Year/ enric hment	numb er								
	1C 1B	12 25	1A 1B 1C	102 108 102	406	82	1.25 8	1.22	1A-60 1B- 6	13.3	-	-
	1B	12	1A	102	270. 1	92	1.28 1	1.34	1A-60 2B- 6	-	23.8	-
3	1B	13	1A 1B	84 6	289. 8	96	1.23 6	1.27	1A-60 1B- 6	-	29.1	32.7
	1B	12	1A 1B	84 12	330. 9	97	1.28 5	1.28	1A-36 4A-24 2B- 6	-	26.2	31.4
	1B	13	1A 1B	102 7	335. 8	95	1.37 5	1.37 2	1A-36 4A-24 2B- 6	-	26.6	33.8
	1B	18	1A	96	293. 8	86	1.28 0	1.29	1A-24 3A-12 4A-24 3B- 6	-	21.9	33.1
	1B	19	1A	90	300. 5	95	1.24 9	1.27	1A-36 2A- 6 3A-12 2 B- 6 ÊÅ-36	-	19.5	32.8
	B	2	A	0	26.3	6	.253	.31	1 A-24 3 A-30 3 B- 6 ÊÅ-36		2.1	2.9

	B	9	A	6	22.5	5	.262	.28	1 A-30 3 A-24 3 B- 6 ÊÅ-36		4.0	4.8
0	B A	6 2	D A	5 1	92.1	2 8	.283	.28	1 D- 8 1 A-22 3 A-24 2 B- 6 ÊÅ-36		4.7	4.9
1	B	6	D A	2 2	10.4	3 2	.283	.26	1 D-25 1 A- 5 3 A-24 3 B- 6 ÊÅ-36		6.1	3.8

## 2. CORE RELOAD DESIGN NEUTRON-PHYSICAL COMPUTER CODES

The adaptation of the existing and the development of new neutron-physical (NP) computer codes and their validation costs a lot of efforts of many Kozloduy NPP specialists and INRNE-BAS scientists during the years [1-14].

At present the computer code complex (Fig.II.1) consisting of WIMS-D4, SPPS-1.6 and HEXAB-2D is mainly being used for In-Core fuel management and analyses.

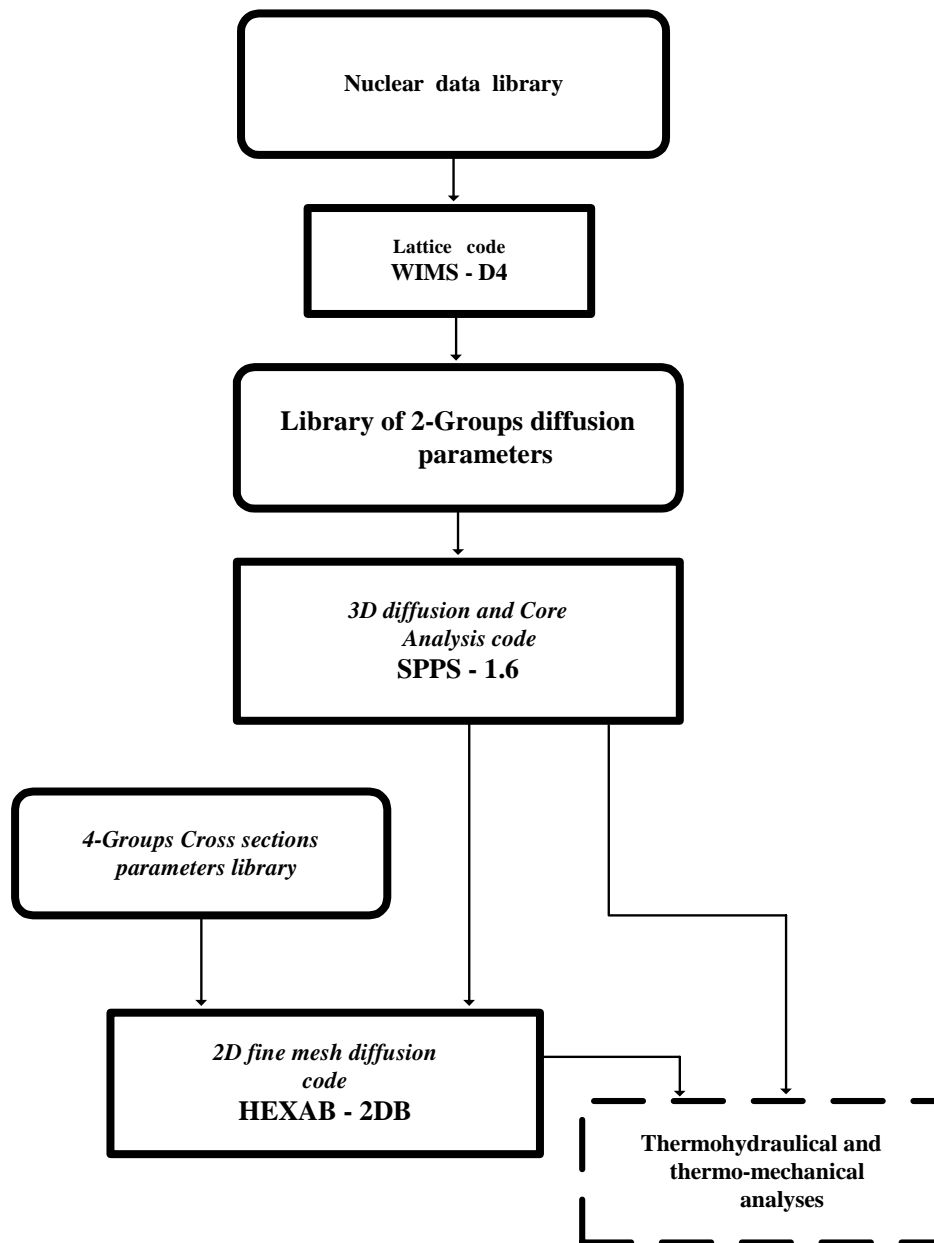


Fig. II.1. WWER-440 reactor computer codes complex for in-core fuel management analysis.

The development of core refueling schemes and determination of the NP characteristics are carried out by means of following computer codes:

- WIMS-D4 calculates the libraries of few-group diffusion parameters for the SPPS-1.6 code;
- SPPS-1.6 is a three-dimensional two-group diffusion code which calculates the core spatial distribution of the neutron flux, power generation, peaking factors and burnup in WWER-440 hexagonal geometry;

- HEXAB-2DB is a fine-mesh two-dimensional diffusion code for calculation of power and burn up pin-wise distribution.

The computer codes have been verified and validated with experimental data; comparative calculations similar to well-known computer codes like HEXBU-3D (Finland), BIPR-7 (Russia), MOBY-DICK (Czech) etc., have been carried out.

The code complex of the fuel supplier (Russia) developed in the RRC “Kurchatov” Institute) is also being applied for comparisons and estimations.

Since 1999 the implementation of the advanced HELIOS spectral computer code has been started in the frame of a PHARE project, its efficient application will give the possibility to assure, verify and license adequately NP parameter libraries for WWER-440 and WWER-1000 reactors to be used in NP and safety calculations of advanced and new design FA.

### 3. KOZLODUY NPP WWER - 440 FUEL UTILIZATION

The achievement of higher burn-up in the WWER-440 reactors is done mainly through:

- introduction of 4-years fuel cycles with 3.6% U-235 enrichment of the FA;
- application of optimal LLLP schemes at reloads;
- transition from 2.4% to 3.6% U-235 CA enrichment;
- operation at power reactivity effect conditions at the end of the fuel cycle, accounting for the fuel supplier technical and safety requirements;
- implementation of fuel with advanced and new design features;

During the last three cycles of 1–4 Units the FA average discharge burn up (Table 3.1.) is:

Unit	Working fuel assemblies	Control assemblies	
	Enrichment 3.6% Burn up [MWd/kgU]	Enrichment 2.4% Burn up [MWd/kgU]	Enrichment 3.6% Burn up [MWd/kgU]
<b>1</b> 17,18,19 cycles	32.0* 32.7**	26.2	-
<b>2</b> 18,19,20 cycles	32.9* 34.5**	26.1	-
<b>3</b> 13,14,15 cycles	35.4* 36.3**	27.4	34.3
<b>4</b> 12,13,14 cycles	36.9* 37.4**	24.9	36.4

\* indicates the realized burnup

\*\* indicates the planned burnup

The introduction of advanced design fuel into the Kozloduy NPP WWER-440 reactors consists of consequent stages preceded by comprehensive theoretical and experimental investigations:

- First stage, completed in 1996-97: implementation of FA with improved design features (decreased shroud thickness, increased internal gas pressure);
- Second stage, ongoing: use of FA with zirconium (Zr) spacer grids (ZSG);
- Third stage in the future: FA with profiled along the radius enrichment and implementation of FA with decreased hafnium (Hf) content in the Zr alloys.

Along with the process of new advanced fuel assemblies implementation, studies with respect to neutron-physics, thermal-hydraulics, safety analyses and fuel cycles costs estimation are carried out.

#### 4. SAFETY ESTIMATIONS OF PARTICULAR NPP KOZLODUY WWER - 440 CORE RELOADS

##### 4.1. Method adopted at Kozloduy NPP

The main purpose of the neutron physics and thermal-hydraulics analyses during reload design is to prove that all important reactor core characteristics are within the range of admissible safety limits [16-24].

Due to introduction of some changes in the fuel assemblies and core design (Zirconium spacer grids, fuel assembly shroud tube thickness and loading pattern) it was found that the reload safety evaluation procedure requires improvements. Currently the new efficient method enabling safety evaluation for each specific core reload has been developed and applied at Kozloduy NPP.

The list of the basic neutron-physics characteristics, which are important for the safety includes:

- fuel type reload characteristics;
- design burn-up;
- maximal power peaking distribution at nominal parameters;
- maximal linear power density;
- coolant temperature reactivity coefficient;
- maximal fuel burn-up at the end of the fuel cycle;
- integral effectiveness of the control assemblies for the fuel cycle beginning and the end;
- emergency protection worth for all control assemblies groups at the core bottom end position with an exception of the most effective absorber, remained stuck at 250 cm, elevation in a hot zero power condition;
- reactor sub-criticality at the beginning of the cycle with 12 g/kg boron coolant concentration, in a hot condition without any power for all withdrawn control assemblies groups;

- reactor negative reactivity provisions while inserting all control assemblies groups into the reactor core with an exception of the most effective absorber, remained stuck at 250 cm elevation, in case of sharp trip from nominal parameters and from zero power at 260°C coolant temperature;
- reactor critical state temperature at the end of the boron cycle, without any power, at 0.001 g/kg boron coolant concentration, when all control assemblies bundles are into the reactor core with an exception of the most effective absorber, remained stuck at 250 cm elevation (repetitive criticality temperature).

A new step to the procedure of core reload design has been added: the check of the key safety parameters as a basis for safety evaluation of the new core characteristics. The method is presented schematically on Fig.IV.1

- It should be confirmed, that neutron-physical (NP) and thermal-hydraulics (TH) key parameters remain within the limiting area in the corresponding accident analysis;
- the key safety parameters are those parameters which are important for the safety analyses and their values could be affected by the core reload design.

The reload safety evaluation method used at Kozloduy NPP is based on following principles:

- Determination of key parameters and their limiting values and conditions. In general, the limiting values are defined on the base of safety analyses, directly by fuel technical specifications or by another regulatory requirements;
- Comparison of the reload design key parameters values with the limiting ones;
- Safety assessment of a new fuel cycle is started on the base of information, obtained at the end of the previous cycle;
- Safety evaluation calculations are done by the use of licensed codes, usually applied at Kozloduy NPP.

If all these parameters are within the area limited by the values of key parameters, then it is evident that the reactor core design meets the safety requirements.

The procedure for comparison of the basic key parameters with their permitted values is demonstrated by a set of tables (Table 4.1).

The documents related to safety evaluation which are prepared for each fuel cycle are:

- Report – Analysis of the forthcoming fuel reload of a defined unit, for evaluation of safety margins of the core design;
- Report – Evaluation of the reactor core design thermal-hydraulics margins.

The last report contains the thermal-hydraulics analysis of reactor core characteristics in a steady state and at a mode of multiple main circulation pumps trips. The thermal-hydraulics calculation is based on the preliminary performed neutron-physics calculation on assembly wise power distribution.

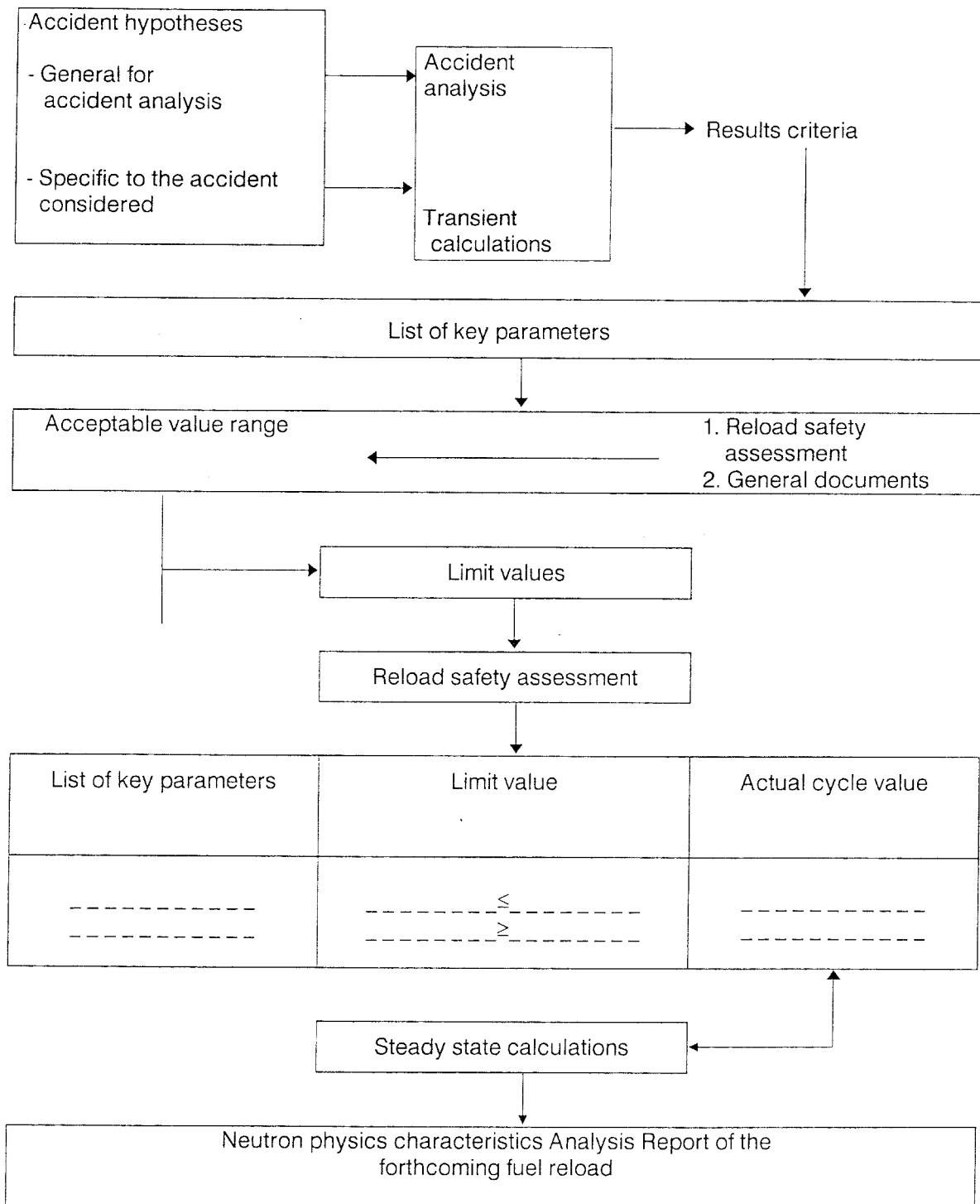


Fig. IV.1 Diagram of reload safety assessment method.

Thermal-mechanical calculations and analyses have been carried out for estimations of the fuel rod performance and behavior.

The final reactor core characteristics design values confirmation is performed on the base of start-up physical experiments.

In general, each test is considered to be successful if the difference between the measurement and the prediction is less than a predetermined criterion.

## 5. COMPUTATIONAL AND EXPERIMENTAL INVESTIGATIONS OF THE FUEL ROD LIMITING MAXIMAL LINEAR POWER AT THE KOZLODUY NPP, 1-4 UNITS WITH WWER - 440 REACTORS, BASED ON THE OPERATION EXPERIENCE

The determination of the fuel rod limiting maximal linear power (LMLP) dependence on burnup during reactor operation, from the viewpoint of preventing the positive feedback between fuel temperature and fission gas release (FGR) increase, is aimed at achievement of better fuel utilization, efficiency and safety grounding at core reloads. The LMLP is closely related to the other thermal limiting parameters, such as fuel temperature, internal gas pressure, etc.

The WWER-440 fuel rod normal operation limiting parameters, presented in Table 5.1., are well known.

On the base of the long-year WWER-440 operation experience and experimental investigations, more detailed fuel rod thermal and cladding deformation criteria have been recently reported [37, 40], as shown on Table 5.2., and recommended for more efficient and safe fuel rod operation.

Different approaches to construct the LMLP curve, applied in all countries operating WWER-440 reactors, based on computational determination of the FGR rate limit (Russia) and on experimental investigations of the 1% FGR limit (Finland) have been analyzed. The LMLP dependencies [33-36] are presented in Fig. V-1.

The LMLP dependence on burnup from thermo-mechanical analyses viewpoint is under preparation using the PIN-micro [39] and the TRANSURANUS [38] codes:

- the PIN-micro code is developed and widely applied for steady-state thermo-mechanical analyses of WWER fuel rods;
- TRANSURANUS is a modern universal thermo-mechanical code for steady-state, transient and accident analyses of fuel rods of different designs, including WWER reactor fuel rods.

Using the experience of the PIN-micro code, the TRANSURANUS-WWER version has been developed and applied under PHARE 92-94 Programme, Project No.95-0587.00.

At present typical operational power histories of highest loaded and highest burnt assemblies and fuel rods of WWER-440 reactors (Kozloduy NPP, Units 1-4) have been analyzed: 9 after one cycle, 7 after two cycles, 12 after three cycles and 10 after four cycles of operation, as shown in Figures V-2 to V-5. All linear heat rates contain a safety factor accounting for the fabrication and technological uncertainties. The application of the safety factor leads to correspondent overestimation of calculated burnup.

Four fuel assemblies, Ass. U1k5, Ass. U2k18, Ass. U3k24 and Ass. U4k36, which have been operated during four fuel cycles and have achieved highest burnup, have been chosen from each reactor operation history and calculated by the TRANSURANUS code [38] with incorporated WWER specific cladding properties.

The highest fuel centerline temperature reached during the first and the second cycles, as shown in Figures V-6a and V-6b, do not exceed 1100°C. The corresponding FGR is less than

0.5% up to the end of the second cycle and about 1% by the end of the fourth cycle, Fig. V-7. The internal gas pressure reaches as maximum 2.5 MPa in hot state and results in ~ 1 MPa by the end of the fourth cycle. The cladding creep-down exhibits onset of the fuel-to-cladding contact by burnup of 40–44 MWd/kgU.

All presented results are obtained using the technological uncertainty safety factor, which leads to overestimation of the burnup (shown on the “x” axis of all figures). The existence of sufficient margins of the thermal and deformation limiting parameters (Table V-2) for steady-state operation has been proved: > 8–10% for the LMLP [33]; > 60% for the maximal fuel temperature; > 5% for the maximal cladding temperature; > 50% for maximal internal gas pressure, up to the local fuel rod burnups of 50 MWd/kgU.

It can be preliminarily concluded by results obtained, that the reasons for possible fuel rod failures cannot be connected with the exceeding of the thermal and deformation operational limits.

The investigations performed up to now allow to make the preliminary conclusion [41] that the non-exceeding of the ~ 3% FGR limit during fuel rod steady-state operation indirectly assures the prevention of a positive feedback onset.

## 6. CONCLUSIONS

During the passed Kozloduy NPP, Units 1–4, operation, significant experience in core design management and fuel performance has been achieved:

- 4-years fuel cycles with FA 3.6% U-235 enrichment has been introduced and higher burnup has been achieved for the discharged assemblies compared to the design one;
- optimal LLLP schemes have been applied at reloads;
- fuel with advanced and new design features has been introduced;

The progressive international experience concerning core and fuel management has been successfully applied;

The development of applied at Kozloduy NPP safety evaluation method is ongoing.

The number of the safety key parameters can be increased through implementation of new safety requirements:

- related to the reduction of fast neutron flux to the reactor vessel;
- related to the limiting maximal linear power depending on fuel burn-up;
- related to the introduction of new type of fuel.

In order to improve the efficiency of the fuel utilization and to enhance its reliability it is reasonable to introduce an united systematic method of approach including complex neutron-physical, thermal-hydraulics and thermal-mechanics analyses, safety estimations and based upon technical-economical conclusions.

**Table I.1 Basic data on the previous 14 fuel cycles carried out on Unit 3**

C y c l e N	Loaded fuel				Cycle life- time  FPD	TPAF %	calc Kq	exp Kq	Core periphery special features	Average burnup of withdrawn assemblies [MWd/kgU]		
	CA		WFA							1.6%	2.4%	3.6%
	Year/ en- rich- ment	num be r	Year/ en- rich- ment	num ber								
1	1C 1B	12 25	1A 1B 1C	102 108 102	406	82	1.258	1.22	1A-60 1B- 6	13.3	-	-
2	1B	12	1A	102	270.1	92	1.281	1.34	1A-60 2B- 6	-	23.8	-
3	1B	13	1A 1B	84 6	289.8	96	1.236	1.27	1A-60 1B- 6	-	29.1	32.7
4	1B	12	1A 1B	84 12	330.9	97	1.285	1.28	1A-36 4A-24 2B- 6	-	26.2	31.4
5	1B	13	1A 1B	102 7	335.8	95	1.375	1.372	1A-36 4A-24 2B- 6	-	26.6	33.8
6	1B	18	1A	96	293.8	86	1.280	1.29	1A-24 3A-12 4A-24 3B- 6	-	21.9	33.1
7	1B	19	1A	90	300.5	95	1.249	1.27	1A-36 2A- 6 3A-12 2B- 6 KE-36	-	19.5	32.8
8	1B	12	1A	90	326.3	96	1.253	1.31	1A-24 3A-30 3B- 6 KE-36	-	22.1	32.9
9	1B	19	1A	96	322.5	95	1.262	1.28	1A-30 3A-24 3B- 6 KE-36	-	24.0	34.8
10	1B 1A	6 12	1D 1A	25 71	292.1	88	1.283	1.28	1D- 8 1A-22 3A-24 2B- 6 KE-36	-	24.7	34.9
11	1B	6	1D 1A	62 22	310.4	82	1.283	1.26	1D-25 1A- 5 3A-24 3B- 6 KE-36	-	26.1	33.8

Table I.1 Basic data on the previous 14 fuel cycles carried out on Unit 3 (cont.)

C y  c l i c l e N o	Loaded fuel				Cycle life- time  FPD	TPAF %	calc Kq	exp Kq	Core periphery special features	Average burnup of withdrawn  assemblies [MWd/kgU]		
	CA		WFA							1.6%	2.4%	3.6%
	Year/ en- rich- ment	num ber	Year/ en- rich- ment	num ber								
12	1B 1A	7 12	1D 1A 1B	75 15 7	327	69	1.296	1.28	1D-20 1A- 4 3A-33 4B- 3 KE-36	-	-	34.7
13	1A	12	1D 1E	96 3	321.5	80	1.267	1.279	1D-36 3D-18 3B- 6 KE-36	-	25.2	35.8
14	1A	12	1D	90	329.8	84.8	1.264	1.250	1G-30 3D- 9 4D-11 3A-6 4A-1 3E-3 KE-36	-	30.1	35.6

CA- control assemblies;  
WFA - working fuel assemblies;  
TPAF- thermal power availability factor;  
FPD - full power days

Table I.2 Basic data on the previous 14 fuel cycles carried out on Unit 4

c y c l e N o	Loaded assemblies				Cycle lifetime  FPD	TPAF  %	K <sub>a</sub>	K <sub>a</sub> <sup>exp</sup>	Core periphery special features	Average burnup of withdrawn assemblies [MWd/kgU]		
	CA		WFA							1.6	2.4	3.6
	year/ enric ment	num ber	year/ enric ment	num ber								
1	1B 1C	25 12	1A 1B 1C	102 108 102	390	0.90	1.287	1.298		12.8		
2	1B	12	1A	102	241.2	0.95	1.269	1.3	1A-60 2B-6		22.2	
3	1B	13	1A 1B	90 6	348.8	0.97	1.372	1.346	1A-36 2A-12 1B-6 3B-12		26.5	33.2
4	1B	12	1A	102	313.7	0.96	1.355	1.270	1A-36 2A-12 4A-12 2B-6		25.6	32.7
5	1B	19	1A	96	354.4	0.96	1.303	1.240	1A-24 3A-12 4A-24 3B-6		21.3	33.9
6	1B	18	1A	96	309.5	0.96	1.302	1.301	1A-12 3A-30 4A-18 2B-6		21.1	34.1
7	1B 1A	7 12	1A	90	244	0.90	1.313	1.288	1A-12 3A-18 4A-30 2B-6		20.3	33.2
8	1B	6	1A	78	350.4	0.91	1.290	1.301	1A-12 4A-48 3B-6		26.4	34.4
9	1A	12	1F 1B 1A 1D	1 6 33 57	295	0.95	1.335	1.330	1A-3 1D-9 4A-48 3B-6		25.9	34.8

CA- control assemblies; WFA - working fuel assemblies; TPAF- thermal power availability factor;  
FPD - full power days

Table I.2 Basic data on the previous 14 fuel cycles carried out on Unit 4 (cont.)

c y c l e N o	Loaded assemblies				Cycle lifetime  FPD	TPAF  %	$K_G$	$K_G^{exp}$	Core periphery special features	Average burnup of withdrawn assemblies [MWd/kgU]		
	CA		WFA							1.6	2.4	3.6
	year/ enric ment	num ber	year/ enric ment	num ber								
10	1B 1A	7 12	1A	90	309.3	0.87	1.308	1.320	1A-12 4A-48 3B-6	13.2	24.3	35.6
11	1B	6	1D	90	332	0.64	1.316	1.317	1D-12 3D-9 3A-3 4A-36 2B-6		28.9	36.1
12	1A	12	1D	96	356.4	0.88	1.315	1.330	1D-12 3A-12 4D-36 3B-6		23.7	36.6
13	1C 1B 1A	1 6 12	1D 1G	78 12	358.7	0.77	1.315	1.300	1D-12 3D-12 4A-36 3B-6		26.1	37.4
14	1B	6	1G 1H	90 6	295.65	0.85	1.340	1.280	1G-12 3A-6 3D-18 4D-30			36.8

CA- control assemblies; WFA - working fuel assemblies; TPAF- thermal power availability factor;  
FPD - full power days

Table 4.1.

Parameters	Limit values	15th cycle values
<p><b>1. Core power peaking factors</b> at full power, Nð=100%</p> <p>1.1. Fuel assembly radial peaking factor,</p> <p style="padding-left: 40px;"><math>K_q</math></p> <p style="padding-left: 40px;"><math>H_{VI} = 200 \text{ cm}</math></p> <p style="padding-left: 40px;"><math>H_{VI} = 250 \text{ cm}</math></p> <p>1.2. Fuel rod radial peaking factor <math>K_{\mu} = K_q \cdot K_{kk}</math>, where</p> <p style="padding-left: 40px;"><math>K_{kk}</math> is the peaking factor of the fuel rod in the assembly</p> <p>1.3. Core volume peaking factor <math>K_v</math>:</p> <p style="padding-left: 40px;"><math>\dot{I}_{VI} = 180 \text{ cm}</math></p> <p style="padding-left: 40px;"><math>H_{VI} = 200 \text{ cm}</math></p> <p style="padding-left: 40px;"><math>H_{VI} = 250 \text{ cm}</math></p> <p>1.4. Axial power peaking factor</p> <p style="padding-left: 40px;"><math>K_v^{\max}</math> <math>K_z = \frac{K_v^{\max}}{K_q}</math></p> <p>1.5. Power peaking factor (total) <math>K_o</math>:</p> <p style="padding-left: 40px;"><math>K_o = K_v \cdot K_{kk} = K_q \cdot K_z \cdot K_{kk}</math></p>	<p style="text-align: center;"><math>&lt; 1.35</math></p> <p style="text-align: center;"><math>&lt; 1.55</math></p> <p style="text-align: center;"><math>&lt; 2.14</math></p>	<p style="text-align: center;"><math>\leq 1.316</math></p> <p style="text-align: center;"><math>\leq 1.312</math></p> <p style="text-align: center;"><math>\leq 1.507</math></p> <p style="text-align: center;"><math>\leq 1.759</math></p> <p style="text-align: center;"><math>\leq 1.701</math></p> <p style="text-align: center;"><math>\leq 1.627</math></p> <p style="text-align: center;"><math>\leq 1.296</math></p> <p style="text-align: center;"><math>\leq 1.921</math></p>

Distribution of the power peaking factors values in the core for the 15<sup>th</sup> cycle, Unit 4.

Table 5.1. WWER–440 fuel rod limiting parameters at normal operational conditions

P A R A M E T E R		V A L U E
Maximal linear power,	W/cm	325
Maximal fuel temperature (fresh fuel),	°C	2800
Maximal cladding surface temperature,	°C	335
Maximal internal gas pressure,	MPa	12.3
Part of the failed fuel rods with gas untightness,%		0.1
Part of the failed fuel rods with direct fuel-to-coolant contact,	%	0.01

Table 5.2.WWER fuel rod limiting (thermal and cladding deformation) parameters for normal operation [40]

Limiting parameter	Limiting value
TC1 – maximum fuel temperature	2800°C for fresh fuel accounting for the decrease dependent on fuel burnup
TC2 – maximum internal gas pressure	12.3 MPa (WWER–440)
TC3 – maximum linear heat rate	325 W/cm for fresh and low burnup fuel accounting for the decrease dependent on burnup
TC4 – maximum quick power increase	80.0 W/cm
DC1 – maximum cladding diameter decrease	0.12 mm
DC2 – maximum cladding elongation	25.0 mm
DC3 – maximum cladding diameter increase	0.4% (≈ 37 micron)

**Fig. V-1.** WWER-440 Fuel Rod Limiting Maximal Linear Power

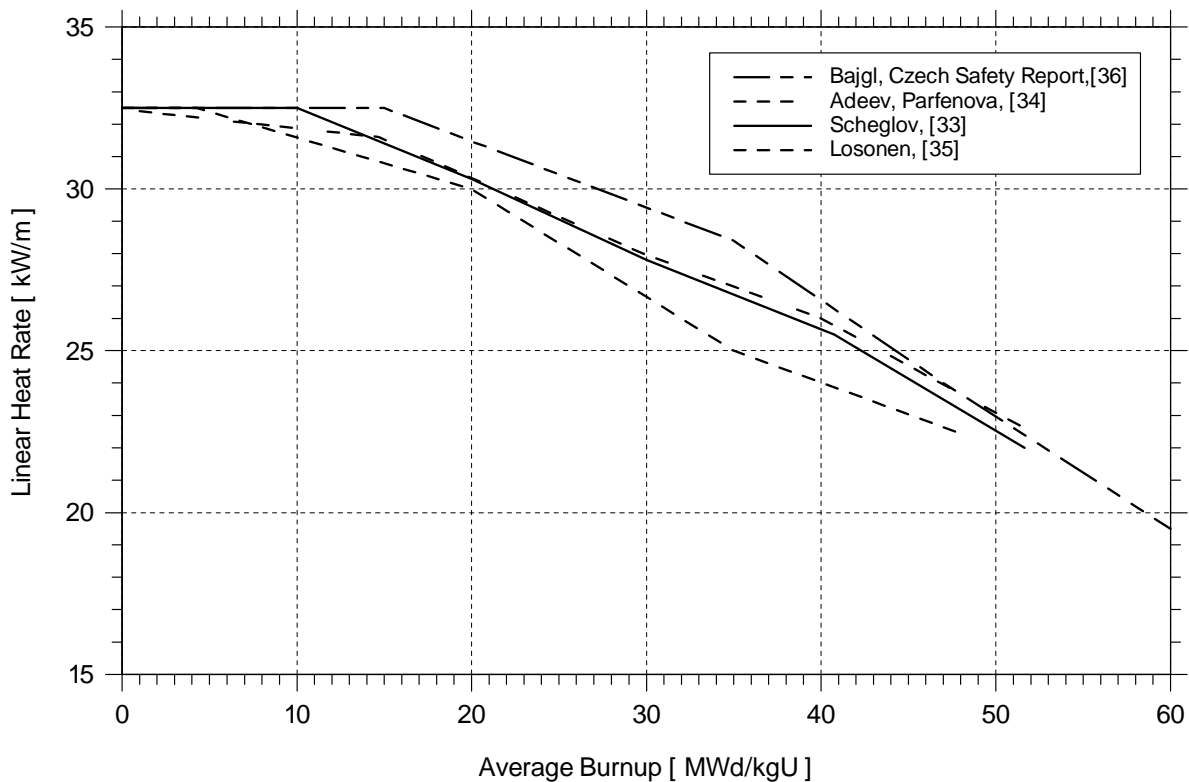


**Fig. V-2.** Power Histories, Unit 1, 14-18 Cycles.

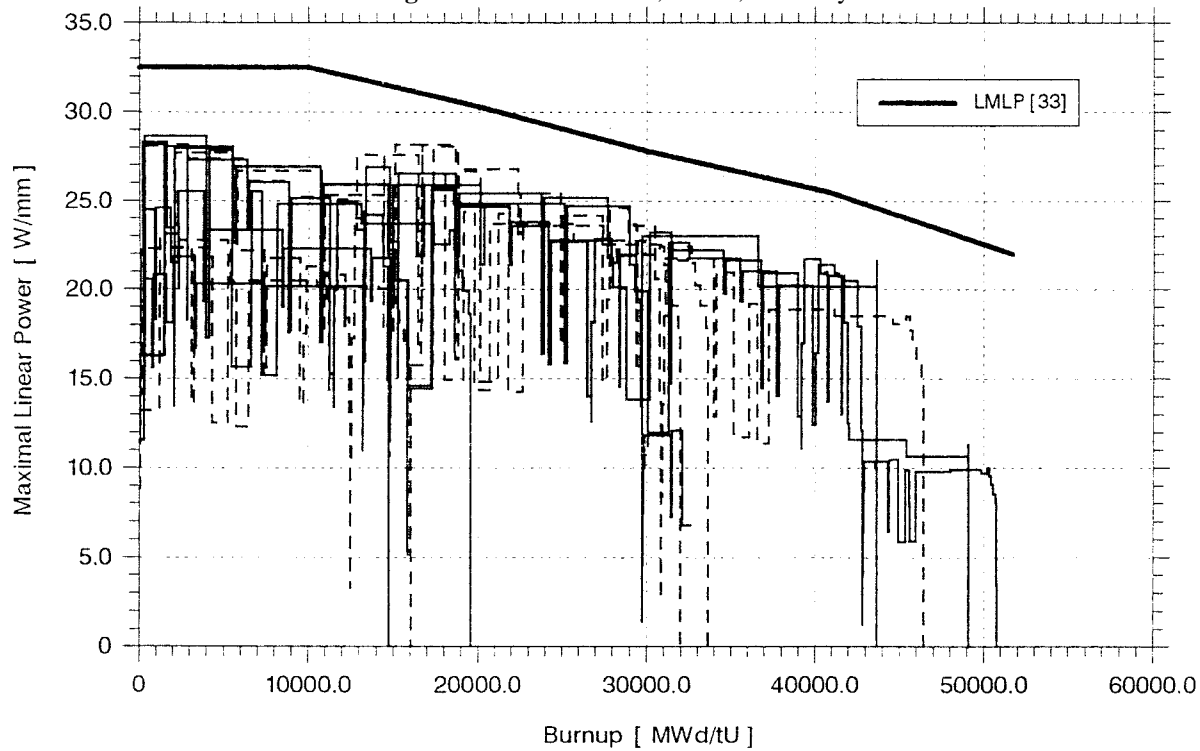


Fig. V-3. Power Histories, Unit 2, 14-19 Cycles.

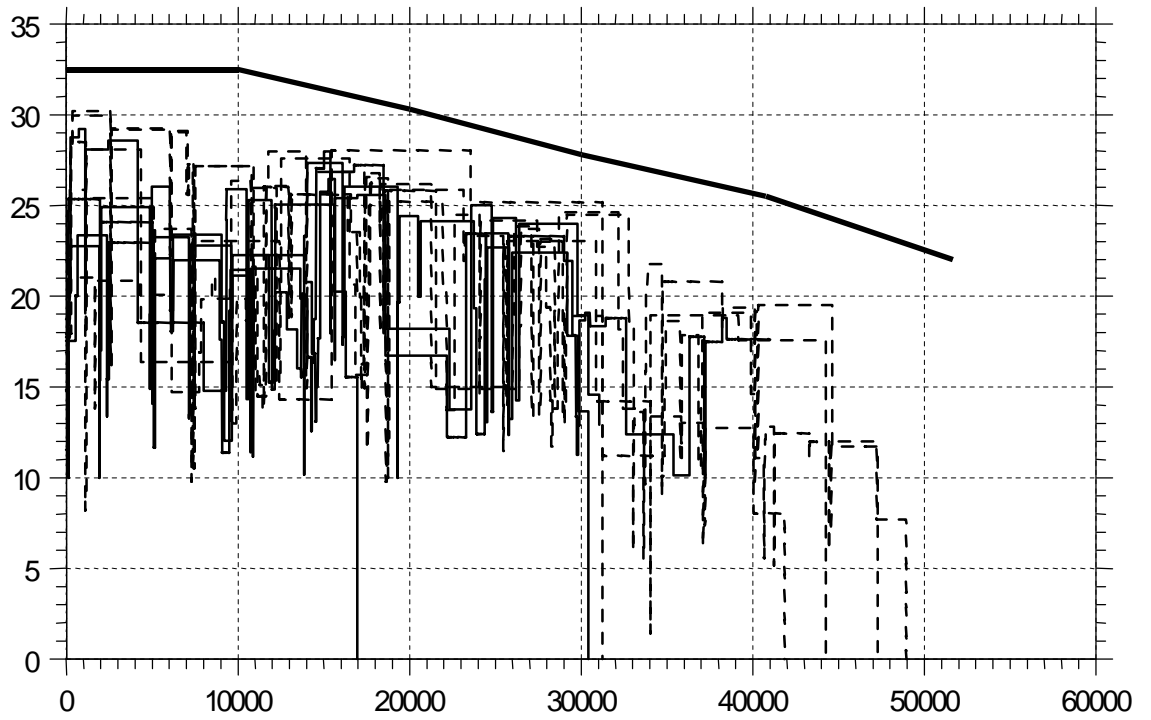


Fig. V-4. Power Histories, Unit 3, 9-13 Cycles

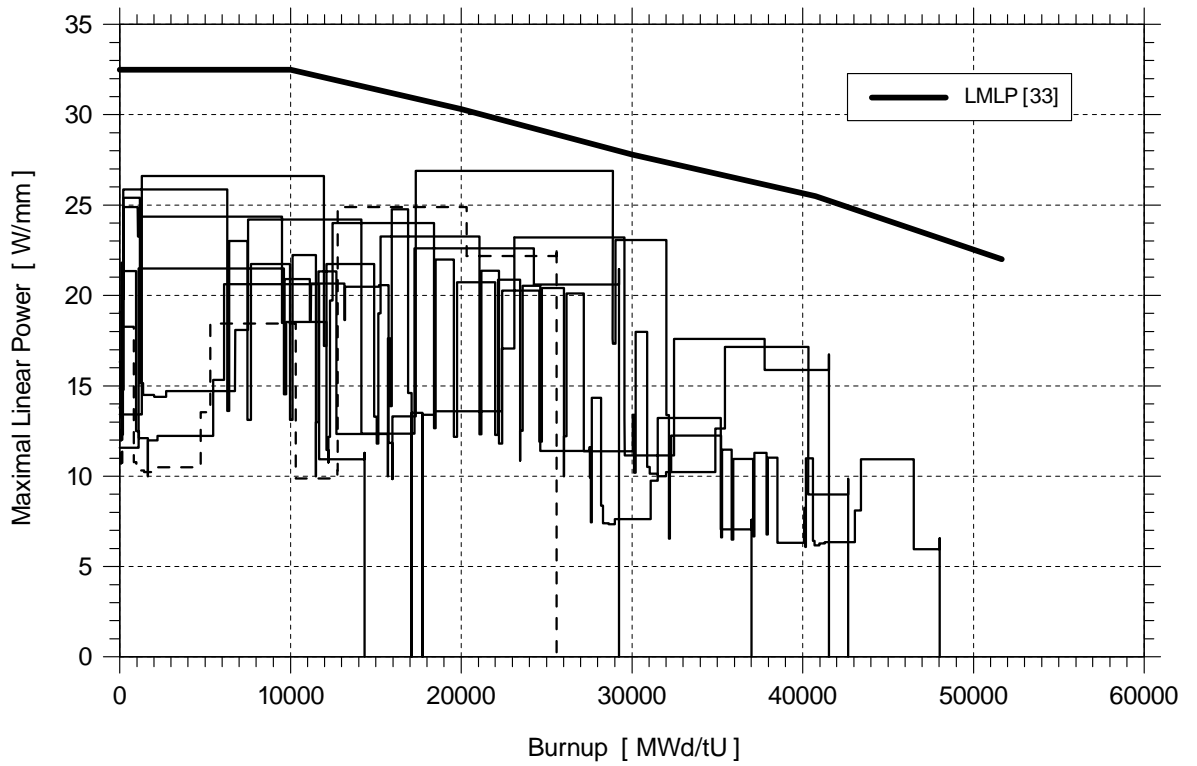


Fig. V-5. Power Histories, Unit 4, 9-13 Cycles

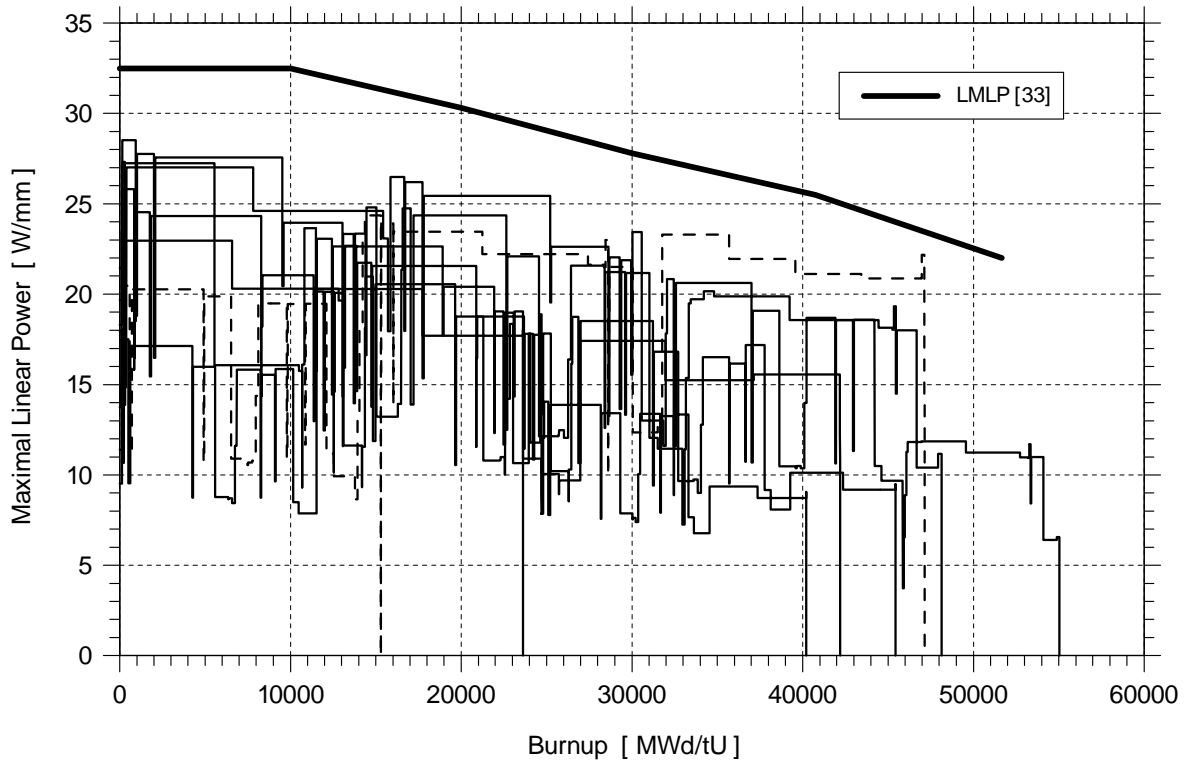
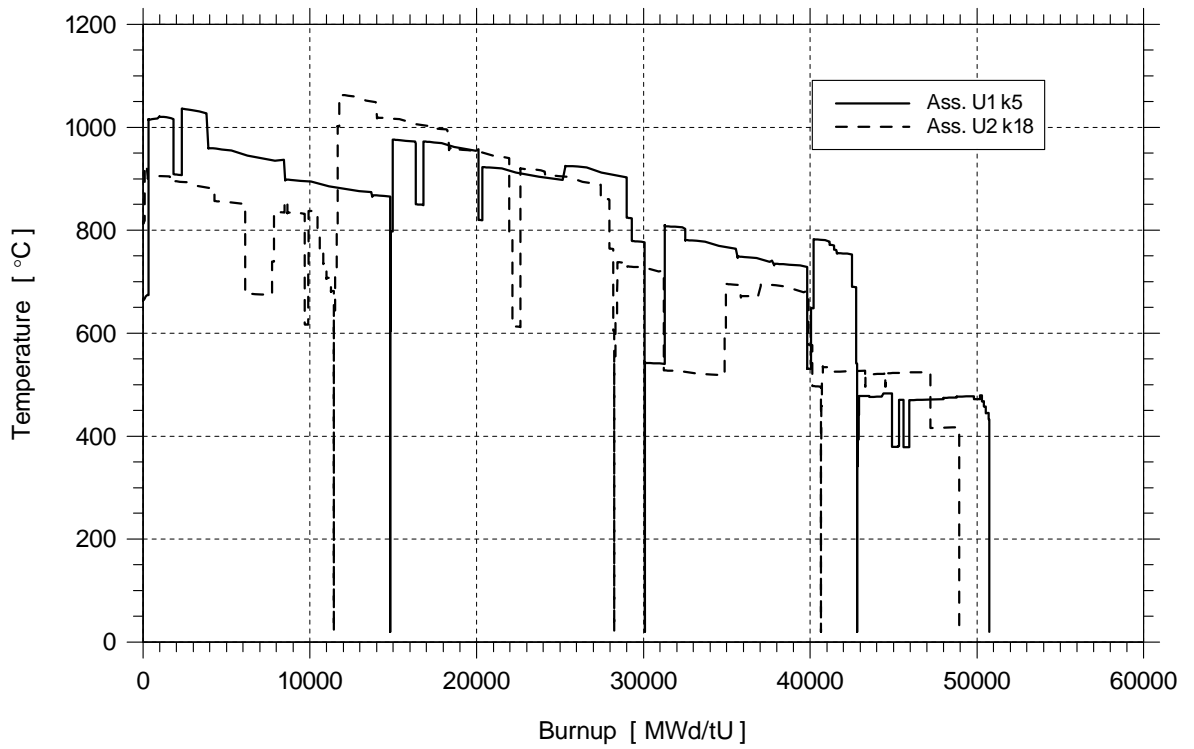
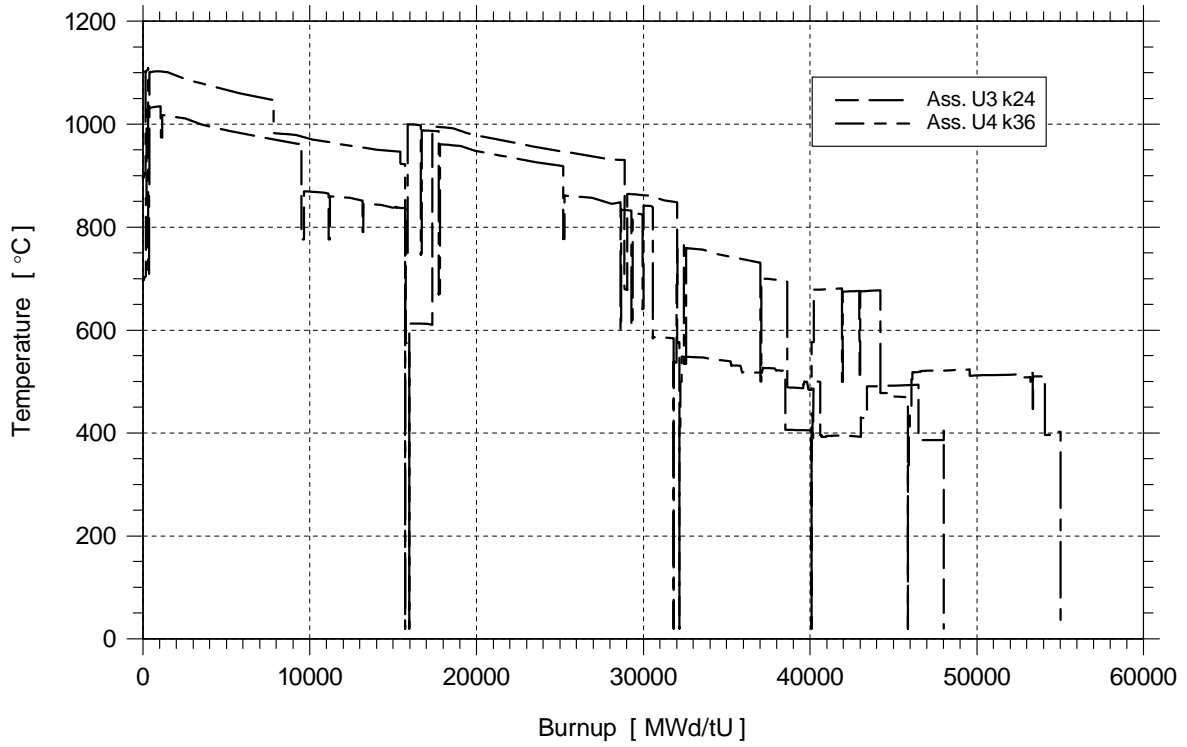


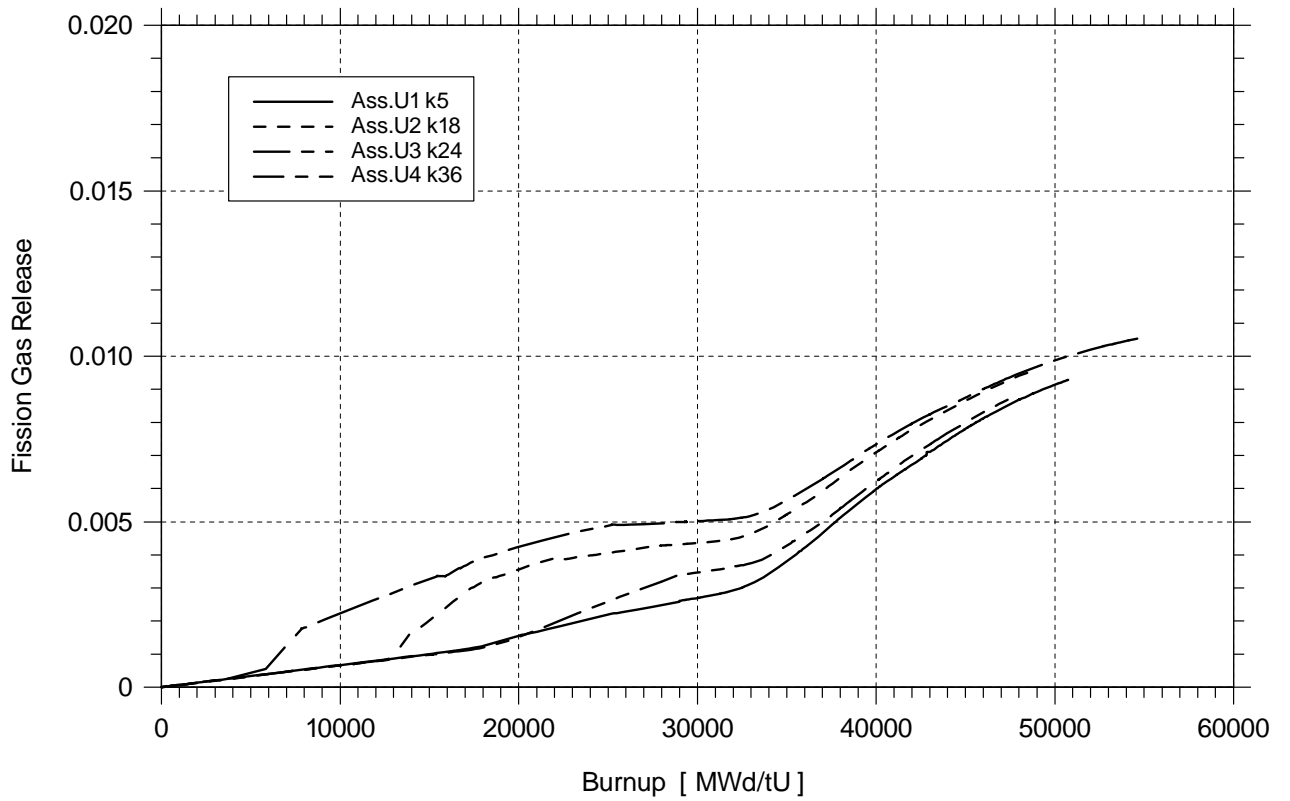
Fig. V-6a. Fuel Centerline Temperature, Units 1 & 2



**Fig. V-6b. Fuel Centerline Temperature, Units 3 & 4**



**Fig. V-7. Fission gas Release, Units 1,2, 3 & 4**



## REFERENCES

- [1] P.T.Petkov. SPPS-1.6 - A 3D Diffusion Code for Neutronics Calculations of the VVER-440 Reactors. Proc. of the Forth Symposium of AER, Sozopol, 10-15 Oct., 1994.
- [2] J.R. Askew, F.J. Fayers, P.B.Kemshel. A General Description of the Lattice Code WIMS.J.BNES, Oct., 1966.
- [3] C.J.Taubman. The WIMS 69 Group Library Tape 166259 AEEW-M1324, 1976.
- [4] Jung - Do Kim. WIMKAL-88. The 1988 Version of WIMS - KAERI Library. IAEA-NDC-92. August 1990.
- [5] A.Trkov, A. Holubar, M.Ravnik. WIMS Library Update Project: Phase Report on Stage 2.IJ S-DP -6243, Nov. 20, 1991.
- [6] P.T.Petkov, Modifications in the WIMS-D4 Code and its Library. Proc. of the Forth Symposium of AER, Sozopol, 10-15 Oct.1994
- [7] “ ”, -1, , 1995 . . . . .  
12  
13-
- [8] -  
175-  
96/05.03.1995 . , - , 1997 .
- [9] A. S.Scheglov, V.N. Proselkov, Y.u K. Bibilashvili. Approach to Detemine Dependence of Permissible Maximum Linear Heat Rates of WWER-440 Fuel Rods versus Burnup, II Internationale Meeting of VVER Fuel Performance Modelling and Experimental Support, Bulgaria, 1995.
- [10] Casal JJ, Stamm’ler RJJ, Villarino E A and Ferri A A, “HELIOS: Geometric capabilities of a new fuel-assembly program,” Intl Topical Meeting on Advances in Mathematics, Computations, and Reactor Physics, Pittsbirgh, 1991, Vol. 2, p. 10.2.1 1-13.
- [11] EDF, D.Leduc. Centrale de Bugey 2/3 - Tranche 3 - Campagne 10. Dossier spécifique d'évaluation de la surete de la recharge - pilotage mode A. D541 90/811.
- [12] A. SCHEGLOV, V. PROSELKOV, YU. BIBILASHVILI, *Approach to Determine Dependence of Permissible Maximum Linear Heat Rates of WWER-440 Fuel Rods versus Burnup*. Proceedings of the Second International Seminar on WWER Reactor Fuel Performance, Modelling and Experimental Support, Sandanski, Bulgaria, 21–25 April 1997.
- [13] V. ADEEV, N. PARFENOVA, V. PROSELKOV et al., *Experience of Kola NPP Fuel Rod Operation*. Proceedings of the Seventh Symposium of AER, Hörnitz near Zittau, Germany, 23–26 September 1997.
- [14] P. LÖSÖNEN, *VVER Fuel Performance, Development, QA and Future Prospects at Loviisa NPS*. Proceedings of an International Seminar on WWER Reactor Fuel Performance, Modelling and Experimental Support, Varna, Bulgaria, 7–11 November 1994.

- [15] J. BAJGL, *Comparison of Profiled FAs Loadings Proposals*. Proceedings of the Seventh Symposium of AER, Hörnitz near Zittau, Germany, 23–26 September 1997.
- [16] P. MENUT, *IAEA Technical Co-operation Program RER 4-019* IAEA RER/4/019 Workshop “Implementation of the WWER version of the TRANSURANUS code and its implementation to the safety criteria”, BAN Hotel, Sofia, 7–11 December 1998.
- [17] K. Lassmann, *TRANSURANUS: a fuel rod analysis code ready for use*. Journal of Nuclear Materials, **188** (1992), p. 295–302.
- [18] R. Pazdera, M. Valach, P. Strijov, K. Dubrovin, V. Murashov, A. Senkin, V. Yakovlev, *User’s Guide for the Computer Code PIN-micro*. UJV 9515–T. Rez, CSFR, November 1991.
- [19] 19.Bibilashvili Yu.K., *WWER Fuel Rod Acceptance / Design Criteria for Safe and Reliable Operation and Their Justification*. IAEA Regional Training Course on WWER Fuel Design, Performance and Back End, Bratislava, Slovak Republic, 21 June, 2 July 1999.
- [20] Contract 2810431/13.07.1999 between NEC EAD Kozloduy NPP branch and INRNE – BAS.

# Core analysis of the first cycle of Chashma nuclear power plant

**Subhan Gul, M. Khan, Waseem Azhar, M. Kamran, Abid Hussain**

Institute for Nuclear Power,  
Islamabad, Pakistan

**Abstract.** The up coming 300 MWe CHASHMA NPP will provide the opportunity to study the burn-up behavior of the fuel. Our experience is limited to the incore fuel management studies when fuel burn-up remains within the design limits. The initial core is loaded in three regions with fuel of three different enrichments 2.4 w/o, 2.67 w/o & 3.0w/o. It is intended to study the enhanced fuel burn-up vis-à-vis the expected cost benefit in due course of time. The core of the Chashma nuclear power plant is that of a typical PWR NPP of 300 MWe capacity. It has 121 fuel assemblies and all of them have identical external dimensions and hydraulic characteristics. The core height is 290 cm and equivalent diameter is 248.6 cm. The core is cooled and moderated by H<sub>2</sub>O and surrounded by a stainless steel baffle. Each fuel assembly consists of 15 x 15 rod array and the assembly pitch is 20.03 cm. The average discharge burn-up is 30,000 MWd/MTU. Core analysis was carried out for the first cycle at hot full power (HFP). Two dimensional calculations were performed for burn-up analysis including core multiplication, flux distribution, burn-up length, isotopic inventory, peaking factor and critical boron concentration to achieve the economical fuel management within the constraints imposed by safe reactor operation. Calculations indicate that expected burn-up of the first cycle is 13479 MWd/MTU equivalent to 485 EFPD, with 25 ppm of boron is still in the system, which is very near to the design value. Similarly assembly power distribution, pin by pin power distribution and reactivity coefficients, calculated are within the acceptable limits. Efforts are on to improve further these calculations.

## 1. INTRODUCTION

Chashma Nuclear Power Plant is a 300MWe two loop PWR presently under construction on the bank of Indus river, at the south of Mianwali, in the Punjab province, about 300 Km from Islamabad. It will be operational some time in the second half of 1999. Incore fuel management programme for Chashma NPP has to be developed in order to have an economical and safe power generation within safety [1,2] limits from the plant. Therefore efforts are underway to have an extensive and reliable incore fuel management programme for the plant.

## 2. REACTOR CORE

### 2.1. Description

The core of the CHASHMA nuclear power plant is that of a typical PWR NPP of 300 MWe rated capacity. It has 121 fuel assemblies and all of them have identical external dimensions and hydraulic characteristics. The core height is 290 cm and the equivalent diameter is 248.6 cm. The core is cooled and moderated by H<sub>2</sub>O and surrounded by a Stainless Steel baffle. Each fuel assembly consist of 15x15 rod array and assembly pitch is 20.03 cm. The cladding material is Zircaloy-4, burnable poison material is Borosilicate Glass, and the control rod material is Ag-In-Cd alloy. The spacer grids and top & bottom fittings hold the fuel rod within the assembly. The fuel assembly is provided with guide thimbles for cluster of control rods. All other details and features are according to the standard PWR assembly [3].

## 2.2. Fuel Enrichment & Loading

Fuel assemblies of three different enrichments are used in the initial core, in order to obtain a favourable radial power distribution and burn-up.

Region I	2.40 w/o U235
Region II	2.67 w/o U235
Region III	3.00 w/o U235

The first two regions, which consist of the lower enrichment are arranged in modified checkerboard pattern towards the center of the core. The third region is arranged around the periphery of the core. Configuration of the core including the burnable poison (BP) and rod cluster control assembly (RCCA) in the standard PWR core.

## 3. METHODOLOGY

### 3.1. Cross-section generation

Core analysis was carried out with a two dimensional computer code using the following sets of cross section:

- 1) 2.4 w/o U235 without BP, with 16 BP and 20 control rods,
- 2) 2.67 w/o U235 without BP, with 8 & 16 BP and 20 control rods,
- 3) 3.0 w/o U235 without BP, with 8 & 16 BP,
- 4) Core baffle,
- 5) Reflector,

Four Group Microscopic Cross section were calculated from Cross Section Generation codes.

### 3.2. Two dimensional analysis

The mesh point scheme in xy plane is shown in figure 1. One fourth core was analyzed for the following cases.

- Criticality analysis as a function of burn-up with no soluble Boron,
- Critical Boron concentration with burn-up,
- Peaking factor as a function of burn-up,
- Burnable poison remaining fraction with burn-up,
- Expected cycle length of first cycle,
- Assembly power distribution as a function of burn-up.

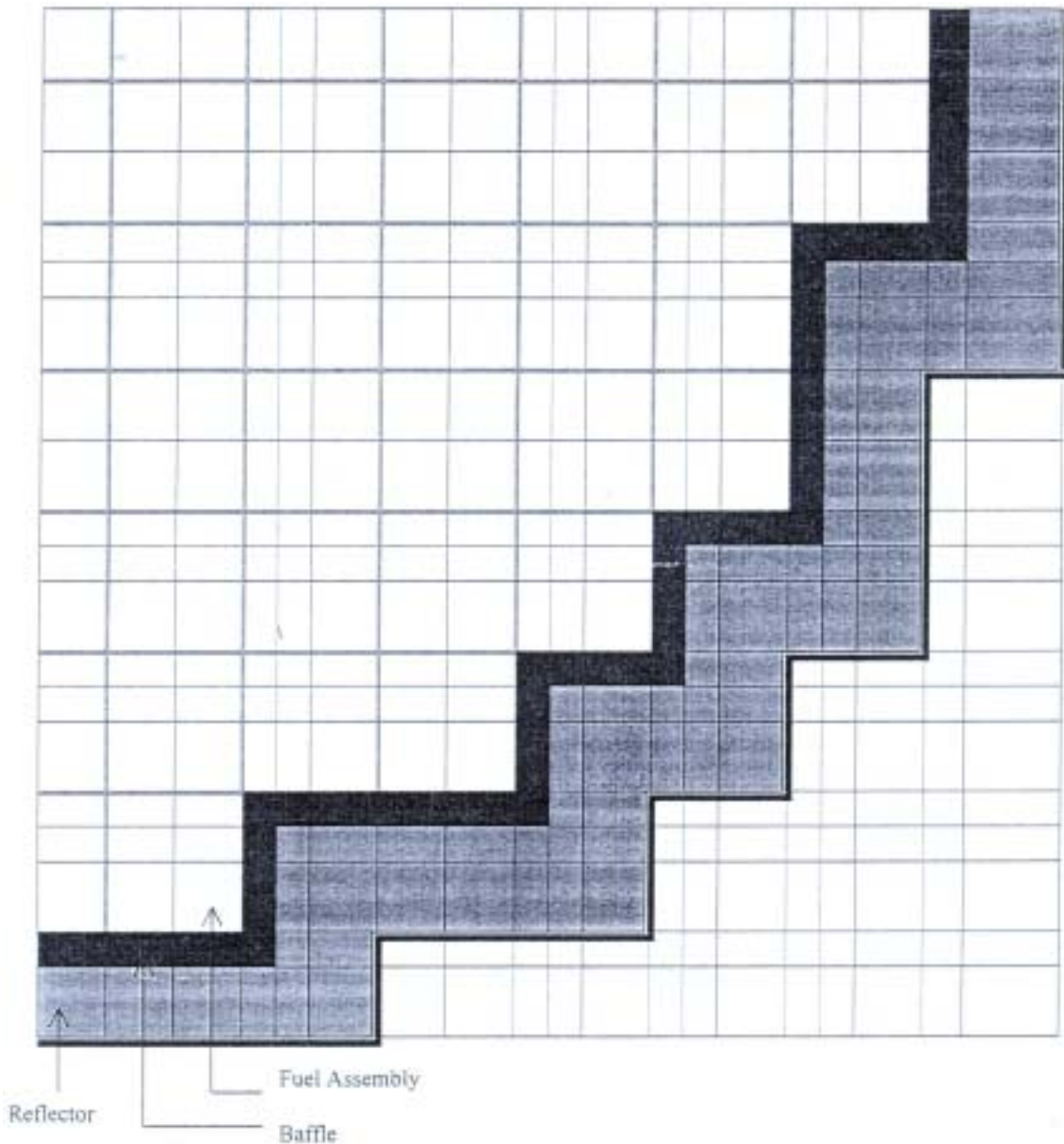


FIG. 1. Meshing scheme in XY plane for the nuclear core of CHASNUPP 300 Mwe.

### 3.3. Reactivity coefficients

During reactor operation, the plant condition variations, operator interventions and abnormal or accidental transients will lead to the corresponding response of the core. The core response is determined by the core kinetics characteristics, which are associated with reactivity coefficients. The reactivity coefficients reflect the change in the neutron multiplication due to varying plant conditions such as power, moderator or fuel temperature or less significantly due to change in pressure or void conditions. A three-dimensional code based on nodal method employing perturbation techniques, calculates reactivity coefficients. Various reactivity coefficients have been calculated at the beginning of life (BOL). Two energy group average cross section have been used in the analysis.

### *3.3.1. Moderator temperature and density coefficients*

The moderator temperature coefficient curves as a function of moderator temperature at BOL, ARO (all rods out) and at boron concentration 0, 500, 1000, 1500 and 2000 ppm were computed. The moderator coefficient is calculated for the various plant conditions by performing two group perturbation calculations, varying the moderator temperature by about  $\pm 1^\circ\text{C}$  each of the mean temperatures. The temperature range covered is from cold  $20^\circ\text{C}$  to about  $320^\circ\text{C}$ . Moderator temperature coefficient has been calculated as a function of boron concentration at Hot zero power (HZP) and hot full power (HFP).

### *3.3.2. Doppler temperature coefficient*

Doppler temperature coefficients as a function of fuel effective temperature were calculated at BOL and ARO for moderator temperature  $280^\circ\text{C}$  and  $302^\circ\text{C}$  with  $1^\circ\text{C}$  change in fuel temperature.

### *3.3.3. Doppler Power coefficient*

Doppler Power coefficient as a function of rated power (0 to 100%) at ARO and BOL were calculated with power change of  $9.989\text{E}06$  Watt. Doppler induced negative reactivity was also calculated at ARO and BOL as a function of Power when boron concentration was 1000 ppm.

### *3.3.4. Total Power coefficient*

Power coefficient at BOL, ARO were calculated as a function of rated power (0 to 100%) when Boron concentrations were 750, 1000 and 1250 ppm. Power defects due to the power increase were also calculated at BOL and ARO with Boron concentration 750, 1000, and 1250 ppm. Differential worth of soluble boron versus power level at BOL ARO were estimated with soluble boron concentration ranging from 750 to 1250 ppm.

## **3.4. Power Distribution**

The axial power distribution and pin-by-pin power distribution in the radial direction has been calculated. A one-dimensional and two-dimensional diffusion theory based computer codes were used for this purpose. Analysis has been performed for various conditions for hot rod assembly, core central assembly and core periphery.

The one dimensional axial computer code calculates the mesh wise axial power distribution for the core. The one-dimensional group constants are converted from two dimensional group constants by space and flux averaging. The effective multiplication factor calculated for two-dimensional core has been adjusted for the one-dimensional configuration by modifying the  $v\sigma_f$  and radial buckling.

The two dimensional diffusion theory based code we use calculates power distribution at desired points in an assembly by using the four group microscopic cross section homogenized for a quarter of the assembly. Power distribution output within an assembly does not include the heterogeneous effect due to different types of cells viz.: fuel, burnable poison, control rod, thimble etc. in an assembly. The shortcoming of the code is overcome by using the pin-by-pin flux distribution obtained from the thermal spectrum calculation code.

The relative (out put of two dimension code, as discussed above) power distribution in each pin is multiplied with relative (out put of spectrum code, as discussed above) flux in the corresponding pin to get the pin-by-pin power distribution map for the complete core. The input of two dimensional codes was prepared in a manner to print the power at every fuel pin center in a quarter of core.

#### 4. RESULTS & DISCUSSIONS

Burn-up analysis was performed and results obtained were analyzed to check their conformity with the well established reactor physics principles.

Criticality analysis as a function of burn-up without Boron is shown in figure 2. Initially decrease in  $K_{eff}$  is due to Xenon-equilibrium. The reactor remains critical at 13000 MWD/MTU. Critical Boron concentration versus burn-up is given in figure 3. The initial decrease in boron concentration up to 135 MWD/MTU is due to the formation of Xenon and after 135 MWD/MTU, the burn-up is consistent with the boron concentration.

Radial Peaking Factor as a function of burn-up is described in figure 4. The graph shows that peaking factor decreases in the beginning and after reaching Xenon-equilibrium peaking factor increases with burn-up up to 6000 MWD/MTU. This increase is due to uneven distribution of burnable poison. At the End of Life (EOL), the power distribution is more flat due to burnable poison depletion with U-235.

Burnable poison remaining fraction with burn-up is depicted in figure 5. Its behavior conforms to the criteria, i.e. 25 ppm of soluble Boron concentration should be present at EOL. Expected burn-up of first cycle is 13145 MWD/MTU, with 25 ppm of Boron still in system. The calculated burn-up is greater than the design value, which is more conservative.

The analysis for moderator temperature coefficient behavior has been studied for the BOL/ARO conditions. Moderator temperature coefficient as a function of moderator temperature is plotted in figure 6 for 0 ppm to 2000 ppm for full range of operation. Here it is observed that increase in temperature of moderator or decreases in boron concentration gives a more negative moderator temperature coefficient by hardening the neutron spectrum. The neutron spectrum is hardened both by increase in moderator temperature as the moderator density decreases reducing moderation and by decreasing boron concentration as the boron density decreases giving a reduced effect of neutron poison. These curves are of importance from stand point of boron dilution/addition.

The Doppler temperature coefficient as a function fuel temperature is shown in figure 7 for the full range of operation for two moderator temperatures 280°C and 302°C. This is because the Doppler coefficient is less negative at higher fuel temperature owing to the saturation of resonance broadening effect. It becomes more negative at higher moderator temperature due to hardening of neutron spectrum.

The axial power distribution results give relative power for various core heights for different core conditions viz.: beginning of life (BOL), middle of life (MOL) and end of Life (EOL), including zero and Equilibrium Xenon at all rod out (ARO) positions. Figure 8 shows Relative axial power distribution at ARO for the no Xe at BOL and Equilibrium Xe at BOL, MOL, EOL conditions whereas Figure 9 shows relative axial power distribution for the BOL core at RCCA inserted at 120 steps. It has been observed that all these vital parameters are well behaved and in good agreement (within  $\pm 5\%$ ) with quoted design values[4]. Efforts are on to improve further these calculations.

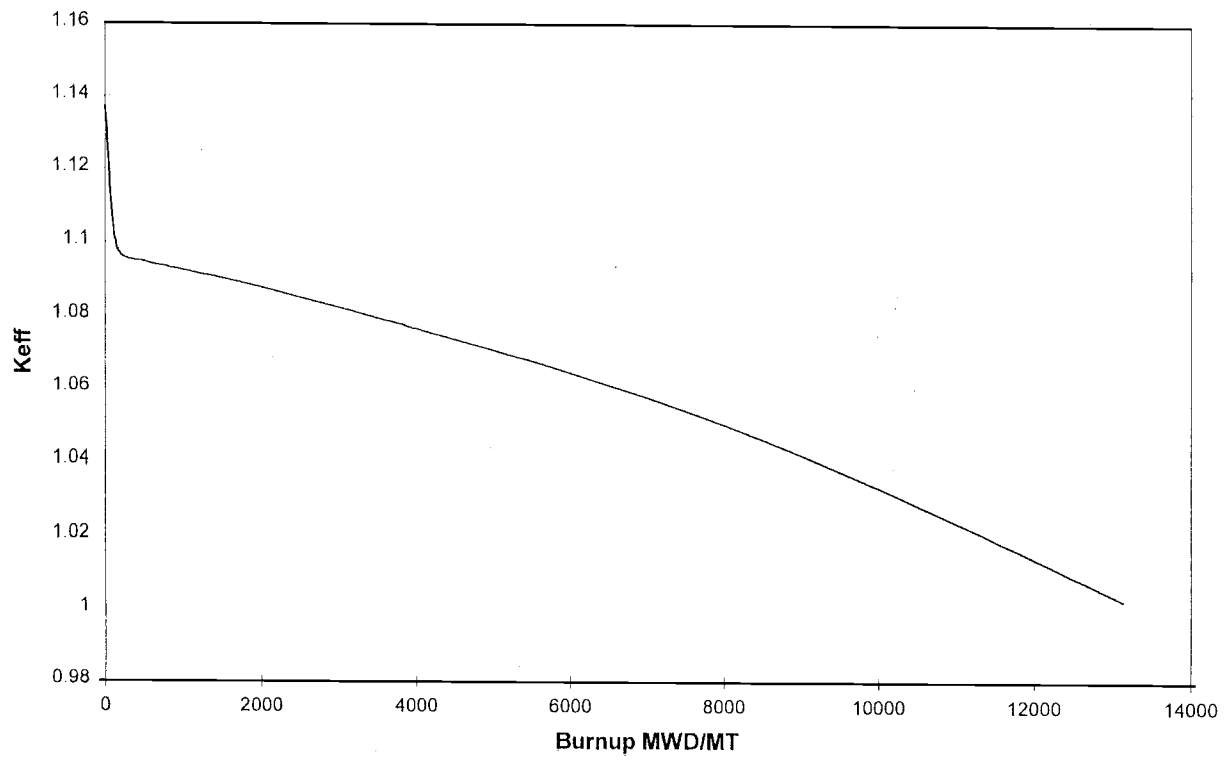


FIG. 2.

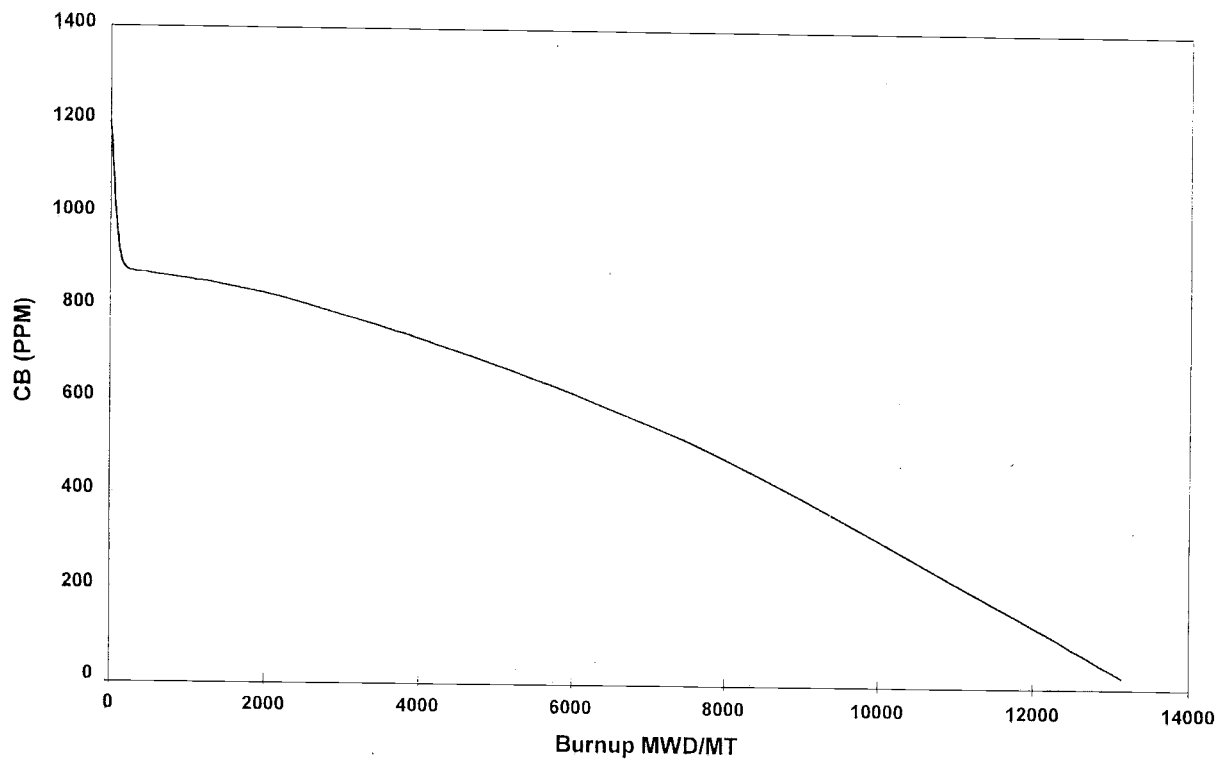


FIG. 3.

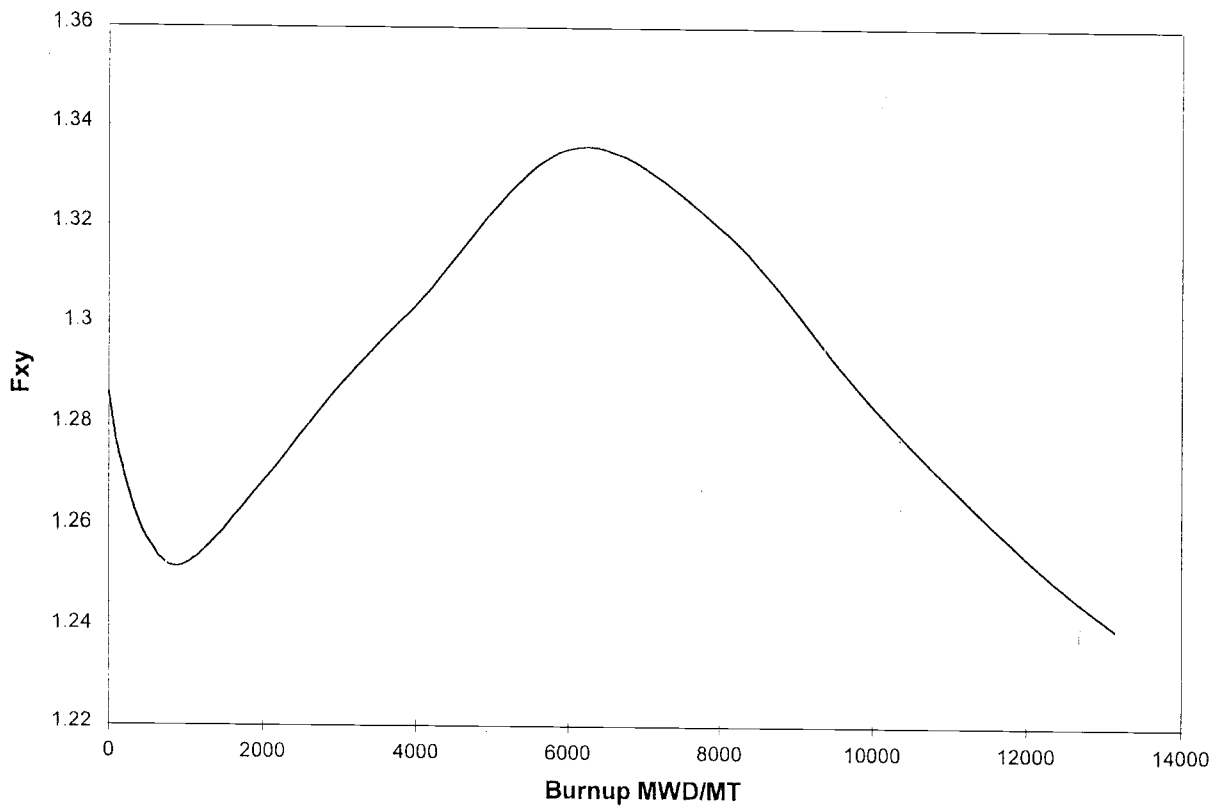


FIG. 4.

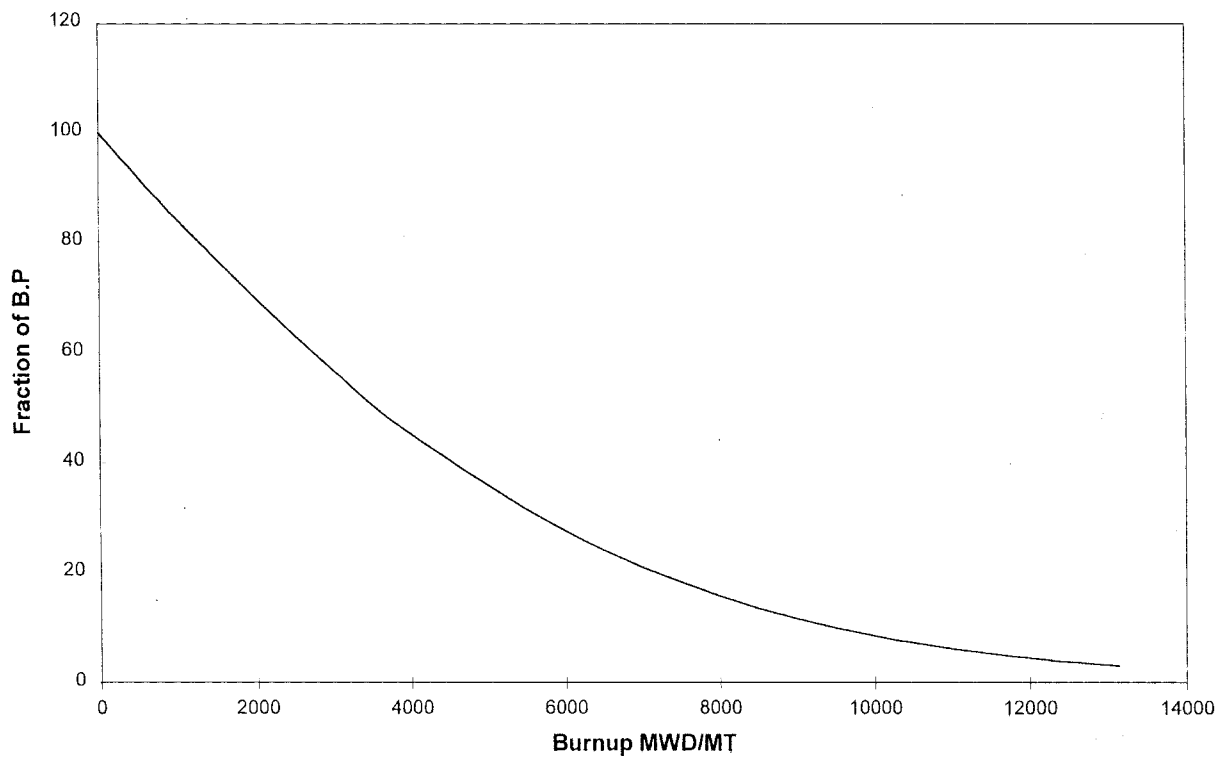


FIG. 5.

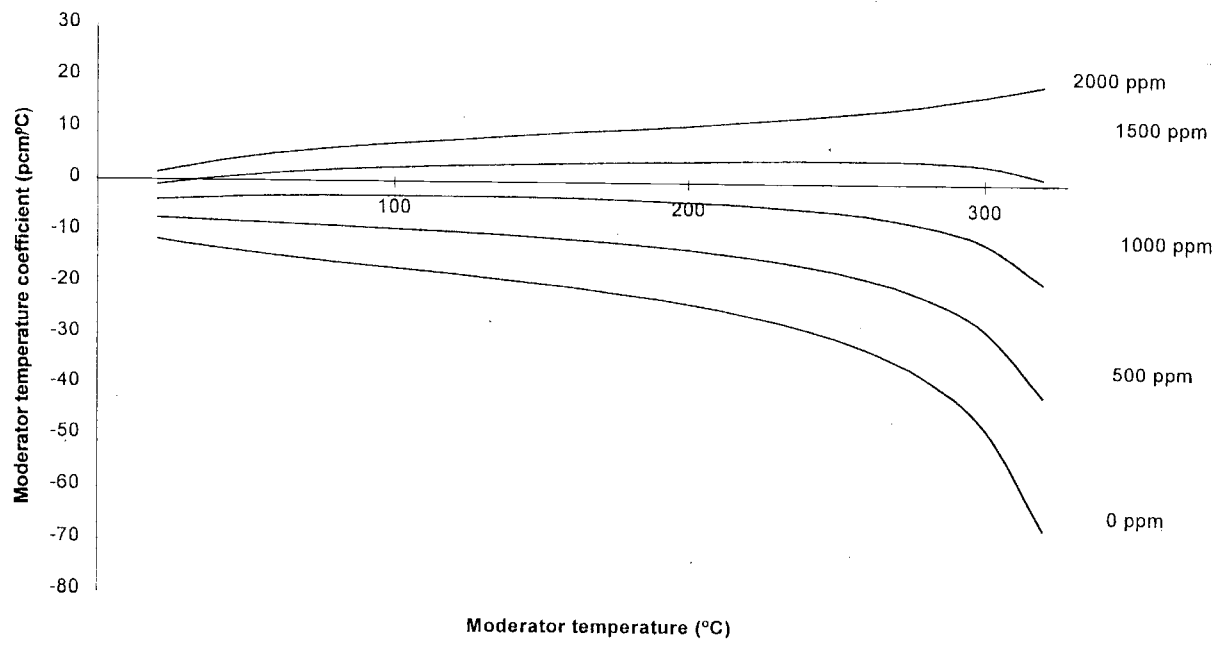


FIG. 6.

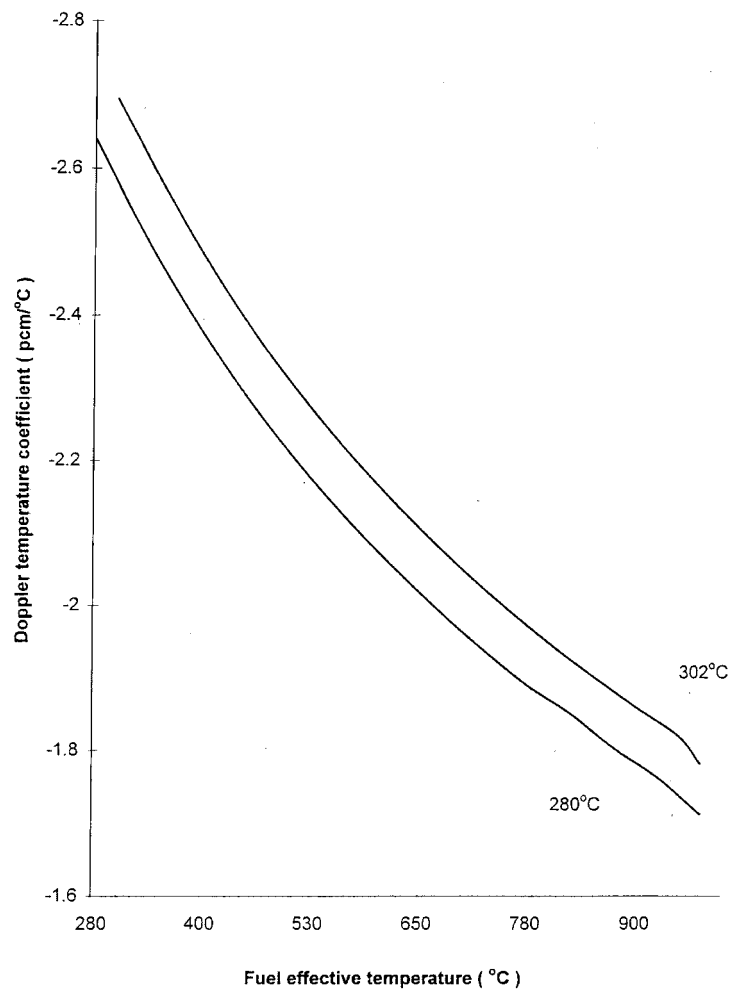


FIG. 7.

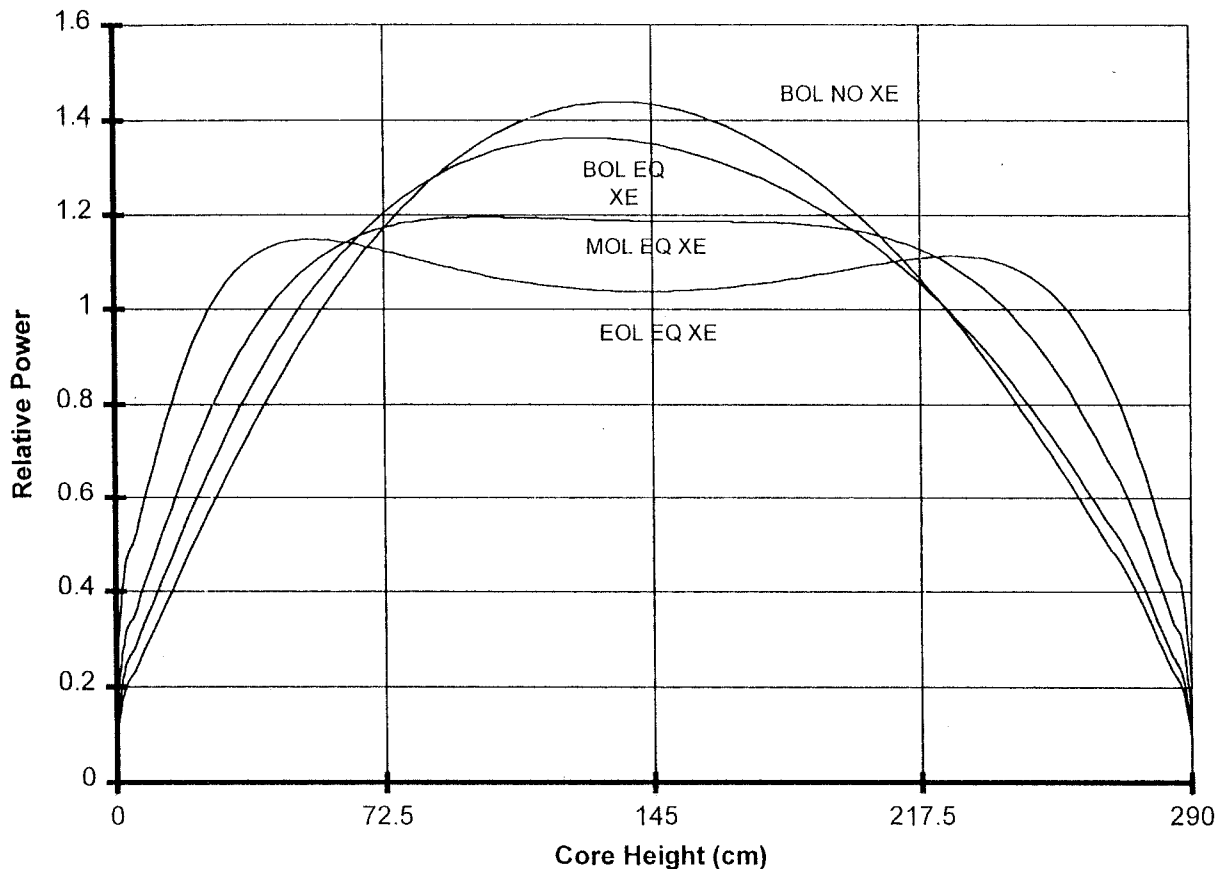


FIG. 8.

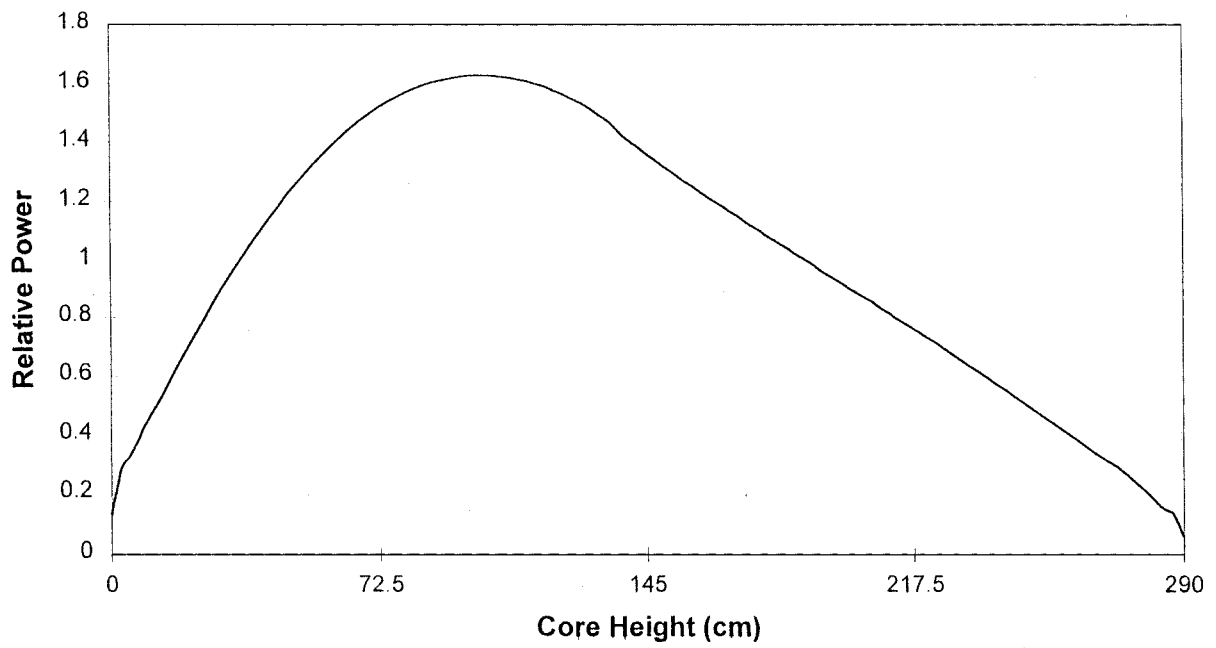


FIG. 9.

## REFERENCES

- [1] IAEA Safety Series No. 50-CD IAEA Safety Standards.
- [2] IAEA Safety Series No. 50-SG-D14 IAEA Safety Standards.
- [3] Chashma Nuclear Power Plant PSAR Chapter 4.
- [4] Nuclear Design Report for CHASNUPP.

# Overview of the SEU project for extended burnup at the Atucha-I NPP. Four years of operating experience

**J.M. Fink, M. Higa, R. Pérez, J. Piñeyro, J. Sidelnik**  
Nucleoeléctrica Argentina S.A. Argentina

**J.A. Casario, L. Alvarez**  
Comisión Nacional de Energía Atómica,  
Buenos Aires, Argentina

**Abstract.** Atucha I is a 357 MWe nuclear station moderated and cooled with heavy water, of German design located in Argentina. Fuelling is on-power and the plant was originally fuelled with natural uranium. To reduce fuel costs a program was initiated in August 1993 to introduce gradually slightly enriched uranium (SEU) fuel (0.85 w% U235) with an associated burnup increase from 5900 MWd/tU to 11300 MWd/tU. The introduction of SEU fuel started in January 1995 and the program was divided in three Phases with an upper limit of SEU FA in the core: 12, 60 and 252 (full core) and licensing documentation was prepared for each Phase. This paper describes the most important aspects of the operating and project experience, and some factors limiting the burnup extension from an operation point of view. After four years of the program and with 181 SEU FA (71%) of the core, the operating experience has been good and without unfavourable effects due to the use of SEU fuel with the only exception of a small increase of the time to reach full power in plant startups or power cycling. In particular, the new criteria to prevent PCI failures in power ramps for higher burnup SEU fuel in refueling operations, plant startups or power cycling has been effective. The average discharge burnup of the SEU fuel taken out of the reactor in 1998 was 11263 MWd/tU. The average discharge burnup of the natural fuel in the same year was 6640 MWd/tU, with an increase of about 12% of the original value for a natural fuel core. The average number of fresh fuel assemblies per full power day was being reduced from 1.31 to 0.92 in 1998 and 0.83 in 1999. The fuel costs dropped gradually during the program from 9.38 (with natural uranium fuel) to 6.57 \$/MWh in the first four months of 1999 (taking as reference the NU and SEU FA costs for 1999). Because of this the SEU program has been an important contribution to the reduction of Atucha I operating costs and to the competitiveness of nuclear power generation against other sources of generation in a deregulated electrical market in Argentina. It is planned to explore in the future the feasibility to increase the enrichment to 0.9 w% with an estimated burnup increase to 13000 MWd/tU, but this is probably the upper limit that the design of Atucha I permits.

## 1. INTRODUCTION

Atucha I is a 357 Mwe (gross) nuclear station, pressure vessel type designed by Siemens (Germany), moderated and cooled with heavy water, located 120 km NW of Buenos Aires. Fuel assemblies (FA) were originally 36 active natural UO<sub>2</sub> (NU) rod vertical clusters, 5.3 meters long. Fuelling is on power. Average FA discharge burnup for NU fuel was  $\approx$  5900 MWd/tU and maximum rod burnup (m.r.b)  $\approx$  8400 MWd/tU. With the objective of reducing the fuel costs a program of utilization of slightly enriched uranium (SEU) (0.85 w% U235) fuel was initiated in 1993 and the introduction of SEU fuel started at the beginning of 1995.

The introduction of SEU fuel was gradual and the Project was divided in different Phases. At the present time 181 fuel channels (72 % of the core) are loaded with SEU fuel and it is planned to reach a full SEU core next year. The operating experience, the fuel performance, and the impact on fuel consumption and fuel costs has been good and the use of SEU fuel proved to be an effective tool to reduce operating costs.

This paper presents a general description of the Atucha I SEU Project activities and the operation experience in the four years of the program and will be mainly oriented to fuel management and operating experience. Activities related with fuel design improvements and fuel performance results will be treated in more detail in another paper of this Technical Committee Meeting [1]

## 2. BRIEF DESCRIPTION OF THE ATUCHA-I REACTOR

Atucha I is the first nuclear station in Argentina and started operation in 1974. It has a gross electrical power of 357 MW and a thermal power of 1179 MW. The reactor core has 252 vertical coolant channels, which contain the FA and separate the coolant from the moderator. The average coolant temperature is 280°C and the average moderator temperature is 200°C. A section of the core can be seen in fig.1.

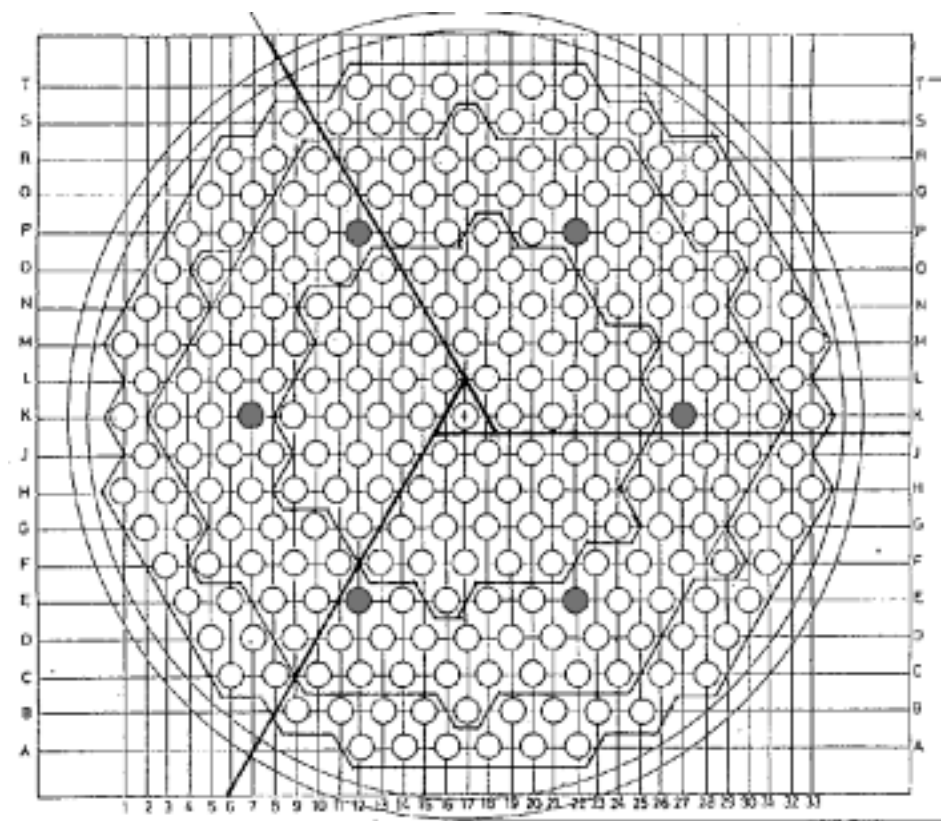


*FIG. 1 Section of the Atucha I core indicating the fuel channels, and the burnup zones for natural uranium fuel. The six channels selected for the introduction of the first fresh SEU FA are also shown*

Power regulation is made through six absorber rods, three made of hafnium, usually called black, and three made of steel, called gray. They normally have an insertion corresponding to an excess reactivity of 6.5 mk in normal operation. Additional 21 hafnium rods are used for shutdown purposes. Power measurements for the regulation, are obtained with four out of core compensated ion-chambers.

The fuel movement scheme is radial. For natural uranium the core was divided in three approximately concentric annular regions (see fig.1). The fresh fuel is introduced in the intermediate zone, left there until it reaches ~2700 MWd/tU, later transferred to the central zone until it reaches ~5100 MWd/tU, then moved to the outer zone, from which it is taken out at ~5900 MWd/tU. In some cases the fuel is moved through four positions instead of three to reduce power ramps.

The coolant flow in the fuel channels is reduced from the center to the periphery of the core according to the channel powers, in such a way as to have approximately constant outlet channel temperatures. The temperature increase in the channels at full power is about 35 °C. No coolant boiling is allowed at the channel outlets. To obtain that there are 8 "hydraulic regions" with different nozzles, numbered 1 to 8, from the periphery to the center. To keep an adequate margin to outlet boiling, channel power limits are defined for each hydraulic region. The reactor has outlet temperature measurements in 28 channels, and 48 in-core vanadium flux detectors give indications of local flux to the operators.

### 3. ECONOMIC INCENTIVES OF USING SEU FUEL IN ATUCHA I

It is well known that in heavy water reactors, initially designed for natural uranium fuel, a slight increase in enrichment from 0.711 w% U235 to values from 0.85 to 1.2 % has a strong improvement in fuel discharge burnup and fuel economy. These advantages have been presented in many reports both for Siemens pressure vessel type and CANDU type heavy water reactors (see for example [2] to [4]). In Germany there was a similar program about 20 years ago with the 50 MWe MZFR reactor in which the fuel, originally NU, had a first transition to 0.85 % enrichment and then a further transition to 1 %.

In Argentina the Atucha-I fuel is manufactured by CONUAR, an Argentine Company and because of the type of design, assembly, dimensions and small scale its fabrication cost is high compared with other reactors of natural uranium and heavy water. For that reason any improvement in the extension of the life of the fuel in the reactor has an important economic impact in the unit energy cost.

Basically the main advantages of using SEU fuel (comparing an equilibrium full NU core with an equilibrium full SEU core), are reflected in four areas:

- a) An increase of the fuel discharge burnup from 5900 MWd/kg U to 11300 MWd/kg U,
- b) A reduction of the new fuel loading requirements from 1.31 to 0.7 FA per full power day (fpd),
- c) A reduction of about 39 % fuel cycle cost if we take as a reference the costs for NU and SEU fuel in 1998 and 1999,
- d) A reduction of the spent fuel volume of about 42 %, which extends the useful life of the spent fuel pools and represent a positive contribution to environment protection..

#### **3.1. Reduction of Fuel Assemblies Required per Year**

The reduction of new fuel requirements per fpd with SEU fuel reduces the yearly FA requirement from 430 to 230 (assuming a load factor of 0.9). This also means an important decrease of fueling machine use.

### 3.2. Reduction in the Unit Energy Cost

The reduction of the number of FA required per year, implies a corresponding decrease in yearly fuel expenses. With natural uranium fuel, the component of the unit energy cost due to fuel was 9.38 U\$\$/MWh. Considering these factors the fuel cost when the full SEU equilibrium core is reached is estimated at 5.70 U\$\$/MWh, a reduction of about 39% (for this cost comparisons 1999 costs for NU and SEU FA were used).

### 3.3. Reduction in the Spent Fuel Volume

The reduction in the consumption of FA implies a decrease in the irradiated fuel volume of about 45 %. Although detailed calculations of final spent fuel storage costs have not been done, if values of 100 U\$\$/kg U given for CANDU fuel in [5], are used as a lower bound, we obtain estimated minimum annual savings of about 2.8 MU\$\$ for this concept.

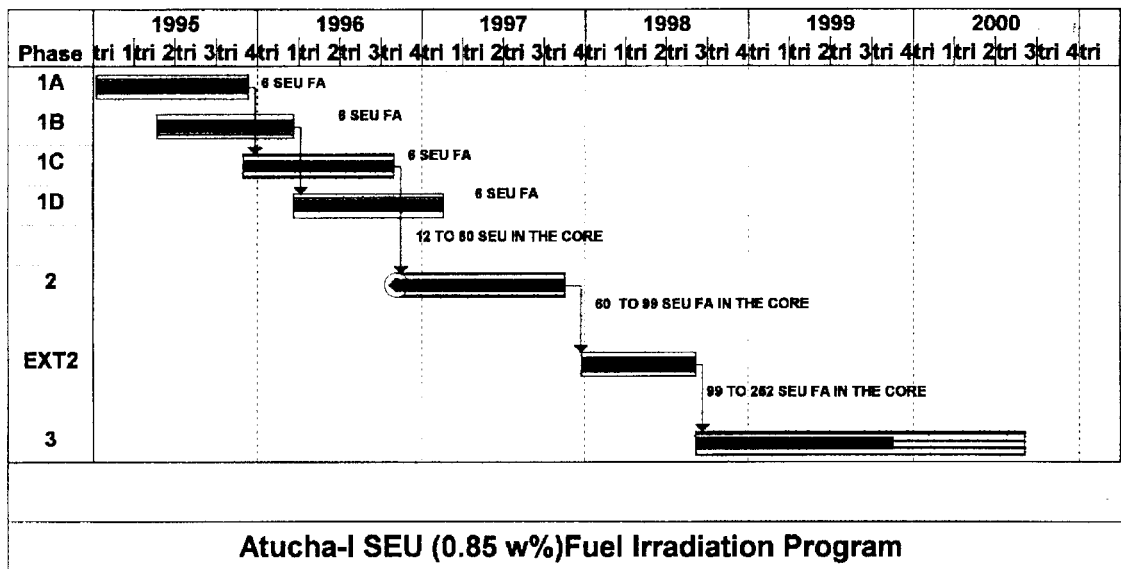


FIG. 2: Different Phases of the Atucha I SEU Fuel Program

## 4. PROGRAM OF INTRODUCTION OF SEU FUEL

Different activities related to the use of SEU fuel, mainly reactor physics and economics calculations, have been carried out in Argentina in the late seventies and eighties without a concrete irradiation program. In August 1993, a SEU Project for Atucha I was created. The program was divided in different Phases with an increasing upper limit of SEU FA in the core. Licensing documentation and authorizations from the Nuclear Regulatory Authority were also associated with each Phase. At the beginning of the Project the Quality Assurance Manual and Procedures were prepared, and also a qualified Independent Revision Group was established for the Project. During 1993 and 1994 the Safety Report for the First Phase was prepared and completed in November 1994. The phases of the irradiation program are shown in figure 2.

Phase 1 consisted in the introduction of SEU FA not exceeding twelve at any time in the core. It began in January 1995 and ended in November 1996. Phase 2 was initially defined as the transition period from 12 to 60, but was later extended to 99. Phase 3, from 100 to full core, was initiated in September 1998 and it is expected to reach the full SEU core in the year 2000. The initial average discharge burnup was set at 10000 MWd/tU.

During Phase 1, the fresh SEU FA were introduced in six predetermined channels (shown in fig.1) selected because they have the following convenient features: A larger margin to the channel power limits which is important to accommodate the higher power increase when introducing fresh SEU fuel. The channel power is relatively high, which reduces the irradiation time, until the FA is transferred to another position. They have outlet channel temperature measurements and five out of the six had in-core detectors in the vicinity. This allows taking measurements of outlet temperatures and in-core detectors to compare with calculations.

The main objectives of the Phase 1 of the irradiation program were:

- a) to verify the performance of the SEU fuel in the core with discharge burnups close to the values expected for the equilibrium full SEU core. In particular, to verify the behavior in power ramps arising in refueling operations, reactor power increases, and startups from low power,
- b) to verify predictions of neutronic calculations like reactivity gain, channel power increase and detector flux increase when introducing SEU fresh FA,
- c) to test operating procedures developed for SEU fuel,

In Phases 2 and 3, the average discharge burnup of the SEU fuel was increased to 11000 MWd/tU, and the maximum average burnup of the bundles located in the center of the core at 10000 MWd/tU.

The main objectives for Phases 2 and 3 were :

- d) to verify the performance of the SEU fuel in the core with exit burnups and burnups at which they are moved from one channel to another in the core similar to the corresponding ones for the full SEU core,
- e) to verify the global behavior of the core with a larger proportion of SEU fuel,
- f) to prepare the location of SEU FA in the core for the transition to a full SEU core.

## 5. FUEL DESCRIPTION AND IMPROVEMENTS IN THE FUEL DESIGN

FA for Atucha-I consist of 36 fuel rods with natural UO<sub>2</sub> pellets and one supporting tube in the outer ring. Fuel rods are set in their positions by solid spacer grids.

Several changes have been introduced to the design of the fuel rod to use UO<sub>2</sub> pellet with SEU. A more detailed description of the fuel design and the improvements developed for SEU fuel can be found in [1].

## 6. FUEL MANAGEMENT

### 6.1. Reactor Physics and Fuel Management Studies

The reactor physics studies were done with the British lattice code WIMS-D4 [6], and the 3D reactor code PUMA [7], developed in Argentina, and presently used for the fuel management calculations of the Atucha-I and Embalse operating stations.

Fuel management studies were done in two steps. The first step was with "time-average" type calculations for a given fuel movement strategy, which give the burnups at which the fuel is moved from one region to another and the discharge burnup and also provides time averages of the flux and power distributions. It does not give fluctuations due to refueling operations. These types of studies are later completed and confirmed with detailed refueling simulations for 6-12 months which permit to make final adjustments.

In Phase 1 (up to 12 SEU FA in the core) the situation can be considered as a relatively small perturbation of the natural uranium core, except for the larger channel powers in the six channels where the fresh SEU FA are introduced.

Before the beginning of Phase 2, "time average" studies for configurations with 12, 30, 60 have been completed. A detailed simulation of 1 full power year was done for the transition period from 12 to 60 SEU FA in the core to verify channel and bundle power limits, and that PCI prevention criteria were met.

To develop the fuel movement strategy for the transition and equilibrium core, it was decided not to modify the nozzles that regulate the coolant flow in the channels that were defined for the power distribution of the natural uranium original fuelling strategy, but rather adjust the burnup zones and fuel movement in such a way that channel power limits could be respected and PCI prevention criteria could be respected.

Later, the efforts were directed to develop the fuel strategy for the full SEU core, first with time average calculations and later confirmed with a detailed simulation of 702 fpd for the transition period from 60 to 252 SEU FA in the core, and continued for the full SEU core up to 803 fpd. This work was done in a very close and fruitful interaction between the Headquarters Physics Group and the Fuel Engineers at the plant. In general, the original idea of introducing fresh fuel in intermediate regions, moving them later to more central regions, and then to the periphery for the last part of the irradiation period was maintained. However in some regions it was found necessary to combine SEU fuel with high and low burnups to avoid local channel power peaking. This fuelling strategy has been applied at the plant during the transition 60 to 181 FA in the core with good results.

These studies confirmed the fuel strategy but provided other results like a) data to estimate the NU and SEU fuel requirements for the following year, which has to be made almost a year in advance. b) Fuel power and burnup histories representative of the transition. c) A decreasing trend of the reactor maximum linear power with the proportion of SEU fuel in the core due to a larger axial flattening of the power distribution.

## 7. LICENSING ASPECTS

For the safety studies complete revisions of the Safety Report (SR) were prepared for each Phase of the Project and were revised by the Independent Revision Group of the Project. Besides, and following the Procedure for Design Changes Related to Safety, they were reviewed by the Internal Safety Committee of Atucha I (that makes recommendations to the Atucha I Manager) and by the Technical Revision Committee (that makes recommendations to the General Manager of NASA) and submitted to the Nuclear Regulatory Authority

## 8. OPERATING EXPERIENCE

### 8.1. Phase 1

The irradiation of SEU fuel at the plant started in January 1995, with the introduction of six SEU FA in the six pre-selected channels described before in the period from the 9th to the 31st. During each introduction, relevant operating data like control rod positions, inlet heat transport system temperatures, outlet heat transport temperatures at the six channels, in-core detectors, etc, were collected. Between May 22nd to June 26th, the first six FA were moved to the central region of the reactor, and another set of 6 fresh SEU FA was inserted. Between October 30th and December 5th, a third group of 6 fresh SEU FA was introduced, and the first group of six taken out of the reactor with an average discharge burnup of about 10 MWd/kgU.

The first SEU fuel assemblies remained in the channel they entered the core until they reached an average burnup of 5.5 to 6 MWd/kgU, and were later moved to the central region, where they remained until the average burnup reached  $\approx 8.0$  MWd/kgU. From there they were transferred to the outer region until they reached 10 MWd/kgU.

The core reactivity gain when introducing fresh SEU fuel was about 0.7 mk (compared with about 0.35 mk for natural fuel), while the channel power increase was about 15 - 20 % (compared with a very small change for natural fuel).

#### *8.1.1. Comparison between Calculations and Measurements of Relevant Parameters*

The data was used for comparisons with neutronic calculations, similar to the ones used for design and fuel management using WIMS-D4 and PUMA. In particular, the relative increase in  $\Delta T$  in the channels with the SEU fuelling was compared to the relative increase of the calculated channel power (Atucha I has no coolant boiling at the outlet of the channels), and the increase in the vanadium detector readings close to the refueled channels were compared with calculated values. The consistency of the calculated and measured reactivity change due to the SEU refuelling was done comparing the calculated core reactivity before and after the refuelling with the corresponding rod positions in each case, which should be the same.

The agreement was good and in most of the cases within the uncertainty of the measurement errors.

### 8.1.2. Fuel Performance

The performance of the 18 SEU FA during the irradiation period was good, without any indication of failures.

After the first 6 SEU FA that completed their cycle were taken out of the core, examinations and measurements were performed showing no abnormalities and that the elongation of the fuel rods was within the expectations considering the larger fuel burnup.

## 8.2. Present Operating Experience (Phases 2 and 3)

### 8.2.1. General Aspects

In 1999 the plant reached 181 SEU FA in the core (71.8 % of the total of 252) with 125 irradiated SEU FA. The operation of the plant was satisfactory. The maximum linear power shows the decreasing trend (about 6 %) anticipated by the fuel management studies. The larger reactivity increase per refueling with SEU fuel makes it easier to normalize operating situations with low reactivity reserve, than when using NU fuel.

### 8.2.2. Effects of the SEU Fuel on the Plant Fuel Consumption

The average consumption of fuel assemblies per full power day showed a decreasing trend since the beginning of the program. During 1993 and 1994 the average fuel consumption with natural uranium fuel per day (fpd) was 1.31 FA/fpd. In 1995 during Phase 1 of the Program the average fuel consumption was decreased to 1.22 FA/ fpd. In 1996, most of the year still in Phase 1, it was 1.23. In 1997 dropped to 1.12 in Phase 2. In 1998 dropped to 0.92 and in the first four months of 1999 to 0.83 getting closer to the value of 0.7 anticipated to the homogeneous SEU core. It is interesting to remark that, during the program the discharge burnup of the natural uranium bundles showed an increase due to the positive contribution to the core reactivity of the SEU FA with a burnup distribution biased toward the fresh side, an effect that had been anticipated before. In 1998 for example it was 6640 MWd/tU, about 12 % more than with a pure natural uranium core.

Table 1. Actual Consumption of Natural and SEU Fuel In Atucha-I during The SEU Fuel Project

YEAR	Energy Produced (FPD)	New NU F.A. Loaded	New SEU F.A. Loaded	F.A. Loaded Total	F.A./FPD	Fuel Cost (U\$/MWh)	Relative Saving vs. NU Fuel
1994 (NU)	313.6	410	0	410	1.308	9.377	0.0%
1995	339.0	394	18	412	1.215	8.767	6.5%
1996	266.3	308	20	328	1.232	8.906	5.0%
1997	341.5	325	59	384	1.124	8.231	12.2%
1998	295.5	139	133	272	0.920	7.036	25.0%
Jan-Apr 1999	120.4	24	76	100	0.831	6.567	30.0%
SEU Core	328.5	0	230.0	0	0.7	5.697	39.2%

Note: Fuel costs are calculated using 1998 and 1999 NU and SEU FA unit cost

### *8.2.3. Effects on Fuel Costs*

The fuel cycle costs (front end), as can be seen in table 1, dropped gradually during the program from 9.38 (with natural uranium fuel) to 6.57 \$/MWh in the first four months of 1999, approaching the value of 5.70 \$/MWh for the homogeneous SEU core.(taking as reference the NU and SEU FA costs for 1999). One interesting thing to remark is that the average consumption of FA per fpd or the cost reductions are associated with the fraction of SEU fuel in the fuel loaded (not the fraction of SEU fuel in the core) so the full benefits are achieved when the loading of NU fuel ends. That occurs about 6 months earlier than achieving a full SEU core.

### *8.2.4. Prevention of PCI Failures*

The existing PCI prevention criteria were developed for natural uranium fuel and were based on estimations of maximum core linear power based on the readings of in-core detectors. For SEU fuel new criteria were developed for fuel of higher burnup based on the verification of the final linear powers and change in linear powers for all the fuel assemblies in the core using data files with burnups and linear powers from the fuel management calculations. These revised criteria was applied to power ramps arising during operation as a result of fuel movements, reactor power increases, and associated control rod movement and as a result of them the time to reach full power in a plant startup was increased from 28 to 35 hours. The overall experience with the new criteria seems good as no fuel failures due to PCI were observed with 125 irradiated SEU FA.

### *8.2.5. Data Bases with Fuel Burnup and Linear Power Histories*

Using results from the plant fuel management calculations a database with local linear powers and local burnups for all the SEU FA that have been irradiated in the program was prepared and is maintained. This data is useful to generate burnup and linear power histories during the permanence of the SEU FA in the reactor for fuel performance evaluation purposes.

### *8.2.6. Plans to Explore the Feasibility of Increasing the Enrichment to 0.9 %*

Given the good operating experience with 0.85 w% SEU fuel, it is planned to explore in the future the feasibility to increase the enrichment to 0.9 w%, extending the fuel burnup to about 13000 MWd/tU. However, it is considered that, due to channel power limits in the hydraulic zones, this is probably the limit that can be reached without changing the core channel flow restrictions.

## 9. CONCLUSIONS

In January 1995, a gradual program to irradiate SEU fuel in the Atucha I nuclear station was started. At the present time, about four years later the operating experience and economic benefits of the SEU program have been good and it can be considered an effective tool to reduce fuel and operating costs at this plant.

The main aspects to remark are:

- a) The operation of the plant, with 181 SEU FA (72 % of the core channels) showed no abnormalities attributable to the use of SEU fuel. The only adverse effect was a small increment of the time to reach full power from a hot shutdown condition or in power cycles due to PCI prevention criteria for higher burnup SEU fuel. It is expected to reach a full SEU core next year;
- b) The fuel consumption of about 1.31 FA/ fpd. with natural uranium was gradually reduced to 0.92 FA/ fpd. in 1998 and 0.83 in the first four months of 1999, getting closer to the value of 0.7 predicted for a full SEU core. The average discharge burnup of the SEU FA in 1998 was 11263 MWd/tU, and the corresponding value for the NU FA was 6640 MWd/tU (about 12% more than in a full NU core);
- c) The front end fuel cycle cost dropped from 9.38 to 7.04 in 1998 and 6.57 \$/MWh in the first four months of 1999, taking as reference the NU and SEU unit FA costs for 1998 and 1999;
- d) At the present time 125 SEU fuel have been taken out of the reactor. With the exception of two isolated cases of failures in FA manufactured in 1997, that are attributed to fabrication causes, the performance of the SEU fuel has been good, particularly with respect to the power ramps that occur in fuelling operations, reactor startups or power cycling. This indicates that the design improvements and PCI prevention criteria developed for SEU fuel seem to be adequate;
- e) The comparison of calculated channel power variations, reactivity increases and detector reading changes with measured values with the introduction of fresh SEU fuel at the beginning of the program showed good agreement.

## **ACKNOWLEDGEMENTS**

The authors are grateful to many individuals of NASA and CNEA that have collaborated in different areas of this Project. In particular, to R.Corcuera for the technical revision of the licensing and technical documentation, to C.Carloni and Y.Simkin for the assistance in documentation and Q.A. aspects of the Project. Also to F.Bassarsky for collaboration with reactor physics calculations and the preparation of the fuel burnups and linear powers database, and to B. Cantalupo for the efficient assistance in preparing technical and licensing documentation.

## **REFERENCES**

- [1] L. A. ALVAREZ et al. Extended Burnup with SEU Fuel in Atucha-I NPP. Paper Presented at this Technical Committee Meeting.
- [2] FRISCHENGRUBER, K., DUSCH, F., Development Potential of Power Reactor Types and Fuel Cycles in KWU type PHWR's. Proceedings of a Technical Committee Meeting, and Workshop on Advanced Light and Heavy Water, Reactor Technology. IAEA - TECDOC - 344. 1985.
- [3] BOCZAR, P.G., et al., Slightly Enriched Uranium in Canada. An Economic First Step towards Advanced Fuel Cycles. Proceedings of a Conference on Nuclear Power Performance and Safety. IAEA Vienna, September 18th to October 2<sup>nd</sup>, 1987.

- [4] BOCZAR, P.G., Benefits from the Use of Slightly Enriched Uranium Fuel In Operating CANDU Reactors. Paper presented at this Technical Committee Meeting. Water Reactor Extended Burnup Study. IAEA Technical Report Series 343. IAEA, Vienna, 1992.
- [5] HALSALL, M.J. A Summary of WIMS-D/4 Input Options. AEEW-M1327 (1980).
- [6] GRANT, C. PUMA, Sistema para la simulación del funcionamiento de reactores nucleares. (PUMA, System for the Simulation of the Operation of Nuclear Reactors). Internal Report CNEA-Re 163, 1980.

# Extended burnup with SEU fuel in Atucha-1 NPP

L. Alvarez (\*), J. Casario (\*),  
Comisión Nacional de Energía Atómica

J. Fink, R. Pérez, M. Higa  
Nucleoeléctrica Argentina S. A.

Buenos Aires, Argentina

## Abstract

Atucha-1 is a Pressurized Heavy Water Reactor originally fuelled with natural uranium. Fuel Assemblies consist of 36 fuel rods and the active length is 5300 mm. The total length of the fuel assembly is about 6 m. The average discharge burnup of natural  $\text{UO}_2$  fuel is 5900 MWd/tU. After the deregulation of the Argentine electricity market there was an important incentive to reduce the impact of fuel cost on the cost of generation. To keep the competitiveness of the nuclear energy against another sources of electricity it was necessary to reduce the cost of the nuclear fuel. With this objective a program to introduce SEU (0.85 %  $^{235}\text{U}$ ) fuel in Atucha-1 was launched in 1993. As a result of this program the average SEU fuel discharge burnup increased to more than 11000 MWd/tU. The first SEU fuels were introduced in Atucha-1 in 1995 and, in the present stage of the program, 71% of core positions are loaded with this type of fuel. This paper describes key aspects of Atucha-1 fuel design and their relevance limiting the burnup extension and shows relevant data regarding the SEU in-reactor performance. At the present time 125 SEU Fuel Assemblies have been irradiated without failures associated with the extended burnup or unfavorable influences on the operation of the power station.

## 1 Burnup extension using SEU fuel

Pressurized Heavy Water Reactors (PHWR) were initially designed for using natural uranium. It was recognized in many papers that a small increase in the enrichment of the fuel produces a significant extension of the discharge burnup and therefore an important improvement in the economy of the fuel cycle.

The advantages of using Slightly Enriched Uranium (SEU) have been reported for pressure vessel heavy water reactors and also for CANDU pressure tube heavy water reactors [1][2][3]. As an example, in Atucha-1, one of the Argentine Nuclear Generating Stations, a 20 % increase on the degree of enrichment produces an increase in the average discharge burnup of about 90 %. The typical burnup for Atucha-1 natural fuel is 5900 MWd/tU. Using 0.85 %  $^{235}\text{U}$  slightly enriched uranium, the average discharge burnup of the fuel assemblies is close to 11500 MWd/tU.

In absolute values this extended burnup is not significant comparing with typical burnups for PWR fuels. But in relative terms the almost 100 % increase clearly shows the relevance of using SEU and justifies the challenges related with this modification in the design of the fuel.

## 2 Brief description of the SEU Project for Atucha-1

A project to extend the fuel discharge burnup in Atucha-1 was initiated in 1993 and the first SEU fuels were loaded in January 1995 [4]. An extensive description of the project is reported in [5].

The advantages from using SEU fuel with extended burnup in Atucha-1 are:

- Reduction of the cost of generation
- Reduction of spent fuel volume
- Reduction of on-power refueling frequency

An additional benefit from using SEU is the increase in the discharge burnup of natural uranium fuel during the transition to a full SEU core. Other advantage might be the reloading of spent natural uranium fuel assemblies currently stored in pools to extend their original (low) discharge burnup.

The program to introduce SEU fuel in Atucha-1 was divided in three stages. During the first stage that started in January 1995, 12 demonstration SEU FA were loaded. The second stage was the transition from 12 to 99 FA. The third stage will be concluded in 2000 – 2001 with the whole core loaded with SEU fuel. At the present 125 FA have completed their irradiation in Atucha-1 and 181 core positions (72 %) are fuelled with SEU fuel.

### 3 The Fuel Assembly for Atucha-1

The fuel assembly for Atucha-1 is a single 36 fuel rods bundle with an overall length of about 6 m. Fuel rods are in a circular array with three concentric rings and one central fuel rod. A structural tube occupies one position in the outer ring. The fuel rods are kept in their positions using Zircaloy solid spacer grids. Fuel claddings are free standing. Bearing pads welded to the outer surface of the sheaths provide the interaction with the spacer grids. Sliding shoes attached to the spacer grids and to the structural tube are used to set the assembly position in the coolant channel. The fuel rods and the supporting tube are hanging from an upper tie plate which is also made of Zircaloy. The bundle fixation at the lower end of the fuel assembly is increased with an additional spring-loaded sliding shoe attached to the lowest spacer grid. It assures proper radial positioning of the bundle end inside the coolant channel even under unfavorable coolant conditions. For neutron economy practically only Zircaloy was used as structural material in the active region. **Figure 1** represents a schematic description of the Atucha-1 fuel assembly.

The internal designs of Atucha-1 and LWR fuel rods are very similar. Each Atucha-1 fuel rod has a 5300 mm long stack of UO<sub>2</sub> pellets, isolating pellets, a gas plenum and a compression spring. The plenum and the spring are in the upper end of the rod. End plugs are welded by tungsten inert gas (TIG) process. The Zircaloy-4 fuel cladding is free-standing (non-collapsible). Fuel rods are pressurized during manufacturing with helium gas at 17 bar. In the outer surface resistance welded wearing pads reduce the risk for fuel rod defects by fretting, facilitate the assembling procedure and are also used in certain outer fuel rods for the axial positioning of the spacers grids. **Figure 2** shows schematically a typical Atucha-1 fuel rod and **Table 1** shows relevant data of both, the fuel assembly and the fuel rod

### 4 Limitations for Atucha-1 fuel burnup extension

The fuel for Atucha-1 was originally designed for a discharge burnup of almost 6000 MWd/tU. At the extended burnup typical for SEU fuel additional constraints are placed upon fuel performance.

In the new boundary conditions the main changes affect the following aspects: burnup discharge, residence time, local burnup at the time of fuel reshuffling (power ramps) and

maximum burnup at high power. Power levels, water chemistry and sheath and coolant temperatures almost remain the same that those for natural uranium.

Therefore the relevant aspects in Atucha-1 fuel performance to be analyzed are mainly those affected by the higher burnup and by the increase in the residence time. Among them can be mentioned:

- Fission gas release and its impact on internal gas pressure
- Fuel cladding creep down and sheath strain
- Relative length changes between the fuel stack and the cladding
- Fuel cladding axial growing
- Fuel assembly structural integrity, including the effectiveness of the interactions between fuel rods and spacer grids and between elastic sliding shoes and coolant channel to hold fuel rods and fuel assemblies in their positions through the whole irradiation.
- Power ramp behavior
- Waterside corrosion and deuterium uptake

## **5 Design analysis and modifications**

The design analysis of the Atucha-1 SEU fuel was performed with the aim of satisfying three key considerations:

- Atucha-1 fuel performance should not be adversely affected.
- Safety margins for SEU fuel should be kept as close as possible to the margins for natural fuel.
- The reduction of the operational flexibility at the power plant must be as low as possible.

Several changes have been introduced in the design of both, the fuel rod and the fuel assembly to optimize them for SEU requirements:

- The plenum length was increased to provide more volume for gas release.
- Bearing pads with longer contact surfaces were adopted to assure reliable interaction between spacers and fuel rods during the whole life of the fuel.
- The ductility of the cladding material was increased to reduce the fuel rod susceptibility to PCI failures on power ramps.
- Regarding the fuel assembly structural design, Inconel 718 was used to replace the original material for spring-loaded sliding shoes (SS A286) to compensate the higher relaxation produced by the increase in neutron fluence. In addition to its superior spring characteristics Inconel was chosen because of its good resistance against stress relaxation, providing similar safety margin for fuel assembly holding in position that in natural uranium fuel. The effect of this modification on the neutron economy is practically negligible.

## **6 Design verifications**

Fuel rod calculations were performed to evaluate the fuel performance in the new operating conditions. The calculations were performed with the CARO-D code [6]. This code was

originally developed by SIEMENS for the analytical investigation and numeric description of LWR fuel rods under authorized operating conditions with higher burnups than those foreseen for Atucha-1 SEU fuel. The code is used as a routine tool in the design of fuel rods, however the desirable degree of conservatism is achieved by means of selecting appropriate input data sets. This includes fuel rod input data and calibration parameters. Conservative power histories are also selected according to the parameter to be verified.

Several power histories representative of different irradiation routes were analyzed. **Figure 3** shows the most conservative history used for these calculations. It represents a maximum power condition during fuel residence before and after the reshuffling. This power history considers that the fuel reaches its discharge burnup in a high power position without the typical second reshuffling to outer low power positions.

The main performance parameters included in the fuel rod calculations are detailed in the following paragraphs :

- **Maximum Fuel Temperature**

As is shown in **Figure 4**, even under the most conservative combination of design parameters and power history the center line temperature remains below 2100 C. It means that the maximum temperature is always well below the melting temperature of  $UO_2$  (about 2800 C). The evolution of the temperature shows the little variation of the heat transfer coefficient between pellet and cladding.

- **Internal Fuel Rod Pressure**

At SEU fuel typical burnup the fission gas release becomes more important than in the natural uranium fuel. Even in this situation the remaining free internal volume allows to keep the internal pressure below the coolant pressure. Therefore no cladding lift-off from the fuel can occur. The pressure build up is produced mainly by the enhanced fission gas release and the reduction of free internal volumes.

- **Long term sheath strain**

In the burnup range considered for SEU fuel the gap between cladding and pellet is not completely closed across its circumference and almost no mechanical interaction with tensile strains is expected. Only under severe combinations of design conditions and cladding creep the code predicts a low amount of cladding total tensile strain (0.3 - 0.4 %).

- **Short term strains**

The maximum linear power allowed for non-steady state conditions is the same for natural fuel and for SEU fuel. The maximum tensile sheath strain calculated for the maximum ramp is well below the 1 % limit accepted for the pure mechanical part of the interaction between pellet and cladding. The relationship between this interaction and the stress corrosion cracking in the presence of chemically aggressive fission products had a special treatment that was included in point 7 of this paper.

- **Waterside corrosion and deuterium pick-up**

Due to the short time of residence, even for SEU fuel, the oxide layer on the fuel sheath

surface remains in the range of a few microns and far below technological limits. Then the sheath corrosion is not a life limiting aspect for SEU fuel.

#### . **Fuel Rod Axial Growing**

The length increase of a Zircaloy cladding comes from 3 different mechanisms: anisotropic creep-down, irradiation growing and pellet-cladding mechanical interaction. For the extended burnup of SEU fuel, as almost there is no mechanical interaction, the main contribution for length increase is the irradiation growth.

**Figure 5** shows the results of Atucha-1 SEU fuel rod length measurements representative of different burnups. These data fits well with model predictions and experimental data from LWR fuel rods. The maximum calculated axial growing was such that the maximum relative displacement between wearing pads and spacer grids was below the limit displacement that reduces the surface contact between them.

#### . **Another parameters**

Another parameters verified during the fuel rod design analysis were the elongations of the pellet stack and the cladding. The maximum relative elongation between them was below the spring compression required for spring spires hard contact.

**Table 2** summarizes relevant results from conservative fuel rod calculations.

### **7 Power ramps**

Because of the higher SEU fuel burnup, the potential of fuel failures by pellet cladding interaction is a specific concern in this type of fuel. The postulated failure mechanism is stress corrosion cracking. As seen in **Figure 6**, in the low burnup range which is representative of natural fuel, the typical power ramps from fuel reshuffling are below a conservative failure threshold. The application of the same conservative criteria to SEU fuel would introduce limitations to the size of the power ramps from fuel shufflings, reactor start ups and power changes. The new burnup dependent criteria is based on the verification of the power ramp size considering also the local burnup just before the ramp and the conditioning power. Data obtained from fuel management calculations is used for this verification.

**Figure 7** shows the power ramps during fuel shufflings to positions with higher linear powers as function of local burnup for all the SEU fuel assemblies irradiated. The distribution clearly shows the application of the new burnup dependent PCI failure criteria. The development of a remedy to prevent PCI-SCC fuel failures consisting in the use of an inner sheath surface coating with graphite is almost completed and will be introduced in the Atucha-1 fuel rod design only if necessary.

### **8 SEU Fuel Performance Evaluation**

SEU fuel performance at this stage of the program was evaluated using the following information:

- Data obtained from fuel management calculations, including local linear power, local burnups, discharge burnup distribution and residence times.

- Visual inspection in a pool-side station of all the discharged SEU fuel assemblies.
- Fuel rod axial growing measurements in some of the irradiated FA.

Since the beginning of the program there were only two failed Fuel Assemblies. Both were correlated with manufacturing defects. Therefore the failure rate was not affected either by the higher burnup or by the higher residence time.

The average discharge burnup is more than 11000 MWd/tU and maximum local burnups are close to 15000 MWd/tU. Without considering two FA that were withdrawn before reaching the discharge burnup, the dwelling time goes from 300 to 500 fpd, almost doubling the corresponding value for natural uranium. **Figure 8** shows the distributions of fuel discharge burnup.

The irradiation behavior of the structural design was satisfactory. Unacceptable spacer grids movements, rod bowing or fretting wears were not detected.

## 9 Conclusions

A project for a gradual transition from natural uranium fuels to slightly enriched fuels (0.85 %  $^{235}\text{U}$ ) is well advanced in Atucha-1 NPP. Licensing studies are completed and more than 70 % of coolant channels are fueled with SEU Fuel Assemblies.

The fuel design was analyzed considering the new boundary conditions associated with the extended burnup. Potential life limiting aspects for the fuel were recognized and several modifications were introduced to optimize the fuel design. An extended criteria to prevent PCI failures was established.

The in-pile performance of SEU fuel assemblies at the present stage of the program is encouraging. Particularly the response to power ramps during on-power refueling and fuel shufflings. As was predicted, the operation of the plant showed no unexpected impacts due to the use of SEU fuels. An evaluation of SEU fuel performance data shows that power ramps, discharge burnups and dwelling times satisfy previous estimations without any negative impact on the fuel performance. The results of post-irradiation pool-side examinations and fuel rod length measurements are satisfactory and in agreement with previous estimations and models.

Relevant data to point out is the increase of the average discharge burnup from 5900 (natural uranium) to 11300 MWd/ tU and the reduction of the refueling frequency from 1.31 to 0.7 FA/fpd. Fuel consumption was reduced from 402 FA during 1997 to 272 FA during 1998. Based on the favorable experience the number of SEU FA in the core will be gradually increased to a full core in about one year (2000-2001).

## ACKNOWLEDGEMENTS

The contributions to this paper by many individuals at both CNEA and NASA is acknowledged; in particular the contributions of F. Bassarsky, for the irradiation data base, and G. Ruggirello for PIE and axial growth measurements, are gratefully acknowledged.

## REFERENCES

- [1] Frischengruber K., Dusch F., Development of Power Reactor Types and Fuel Cycles in KWU type PHWR's. Proceedings of a Technical Committee Meeting and Workshop on Advanced Light and Heavy Water Reactor Technology, IAEA-TECDOC-344, (1985).
- [2] Boczar P. et al, Slightly Enriched Uranium in Canada. An Economic First Step Towards Advanced Fuel Cycles. Proceedings of a Conference on Nuclear Power Performance and Safety. IAEA, Vienna, Austria, (September 1987).
- [3] Boczar P., Benefits From the Use of Slightly Enriched Uranium Fuel in Operating CANDU Reactors, Sesion I.2/Paper 16 at this meeting.
- [4] M. Higa et al, Reducing Operating Costs by Using Slightly Enriched Uranium (SEU) Fuel in the Atucha-1 Nuclear Station. Economic and Technical Aspects after 18 Months of the Irradiation Program, Proceedings of an International Conference on Nuclear Power Competitiveness in the Next Two Decades, Buenos Aires, Argentina, (November 1996).
- [5] Fink J. et al, Overview of the SEU Project for Extended Burnup at the Atucha-1 NPP. Four Years of Operating Experience. Paper presented at this meeting.
- [6] Eberle R. et al, The KWU Fuel Rod Code CARO. IAEA Specialist Meeting on Fuel Element Performance Computer Modelling, Blackpool, UK, March 1978.

**Table 1: Relevant data of the Atucha-1 Fuel Assembly and Fuel Rod**

---

Assembly Geometry	Circular Array
Active Fuel Rods	36
Supporting Tube	1 (Zircaloy-4)
Rigid Spacer Grids	15 (Zircaloy-4)
Tie Plate	1 (Zircaloy-4)
Cladding Material	Zircaloy-4
Outside diameter	10.90 mm
Cladding wall thickness	0.55 mm
Active length	5300 mm
UO <sub>2</sub> sintered pellet density	10.60 g/cm <sup>3</sup>
Fuel pellet diameter	10.62 mm
Gas pressure (as manufactured)	17 bar

---

**Table 2: Relevant results from conservative fuel rod calculations**

---

Maximum fuel center line temperature	2040	K
Maximum long term tensile sheath strain	0.41	%
Linear Power for gap closure	510	W/cm
Maximum equivalent sheath strain	0.51	%
Maximum relative elongation	23.2	mm
Maximum relative displacement between fuel rods	4.5	mm
Maximum corrosion layer thickness	5	μm

---

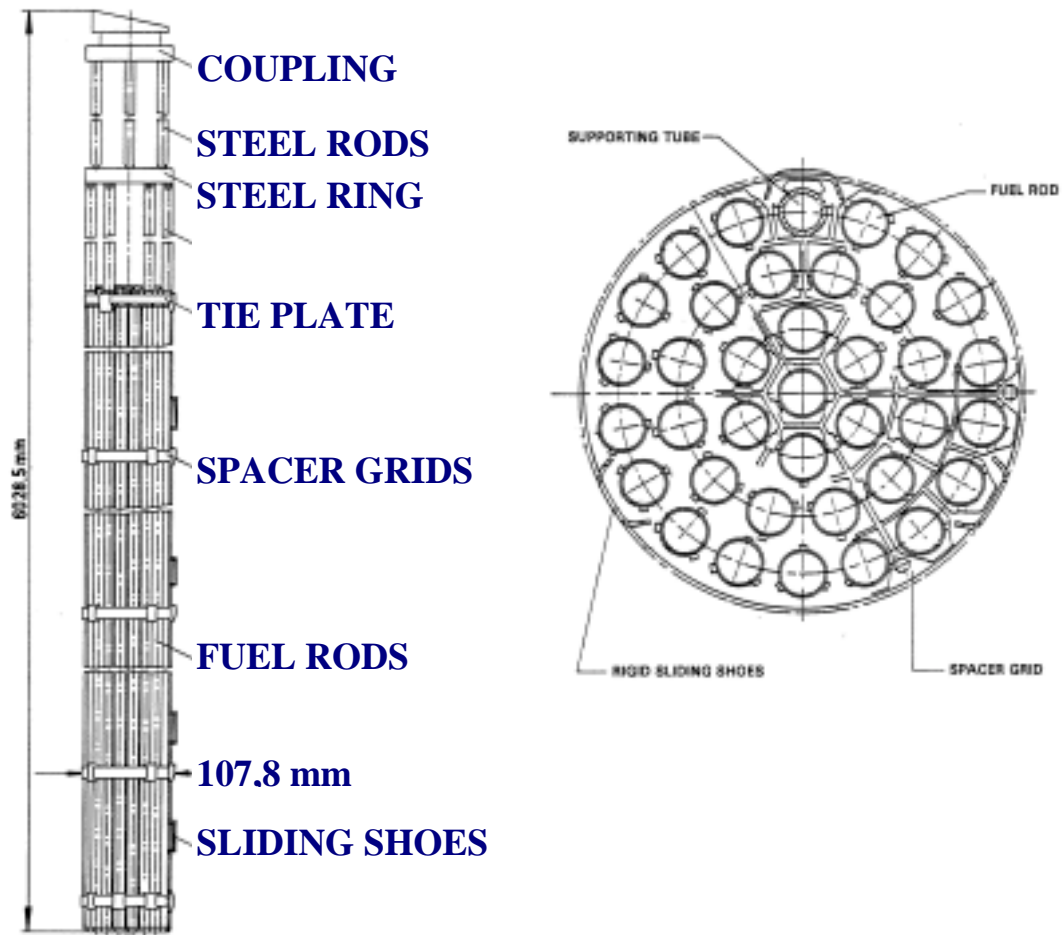


Figure 1: Schematic description of the Atucha-1 fuel assembly

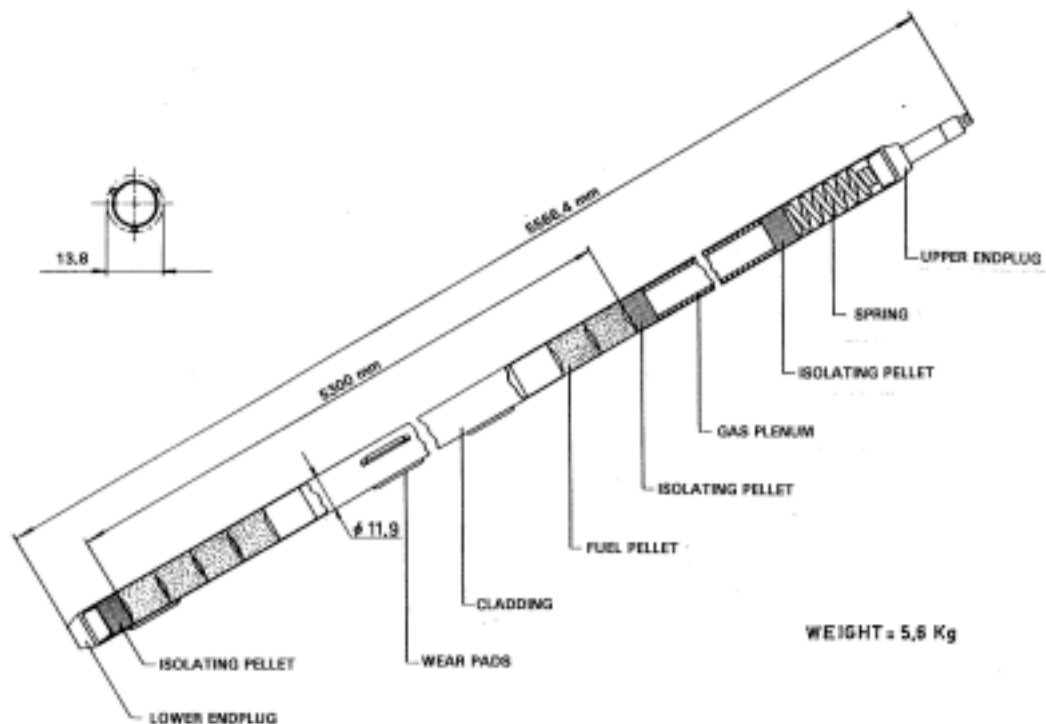


Figure 2: Typical Atucha-1 fuel rod

### LINEAR POWER [W/CM]

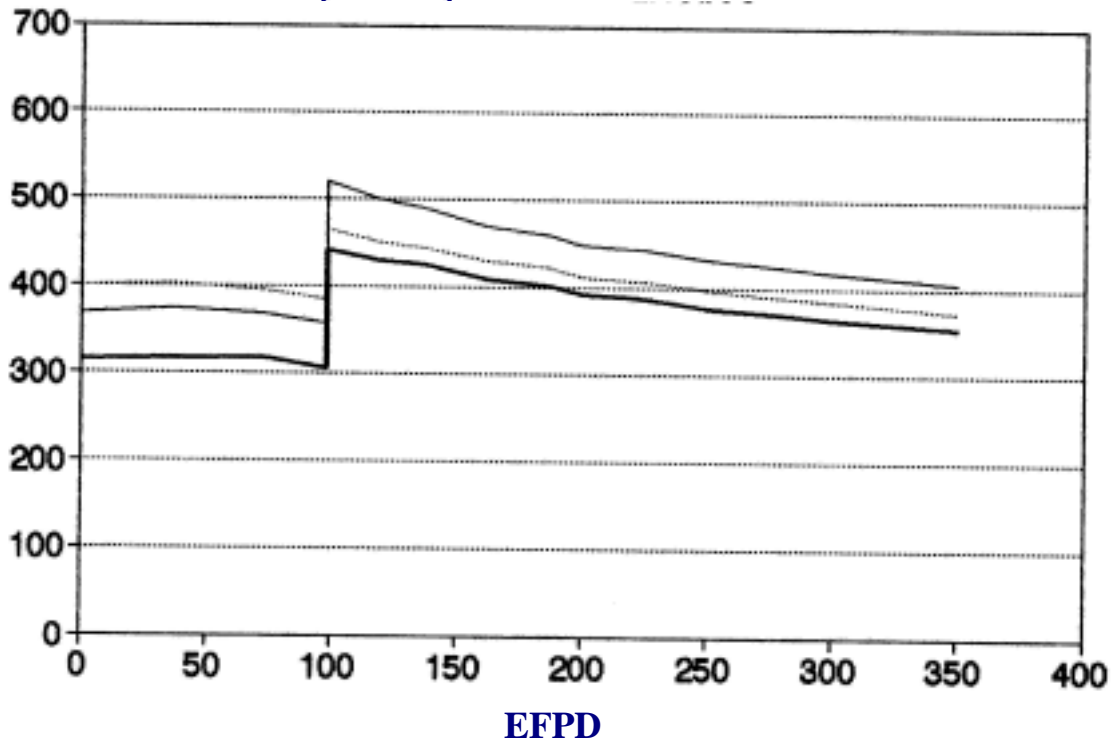


Figure 3: Conservative power history used for calculations

### TEMPERATURE [C]

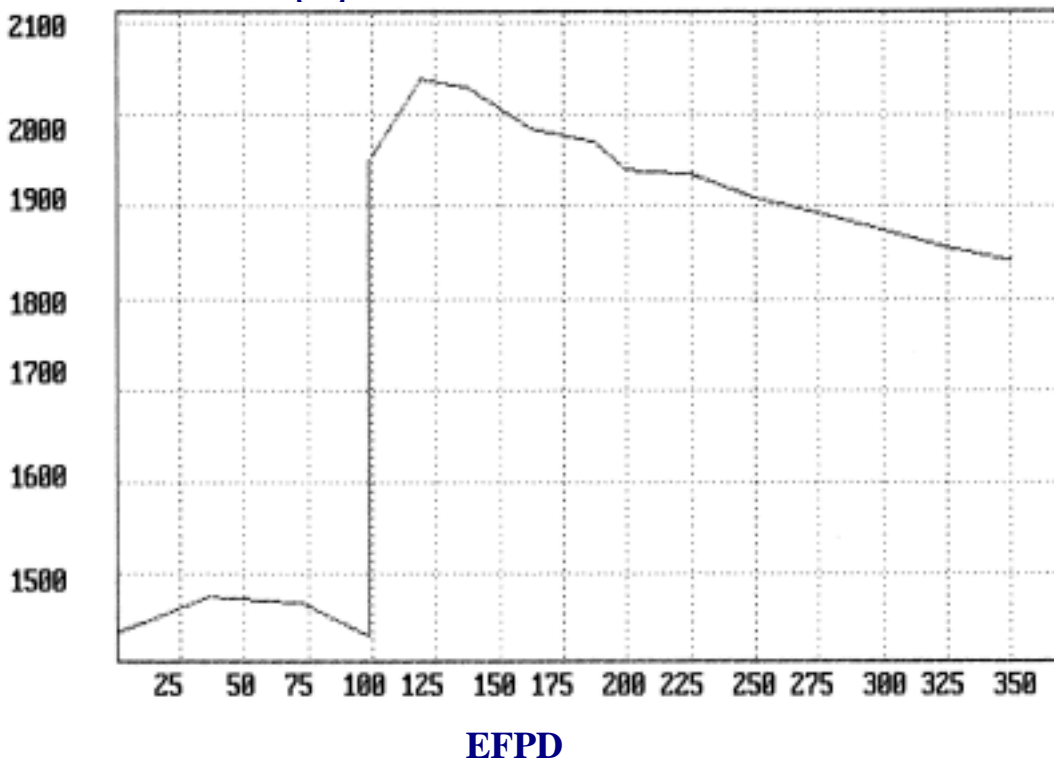


Figure 4: Evolution of calculated Center Line Fuel Temperature

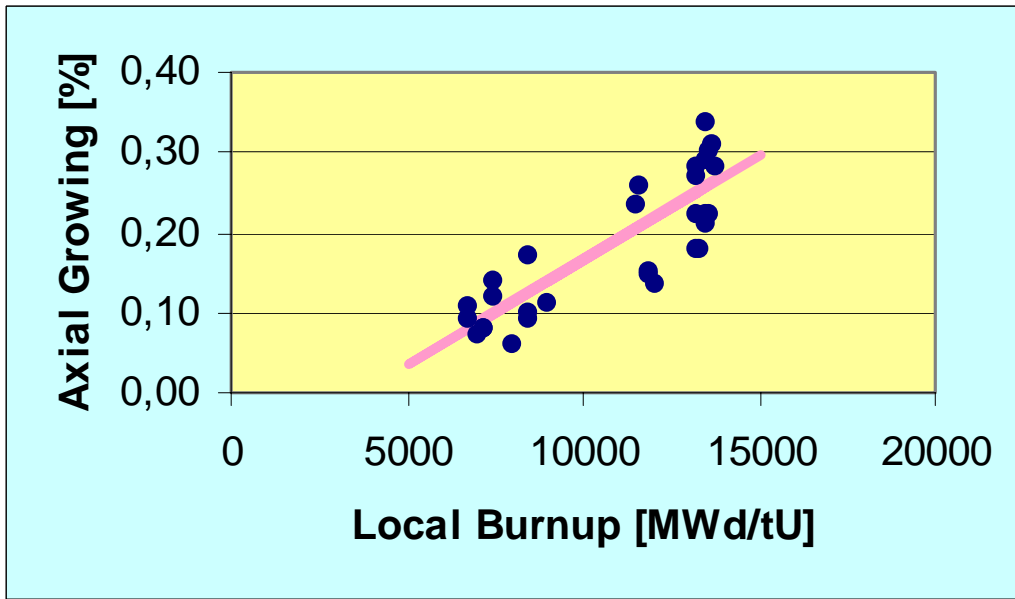


Figure 5: Aucha-1 SEU fuel rod axial growing measurements at different burnups

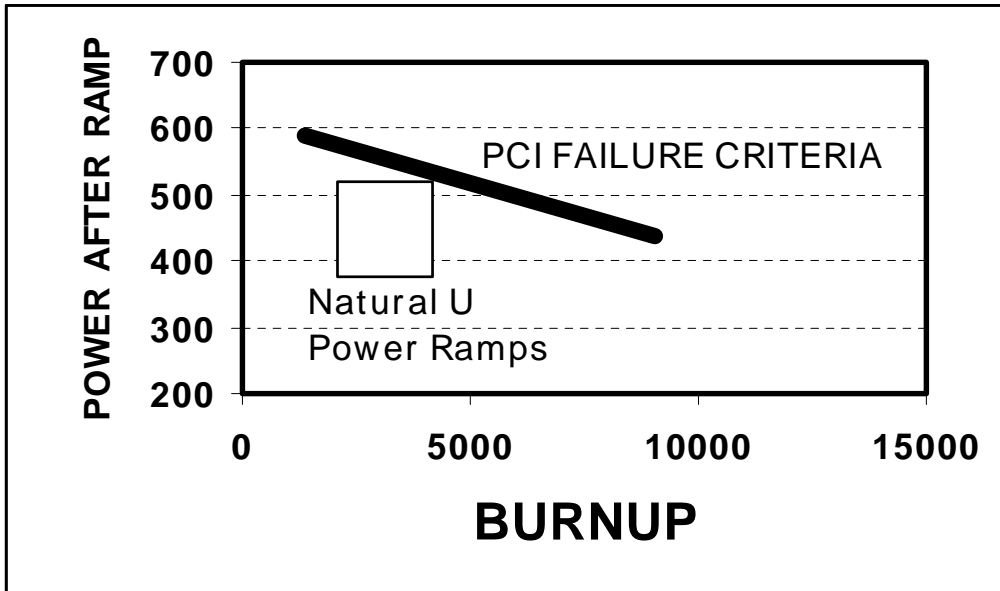
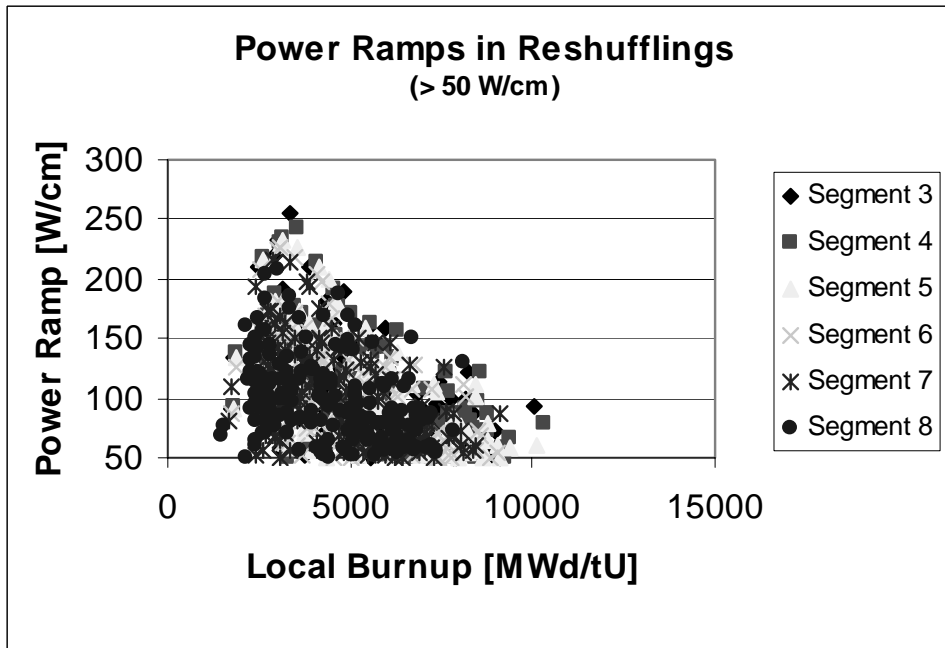
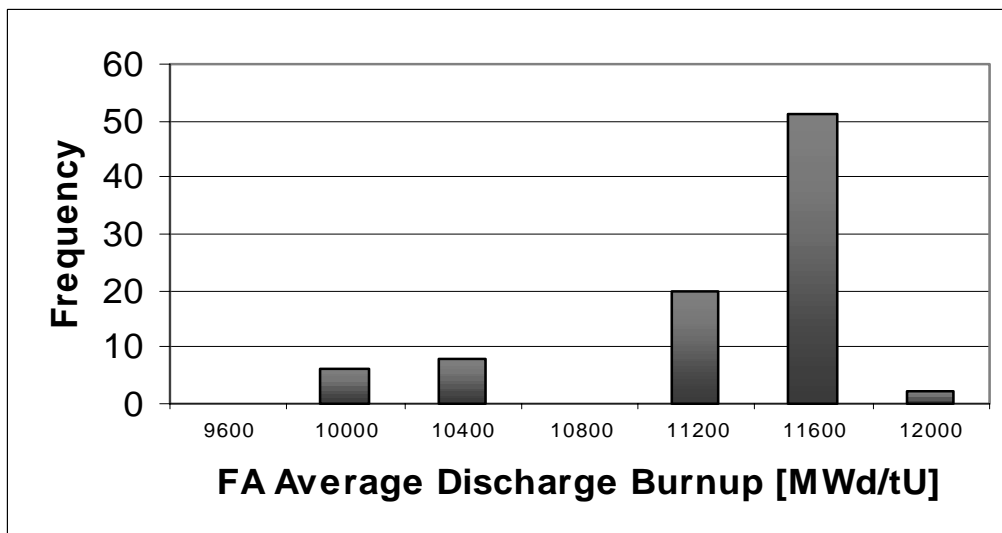


Figure 6: Schematic representation of typical power ramps in the low burnup range representative of natural uranium fuel



**Figure 7: Power ramps during fuel reshufflings as function of local burnup for SEU fuels irradiated in Atucha-1**



**Figure 8: Distribution of fuel discharge burnup**

# Technologies for manufacturing $\text{UO}_2$ sintered pellets to fuel burnup extension

**D. Ohai**

Institute for Nuclear Research,  
Pitesti, Romania

## Abstract

The actual tendency all over the world is to manufacture fuel bundles capable to resist high burn-up. The factors affecting the burn-up increase are: the pellet-cladding mechanical interaction (PCMI), the oxidation and hydriding of the Zircaloy-4 sheath, the increase of internal pressure, stress corrosion cracking, Zircaloy-4 irradiation growth, fuel swelling. A way to increase fuel burn-up is to diminish the elements internal pressure by adequate  $\text{UO}_2$  fuel pellet structure (large grain or controlled closed porosity). In the large grain size  $\text{UO}_2$  pellets, fission gas release rate decreases and the elements internal pressure increase slowly. Similarly, in the  $\text{UO}_2$  sintered pellet with controlled closed porosity the fission gas accommodation is better and the elements internal pressure increases slowly. The paper presents a literature review related to the technologies and the methods for manufacturing  $\text{UO}_2$  sintered pellets to fuel burn-up extension. The flowsheets for large grains and controlled closed porosity  $\text{UO}_2$  sintered pellets obtained by  $\text{Nb}_2\text{O}_5$  dopant respectively pores former addition in  $\text{UO}_2$  sinterable powder, pressing and sintering in  $\text{H}_2$  atmosphere are exposed. In the diagrams are presented the dependency of the main sintered pellet characteristics (pore radius distribution, pores volume, density, grains size) as function of the  $\text{Nb}_2\text{O}_5$  dopant concentration,  $\text{UO}_2$  sinterable powder nature and sintering temperature. Other sintered pellets characteristics (electrical conductivity, Seebeck coefficient, high temperature molar heat capacity and thermomechanical properties) are presented. The technologies for sintered pellets manufacturing for RU, DUPIC, MOX fuel cycles are presented. A proposal related to fuel manufacturing from Uranium compound resulted in LWR spent fuel reprocessing is also given.

## 1. INTRODUCTION

A main concern all over the world is to increase fuel burn-up for reducing nuclear electricity costs and the high level waste (spent fuel) amount. Very good results were obtained in the removing or the diminishing of the factors affecting the burn-up increase and the theoretical and practical (experimental results) solutions proposed to diminish adverse effects.

Table 1 presents some factors affecting the burn-up increase and the solutions.

A way to increase fuel burn-up is to diminish the elements internal pressure by adequate  $\text{UO}_2$  fuel pellet structure (large grain or controlled closed porosity). In the large grain size  $\text{UO}_2$  pellets, fission gas release rate decreases and the elements internal pressure increases slowly. Similarly, in the  $\text{UO}_2$  sintered pellet with controlled closed porosity the fission gas accommodation is better and the elements internal pressure increases slowly.

Table 1. Factors affecting burnup increase

Factor	Solutions
Increasing of internal temperature	<ul style="list-style-type: none"> <li>- reducing of elements diameter [1]</li> <li>- pellets with central hole [2]</li> <li>- duplex pellets [3]</li> <li>- graphite discs between pellets [4-5]</li> </ul>
increasing of internal pressure	<ul style="list-style-type: none"> <li>- large grain size pellets [6-8]</li> <li>- controlled closed porosity</li> </ul>
pellet-cladding mechanical interaction (PCMI)	<ul style="list-style-type: none"> <li>- pellet length/diameter &lt; 1 [9]</li> <li>- pellet geometry improvement [10]</li> </ul>
stress corrosion cracking	<ul style="list-style-type: none"> <li>- Zy-4 sheath covered with pure Zr [11]</li> </ul>
oxidation and hydriding of the Zircaloy-4 sheath	<ul style="list-style-type: none"> <li>- new microstructure for Zy-4 [12]</li> <li>- new Zr alloys (ZIRLO- Nb1%, Sn1% and Fe 0.1%) [13]</li> </ul>

Other way to reduce fission gas release rate is to use composite fuels. Two type of disperse fuels for water reactors are known:

- **ceramic – metallic** (cermet) where inert matrix are metals (Zr, Al, Mo) and ceramic fissile materials ( $^{235}\text{U}$  and Pu compounds with O<sub>2</sub>, Si, C);
- **ceramic – ceramic** (cercer) where inert matrix may be ceramics (MgO, MgAl<sub>2</sub>O<sub>4</sub>) and the ceramic fissile materials are the same like cermets.

The increasing of internal temperature appears because the fuel thermal conductivity decreases with the burn-up and heat removing is worsened. The solutions are reducing of element diameter [1], pellets with central hole [2], duplex pellets [3], graphite discs between pellets [4-5] and others.

Some solutions proposed for pellet cladding mechanical interaction (PCMI) reduction are pellet length/diameter < 1 [9], pellet geometry optimization [10].

The internal and external corrosion issue are resolved by Zy-4 sheath covered with pure Zr [11], new microstructure for Zy-4 [12], new Zr alloys (ZIRLO- Nb1%, Sn1% and Fe 0.1%) [13].

The RU, DUPIC, MOX fuel cycles and CANFLEX fuel type concept are modern ways to extend burn-up. Much solution for burn-up extension bad effects removing, presented above, retrieves in these modalities.

## 2. TECHNOLOGIES FOR $\text{UO}_2$ LARGE GRAINS MNUFACTURING

One of the ways to increase pellets grain size without increasing sintering temperature and time is the addition of small quantities ( $< 1\%$  wt M/U) of sintering additives (aliovalent metal or rare earth oxide).

By the addition of certain dopants in the  $\text{UO}_2$  powder ( $\text{TiO}_2$ ,  $\text{Nb}_2\text{O}_5$ ,  $\text{Cr}_2\text{O}_3$ ,  $\text{CaO}$ ,  $\text{V}_2\text{O}_5$ .) the grain size, porosity and the mean free diffusion path are increased, whereas the grain boundary area is reduced [14–18].

At the Institute for Nuclear Research (ICN) - Pitesti a technology for obtaining large grains size  $\text{UO}_2$  pellets using dopants [19] was developed. The manufacturing flowsheet is presented in Figure 1.

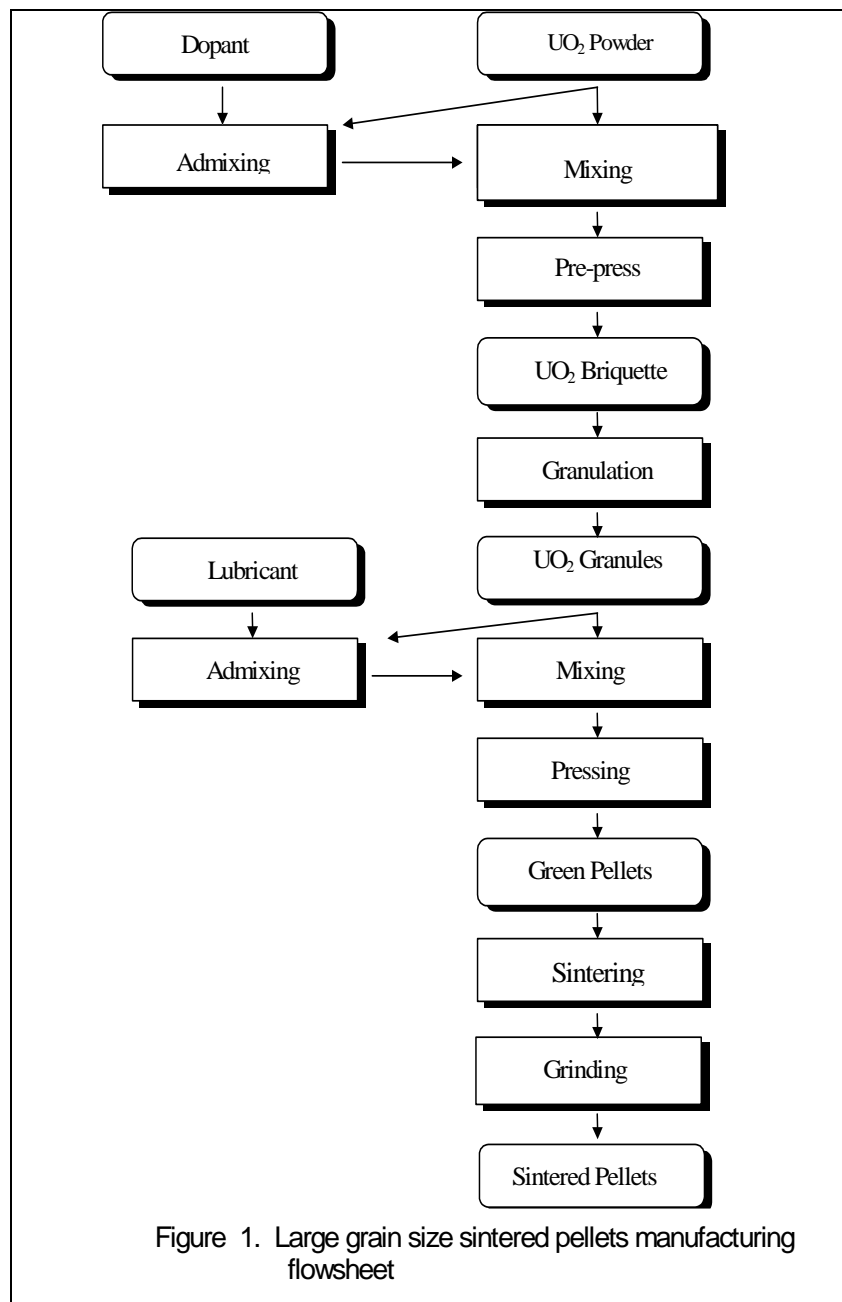


Figure 1. Large grain size sintered pellets manufacturing flowsheet

The  $\text{UO}_2$  non-free flowing powder, manufactured by ADU route, was mixed with  $\text{Nb}_2\text{O}_5$  in an Y - con master mix. The blended powder was pre-pressed and granulated using a 0.5 mm sieve. The resulted granules were mixed with Zn stearate as lubricant. The green pellets were manufactured by bilateral pressing. The compacts were directly sintered (4 hours at  $1700^\circ\text{C}$ ) in standard continuous sintering furnace with a dewaxing step at  $900^\circ\text{C}$ .

For the production of niobia doped  $\text{UO}_2$  fuel the “direct pelletizing process” which has been developed in relation with the AUC powder technology can be applied without any change beside the admixture of niobia to the  $\text{UO}_2$  powder.

In a master mix  $\text{UO}_2$  and  $\text{Nb}_2\text{O}_5$  powders are added and homogenized. The blended powder is directly pressed without the addition of a lubricant. The green pellets are sintered in a sintering furnace. Under the same sintering conditions, the density of the pellets can be adjusted by  $\text{U}_3\text{O}_8$  addition,  $\text{UO}_2$  -  $\text{Nb}_2\text{O}_5$  pellets with densities between  $9.9 - 10.75 \text{ g/cm}^3$  and grain size between  $2 - 50 \mu\text{m}$  being obtained [20].

Other methods to obtain uranium dioxide pellets with large grain sizes are:

- heating sintered pellet of uranium dioxide at temperatures higher than  $1700^\circ\text{C}$  in hydrogen stream containing silicate vapors, resulting from the aluminum silicate decomposition. The grain size values can be increased to more than  $50\mu\text{m}$  [21];
- production of sintered uranium dioxide pellets by the addition of sintering agent (10 - 55wt%  $\text{MgO}$  and 90 - 45wt% $\text{SiO}_2$ ) or precursor thereof in the composition ranging from 0.1 - 0.8wt% of a sinterable mixture. The resulting mixture is turned into a compact. The sintering process is performed at a temperature where the sintering agent forms a liquid phase to produce a sintered product. The precursor is thermally decomposed below the sintering temperature [22];
- obtaining of sintered  $\text{UO}_2$  nuclear fuel pellets, with the average grain size ranging from about  $30\mu\text{m}$  to about  $80\mu\text{m}$  by the addition of magnesium aluminosilicate in uranium dioxide powder. The pores volume is ranging between 2 and 10% [23];
- addition of  $\text{Cr}_2\text{O}_3$  or  $\text{Al}_2\text{O}_3$  and of small quantities of  $\text{SiO}_2$  into the uranium dioxide powder [24].

The physical, thermal, electrical and mechanical properties of  $\text{Nb}_2\text{O}_5$  - doped  $\text{UO}_2$  pellets are affected, as compared to the undoped ones.

The variation in density of  $\text{Nb}_2\text{O}_5$  - doped  $\text{UO}_2$  pellets as a function of Nb content is presented in Figure 2. A very small concentration of  $\text{Nb}_2\text{O}_5$  (0-0.1%Nb/U) leads to a minimum value of the  $\text{UO}_2$  pellet density. The density of  $\text{UO}_2$  pellets increases with the increase of the Nb content for low concentrations (0.1  $\pm$ 0.2% Nb/U). At concentrations higher than 0.2%Nb/U, the density values are different, depending on the manufacturing routes: the increase of the Nb concentration slowly diminishes the density ( $P_1$  -ADU route) or remains constant ( $P_2$  - IDR route). Figure 3 displays the grain size dependence of the  $\text{UO}_2$  pellets on the Nb content [19]. The dopant addition determines a significant grain growth. The average grain size, versus concentration, shows an increase up to a maximum value (0.5%) followed by a constant value.

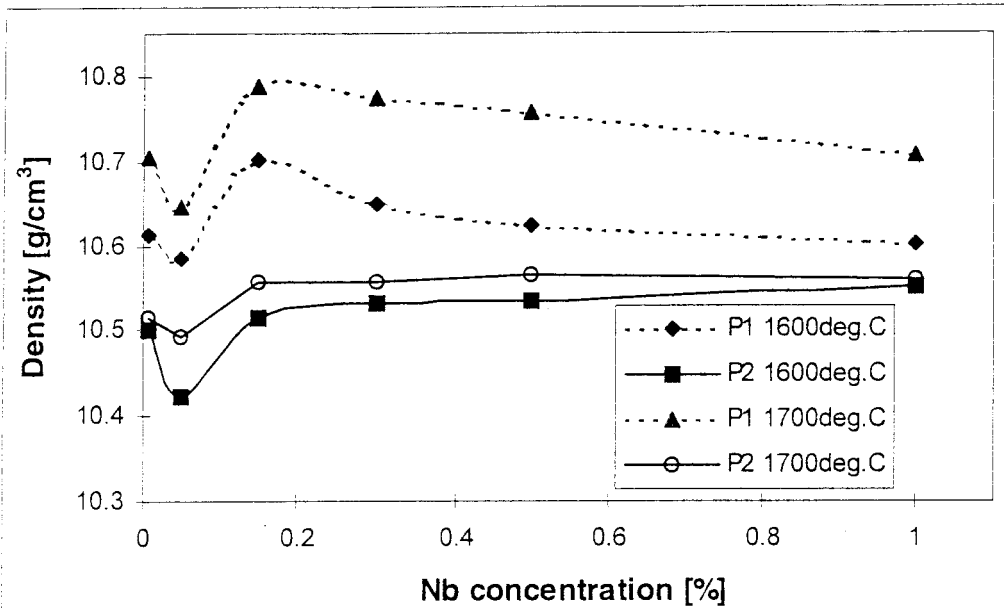


**Figure 2. Density of sintered pellets versus Nb concentration**

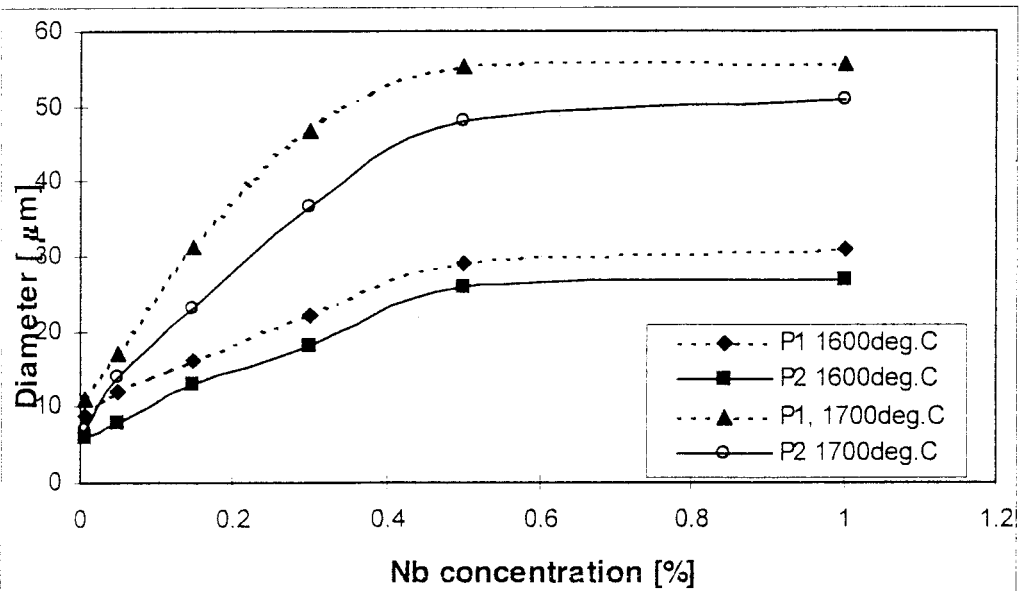


**Figure 3. Grain size dependence versus Nb concentration**

The addition of dopant brings changes into the porosity of sintered pellets. The total pores volume evolution versus Nb concentration in Nb<sub>2</sub>O<sub>5</sub> - doped UO<sub>2</sub> sintered pellets is presented in Figure 4 [19].

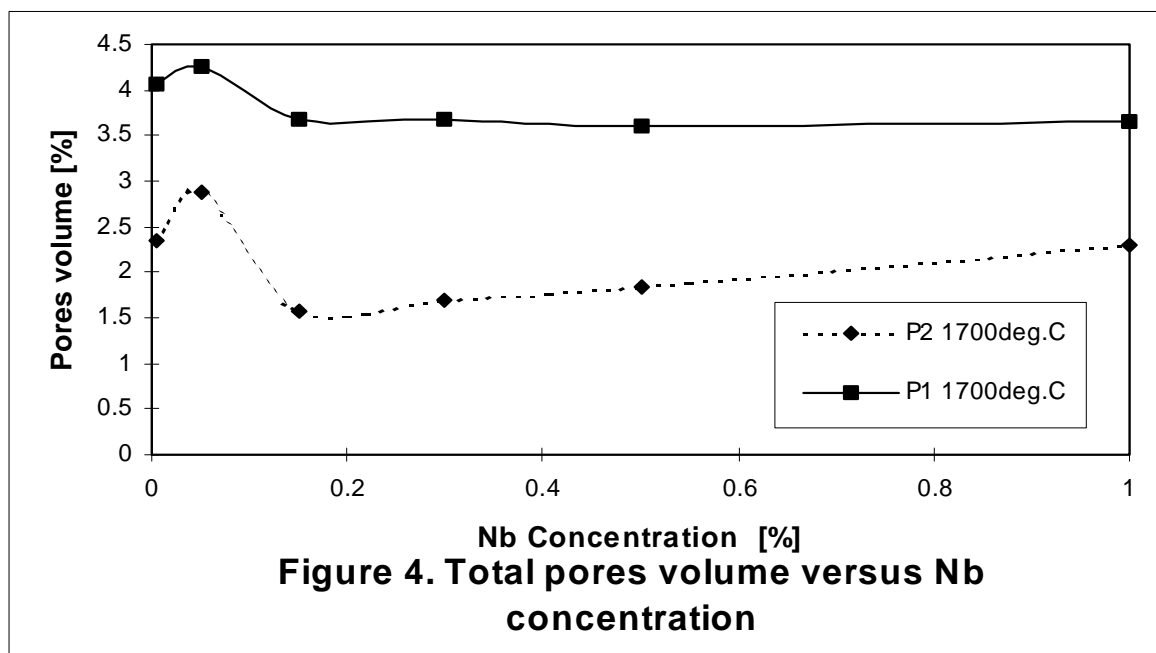
At low Nb concentrations the pores volume is distributed in small pores. If the Nb concentration increases, the pores volume is distributed in large pores, that prevail, while small pores volume is negligible [19].

Nb addition affects the UO<sub>2</sub> pellets mechanical properties [19], [25] as shown in Figure 5.

The transgranular fracture observed at low temperature ( $\leq 400^\circ\text{C}$ ) points out the intense cohesion between the grains. If the temperature increases the intergranular fracture is dominant and only this type of rupture takes place at high temperature ( $\geq 850^\circ\text{C}$ ), Figure 6.

The electrical conductivity and Seebeck coefficient of Nb<sub>2</sub>O<sub>5</sub> - doped UO<sub>2</sub> have been measured and compared with undoped UO<sub>2</sub>. Niobium acts as a donor impurity in UO<sub>2</sub>, but is not completely ionized and does not lead to n-type extrinsic behavior. On the contrary, intrinsic conductivity is observed and this is attributed to Nb compensating for acceptor levels due to slight excess oxygen nearly stoichiometric UO<sub>2</sub>. The value of the band gap in UO<sub>2</sub> is measured to be 2.14eV for undoped material and 2.26 eV for doped UO<sub>2</sub> [26].

High temperature molar heat capacity of Nb<sub>2</sub>O<sub>5</sub> - doped UO<sub>2</sub> are practically the same as that of UO<sub>2</sub>, [27].



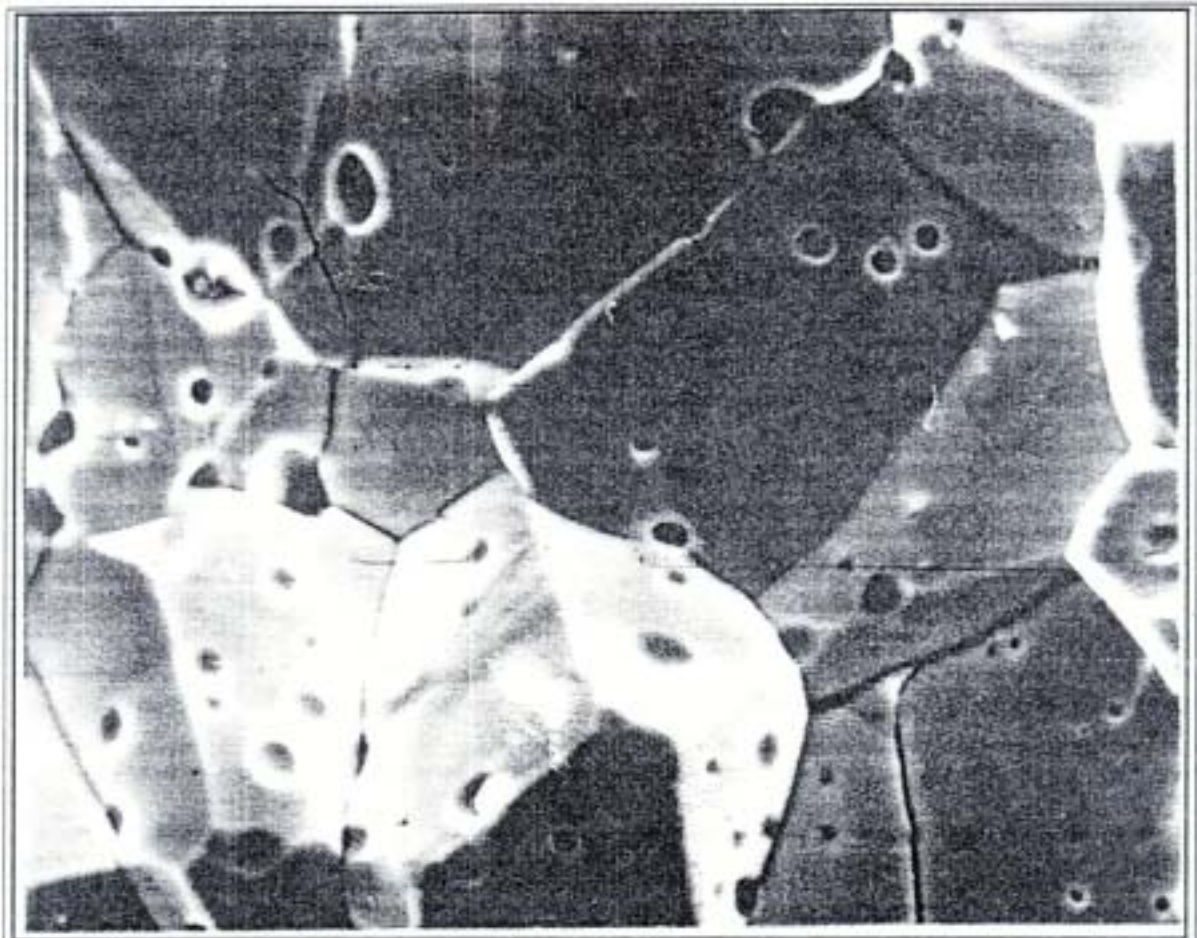
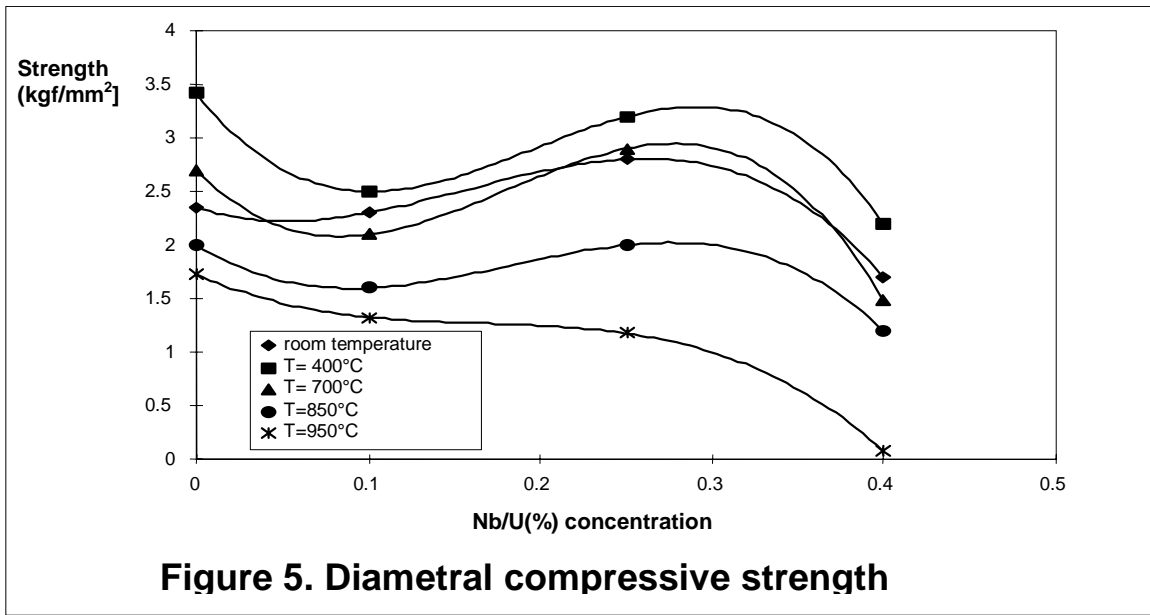


Figure 6. Intergranular fracture

### 3. OBTAINING OF UO<sub>2</sub> SINTERED PELLETS WITH CONTROLLED POROSITY

The technology for manufacturing of UO<sub>2</sub> sintered pellets with controlled porosity is relatively simple using pores former. UO<sub>2</sub> sinterable powder is mixed with pores former and thereafter the sintered pellets are elaborated by usually methods.

The common pores former can be organic compounds, UO<sub>2</sub> powder precursors (ADU, UO<sub>3</sub>, U<sub>3</sub>O<sub>8</sub>) or powder resulted from sintered pellets calcination.

In the Figure 7 [28] is presented a flowchart for UO<sub>2</sub> sintered pellets with controlled porosity, manufactured from no free flowing UO<sub>2</sub> sinterable powder.

The powder homogenization is very important to obtain uniform porosity. If the mix powder – pores former is non-adequate it appears connected pores and grouping porosity. Therefore, the first step is to make a preliminary admixing of pores former with about 10%wt of batch powder and thereafter this is mixed with the rest. The manufacturing is continued with compacts pre-pressing and granulation, granule homogenization with Zinc stearate, green pellets pressing and sintering in hydrogen atmosphere. The sintered pellets are grinded in a centerless grinding machine. The washing, the drying and the quality control of the grinded pellets are the last steps in the obtaining process.

The pores structure and volume are dependent on pore former amount, pre-pressing and pressing pressure and thermal treatment conditions. If the technical conditions will be well selected, desired microstructure will be obtained.

UO<sub>2</sub> sintered pellets with homogenous controlled porosity can be obtained directly from the UO<sub>2</sub> powder. UO<sub>2</sub> sinterable powder thermal is treated (few hours) in hydrogen above the reduction temperature and thereafter the sintered pellets are manufactured by usual way. Desired pores structure and volume are obtained in terms of the technical conditions.

### 4. UO<sub>2</sub> PELLETS MANUFACTURING FROM RECOVERED URANIUM

Recovered Uranium (RU) resulted like by-product from conventional reprocessing of LWR spent fuel for Pu obtaining. The enrichment of RU is about 0,9% U<sup>235</sup> and it contain Uranium daughter products and traces of transuranic elements [29] (Table 2).

Table 2. Uranium daughters and transuranic elements in RU.

U daughters	Contents	U <sub>nat.</sub>	Nuclide	Range g/gU)
U <sup>232</sup>	0.15 - 1 ppb	0.0055%	Np	3.10 <sup>-6</sup>
U <sup>234</sup>	0.014 - 0.018%		Pu	3.10 <sup>-6</sup>
U <sup>235</sup>	0.85 - 0.95%	0.711%	Am	1.10 <sup>-8</sup>
U <sup>236</sup>	0.28 - 0.4%		Cm	1.10 <sup>-9</sup>
U <sup>238</sup>	98.856 - 98.632	99.289		

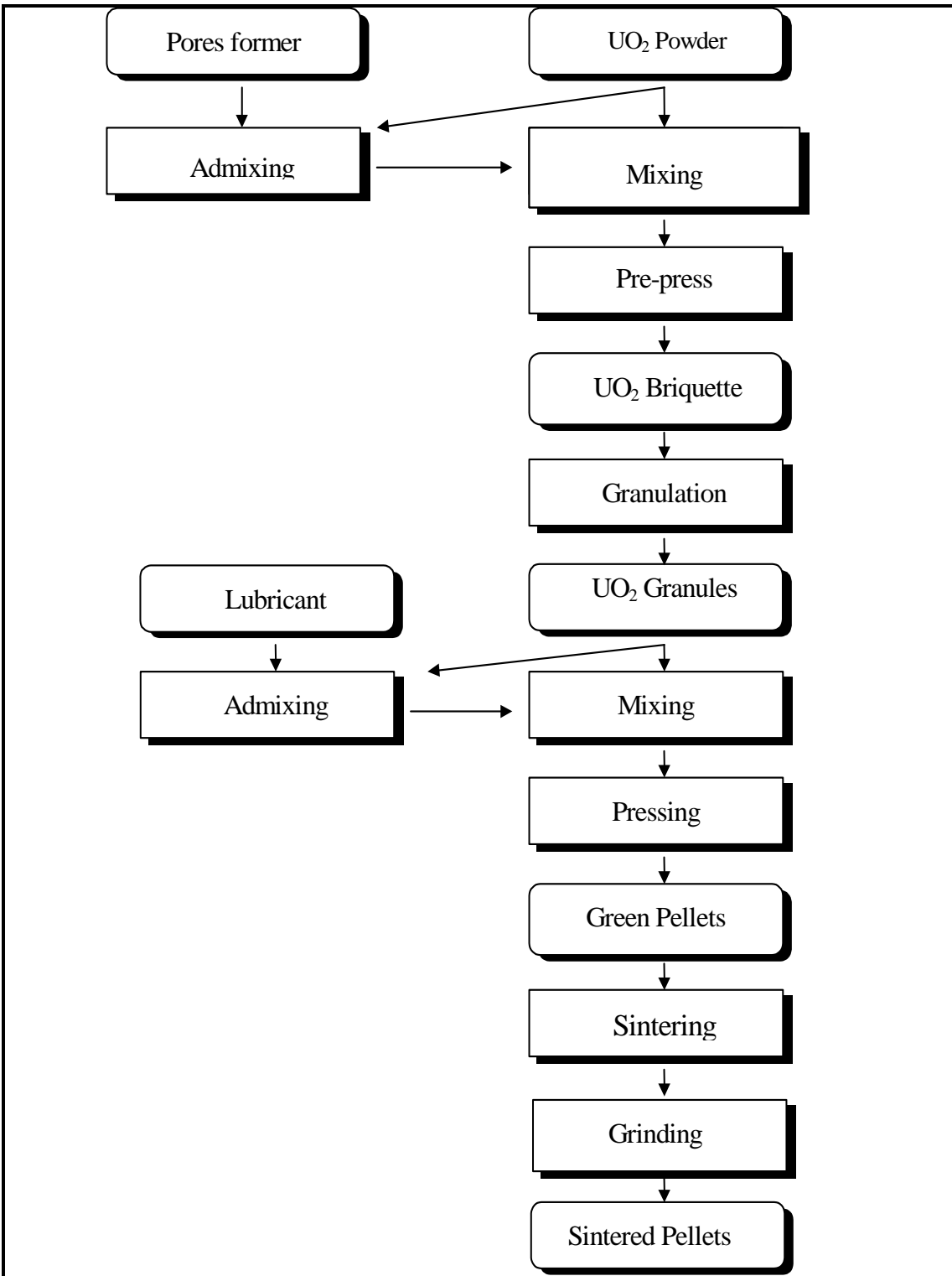


Figure 7. Controlled porosity sintered pellets manufacturing flowsheet

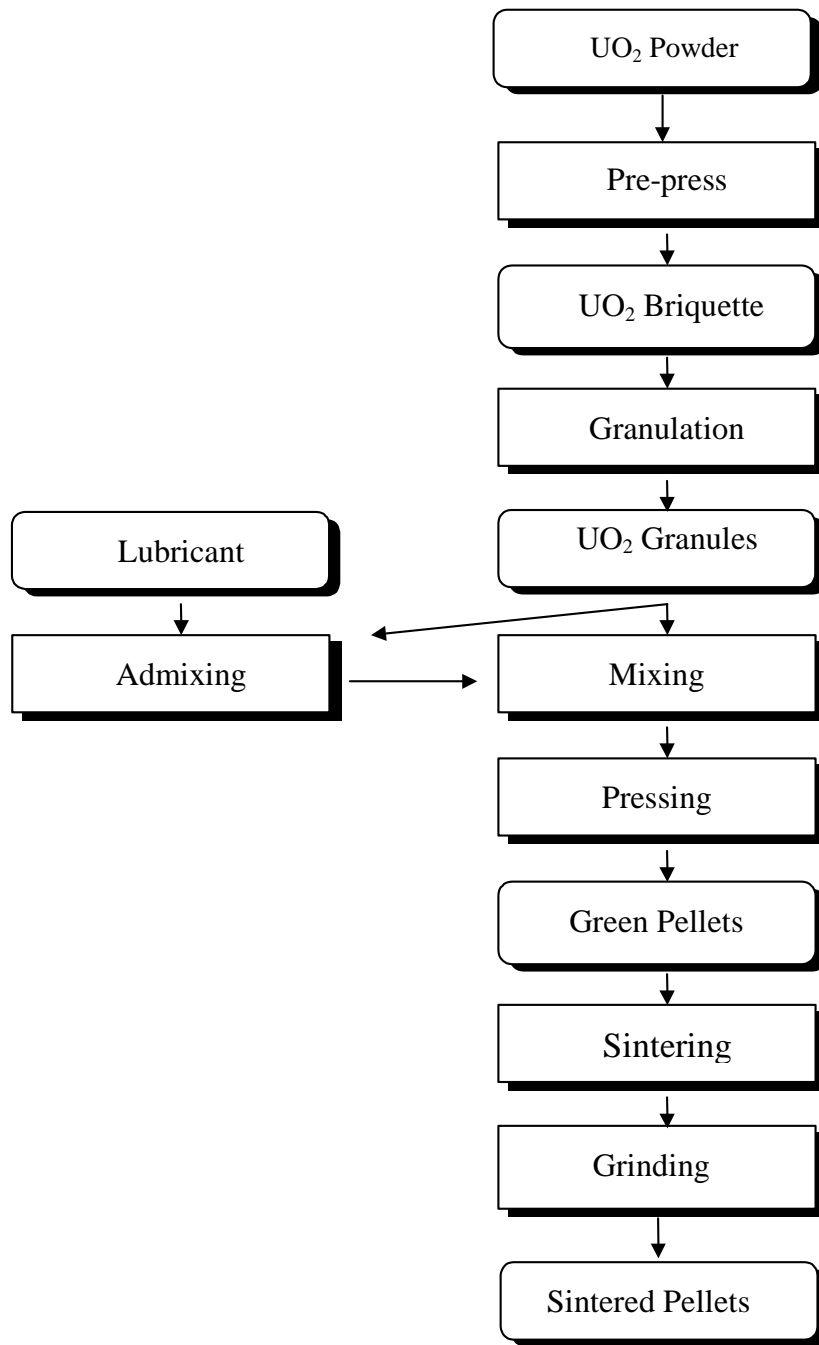


Figure 8. Sintered pellets manufacturing from no free flowing powder (flowsheet)

The quantity of RU in Europe and Japan is about 25.000 t [29].

RU resulted from reprocessing is Uranium Nitrate (UN). UN is converted in  $UO_3$  by denitration (BNFL) or in  $U_3O_8$  by ADU route (COGEMA). The manufacturing of  $UO_2$  pellets is usually.  $UO_2$  powder is manufactured by reduction of  $UO_3$  or  $U_3O_8$  with hydrogen. If  $UO_3$  is converted to  $UF_6$  (for enrichment), the Integrated Dry Route (IDR) is applicable.  $UO_2$  sintered pellets can be manufactured anywhere it exists facilities, devices and technologies for  $UO_2$  no free flowing powder manufacturing (Figure 8).

The difference between powder and pellets manufacturing from natural uranium and RU is the radiological inventory of RU, dependent of the fuel history (reprocessing, aging stage, burnup). In every process, volatile fission product can be released. That imposes supplementary measures for operators and environment protection. During sintering the release of  $^{137}\text{Cs}$  and other volatile products was detected. But AECL concludes that no significant radiological field in a commercial fuel manufacturing plant would build up due to release of volatile products.

An international collaboration between **K**orea **A**tomic **E**nergy **R**esearch **I**nstitute (KAERI), **A**tomic **E**nergy of **C**anada **L**imited (AECL) and **B**ritish **N**uclear **F**uel **plc** (BNFL) to use RU was developed. KAERI and AECL have introduced the Canadian Flexible (CANFLEX) fuel concept as a vehicle for this fuel cycle. A very attractive alternative to use RU in CANDU Reactors appears. Theoretically [29] the quantity of 25.000 t of RU would provide sufficient fuel for 500 CANDU reactor years of operation, knowing that the annual refuelling requirement for a RU fuel burnup 13 MWd/KgU is around 50 t/an comparatively with 85 t/an for NU.

## 5. SINTERED PELLETS FABRICATION FOR DUPIC [30-32]

The DUPIC (**D**irect **U**se for spent **P**WR fuel in **C**ANDU) is the fuel cycle where the spent PWR fuel is dry processed into CANFLEX fuel for the additional burnup of about 15 MWd/KgUHE (**H**eavy **E**lement) in CANDU Reactor. AECL, KAERI, USDOE and USDOS proposed the DUPIC fuel cycle concept. The PWR spent fuel, having a nominal burnup of 35 MWd/KUHE contain 0.9wt% fissile uranium and 0.6wt% fissile plutonium, more than natural uranium with 0.711wt% fissile content.  $\text{UO}_2$  powder, from PWR spent fuel manufacturing is based on OREOX (**O**xidation **R**eduction of **O**xide **F**uel) process (Figure 9). When  $\text{UO}_2$  is oxidized to  $\text{U}_3\text{O}_8$ , the crystallographic system is changed elemental cell volume increase, the stresses appear and pellets are broken themselves. The process is repeated to obtain a very fine powder.

The powder resulted from OREOX process is conditioned by milling to increase the sinterability. The sinterable powder is pressed into pellets and green pellets are sintered to 95 - 98 % TD (**T**heoretical **D**ensity). The sintered pellets are grounded on centerless grinding machine (dry process only) to final diameter and surface.

The DUPIC being a dry processing technology to manufacture CANDU fuel from PWR spent fuel without separating fissile materials and stable fission products from the spent fuel needs experimental works to verify the performance. In Korea, the simulated sintered pellet where manufactured, the irradiation testing program will be started in 2000.

## 6. MOX SINTERED PELLETS MANUFACTURING

The MIMAS (**M**icronized **M**ASter blend) process for MOX fuel obtaining (for LWRs) was developed by BelgoNucleaire (BN) in the Dessel plant. The MIMAS MOX pellets are a solid solution of  $\text{UO}_2$  and  $\text{PuO}_2$ , homogeneously dispersed in a  $\text{UO}_2$  matrix [33]. Schematically the process is presented in the Figure 11.

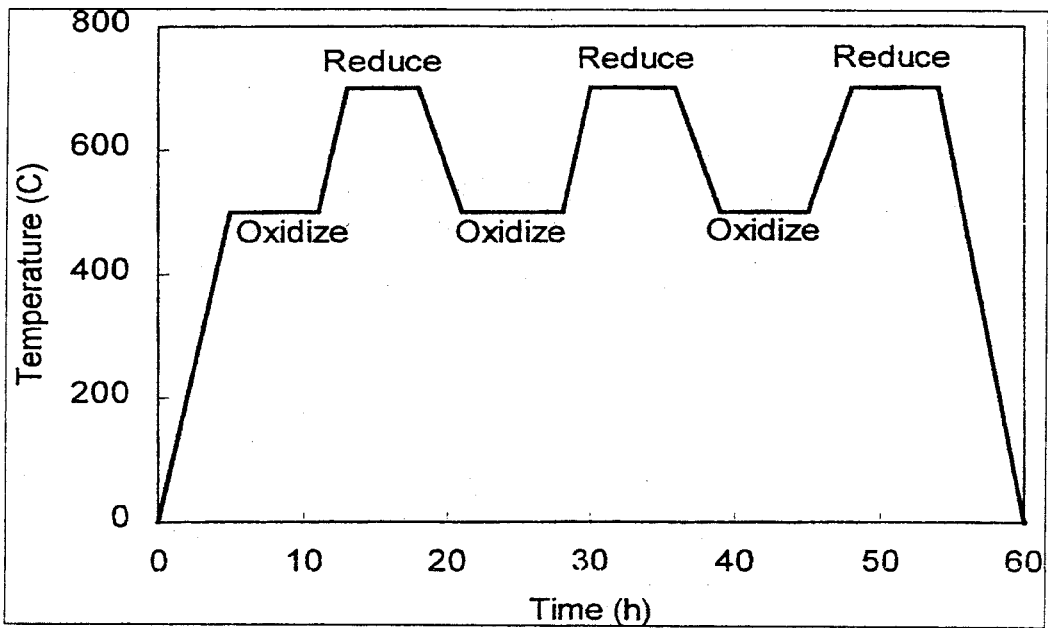


**Figure 9. OREOX Process**

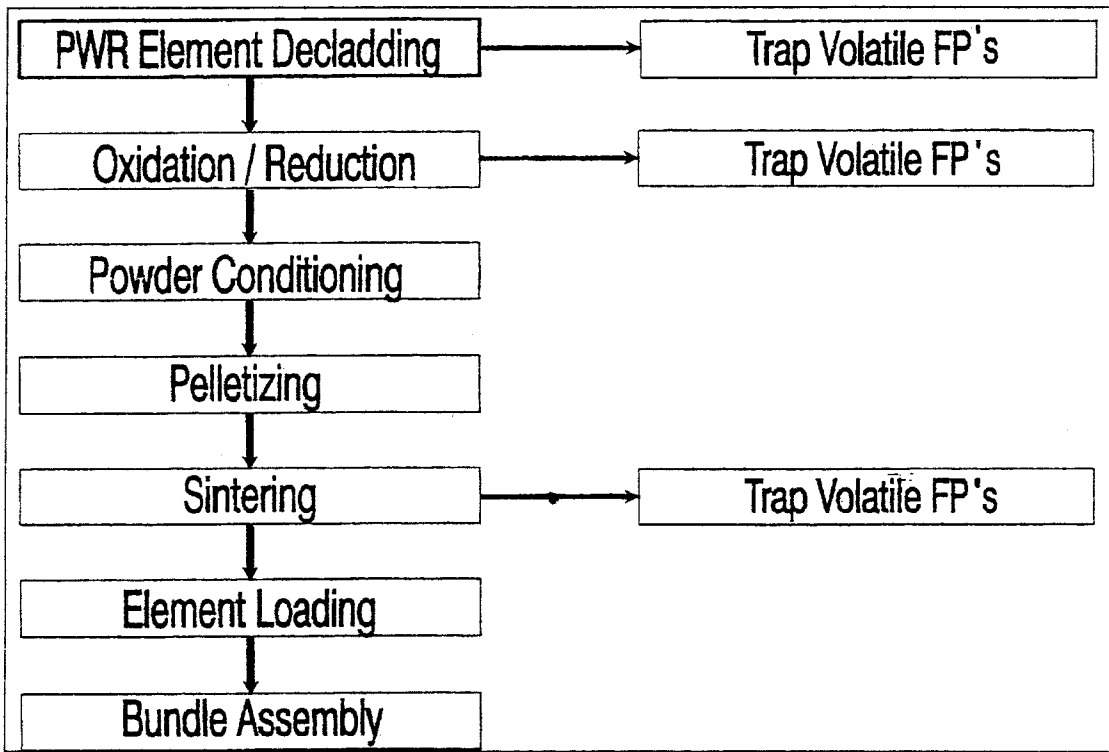


**Figure 10. DUPIC process**

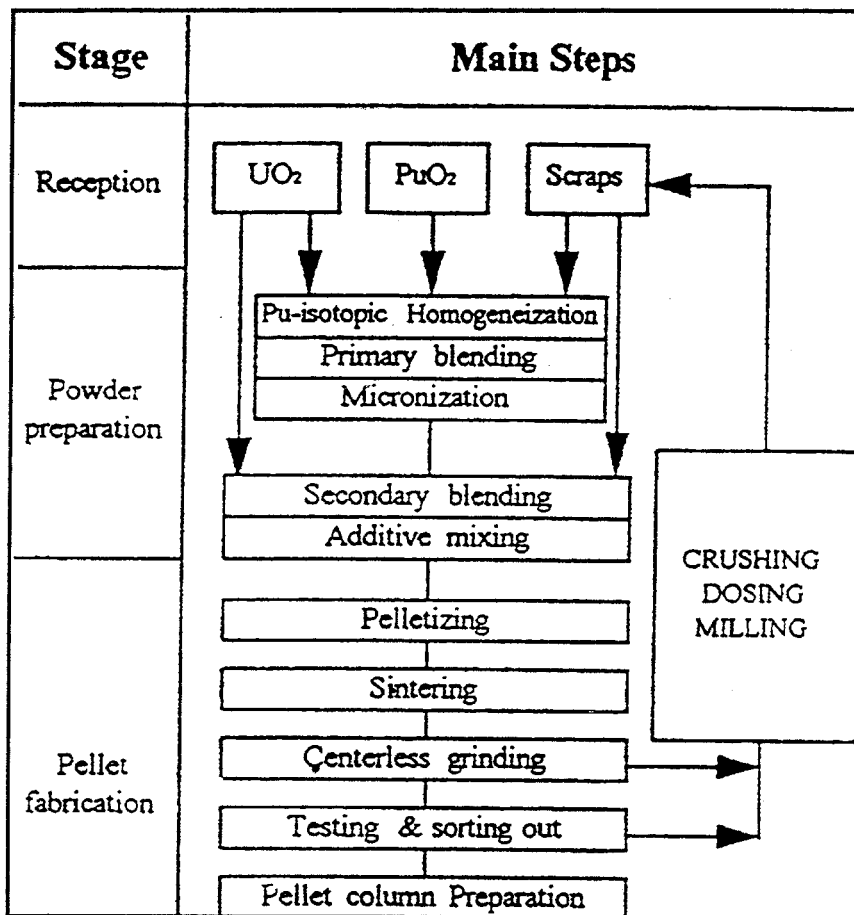


Figure 11. Sintered pellets obtaining by MIMAS process

The powder preparation has two blending steps: the primary (master) blend obtained by ball milling (micronization) and secondary (final) blend. The powder obtained is pelletized. The green pellets are sintered in H<sub>2</sub>/Ar atmosphere and the sintered pellets are dry grinded.

The MIMAS process can lead to excellent isotopic homogeneity of the Pu in the product even with Pu of various origins, forms and batch sizes because it has double blending.

A way to manufacture MOX fuel (for FBRs) is the microsphere obtaining and densification by vibro-compacting [34].

The concentrated solution of U and Pu nitrate mixed with the organic gelling agent is added in ammonia like small drops. The obtained microsphere are washed in water, dried, calcinated and sintered. The pin is filled with sintered microsphere by vibrocompacting.

In Canada, AECL MOX fuel fabrication activities are conducted in the **Recycle Fuel Fabrication Laboratories (RFFL)**. The RFFL fabrication process [35] is presented in Figure 12.

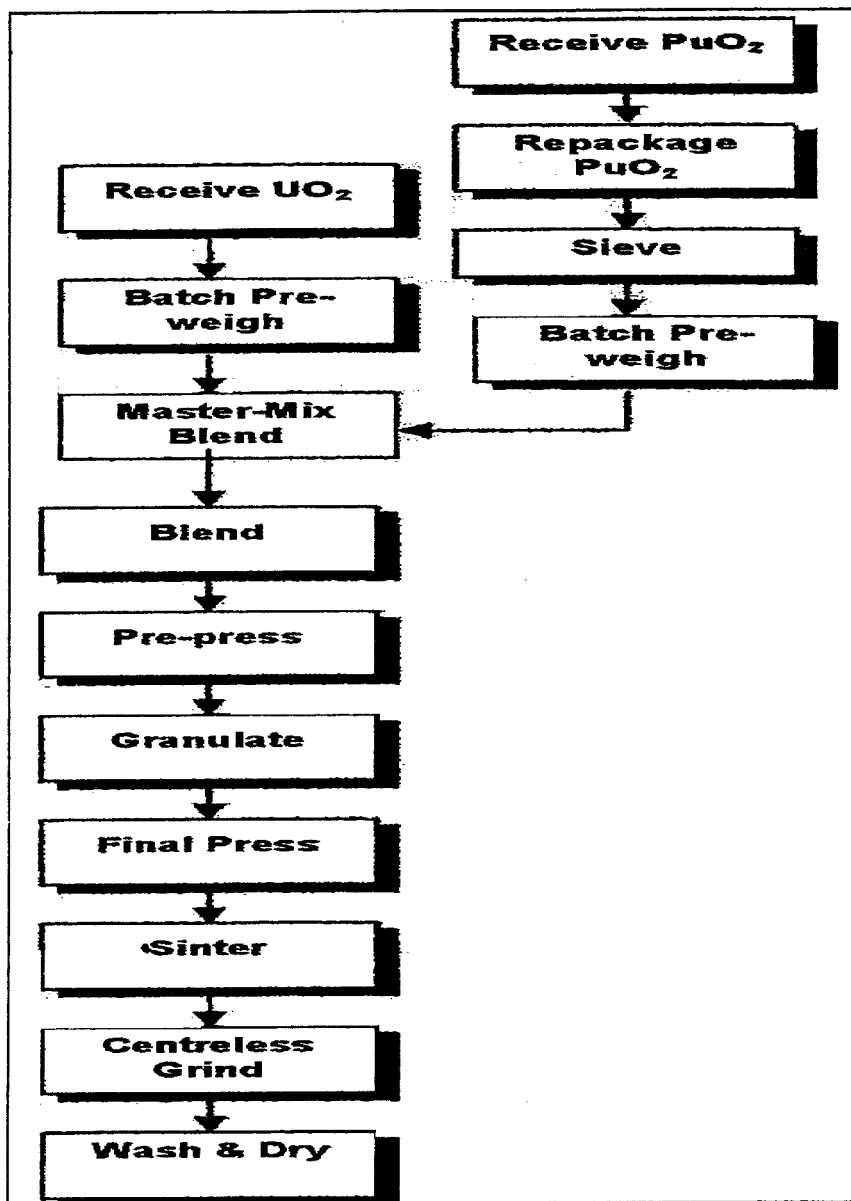


Figure 12. . Sintered pellets obtaining by RFFL process

The process consists in blending of  $UO_2$  and  $PuO_2$  powders in Master-Mix blend followed by usual manufacturing of sintered pellets from no free flowing powder. Therefore, the powder is pre-pressed and obtained compacts are granulated. The granulation process is necessary to adapt the powder flowability for transport and filling of the pressing tools. The granules are pressed and green pellets are sintered in hydrogen atmosphere. The sintered pellets are grinded in a centerless grinding machine.

The Indian option for MOX sintered pellets manufacturing is approximately the same [36].

## 7. PROPOSAL FOR FUEL MANUFACTURING FROM RU

For CANDU owners, the utilization of fuel based on the RU way seems to be very attractive particularly having in view the shorten time necessary to develop adequate manufacturing

processes to perform suitable tests. Romania is interested to enlarge the existing R & D activities in this field.

Romania have some important facilities necessities for the fuel development, such as:

- Nuclear fuel plant;
- TRIGA reactor (14 MW) for materials testing;
- Post-irradiation laboratories;
- Out of pile facilities;
- Competence and experience in CANDU fuel type manufacturing.

We are open for a co-operation in order to obtain all the information needed for industrial implementation.

## 8. CONCLUSIONS

In the nuclear word, many efforts for fuel manufacturing resistant to extended burn-up were make. Many new technology offer the possibility to use the available manufacturing equipment and quality assurance programs from commercial production without specially modifications. The technologies for extended burn-up fuel manufacturing are available. The main direction in this field will be to adapt the existent facilities for this reason.

Increasing burn-up, which allows the utility to get the same kWh output with a reduced amount of higher enriched fissile material, provides a saving not only in the cost of fuel fabrication but also in the cost of disposal of the irradiated fuel. This latter cost is two to four times higher than that of fuel fabrication. Reducing the quantity of irradiated fuel also has a positive impact on the environmentally acceptable solution adopted for its disposal.

This is true not only for fresh uranium fuel, but also for mixed oxide (MOX) fuel. For MOX fuel, the goal is to achieve the same higher burnups as with uranium fuel. Higher burnups make MOX fuel more competitive in comparison with fresh uranium fuel, because the latter requires more uranium feed and enrichment to achieve higher burnups. Meanwhile, the safety authorities are increasing their requirements to license higher burnup fuels, asking for more representative material tests under accidental conditions, more feedback from experience and testing, before granting a license.

## REFERENCES

- [1] H. GROSS, R. EBERK, "LWR Fuel Nods Extended Burnup: Design And Experimental Basis", Proc. IAEA Tech. Com. Meet on "Improved utilization of water reactor fuel with special emphasis on extended burnup and Pu - recycling" Mol, Belgium, (1984).
- [2] T.J CARTER, "The Effects Of UO<sub>2</sub> Pellet Shape On Strains Induced In Collapsible Zy Cladding", Rapport AECL 5978 (1977).

- [3] J.D. PALMER, K.W. HESKETH, P.A. JACSON, "Water Reactor Fuel Element Performance Computer Modelling", Applied Science, UK (1983) 221.
- [4] W.B. LEWIS, "Large Scale Nuclear Energy From The Th Fuel Cycle", Rapport AECL 3980 (1971).
- [5] MACDONALD, R.J. HASTINGS, "Graphite Disk UO<sub>2</sub> Fuel Element Designed for Extended Burnup At High Power", Nucl. Tech., 71 (1985) 430.
- [6] S. DOI et al, "Improvement Of Fuel Pellet For High Burnup", IAEA-TCM "Fuel Performance at High Burnup for WRs", Studsvik, Suedia (1990).
- [7] I. HARADA, S. DOI, S. ABETA, K. YAMATA, "Behaviour Of Large Grain UO<sub>2</sub> Pellet By New ADU Powder, Proc. IAEA Tech. Com. Meet on "Water Reactor Fuel Element Modeling at High Burnup and its Experimental Support", Bowness on Windermere, UK (1994).
- [8] J. A. TURNBULL, "The Effect Of Grain Size On The Swelling And Gas Release Properties Of UO<sub>2</sub> During Irradiation", J. Nucl. Mater. 50 (1974)62.
- [9] T. J. CARTER, "Experimental Investigation Of Various Pellet Geometries To Reduce Strains In Zirconium Alloy Cladding", Nucl. Tech., 45 (1977) 166.
- [10] E. ROLSTAD K.D. KNUDSEN, "Studies Of Fuel-Clad Mechanical Investigation At The Resulting Interaction Failure Mechanism", Technology, 13 (1972) 168.
- [11] S. ROSENBAUM, T. C. ROWLAND, "Large-Scale Demonstration Of Zy - Barrier Fuel", Proc. IAEA Symp. On "Improvements in Water Reactor Fuel Technology and Utilization" Stockholm (1986).
- [12] F. GARZAROLLI, R. HOLZER, "Waterside Corrosion Performance Of Light Water Power Reactor Fuel", Nucl. Energy, 31 (1992) 65.
- [13] G. R. KILP et al., "Corrosion Experience With Zircaloy And ZIRLO<sup>TM</sup> In Operating PWRs", Proc. ANS/ENS Topical Meeting on LWR Fuel Performance, Avignon, France (1991).
- [14] K.C. RADFORD, J.M. POPE, "UO<sub>2</sub> Fuel Pellet Microstructure Modification through Impurity Additions", J.Nucl.Mat, 116, (1983), 305-313.
- [15] M.EL.SAYED, R.LORENZELLI, "Kinetics Of Initial Stage Of Sintering Of UO<sub>2</sub> And UO<sub>2</sub> With Nb<sub>2</sub>O<sub>5</sub> Addition", J.Nucl.Mat, 87, (1979), 90-96.
- [16] D. DIACONU, D. OHÂI, V. BĂLAN, "Microstructural Aspects Of Grain Growth Induced By The Dopants In UO<sub>2</sub> Sintered Pellets", Mat.Sci.Forum 126-128 (1993), 427.
- [17] D. OHÂI, D. DIACONU, V. BĂLAN, I. MIRION, "Sintered Pellets Having Large Grains Structure For Advanced Nuclear Fuels", Proceedings of National Energy Conference CNE'94-Neptun, 1994, Romania.
- [18] "Effects Of Nb<sub>2</sub>O<sub>5</sub> Addition On Grain Growth And Densification In UO<sub>2</sub> Pellets Under Reducing And/Or Oxidizing Atmospheres", J. Nucl. Mat, 209, (1994), pp.280-285.
- [19] D. OHAI, "Contribution To Fuel Manufacture Technologies For Advanced Reactors", Ph.D. Thesis, Institute for Atomic Energy, Bucharest-Romania, 1997.
- [20] H. ASSMANN et.al., "Doping UO<sub>2</sub> With Niobia - B Beneficial Or Not?", J. Nucl. Mat. 98, 1981, 216.
- [21] I. TANABE, M. OGUMA, H. MASUDA, JP patent document 3-287096/A/, JP patent document 2-87578.
- [22] K.W. LAY et.al. US patent document 4, 869, 868/A/.
- [23] K.W. LAY et.al. US patent document 4, 869, 867/A/.
- [24] P. DEHAUDT, A. CHOTARD, Nuclear Europe Worldscan, No 11-12, Nov.-Dec. 1997, 65.

- [25] M. ROTH, V. RADU, D. OHÂI, D. DIACONU, V. BĂLAN, "Mechanical Behaviour Of Large Grains UO<sub>2</sub> Pellet" - Proceedings of Romanian First International (4<sup>th</sup> National) Conference on Powder Metallurgy, 4-7 July 1996, Cluj-Napoca.
- [26] J.C. KILLEEN, "The Effect Of Niobium Oxide Additions On The Electrical Conductivity Of UO<sub>2</sub>", J. Nucl. Mat. 88 (1980),185-192.
- [27] M. ASOU, Y. TAKAHASHI, "High-Temperature Heat Capacity Of Nb-Doped UO<sub>2</sub>", J. Nucl. Mat. 195, (1992), 317.
- [28] D. OHAI, "Obtaining Of UO<sub>2</sub> Sintered Pellets With Controlled Porosity", will be presented to Second International Conference on Powder Metallurgy, Cluj-Napoca, Romania, 2000 July 6-8.
- [29] H.C. SUK, J.H. PARK, B.J. MIN, K.S. SIM, W.W. INCH, T.G. RICE, "Technical Aspects And Benefits Of The Use Of RU In CANDU Reactors", Proceedings of Sixth International Conference on CANDU Fuel, 1999 September 26-30, Niagara Falls, Canada, vol.1, pag.444-459.
- [30] J.D. SULLIVAN, D.S. COX, "AECL's Progress In Developing The DUPIC Fuel Fabrication Process", Proceedings of 4<sup>th</sup> International Conference on CANDU Fuel, 1995 October 1-4, Pembroke, Canada, pag. 4A\_49-4A\_58.
- [31] J.D. SULLIVAN, M.A. RYZ, J.W. LEE, "AECL's Progress In DUPIC Fuel Development", Proceedings of 5<sup>th</sup> International Conference on CANDU Fuel, 1997 September 21-25, Vol.1, pag. 300-310.
- [32] K. BAE, K. KANG, M. YANG, H. PARK, "Irradiation Plan Of DUPIC Fuel At Hanaro", Proceedings of Sixth International Conference on CANDU Fuel, 1999 September 26-30, Niagara Falls, Canada, vol.1, pag.460-469.
- [33] D. HAAS, "MOX Fuel Fabrication Experience At Belgonucleaire", IAEA-TECDOC-941, May 1997, pag. 77-89.
- [34] P. PARKES, "Use Of Vibrocompacted MOX Fuel In Thermal Reactors", IAEA-TECDOC-941, May 1997, pag.93-98.
- [35] F.C. DIMAYUGA, "AECL's Experience In MOX Fuel Fabrication And Irradiation", IAEA-TECDOC-941, May 1997, pag.373-385.
- [36] K. KUMAN, H.S. KAMATH, "MOX Fuel Development For The Indian Nuclear Power Program, IAEA-TECDOC-941, May 1997, pag. 47-56.

# Technological problems and counter-measures on equipment materials for reprocessing of high burnup fuels

**K. Kiuchi, T. Kato, H. Motooka, S. Hamada**

Japan Atomic Energy Research Institute,  
Japan

## Abstract

The reliability of structural materials is considered as one of the most important technological issues on the commercial reprocessing of high burnup fuels. The durability prediction study of equipment materials used in commercial purex process has been conducted in the JAERI. From the experimental results obtained by scaled mock-up tests and laboratory tests, the stress corrosion cracking (SCC) for a dissolver made of zirconium and the trans-passive corrosion of heat transfer tubes for evaporators made of austenitic stainless steels have been clarified as critical issues on the reliability. The susceptibility to these failures increases with THE amount of TRU and FP elements included in spent fuels, because Np, Pu, Ru, Pd act as strong oxidizers. As counter-measures against these problems, the development of the modified alloys is going on in the JAERI. It has been found that the intergranular corrosion resistance of stainless steels is possible to be completely improved by purifying the electron beam melting process and by modifying the metallographic structure. The other counter measure is to inhibit the trans-passive corrosion by addition of oxide film former elements such as W and Si. It has also been found that the susceptibility to SCC of Zr can be improved by addition of titanium. However, the addition of titanium decreases the corrosion resistance of Zr. We selected niobium alloys as alternative materials to zirconium. By addition of tungsten to the niobium, the corrosion resistance and the mechanical strength have been improved. This niobium alloy can be used in heavily corrosive nitric acid contaminated with fluorine. It is considered that the difference between corrosion resistance of Zr and Nb-alloys is attributed to the chemical stability of the oxide films ( $\text{MO}_2$  on Zr and  $\text{M}_2\text{O}_5$  on Nb).

## 1. GENERAL SITUATION OF PUREX TYPE REPROCESSING FOR HIGH BURNUP FUELS

From economical reason and practical experiences, the present commercial reprocessing plant using the purex process would be able to apply for reprocessing high burn-up and MOX fuels more than 45GWd/t used in advanced water cooling reactors. The development of life prediction techniques and corrosion resistant alloys is considered to be required for improving the safety and performance of equipment materials used in highly corrosive nitric acid solutions<sup>(1-5)</sup>. Its corrosiveness is enhanced by enriching TRU and FP elements derived from high burnup spent oxide fuels<sup>(6)</sup>. From the fundamental life prediction study<sup>(4-5)</sup> and failure analyses of mock-up testing data of Tokai and Rokkasho reprocessing devices<sup>(5)</sup>, the corrosion mechanism and controlling factors on the performance of equipment materials have been elucidated<sup>(3)</sup>. The corrosion problems have been observed in component materials used in heavily oxidizing conditions like heat conducting tubes<sup>(6)</sup>. This mechanism is considered to be formed by the high oxidizing atmosphere due to  $\text{NO}_x$  gas by the thermal decomposition of nitric acid itself at boiling surfaces. It is enhanced with dependent on the vaporization rate and formation rate of oxidizer ions from dissolved species of TRU and FP. Ultra-low carbon austenitic stainless steels such as types 304ULC and 310Nb designed for the present reprocessing process like evaporators would be suffered from grain boundary attack with increasing oxidizer ions formed at heat conducting surfaces, even if evaporators operated at low boiling points<sup>(7-9)</sup>.

On the other hand, zirconium and titanium alloys have been used in dissolver and evaporators operated at ambient pressure<sup>(10)</sup>, instead of stainless steels with the inherent property of trans-passive corrosion. However, these materials have a high susceptibility to local attacks and environmental cracking due to the low chemical stability and low repassivation rate of oxide film<sup>(11-16)</sup>. Zirconium of 702 grade has a high susceptibility to trans-granular type stress corrosion cracking which propagate along (0001) planes, even if it is nitric acid solutions with low concentration less than 65% as described later. Although the resistance to SCC of zirconium is able to improve by alloying like Ti, it is difficult to improve without decreasing the corrosion resistance. This limitation is due to the spinodal decomposition in relation to the cph type crystal structure composed of ABAB stacking. On the other hand, Ti-5Ta alloy with relatively high solubility in nitric acid has the low corrosion resistance at liquid-vapor interface exposed to the condensed nitric acid and shows mass-transfer of volatile corrosion products.

We have been developed two kinds of advanced technologies concerning the purex reprocessing materials aiming at high burnup spent fuels. One is to develop quantitative techniques for life prediction of major equipment materials. It is composed of three major programs, namely, the mock-up tests by using the small-scaled devices simulated to the practical design, laboratory tests for examining corrosion controlling factors by using small specimens and the establishment of data base system for evaluating reliability. The other one is to develop advanced materials with high corrosion resistance against highly oxidizing nitric acid solutions.

For minimizing the trans-passive corrosion of stainless steels, two kinds of advanced alloys have been developed. One is to modify these steels into immunity against grain boundary attacks by minimizing grain boundary segregation of harmful elements. It was achieved by means of modifying the steel making process, so-called the EB-SAR treatment, that is composed of the following processes:

- adjusting the chemical composition,
- refining by electron beam melting,
- stabilizing minor impurities through the thermo-mechanical treatment so-called SAR process (strained, aged and recrystallized)<sup>(7, 8)</sup>.

The other is a new Cr-W-Si Ni base alloy so-called RW alloy. This alloy composition was designed for inhibiting the trans-passive corrosion by enriching oxide former elements such as Cr, W and Si with different electrode potential for forming the protective film. On the other hand, niobium alloys were selected for the most promising alternative materials instead of Zr and Ti alloys which have a high susceptibility to local attacks and environmental cracking as stated above.

## 2. LIFE PREDICTION STUDY FOR REPROCESSING EQUIPMENT MATERIALS

Table 1 shows the outline of life prediction study concerning the RRP equipment materials as reported in elsewhere<sup>(16)</sup>. The evaporator for nitric acid recovery made of type 304ULC austenitic steel and the dissolver made of type 702 metallic zirconium were selected for testing the reliability. This study is composed of three major programs, namely, the mock-

up tests by using the small-scaled devices simulated to the practical design, laboratory tests for examining corrosion controlling factors using small specimens and the establishment of data base system for life prediction. Important parameters on this study were extracted by analyzing the past data obtained from the life prediction study on the Tokai reprocessing equipment materials. The mock-ups were designed by considering the most important parts on objective devices with respect to the quantitative life prediction, namely, heat conducting tubes in an acid recovery evaporator and the thermal jacket in a dissolver. The mock-up of thermo-siphon type acid recovery evaporator consists of seven heat conducting tubes with the practical scale and it has been operated in the maximum corrosive condition expected in the steady state operation. From pre-examination tests for clarifying the effect of metallic ion species on nitric acid solution chemistry, the corrosion mechanism was elucidated with based on thermodynamic analysis and thermal-fluid dynamics. Mock-up testing conditions and corrosion monitoring methods were selected based on the plant operation planning and pre-examination data. This mock-up was constructed as shown in Fig. 1. After the PSI (pre-service inspection test), the operation started from April 1997 by simulating the steady state operating conditions. The mock-up of a dissolver is designed for simulating a thermal jacket made of metallic zirconium by focusing on the heat conducting surfaces (Fig. 2). Laboratory testing methods were programmed to obtain reference data of the important corrosion parameters expected in stainless steels and metallic zirconium used in the practical equipment, by considering the effect of radio-active elements like FP and TRU. The computer simulation is planned to develop the evaluation codes that are required for the life prediction based on experimental data. Compared with the practical equipment, the simulation rate of mock-ups is evaluated with computer simulation like thermal-fluid dynamics. Major parameters that control the corrosion rate of heat transfer tubes in a nitric acid evaporator were evaluated as shown in Fig.3. The corrosion mechanism at heat transfer surfaces is schematically shown in Fig. 3-A. The corrosion parameters found in Fig. 3-A is evaluated by thermal-fluid dynamics as Fig. 3-B. The accelerated effect of corrosion on heat transfer surfaces was experimentally clarified by results of 1st ISI as shown in Fig. 3-A schematically. Even if the corrosion is at low boiling temperature, the rate is mainly controlled with the heat flux. It shows the remarkable difference in the corrosion mechanism between immersion and heat transfer conditions as shown in Fig. 3-A.

### 3. DEVELOPMENT OF CORROSION RESISTANT MATERIALS FOR REPROCESSING

The outline of development study of corrosion resistant materials applied for oxidizing nitric acid environments is shown in Table 2 as the historical sequence of commercial material development. The corrosion problems have been gradually elucidated with dependent on the specific burnup of spent fuels. It means that the corrosiveness of reprocessing nitric acid increases with TRU and FP contents in spent fuels as stated above.

#### 3.1. Advanced Materials for Devices Operated at Low Boiling Point

- 1) The development process of EB-SAR treated type 304ULC steel is shown in Fig. 4, compared with the corrosion data of commercial one. To attain complete immunity to intergranular attack, the combined method of both refining and modifying the metallographic structure is required. This steel has the annealed fine grain structure with clean grain-boundaries recrystallized. The small amount of Ti acts as scavenger elements for stabilizing harmful trace impurities. The mechanical strength of the purified steel is

able to maintain by the Hall-Petch effect and dispersion hardening of fine precipitates. As shown in Fig. 5, alloying of several metallic elements which act as the stable oxide former would be required to attain the sufficient corrosion resistance over a wide range of the corrosion potential expected in reprocessing nitric acid environments. According to this principle, high Cr-W-Si Ni base RW alloy which contains Cr, W and Si as oxide former alloying elements have been developed in our study. Electron beam melting is the most effectively practical means for enhancing the maximum solubility limit of these elements by improving the workability;

- 2) The corrosion resistance of EB-SAR treated type 304ULC and Cr-W-Si Ni base RW alloy with the chemical composition of Table 3 was compared with that of commercial grade 304ULC by corrosion tests simulated to heat conducting surfaces in nitric acid solutions controlled at low boiling points. Markedly difference in the corrosion rate among above alloys was observed in Cr<sup>66</sup> bearing nitric acid solutions as seen in Fig. 6. The corrosion rate of commercial type 304ULC increased markedly with testing time up to equilibrate with the consumption rate of Cr<sup>66b</sup>. Compared with results of EB-SAR treated type 304ULC steels, it is clear that it is able to minimize the corrosion rate by inhibiting grain boundary attacks. Moreover, the corrosion rate of RW alloy is promptly astringent in the low corrosion rate. The modification method of these modified alloys is considered to be an effective means to inhibit the heat conducting surface corrosion.

This modified EB-SAR treated type 304ULC steel would be limited to a practical use with respect to cost and the mechanical strength due to refining. To minimize these problems, the appropriate cladding technique of this steel on type 304L steel which is faced to the steam heating side, was investigated. Several means of cladding technologies like the HIP, continuous EB melting and the diffusion bonding were examined. The diffusion bonding is selected as the most promising technique. Diffusion bonding behavior by hot rolling was minutely examined at several temperatures higher than 825se which corresponds to the grain growth temperature, by changing the reduction ratio within 60%. An appropriate diffusion bonding region without defects is selected by examining metallographically after bending tests of cladding specimens as shown in Fig. 7. An appropriate cladding temperature region by diffusion bonding of high Cr-W-Si Ni base RW alloy on type 304L steel is limited by austenite phase stability of RW alloy, because of the formation of eutectics at high temperature and the precipitation of silicides at low temperatures. The workability of RW alloy was examined from the ductility loss by tensile tests as a function of heating temperatures. From these results, an appropriate temperature region with stable austenite phase was selected as near 1100en as shown in fig. 7. A suitable bonding at 1100 a was obtained by the reduction ratio of 50% by hot rolling .

### **3.2. Advanced Materials for Devices Operated in Ambient Pressure**

As alternative materials of type 300 series austenitic stainless steels with characteristics of trans-passive corrosion, metallic zirconium has been used for devices operated in ambient pressure. However, it has the susceptibility to SCC as stated already. The SCC is strongly dependent on the texture of cph crystal structure as shown in Fig. 8. The propagation of SCC along L direction is easier than it is along T direction, because of preferential allay of (0001) planes. Therefore, the texture of reprocessing grade zirconium is controlled to minimize the susceptibility to SCC. However, TIG weld joints are difficult to control the crystal texture. As shown in the right picture of Fig. 9, the susceptibility increases with increasing nitric acid concentration. This tendency of T specimens is more clearly than that of L specimens. On the

other hand, the susceptibility of TIG weld joints depends on the crystal texture of each position, namely, HAZ(heat affected zone) > Base metal > DEPO(deposit metal). From the crack propagation rate evaluated by fatigue tests in boiling 3N HNO<sub>3</sub>, the difference is not observed (Fig.10). It means the difference of acceleration mechanism between the crack initiation and the crack propagation. The rearrangement of crystal texture due to local plastic deformations is considered to be easy at the front of fatigue cracking with high stress field. From electrochemical measurements and mechanical tests, it is clear that the susceptibility to SCC of zirconium is controlled by the low repassivation rate and deformation behavior accompanied with low temperature creep<sup>(12-15)</sup>. It is considered to be enhanced at heat transfer surfaces with the high oxidizing potential

The corrosion resistance in nitric acid solutions with high oxidizing potential near 1.8V like heat transfer surfaces under ambient pressure is considered to be dependent on the chemical stability of oxide films with the most high valence. The corrosion rate of refractory metals depends on the solubility of this oxide film in nitric acid solutions and that was clarified. The saturation solubility of above oxide powder with extra-pure grade in boiling nitric acid in the concentration range of 3N to 14.4N was examined as the corrosion index of major refractory metals. Nb and Ta showed the lowest value as shown in Fig. 11. Nb as same as Ta is easy to form high valence oxide films like M<sub>2</sub>O<sub>5</sub> that shows the minimum solubility in nitric acid solutions, even if it is in fluorine doped nitric acid, compared with MO<sub>2</sub> oxide formers like Ti, Zr and MO<sub>3</sub> oxide formers like Mo,W as shown in Fig. 12. From pre-examination results, the applicability as structural materials including workability and alloying was examined and niobium was selected as a base metal for this purpose. To modify the mechanical strength of niobium with bcc type crystal structure by alloying is easier than that of Ti or Zr with hcp type crystal structure. Several niobium base binary alloys were made by electron beam melting for examining the appropriate alloying composition. The mechanical strength of this metal was improved by alloying refractory metals with a large metallic ion size like W and Hf. The corrosion resistance of this metal was improved by adding Ta and W with the low solubility in nitric acid solutions. Accordingly, alloying of 5-10 atomic %W is considered to be the most effective means for modifying both properties of Nb as shown in Fig.13.

#### 4. Conclusions

Technological problems and counter-measures on equipment materials for reprocessing using purex process aiming at high burnup fuels were discussed based on the present JAERI research project. The development of experimental techniques is necessary for the quantitative life prediction of equipment materials used in heavily corrosive nitric acid. The performance of evaporators made of ULC grade stainless steels operated at low boiling point is controlled by trans-passive corrosion at heat transfer surfaces. The performance of dissolver and evaporators made of Zr is controlled with the resistance against stress corrosion cracking. The arrangement of sufficient database for modeling aging degradation and the development of ISI techniques are required for the life prediction of these equipment materials with respect to high burnup fuels reprocessing. New corrosion resistant alloys and cladding materials have been developed and evaluated by considering the application to the advanced purex reprocessing equipments as follows:

- 1) Compared with commercial grade type 304ULC steels, EB-SAR treated type 304ULC steel and high Cr-W-Si Ni base RW alloy showed excellent corrosion resistance in oxidizer

doped nitric acid solutions under heat flux control. To inhibit grain boundary attacks and to form stable passive films countermeasures to modify the corrosion resistance of components materials exposed to oxidizing nitric acid under heat flux are considered to be effective. The applicability to the practical use of these alloys is possible to expand by cladding with type 300 series austenitic stainless steels as a heater side material. The appropriate diffusion bonding condition of each developed alloy was selected by hot rolling tests.

- 2) Niobium with bcc type crystal structure was selected as one of the most promising refractory metals applied to heavily corrosive nitric acid, because it forms  $M_2O_5$  stable oxide film. Both the corrosion resistance and the mechanical strength of metallic niobium was improved by alloying wolfram .

### ACKNOWLEDGEMENT

This research was promoted as one of the atomic energy research on nuclear energy promoted by the Science & Technology Agency. The life prediction study was referred from the opened reports. The steel refining process by EB-CHR method was made by the collaboration with Japan Energy Corp. Limited.

### REFERENCES

- [1] K.KIUCHI et.al.: RECOD`91, Vol.2(1991)549 &1054.
- [2] K.OKUBO et.al. ; RECOD`87 ,Vol.2,p1181(1987).
- [3] K.KIUCHI; J. Atomic Energy Society of Japan,31(1989)229.
- [4] K.KIUCHI et.al.: RECOD`94,Vol.3,Materials selection(1994).
- [5] K.KIUCHI et.al.; JAERI-M 92-207(JAERI-CONF 1)(1992)581.
- [6] R.SHAW et.al.; British Corrosion Journal,Vol.25(1990)87.
- [7] K.KIUCHI et.al.; Journal of Tetsu to Hagane 70(1984)112.
- [8] K.KIUCHI et.al.; Journal of Nuclear Materials, 212-215 (1994)551.
- [9] J. A. BEAVERS et.al.; Corrosion 36(1981)292.
- [10] P.FAUVET et.al.; EUROCORR`92 SECN/14157(1992).
- [11] K.KIUCHI et.al.; Proc.of Int.Symp. on Plant Aging and Life Prediction (1995)861.
- [12] C.KATO et.al.; ibid (1995)883.
- [13] M.SAKAIRI et.al.; ibid (1995)875.
- [14] T.MOTOOKA et.al.;Proc. of 13th Int. Corrosion Conf. Australia(1996)223.
- [15] A.TOYAMA et.al.; JAERI-Research 96-021(1996).
- [16] K.KIUCHI et.al.; RECOD`98,Vol.3 (1998)859, 867.

## CARA design criteria for HWR fuel burnup extension

**P.C. Florido, R.O. Cirimello, J.E. Bergallo, A.C. Marino, D.F. Delmastro,  
D.O. Brasnarof, J.H. Gonzalez, L.A. Juanicó**

Centro Atómico Bariloche,  
Comisión Nacional de Energía Atómica,  
Bariloche, Argentina

### Abstract

A new concept for HWR fuel bundles, namely CARA, is presented. The CARA design allows to improve all the major performances in the PHWR fuel technology. Among others, it reaches higher burnup and thermohydraulic safety margins, together with lower fuel pellet temperatures and Zry/HM mass ratio. Moreover, it keeps the fuel mass content per unit length and the channel pressure drop by using a single diameter of fuel rods.

### 1. INTRODUCTION

In Argentina, there are two operating NPPs (Atucha and Embalse). Both of them are cooled by pressurized heavy water and are fueled with natural uranium, but they have very different design for the primary system. Embalse is a standard CANDU 6 reactor (horizontal pressure tube, see figure 1), and Atucha I have vertical fuel channels inside a pressure vessel reactor (Siemens' design, see figure 2). Therefore, their nuclear fuel elements are strongly different (see figures 3 and 4). Embalse uses a national developed CANDU 37 rods fuel element, and Atucha uses a long bundle similar to PWR rod type, both supplied by a private owned fuel -manufacturing company, namely CONUAR. This diversified scenario leads to several complications from the point of view of the production at commercial scale, especially when the competitiveness is a main task in electricity generation costs.

Nowadays, the CANDU fuel design is a very active area with a new bundle generation (CANFLEX) [1] following the present LWR trends, enabling to reach higher burnup with smaller rod diameter and, consequently, lower central temperature, linear and surface heat flux. Taking into account that the Argentinean electric system dispatch for fuel marginal cost, it is reasonable to have a new generation of advanced nuclear fuels. These fuels must lead, the most ambitious goals described, with an additional one: one fuel element for both types of NPPs in order to achieve the smallest costs at small-scale commercial production.

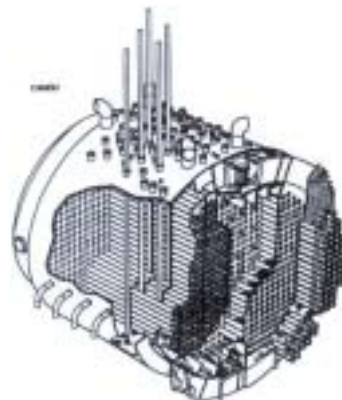


*FIG. 1. CANDU reactor.*



## 2. INITIAL CRITERIA FOR A NEW BUNDLE CONCEPT

Instead of small changes in fuel element improvements, we analyze the feasibility study of a completely new fuel element, for both types of NPPS, namely CARA (Advanced Fuel for Argentinean Reactors).

This fuel element was set up with the following objectives:

- 1- To fit for both NPPS,
- 2- Increasing the heated perimeter,
- 3 - Using a single type of fuel rod diameter,
- 4- Decreasing the fuel center temperature,
- 5 - Decreasing the Zry/Uranium mass ratio,
- 6- Keep the higher uranium mass per fuel length unit,
- 7- Do not change the hydraulic pressure drop of each NPP core,
- 8- Burnup extended using SEU (Slightly Enriched Uranium),
- 9- Do not exceed the fabrication cost of the CANDU fuel.

As in the CANFLEX design, which has many of the same objectives using two different rod diameters, the CARA fuel must explore new choices. Increasing the fuel rod number, the distributed friction is increased, related to the smaller hydraulic diameter. To keep constant the core pressure drop leads to the CANFLEX solution, losing a single rod diameter (condition number 3), or use one type of rod diameter losing uranium mass (condition number 6). The key in the CARA solution is a fuel element length twice the present CANDU fuel substituting a couple of elements for a single one in the refueling machine in order to decrease the concentrated pressure drop and using this handicap to create a new bundle of many thin fuel rods.

At present, the Atomic Energy Commission of Argentina (CNEA) is developing the CARA together with the fuel manufacturing company (CONUAR) and the interest of the nuclear power operator utility (NASA) in Argentina. The scope of the present project is to develop the CARA with the commercial production of CARA bundle using 0.9 % enrichment fuel.

## 3. GENERAL CHARACTERISTICS

### 3. 1. Fuel Rods Definitions

Analyzing the pressure drop of an Embalse fuel channel [2], and subtracting the distributed pressure drop [3, 4], we could find the concentrated pressure drop of one CANDU bundle (end plates and spacers). In reference [5] several changes in the CANDU fuel are studied and, using these data, pressure drop of the end plates and the spacers in present CANDU 37 rods bundle could be calculated and checked with our own data set.

An important pressure drop is concentrated on the end plates, and if we consider a bundle with twice of length of the usual CANDU fuel (without compatibly problems with CANDU 6 refueling machine), we could decrease the hydraulic diameter, increasing the number of rods.

To check this approach, two type of curves were developed for a given fuel channel in which the radius was changed in order to keep constant the uranium mass (mass constant curve) or

hydraulic pressure drop ( $\Delta p$  constant curve) for different number of rods. Clearly both curves monotonously decrease for higher rod diameters, and if standard CANDU 6 bundle is taken as a basis, both curves have the same radius at 37 rods number. At higher rod number, if the  $\Delta p$  is kept constant, uranium mass must decrease (mass constant curve above the hydraulic pressure drop curve).

But if a twice length bundle is used, both curves cross at 66 rods number. The  $\Delta p$  gain for the end plates number reduction, gives a  $\Delta p$  credit for the distributed friction together with a new concept for spacer function with only 33 % pressure drop reduction. As CARA fuel element must be compatible with two types of fuel channels, the most restrictive curve must be used for mass and  $\Delta p$  curves. Atucha has the most restrictive  $\Delta p$  requirements, and Embalse has the most restrictive mass requirements. Using both curves, with 1 meter long bundle, approximately 50 rods could be used for both NPPS, as is shown in figure 5.

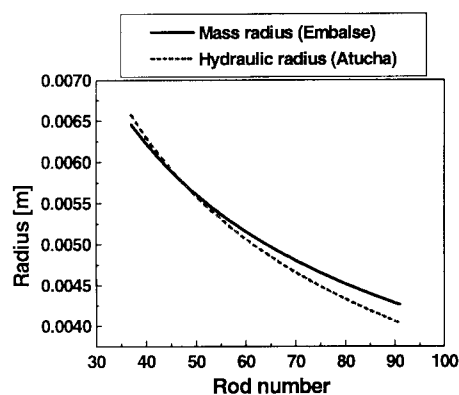


FIG. 5. Curve with the “mass” and “hydraulic” radius of CANDU and Atucha.

### 3.2. Bundle Geometry

For the study of different bundle geometries, symbolic algebra languages enable very simple and fast evaluation; including rod ring rotation and different central rod number. Using this type of approach, 4 final geometries were studied, with 48 to 52 fuel rods. Finally, a 52-bundle geometry was selected, for the good symmetry and compactness of the array. This geometry, shown in figure 6, has 4, 10, 16 a 22 rods per ring. The reduction of number or plugs and end plates gives a uranium credit that could be used to increase the bundle uranium mass.

The corresponding pellet diameter is very similar to present smallest CANFLEX one, but with slightly thinner clad thickness and present gap clearance of CANDU 37 rods bundle.

### 3.3. Mechanical Concept

General dimensions of the first prototype series are based in simple engineering solutions, in order to perform different tests and produce an extensive engineering feedback in the design concept. Using an outside diameter of 10.86 mm and 0.35 of clad thickness, the bundle has a double total length of the CANDU fuel.

Present prototypes use three spacer grids and two dismantlable end plates at both ends, both shown in figure 7 and 8. Each fuel rod is fixed in its position for one elastic spring and two fixed dimples. The rods end caps could be easily dismantled from the end plate using specially designed screw. Each loaded springs and fixed supports are built in the spacer itself, in order to drastically reduce the number of welds over the cladding length, with only four rods welded to the spacer grids in order to fix its axial position.

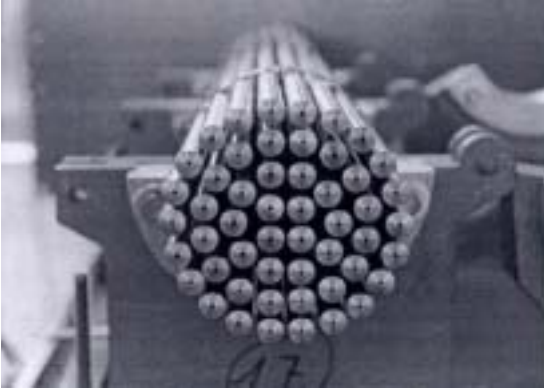


FIG. 6. Geometry of the CARA bundle with 52 fuel rod.



FIG. 7. CARA bundle spacer grid with 52 fuel rods.



FIG. 8. Dismountable end plates of the CARA bundle with 52 fuel rods.

External pads in the spacers fixed the bundle in the CANDU pressure tube for Embalse, and in an Zircalloy alloy external metal jacket or basket in order to build using 5 bundles an Atucha type fuel element. This external basket reduce the effect of the external water bypass due to the small differences in both fuel channels (the Atucha channel have an internal diameter slightly greater than Embalse).

The dismountable end plates able to easily dismount each rods after the different loop tests in order to measure any type of dimensional change and the effect of different elastic spring loads. A general view of one of the first prototypes presently tested in the hydraulic low-pressure test loop is shown in figure 9.

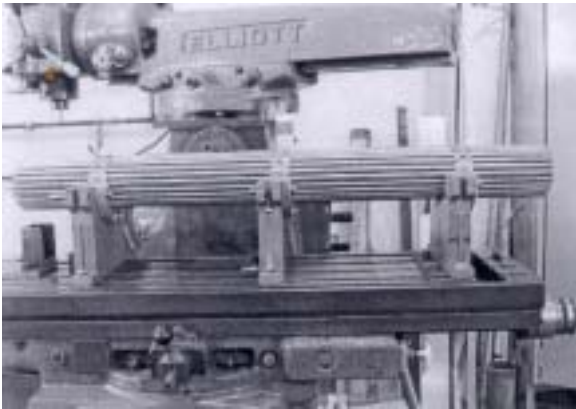


FIG. 9. External view of one of the prototypes of CARA bundle with 52 fuel rods.

4. FUEL PERFORMANCE MODELING

4. 1. Neutronic Behavior

The neutronic fuel element behavior was estimated using WIMS D/4 [6] as a neutronic cell code. Differences in pitch and pressure tube thickness were considered in the equivalent cell. Burnup could be estimated using cell reactivity evolution, and an adequate criteria for continuum refueling NPPS (figure 16). Power peaking factors for the four pin annulus were also determined as a function of burnup (figure 16)[7]. Considering the fuel rod definitions in section 3. 1, the proper power densities, dimensions and geometrical bucklings are calculated and inserted in the WIMS D4 input to estimate the CARA fuel element neutronic behavior. These points are detailed in the following subsections.

4.1.1 Average cell

The geometric fuel dimensions of CARA fuel element are the following:

Fuel element geometry	Cluster
Number of fuel rods per fuel element	52
Number of uranium fuel rods	52
Total length	990.6 mm
Fuel element radii	51.285 mm
Fuel rod length	981.5 mm
Clad external radii	5.43 mm
Clad thickness	0.34 mm
Pellet radii	5.045 mm
Pellet length	10.78 mm

The input cell for WIMS-D4 code was built using the dimensions detailed above, as the following figures show (figures 17 a and b):

#### 4.1.2. Core burnup

The radial buckling will remain constant for each NPP, as it is related with the core radii. However, for CNA, the axial buckling will change as the total fuel element length will be 5 meters instead of 5.3 meters and, in this condition, the new buckling will be  $2.7778 \cdot 10^{-5} \text{ cm}^{-2}$ .

For the CNA power density, the value used for the original fuel element was scaled considering the  $\text{UO}_2$  mass rate between this fuel element and CARA. The original power density was  $d = 29.644 \text{ MW/tU}$ . Considering an  $\text{UO}_2$  mass of 211.37 kg for five CARA elements, the new power density will be:  $24.431 \text{ MW/tU}$ .

Finally, to estimate these results, the core burnup could be calculated as the burnup that equalized the mean reactivity of core of an average cell to the required excess reactivity for operation.

To apply these criteria, old working reactivity values from both NPP data were used. For instance, in CNA NPP for a core reactivity burnup of 6100 MWd/tU, a working reactivity  $k_w = 1.019950$  resulted, and was used to obtain the core burnup with CARA fuel element, as figure 16 show.

Table 1 shows fuel burnup and power peaking factors for both NPP, with both fuel elements, and for natural and 0.9 enriched uranium.

The BOL excess reactivity, power peaking factor and burnup level could be seen in table 1, for natural uranium or SEU rods, for both types of Argentinean NPPS.

Using the power evolution, burnup level and peaking factor calculated with WIMS, together with all the geometric and compositions, a complete thermomechanical behavior could be calculated for the most restrictive CARA rods.

Table 1. Wims results, neutronic differences between the CARA fuel element for CANDU (CNE) and Atucha 1 (CNA 1).

Characteristic	CANDU37	Atucha I	CARA (in the CNE)	CARA (in the CNA I)
Natural Uranium Burnup [MWd/THU] Peak Factor [a.U.]	7500 1.1261	6100 1.0936	7529 1.1359	6368 1.1483
Uranium 9 % Burnup [MWd/THU] Peak Factor [a.U.]	14537 -	13466 -	14576 1.1484	14524 1.1577

## 4.2. Fuel Rod Thermo-mechanical Behaviour

The power history for a CANDU fuel used for calculation is included in the Figure 10. The power history sketched reaches high power (and then high temperature) and it includes two shutdowns with a step-by-step increase in the power level after the second shutdown. This hypothetical, but realistic, power history was defined with demand conditions of irradiation for a real fuel element and for the BACO code simulation [8]. Starting with that power history we extrapolate the respective history for the equivalent CARA fuel conditions in a CANDU reactor correcting by the neutronic cell calculation model. The extrapolation is based on the burnup extension and the adaptation of linear power levels of the CARA fuel. The extension in burnup is 15000 MWd/tUO<sub>2</sub> and the linear power is reduced up to a 72 % of the original value.

The Figure 11 represents the BACO code output for the temperature center of the UO<sub>2</sub> pellet for a CANDU fuel rod and for the equivalent CARA fuel using its associated power history (Figure 10). CARA fuel allows a decrement of temperature of 500°C at the maximum power level. The Figure 12 represents the local power history of the seventh axial segment of a 5 meter long Atucha I fuel element (from the top of fuel and taking into account ten axial segments). The seventh segment is the axial section most demanded during irradiation, it include a maximum power level of 547 W/cm. The CARA fuel extrapolation corresponds with the forth module of a CARA assembly in Atucha I (the forth CARA module is equivalent with the seventh Atucha segment). The burnup at end of life is 14750 MWd/tUO<sub>2</sub> and the power level is reduced a 73.4 % of the original Atucha fuel value.

The maximum calculated pellet temperature for the Atucha fuel is 1850°C during the maximum power level (see Figure 13). The temperature for the equivalent CARA module is 1340°C, conversely, a decrease of 510°C.

The BACO code calculations shows: temperature decreasing, smallest fission gas release, no restructuring and no central hole, lowest thermal expansion, and finally a best tolerance of the CARA's dimensional parameters. This allows to best manufacturing tolerance with an improvement in the dishing and shoulder of the pellet, and small plenum.

BACO code validity is sustained with the participation in international code benchmarking, the Atucha and CANDU experience, irradiation provided by international literature and own experimental irradiation [9].

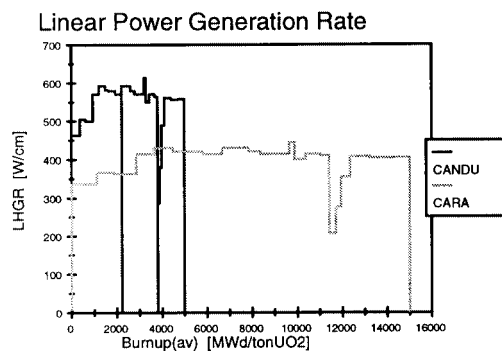


FIG. 10. Averaged power history for a CANDU fuel rod and CARA fuel in CANDU NPP.

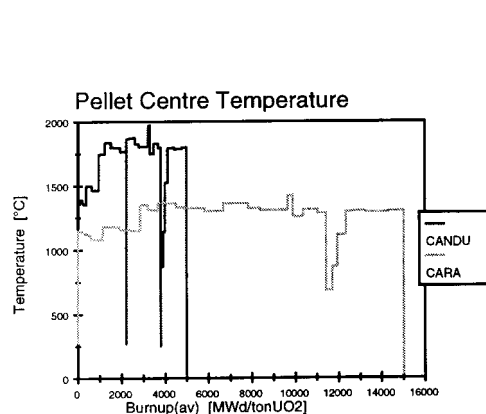


FIG. 11. Averaged temperature at the pellet center of a CANDU fuel rod CARA fuel.

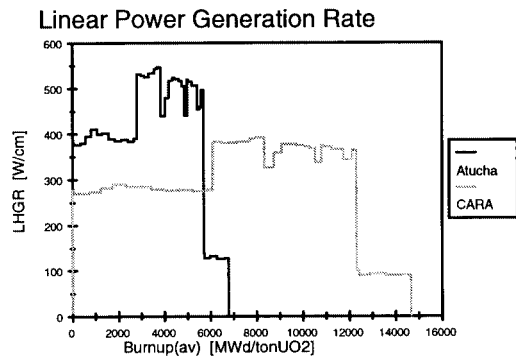


FIG. 12. Local power history for the seventh segments of a fuel rod of the Atucha I NPP and CARA fuel.

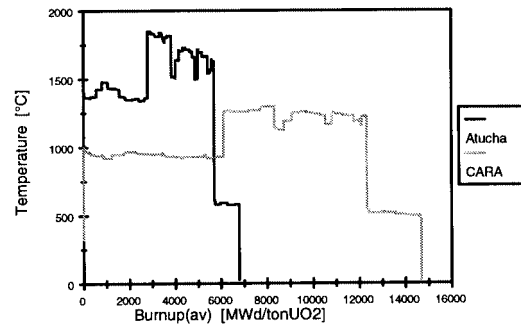


FIG. 13. Local temperature in the seventh segments of a fuel rod for Atucha I CARA fuel.

### 4.3. Hydraulic Pressure Drop

The hydraulic pressure drop along a fuel channel is due to two general components: concentrated and distributed friction losses. A complete analytical hydraulic pressure drop model was developed. It considers the contribution of the end plates, grid spacers and fuel rods to friction loss.

For the case of grid spacer, it was considered local obstructions relates to strap, dimples and springs, following previous approach. [11, 12]

The particular cluster geometry of the CARA bundle need experimental validation of this model. Experiments were carry out in a low pressure loop with two prototypes, finding good agreement with theoretical predictions. After that, the spacer grid design was improved considering the thermohydraulic performance of the fuel element.

An analytical model of pressure drop for the misalignment angle of junction between neighbors fuels has been developed [10] and tested using published [5] and CNEA measured experimental data. The excellent agreement between the model and published experimental data for CANDU have been shown in figure 14.

Using this model, the CARA coefficient pressure drop has been calculated for both Embalse and Atucha I power plants, and present calculated values are 18 to 6 % lower than the respective maximum pressure drop. Figure 15 illustrate this behavior for Embalse. For the Atucha I fuel channel, the theoretical prediction of pressure drop, taking into account the assembling device (by coupling five CARA fuel elements in order to fill the vertical channel), shows good agreement with the core pressure drop.

The critical heat flux assessment of the CARA fuel is a qualify test, rather than a developing test, due to improved heated surface (18% greater than CANDU one) with a single rod diameter homogeneous bundle.

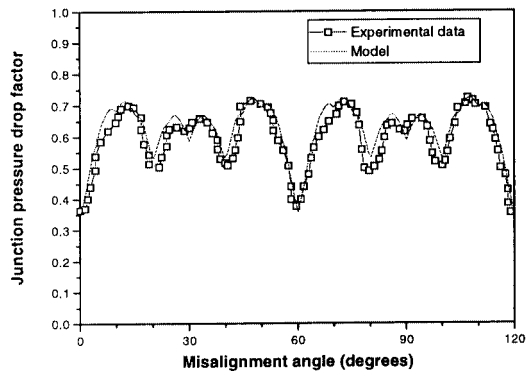


FIG. 14. Comparison of CANDU end plate friction factor coefficient between experimental and the developed model.

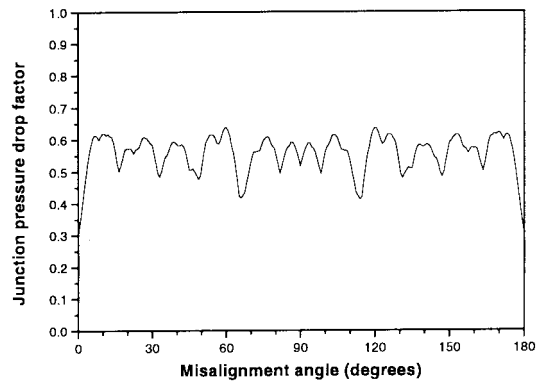


FIG. 15. Calculated end plate friction factor coefficient for CARA fuel using the developed model.

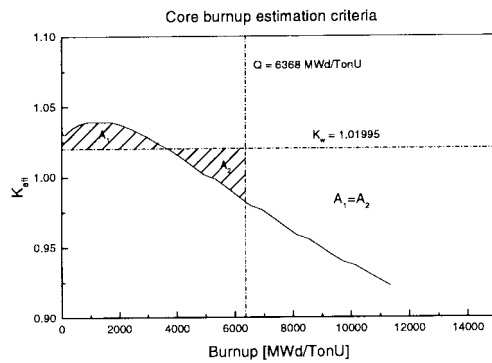


FIG. 16. Core burnup estimation criteria.



FIG. 17. Average cell for CAN NPP (A), and for CNE NPP (B).

## 5. CARA DEVELOPMENT PROJECT

The CARA design, attracted the interest of the nuclear power operator utility in Argentina (NASA), and the fuel element manufacturing company (CONUAR). Then a new project is right now under planning with the cooperation of three partners (CNEA -NASA - CONUAR) in order complete the whole development program in the shortest time, finishing in the commercial production of CARA fuel bundle for both type of reactors.

The strong economical advantages of the new fuel, together with the excellent experience for the close to commercial SEU Atucha program, put strong incentives for the fastest fuel development up to commercial level.

The present CARA project, including an Atucha and Embalse program irradiation and post irradiation analysis, looks for ambitious tasks of 4 years of time span.

The following projects milestones have been achieved:

- Conceptual design of fuel bundle,
- Basic design of fuel bundle,
- First demonstration bundle,
- First CARA bundle,
- Low pressure loop test,
- Detailed design of fuel bundle,
- Detailed design of coupling system for Atucha I,
- Agreement for fuel rod irradiation tests.

## 6. CONCLUSIONS

The feasibility study of an advanced SEU fuel element, compatible with CANDU 6 and Atucha type reactor have been successfully done, using a single rod diameter, as an essential task for economic production in Argentina.

The condition of the present project is to develop the CARA fuel element at the shortest time, finishing with the commercial production of CARA bundles.

## REFERENCES

- [1] LANE A.D., GRIFFITHS J. & HASTINGS I.J., "The Role of the New Canflex Fuel Bundle in Advanced Fuel Cycles for CANDU Reactors.", *CNS 10th Annual Conference*, 1989.
- [2] Central Nuclear Embalse, Córdoba, *Station Data Manual*. Compiled by F.T. CLAYTON. L6K 1B2.
- [3] STEGEMANN D., "*Diseño de centrales nucleares*", Centro Atómico, San Carlos de Bariloche, 1982
- [4] GACES M., ORPEN V. C. & OLDAKER I. E., "Candu fuel design: Current Concepts", *IAEA/CNEA International Seminar on Heavy Water Fuel Technology*, San Carlos de Bariloche, Argentina, June 27 - July 1, 1983, AECL-MISC 250 (1983).
- [5] MAC DONALD I. P. L., "Enhancement of Critical Heat Flux in CANDU 37 Element *CNS 8th Annual Conference*. (1987).
- [6] ASKEW J. R., FAYERS F. J. & KEMSHELL P. B., *J Brit. Nucl. Energy Soc.* 4, 564 (1966).
- [7] FLORIDO P. C. & BERGALLO J. E., "El uso de venenos quemables en los reactores de potencia de nuestro país.", *Argentina Nuclear Vol. 35*, p20 (1993).
- [8] MARINO A. C., SAVINO E. J. & HARRIAGUE S., "BACO (Barra Combustible) Code Version 2.20: a thermo-mechanical description of a nuclear fuel rod", *Journal of Nuclear Materials Vol. 229*, April 11, 1996 (p. 155-168).
- [9] MARINO A. C., "Probabilistic safety criteria on high burnup HWR fuels", *this meeting*.

- [10] BRASNAROF D, DELMASTRO D., "CARA fuel pressure drop characterization", Informe , *XXV Reunión Científica de la Asociación Argentina de Tecnología Nuclear (AA TN 98)*, Buenos Aires, Argentina, 1998.
- [11] NAE-HYUN KIM, S. K. LEE AND K.S. MOON, "Elementary model to predict the pressure loss across a spacer grid without a mixing vane". Nucl. Tech., vol. 98, 349-353, 1992.
- [12] Klaus Rehme, "Pressure drop correlations for fuel element spacers", Nucl. Tech., vol. 17, 15-23, 1973.

## Experimental programmes related to high burnup fuel

**P.R. Vasudeva Rao, R. Vidhya, K. Ananthasivan**

**T.G. Srinivasan, K. Nagarajan**

Fuel Chemistry Division,

Indira Gandhi Centre for Atomic Research,

Kalpakkam, India

### Abstract

The experimental programmes undertaken at IGCAR with regard to high burn-up fuels fall under the following categories: a) studies on fuel behaviour, b) development of extractants for aqueous reprocessing and c) development of non-aqueous reprocessing techniques. An experimental programme to measure the carbon potential in U/Pu-FP-C systems by methane-hydrogen gas equilibration technique has been initiated at IGCAR in order to understand the evolution of fuel and fission product phases in carbide fuel at high burn-up. The carbon potentials in U-Mo-C system have been measured by this technique. The free energies and enthalpies of formation of  $\text{LaC}_2$ ,  $\text{NdC}_2$  and  $\text{SmC}_2$  have been measured by measuring the vapor pressures of CO over the region  $\text{Ln}_2\text{O}_3\text{-LnC}_2\text{-C}$  during the carbothermic reduction of  $\text{Ln}_2\text{O}_3$  by C. The decontamination from fission products achieved in fuel reprocessing depends strongly on the actinide loading of the extractant phase. Tri-n-butyl phosphate (TBP), presently used as the extractant, does not allow high loadings due to its propensity for third phase formation in the extraction of Pu(IV). A detailed study of the allowable Pu loadings in TBP and other extractants has been undertaken in IGCAR, the results of which are presented in this paper. The paper also describes the status of our programme to develop a non-aqueous route for the reprocessing of fast reactor fuels.

### 1. INTRODUCTION

Mixed carbides of uranium and plutonium are candidate fuel materials for Fast Breeder Reactors. The Fast Breeder Test Reactor (FBTR) at Kalpakkam is fuelled by a mixed carbide of uranium and plutonium, with Pu/(U+Pu) ratios of 0.7 (Mark I) and 0.55 (Mark II). The fuel has already reached a burn-up of 50,000 MWd/T. Continued irradiation of the fuel to higher levels of burn-up is envisaged. As uranium and plutonium undergo fission, a number of fission products (f.p.) are formed with different affinities for formation of binary and ternary carbides. Fission products with high yield may alter the carbon balance, and influence clad carburization. Data on the Gibbs energies of formation of the compounds in the system U-Pu-f.p.-C will be useful in understanding and predicting the evolution of the fission product carbide phases in the irradiated fuel. We have initiated a programme to study the thermochemistry of the (U-Pu)-f.p.-C systems. In this paper, we describe the results of our studies on U-Mo-C system, and the Ln-C system where Ln = La, Nd, Sm.

The reprocessing of fuels with high burn-up and short cooling time, which is a requisite for achieving short doubling times and low fuel cycle costs, is another challenging aspect of the fast reactor fuel cycle. The decontamination from fission products achieved in aqueous fuel reprocessing depends strongly on the actinide loading of the extractant phase. Higher loading of the actinides, U and Pu, in the extractant phase leads to increased decontamination from the fission products. Tri-n-butyl phosphate (TBP), presently used as the extractant in fast reactor fuel reprocessing by aqueous route, does not allow high loading of Pu, due to the tendency for formation of a third phase in the extraction of Pu(IV). However, the higher homologues of trialkyl phosphates permit higher actinide loadings without the attendant problem of third

phase formation. A detailed study of the allowable Pu loadings in tri-amyl phosphate (TAP) and other extractants has been undertaken in IGCAR, the results of which are presented in this paper.

Finally, the reprocessing of fast reactor fuels by non-aqueous routes presents a number of advantages arising out of their compatibility with short cooled, high burn-up fuels, compactness of the equipment, less waste generation etc. This paper describes the status of the programme at IGCAR to develop a non-aqueous route for the reprocessing of fast reactor fuels.

## 2. STUDIES ON U-MO-C SYSTEM

There are two ternary carbides in the system U-Mo-C:  $UMoC_{1.7}$  and  $UMoC_2$  according to a recent review [1]. The isothermal section of the ternary phase diagram for U-Mo-C system at 1773 K is shown in Fig. 1.

In our laboratory, the carbon potentials in two three-phase fields in the system U-Mo-C were measured by using the methane-hydrogen gas equilibration technique in the temperature range 973 to 1173 K. From the experimentally measured values of the chemical potential of carbon in the ternary phase fields  $UC + Mo + UMoC_{1.7}$  and  $UC + UMoC_{1.7} + UMoC_2$ , and data for UC from the literature, the Gibbs energies of formation of the two ternary carbides were derived.

### 2.1. Experimental details

#### 2.1.1. Preparation of samples

Dimolybdenum carbide ( $Mo_2C$ ) was procured from Alfa products, USA. The three-phase mixtures were prepared from the elements by arc melting. After annealing, the alloys were characterised by chemical analysis and XRD, the results of which are given in Table I

#### 2.1.2. Determination of Carbon Potential

High purity hydrogen was allowed to react with the sample at the desired temperature for about 24 h. The pressure of the gas in the reaction chamber was maintained constant at 0.1 MPa. The gas phase over the carbide sample was continuously circulated and the concentration of methane in the gas phase at equilibrium was measured employing a flame ionization detector.

### 2.2. Results and discussion

The experimental method was validated by measuring the temperature dependence of carbon potential of the biphasic mixture  $Mo/Mo_2C$ . Third law analysis of this data showed that the technique can be used to measure the free energies within an uncertainty of  $\pm 2$  kJ/mole [2].

### 2.2.1. Gibbs energy of formation of UMoC<sub>1.7</sub>

The measured values of the carbon potential in the phase field UC + Mo + UMoC<sub>1.7</sub>, relative to graphite as standard state is shown in Fig. 2. The chemical potential of carbon is calculated from the equilibrium using the expression:

$$\Delta\mu_C = RT \ln a_C = \Delta_f G^\circ (\text{CH}_4) + RT \ln \frac{P_{\text{CH}_4}}{P_{\text{H}_2}^2} \quad (1)$$

Linear least-squares regression analysis of the data leads to the expression:

$$\Delta\mu_C = -52,210 - 19 T (\pm 7300) \text{ J mol}^{-1} \quad (2)$$

The chemical potential of carbon in the three-phase field is established by the reaction:



In view of the limited solubility of Mo in UC, and the limited solubilities of U and C in molybdenum [3] in the temperature range 973 to 1173 K, the activities of UC and Mo may be assumed to be unity. By combining the carbon potential data with the Gibbs energy of formation of UC reported in the literature [4], the Gibbs energy of formation of UMoC<sub>1.7</sub> in the temperature range 973 to 1173 K can be calculated as:

$$\Delta_f G^\circ \text{UMoC}_{1.7} = -146,630 - 15.0 T (\pm 8000) \text{ J mol}^{-1} \quad (4)$$

The value of the Gibbs energy of formation of UMoC<sub>1.7</sub> at 1073 K, obtained in this study is 10 kJ / mol more positive than the estimate of Ugajin et al. [3]. Since the uncertainty in the values estimated by these authors is rather large, the Gibbs energy of formation obtained in this study, is considered to be more accurate.

### 2.2.2. Gibbs energy of formation of UMoC<sub>2</sub>

The temperature dependence of the carbon potential in the three-phase field UC + UMoC<sub>1.7</sub> + UMoC<sub>2</sub> obtained from this study is shown in Fig. 2. Linear least-squares regression analysis of the data in the temperature range 973 to 1173 K gives the expression:

$$\Delta\mu_C = -17,770 - 2.0 T (\pm 4600) \text{ J mol}^{-1} \quad (5)$$

The carbon potential in this three-phase field is established by the reaction;



By combining the measured values of the carbon potentials in the three-phase field UC + UMoC<sub>1.7</sub> + UMoC<sub>2</sub> with the Gibbs energy of formation of UMoC<sub>1.7</sub>, given by the expression (4), the Gibbs energy of formation of UMoC<sub>2</sub> was found to be:

$$\Delta_f G^\circ \text{UMoC}_2 = -151,960 - 13.7 T \text{ J mol}^{-1} \quad (7)$$

The carbon potential over the three-phase field UC + UMoC<sub>1.7</sub> + UMoC<sub>2</sub>, determined in this study is found to be a very weak function of temperature. Our data suggest that in the ternary system U-Mo-C the two ternary carbides may not coexist with molybdenum at 1773 K. This is consistent with the review [1].

### 2.2.3. Implications with regard to FBTR fuel at High Burn-up:

Lorenzelli and Marcon [5] have predicted that, ~2 at% Mo would be present in a mixed carbide fuel at a burn up of approx. 10 at%. Experimental investigations [6] on the system U-Mo-C, indicate that molybdenum has a maximum solubility of 2 at%, in uranium monocarbide. There is only one ternary compound PuMoC<sub>2</sub>, in the system Pu – Mo – C [1]. The Gibbs energy of formation of this ternary compound has not been reported so far. The solubility limit of Mo, in the monocarbide of plutonium has not been determined. The solubility of molybdenum in the monocarbide phase increases from 2 at% in pure uranium

monocarbide to about 3.5 at% in a mixed carbide of uranium and plutonium with  $\{Pu / (U+Pu) = 0.2\}$  [7]. Since the FBTR fuel has a higher fraction of plutonium, a molybdenum solubility in excess of 3 at% is expected. The quasi-ternary compound  $MMoC_2$  would be precipitated in the irradiated fuel, only when the terminal solubility is exceeded.

The difference between the values of the Gibbs energies of the two ternary carbides in the system U-Mo-C, is quite small. By assuming that the stabilities of these carbides are similar to those in the system Pu-Mo-C, and further that the ternary carbides form ideal solid solutions, the trend in the variation of the carbon potentials in the fuel system can be predicted.

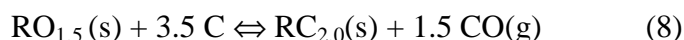
There are two isograms in the pseudo ternary system  $M - Mo - C$   $\{M=(U,Pu)\}$ , viz. the one along which the two phases  $MC$  and  $MC_{1.5}$ , and the one along which the phases  $MMoC_2$  and  $MMoC_{1.7}$  coexist. The carbon potential in the "three-phase" field  $MC + MC_{1.5} + MMoC_2$  would be controlled by the  $MC/MC_{1.5}$  system, while that in the three-phase field  $MC + MMoC_2 + MMoC_{1.7}$  would be controlled by  $MMoC_2 + MMoC_{1.7}$ . The carbon potential along the isogram which involves  $MC_{1.5}$ , corresponds to that of the unirradiated fuel, while the carbon potential along the latter is expected to be around  $-20$  kJ / mol at 1000 K. Since this value is more positive than the carbon potential of the mixed carbide fuels employed in FBTR, the quasi-ternary compound  $MMoC_{1.7}$ , will not be formed in the FBTR fuel. In order to ascertain these predictions, data on the Gibbs energy of formation of the plutonium bearing ternary carbide as well as the quasi ternary carbides bearing U and Pu are required. Further studies are planned in this direction.

### 3. GIBBS ENERGIES OF FORMATION OF THE DICARBIDES OF LANTHANUM, NEODYMIUM AND SAMARIUM

The lanthanides constitute an important group of fission products, since they are formed at a high yield. Thus, a study of the lanthanide-carbon systems is essential for predicting the chemical state of the irradiated fuel [8]. There is considerable discrepancy in the thermodynamic data available in the literature on the rare earth-carbon systems. In continuation of our studies to generate thermodynamic data on fission product - carbide systems we have measured the Gibbs energies of formation of the dicarbides of La, Nd and Sm.

#### 3.1. Experimental

A detailed description of the experimental set up and the procedure adopted are given elsewhere [9]. The carbides of La, Nd and Sm were generated "in situ" in a high vacuum chamber by the carbothermic reduction of the corresponding oxides and the  $CO(g)$  effusion pressures were measured by means of a quadrupole mass spectrometer. From the  $CO(g)$  pressure data, the equilibrium  $CO(g)$  pressure,  $P_{CO}$ , for that temperature was deduced, and thus, the  $\Delta G$  of the reaction 8:



could be obtained. From the  $\Delta G$  of the reaction (8), the  $\Delta G_f$  of  $RC_{2.0}(s)$  was calculated by taking the Gibbs energy data of  $RO_{1.5}(s)$ , graphite and  $CO(g)$  from ref. 10. The  $\Delta H_f$  (298.15 K) of  $RC_{2.0}(s)$  was calculated by second and third law methods by using the enthalpy functions and free energy functions from literature [10-13]

## 3.2. Results and Discussion

The temperature dependence of  $\ln(P_{CO})$ , along with the corresponding range of temperatures in which the measurements have been done is shown in table II. The values of the enthalpy of the reaction (8) according to II and III law calculations are also given in table II. Table III provides the Gibbs energy and the enthalpy of formation of the individual carbides derived from the data in table II.

### 3.2.1. Lanthanum Carbide

As seen from table II, the second law and third law enthalpies of the reaction (8), are in close agreement. The third law value for the enthalpy of formation is in agreement within the error limits with that reported by Meschel et al [13] and Anderson et al [14]. It is also within the error limits of the II law results of Stearns et al [15]. The average of second and third-law results is chosen to be the recommended value considering the fact that Gibbs energy functions of  $LaC_{2,0}(s)$  are estimated values.

### 3.2.2. Neodymium dicarbide

The second and third law enthalpies of the reaction (8) obtained from the present study are in good agreement with each other. We did not observe any significant influence of temperature on the third law enthalpy of reaction, indicating the reliability of the thermodynamic data obtained. The average of second and third-law results is chosen to be the recommended value for the enthalpy of formation, considering the fact that Gibbs energy functions of  $NdC_{2,0}(s)$  are estimated values.

### 3.2.3. Samarium dicarbide

There is a reasonable agreement between the second and third law enthalpies of formation of the dicarbide determined in our study. The Gibbs energy of formation and the enthalpy of formation determined in this study are close to the literature data [12,16,17].

### 3.2.4. Implications with regard to FBTR fuel at High Burn-up:

Among the lanthanides studied, neodymium has the highest yield. It is therefore appropriate to use the data on Nd-C system to explore the application of the thermochemical data to the chemical state of lanthanides in the fuel. However, the phase diagram of the Nd-C system has not been reported so far. From a comparison with the phase diagram of La-C system [18] it can be concluded that in the temperature range expected in the FBTR fuel ( $< 1800$  K),  $NdC_2$  will be in equilibrium with  $Nd_2C_3$ . The carbon potential of this phase field, estimated by taking the free energy of formation of  $Nd_2C_3$  from literature[18] and utilizing the data on  $NdC_2$  from the present work, is plotted in Fig.2 along with the data on carbon potential for the FBTR fuels [19]. Data for  $Sm_2C_3$ - $SmC_2$  system are also plotted in this figure. It is seen that the carbon potential corresponding to the  $Ln_2C_3$ - $LnC_2$  systems is of the same order, or more than, that of the Mark I FBTR fuel. Thus, in Mark I FBTR fuel, the lanthanide dicarbide is not expected to be formed. Since solubilities of both  $LnC$  and  $Ln_2C_3$  phases in the corresponding fuel phases are expected to be more than the lanthanide content of the fuel at 10 % burn-up [8], the lanthanide could exist in solid solution in either of the phases. A more clear picture is

possible only if the carbon potential of  $[\text{LnC}]_{\text{MC}} - [\text{Ln}_2\text{C}_3]$  system is evaluated. In the case of Mark II fuel, the  $\text{NdC}_2$  phase could be precipitated at high burn-up since the carbon potential of the fuel is higher than that of the lanthanide system.

#### 4. STUDIES ON THIRD PHASE FORMATION AND ALTERNATE TRIALKYL PHOSPHATES

In the phenomenon of third phase formation, the organic phase splits into two, when the “Limiting Organic Concentration (LOC)” for the metal is exceeded. In our laboratory, a systematic investigation of the phenomenon of third phase formation was carried out to establish the LOC values for different homologues of TBP.

##### 4.1. Experimental

The details of the experimental procedure used for measuring the LOC values are given in ref. 20. The third phase formation was induced by loading the extractant phase initially with high concentration of the actinide and then dissolving the third phase carefully by adding either the extractant solution or nitric acid. The organic and aqueous phases were analysed for the actinide and nitric acid at the point of disappearance of the third phase, to obtain the LOC.

##### 4.2. Results and Discussion

Our studies on Pu extraction indicated that no third phase formation takes place during extraction of Pu(IV) from nitric acid medium by TAP and higher homologues whereas third phase is formed during extraction by TBP. To understand more quantitatively the effect of the nature of the extractant on the LOC, studies were carried out on the Th(IV) extraction system, where third phase is formed more readily. Figure 3 depicts the variation of LOC for the extraction of Th(IV) as a function of the aqueous nitric acid concentration for Tri-n-amyl Phosphate (TAP), Tri-n-Hexyl Phosphate (THP) and Tri-n-isoamyl Phosphate (TiAP) [20]. The LOC data are compared with the data for TBP. It is clear from the figure that the higher homologues permit significantly higher loading. In fact, no third phase formation could be induced in the case of THP for Th(IV) also, and the data shown correspond to the maximum loadings achieved. It is clear that use of TAP or TiAP will be advantageous when high Pu loading in extractant phase has to be realised, as in the case of reprocessing of fast reactor fuels. In fact, Russian workers have reported [21] the use of TiAP for reprocessing of U,Pu mixed oxide fuel irradiated to 1,00,000 MWd/T burn-up.

#### 5. LABORATORY SCALE STUDIES RELATED TO PYROCHEMICAL REPROCESSING

##### 5.1. Introduction

Pyrochemical reprocessing methods offer several advantages over the conventional PUREX process for reprocessing short cooled fast reactor fuels with high burn-up. Molten salt electrorefining, one of the pyrochemical reprocessing methods, has received considerable attention, especially for reprocessing of the irradiated metallic fuels as well as the nitride fuels [22]. This process was first developed as a part of the Integral Fast Reactor program, in the

Argonne National Laboratory [23]. In this process, the electrochemical separation of the fuel materials from the fission products is achieved by utilizing the large differences in the thermodynamic stabilities of the respective chlorides. Molten cadmium is used as the anode, an eutectic of LiCl-KCl containing about 2 mol% of uranium and plutonium chlorides as the electrolyte and a low carbon steel rod/molten cadmium is used as the cathode. During the process, uranium and plutonium are selectively electrotransported and deposited on the cathode, leaving behind most of the fission products in the salt and the anode. The recovery of the actinides from the cathode deposits is achieved by heating them to 1300<sup>0</sup>C to distill off the cadmium and consolidate the actinides into an ingot.

## **5.2. The laboratory scale facility for pyrochemical reprocessing studies and the associated systems**

A laboratory scale facility for carrying out pyrochemical reprocessing studies on radioactive materials has been designed, set up and is being operated in our laboratory. The facility has been designed to facilitate studies on all the process steps associated with the molten salt electrorefining process. It comprises an argon atmosphere glove box train (Fig.4) housing all the equipment. An electrorefining cell is positioned inside the furnace well attached to the bottom of one of the glove boxes. The electrorefining cell consists of an S.S. 304 vessel, a cylindrical SS 430 crucible as the anode container, and a solid mild steel rod as the cathode. A consolidation set up, a cadmium distillation set up and an injection casting set up are also incorporated in the facility.

The electrorefiner cell has been regularly operated on a 200 g scale. The potential of the cell was controlled between 0.8 to 1.0 V. Maximum cathode current densities of 50 mA/cm<sup>2</sup> were obtained in these runs. Initial deposition rates were about 5-6 g per hour which reduced to a value of about 2 g per hour as the anode content of uranium comes down. Collection efficiencies ranging from 60 to 85 % were obtained in different runs. Studies are in progress to optimise the parameters to improve the current efficiency.

Investigations were carried out on the effect of the concentration of UCl<sub>3</sub> on the current in the cell to arrive at an optimum value for maximising the current. The concentration of UCl<sub>3</sub> in the electrolyte was varied from 0.5 mol % to 3.2 mol %. An optimum current was obtained at a concentration of 1.0 mol% which increased slightly with increase in concentration until 3.0 mol% and beyond this value the increase in current was not appreciable.

## **5.3. Studies on the recovery of U from UC**

Investigations were carried out on the recovery of U from UC. UC pellets prepared by the carbothermic reduction of U<sub>3</sub>O<sub>8</sub> were taken in an alumina crucible to the bottom of which a layer of cadmium was added for ensuring better electrical contact. A tantalum wire was introduced into the crucible which was made the anode. A low carbon steel rod was used as the cathode. The recovery of uranium was about 90%.

#### **5.4. Studies on the separation of Zr, Ce and Pd from uranium**

The separation of uranium from U-10 % Zr and U-Ce-Pd alloys was studied, with LiCl-KCl eutectic salt mixture loaded with about 5 wt.%  $\text{UCl}_3$ , the uranium alloy kept immersed inside the cadmium pool as the anode, and solid mild steel rod as the cathode. The anode, salt and the deposit were periodically analysed for the elemental concentrations. The Zr content in the deposit was as low as 0.02-0.03 %. The amount of cerium transported to the cathode was very less and almost all the cerium in the initial feed was transferred to the electrolyte. Palladium stayed in the anode itself, and very low amounts were only transferred to the cathode. The overall recovery of uranium was only 76 % in our experiments, which could be improved by controlling the ambient conditions in the glove box.

Table 1. Composition of the u-mo-c ternary alloys studied

Alloy composition				Phases identified in XRD
U (wt%)	Mo (wt %)	C (wt %)	O (ppm)	
66.40	27.83	5.45	500	UC, UMoC <sub>2</sub> , UMoC <sub>1.7</sub>
17.80	81.21	0.96	500	UC, Mo, UMoC <sub>1.7</sub>

Table 2. Equilibrium Co (G) Pressures Over Ln<sub>2</sub>O<sub>3</sub>-C-LnC<sub>2</sub> Phase Fields

Condensed Phase	Vapour Pressures ln P <sub>CO(g)</sub> *	Temperature range(K)	ΔH of reaction at 298 K (II law) †kJ/mol	ΔH of reaction at 298 K(III law) † kJ/mol
La <sub>2</sub> O <sub>3</sub> (s) - C(s) - LaC <sub>2</sub> (s)	-50130(658) / T + 22.9 (0.4)	1342 – 1642	632.1 ± 8.4	637.1 ± 2.7
Nd <sub>2</sub> O <sub>3</sub> (s) – C(s) - NdC <sub>2</sub> (s)	- 53012.9(698)/ T+ 23.5 (0.46)	1403 – 1588	668.0 ± 8.7	670.8 ± 1.0
Sm <sub>2</sub> O <sub>3</sub> (s) -C(s) -SmC <sub>2</sub> (s)	-52000.3 (895)/T+ 22.6 (0.58)	1427 – 1666	665.8 ± 11.1	673.9 ± 2.9

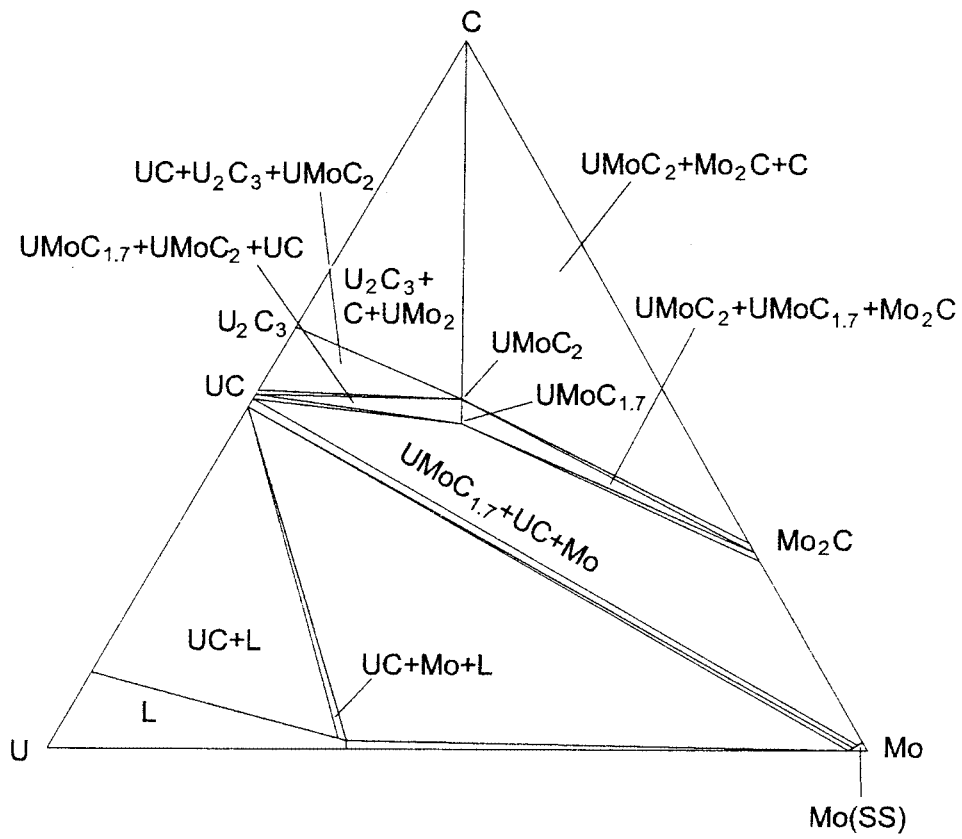
\* - The error in the parameters of the linear fit are given in brackets.

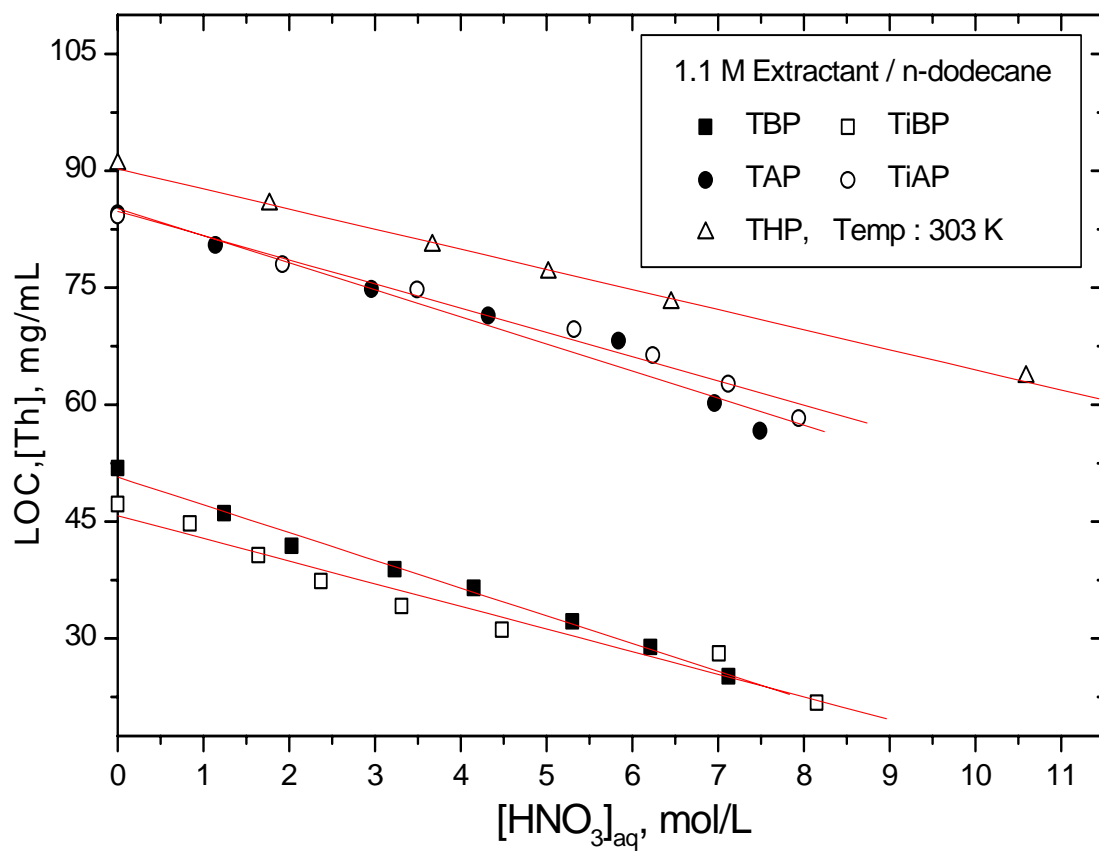
† - The overall errors in the parameters are indicated.

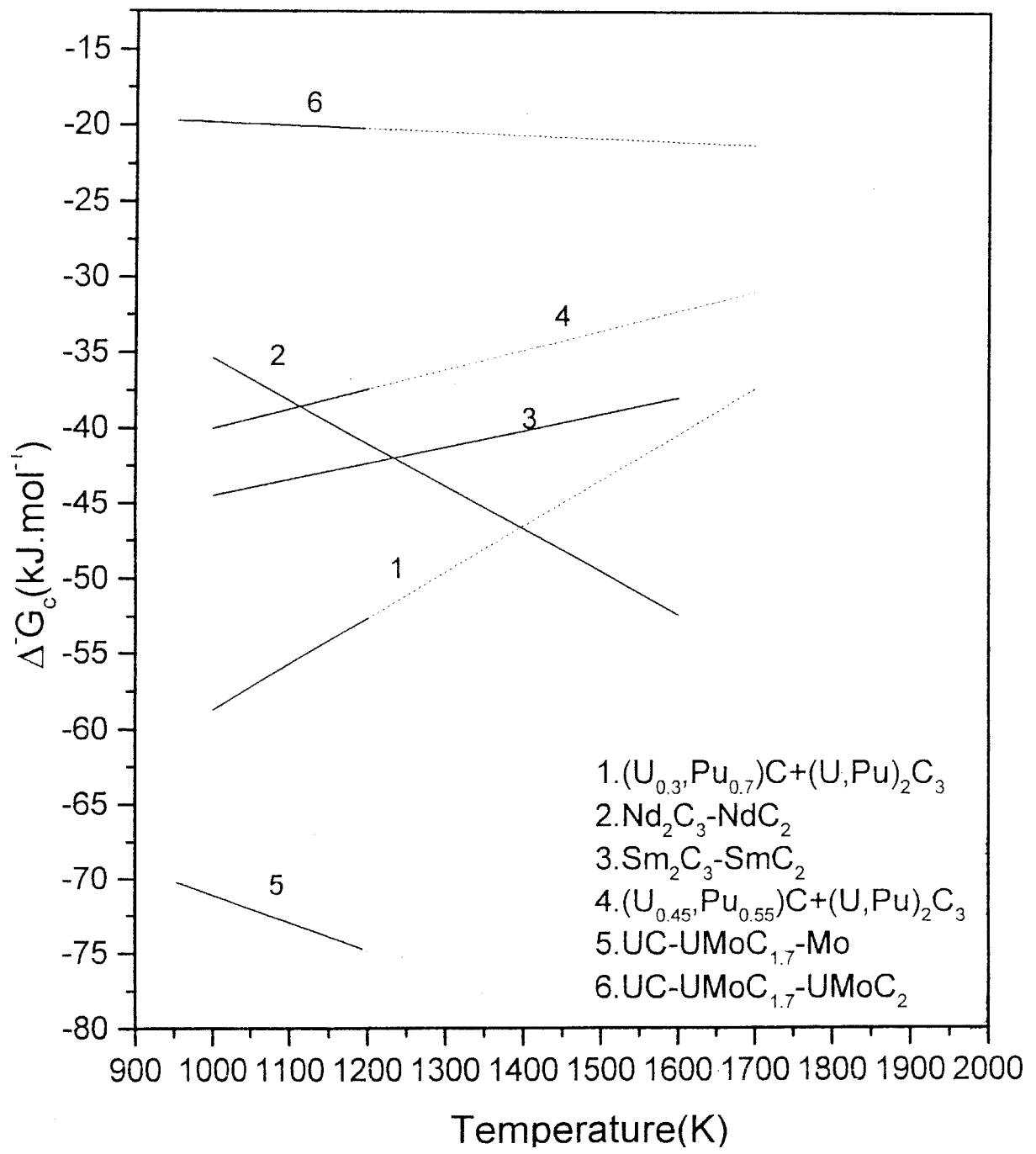
Table 3. GIBBS energies and enthalpies of formation of the rare earth dicarbides

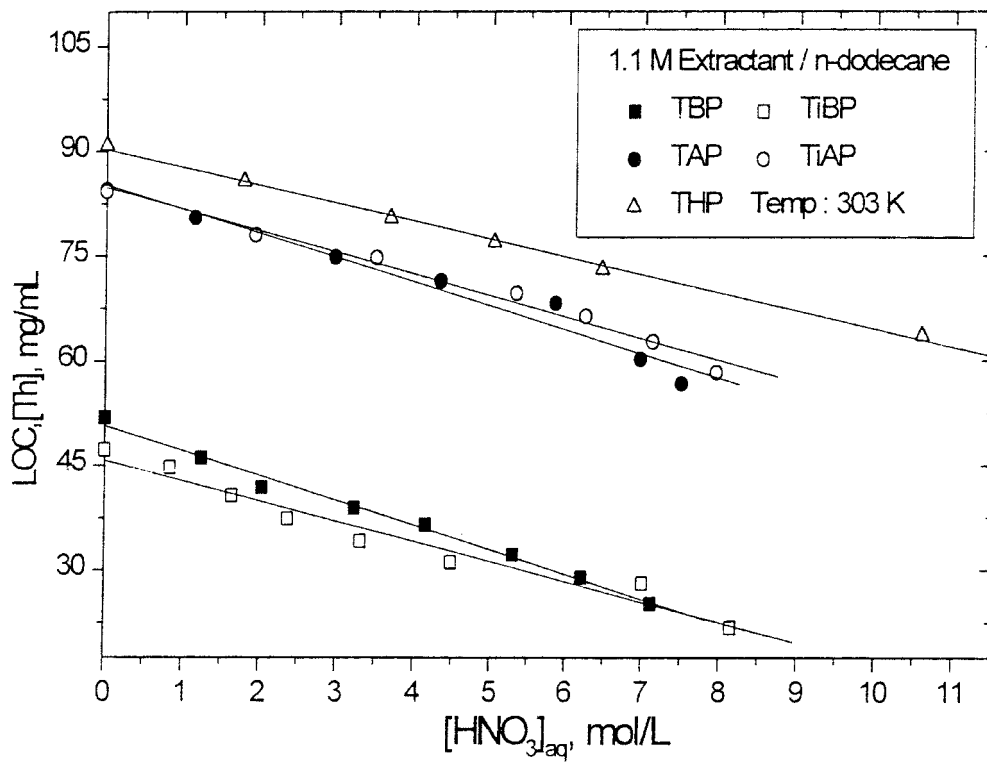
Phase	ΔG <sub>f</sub> <sup>o</sup> (298.15 K), kJ.mol <sup>-1</sup>	ΔH <sub>f</sub> <sup>o</sup> at (298.15 K), kJ.mol <sup>-1</sup>		
		II Law	III Law	SELECTED*
LaC <sub>2</sub> (s)	-103.1	-90.6±8.4	-80.1±3.6	-85.6±10
NdC <sub>2</sub> (s)	-65.3	-70.1±8.7	-67.3±1.0	-68.7±10
SmC <sub>2</sub> (s)	-87.6	-81.2±11	-71.6±2.5	-76.4±12

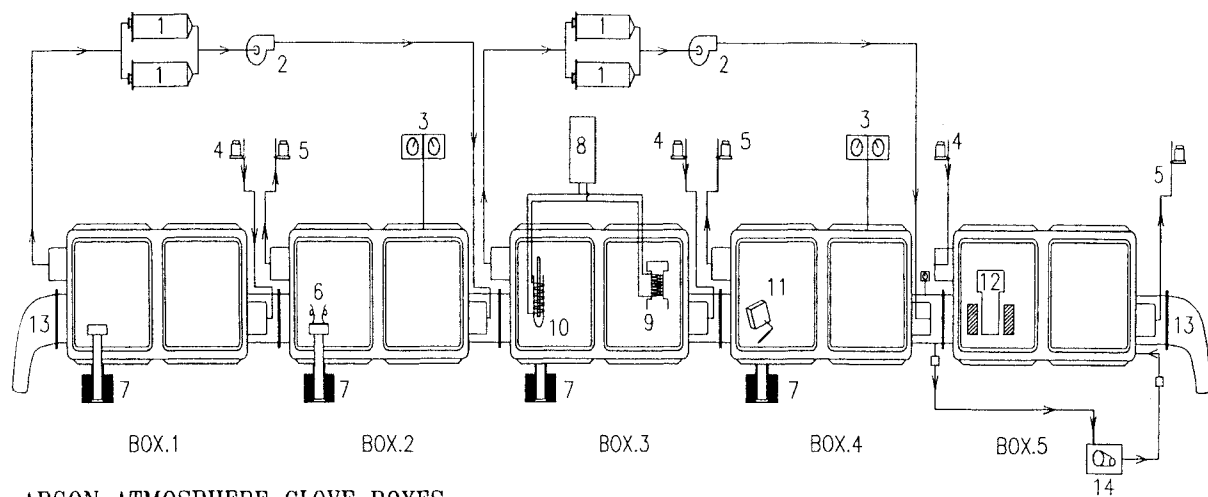
\* Recommended value with the overall estimated error in the measurement











**ARGON ATMOSPHERE GLOVE BOXES**

- BOX.1 ELECTROLYTE SALT PREPARATION
- BOX.2 ELECTROREFINING EXPERIMENTS
- BOX.3 INDUCTION MELTING
- BOX.4 METAL/ALLOY TREATMENT

**AIR ATMOSPHERE GLOVE BOX**

- BOX.5 TRANSIT AIR BOX / CADMIUM DISTILLATION

- 1. PURIFICATION TOWER
- 2. BLOWER
- 3. PHOTOHELIC GAUGE
- 4. VACUUM BREAKER(INLET)
- 5. VACUUM REGULATOR(EXHAUST)
- 6. ELECTROREFINING CELL
- 7. GLOVE BOX FURNACE ATTACHMENT
- 8. INDUCTION GENERATOR UNIT
- 9. CONSOLIDATION SET UP
- 10. INJECTION CASTING SET UP
- 11. POLISHING INSTRUMENT
- 12. CADMIUM DISTILLATION SET UP
- 13. BAG-IN/BAG-OUT PORT
- 14. VACUUM PUMP

## FIGURE CAPTIONS

- Figure 1. Isothermal section of U-Mo-C phase diagram at XXX K
- Figure 2. Temperature dependence of the carbon potential in fuel and fission product systems
- Figure 3. Limiting Organic Concentration for third phase formation in extraction of thorium(IV) by trialkyl phosphates from nitric acid medium.
- Figure 4. Schematic diagram of inert atmosphere glove box train housing facilities for studies on pyrochemical processes

## REFERENCES

- [1] HOLLECK, H., in Handbook on the physics and chemistry of the actinides, A. J. Freeman and C. Keller (Eds.), Elsevier Science Publishing Company Inc., New York, U.S.A., Vol. 4, Ch. 6, (1986 ) 209.
- [2] ANANTHASIVAN, K., KALIAPPAN, I., ANTHONYSAMY, S., CHANDRAMOULI, V., VASUDEVA RAO, P.R., MATHEWS, C.K. and JACOB, K.T., J. Alloys and Compounds 245 (1996) 40.
- [3] UGAJIN, M., ABE, J. and KURIHARA, M., J. Nucl. Sci. Tech., 12[9] (1975) 30.
- [4] STORMS, E.K. and ACKERMANN, R.J., IAEA Panel on Thermodynamic Properties of the UC, PuC and (U,Pu)C systems, Grenoble, France (1974).
- [5] LORENZELLI, N. and MARCON, J.P., Panel on the behaviour and chemical state of fission products in irradiated fuel, Vienna, (1972) 7-11, Translated in ANL-trans-920.
- [6] CHUBB, W., J. Nucl. Mater. 23 (1967) 336.
- [7] YASUO ARAI, TOSHIHIKO OHIMICHI, SUSUMU FUKUSHIMA and MUNEKO HANDA, J. Nucl. Mater. 170 (1990) 50.
- [8] FEE, D.C. and JOHNSON, C.E., ANL report no. ANL-AFP-10, 1975.
- [9] VIDHYA, R., ANTONY, M.P. and MATHEWS, C.K., J.Phys.Chem. 99 (1995), 16468.
- [10] KUBASCHEWSKI, O., KNACKE, O. and HESSELMAN, K., *Thermochemical properties of Inorganic substances*, 2<sup>nd</sup> ed.; Springer-Verlag ; London, 1991.
- [11] FAIRCLOTH, R.L., FLOWERS, R.H. and PUMMERY, F.C.W., J.Inorg.Nucl.Chem. 30, (1968), 499.
- [12] STOUT, N.D., HOENIG, C.L. and NORDINE, P.C., J.Am.Cer.Soc. 52 (1969),145.
- [13] MESCHEL, S.V. and KLEPPA, O.J., J.Alloys.Compds. 205 (1994), 165.
- [14] ANDERSON, J.S. and BAGSHAW, A.N., Rev.Chim.Miner. 115 (1972).
- [15] STEARNS, C.A. and KOHL, F.J., J.Chem.Phys. 54 (1971), 5180.
- [16] AVERY, D.F., CUTHBERT, J. and SILK, C., Brit.J.Appl.Phys. 18 (1967), 1133.
- [17] GSCHNEIDNER Jr. K.A., and KIPPENHAN, N.; *US Rare Earth Information Center, Iowa rept. IS-RIC-5*, 1971.
- [18] ADACHI, G., IMANAKA, N. and FUZHONG, Z., in "Handbook on the Physics and Chemistry of Rare Earths", Vol.15, GSCHNEIDNER Jr. K.A. and EYRING, L.(Eds), Elsevier Science Publishers, 1991, p.61.
- [19] ANANTHASIVAN, K., KALIAPPAN, I., ANTHONYSAMY, S., CHANDRAMOULI, V., VASUDEVA RAO, P.R., MATHEWS, C.K. and JACOB, K.T., J. Nucl. Mater., 223 (1995) 20.
- [20] SURESH, A., SRINIVASAN, T.G. and RAO, P.R.V., Solvent. Extr., Ion Exch., 12, (1994) 727.
- [21] NIKIFEROV, A.S., ZAKHARIN, B.S, RENARD, Kh.V., ROZEN, A.M. and SMETANIN, Eh.Ya., "Actinides'89 ", Tashkent, USSR, September 1989, pp.20-21.
- [22] CHANG, Y.I., Nucl. Tech. 88 (1989) 129
- [23] BURRIS, L., STEUNENBERG, R.K., and MILLER, W.E., in Proc. A.I.Ch.E Symposium on Electrochemical Engineering Applications (1986), A.I.Ch.E Series 254, Vol.83 (1987) p.135.

ECONOMIC LIMITS  
**(Session II)**



# Fuel with burnable absorber for RBMK-1500

**G. Krivosein**

Ignalina NPP,  
Lithuania

## Abstract

Following the accident at the Chernobyl Unit 4, the priority measures to improve RBMK's safety were developed. Under this program, the measures to reduce the void reactivity coefficient were executed on the stage-by stage terms: As a result of these measures, the void reactivity coefficient was reduced below  $+1.0\beta$ . But there was decrease in fuel burnup to  $14.0\div 14.5$  MW.d/kg, (design value  $\sim 21\div 22$  MW.d/kg). High power level of a fresh fuel assembly did not allow to employ fuel with higher enrichment without any compensatory measures. The different types of burnable absorbers were considered to be used. From the results of the anticipated calculations, it was specified that the most efficient power neutron flux flattening between fuel channels could be achieved when erbium was used. Ignalina NPP has used 2.4 % enriched fuel assemblies with burnable absorber since 1995. The fuel burnup has been increased by 60 %. The obtained experimental results are analyzed.

## I. INTRODUCTION

The Ignalina nuclear power plant is located in the northeast corner of Lithuania, close to the borders with Belarus and Latvia. Now, there are 2 units at INPP, each of which is equipped with RBMK-1500 reactor. The RBMK-1500 reactor is the most advanced version of RBMK design [1]. The RBMK-1500 is a graphite moderated, channel-type, boiling water reactor. Its design thermal power is 4800 MW. However, for safety reasons, these reactors are currently running at reduced power of maximum 4200 MW. Each fuel assembly is located in a separately cooled fuel channel (pressure tube). The total number of such channels is 1661 and the cooling water must be equally divided among that number of feeder pipes. Past the core, these pipes are brought together to feed the steam-water mixture to the steam separators.

Each reactor is divided into two halves. Each half is cooled by a main circulation circuit provided with flow from three operating main circulation pumps. The schematic representation of the principal features of the RBMK fuel assembly is shown in Fig. 1. The assembly contains two fuel bundles. Each bundles has 18 fuel rods arranged within two concentric rings in a central carried rod. The lower bundle of the fuel assembly is provided with an end grid and ten spacing grids. The top bundle has additionally 18 specifically design spacers, which act as turbulence enhancers to improve the heat transfer characteristics. The main parameters of the RBMK fuel assembly are presented in Table 1.

## 2. CORE DESIGN IMPROVEMENTS AFTER THE CHERNOBYL ACCIDENT

After the Chernobyl accident, the prime safety improvement measures on RBMK NPP were developed, within the framework of which the step-by-step reduction of the void reactivity coefficient was executed. The first two basic stages on its reduction were:

- increase of an operative reactivity margin till 53-58 manual control rods, as a result, void reactivity coefficient decreased up to  $+1.7\beta_{\text{eff}}$  ;
- installation in the core of 53 additional absorbers, as a result, void reactivity coefficient decreased up to  $+1.0\beta_{\text{eff}}$  .

However, after that, economic parameters of units suffered considerably because of decrease of fuel burnup up to 14.0-14.5 MWdays/kgU (compared to design value of 21 MWdays/kgU).

The loading of 2.4 % enrichment fuel like at the units with RBMK-1000 was impossible for RBMK-1500 because of significant growth of channel power after refueling.

The following step on the reduction of the void reactivity coefficient was the implementation of 2.4 % enrichment fuel with a burnable absorber at RBMK-1500. The given measure was of the highest importance for the further existence of RBMK reactors, because it allowed not only to improve their safety, but also to improve considerably the technical and economic characteristics. Although it was suggested some time ago, the anticipated calculation did not give favorable results. It was not until the end of 1992, with the aid of WIMS code, that the efficiency of burnable absorber use was proved. The different type of burnable absorbers were considered to be used, namely, boron, dysprosium, hafnium and erbium. Gadolinium was not considered because some preliminary tests proved to be inefficient in the neutron flux flattening comparing with boron. In addition, in the case of gadolinium, there was no significant decrease of the void reactivity coefficient.

Based on the results obtained, it was specified that the most efficient neutron flux flattening between fuel channels, could be achieved when either erbium nor boron was used. The advantage of erbium is in decrease of the average void reactivity coefficient of three times comparing to boron.

### 3. FUEL WITH ERBIUM

The natural erbium contains six isotopes: Er-162 - 0.14 %, Er-164 - 1.56 %, Er-166 - 33.4 %, Er-167 - 22.9 %, Er-168 - 27.1 %, Er-170 - 14.9 %. From neutron physics point of view, only these isotopes represent interest which have a considerable contribution to the total neutron absorption by natural erbium. Such isotopes are Er-166 and Er-167. The contents of Er-162 and Er-164 in natural erbium are small. Furthermore, these isotopes have small values of the absorption cross sections. The absorption cross section of Er-162 in the thermal range is 2 barns and 100 times smaller than average value for natural erbium. The neutron absorption by Er-170 is not negligible. The cross section in the thermal range equals approximately 9 barn. The main role in the neutron absorption belongs to Er-167 which has the cross section ten times greater than Er-166. At the energy  $E=0.47\text{eV}$ , Er-167 has a resonance with the maximum value of the cross section  $\sim 8 \cdot 10^3$ , Figure 2. The core calculations have shown that the location of erbium directly in the fuel is optimum. The natural mixture of erbium isotopes in form of  $\text{Er}_2\text{O}_3$  was advised to add into fuel matrix.

The optimal weight content of erbium in the new fuel was selected on the basis of the following conditions:

- The unloaded fuel burnup is not less 22 MWd/kg when there are no additional absorbers in the core;
- The void reactivity coefficient is not higher + 1.0  $\beta_{\text{eff}}$ ;
- The maximum power level of a fresh fuel assembly with 2.4 % enrichment does not exceed the corresponding power level of a fuel assembly with 2.0 % enrichment.

The first condition defines the upper limit of initial weight content of erbium which is equal to 0.48 %. The other two conditions define the lower boundary 0.4 %. On the basis of the calculations, 0.41 % was selected as the value of the erbium optimal weight content.

Mechanical and thermo-physical properties of uranium-erbium fuel pellets and their compatibility with the Zr+1 %Nb alloy were tested. Finally, the properties of the new enriched fuel appeared to be insignificantly different from the old fuel and therefore the decision was made that it would be unreasonable to modify either fuel assembly or fuel rod design.

As a result of large amount of investigations executed by Kurchatov Institute, RDIPE and other research organizations since 1992, it was determined that the increase of fuel enrichment in fuel assembly of RBMK-1500 up to 2.4 % with addition of 0.41 % of erbium allows to receive the following advantages:

- to improve the reactor safety;
- to increase the unloaded fuel burnup;
- to decrease the fuel consumption;
- to unload all additional absorbers from the reactor.

#### 4. REACTOR REFUELING

After a detailed substantiation of an opportunity to use such fuel in 1995-1996 years, the loading of the first experimental batch of 150 assemblies with uranium-erbium fuel was carried out at INPP unit 2. The first 150 experimental fuel assemblies were loaded in a step of 25. The void reactivity coefficient  $\alpha$ , fast power reactivity coefficient  $\beta_w$  and period of the first azimuthal harmonic changing  $\omega_1$  were carefully measured after each step of loading. After the completion of 150 experimental fuel assembly loading, the void reactivity coefficient was decreased from  $0.8\beta_{\text{eff}}$  to  $0.5\beta_{\text{eff}}$ ; the power reactivity coefficient was altered from  $(-1.8) \cdot 10^{-4} \beta/\text{MW}$  to  $(-2.1) \cdot 10^{-4} \beta/\text{MW}$ , period of the first azimuthal harmonic changing increased from 22 minutes to 26 minutes.

After thus experimental check of correctness of preliminary theoretical investigations, the step-by-step U-Er fuel implementation was begun (by batch of 200-500 fuel assemblies), during which the gradual unloading of an additional absorbers from the core took place. Up to the present time at unit 1, the share of uranium - erbium fuel is approximately 50 %, at unit 2, approximately 85 %.

The implementation process is accompanied by the monitoring of the reactors neutron-physical characteristics obtained by means of experimental measurements. The void and power reactivity coefficients, stability of radial-azimuth power distribution, reactor sub-criticality and other parameters are measured. In the intervals between experiments, the neutron-physical reactors characteristics are monitored using STEPAN code (Kurchatov Institute). The received experimental data are compared with the predicted calculated data produced by Kurchatov Institute before the loading of the next batch. It is necessary to note their satisfactory consent. The difference of the experimental and anticipated calculated data does not exceed the value of  $0.2 \beta$  for void reactivity coefficient.

The sequence of fuel assembly loading and additional absorber unloading was selected to maintain the reactor safety parameters within the allowed limits. The data for some basic

parameters are presented in Table 2: void and power reactivity coefficients, the period of the first radial-azimuth harmonic changing, cold poisoned reactor sub-criticality.

The results show that during the new fuel loading, the void of reactivity coefficient was reduced to the value less than  $1 \beta_{\text{eff}}$  and was kept at a level  $0.6 - 0.7 \beta_{\text{eff}}$ . The absolute value of the power reactivity coefficient has increased. The increase of the period of the first radial-azimuth harmonic changing means the stabilization of the power distribution in the reactor. The cold poisoned reactor sub-criticality was increased also.

The process of U-Er fuel loading into 1 and 2 units reactors, accompanied by an additional absorbers unloading, is submitted on the Figures 3 and 4 as dependence of loaded fuel assemblies amount versus effective time of reactor operation starting from the beginning of the process. On the diagrams, the moments of replacement of control rods groups (2091 design to modernized 2477 one) are also marked. As a result, the voiding effect of the Control and Protection System circuit under operating conditions decreases. These replacements result in void reactivity coefficient increase approximately by  $0.1 \beta_{\text{eff}}$  per every 24 rods group. It was taken into account also when new fuel loading process was planning.

The use of the U-Er fuel has allowed to increase considerably fuel assembly burnup. Though during the initial stages of new fuel loading the average fuel assembly burnup in the core decreased a little (because a fresh U-Er fuel assembly has lower multiplication factor in comparison with regular one), subsequently the average fuel assembly burnup growth is observed in the core (Figures 5 and 6). The growth for unit 1 is 25 %, for unit 2, 44 % in comparison with initial value. In the same diagrams, the burnup of unloaded fuel is shown, for which the tendency to increase is also well visible.

## 5. CONCLUSION

The implementation of uranium-erbium fuel at Ignalina NPP shows very good results:

- the significant increase of fuel burnup,
- additional absorbers unloading,
- decrease of reloading rate,
- improvement of the reactor safety characteristics and keeping them within established limits.

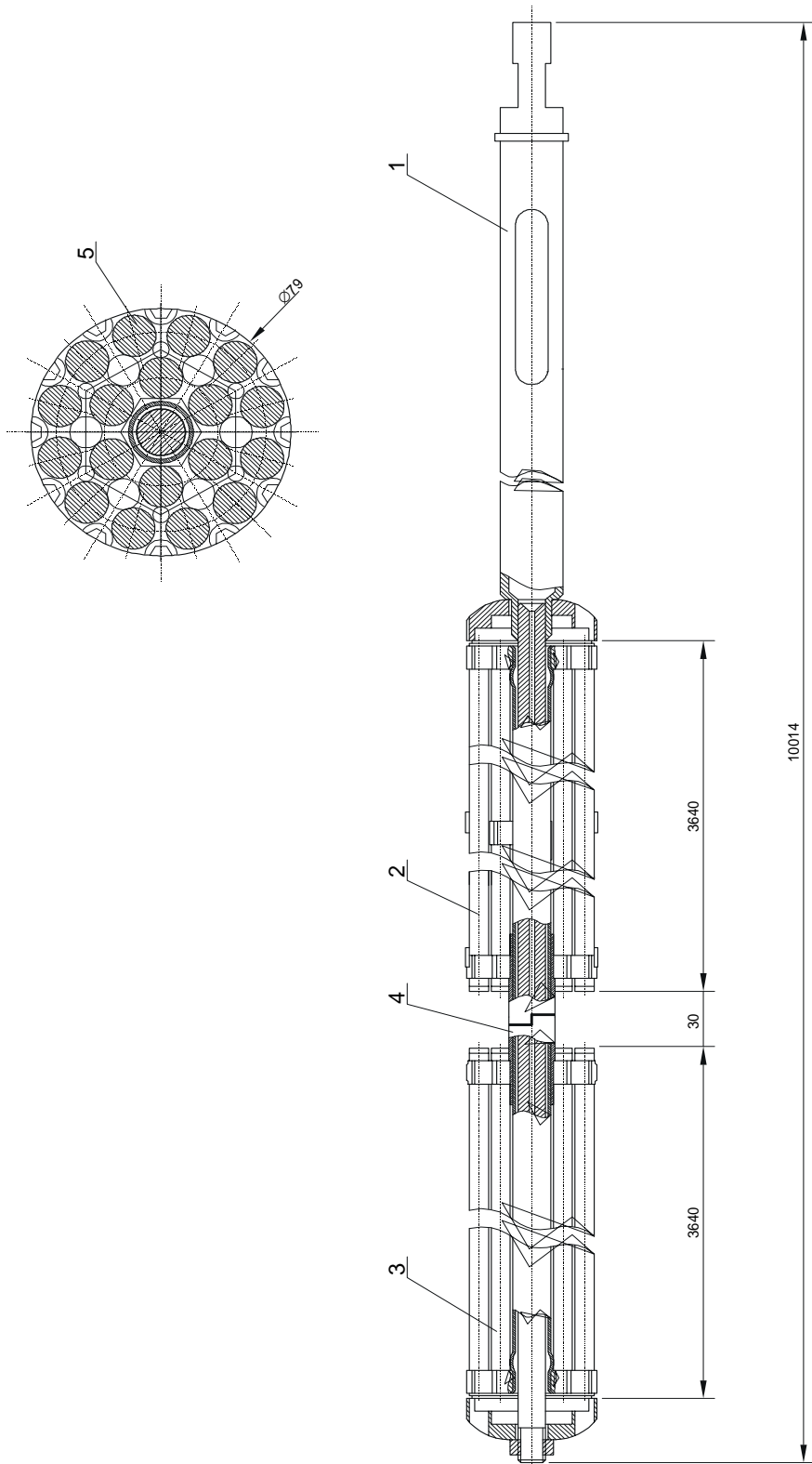
TABLE I. RBMK-1500 fuel assembly parameters

<b>Fuel pellet</b>	
Fuel	Uranium dioxide
Fuel enrichment, % of U <sup>235</sup>	2, 2.4
Fuel pellet diameter, mm	11.5
Fuel pellet length, mm	15
Pellet central orifice diameter, mm	2
<b>Fuel element</b>	
Cladding material	Zr+1%Nb
Outside diameter, mm	13.6
Length, m	3.64
Cladding thickness, mm	0.825
Pellet/clad gap, mm	0.22-0.38
Helium pressure in the cladding, MPa	0.5
Maximum linear heat generation rate, W/cm	485
<b>Fuel assembly</b>	
Number of bundles	2
Number of fuel rods per bundle	18
Diameter (in the core), mm	79
Mass of uranium within fuel pellet, kg	111.2
Mass of uranium within edge fuel pellet, kg	1.016
Maximum permissible power of fuel channel, MW	4.25

TABLE II. BASIC REACTOR PARAMETERS

Number of U-Er fuel assemblies	Void reactivity coefficient,, $\beta_{\text{eff}}$	Power reactivity coefficient, $10^{-4}\beta$ /MW	Period of azimuthal harmonic changing, min	Subcriticality, $\beta_{\text{eff}}$
<b>Unit 1</b>				
0	1.0	-1.6	20	4.6
500	0.6	-2.0	38	5.5
550	0.7	-2.0	20	-
663	0.6	-2.6	26	-
690	0.8	-2.3	25	-
759	0.7	-2.3	27	7.0
775	0.6	-2.8	37	-
<b>Unit 2</b>				
0	0.8	-1.8	22	5.8
150	0.5	-2.1	26	5.7 (74)*
650	0.6	-2.2	35	6.8 (752)
840	0.7	-2.2	38	7.4 (851)
1060	0.7	-2.0	50	-
1170	0.8	-2.0	48	-
1251	0.9	-2.1	68	6.3
1350	0.6	-2.5	69	-

\* - the FA amount specified in brackets means the value at which the subcriticality measurements were done



1-coupling rod; 2-upper bundle; 3-lower bundle; 4-carrying rod (or tube); 5-fuel rod.

*Fig. 1. Fuel assembly.*

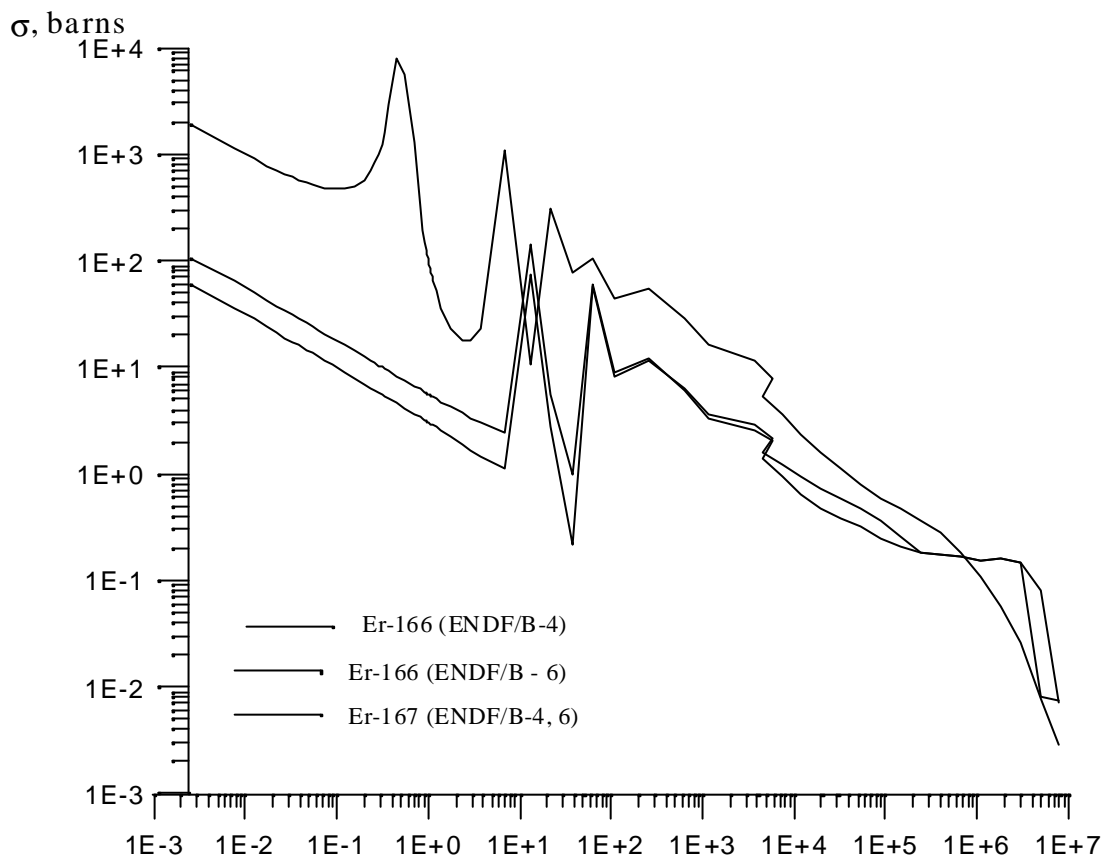


Fig. 2. Cross sections of Er.

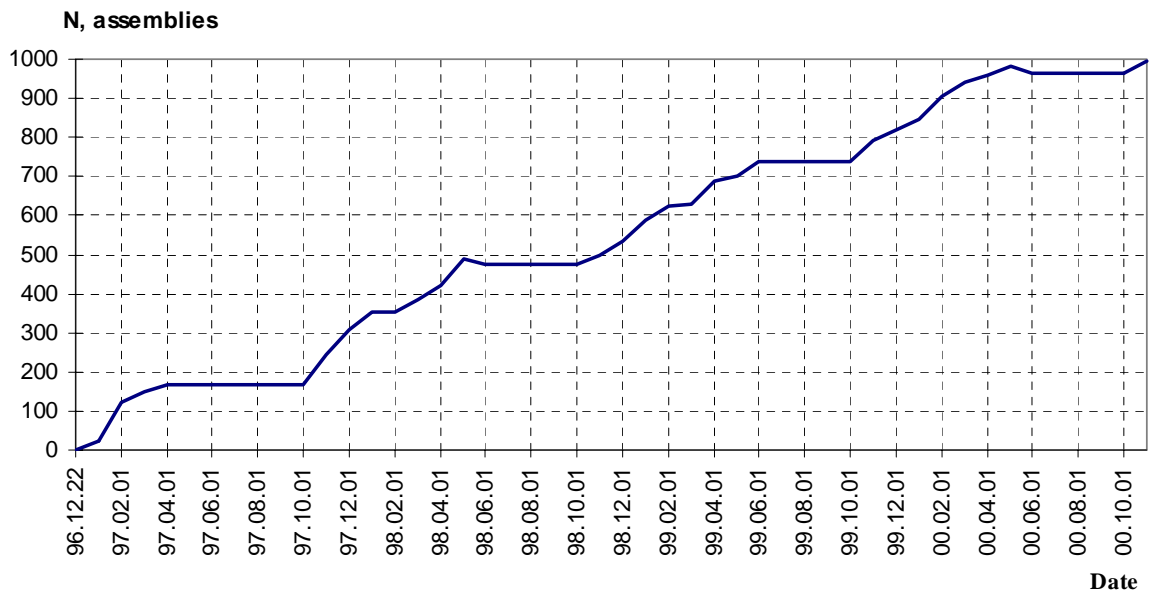
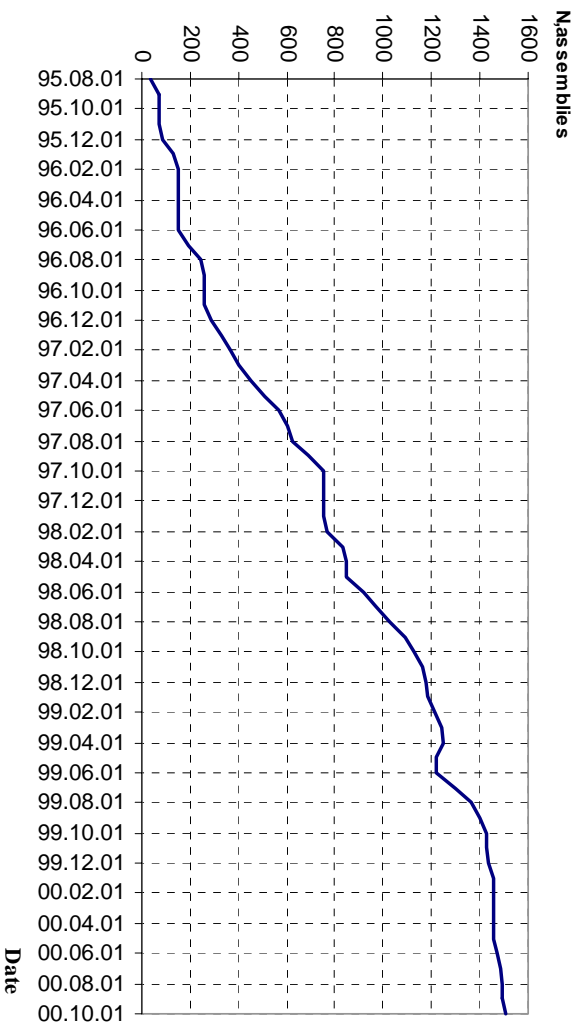
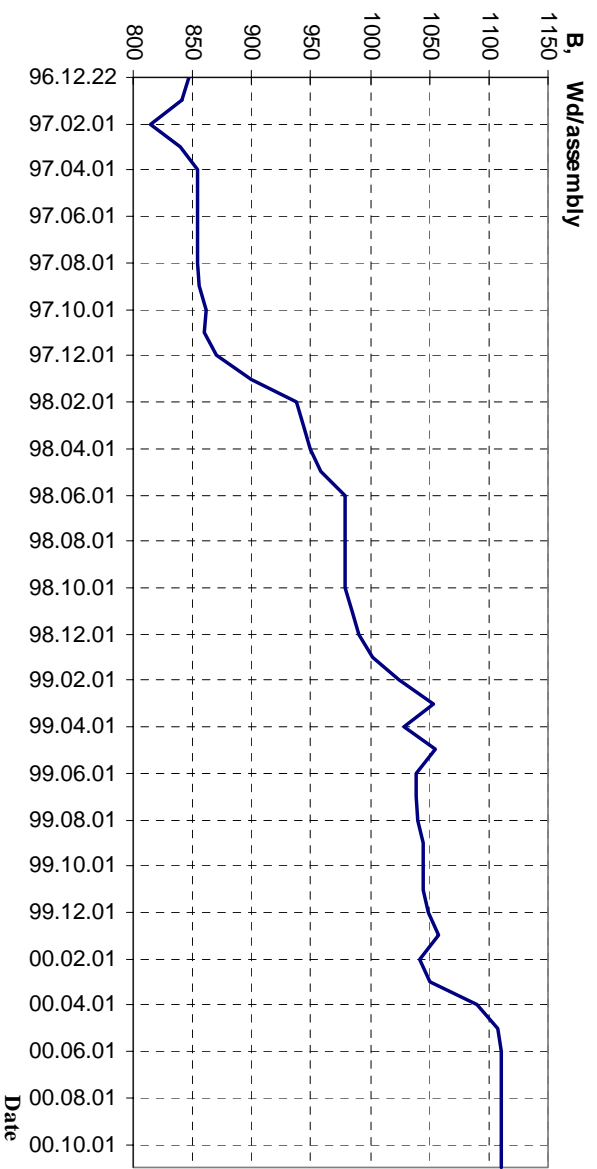


Fig. 3. Number of U-Er fuel assemblies in Unit 1.



*Fig. 4. Number of U-Er fuel assemblies in Unit 2.*



*Fig. 5. Average fuel burnup in Unit 1.*

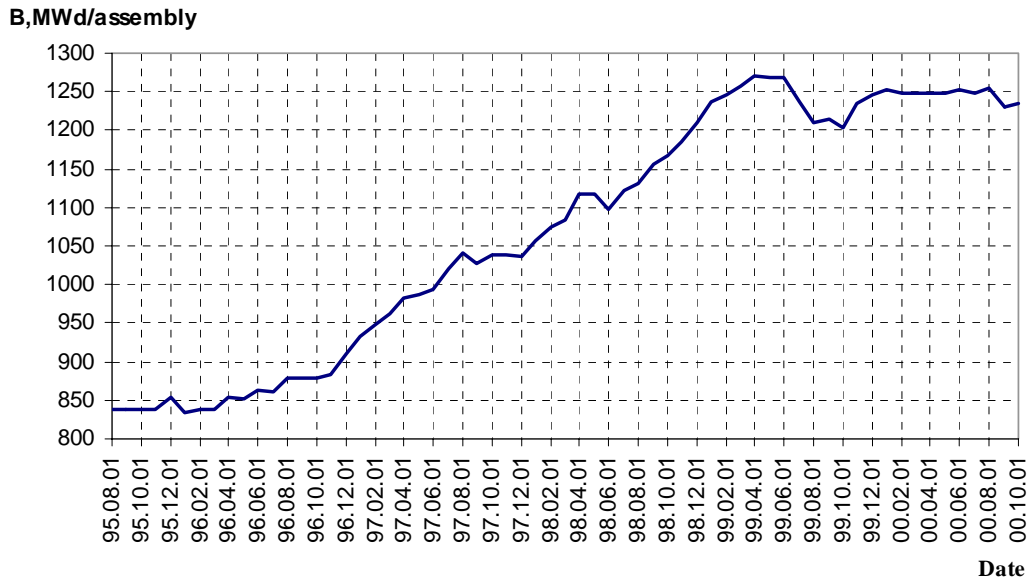


*Fig. 6. Average fuel burnup in Unit 2.*

### REFERENCE

- [1] ALMENAS K., KALIATKA A., USPURAS E., Ignalina RBMK-1500 a Source Book. Lithuanian Energy Institute, Lithuania, 1998.

# **The adequacy of methods used for the approval of high burnup core loading**

**H.G. Sonnenburg**

Research Centre,

Gesellschaft für Anlagen- und Reaktorsicherheit (GRS) mbH,

Garching, Germany

## **Abstract**

New fuel assembly designs and new core loading strategies are foreseen by most utilities, optimising the use of nuclear fuel in nuclear power plants. Increasing the burn-up to high values above 50 MWd/kg affects the fuel and cladding conditions, which could have safety relevant consequences. It is the task of the safety authorities to assess the impact of these changes with respect to compliance with safety regulations. Usually this assessment is based on code analyses which contain models developed at a time when the burn-up was significantly lower. Because the high burn-up is accompanied with the development of new phenomena like the rim effect on fuel pellets, the codes' models need to be revised for the representation of these new phenomena. The objective of this paper is to present a review of the knowledge base of the fuel phenomena under high-burn-up conditions as seen from safety aspects. The safety relevant fuel rod phenomena will be discussed. It will further provide an assessment of the limitations of the methodologies so far applied in the context of LOCA and RIA transients. The recently started research activities in Germany to improve the methodologies will be presented.

## **1. LICENSING PRACTICE IN GERMANY**

According to safety codes and guides (RSK guidelines for pressurised water reactors [GRS 81], KTA rules) there is no explicit limitation of the fuel burn-up foreseen in Germany. In practice the applicant has to demonstrate the compliance with existing requirements by submitting related documents to the technical inspection agency (TÜV) for approval.

With respect to the Loss of Coolant Accident (LOCA) the RSK guidelines are basically identical with the United States Code of Federal Regulations, Title 10, Section 50 (10 CFR 50) appendix K "ECC evaluation models". That is, under LOCA condition, the maximum fuel rod cladding temperature allowed is 1200 °C, the local oxidation depth as a fraction of actual cladding tube wall thickness shall not exceed 17 %, the maximum fraction of zirconium of all cladding tubes reacting with water shall not exceed 1%, long-term cooling and sub-criticality of the core shall be maintained. Beyond these acceptance criteria the RSK guidelines require that the core damage extent during a LOCA shall not exceed 10 % of all rods.

In particular, the latter has to be proven by a core damage analysis. In contrast to the licensing practise in other countries the applicant is requested to show the compliance with this requirement for each core loading cycle.

This analysis consists of two parts, the thermal hydraulic analysis and a subsequent fuel rod failure analysis using the hot channel boundary conditions derived from the thermal hydraulic part. The subsequent fuel rod failure analysis is very detailed and subdivides the entire number of fuel rods into two classes: a) power class and b) burn-up class.

Concerning the definition of power classes an extreme power status of the core is supposed which reflects a distorted power profile of the core before the accident. This power profile is

bound by a maximum linear rod power rate of e.g. 440 W/cm. This value is called the "LOCA peak value" of linear power generation rate. It is defined in order to cope with uncertainties in the core power distribution and their measurement. It depends on the specifics of a reactor core. The reactor surveillance system assures that this LOCA peak value cannot be exceeded during normal operation at any location of the core.

For each class the steady state operational parameters like fuel rod internal pressure, the gap conductivity between pellet and cladding as well as the status of corrosion has to be provided as input for the fuel rod failure analysis. That is, all fuel rod properties including the effects caused by burn-up are explicitly taken into account when judging on the acceptance of a core loading.

The applicant performs for all of these fuel rod classes calculations which even consider statistical effects in order to demonstrate with high confidence that the compliance with this 10% failure criterion is fulfilled. As an example see also paper 7 of this Technical Committee Meeting by C. Fenzlein which illustrates the statistical technique applied by the fuel rod vendor SIEMENS.

The technical inspection agency on the regulatory side uses the fuel rod analysis code TESP (Temperature and Strain Probabilistic Analysis code) which has been developed by GRS in the 80's in order to independently assess the results submitted by the applicant.

## 2. CONCEPT OF THE FUEL ROD FAILURE ANALYSIS CODE TESP

The basic concept of the TESP code [ULL 80, ZIR 81] is to determine the temperature distribution in a cross-section of a fuel rod and to deduce from the resulting cladding temperatures the strain rate and the related hoop stress. The fuel rod is assessed to be failed when the hoop stress exceeds the ultimate hoop stress. The ultimate hoop stress is determined by a correlation which has been developed at KfK Karlsruhe for Zircaloy-4 in the early 80's [ERB 80].

The straining due to the thermal creep of the zircaloy cladding is assumed to have an eccentricity because the cladding material is characterised by a texture with respect to grain size and orientation. Due to this eccentricity both an azimuthal temperature distribution and an azimuthal strain distribution in the cladding is to be calculated.

The thermal hydraulic condition of coolant surrounding the cross-section of the fuel rod is provided by a thermal hydraulic code analysis for a so-called hot channel condition. This hot channel is simulating the coolant channel of a fuel element with the highest rod power among the others.

Both the initial value of the internal pressure and the initial value of the gap conductivity between pellet and cladding are provided as input values to this fuel rod code TESP.

## 3. PRESENT LIMITATIONS OF THE TESP CODE REGARDING THE HIGH BURN-UP REGIME

However, the fuel rod failure analyses are reliable to that extent which is still supported by the related experimental data base underlying the analysis code. The international discussion on fuel rod failure limits under LOCA and RIA (Reactivity Initiated Accident) conditions

motivated us to reconsider the methods applied so far. This reconsideration led to the conclusion that the TESPAC code applied in the licensing process has to be updated in order to account also for the recent developments in fuel rod fabrication and burn-up levels.

Therefore a developmental project has been started this year at GRS which will provide at the end of the project a renewed analysis tool for future safety assessments. Particular emphasis in this developmental work will be given to the effects which correspond to the high burn-up regime.

With respect to the failure analysis under LOCA condition the detrimental effects of the high burn-up increase on the pellet material properties and their consequences for the modelling of the TESPAC code will be discussed next.

### **3.1. Findings from experiments related to LOCA analysis**

The fuel rod tests under reactivity initiated accident (RIA) condition performed in France, Japan and Russia demonstrated that the failure threshold might be lowered when the burn-up level of the fuel rod is increased. Further experimental investigations have been undertaken in order to isolate certain phenomena which may provoke this burn-up effect. The investigations concentrated on the fission gas release from the fuel matrix as well as on the embrittlement of the fuel rod cladding. For both phenomena detrimental effects to the failure threshold have been identified and partly quantified.

The investigations in Halden e.g. have shown [TUR 99] that the fission gas temperature threshold continuously decreases with increasing burn-up. This threshold is responsible for an immediate fission gas release from the fuel matrix (Vitanza threshold). The experiments identifying this threshold have reached burn-up values of about 80 MWd/kg UO<sub>2</sub>.

Measurements confirm that an averaged fuel rod burn-up of 30 MWd/kg leads to a release of 6% fraction of the generated fission gas while a burn-up of 70 MWd/kg even leads to a release of a 10% fraction. That is, the decrease of power with burn-up due to a loss of reactivity does not necessarily compensate the effect of a progressive fission gas release.

Due to the permanent reactor operation and consequently due to the burn-up increase, there exists a more and more extending central part of the pellet, which is affected by lowering fission gas temperature threshold. Simultaneously this fission gas release is additionally supported by the continuously lowering thermal conductivity which increases the central temperature of the pellet.

As a consequence from these burn-up developments the internal fuel rod pressure progressively increases. Therefore, it cannot be excluded that the rod internal gas pressure of high burn-up rods might even reach values close to or above the environmental pressure under reactor operation. Thus we are faced with high burn-up fuel rods having relative high fuel rod internal gas pressures as initial condition in our fuel rod failure analyses.

However these investigations do not quantify the effect of fission gas release during a rapid temperature transient like that one of a LOCA transient. Fig. 1 illustrates the rapid temperature rise in a rim near to the pellet periphery within the first ten seconds of a LOCA transient.

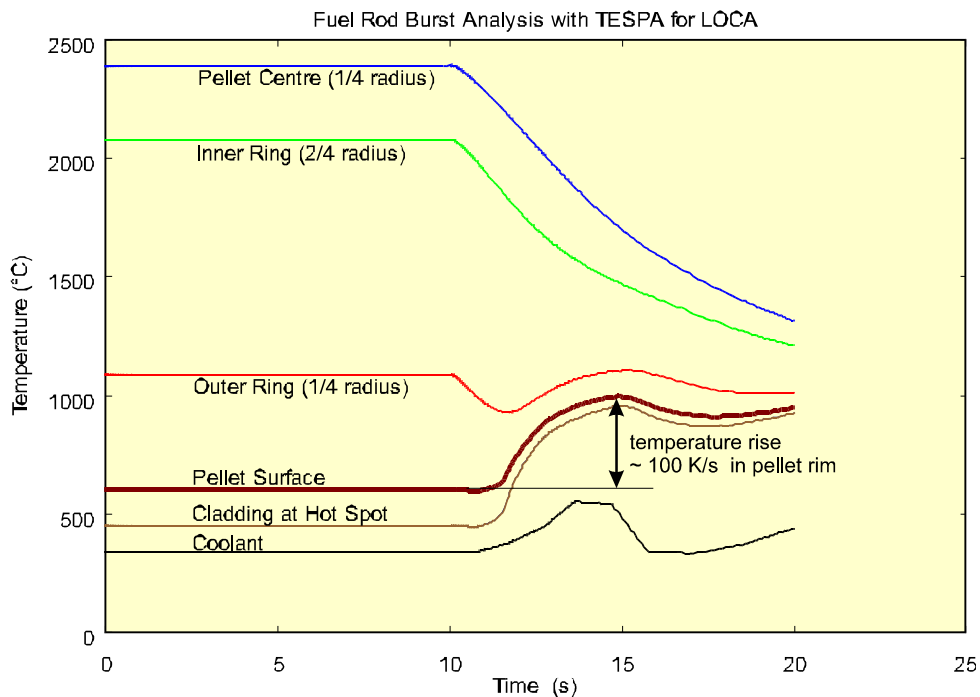


Fig. 1: Temperature development of the pellet during the LOCA transient.

Although the rim temperature still stays below the Vitanza threshold, it cannot be excluded that this rim region will release the stored fission gas and therefore additionally support the fission gas pressure development during the LOCA transient.

Up to now the behaviour of the rim region concerning gas release during accidental conditions is not well understood. Therefore an uncertainty margin on the rod internal pressure needs to be taken into account until a better estimation of this transient fission gas release is available.

From experimental investigations at the ITU Karlsruhe (Germany) [LAS 95] it became evident that a pellet rim region develops when the burn-up value exceeds 40 MWd/kg. This region is characterised by a new structure of the fuel matrix and has a different fission gas storage behaviour. The porosity of this rim region is drastically increased. The grain size is decreased to about 0.2  $\mu\text{m}$ .

The experimental data suggest that an inter-granular storage of fission gas still exist. This region is further characterised by an increased power density and an increased burn-up. It also shows a larger content of Plutonium.

We conclude from these experimental findings that the TESPA prediction of the radial pellet temperature distribution requires an enhanced spatial resolution in order to account also for the pellet rim characteristics.

The fission gas flow within the fuel rod also plays an important role in the same context. Up to now the TESPA code simulates the behaviour of a fuel rod cross-section only. The code ignores the rod internal gas flow coming from or going to the fuel rod gas plena. Because it can be expected that these gas flows have a relevant impact on the fission gas pressure development during the LOCA transient, it is planned to extend the TESPA code to a fuel rod code describing the entire fuel rod.

#### 4. FINDINGS FROM EXPERIMENTS RELATED TO RIA TRANSIENTS

The findings above have also relevance for the fuel rod behaviour under RIA conditions, but it appears that the loading of the fuel rod under RIA condition challenges the fuel rod cladding in a different way as under LOCA condition.

Concerning the corrosion behaviour of the fuel rod cladding there is a permanent activity on the fabrication side to improve the corrosion performance. The amounts of niobium and tin have been varied to improve this performance. Up to now it is not clear whether these modified alloys will provide the same yield strength as the elder Zirkaloy-4 which has been extensively investigated in LOCA burst tests.

Under LOCA condition the thermal creep of the cladding finally leads to the rod failure. When looking on the RIA transients which may have a duration of less than one second, the cladding will be strained by the thermal expansion of the pellet and additionally by a rapid fission gas release resulting in a rapid internal pressure increase. This straining process may reach the limits of the plasticity of the cladding before the thermal creep of the cladding is significantly active.

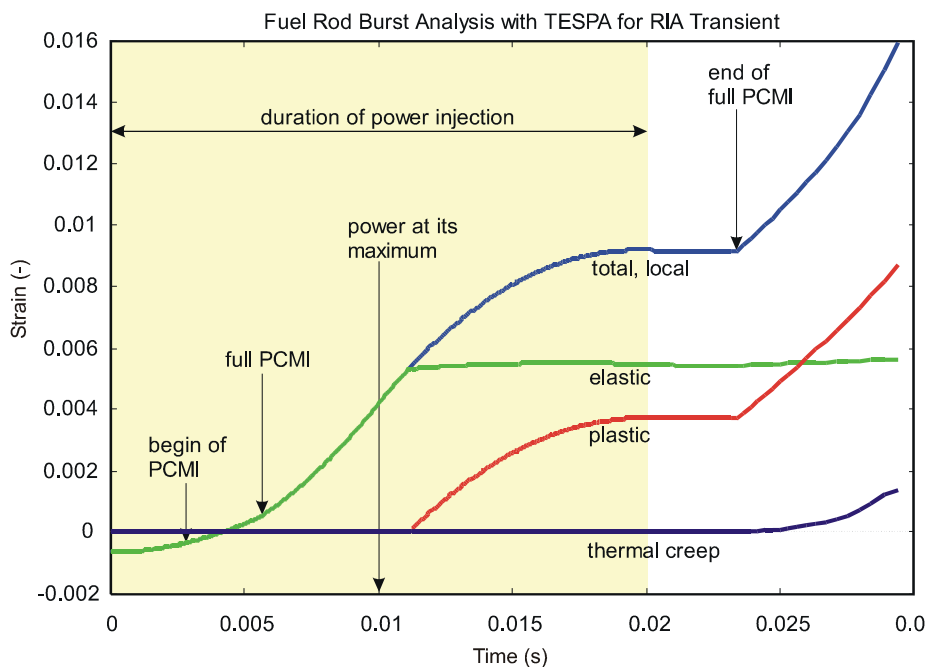


Fig. 2: Possible strain development of the cladding during a fast RIA power pulse.

Figure 2 illustrates the strain prediction for a RIA transient with a pulse half-width of 10 ms. The example shown is related to a high burn-up fuel rod with almost complete radiation hardening. The plastic deformation occurs rather late. Due to continues temperature increase of the cladding, thermal creep starts almost simultaneously with a progressive plastic strain which ultimately leads to the rod failure.

The failure mode in this case is not attributed to the Pellet Cladding Mechanical Interaction (PCMI). It is attributed to the rising fission gas pressure.

Depending on the transient duration of the RIA transient the creep of the cladding more or less superposes the plastic straining but it may not dominate the failure mode. Therefore the

interpretation of experimental results from RIA tests is more difficult than for LOCA related fuel rod tests.

Therefore RIA tests require accurate post test examinations of the cladding in order to identify the failure modes. These tests furthermore require a thorough pre-test qualification of the fuel rods in order to determine the corrosion status of the cladding.

The pre-test information about the burn-up value is only an indirect measure of the status of the cladding. Radiation hardening occurs relative early and a continuation of the burn-up provokes no further hardening. The determination of the cladding parameters like the hydride content, the oxide layer thickness and stress-strain curves from relevant cladding materials are decisive for a successful failure analysis.

We believe that the high burn-up RIA tests in the CABRI test facility and associated tests in France will provide the necessary quality of the experimental data. Therefore, Germany including the German utilities are taking part in the international CABRI test series.

## 5. SUMMARY AND OUTLOOK

The growing economic competition leads to cost optimisation on the fuel cycle costs. Both burn-up increase and an upgrade of the thermal power of the reactor core is a consequence of this optimisation process. It is the obligation of the safety authorities to accompany and assess the optimisation steps taken by the utilities in order to keep the safety standards.

Because the burn-up increase provokes new fuel rod phenomena, the inspection tools applied for the safety assessment require an adequate modelling. TESPAs is the code which is applied for the fuel rod failure analysis by the technical inspection agencies in Germany. The international discussion on high burn-up primarily related to RIA transients motivated us to reconsider the code's applicability to the high burn-up regime.

This reconsideration identified several high burn-up related phenomena which are not well or not at all represented in this code. In particular it is found that the fission gas release during a LOCA transient and the resulting fuel rod internal pressure have to be modelled in this code adequately.

According to the German safety codes and guidelines the compliance with safety standards has to be demonstrated for each core loading. This safety assessment is focused on the fuel rod damage which might occur under a loss of coolant accident (LOCA).

The fuel rod failure assessment under RIA transients is only performed for representative core loadings using various conservative assumptions (inserted reactivity by control rod ejection, kinetic parameters and power density distribution). For each fuel cycle the applicability of the generic RIA analysis is assured, but no stress and strain analysis is performed.

A developmental project has been initiated this year to determine the failure threshold and the phenomena for high burn-up fuel rods from planned international CABRI tests. In addition, these RIA related investigations will also help to quantify the transient fission gas release which might be of relevance for the fuel rod failure assessment of LOCA transients. This project will improve the TESPAs code's performance. It is expected that after this developmental work the TESPAs code is available for assessments of RIA and LOCA transients.

## REFERENCES

- [1] Gesellschaft für Reaktorsicherheit (GRS mbH):Translations – Safety Codes and Guides. Edition 5/82, RSK Guidelines for Pressurized Water Reactors, 3<sup>rd</sup> Edition, Oktober 1981 [GRS 81].
- [2] ULLRICH, R.: Status der Entwicklung und Verifikation des Brennstabverhaltensprogramms TESPА zur gekoppelten Dehnungs- und Temperaturanalyse, GRS-A-415, Januar 1981 [ULL 80].
- [3] ZIPPER, R.: Reorganisation des Programmsystems TESPА zur gekoppelten Temperatur- und Dehnungsanalyse von Reaktorbrennstäben, GRS-A-567, März 1981 [ZIR 81].
- [4] TURNBULL, J.A.: An assessment of fission gas release and the effect of microstructure at high burn-up. OECD Halden Reactor Project, Work Report HWR-604, March 1999 [TUR 99].
- [5] LASSMANN, K.; WALKER, C.T.; VAN DE LAAR, J.: Modelling the high burn-up UO<sub>2</sub> structure in LWR fuel, J. Nucl. Mat. 226, pp. 1-8., 1995 [LAS 95].
- [6] ERBACHER, F.; NEITZEL, H.J.; ROSINGER, H.; SCHMIDT, H.; WIEHR, K.:Burst criterion of zircaloy fuel claddings in a LOCA. ASTM 5<sup>th</sup> International Conference on Zirconium in the Nuclear Industry, Boston, Massachusetts, USA, August 4-7, 1980 [ERB 80].

# Probabilistic Safety Criteria On High Burnup HWR Fuels

**A.C. Marino**

Grupo Diseño Avanzado y Evaluación Económica,  
Comisión Nacional de Energía Atómica,  
Bariloche, Argentina

## Abstract

BACO is a code for the simulation of the thermo-mechanical and fission gas behaviour of a cylindrical fuel rod under operation conditions. Their input parameters and, therefore, output ones may include statistical dispersion. In this paper, experimental CANDU fuel rods irradiated at the NRX reactor together with experimental MOX fuel rods and the IAEA'CRP FUMEX cases are used in order to determine the sensitivity of BACO code predictions. The techniques for sensitivity analysis defined in BACO are: the "extreme case analysis", the "parametric analysis" and the "probabilistic (or statistics) analysis". We analyse the CARA and CAREM fuel rods relation between predicted performance and statistical dispersion in order of enhanced their original designs taking account probabilistic safety criteria and using the BACO's sensitivity analysis.

## 1. INTRODUCTION

To get nuclear power generation within safety and economic criteria requires a deep knowledge on fuel behaviour under many different situations. The economic of the energy production might be greatly improved by means of relatively minor corrections on the design, fuel processing and operating conditions. These options require to check carefully the fuel design. This fact must consider the performance of parts as well as their in service thermo-mechanical coupling. The classical tool, which has been used to study these coupling, is the numerical simulation on computer codes to obtain qualitatively results and even quantitatively valid. Numerical predictions are strongly influence by realistic modelling.

BACO is a code for the simulation of the thermo-mechanical and fission gas behaviour phenomena in a cylindrical fuel rod under operation conditions. The 2.40 is the present version of the code. Our modelling approach is based on using simple models, which are however sustained on phenomenological ideas and critical evaluation of their consistency. Input parameters and, therefore, output ones may include statistical dispersion.

To better understanding the uncertainties and their consequences, the mechanistic approach must be augmented by probabilistic analysis. BACO includes a probabilistic analysis within their structure including uncertainties in fuel rod parameters, code parameters and fuel models. These characteristics are emphasised in this paper. They do not only related to fuel rod knowledge and modelling, but can also be applied in safety and economics assessments to define the operation conditions and to asses further developments. BACO has been used for simulating PWR, CANDU, BWR, MOX, and experimental fuel rods. In the same way, it is used for the design of advanced fuels (CARA and CAREM). The code performance was tested against other ones of similar features. BACO has participated in several co-ordinated round robin benchmarks of fuel code predictions against experimental results (D-COM and FUMEX).

Argentina has two nuclear power stations under operation: Atucha-I (a Pressure Vessel PHWR) and Embalse (CANDU 600 type), and another one under construction (Atucha II). Basic fuel design is different in both cases. Predicting the thermal and mechanical performance of the CANDU fuel is challenging for computer codes not designed “ad hoc”, from the fuel performance characteristics (collapsible cladding, filling gas pressure, cladding creep down during irradiation, etc.). The CARA Fuel Project [1] and the CAREM Reactor Project [2], where BACO is embedded, require a code with HWR extended burnup and probabilistic capabilities.

## 2. BACO CODE

The BACO code structure and models in its present versions have already been described by Marino et al. [3], including steady state and transient thermal analysis. Nowadays, the number of instructions is about eleven thousand FORTRAN 90 sentences. Data post-processing improves the code’s performance and analysis of results.

On modelling the UO<sub>2</sub> pellet phenomena, such as elastic deformation, thermal expansion, creep, swelling, densification, restructuring, cracks and fission gas release are included. While for the Zry cladding, the code models elastic deformation, thermal expansion, anisotropic plastic deformation, and creep and growth under irradiation. The modular structure of the code easily allows added of different material properties. It can be used for any geometrical dimensions of cylindrical fuel rods with UO<sub>2</sub> pellets (either compact or hollow, with or without dishing) and Zry cladding.

Fuel rod power history and either cladding or coolant outside temperatures must be given to the program. Rod performance is numerically simulated using finite time steps (finite differential scheme). The code automatically selects time steps according to physical criteria. Temperature profile within pellet and cladding, main stresses at pellet and cladding, radial and axial crack pattern in the pellet, main strains and hot geometry of pellet and cladding, change in porosity, grain size and restructuring of the pellet, fission gas release to the free volume in the rod, trapped gas distribution in the fuel and in the UO<sub>2</sub> grain boundary, internal gas pressure and current composition of the internal gas, dishing shape evolution, are calculated. The output contains the distribution along the rod axis of these variables.

We assume azimuthal symmetry in cylindrical coordinates for the fuel rod; our model is bidimensional and angular coordinates are not considered. However, angular dependent phenomenon, as well as radial cracking, is simulated via some angular averaging method. For the numerical modelling the hypotheses of axial symmetry and modified plane strains (constant axial strain) are adopted. The fuel rod is divided in axial sections in order to simulate its axial power profile dependence. The mechanical and thermal treatment and the pellet, cladding and constitutive equations are available from Reference [3].

## 3. BACO CODE SENSITIVITY ANALISYS

The uncertainties on results of a validated fuel computer code with an experimented user come from many different sources:

- 1) Input data of the codes:
  - a) Neutronic and reactor data,
  - b) Power history of the irradiation,
  - c) Fuel data:
    - i) Dimensional data
    - ii) Material properties
- 2) Internal data of the code (and code structure):
  - a) Code parameters,
  - b) Modelling,

- i) Physical constants,
- ii) Parameters of the model,
- iii) Field of application of the model.

Also, we can join these data around the point of view of its influence on the uncertainties:

- 1) Modelling and its empirical or theoretical parameters,
- 2) Data provided by direct measures due to in reactor irradiation and fuel test, and
- 3) Fuel manufacturing data and fuel design data.

We can require best models for our codes and then we solve the first point. We can require best measurements during irradiation, material testing and reactor parameters. That means it is possible an improvement of code results from modelling, reactor and material data.

The same does not happen with the parameters of the fuel due to manufacturing process. The tolerances of fuel dimensions are a consequence of their process and they are sustained by the basic design. Then we must include the treatment of this source of uncertainties.

The first and easy way to analyse these topics is the definition of a set of worst cases. Those cases are the coupling of the variations of fuel parameters taking account the tolerances in order to produce the worst situations (such as maximum stress, maximum strains, extreme temperatures, etc.).

Several fuel performance codes include a probability analysis within their structure covering uncertainties in input, fabrication, parameters and models [4, 5, and 6]. The BACO code (version 2.40) includes probabilistic analysis with statistical dispersion of the fuel rod parameters.

A BACO's probabilistic analysis of power fuel reshuffling have been performed to the Atucha I NPP [7], where we analyse the susceptibility of hoop stress during fuel reshuffling at different powers and burnups. Here we reproduce the recommendation of the designer for fuel reshuffling with simplified rules. The fuel for the Atucha I NPP are analysed in the Reference [8] and, the fuel for the EMBALSE NPP (CANDU type, Argentina), are analysed in Reference [9].

We use three different techniques for sensitivity analysis:

- 1) Extreme cases analysis.
- 2) Parametric analysis.
- 3) Probabilistic (or statistical) analysis.

The “extreme cases analysis” consists in finding which combination of fuel rod parameters their possible extreme values (code input data) produce the worst situation about fuel rod behaviour. With this analysis we could define the tolerance of the fuel rod parameters. This technique is the first step in order to define the as-fabricated tolerances of the fuel element.

The “parametric analysis” is the study of the individual influence of each fuel rod parameter in the fuel rod behaviour (temperatures, stresses, deformations, pressures, etc.). With this analysis we find the correct weight of each fuel rod parameter in order to understand the fuel behaviour with a far and wide scope. This technique is the second step in order to tune the as-fabricated tolerances with an engineering overview specially when we are designing fuel elements.

The “probabilistic analysis” is a Monte-Carlo technique, which combine several random of fuel parameter (input data) with its statistical distribution. Each probable input data could be a real fuel rod, and the series of M-C calculation have a significant impact on the calculated results.

## 4. BACO CODE VALIDITY TEST AND PROBABILISTIC APPLICATIONS

### 4.1. CO-ORDINATED RESEARCH PROJECT ON FUEL MODELING AT EXTENDED BURNUP

The IAEA’s CRP FUMEX (Co-Ordinated Research Project on Fuel Modelling at Extended Burnup) is a blind-test developed on a set of experiments in order to compare fuel performance with code predictions. The OECD-HALDEN reactor (Norway) provided data. A set of fuels are instrumented following the evolution of some parameters (pellet centre temperature, inner pressure of the rod, cladding elongation, fission gas release, cladding diameter). The experiments include PIE (post-irradiation) analysis. The final burnup reached for the rods were intermediate (25 MWd/kgU) and high (50 MWd/kgU) [10, 11].

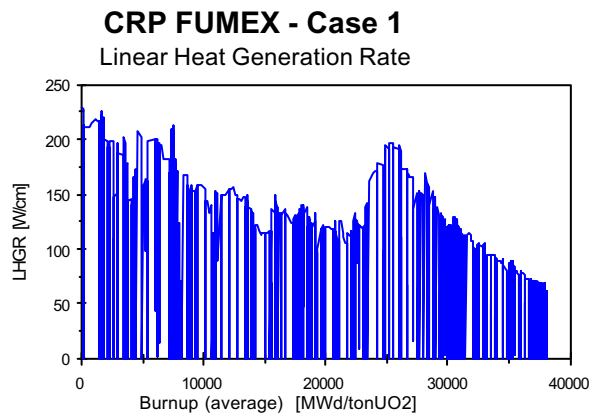


Figure 1: Linear Heat Generation Rate (power history) as a function of the averaged burnup of the fuel rod.

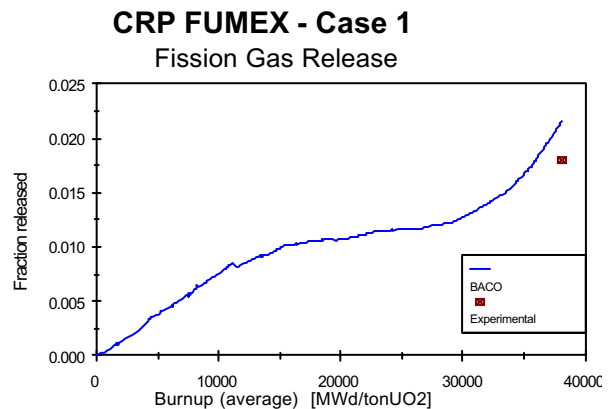


Figure 2: Fraction of fission gas released as a function of averaged burnup of the fuel rod. BACO code version 2.20 (before FUMEX version).

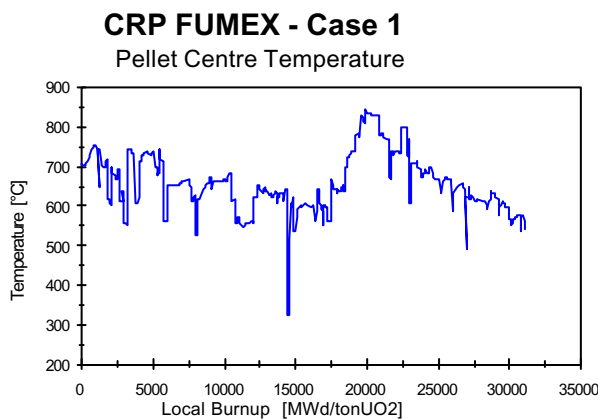


Figure 3: Pellet centre temperature. CRP FUMEX Case 1. “On line” temperature measured at the OECD Halden Reactor.

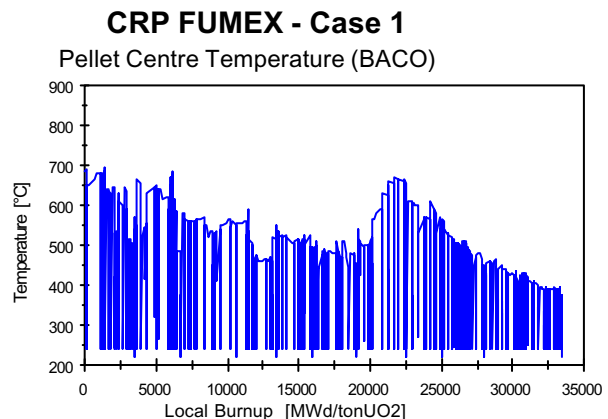


Figure 4: BACO output for the pellet centre temperature. CRP FUMEX Case 1. BACO code version 2.20 (before FUMEX version).

As an example of the BACO Code performance during the CRP FUMEX we include some of our results for the first exercises (FUMEX Case 1). The figure 1 shows the power history (input data) for that case. The calculated fraction of fission gases released at EOL (End Of Life) is 2.2 % (and the predicted value during the “blind test” stage was 2.5 %). The experimental value was 1.8 % (see figure 2). Figure 3 shows the measurement during irradiation of the temperature at the pellet centre (top of the nuclear fuel rod). The temperature monitoring was made each fifteen minutes along the irradiation. The measurement uncertainty was  $\pm 50$  °C. Figure 4 includes the BACO code calculation [12]. The CRP FUMEX case 1 looks equivalent as the fuel for the CAREM Reactor [2].

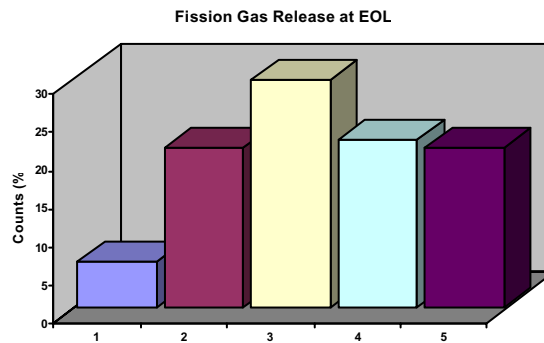


Figure 5: Histogram with the Fission Gas Release at End of Life (EOL) calculated with BACO code 2.40

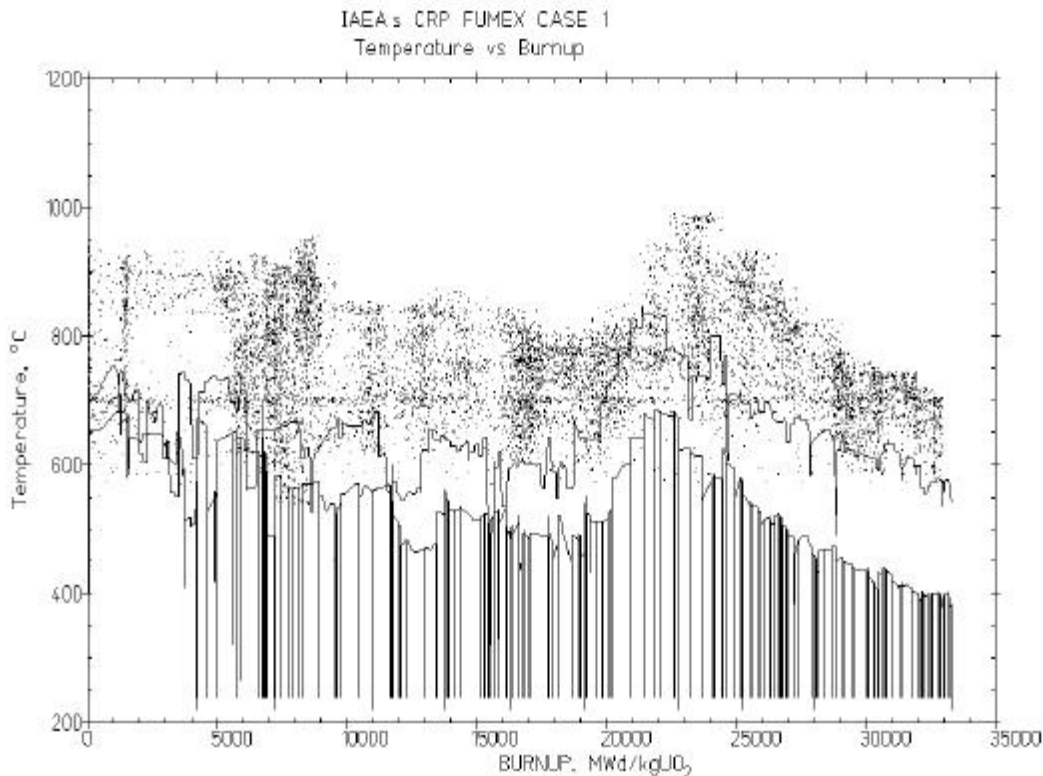


Figure 6: Probabilistic analysis of the pellet centre temperature (FUMEX Case 1) including the measurements and the BACO code v2.20 result.

The probabilistic analysis was done using the present version of the code for the fission gas release and the temperature of the pellet at the thermocouple position. The Figure 5 shows the histogram with the fission gas release. The Figure 6 shows the M-C evaluation for the pellet centre temperature. The curves calculated (dot lines) shows an overpredicted average with a great dispersion not easy to follows due to the big numbers of shutdowns and start-ups. We are using the uncertainties assumed during the CRP FUMEX ( $\pm 5\%$  uncertainty in power,  $\pm 5\ \mu\text{m}$  in initial gap and  $\pm 5\%$  in  $\text{UO}_2$  thermal conductivity) [11]. Here we are introducing the coupling of uncertainties due to irradiation data, as-fabricated tolerance and modelling. The same calculation produces a very small dispersion if we take accounts just the as-fabricated tolerance in the gap.

#### 4.2. EXPERIMENTAL IRRADIATION AT THE NRX REACTOR (Notley, 1980)

The work reported by Notley [13] was used for testing the BACO code and results reported References [3, 14]. In Notley's work six Zircaloy-sheathed  $\text{UO}_2$  fuel elements were irradiated at

power outputs between 760 and 600 W/cm to a burnup of about 5500 MWd/tonU. Then both of them and another pair of new rods were irradiated at lower powers for a further 1250-1700 MWd/tonU. The experiment was irradiated in the X-2 loop of NRX reactor. All elements were destructively examined and some of them were measured during the irradiation. The predicted and measured rod radius change  $\Delta R/R$ , fission gases released, columnar and equiaxed grains and central hole are provided by Notley [13] and calculated with BACO [3, 14].

From the point of view of the codes the couples of rod namely HZB-HZC and HZF-HZZ are identical, but, of course, the fission gas release reported was different. Nevertheless, the probabilistic analysis shows small dispersion for these values (see Table 1).

The discrepancy between measurements and calculation is not explained with probabilistic analysis. We must enhance the fission release model because the Notley's irradiations are close to the limit of validation.

Table 1: Volume of fission gases released. (Units: cm<sup>3</sup> STP)

	HZB	HZC	HZF	HZZ
Vol. (gas) [Experimental.]	10.6	11.5	17.4	13.7
Vol. (gas) [BACO]	7.94		11.12	
$\sigma$ [BACO]	0.04		0.05	

### 4.3. MOX de PETTEN

Within our interest on studying MOX fuel performance, the irradiation of the first Argentine prototypes of PHWR MOX fuels began in 1986 with six rods fabricated at the  $\alpha$  Facility (CNEA, Argentina). These experiences were made in the HFR-Petten reactor, Holland. The goal of this experience was to study the fuel behaviour with respect to PMCI-SCC. An experiment for extended burnup was performed with the last two MOX rods. During the experiment the final test ramp was interrupted due to a failure in the rod. The posirradiation examinations were indicated that PCI-SCC was a mechanism likely to produce the failure [15]. That analysis was predicted with the calculated stresses [16]. The parameters of the MOX irradiation, the preparation of the experiments and post-irradiation analysis were sustained by the BACO code predictions.

#### 4.3.1. "EXTREME CASES" ANALYSIS OF THE MOX FUEL ROD

The purpose of this exercise is considering how the combination of assumed extreme rod dimensions conditions, but within reasonable tolerance for its fabrication, can affect performance. In this case we define two extreme situations:

- 1) A rod with the largest gap between pellet and cladding compatible with the as-fabricated tolerances, and
- 2) A rod with the smallest gap.

The first situation should have to rise up the maximum temperature in the fuel, and the second to maximum stress between pellet and cladding.

For the same power history of figure 7, figure 10 includes the pellet centre temperature to the maximum gap situation at the bottom of the fuel rod. The largest temperature attained in this case is 1675 °C (against 1600 °C for the minimum gap situation). Figure 12 includes the BACO calculation of hoop stress with a minimum gap situation. Here we have not seen a big change; the wide range between both situation at the middle of life is due to the hard contact happens. The curves calculated have shown a narrow band due to the strict QA under lab conditions. We obtain a stable solution, with the three parameters mentioned, which probes that the BACO code is a good tool to be used for fuel rod design.

### 4.3.2. PROBABILISTIC ANALYSIS OF THE BU15 EXPERIMENT

As it was noted in the Introduction, the flexibility and computer time saving capabilities of the BACO code allows performing systematic statistical analysis. Using allowed fabrication dimensional limits and a statistical distribution of values within those; several runs (a minimum of 1000) are performed with different set of initial values for the rod dimensions [15]. We study the predicted variations in:

- 1) Pellet center temperature,
- 2) Cladding hoop stress, and
- 3) Gas pressure predictions.

The rod input data were randomly selected within assumed deviations for pellet diameter and height, inner and outer diameter of the cladding and pellet density. The random selection of input values was done assuming a Gauss distribution limited with maximum and minimum values. See Table 2 and figures 8 and 9.

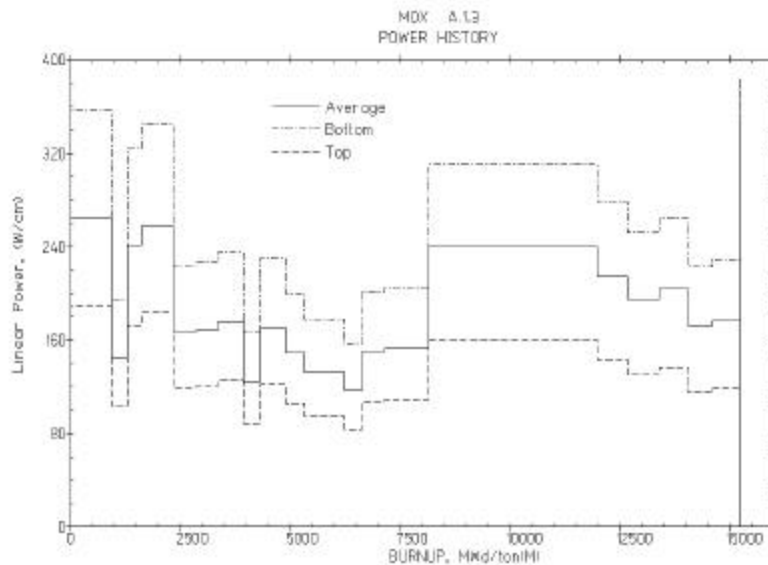


Figure 7: Linear heat generation rate in function of burnup for the A.1.3 fuel rod. The curve upper curve correspond with the top of the fuel, the lower curve correspond with the defective zone of the rod. The maximum during the last power ramp corresponds with the “bottom” of the rod.

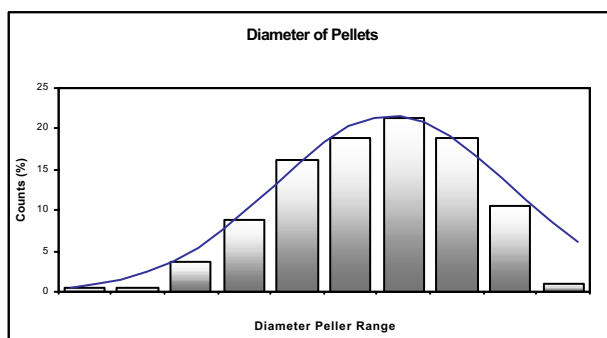


Figure 8: Histogram of the pellet diameters. The columns are between the maximum and minimum specified values [ $\varnothing_p = (1.040 \pm 0.001)$  mm]. The curve is the associated Gauss distribution.

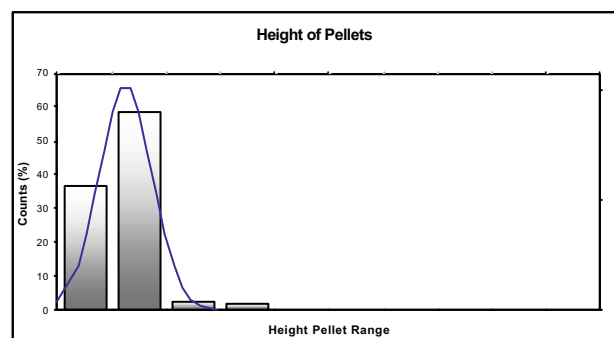


Figure 9: Histogram of the pellet heights. The ten columns are between the maximum and minimum specified values [ $h_p = (11. \pm 1.)$  mm]. The curve is an approximated Gauss distribution.

The Figures 10, 12 and 14 represent the BACO code sensitivity analysis of some performance parameters in the MOX fuel rod A.1.3. We plot in the curves:

- 1) Standard parameters of input data of the rod,
- 2) The parameters of the maximum gap situation,

- 3) The parameters of the minimum gap situation, and
- 4) The points of the Monte-Carlo selection (probabilistic analysis).

**Table 2:** MOX fuels irradiated at Petten reactor.  
Some statistical parameters of the fuel rods.

<i>Pellets</i>	Main Value (or specification)	Standard Deviation	Minimum Value	Maximum Value
Pellet diameter (cm)	1.0402	0.0005	1.0390	1.0414
Pellet height (cm)	1.1217	0.0204	1.1000	1.3000
Density (gr/cm <sup>3</sup> )	10.522	0.048	10.350	10.650
...	...	...	...	...
<i>Cladding</i>				
Cladding inner diameter	1.170 cm	...	1.166	1.174
...	...	...	...	...

Figure 10 is the BACO code calculation for the pellet centre temperature to the same previous history of Figure 1. All the random points calculated are between the extreme values in as-fabricated tolerances, taken with approximate realistic values. There is convergence of dots at EOL (End of Life) due to pellet-clad contact. Figure 11 shows a histogram of the pellet centre temperature at EOL, after the final ramp.

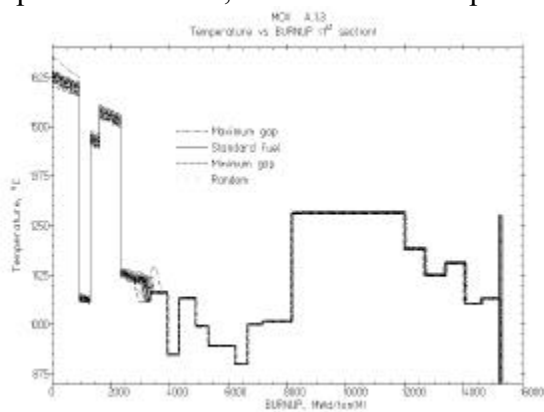


Figure 10: Pellet centre temperature in the first segment of the fuel for the BU15 experiment (A.1.3 rod)

**Pellet Center Temperature at EOL**

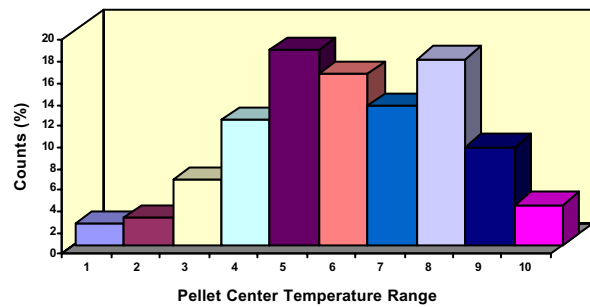


Figure 11: Histogram of the pellet centre temperature at End of Life (EOL). The columns are between the maximum and minimum calculated values (1275-1278°C).

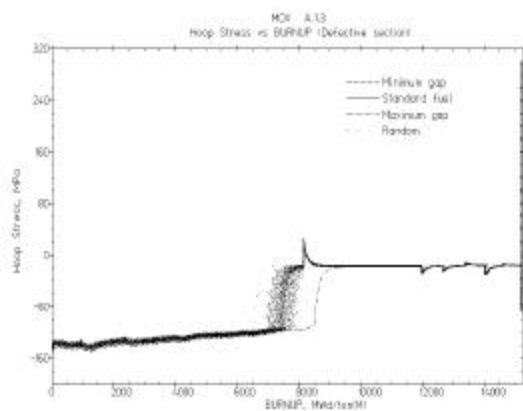


Figure 12: Hoop stress at the defective segment of the fuel rod for the BU15 experiment (A.1.3 rod)

**Histogram of Hoop Stress at EOL**

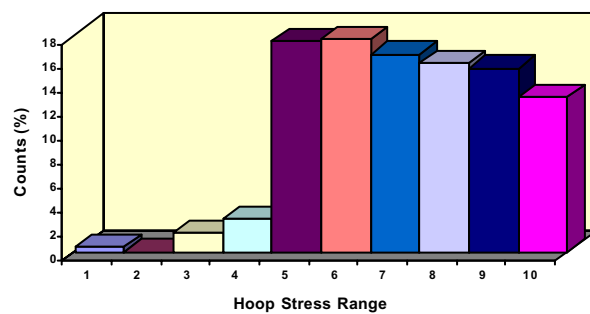


Figure 13: Histogram of the hoop stress at End of Life (EOL). The columns are between the maximum and minimum calculated values (292-302 MPa).

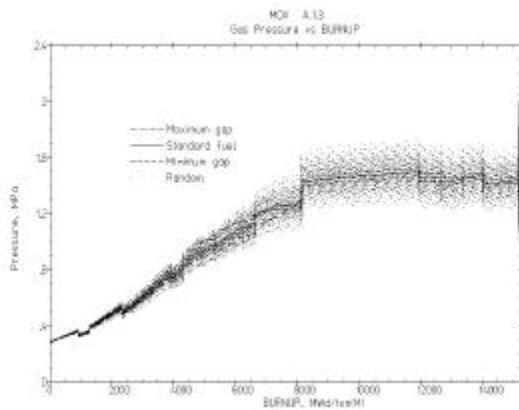


Figure 14: Gas pressure of the free gases in the fuel rod for the BU15 experiment (A.1.3 rod)

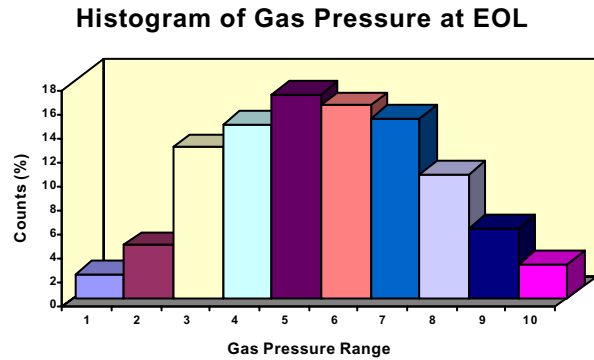


Figure 15: Histogram of the gas pressure of the free gases in the rod at End of Life (EOL). The columns are between the maximum and minimum calculated values (1.60-2.07 MPa).

Figure 12 shows the cladding hoop stress dispersion with the same inputs as the previous plot. The points show a great dispersion at the middle of life due to the pellet-cladding contact situation. There are points out of the extreme limits of the previous analysis. The calculation shows that the hoop stresses converge during the irradiation that is clearly demonstrated by the small dispersion at EOL previous at the final ramp (see figure 13).

Figure 14 is the free gas pressure at the fuel rod. The gas pressure calculation takes account of the thermal calculation, dimensional calculation (stresses), fission gas release, etc. That is the coupling of all fuel rod parameters (input data and behaviour modelling). There is a small dispersion at BOL. The calculated values of pressure diverge during irradiation. Finally, after 4000 MWd/ton(M), there are values both smaller and larger than those predicted at the extreme conditions of the “gap” size situation. Figure 15 is a histogram of the rod gas pressure of the free gases at EOL. The main value agrees with the one calculated for the standard fuel parameters.

The laboratory condition produces a narrow dispersion due to the adjustment, tuning and QA of the fuel rod parameters, as well as, the irradiation conditions. Nevertheless, the standard calculation and the “extreme case analysis” do not reproduce exactly the fuel behaviour.

## 5. FUEL ROD DESIGN USING PROBABILISTIC SAFETY CRITERIA. CALCULATION WITH BACO CODE.

### 5.1. CANDU and ATUCHA I FUEL ROD SENSITIVITY ANALYSIS

A sensitivity analysis of a CANDU fuel is detailed in Reference [9]. And, for the Atucha I fuel, in the Reference [8]. The main finding of sensitivity analysis calculation, when we are focussed in the pellet centre temperature, cladding hoop stress and gas pressure (due to illustrative purposes), are:

- 1) Random temperature curves are between “extreme limits” curves.
- 2) There are some curves of cladding hoop stress either smaller or greater than the “extreme limits”.
- 3) Great dispersion at the starting of the irradiation for cladding hoop stress.
- 4) The cladding hoop stress curves converge with the burnup.
- 5) There are gas pressure curves either smaller or greater than the “extreme limits”.
- 6) The dispersion of the pressure of free gases increases with the burnup.

“Extreme case analysis” was the aim of their original designs. The sensitivity analysis applied on a very well known fuel conduct us to conservative curves. Nevertheless, we find several suggestions about the fuel operation when SEU is done in Atucha I [8, 18, and 19].

## 5.2. CARA FUEL ROD: A PARAMETRIC ANALYSIS APPROACH

An approach to the parametric analysis of a CARA fuel rod is sketched in Figures 16 to 19. We are finding the weight of the different rod parameters in order to identify its proper influence on fuel behaviour. Figures just include the most significant parameters at the present calculation: pellet radius,  $UO_2$  density, clad inner radius, pellet height and dishing depth.

In Figure 16 we analyse the response about the pellet centre temperature during a powerful ramp at beginning of life (BOL). The X-axis is between 0 and 1 (minor and mayor values of the parameter). The lowest  $UO_2$  density produces the highest temperatures due to densification. (Densification increases the gap pellet-cladding, so reduce the conductance increasing the temperature.)

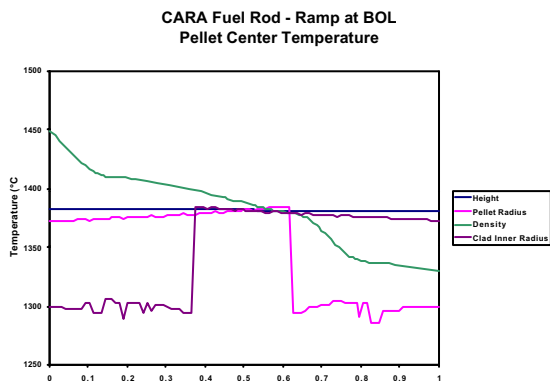


Figure 16: Parametric analysis of the susceptibility on the pellet centre temperature of a CARA fuel rod.

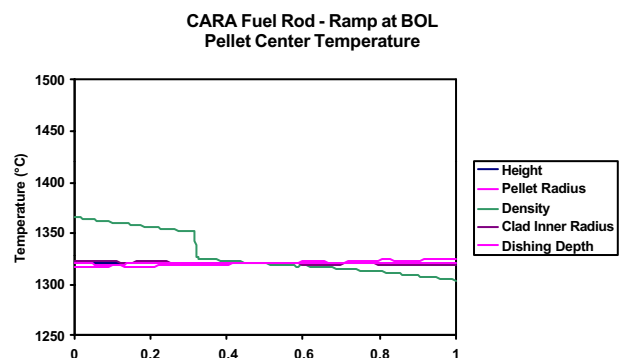


Figure 17: Parametric analysis of the susceptibility on the pellet centre temperature after tuning parameters of the CARA fuel and "feedback" with the manufacturer.

Figure 18 includes the susceptibility with the hoop stress at the inner surface of the cladding during a powerful (and possible) reshuffling during irradiation. Figures 16 and 18 are the "parametric analysis" after "extreme case analysis".

The pellet reaches its minimum temperature when the pellet or the inner clad diameters have the smallest gap. Nevertheless, we lost the handicap of these particular diameters when we execute the corresponding analysis of the "hoop stress". Those diameters reach the highest stresses on the cladding. That stresses are incompatible with safety margins for the cladding integrity.

We repeat the calculation of susceptibility with many different stresses, pressures, deformations, temperatures, etc. under different irradiation conditions. This procedure allows obtain a deep knowledge of the influence of each individual parameter into the fuel behaviour.

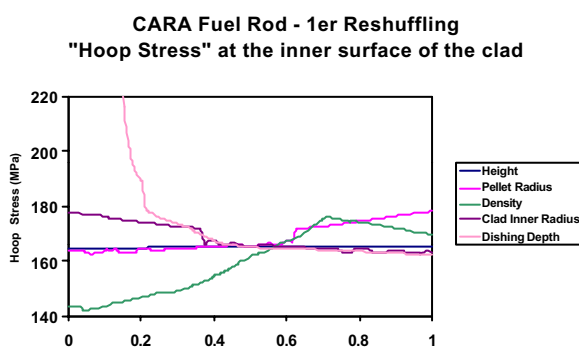


Figure 18: Parametric analysis of the susceptibility on the "hoop stress" at the inner surface of the cladding of a CARA fuel rod.

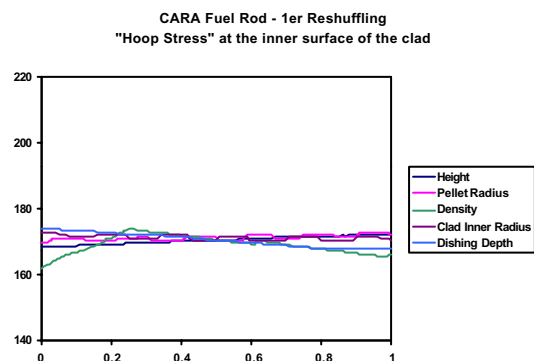


Figure 19: Parametric analysis of the susceptibility on the "hoop stress" after tuning parameters of the CARA fuel and "feedback" with the manufacturer.

With these results we tune up the parameters and we obtain a new set of parameters with a new response. The Figures 17, 19 and 20.b show the new calculation after tuning the parameter of the CARA fuel and including “feedback” with the manufacturer.

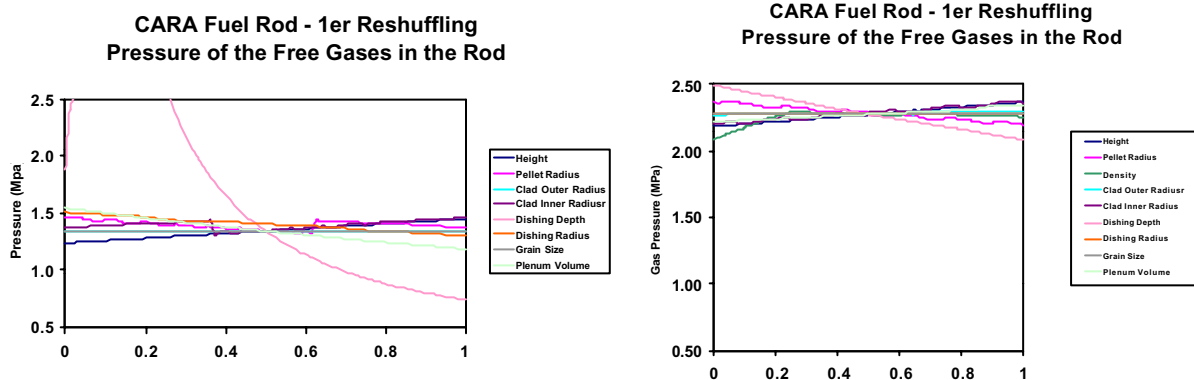


Figure 20.a: Parametric analysis of the susceptibility on the gas pressure of the free gases.

Figure 20.b: Parametric analysis of the susceptibility on the gas pressure of the free gases after tuning parameters of the CARA fuel and “feedback” with the manufacturer.

A realistic definition of some results could be an increment of its values. Nevertheless, those increments produce a stable solution within safety levels. These are the output shown in Figures 20.a and 20.b (gas pressure of the free gases in the fuel rod).

At present, due to this analysis some of the main parameters of the CARA fuel rod are pellet radius, dishing depth and clad inner radius. Dishing radius and density of  $UO_2$  were significant. Volume plenum and pellet heights were not negligible. Finally, the rest of parameters were negligible or they are out of the scope of the BACO code.

These calculations enable us to determine the first appreciation of values of parameters and its extreme values (or as-fabricated tolerances) with an engineering point of view.

### 5.3. CAREM FUEL ROD: A PROBABILISTIC ANALYSIS APPROACH

A probabilistic analysis could be performed without the above calculations with the BACO code. Nevertheless the computational cost of the Monte-Carlo calculation can be reduced when the influence of the parameters had been tested. We present the first probabilistic results with the fuel rod for the CAREM reactor after a wide set of “parametric analysis”.

The Figure 21.a shows the pellet centre temperature for that fuel at the most demanding position into the core. The same happens with Figure 22.a for the “hoop stress” and Figure 23.a for the pressure of the filling gases (plus released gases during irradiation). We find conservative curves in the three plots. The Figures 21.b, 22.b and 23.b includes the average curve, the curve of the standard calculation and the curves of the average plus and less the standard deviation.

The temperature calculation shows a small dispersion during irradiation and converges of curves at EOL (End of Life). The average (of the random calculation) curve and the standard curve look equivalent (See Figures 21.a and 21.b).

The “hoop stress” calculation (Figures 22.a and 22.b) shows a great dispersion between 6000 and 14000 MWd/ton $UO_2$ . This situation is emphasised in the Figure 22.b; here there is a strong difference between average curve and standard curve and a wide field between the curves plus and less deviation. The average curve does not reproduce a real situation. That curve is included with illustrative purposes. Nevertheless, the appearance of an increment of the dispersion of the curves could be the key to understand this kind of situation. The different size of gap pellet-cladding at BOL (Beginning of Life) produce the contact at different time. The coupling

of results with and without contact is the responsible of that increment of dispersion. An equivalent analysis can not be reproduced with the calculation of gas pressure of the free gases. The increment of the dispersion is not easy to explain due to the coupling of all the process during irradiation were the gases pressure calculation is embedded.

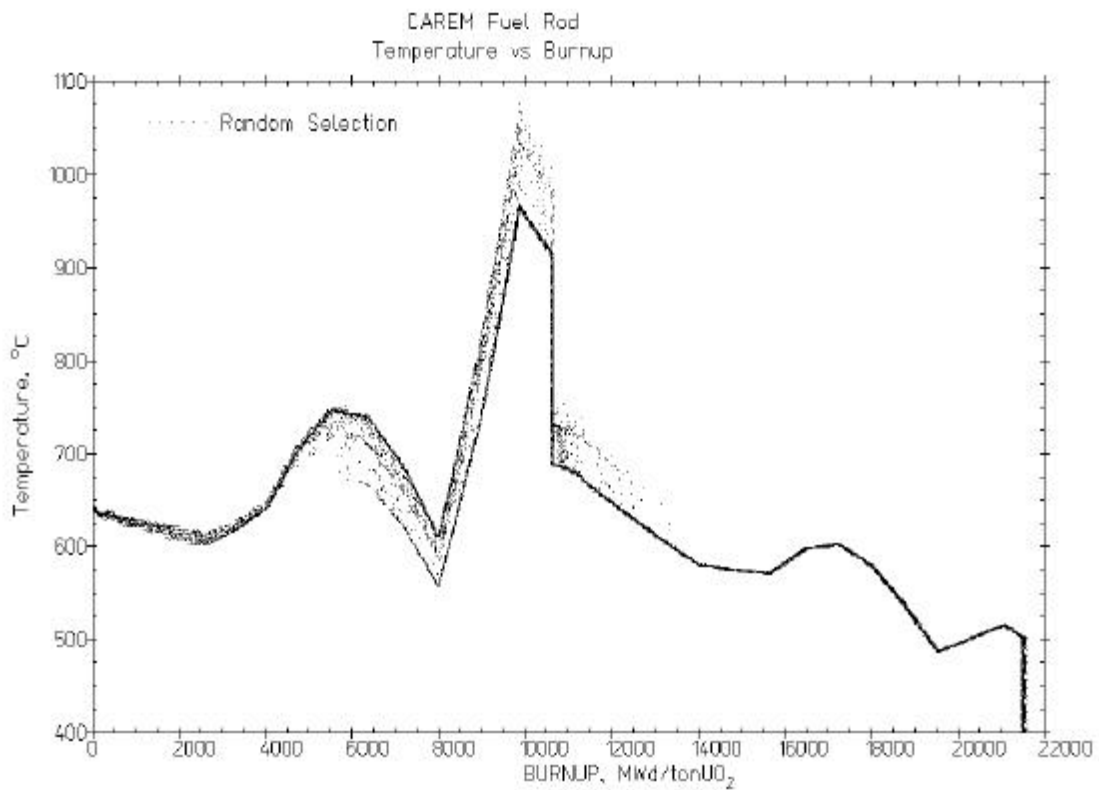


Figure 21.a: Probabilistic analysis for the pellet centre temperature of a CAREM fuel rod.

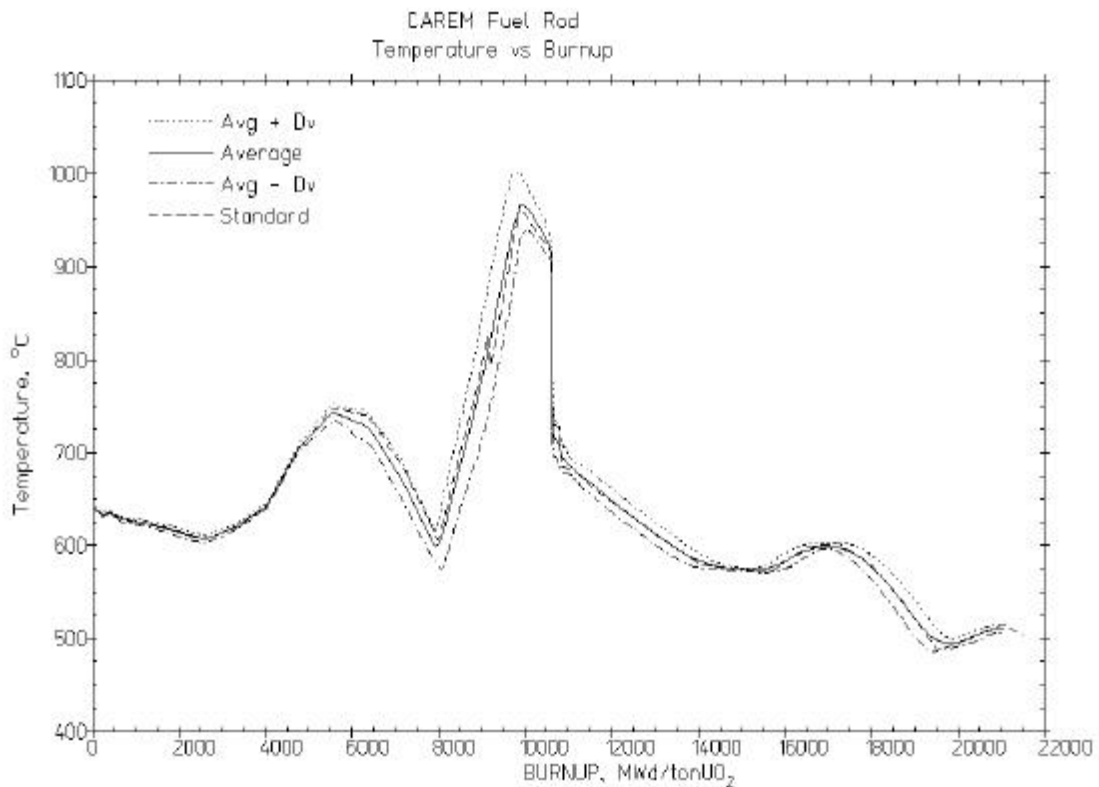


Figure 21.b: Probabilistic analysis for the pellet centre temperature of a CAREM fuel rod.

Further study could analyse the influence in the behaviour of the stress reversal at the maximum power during irradiation or the increment of the dispersion with burnup of the gas pressure.

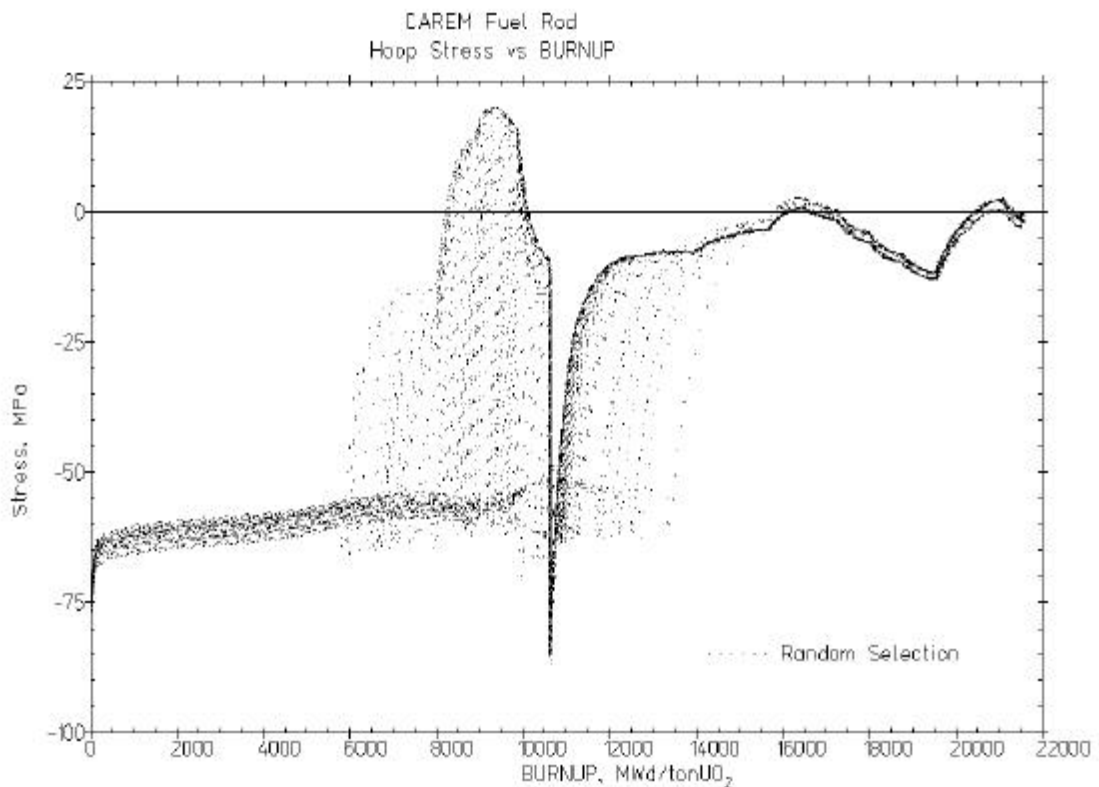


Figure 22.a: Probabilistic analysis for the “hoop stress” of a CAREM fuel rod.

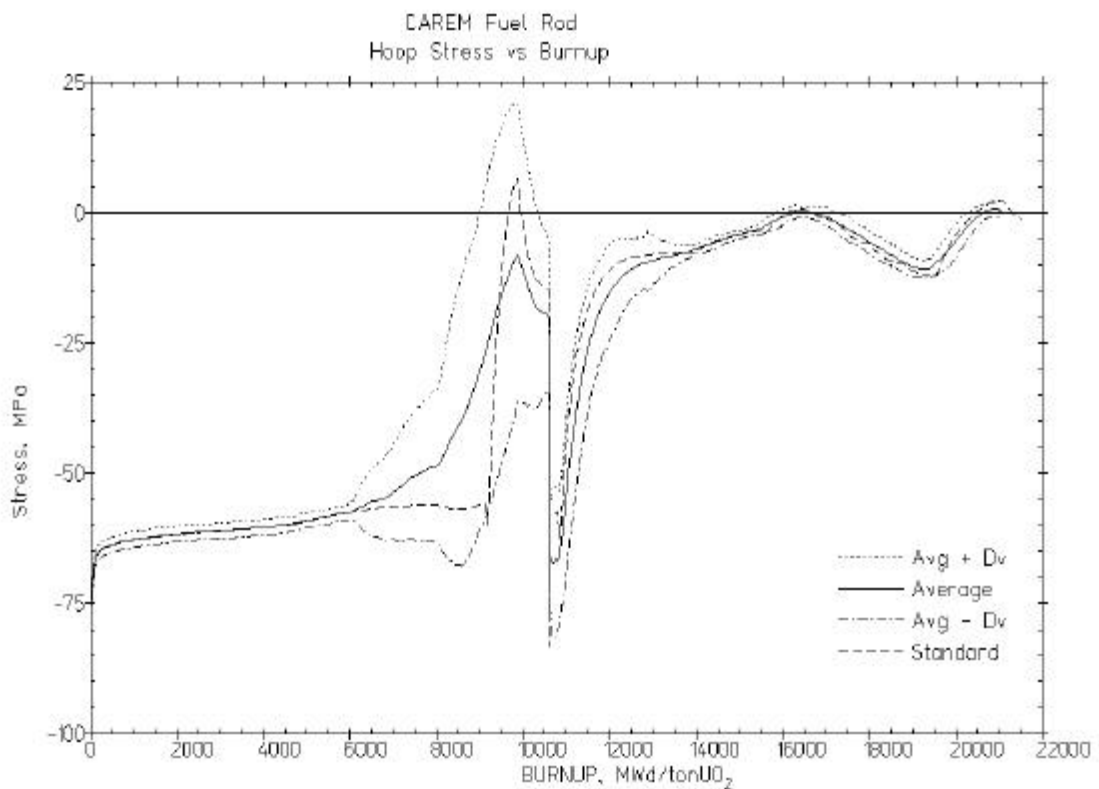


Figure 22.b: Probabilistic analysis for the “hoop stress” of a CAREM fuel rod.

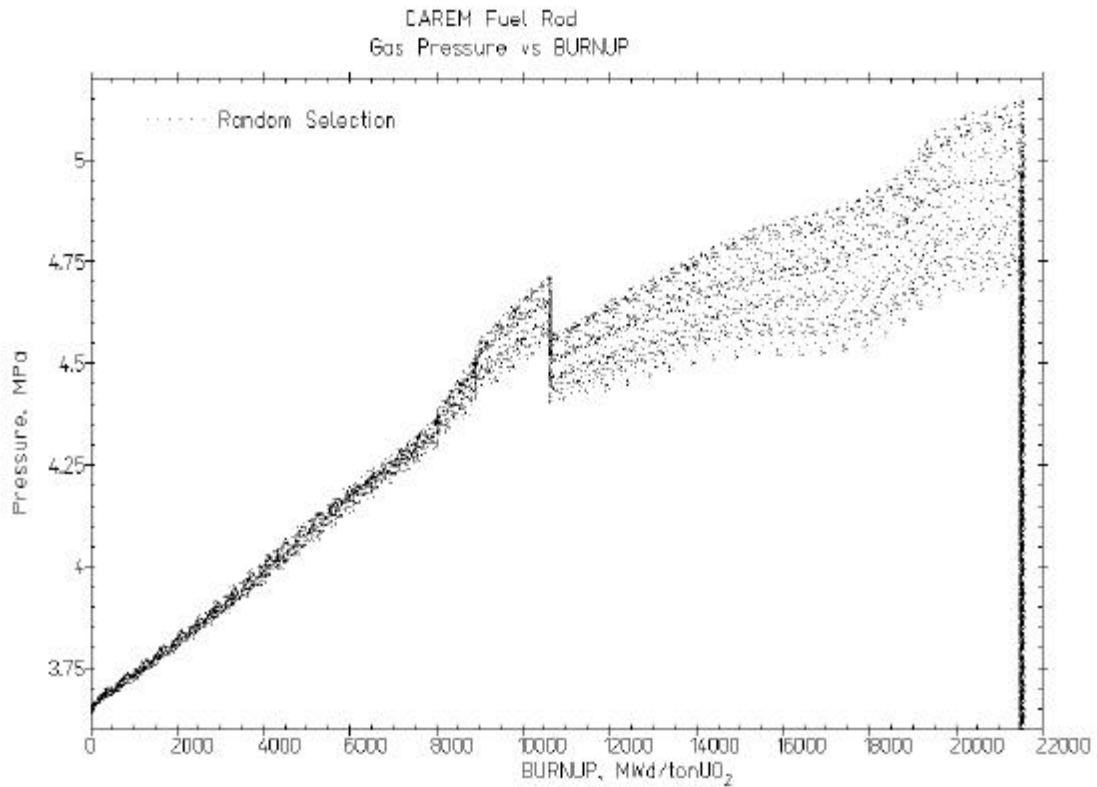


Figure 23.a: Probabilistic analysis for the gas pressure of a CAREM fuel rod.

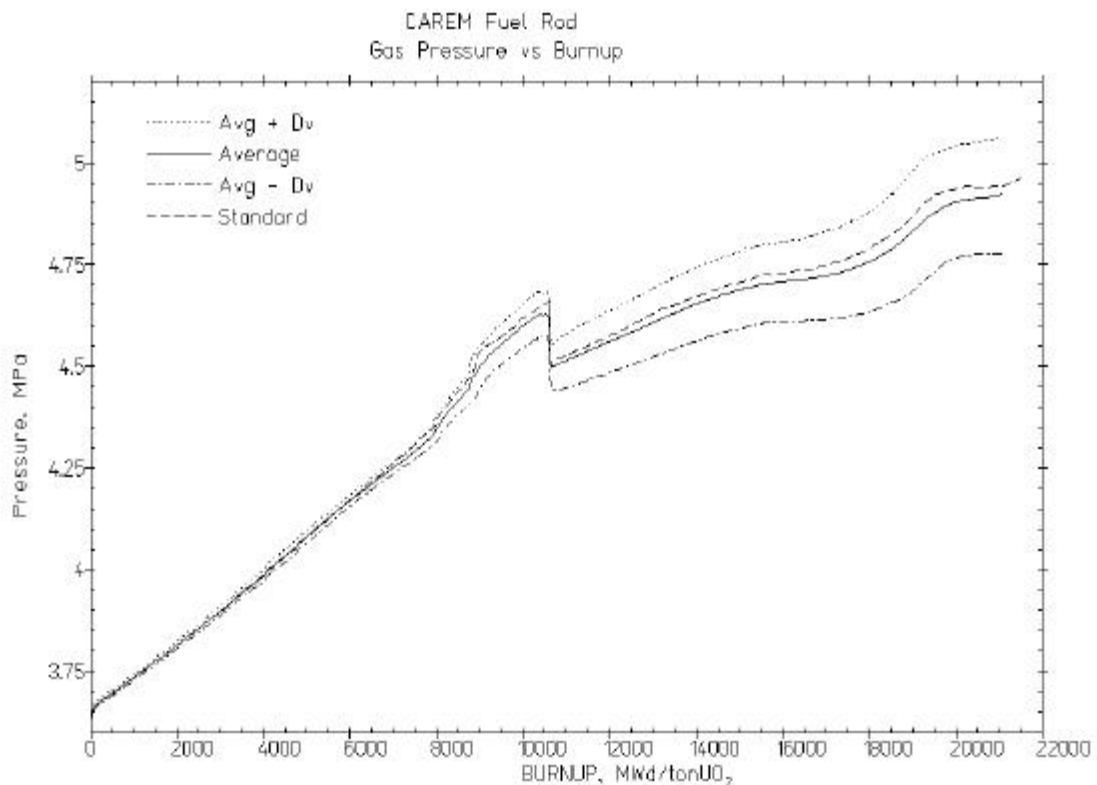


Figure 23.b: Probabilistic analysis for the gas pressure of a CAREM fuel rod.

## 6. CONCLUSIONS

The schedule sketched in this paper begins with a validated code for the simulation of the fuel rod behaviour under irradiation, almost for the internal use in the institution. The helpful due to international project as the CRP FUMEX are relevant at this point. An example of

institutional benchmarking of the BACO code was presented with the NRX irradiation. Here we show that the sensitivity analysis could not be enough to understand the discrepancies between experiments and modelling.

A MOX fuel rod failure due to PCI-SCC was presented. The BACO code was the computing tool during all the stages of the experiments. The original scope of the MOX irradiation was the correct research, developing and manufacturing of MOX fuels in the  $\alpha$  Facility (CNEA). An additional developing was the induction of fuel failures due to SCC mechanism and the simulation of burnup extension with synthetic products (CsI and Iodine).

We have showed that is not enough a simple running code in order to simulate the behaviour of a fuel rod. "Parametric analysis" and "extreme cases" calculations must be done. But the analysis sketched shows that is not enough the study of that cases. The smallest dispersion found in the selected parameter (temperature, hoop stress and gas pressure) is due to the QA procedures into the laboratories. Nevertheless, it is easy to see that the probability distributions of the fuel rod parameters must be known and statistical analysis must be included in order to follows the correct influence of the manufacturing QA procedure of fuel elements. A complete fuel element design must consider the dispersion in rod dimensions due to fabrication. Changes in the rod design related to fabrication uncertainties must be tested. This exercise shows, on one hand, the sensitivity of the predictions concerning such parameters and, on the other hand, the potentiality of the BACO code for a probabilistic study.

The increment of the dispersion with burnup that we find in the calculation performed with BACO is an advice that we must include probabilistic safety criteria in the design of fuel elements. The design of both the CARA fuel and the CAREM reactor fuel are being developed using strongly the techniques of calculation and criteria sketched in this paper.

## ACKNOWLEDGEMENTS

The author acknowledges to Dr Luis Juanicó for critically reading the manuscript and several suggestions.

The present research has been partially supported by CONUAR SA.

## REFERENCES

1. Florido P. C., Cirimello R. O., Bergallo J. E., Marino A. C., Delmastro D. F., Brasnarof D. O., Gonzalez J. H., Juanicó L. A., "*CARA Design criteria for HWR fuel burnup extension*", this meeting.
2. Ordoñez J. P., Abbate P., Lolich J., "*The CAREM Reactor: Bridging the gap to nuclear power generation*", International Conference of the AATN (Asociación Argentina de Tecnología Nuclear), Buenos Aires, Argentina, 18-21 November, 1996.
3. Marino A. C., Savino E. J. and Harriague S., "*BACO (Barra Combustible) Code Version 2.20: a thermo-mechanical description of a nuclear fuel rod*", Journal of Nuclear Materials Vol. 229, April II, 1996 (p155-168).
4. Laßmann K. et al., "*Probabilistic Fuel Rod Analysis using the TRANSURANUS Code*", IAEA, TCM on "Water Reactor Fuel Element Modelling at High Burnup and Experimental Support", paper 5/2, Windermere, UK, 1994.
5. Bull A. J., "*A probabilistic analysis of PWR and BWR fuel rod performance using the code CASINO-Sleuth*", Nuc. Eng. and Design 101 (1887) 213.
6. Moscalu D. R., "*CANDU type fuel behaviour – A probabilistic approach*", 4<sup>th</sup> International Conference on CANDU fuel, Pembroke, Canada, September 1-4, 1995.
7. Marino A. C. and Savino E. J., "*Applications of simple rules of fuel failure in a computer model simulation for nuclear fuel behaviour and performance*", Log#31, International

- Topical Meeting on Light Water Reactor Fuel Performance, Portland, Oregon, USA, 2-6 March, 1997.
8. Marino A. C., Savino E. J., “*Sensitivity analysis applied to nuclear fuel performance related to fabrication parameters and experiments*“, 14<sup>th</sup> International Conference on Structural Mechanics in Reactor Technology, Paper C01/7, SMiRT 14, August 17-22, 1997, Lyon, France.
  9. Marino A. C., “*Computer simulation of the behaviour and performance of a CANDU fuel rod*“, 5<sup>th</sup> International Conference on CANDU fuel, Toronto, Ontario, Canada, September 21-24, 1997.
  10. Chantoin P., Turnbull J. and Wiesenack W., “*Summary of findings of the FUMEX program*“, IAEA’s TCM on Water Reactor Fuel Element Modelling at High Burnup and Its Experimental Support”, Windermere, UK, 19-23 Sept. 1994.
  11. “*Fuel Modelling at Extended Burnup*“, Report of the Co-Ordinated research Programme on Fuel Modelling at Extended Burnup - FUMEX 1993-1996, IAEA-TECDOC-998, January 1998.
  12. Marino A. C., “*Proyecto FUMEX (Fuel Modelling at Extended Burnup) de IAEA: Evaluación final de la participación del código BACO (Irradiaciones en el OECD Halden Reactor)*“, XXIV annual meeting of the AATN (Asociación Argentina de Tecnología Nuclear), Buenos Aires, Argentina, 10-12 November, 1997.
  13. Notley M., “*Zircaloy-sheathed UO<sub>2</sub> fuel irradiated with a declining power history to determine its effect on fission product gas release*“, Atomic Energy of Canada Limited, AECL-6585 (1980).
  14. Marino A. C., Savino E. J. and Harriague S., “*Thermo-mechanical description of a nuclear pin, BACO code version 2.20*“, 13<sup>th</sup> International Conference on Structural Mechanics in Reactor Technology, (SMiRT 95), Universidade Federal do Rio Grande do Sul, Porto Alegre, Brazil, August 13-18, 1995.
  15. Marino A. C., Pérez E. E. and Adelfang P., “*Irradiation of Argentine MOX fuels. Post-irradiation results and analysis*“, IAEA’s TCM on Recycling of Plutonium and Uranium in Water Reactor Fuel, Newby Bridge, Windermere, United Kingdom, 3-7 July 1995.
  16. Marino A. C., Pérez E. E. and Adelfang P., “*Argentine Nuclear fuels MOX irradiated in the Petten Reactor, Experiment analysis with the BACO code*“. IAEA’s TCM on Water Reactor Fuel Element Modelling at High Burnup and Its Experimental Support, paper 1/6, Windermere, 1994.
  17. Marino A. C., “*A PCI failure in an experimental MOX fuel rod and its sensitivity analysis*“, A. C. Marino, International Atomic Energy Agency Technical Committee Meeting (TCM) on “Fuel Chemistry and Pellet-Clad Interaction Related to High Burnup Fuel”, Nyköping, Sweden, 7-10 September 1998.
  18. Marino A. C., Savino E. J., “*Fuel Modelling and its Economical Competitiveness*“, Proceedings of the International Conference on “Nuclear Power Competitiveness in the Next two decades”, (AATN 96), November 18-21, 1996, Buenos Aires, Argentina.
  19. Alvarez L. A., “*Extended burnup with SEU Fuel in Atucha 1 NPP*“, this meeting

# **Fuel burnup extension effect on the fuel utilization and economical impact for a typical PWR plant**

**S. Gomez**

Comisión Nacional de Energía Atómica,  
Buenos Aires, Argentina

**T. Yoshizu**

Engineering Development Co., Ltd,  
Yokohama, Japan

**Y. Komano, T. Kanagawa**

Mitsubishi Heavy Industries, Ltd,  
Yokohama, Japan

**K. Goto**

The Kansai Electric Power Co., Inc.,  
Osaka, Japan

## **Abstract**

Currently in Japan, fuel assembly average burn-up is limited to 48GWd/t and is going to be extended to 55GWd/t in these years. Moreover, R&D programs for further extension are under operation. Simultaneous extension of fuel burn-up limitation and cycle length reduces the number of fuel required to produce a given amount of energy reducing the radioactive waste generation, the occupational radiation exposure and the electricity generation cost. In this paper, the effect of fuel burn-up and operation cycle length extension is estimated from the view point of electricity generation cost and amount of discharged fuel assemblies, and the desirable burn-up extension in the future is studied. The present 5wt% uranium-235 enrichment restriction for commercial reactors divides the burn-up extension implementation in two steps. The fuel burn-up achievable with the present 5wt% enrichment limitation and without it is analyzed. A standard 3 loop PWR plant loading 17x17 fuel assemblies has been chosen for the feasibility study of operation cycle longer than 15 months and up to 24 months under extended fuel burn-up limitation. With the 5wt% enrichment limitation, the maximum assembly average burn-up is between 60GWd/t and 70GWd/t. Three batches reload fuel strategy and 18 months operation cycle allow the electricity generation cost reduction in about 4% and the number of fuel assemblies discharged per year is reduced in approximately 15% compared with the current 48GWd/t fuel. Relaxing the enrichment limitation, for the 24 months operation cycle with 3 batches reload fuel strategy, the maximum assembly average burn-up become 80GWd/t. The electricity generation cost reduction is about 8% and the number of fuel assemblies discharged per year is reduced in approximately 35% compared with the current condition. This study shows the contribution of simultaneous extension of fuel burn-up limitation and operation cycle length to reduce the electricity generation cost and the number of discharged fuel assemblies. The results indicate the target and the scheme of high burn-up fuel development for the future.

## **1. INTRODUCTION**

In the next century, LWR will be the main stream of nuclear power generation in Japan. To insert the nuclear power in the 21 century society, to deal with the economic problems and to contribute globally, the direction of the effort in the development of the future LWR were

established as follows at the committee for LWR improvement in the Ministry of International Trade and Industry of Japan (MITI):

- 1- to keep and improve safety,
- 2- to improve economic competitiveness,
- 3- to reduce human effort,
- 4- to reduce the amount of radioactive waste,
- 5- to establish a next generation of LWR for international cooperation.

Furthermore, to concrete the design target, the simultaneous extension of operation cycle (18~24EFPM) and fuel burn-up have been proposed.

Without affecting the security, longer operation cycles have not only merit from the electricity generation cost but also from the reduction of the human effort by reducing the plant maintenance and occupational doses and the harmonization with the environment by reducing the nuclear waste amount. So, fuel burn-up and operation cycle extension must be one of the main design requirements for the next LWR generation.

In Japan, the length of power operation between maintenance and inspection outages is limited to 13 months by the law. The fuel assembly burn-up limit is 48GWd/t, with a prospect to extend it to 55GWd/t in a near future. In order to establish the maximum fuel burn-up aim, economical and radioactive waste evaluations by taking into account longer cycle operation, regulation and technological problems must be considered.

## 2. ENRICHMENT REQUIREMENTS

In Japan, the present fuel assembly burn-up limit is 48GWd/t considering a cycle length of about 15 months including approximately 1.5 months for programmed outage for maintenance and inspection. The relationship between fuel enrichment, number of batches and maximum fuel burn-up had been evaluated considering cycles between 18 and 24 months (including programmed outage). Fuel enrichment must be increased and fuel burn-up must be extended to achieve longer cycle without changing the batch size (Figure 1).

In other hand, the fuel enrichment is limited to be less than 5wt% both in Japan and other countries, and going beyond this limit will require extensive re-analysis and restructuring of the fuel fabrication facilities, fuel transportation and reprocessing facilities with the consequent licensing process. In the U.S. a movement to relax the enrichment limitation had began and the Japanese movement will depend on the U.S. results in this matter. The future fuel burn-up extension will be strongly affected by the persistency or not of this enrichment restriction.

By considering the actual 5wt% enrichment limit, for a standard 3 loop PWR plant the 18 months cycle can be achieved adopting a fuel management strategy of 3 batches, and 2 batches fuel management strategy must be adopted for a 24 months cycle (Figure 2). Then, the maximum assembly burn-up is between 60GWd/t to 70GWd/t.

By considering the future relaxation of the fuel enrichment limitation, a fuel enrichment of about 6.5wt% could allow 24 months cycles with 3 batches fuel strategy. Then the maximum assembly burn-up is about 80GWd/t.

The hardening of the neutron spectrum due to the fuel enrichment increase also reduce the boron reactivity worth and the control rod reactivity worth. For cores designed using fuel limited to 5wt% uranium enrichment, no changes are required from the viewpoint of the plant components and equipment, and the possible shut-down margin reduction problem can be solved by the selection of appropriate fuel loading patterns.

The utilization of 6.5wt% enriched uranium fuel to achieve the 24 months cycle with 3 batches fuel management strategy will produce large changes in the core characteristics, with the consequent requirement on the review of the safety design and possible changes on the plant components and equipment.

The sub-criticality requirements for fresh fuel transportation and fresh fuel storage were checked. Fresh fuel elements enriched up to 5wt% inserted in water without absorbent material satisfy the sub-criticality requirement for fuel transportation ( $k_{eff} < 0.93$ , Figure 3). For enrichment larger than 5.7wt%, fuel assemblies with burnable absorbers rods will be required to assure the criterion for fuel transportation and for fresh fuel storage sub-criticality ( $k_{eff} < 0.95$ ). Then all the fuel assemblies used to achieve the 24 months cycle by adopting the 3 batches fuel strategy must be designed to have burnable absorber rods.

### 3. BURNABLE ABSORBER DESIGN

The design of longer operation cycles requires to load more reactivity at the beginning of the cycle (BOC) with a consequent increase on the initial critical boron concentration. The moderator temperature coefficient (MTC) becomes more positive with the increase on the BOC critical boron concentration. And the cycle length extension produces a larger reactivity difference between fresh fuel and irradiated fuel, then the peaking factor became worse.

In order to reduce the initial critical boron concentration and to keep the MTC negative in case of cycle length extension, the increase on the number of gadolinium rods inside a fuel assembly becomes necessary (in Japan, natural gadolinium has been used as burnable absorber). And in order to reduce the power peaking factor, the utilization of higher content gadolinium becomes necessary.

Presently, the Japanese PWR operating with a cycle length of 15 months utilizes fuel with 6wt% natural gadolinium oxide. For operation cycle length of 24 months, the number of gadolinium rods inside the assembly became larger but it is still possible to flatten the power distribution by the utilization of fuel rods with 10wt% gadolinium oxide.

### 4. BURN-UP EXTENSION EFFECT ON THE FUEL UTILIZATION

Operation cycle length extension without fuel burn-up extension produce an increase in the number of fuel discharged per year due to the increase on the number of reloaded fuel assemblies. The fuel burn-up extension allows the reduction on the number of fuel discharged per year with the consequent decrease on the high level nuclear waste volume.

Figure 4 shows the number of fuel assemblies discharged per year as a function of the maximum fuel assembly burn-up for a standard 3 loop plant with a reload fuel strategy of 3 batches. On this figure, the number of fuel assemblies discharged for the current 15 months operation with 48GWd/t fuel is used as reference (100%).

In the case where the maximum burn-up is limited by the 5wt% uranium enrichment restriction, the 18 months cycle reduces approximately 15% the averaged number of fuel assemblies discharged per year with the maximum burn-up around 60GWd/t.

The relaxation of the uranium enrichment limitation allows the 24 months cycle with 3 batches fuel strategy by increasing the uranium enrichment to 6.5wt%. In this case the maximum assembly burn-up is expected to be around 80GWd/t and it will reduce the number of fuel assemblies discharged per year in approximately 35% respect to the current condition.

The result shows that the reduction on the number of fuel assemblies utilized will have a big effect on the reduction of high level waste. In addition, the reduction on the number of reloaded fuel achieved by fuel burn-up extension as well as the operation cycle length extension have an important effect on the electricity generation cost reduction. The effect on the electricity generation cost reduction is discussed below.

## 5. ELECTRICITY GENERATION COST

To evaluate the electricity generation cost, the capital cost, the operation and maintenance cost, and the fuel cycle cost were evaluated. Three batches fuel strategy and simultaneous change in the cycle length and the maximum fuel assembly burn-up were considered. In all cases relative variations of the cost per kWh are presented compared with the current condition (15 months operation with 48GWd/t burn-up limitation).

The capital cost includes mainly the construction cost, the components cost, capital repay and insurance. Longer operation cycles increase the utilization factor by reducing the frequency of the programmed outage. It allows the power plant to produce more electricity during the plant lifetime, and the capital cost per kWh decreases with the cycle length increase (Figure 5). The increase in the cycle length from the actual 15 months to 18 months reduces the capital cost per kWh in approximately 2%. The cycle length extension to 24 months reduces the capital cost by approximately 4%.

The operation and maintenance cost includes basically the normal operation cost and the shutdown cost, labor cost and repair cost. Normal operation cost and labor cost are necessary to operate the nuclear power plant and the operation cycle length increase does not have an important effect on these costs. Shutdown cost and repair costs are regular costs and occur during the plant shutdown. Operation cost decreases with the cycle operation length increase because the programmed outage became less frequent with the consequent reduction of the inspection cost (Figure 6). The operation cost per kWh can be reduced respect to the actual cost by approximately 4% for a cycle length increase from 15 months to 18 months, and the reduction became approximately 11% for 24 months cycles.

The fuel cycle cost includes the uranium mining, conversion, enrichment and fabrication as the front-end cost and waste transportation, reprocessing and waste disposal as the back-end cost. Uranium and plutonium credits were also considered. The cost data used in the analysis are from the Committee on Energy Research and Development for the year 2000 (Table 1). The operation cycle length can be enlarged by increasing the fuel enrichment or by increasing the number of fresh fuel assemblies reloaded in the core (batch number reduction). The first option carry out an increase in mining and enrichment cost but produces an offset from the energy production point of view. The second one carry out an increase not only in mining and

enrichment cost but also in the fuel fabrication cost and reprocessing cost, with the consequent disadvantage with respect to the first option. In this study, the 3 batches fuel strategy was fixed then the uranium enrichment and the fuel assembly maximum burn-up should be increased to extend the operation cycle length. Figure 7 shows the relative fuel cycle cost per kWh variation with the maximum fuel assembly burn-up. The fuel cycle cost per kWh for the 80GWd/t maximum fuel burn-up can be reduced by 15% respect to the 48GWd/t maximum fuel burn-up when the fuel enrichment is not restricted. By restricting the fuel enrichment to 5wt% the maximum fuel burn-up is about 60GWd/t and the fuel cycle cost per kWh can be reduced by 8% respect to the 48GWd/t maximum burn-up.

The electricity generation cost is the result of the summation of capital cost, operation cost and fuel cycle cost. To evaluate these costs, plant lifetime of 30 years, 3 batches fuel strategy (fixed) and a maximum fuel burn-up dependant with the operation cycle length were assumed. The electricity generation cost as a function of the cycle length and the maximum fuel burn-up is shown on figure 8. Longer operation cycle and the fuel burn-up extension reduces the electricity generation cost per kWh because the increase of the plant load factor reduces the capital cost, the decrease on the number of programmed shutdown reduces the operation cost and the fuel burn-up extension reduces the fuel cycle cost. But the load factor variation as well as the fuel cycle cost saturate and the electricity generation cost reduction became smaller for operation cycles longer than 24 months. The cycle length and fuel burn-up extension from 15months-48GWd/t to 18months-60GWd/t will reduce the electricity production cost reduction per kWh about 4%. The 24 months cycle with a burn-up extension up to approximately 80GWd/t will allow an electricity production cost reduction of about 8% compared with 15 months, 48GWd/t operation.

## 6. TASK

The fuel enrichment limitation affects the future burn-up extension and divides the implementation in 2 cases.

Case 1: By considering the 5wt% enrichment limitation the maximum burn-up is limited to approximately 60~70GWd/t. Fuel rods with 10wt% gadolinium enrichment without any other large modification or technologic requirement are expected to be necessary for the core design. The only one requirement to extend the cycle length is the relaxation of the actual 13EFPM limitation in the Japanese law.

Case 2: The relaxation of the 5wt% enrichment limitation is a requirement to achieve the 24 months cycle with 3 batches fuel strategy because approximately 6.5wt% enrichment is necessary. The maximum fuel burn-up will be approximately 80GWd/t and to achieve this, goal modifications or developments will be required.

- From the nuclear design point of view, compared with the present core characteristics, boron worth and control rod worth will be reduced. As a consequence of these facts, from the viewpoint of the safety design a design review will be necessary;
- The high fuel enrichment will require the utilization of burnable absorber rod in all the fuel assemblies to satisfy the sub-criticality requirement.;

- The fuel enrichment required to achieve this fuel burn-up is beyond the 5wt% design limit for the fuel manufacture, transportation, storage and reprocess facilities from the view point of criticality, shielding and heat removal. The fuel cost will be increased due to the facilities modification cost and the fuel demand decrease;
- The fabrication of fuel with uranium enrichment larger than 5wt% will require the enrichment limitation relaxation and the safety regulatory system to relax the enrichment limitation.

## 7. CONCLUSIONS

To extend the operation cycle length without penalizing the fuel cycle cost, it is necessary to increase the fuel enrichment and at the same time to extend the maximum fuel burn-up. Simultaneous extension of the maximum fuel burn-up and cycle length reduce the number of fuel required to produce a given amount of energy, reducing considerably the amount of fuel to be fabricated and the number of spent fuel.

The fuel enrichment limitation plays a role in the set-up of the future fuel burn-up target. In this paper, the application and the relaxation of the present 5wt% fuel enrichment limitation were the conditions used to analyze the fuel burn-up targets. Burn-up target, impact and task are summarized below.

Under the 5wt% enrichment limitation, the maximum fuel burn-up will reach 60~70GWd/t. Comparing the 3 batches, 18 months operation strategy with the present one, a reduction of about 4% in the electricity production cost and around 15% in the number of fuel discharged per year are expected. From the viewpoint of the burn-up extension, the tasks are few and the target could be achieved with the present technology.

The future cycle length target will be around 24 months. The maximum fuel burn-up will reach 80GWd/t, when a 3 batches fuel strategy is applied and the 5wt% fuel enrichment limitation is relaxed. The future strategy will allow an electricity production cost save of around 8% and a reduction of the spend fuel of around 35%. However, this burn-up extension and enrichment increase step produce large effect and require R&D process to solve the technologic problems and problems associated with related facilities and the safety regulatory system.

From this study it can be concluded that the simultaneous operation cycle and fuel burn-up extensions have a large effect on the electricity generation cost and the amount of spent fuel.

For the nuclear power generation, reduction of energy generation cost, occupational radiation exposure and radioactive generation waste are required. The extension of cycle length and fuel burn-up are expected to fulfil these requirements.

Figure 1: Fuel enrichment versus batch number

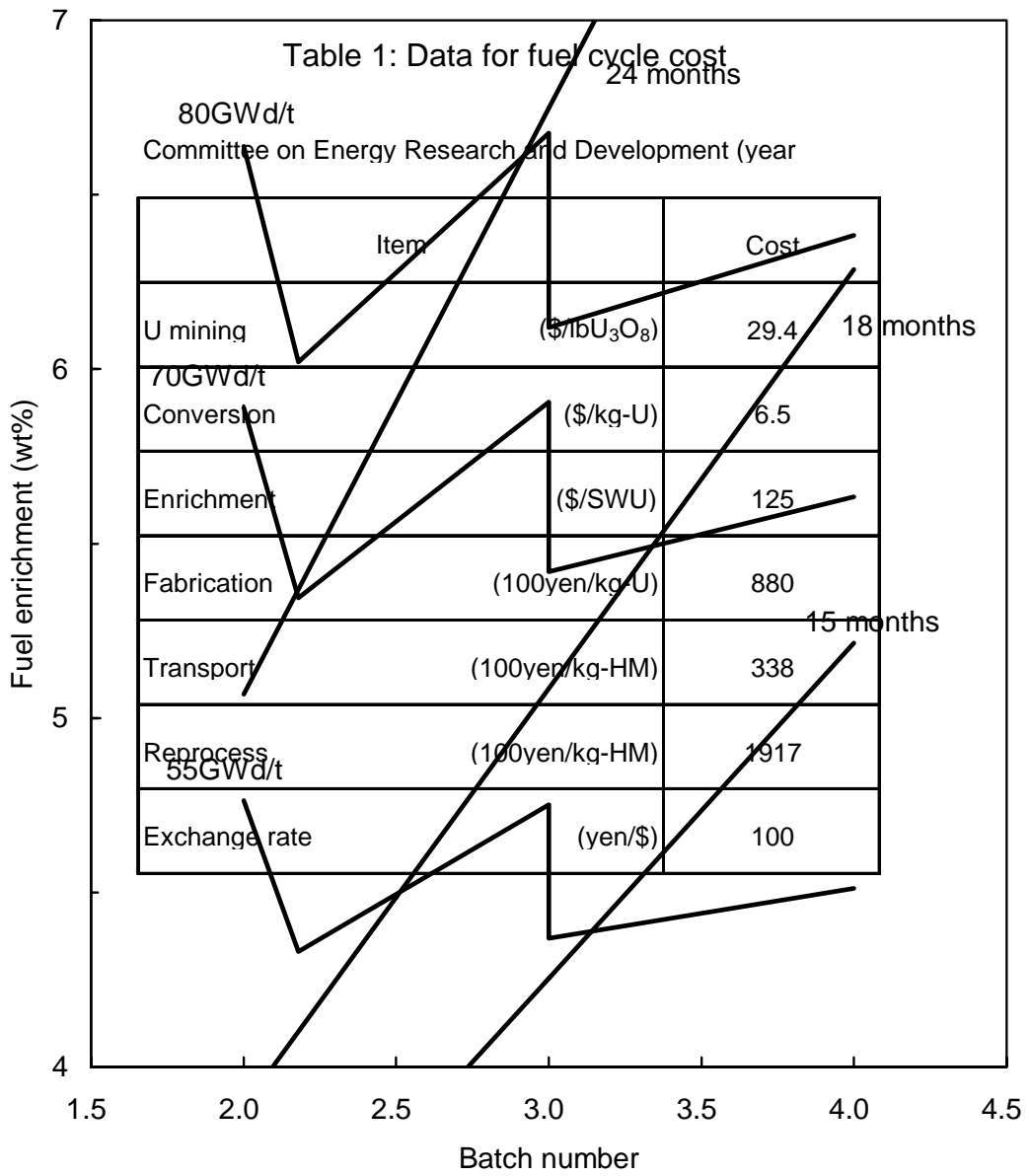


Figure 2: Maximum fuel assembly burn-up as a function of the batch size (uranium enriched is limited to 5wt%)

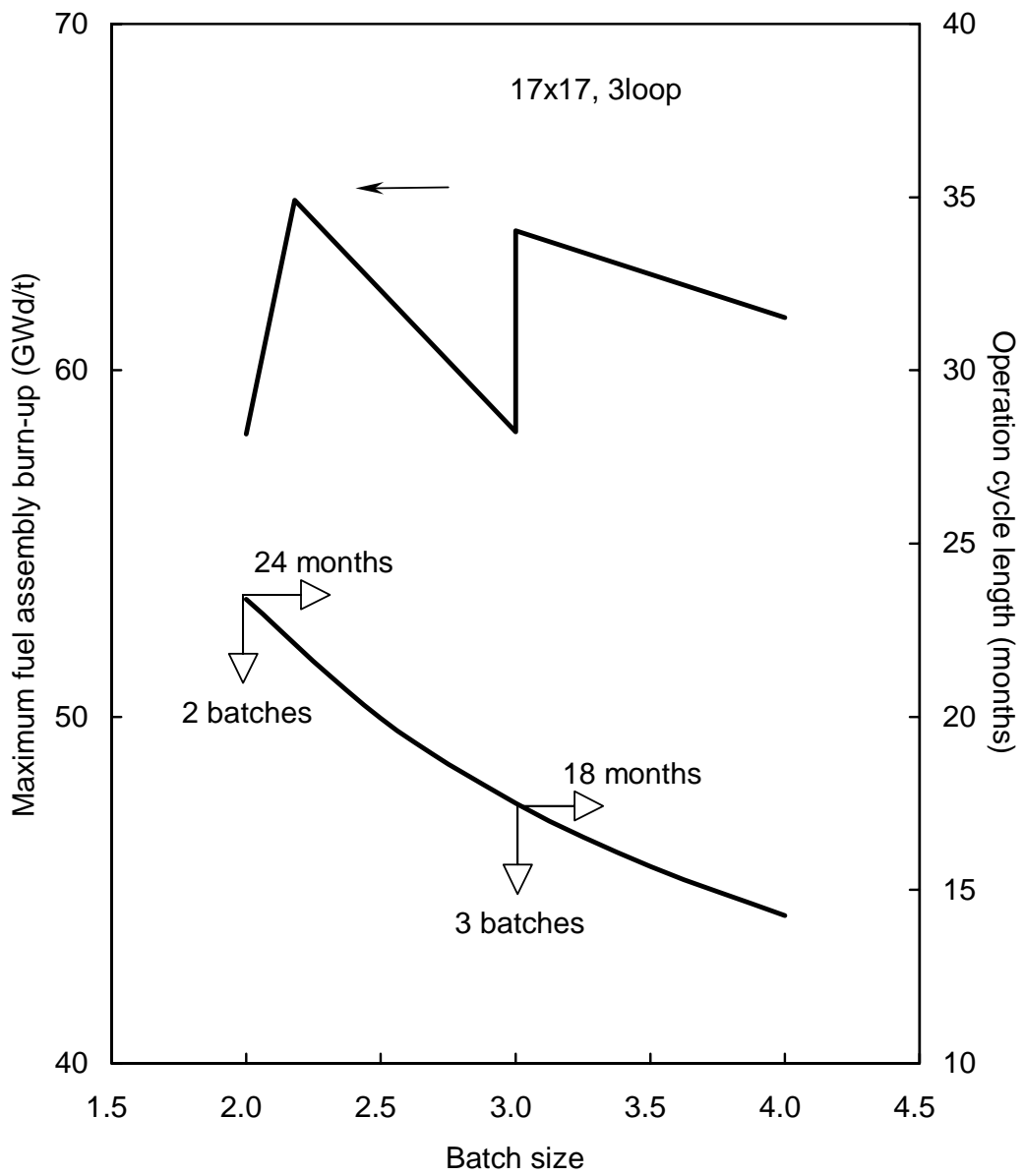


Figure 3: Effective multiplication factor for a 17x17 fuel assembly inserted in water without burnable absorber as a function of the fuel enrichment

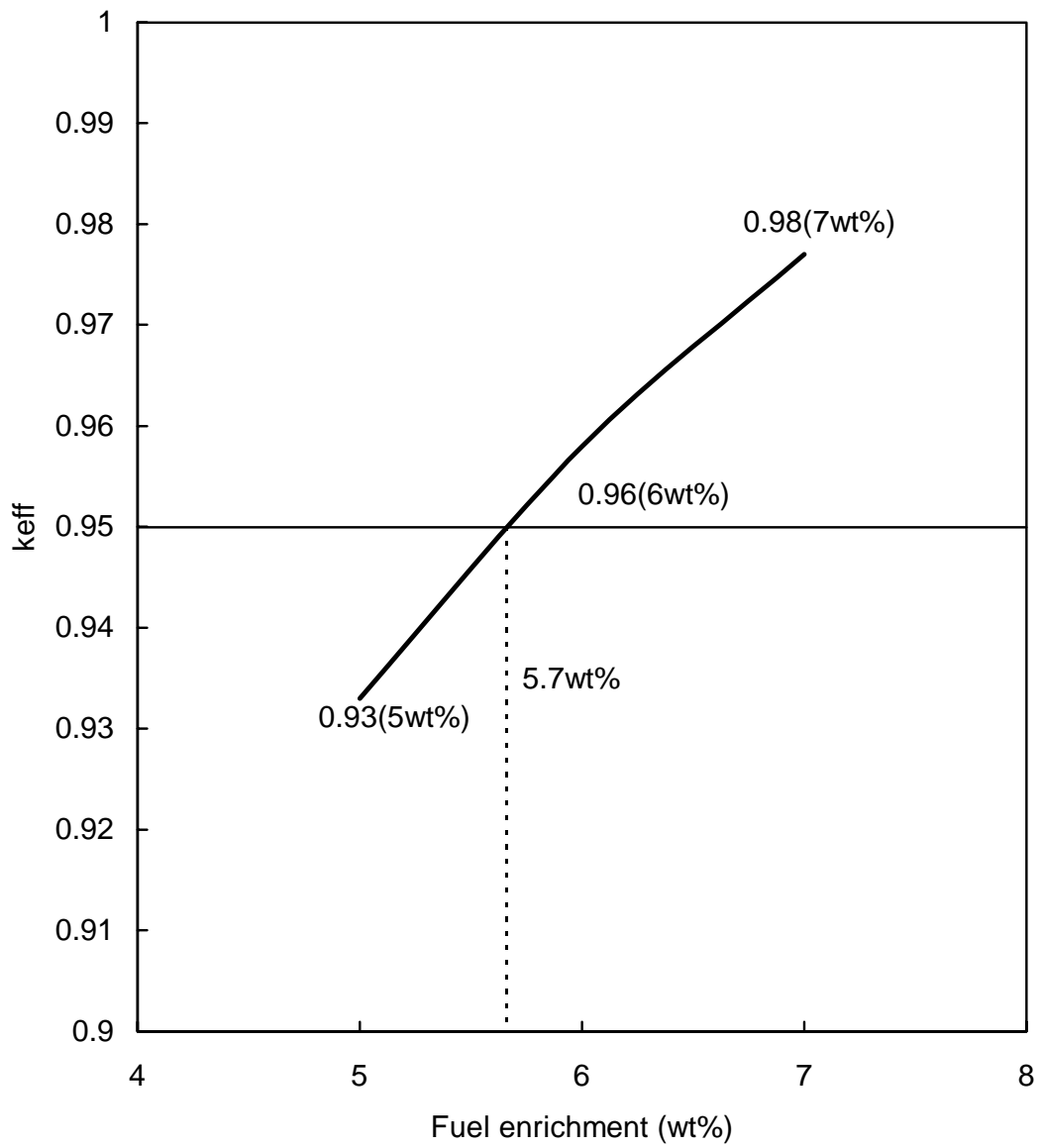


Figure 4: Reduction on the fuel assemblies discharged per year as a function of the maximum fuel assembly burn-up

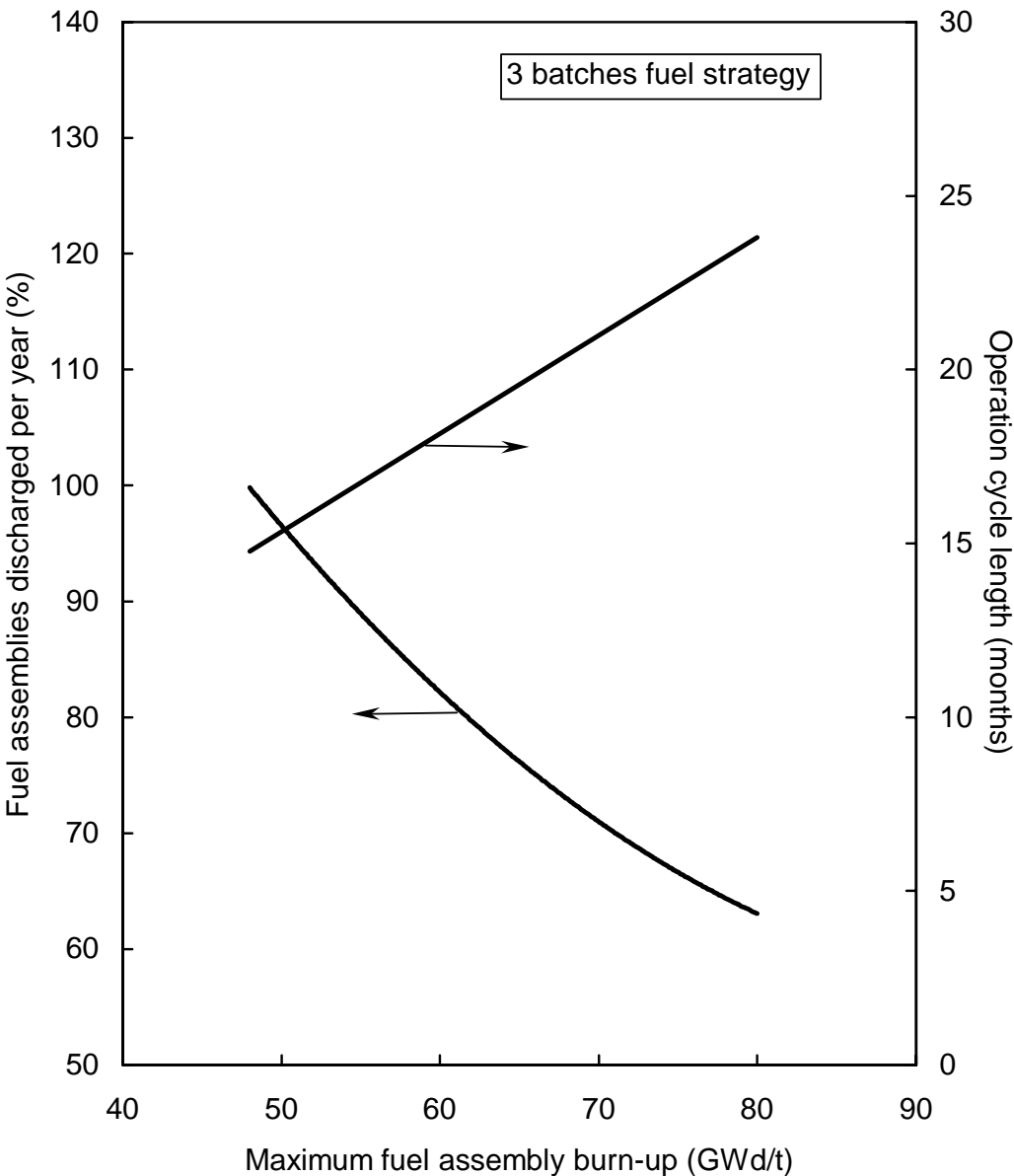


Figure 5: Capital cost reduction per kWh as a function of the maximum fuel assembly burn-up

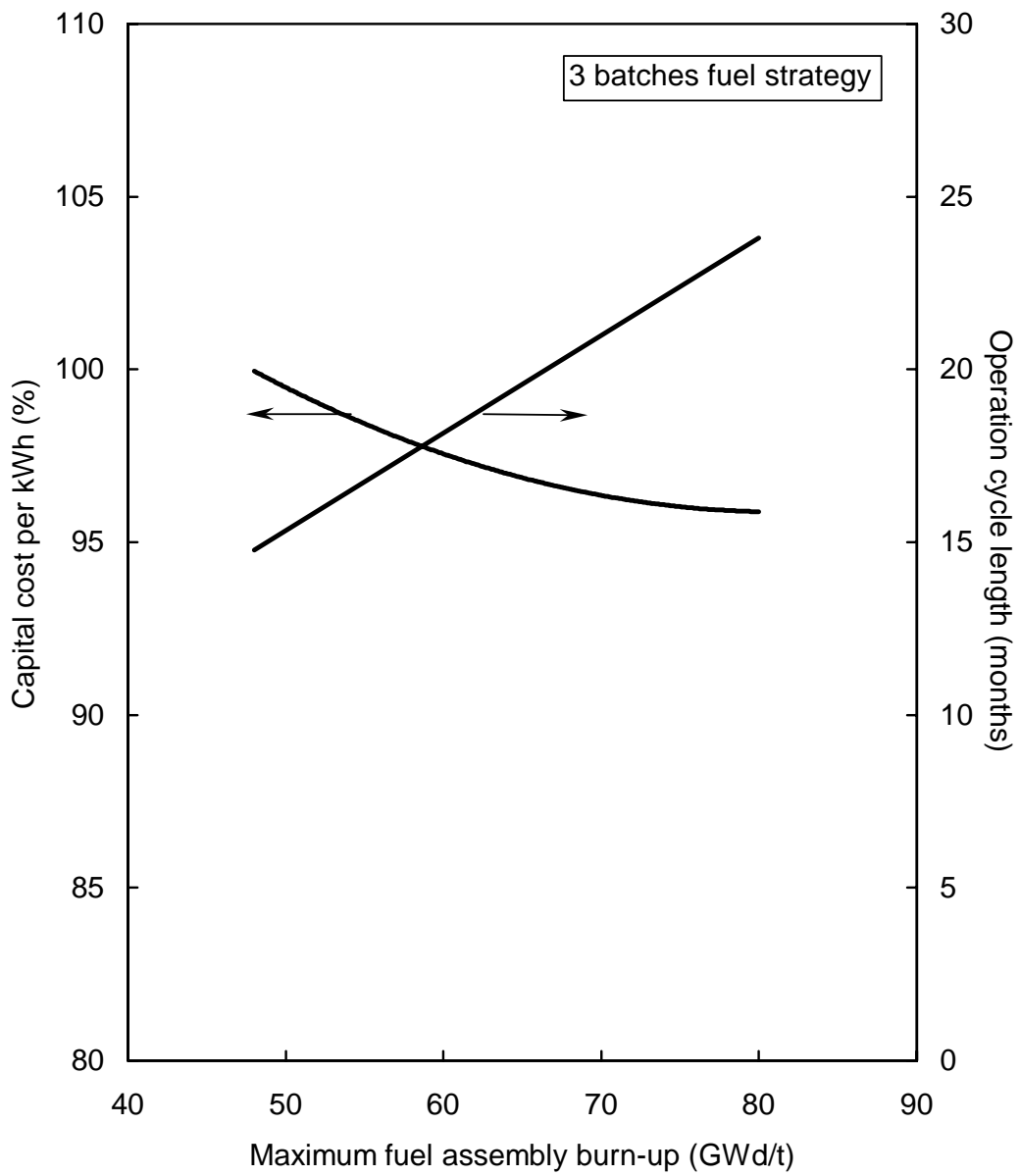


Figure 6: Operation cost reduction per kWh as a function of the maximum fuel assembly burn-up

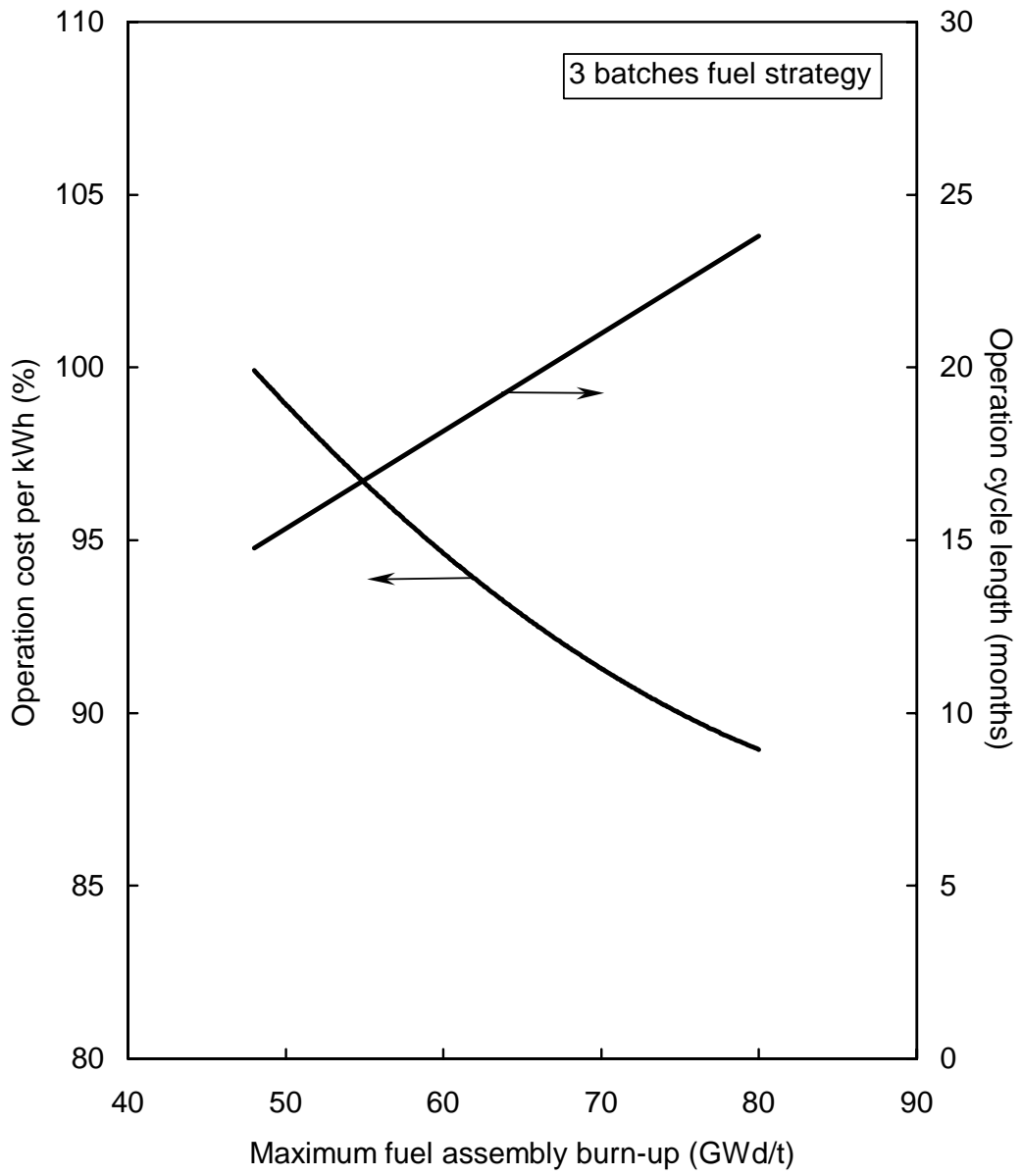


Figure 7: Fuel cycle cost reduction per kWh as a function of the maximum fuel assembly burn-up

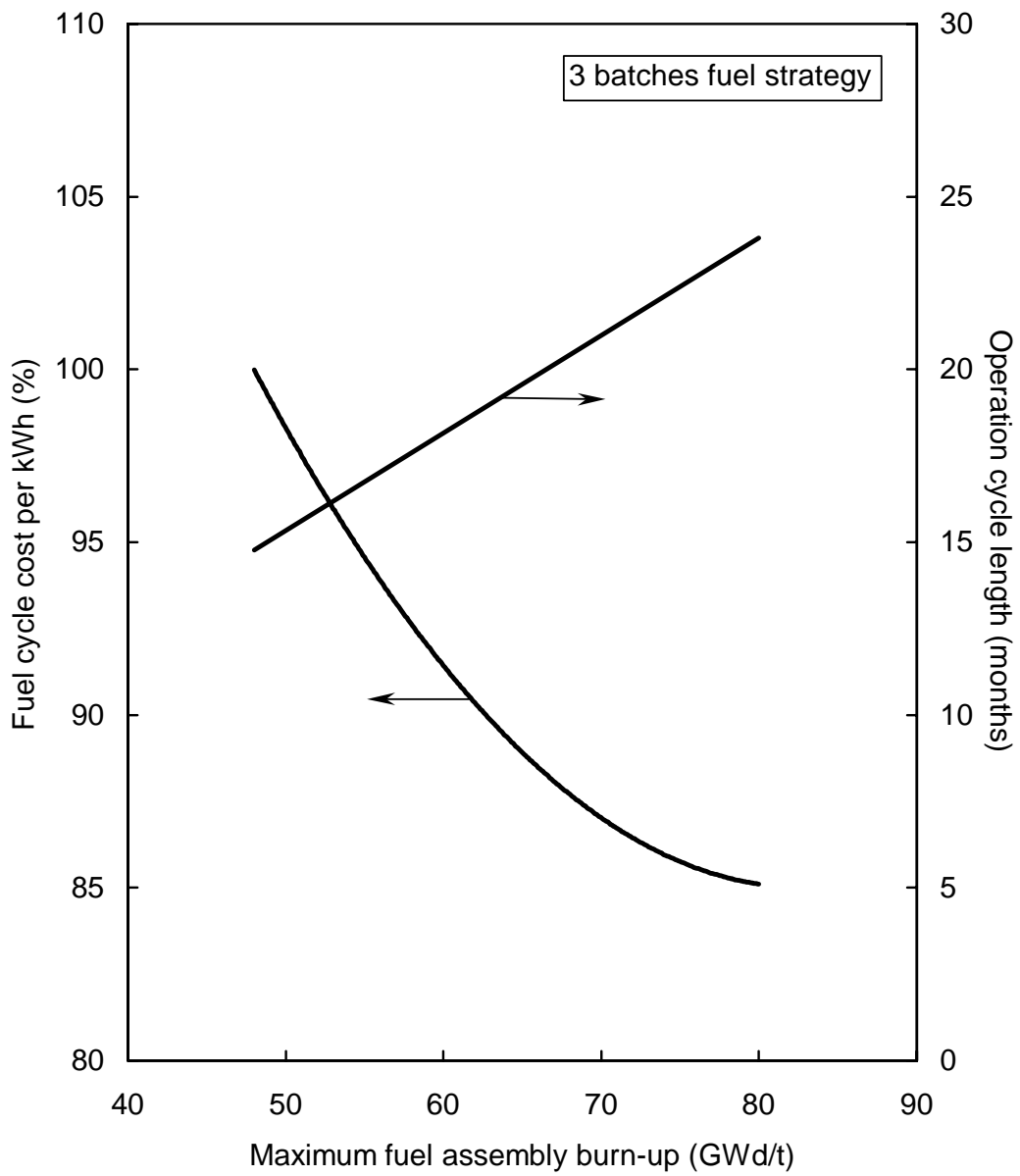
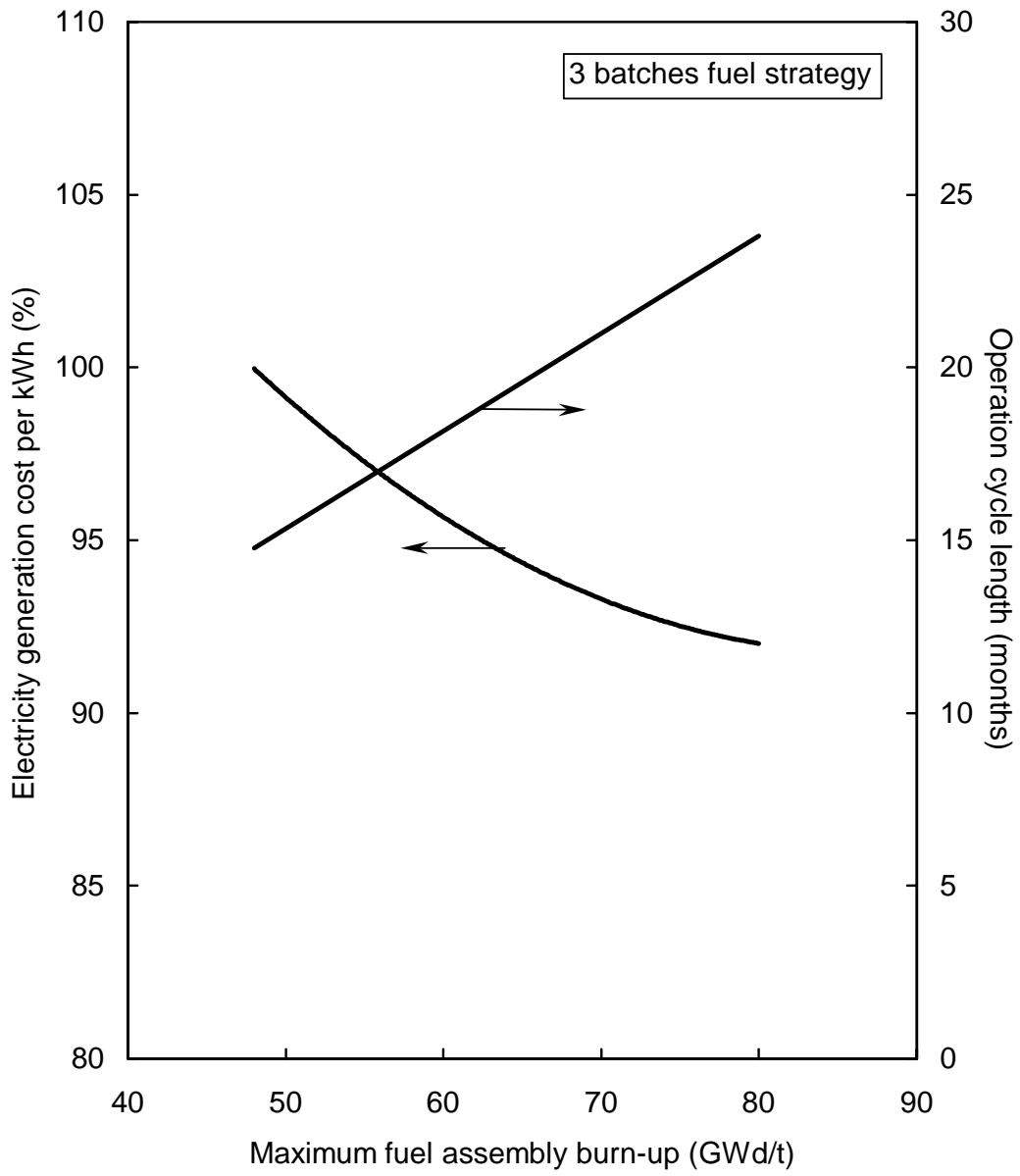


Figure 8: Electricity generation cost reduction per kWh as a function of the maximum fuel burn-up



# The commercial impact of burnup increase

**C. Fenzlein, W. Schricker**

Siemens AG (KWU),

Erlangen, Germany

## 1. INTRODUCTION

Deregulation is driving electricity prices downward in USA. Similar effects are becoming apparent in Europe as deregulation is realized. The expected progress will continue to demand the minimization of electrical production costs and rapid depreciation of NPPs to maintain a competitive position vis-a-vis coal, natural gas, and oil.

Reactor operators struggling to survive in such environment will continue to value fuel cycle cost savings as a strong contributor to reduced production costs, although contributing only about one-third to the whole electricity generating costs (Figure 1).

Besides the self-evident requirement for reliable fuel with always the highest priority, the requirement for increased discharge burn-up is still getting a higher priority.

What is going to happen in the deregulated German market can be learnt from the Scandinavian countries.

The deregulation in the Nordic electricity market started about 1994 and there has been a transition from a regulated market to a complete deregulation. This transition to a completely open market has had dramatic influence on production, on selling and on buying of electricity. Today there is a split between power generation and grid companies. There is a competitive electricity exchange with a spot market, financial instruments and traders. New actors have shown up in the different areas. All consumers have the free choice of a power supplier.

As one consequence the average spot price of electricity has fallen dramatically, now down to roughly 45% of what it was a few years ago. A not unlikely scenario for the next years is even lower prices but the price will at least not increase. In other words, there is a completely new situation for the power producers, the owners and the consumers. The situation is even more dramatic than predicted when the process was started, although the experiences from deregulation of other markets were available.

And in fact, deregulation in Germany is just happening at a much higher pace than expected. Even private households, which were planned to follow later, can now choose their electricity supplier. The result is, that the electricity prices offered have dropped by 40 % within weeks. Such rapid changes in deregulated environments are a real challenge for the nuclear fuel business with its long lead times and relatively low reaction speed.

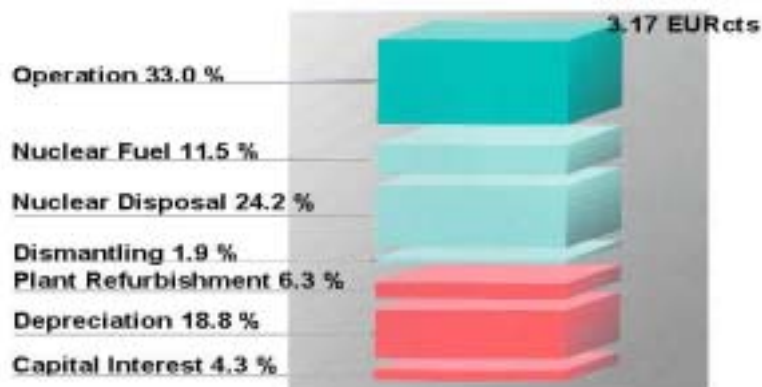


Fig. 1.: Electricity Production Cost Breakdown for a 1000 MWe PWR

## 2. UTILITY PRIORITIES

The fundamental requirement for the utilities in a deregulated market is to reduce the cost of electricity production. Focus in an oversupplied market is on reduced cost for each produced unit rather than on increased production since cheap replacement power is available on the spot market, sometimes offered below the fuel cost of a power plant. This leads to a willingness to take higher risks in production. The situation calls for shorter lead times in order to reduce the inventories at all stages of nuclear fuel materials, manufacturing and delivery. Reduced prices at all stages are of course also of major interest, but have to be valued regarding the optimization of the overall costs.

The improvement of the fuel utilization is also a very cost-effective measure. The value of fuel free of failure increases due to the contribution to cost reductions, e.g. no need for extra inspections, repair, core redesign, no increased personnel dose rates and so on.

Nuclear safety issues, when they occur, also if this is quite an improbable event, would have a negative impact on consumer priorities.

Flexibility is called for to meet the new demands from the power market. Variations in cycle length, power variations during the year, even load follow (weekly and daily) are required from nuclear power plants in some markets. Improved loading patterns also contribute to cost reduction to the extent that safety margins are not jeopardized.

In countries like Sweden there is a continued and even larger interest in fuel technical margins due to the deregulated market flexibility requirements. German operators, with NPP mostly operating at base load, tend to make use of margins to reduce power generation costs.

### 3. THE ECONOMICS OF THE FUEL CYCLE

In order to evaluate the complex interaction of parameters in the fuel cycle as they relate to its economy, all of the technical and commercial parameters are determined and attributed to a single representative quantity, called “*specific fuel cycle costs*”. The technical parameters cover factors such as plant output, load factor, nuclear fuel quantity and enrichment. The commercial parameters include costs incurred at the various stages of the fuel cycle, the lead and lag times for payments, interests and escalation factors.

Fuel cycle costs are defined as the ratio of the total costs of a specific quantity of nuclear fuel and the energy obtained from that quantity. In other words, the product of fuel cycle costs and energy produced exactly covers the total cost of the corresponding quantity of nuclear fuel.

In addition to the large number of parameters, fuel cycle costs have another special characteristic: The individual nuclear fuel cost components are distributed over a period of several decades, so that interest, fiscal regulations, discount or escalation effects can have a significant impact. Consequently, when comparing results from fuel cycle cost analyses, the methodology must be known as well as the application of interest, discount and escalation factors that yield the monetary value.

Thus a direct comparison of the values of the absolute fuel cycle costs is only possible, if the calculations were performed using identical methods, or if sufficient background information on the methods applied is available.

A commonly used method of calculating fuel cycle costs over the commercial lifetime of the NPP is the so-called “*present worth method*”. In this method, all expenditures associated with nuclear fuel during the life of a plant, as well as all revenues derived from the sale of generated power are discounted on an identical reference point in time. As a result, this approach allows, for example, correction for the effects of interest.

### 4. TYPICAL FUEL CYCLE COSTS OF A GERMAN NUCLEAR POWER PLANT

The results of an exemplary calculation of fuel cycle costs for a German 1300-MWe NPP equipped with a pressurized water reactor show that actually more than half of the costs (Figure 2) are related to fuel disposal.

Notable also is the fact that the costs for the fabrication of fresh uranium fuel assemblies account for only about 10 % of the fuel cycle costs. This is in so far remarkable as the product fuel assembly significantly affects the overall fuel cycle economy.

In the past years, fuel cycle costs at German NPPs have undergone considerable change. Initially they increased sharply, but in recent years have tended to decrease. Figure 3 shows that the individual cost components have also evolved differently.

Whereas disposal costs were initially considered to make up a comparatively small percentage of the fuel cycle costs, they have risen sharply over recent years as a result of increasing experience and demanding, sometimes politically motivated licensing requirements.

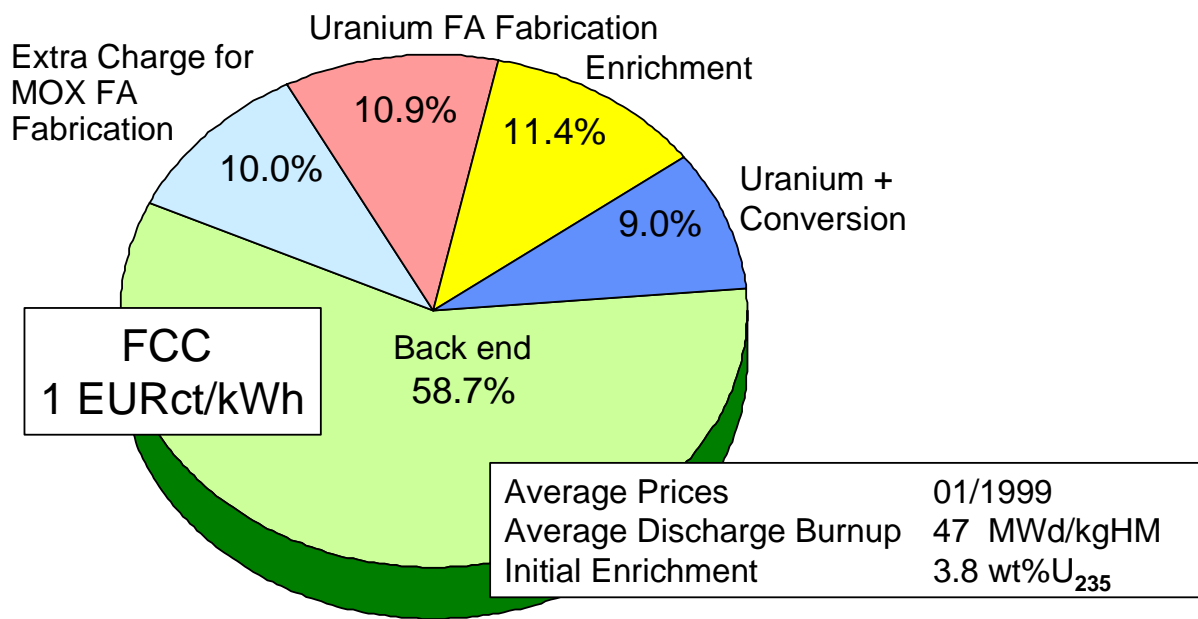


Fig. 2. Fuel Cycle Cost Calculation for a German 1300 MWe PWR

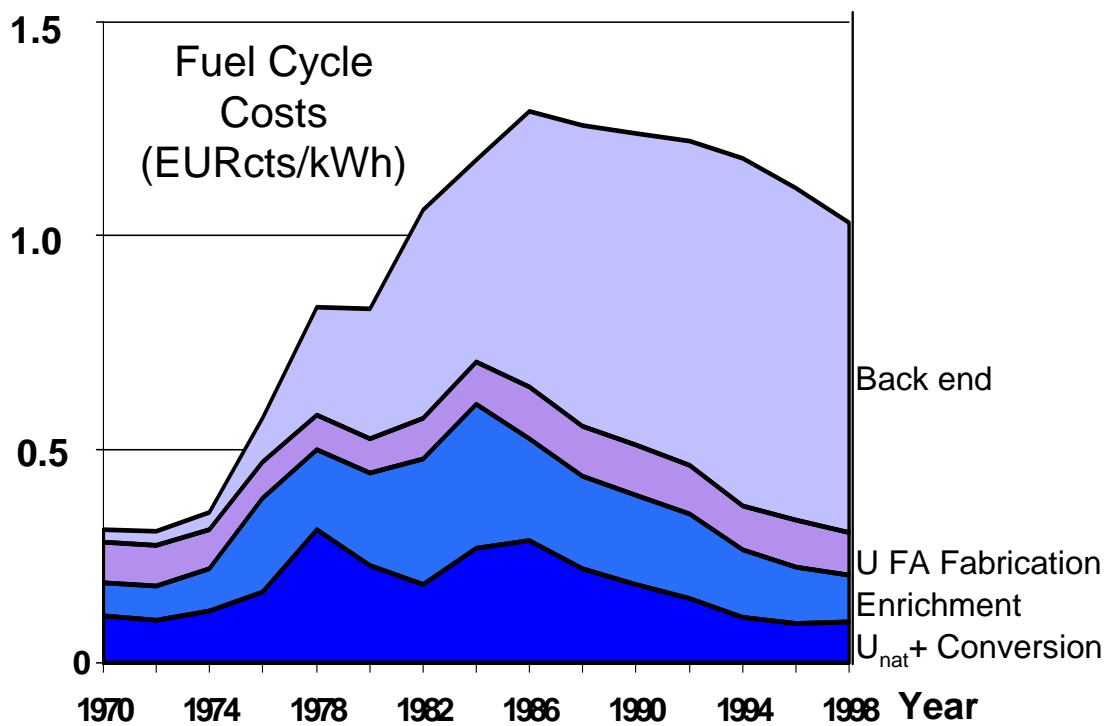


Fig. 3: Historical Development of the Fuel Cycle Costs in Germany

Currently disposal costs constitute the major portion of fuel cycle costs. The natural uranium and fuel enrichment costs exhibit a high degree of volatility. In contrast, the costs for fabrication of fuel assemblies have remained essentially stable or have even decreased recently as a result of successful cost management strategies and advances in fuel assembly technology.

Risks and the consequences of failures deter some utilities in the German situation of politically motivated phase-out discussions from undertaking licensing measures to increase enrichment.

## 5. REDUCTION OF FUEL CYCLE COSTS - A COMPLEX TASK

The reduction in fuel cycle costs can be traced to two major factors:

- lower purchase prices for source materials and services, and
- increased fuel energy yield.

The prices for many services and source materials at certain stages of the fuel cycle process have fallen significantly in recent years and have now already reached rock-bottom in some cases. The reasons are many, but the major factor is over-capacities in a shrinking market.

Efforts to increase energy yields have been largely driven by the fuel cycle cost structure. Against the backdrop of sharply increasing disposal costs in recent years, an increase in discharge burn-up through greater enrichment was one of the most important objectives of fuel assembly development efforts.

Further increases in energy yield became possible as fuel utilization was improved through measures which reduce neutron losses and improve neutron economy. These measures include reducing the amount of neutron absorbing materials in the fuel assembly, improving moderation behavior and use of neutron saving in-core fuel management strategies.

The increase in discharge burn-up due to greater enrichment reduces the size of reload batches and thus reduces particularly the disposal costs, which in Germany depend directly from the fuel mass to be disposed. Improved fuel utilization reduces the demand for natural uranium and enrichment, thus leading to a further increase in discharge burn-up.

Another important factor for economic considerations is the long periods of time required by the fuel as it passes through the various stages of the fuel cycle. The greatest possible fuel economy therefore also depends on a long-term and farsighted strategy, becoming more and more difficult task in a quick changing environment.

## 6. ACHIEVEMENTS OF ECONOMIC BENEFIT BY BURN-UP INCREASE

The optimum for a fuel cycle means to utilize the fuel to the highest economic degree, i.e. in-core fuel management has to achieve the highest possible **average** discharge burn-up. Theoretically ideal would be to operate each fuel assembly to the highest burn-up technologically feasible within defined licensing limits.

Measures such as low-leakage loading, use of low neutron absorbing structural materials or new cladding materials and increase of U235-enrichment have all served to generate a considerable improvement of the fuel cycle economy, resulting essentially from a considerable discharge burn-up increase.

Up to now considerable savings in fuel cycle costs of up to 35 million EUR per year have been achieved.

The easiest and cheapest way of increasing the average burn-up is the reduction of cycle length, although this is normally not discussed as a burn-up increase measure. As far as fuel utilization is concerned, the following statement applies:

The shorter the cycle, the higher the average discharge burn-up achievable with a given U235-enrichment of the fuel assemblies. This in turn, means better fuel utilization and lower specific fuel cycle costs.

The trend of extending plant operating cycles in various countries - e.g. in the USA and in Spain, where some plants are operated at up to 24 months cycles - has a counteracting effect regarding fuel utilization. As we have seen before: The higher the cycle length the worse is the fuel utilization. Longer cycles are favored by utilities, who are not in a position to achieve reliably short outages, e.g. as a consequence of licensing induced restart delays. That means by reducing the average outage time thus improving the plant load-factor, a reduction of the overall power generating cost can be achieved with longer the cycles, depending on the level of replacement power cost.

The gain from burnup increase is especially high in countries with high back-end costs like Germany or Switzerland. In those countries the costs are related to the mass (kg) to be disposed. In countries where the costs are quantity independent like in USA or Spain, there is, in principle, no incentive for burnup increase. Nevertheless in both countries utilities are increasing burnup; in USA because of the lacking storage capacity for spent fuel; in Spain because utilities fear a change of legislation towards volume dependent costs.

German plants have until now not followed the trend towards longer cycles claiming that under German boundary conditions even shorter than annual cycles are economically attractive.

The very short outage times along with the high service time availability of German reactors has in one case already lead to a strategy of alternating one year and half year cycles. A Swiss reactor operator, having applied longer cycles in the past, is in the process of changing its strategy to so-called hybrid annual cycles, i.e. having by turn in one year a service outage and the next year a pure refueling outage.

While the consequences of purely physical – and therefore universally applicable – relationships are identical for all light water reactors their effects may change to a greater or lesser degree, when different **licensing environments** have to be considered.

In contrast to German plants – for which fuel assembly integrity is safeguarded by means of a highly complex monitoring and inspection concept – assurance of fuel integrity is often provided in other countries through the less verification-intensive, yet more restrictive, approach of imposing a limit on fuel burn-up. With limits of this kind, modifications to cycle length often have a significantly smaller impact on the cost-saving potential than at German plants. Figure 4 gives an overview on burn-up limits in different countries.

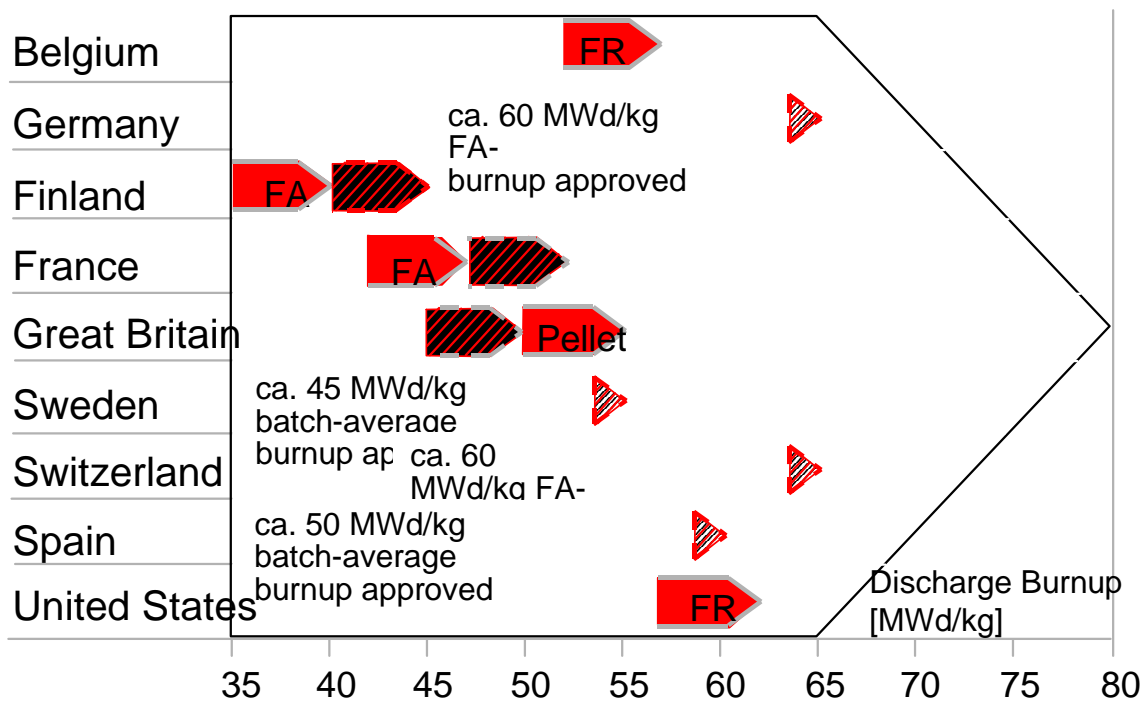


Fig. 4: Burn-up Limits in Different Countries

## 7. ENVIRONMENT FOR FURTHER BURNUP INCREASE

The positive economic effect of burn-up increase is the result of the change of physical parameters in a given environment of commercial and technical boundary conditions. This is referred to in this presentation as the economic “*potential of burn-up increase*”.

Considerable expenditure or additional costs may be connected with a further increase of burn-up, which is progressively counteracting to the above potential, if an advanced burn-up level is already reached. Such possible negative effect is in the following called “*penalties of burn-up increase*”.

The economic potential of burn-up increase is formatively influenced on the one hand by the disposal concept and the financial cost treatment and the burn-up already reached on the other hand.

When we plot fuel cycle costs as a function of discharge burn-up (Figure 5), they are of a hyperbolic character. This means a relatively strong decline of the fuel cycle cost at lower burn-up and a smaller decline at higher burn-up.

Thus, the economic potential of burn-up increase is shrinking significantly, if one has reached already a certain level.

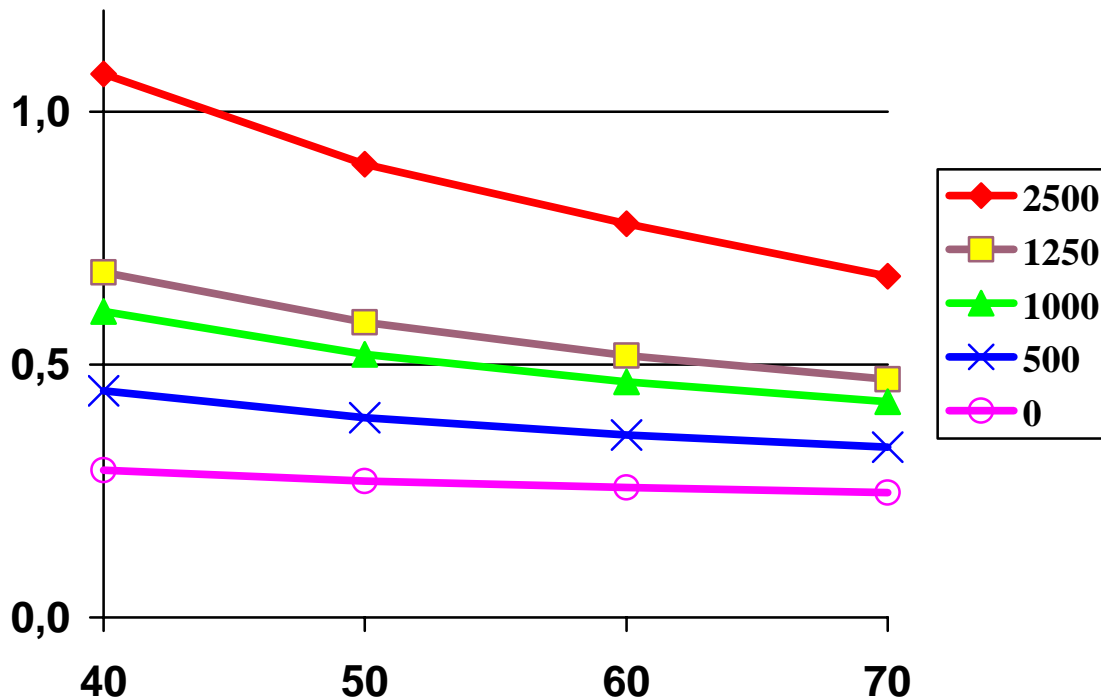


Fig. 5: Fuel Cycle Costs as a Function of Burn-up

Burn-up increase reduces the need for enriched uranium and fuel assemblies for a given amount of energy production, i.e. the economic potential depends also from the actual price level for fuel assembly fabrication and disposal.

In case of disposal costs being directly related to the uranium mass it is obvious that the economic effects increase with a higher price level. Therefore the economic potential of burn-up increase is especially big in countries where disposal costs are assumed relatively high like in Germany. Considering disposal via the reprocessing path the total costs for all disposal steps are calculated around 2500 EUR/KgU.

On the other side there is no contribution to the economic potential of burn-up increase by the disposal costs in countries where they are quoted in currency per produced energy.

Besides the parameters discussed before, the economic potential is also influenced by interest rate, cycle length or reactor type. However, the influence of these parameters is relatively small compared to disposal cost and burn-up level.

Especially when approaching the technological and physical limits it becomes evident that also the efforts and the risks are increasing, which may result in considerable penalties for burn-up extension. To avoid the risk of negative impact on operation, e.g. caused by fuel failures, the efforts for technological improvements with correspondingly high R&D costs on the supplier's side and for additional operation control on the utility side have increased. Depending on burn-up level, fuel assembly design or country-specific boundary conditions, penalties may arise in the areas listed in Table 2&3:

Enrichment (%U235)* PWR	4 - 4.4	4.4	>5.0
1. Fuel Assembly Development	Material- and Product-Development (Fuel Rod, FA-Structure, Fuel) Accident Analyses, Tests, Lead Assemblies, Post Irradiation Excerminations  Validation of Design Codes		
2. Fuel Utilization, Product Costs	Criticality Limit 16x16, 18x18 (Penalty: Neutron Economy) FA-Power Histories Product Design		
3. Reactor Core, Plant	Core Design Calculations for Normal Operation and Accidents (Reactivity Coefficients, Temperature Coeficients, Power Peaking Factors, Control Rod Worth, Boron Concentration, Transients); Reduced Operating Margins  Fuel Store (dry, wet), Residual Core, Licensing  Validation Design Codes; Experimental Programme  FA-Clearance in Core Structure		

\*) Without condieration of tolerances of approx. 0.05% U235

Tab. 2: Determination of Penalties: Structure of the Examination

Problems deriving from non-fulfillment of requirements in those areas may create considerable penalties for:

- Fuel assembly repair,
- Premature unloading and disposal of fuel assemblies (loss of energy),
- Reduced plant availability,
- Increased contamination of primary circuit,
- Increased refueling outage due to handling problems with fuel assemblies.

On the other hand costs or penalties expected from fulfillment of the licensing requirements or technical/physical conditions may discourage utilities from increasing the discharge burn-up.

Since NRC has ceiled the initial enrichment at 5% U235, all the plants and the transport systems in the various stages of the fuel cycle have licenses reflecting this enrichment level. To overcome this ceiling would cause a considerable effort. Therefore it is improbable that initial enrichments will exceed the 5% value in the foreseeable future.

Enrichment (%U235)* PWR	4 - 4.4	4.4 - 5.0	>5.0
4. Front End			
4.1 Transports (UF6, FA)			Hardware, Licensing Validation Design Code
4.2 FA Manufacturing	Capacity Utilization		Technology, Criticality Safety Licensing
4.3 Uranium Enrichment			Licensing
5. Back-end			
5.1 Transports (Spent FA)	Residual Heat, Neutron Radiation, Actinides (Shielding, Volume Utilization)		
	Hardware, Licensing		
5.2 Intermediate Storage	FA Handling after Long-Term-Storage		FA-Storage license
5.3 FA-Conditioning	Licensing Hardware		
5.4 Reprocessing			Solvent, Criticality
5.5 Final Disposal (Conditioned FA, Waste)	Volume Utilization, Shielding		
5.6 Refabrication (U, Pu)	Neutron Dose Rate at FA Manufacturing, Neutron Absorption in Fuel by Fission Products		
6. Others			Revision of Licensing Requirements (GRS)

Tab. 3: Determination of Penalties: Structure of the Examination

Nevertheless, with an enrichment of 5% U235 discharge burn-ups of about 67 MWd/kgU for a PWR and 63 MWd/kgU for a BWR reactor can be achieved in annual cycles.

Some fuel assembly designs, like the Siemens 16x16 and 18x18 designs would already need below 5% additional poisoning measures, because of their lower criticality limits.

BWR fuel assemblies, because of their heterogeneity reach only an average initial enrichment of 4.6 %U235 per bundle, resulting in the lower achievable discharge burn-up mentioned above.

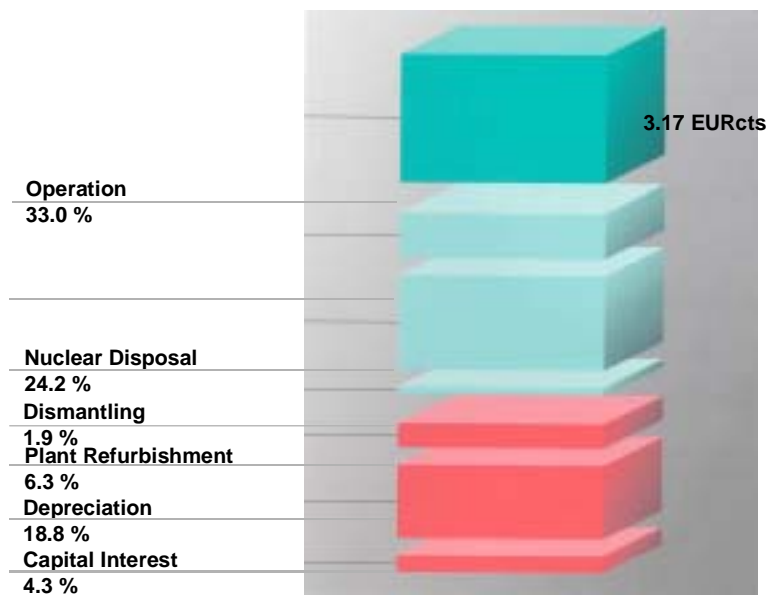
## 8. CONCLUSIONS

Deregulation has a dramatic effect on competition in the electricity markets. This will lead to a continued pressure on the prices in virtually all areas of the nuclear fuel cycle and will encourage further optimization, technical and technological progress and innovations with respect to further cost reductions of power production.

The permission of direct disposal, in Germany legally granted in 1994 as an alternative to the reprocessing path, made possible cost savings and has consequently resulted in a decline of reprocessing prices. In addition, suppliers as well as operators are making considerable efforts to reduce the disposal costs fraction by optimizing disposal technologies and concepts.

The increase of discharge has essentially contributed to the reduction the disposal cost fraction. Compared to former scenarios, the economic potential of burn-up increase is decreasing.

As the incentive of burn-up extension depends on a great variety of parameters and boundary conditions of a further burn-up potential. For the actual economic incentive for a limit of 5% U235.



governed by the lack of

the profitability of a  
extension of core and plant

and intensive continued

safety aspects calls for  
regulators. This may become

# Fuel cycle economical improvement by reaching high fuel burnup

**A. Afanasyev, G. Raspopin**

State Department on Nuclear Energy,

Ministry of Energy,

Kiev, Ukraine

## Abstract

Improvements of fuel utilization in the light water reactors, burnup increase have led to a necessity to revise strategic approaches of the fuel cycle development. Different trends of the fuel cycle development are necessary to consider in accordance with the type of reactors used, the uranium market and other features that correspond to the nuclear and economic aspects of the fuel cycle. The fuel burnup step-by-step extension Program that successfully are being realized by the leading, firms - fuel manufacturers and the research centres [1], [2], [3], [4], [5], [6], [7] allow to say that there are no serious technical obstacles for licensing in the near future of water cooling reactors fuel rod burnup (average) limit to 65 -70 MWd/kgU and fuel assembly (average) limit to (60-65) MWd/kgU. The operating experience of Ukrainian NPPs with VVER-1000 is 130 reactor \* years. At the beginning of 1999, a total quantity of the fuel FA discharged during all time of operation of 11 reactors was **5819** (110 fuel cycles). Economical improvement is reached by increase of fuel burn-up by using of some FA of 3 fuel cycles design in 4-th fuel loading cycle. Fuel reliability is satisfactory. The further improvement of FA is necessary, that will allow to reduce the front- end fuel cycle cost (specific natural uranium expenditure), to reduce spent fuel amount and, respectively, the fuel cycle back end costs, and to increase burn-up of the fuel.

## 1. INTRODUCTION

In Ukraine there are fourteen water-cooled power reactors in operation (11 VVER-1000, 2 VVER-440 and 1 RBMK-1000) with a total installed capacity of 12880 Mwe. This is about 25% of the total installed capacity of the electric power stations. Four VVER-1000 units are under construction. In 1998 NPPs produced  $75,239 \times 10^9$  kW.h of electricity (43,5% of electricity in the country).

The share of electricity produced by NPPs constantly increases because of the economic crisis and cheaper electric power production by the NPPs (See Fig 1.).

In Ukraine it's most probably the VVER-1000 reactors will have been generating up to 93-96 per cent of all NPPs electric power and about 40-50 per cent of the total electricity produced during 2000- 2010.

For the electricity utility today operating an existing nuclear power plant, economic optimization means minimizing the costs of producing electricity, based on a high degree of plant reliability, operational flexibility and maximum fuel utilization. This will include the costs of spent fuel management and eventual plant decommissioning.

## Electric power production in Ukraine

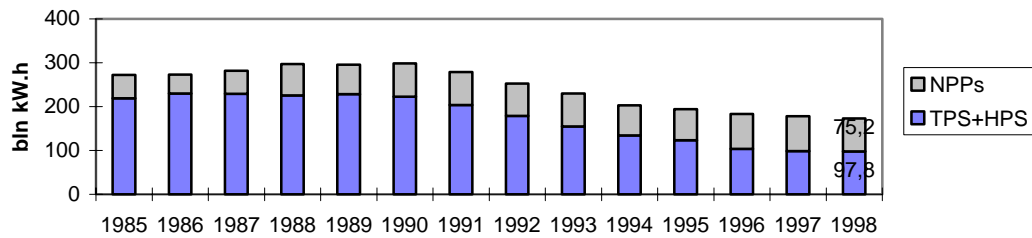


Fig. 1

## 2. EXPERIENCE OF VVER -1000 FUEL OPERATION

### 2.1. Evolution of design limits for VVER-1000 fuel utilization and fuel cycle economical improvement.

The VVER reactor units operating now were designed for base-load operation in the common system of the former Soviet Union.

Originally, according to the design, the VVER-1000 units were operating in 2-years fuel cycle using the fuel of 3.3% enrichment, the burn-up limit of which is 38 MWt.day/kg U. By the year 1989 the 3-years fuel cycle was calculated and supplied by fuel. According to the decision of the Chief Designer of the Reactor Facilities, the units started operating in 3 year cycle using the fuel of 3.6+4.4% and 4.4% enrichment for the units of design B-338, B-320 with 61 RCCA in the core.

Then we began to use the fuel of 3.6+4.4% and 3.6% enrichment for the unit B-302 with 49 control rods in the core (South Ukraine NPP unit 1). Since 1996 fuel assemblies (FA) with enrichment 3.6% are used at South Ukraine NPP units 2 and 3. The design burn-up limit of the fuel is up to 49 MWt.day/kg U. Total FA operating time in the reactor is up to 21000 hours. Number of cycles of increased capacity of 2% comparing to the stationary value does not exceed 70 during all the assemblies operating time. The safety limit when the reactor has to be shut down was  $1.5 \cdot 10^{-2}$  Ci/l iodine.

After the split up of the USSR and of the energy systems it became impossible to implement the design duration of the fuel cycles and to hold the planned refuellings in spring and summer period. The average burn-up of the fuel in VVER-1000 3-years fuel cycle in Ukraine is essentially lower than designed, the fuel utilization is ineffective (Fig. 2 - burn-up distribution in the unloaded FA).

It was decided to use some of the fuel FA for the fourth year for the purpose of higher burn-up, better fuel utilization, flexibility of core layout solutions that allows to vary the duration of the fuel cycle.

The total quantity of 560 FA were used during four years of operation at the Ukrainian NPPs during 1992-96. 72 of them, used in South Ukraine NPP unit 1 are of 3.3% enrichment and designed for 2-years cycle, 478 FA of 3.6+4.4% and of 4.4% enrichment and designed for the 3-years cycle operation.

Up to 1997 significant experience of so-called the experimental-industrial (trial) FA operation in 4 fuel cycles was accumulated, that has allowed the main designer of FA and main designer of the reactor to change design limits for the FA:

Total FA operating time in the reactor was extended from 21000 up to 28000 hours.

The allowed amount of FA in the core, which are operated in 4 years -36 pieces.

**Figures 2, 3** shows burn-up distribution in the unloaded FA. Average fuel burn-up at Ukrainian NPPs with VVER-1000 is 4-10 % higher than that at NPPs with VVER-1000 in other countries.

Analyzing fuel loadings of Ukraine reactors it is possible to state, that the use some FA in 4-fuel cycles has allowed to increase unloaded FA average burn-up from 38 -39 MWt.day/kgU up to 41,5 MWt.day/kg U. It makes possible to reduce spent fuel amount and, respectively, the fuel cycle back end costs.

The comparative fuel performances of the realized fuel cycles of Ukraine VVER- 1000 are shown in table 1.

**Burnup Distribution of Discharged Ukrainian WVER-1000 FAs (3,6+4,4)% & 4,4% enrichment during all time of operation (1992-01.01.1999). Number of Fuel cycles was 58, number of FAs was 2273, 786 of them used in four Fuel cycles.**

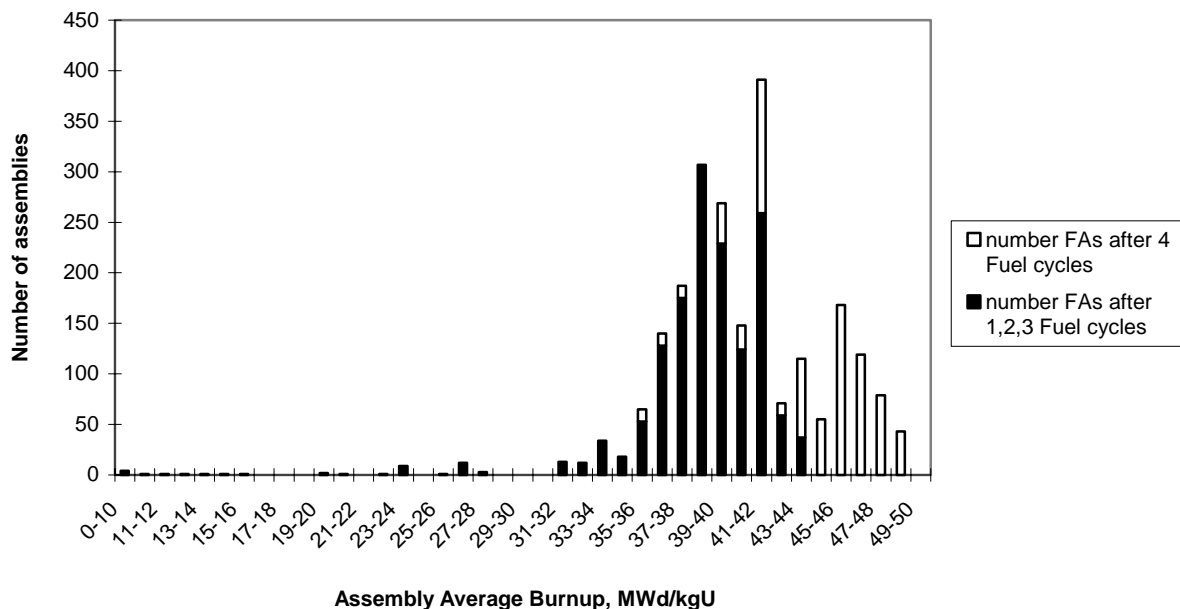


*FIG. 2. FA burnup distribution of Ukrainian VVER-1000*

**Burnup Distribution of Discharged ZNPP FAs (3,6+4,4)% & 4,4% enrichment during all time of operation (1992-01.01.1999). Number of fuel cycles was 21, number of FAs was 1253, 401 of them used in four Fuel cycles.**

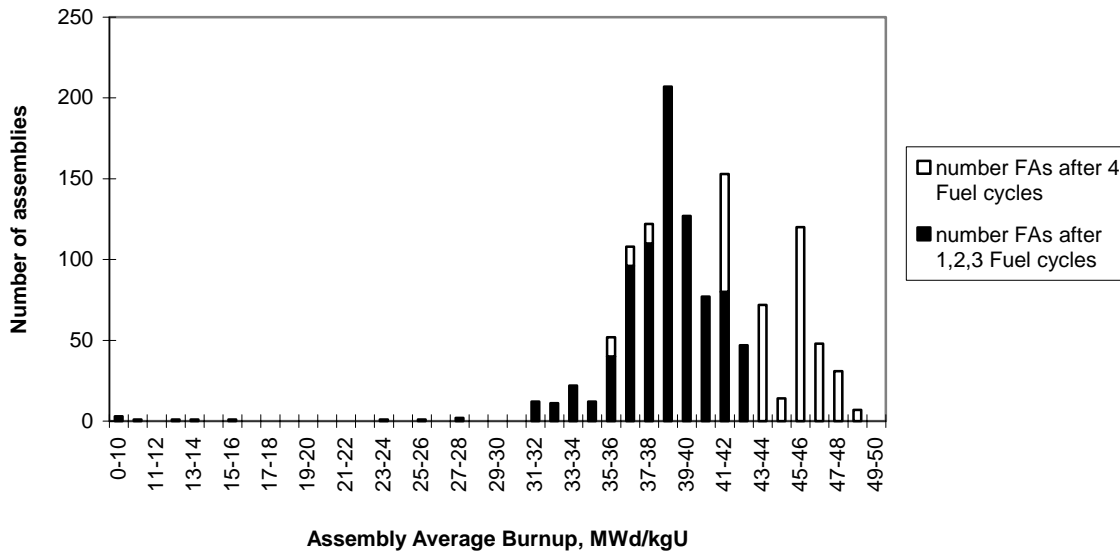


*Fig. 3. FA burnup distribution of Zaporozhye VVER-1000.*

Table 1. The comparative fuel performances of the realized fuel cycles

Type of fuel loading cycle	Enrichment of FA, %	Uranium mass in FA, kg	Average fuel burn-up MWt.day/kg U	Specific natural uranium expenditure, kg/ MWt.day	Front- end fuel cycle cost, mills /kWh (Initial core and services is not included)	Back- end fuel cycle cost/Total fuel cycle cost, mills/ kWh
2years cycle	3,3%	429,5	28,5	0,263	4,37	2,87/7,23
3years cycle	4,31%	401,6	39	0,256	4,16	2,11/6,27
3years cycle and some FA are used in 4-th loading cycle	4,31%	401,6	41,5	0,240	3,83	1,93/5,76

The following data are used for natural uranium expenditure and FA price (Front-end fuel cycle cost) calculation:

Uranium purchase	30 US\$/kg
Conversion	6 US\$/kg
Enrichment	95 US\$/SWU.kg ( tail - at 0,3% wt U235)
Fabrication	275 US\$/kg
Technological losses of uranium	2,5 % wt

The back end fuel cycle cost is evaluated on different way in the different countries depending on already existing capital investments , current state of economy, living standards , public relation and etc.

The German experts evaluate the fuel cycle cost of as follows:

- Natural uranium & conversion - 19%;
- Enrichment - 19%
  - Fabrication - 12%
  - Storage & final disposal -50%

In other words the front end fuel cycle cost (1100 - 1300 US\$/kg) is accepted as equal to the back end fuel cycle cost.

The Swedish experts, having broad experience in the fields of the construction and operation of the central wet interim storage facilities (CLAB) and the disposal canister and the encapsulation plant, evaluate the back end fuel cycle cost (including spent fuel transportation, storage, encapsulation and disposal as equivalent of 700 - 800 US\$/kg.

The experts OECD/NEA recommend the reference unit price and sensitive range of price for the fuel cycle cost evaluation.

The data from 1994 study on the economics of the nuclear fuel cycle [9]and back- end fuel cycle components cost data represented by Cogema (France) [10] in Krasnoyarsk-26 (Zheleznogorsk), (February 1996) are shown in table 2. The value equal to 610 US\$/kgU is accepted for the back- end fuel cycle cost evaluation of the Ukrainian VVER.

Table 2. The data back-end fuel cycle components cost

LWR fuel cycle unit prices (basis assumption for PWR)			
OECD/ NEA (BNFL/UK):			Cogema (France)
Component	Reference unit price, US\$/kgU	Sensitive range, US\$/kgU	Reference unit price, US\$/kgU
<b>Reprocessing option:</b>			
- spent fuel transport	62	25 - 99	54
- reprocessing (Including disposal of LLW & ILW & the vitrification & storage of VHLW)	893	670 - 893	640
- VHLW disposal	109	109 - 719	60
Value of recycled (extracted) UO <sub>2</sub> & PuO <sub>2</sub>	- 130	- 120 - 140	- 133
<b>total:</b>	1064 (934*)	804 -1711 (684 - 1571*)	754 (621*)
<b>Direct disposal option:</b>			
- spent fuel transport & storage	285	74 - 359	
- encapsulation (conditioning) & disposal	755	173 - 829	
<b>total:</b>	1040	247 - 1188	

\* The value of recycled (extracted) UO<sub>2</sub> & PuO<sub>2</sub> is taken into account

## 2.2. Fuel pin failure

The fuel reliability is necessary to consider in a context with the purpose to increase of fuel burn-up.

In the beginning of 1999 a total quantity of the FA discharged during all time of operation of 11 reactors was **5819** (110 fuel cycles). 194 of them were identified as leaking.

34 of them (17,5 %) were returned to the reactor core for using in the following fuel loadings.

138 of them (71,1%) were unloaded in the scheduled order (i.e. before test leaking these assemblies were not planned to use in the following cycles)

4 FA (2,1%) reached the unloading criteria ahead of schedule. 18 FA (9,3%) were unloaded ahead of schedule according to the conservative approach by the decision of the NPP management. 9 FA were unloaded because of the mechanical damage (see Table 2 ).

Table 3. Summary information on all unloaded fa

NPP	Number of Unit	Number of fuel cycles	Number of unloaded FA	Number of tested FA/ average share (%) of tested FA ( after each cycle of operation)	Number of leaking FA after 1/2/3/4 cycles of operation/ total	Number of FA which reached the criteria of unloading ahead of schedule/ were unloaded ahead of schedule according to the decision of the NPP management/total	Number of FA unloaded ahead of schedule because of the mechanical damages
Zaporozhye NPP (ZNPP)	1	11	590	939/ 52,4	15/ 8/ 1/ 0/ 24	0 / 2/ 2	3
	2	11	560	884/ 49,3	1 / 4/ 5/ 0/ 10	0/1 / 1	0
	3	11	589	1245/ 69,4	2 / 11/ 10/ 0/ 23	1/ 4 / 5	0
	4	11	550	706/ 39,4	4/ 1 / 7 / 0/ 12	1/ 0 / 1	0
	5	9	418	726/ 49,5	0/ 2/ 4 / 0/ 4	1/ 0 / 1	0
	6	2	102	0 / 0	0/ 0/ 0/ / 0/ 0	0/ 0 / 0	0
<b>Total for ZNPP</b>		<b>55</b>	<b>2809</b>	<b>4500/ 50,2</b>	<b>22/26/27 / 0/ 75</b>	<b>3/ 7 /10</b>	
South Ukrainian NPP (SUNPP)	1	14	801	1083/ 47,5	5/ 11/ 11 / 1 /28	1/ 0 / 1	0
	2	11	580	1121/ 62,5	7/ 9/ 9 / 1/ 26	0/ 4 / 4	2
	3	9	455	280/ 19,1	0/ 2/ 0 / 0/ 0	0/ 0/ 0	1
<b>Total for SUNPP</b>		<b>34</b>	<b>1836</b>	<b>2484/ 44,8</b>	<b>12/22/19/ 2/ 55</b>	<b>1/ 4 / 5</b>	
Khmelnith. NPP	1	10	529	1210/ 74,2	3/ 6/ 6 / 7/ 22	0/ 6 / 6	0
Rovno NPP	3	11	645	882/ 49,2	5/ 11/ 24/ 2/ 42	0/ 1 / 1	3
<b>Total</b>		<b>110</b>	<b>5819</b>	<b>9076/ 50,6</b>	<b>42/65/76/11/ 194</b>	<b>4/18/22</b>	<b>9</b>

Based on this data of Ukrainian VVER-1000 FA operation we can state, that the probability of FA leaking detection after first, second, third and fourth year of operation will be distributed as follows:

- after the first year of operation -  $42/194=21,6\%$  ;
- after the second year of operation -  $65/194= 33,5\%$  ;
- after the third year of operation -  $77/ 194= 39,2\%$  ;
- after the fourth year of operation -  $11/ 194= 5,7\%$ .

However, the represented statistics are not correct for the determination of fuel burnup influence to fuel pin failure rate, because the average share of tested FA after the first and second fuel cycles has 30 - 50 %, after the third cycle - 60-80 % and after the fourth cycle -90 - 100 % (The rejection criterion of leaky FA is the value of iodine-131 activity  $=1\cdot 10^{-4}$  Ci/l in water of testing system.).

Detection of leaky spent fuel is put into practice under requirements of "Instruction for detection of the fuel rods tightness of VVER-1000 type reactors in operation and after shut down" (0401.00.00.000 DNG), which were issued by Russian competent institutes, OKB Hidropress and Russian Research Center "Kurchatov Institute" accordingly.

Requests of the Instruction are the following:

- 1) The FA can not be tested, if both  $I^{131}$  and  $I^{134}$  coolant activity did not exceed  $10^{-6}$  Ci/l during a fuel cycle;
- 2) All FA must be tested, if the Iodine coolant activity ( $I^{131} + I^{132} + I^{133} + I^{134} + I^{135}$ ) exceeded  $2\cdot 10^{-4}$  Ci/l or the  $I^{131}$  coolant activity exceeded  $10^{-5}$  Ci/l during a fuel cycle;
- 3) It is necessary to test only those assemblies, which will be unloaded according to the schedule, if the Iodine coolant activity has exceeded the requirements stated in item 1, but has not exceeded the requirements of item 2.

The assemblies were not tested after completion of eight fuel cycles i.e. in these cases the requirements stated in item 1 were not executed.

In most fuel cycles the primary circuit coolant activity was about  $(1-5)\cdot 10^{-5}$  Ci/l iodine. Fig. 5, 6, 7 shows the change in the primary circuit coolant activity for some NPP units. The safety limit of  $1.5\cdot 10^{-2}$  Ci/l iodine when the reactor has to be shut down, has never been reached.

In 1998 the main designer of FA and main reactor designer has strengthened the safety limit of iodine primary coolant activity from  $1.5\cdot 10^{-2}$  Ci/l iodine to  $5\cdot 10^{-3}$  Ci/l iodine.

The operational limit is  $1.0\cdot 10^{-3}$  Ci/l iodine.

However the rejection criterion of leaky FA ( $I^{131}$  activity  $\geq 1\cdot 10^{-4}$  Ci/l in water of testing system) remains former, that obliged the technical manager of NPP to use the more conservative approach in FA failure determining and FA unloading ahead of schedule.

Fig. 4 , 5, 6, 7 shows the time evolution of the average fuel pin failure rate (FPFR). The average FPFR is defined as follows:

$$FPFR = NFA/NA\cdot 312$$

NFA - the number of leaking FA during one year

NA - total quantity of FA in reactors

312 - number of pins in assembly, it is assumed that the leaking assembly has only one leaking pin.

Summarizing represented data we can state, that the increase of Ukrainian VVER-1000 fuel burn-up has not worsened fuel reliability.

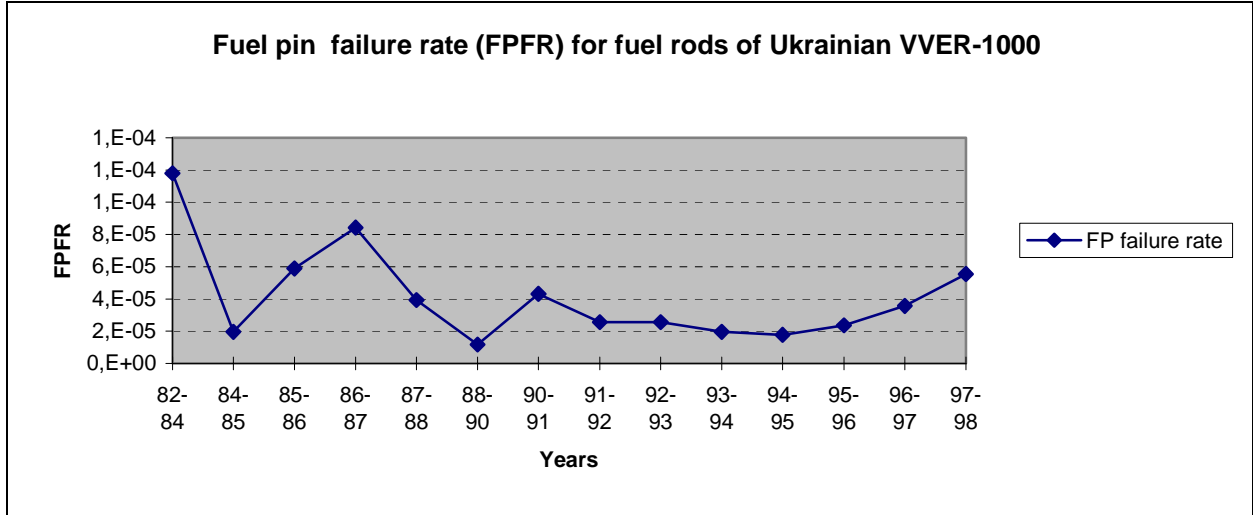


Fig.4. Fuel pin failure rate for fuel of Ukrainian VVER-1000.

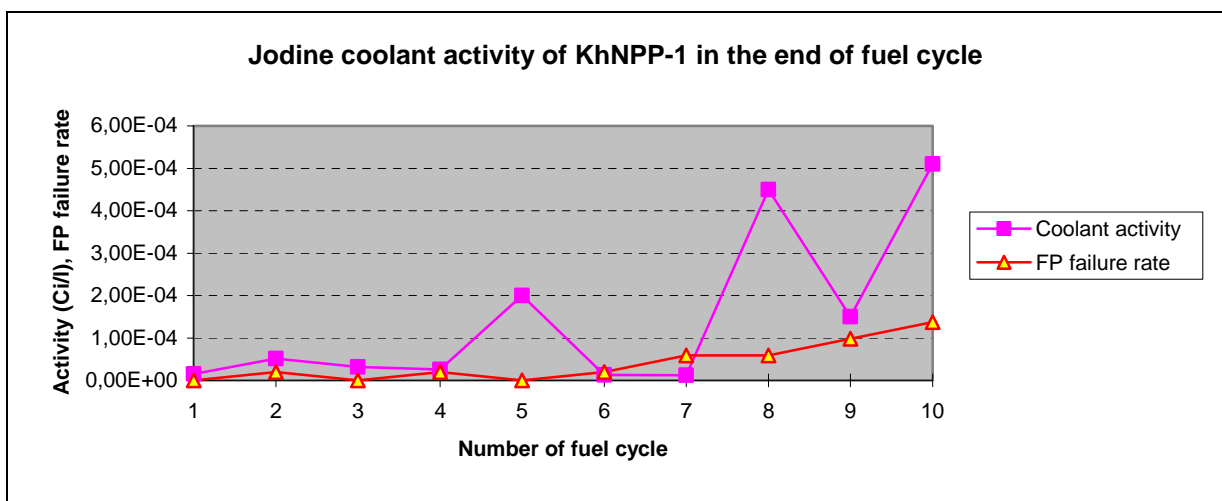


Fig.5. Fuel pin failure rate and iodine coolant activity for fuel of Khmel'nitskaya. VVER-1000.

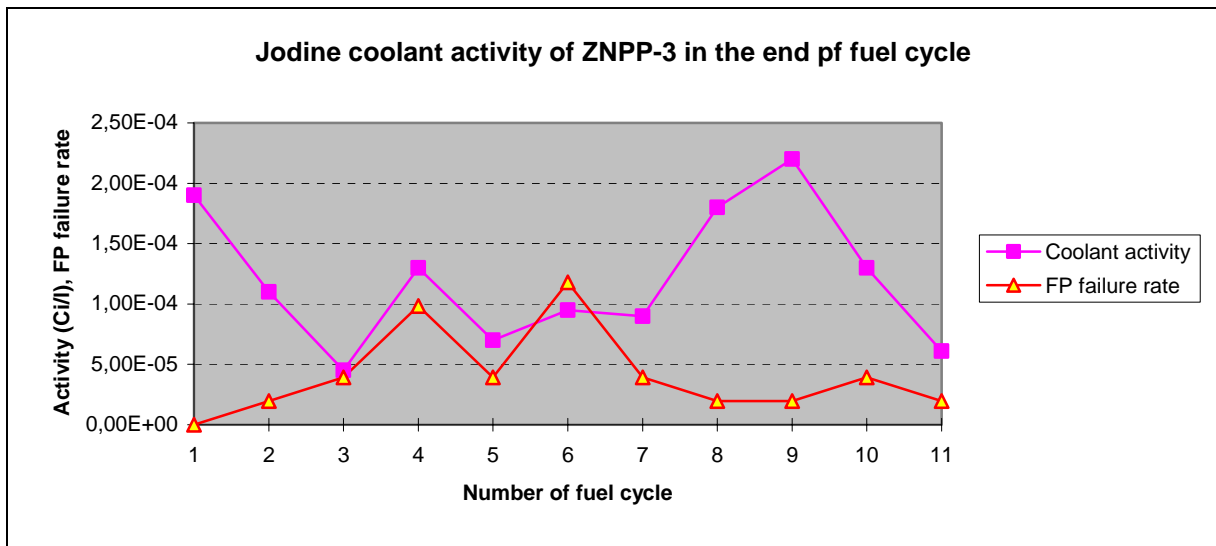


Fig.6. Fuel pin failure rate and iodine coolant activity for fuel of Zap-3. VVER-1000

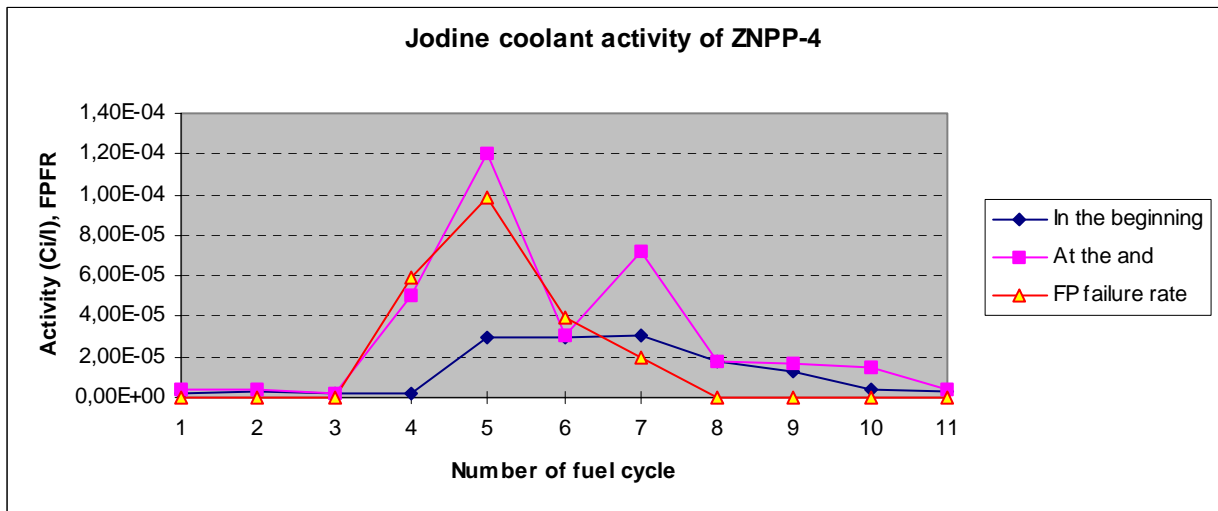


Fig.7. Fuel pin failure rate and iodine coolant activity for fuel of Zap-4. VVER-1000

### 2.3 Fuel assembly bow problems

The main problem of core operation of the last years have been consisted in incomplete RCCA insertion because of Fuel Assembly bow in reactor core.

To 1998 the measurements of FA bow located in VVER-1000 reactor core have been performed in Ukraine, Russia and Bulgaria.

There are 2350 FA measurements for estimate more then 10 000 water gaps.

Only one case had given significance of FA bow - 18,6 mm, two cases 15 mm and the rest gave up to 12mm].

So, the following sequences of FA bow development becomes evident:

At strong position of lower head while the FA bow size reaches 8 - 10 mm and the FA twists around its vertical axis, all deflection vectors are setting onto one direction. By other words, the vectors are rotating to the same direction around the core center, that is shown on figure 8. Rotation direction is considered as a random factor.

Implementation of compensatory technical measures:

- modification upgrading of the bundle safety tubes (BST) in order to correct BST position and to correct axial compression of FA;
- drilling of RCCA drivers bars in order to reduce force of hydrodynamics friction during the input of RCCA in the reactor core;
- utilization of the new designed heavier RCCA with gadolinium or titanat of dysprosium in Rovno NPP and Zaporozhye NPP and RCCA driver bar with increased dead load;
- organizing of the core loading pattern with advanced FA with zirconium (Zr -Nb and Zr - Nb- Sn -Fe alloy) guide thimbles and grids and with increased (comparatively with initially designed) FA head spring gain,

has allowed decreasing the probability of incomplete RCCA operation and allows us step-by-step to reduce FA bow in reactor core.

Currently is proved, that the increase of fuel burn-up under compensatory technical measures implementation does not worsen FA bow situation.

### 3. INVESTIGATION OF THE IRRADIATED FUEL IN HOT CELL

Besides the results of the operation of the fuel assemblies during four years we have the results of material testing. In the Research Institute of Atomic Reactors (Dimitrovgrad, Russia) the investigations of three assemblies from Zaporozhye NPP used in the reactor for four years have been held.

Table 4. Summary of irradiated fa ( <sup>11</sup> 0325, 0328, 0329) examination results

Parameter	FA <sup>11</sup> 0325	FA <sup>11</sup> 0328,0329
1.Average FA/"hottest" fuel rod burnup , MWd /kgU	48.9/ 51,3	44.0/ 46,5
2. Fuel rod parameters:		
2.1.Elongation, mm	12.3-18.6	11.0-17.3
2.2.Decrease in diameter, mm	0.05-0.08	0.04-0.07
2.3. Fuel-cladding gap. μm	3-43	no data
2.4. Fuel rod plenum, cm <sup>3</sup>	31.5-33.6	31.0-34.0
2.5.FGR, %	0.19-2.50	0.52-1.94
2.6. Pressure of gas, MPa	2.46-2.72	2.39-2.64
3.Maximal thickness of oxide film, μm		
outside	7-10	5-7
inside	5-10	5-10
Hydrogen content in the cladding, %	(0.88 - 1.6)·10 <sup>-2</sup>	(0.3 - 1.2)·10 <sup>-2</sup>
4. Fuel pellet parameters:		
4.1. Central hole diameter, mm	2.3-2.4	2.3-2.4
4.2. Average grain size, μm	3.8-5.8	~ 10
4.3. Fuel rod density, g/cm <sup>3</sup>	10.21-10.52	10.39-10.47

The averaged values of elongation, diameter decrease and fuel-cladding gap for all fuel rods of FAs correspond to the earlier determined dependencies obtained during examination of FA bow location before 10-th fuel cycle of unit 1 ZNPP on the half height of core.

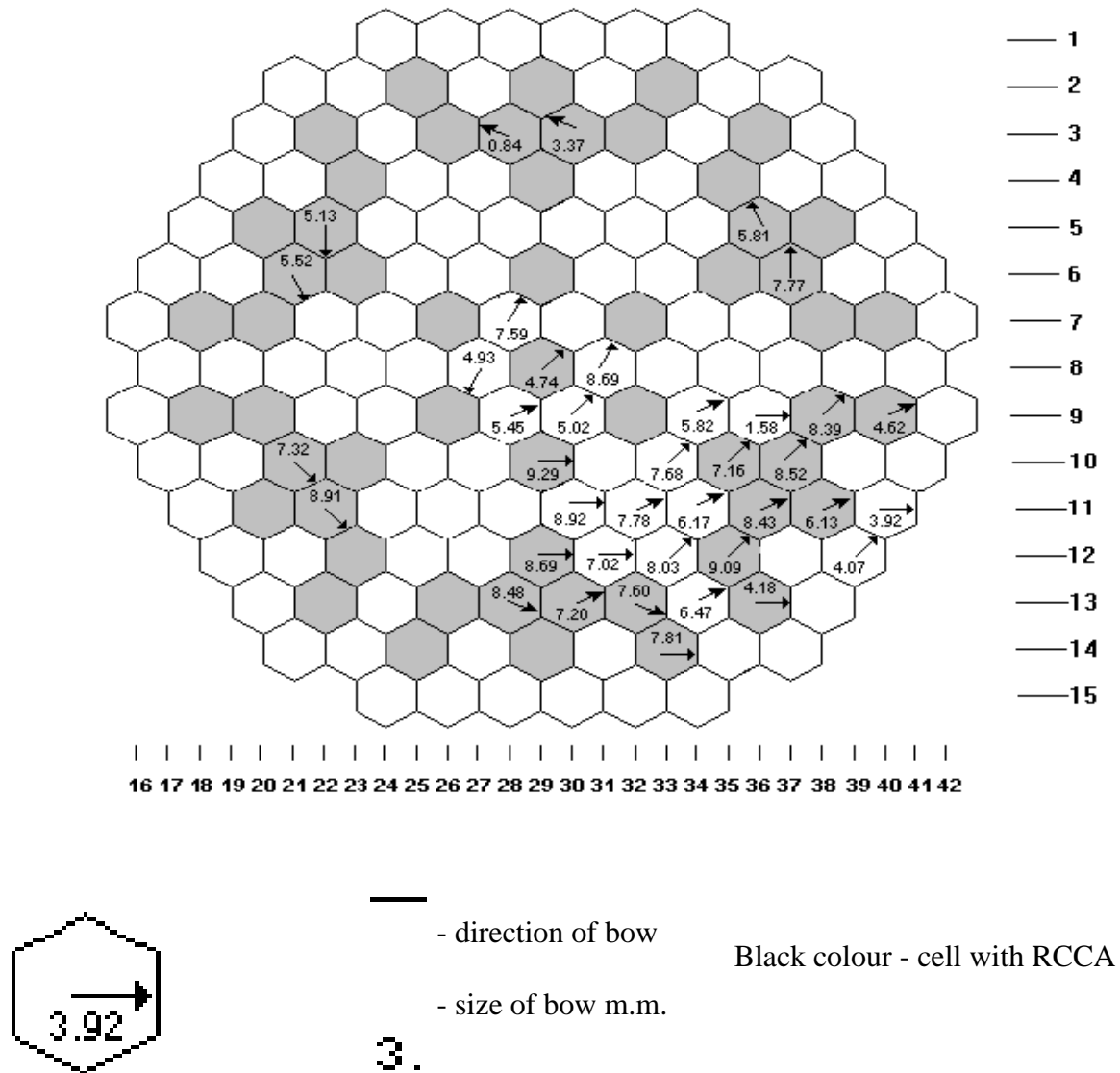


Fig 8.

the VVER-1000 fuel rods with a burn-up of 13.6 up to 46 MWd /kgU and operation time of 1-3 years . This fact indicates the absence of significant axis deformation due to fuel-cladding interaction, as well as radial deformation due to swelling, fuel pressure. Mechanical fuel-cladding interaction is exhibited at the initial stage and expressed in the presence of the local cladding deformation with a period equal to the cladding growth [4].

The state of fuel pins of all tested assemblies is satisfactory. All controlled parameters (elongation and diameter change, corrosion state of the claddings, their mechanical properties,

gas fission fragments' release and pressure inside the pins, ballooning of the fuel, etc.) comply with the requirements in accordance with the design for the WWER-1000 fuel pins [1], [4].

The principal results of the irradiated FAs examination allow to approve a possibility of further fuel burnup increase.

#### 4. THE FURTHER INCREASING OF FUEL BURNUP AND FA IMPROVEMENT

For continuous improvements of VVER-1000 fuel utilization it is necessary to implement advanced uranium- gadolinium ( $\text{UO}_2\text{-Gd}_2\text{O}_3$  fuel) assemblies with Zr alloy guide tubes (GT) and Zr alloy spacer grids (SG). It is assumed to improve fuel assembly dimensional stability and to save uranium expense by increasing of the uranium utilization.

According to the calculations the substitution of the steel by Zr alloy in materials of guide tubes and spacer grids increases the fuel utilization efficiency by 8.2%.

The use of the  $\text{UO}_2\text{-Gd}_2\text{O}_3$  fuel (Integrated Burnable Absorber Fuels, - IFBA) instead of the fuel with the Separated Burnable Absorber and narrowing of the fuel pellet central hole diameter from 2,4 mm to 1,4 mm allow to improve the fuel utilization efficiency by 2.4% and by 4% respectively. Advanced fuel implementation allows to reduce the initial enrichment of fuel by 5 -7 % in comparison with existing value and in the same time to increase fuel burnup by 5 - 7 %.

#### 5. THE CRITERION FOR FUEL CYCLE OPTIMIZATION

The four most important criterions are possible to define for fuel cycle optimization. They are arguable economics, sustainability and security of energy resources, environmental, and proliferation resistance. Safety is not included in the list of potential criteria, as all fuel cycle options must meet the highest levels of safety, and there is usually little to differentiate between different fuel cycle options on the basis of safety.

The resource optimization criterion includes several factors: the cost, availability, and sustainability of the world's natural resources; local or national energy-resource independence and security of supply (whether natural or enriched uranium); diversity of energy resources (Including non-nuclear). Some contend that nuclear power is now repeating the mistakes of the exploitation of other energy resources, such as coal, oil and gas, where market-controlled exploitation has taken place with little regard for its sustainability into the longer term. In an extreme view, optimization of the nuclear fuel cycle considering only the resource optimization criteria would only take place when the maximum amount of energy is extracted from each kilogram of uranium. Based on current operational fuel cycles, this is clearly not taking place, which implies that over the longer term, the process must have a strictly limited life. Uranium reserves may currently appear extensive, but an upsurge in nuclear power based on current fuel cycles may have a limited life of only fifty years or so.

The identification of non-proliferation optimization criteria is even more controversial. In the context of reactor and fuel cycle choices and future technological development in the civil nuclear power sector, the nuclear non-proliferation regime has been able to provide the

necessary assurances, irrespective of the nuclear technology chosen, and should be able to do so in the future. In other words, nuclear fuel cycles and their facilities can be safeguarded.

The establishing of the criteria relating to impact on an environment is difficult.

For example. One often-quoted waste management measure-of-merit is the volume of spent fuel or high level radioactive waste. In fact, it is well established that in a geological repository, such as that envisioned by Canada or Sweden, it is the decay-heat loading of the spent fuel or high level waste, rather than the volume, that is the main determinant in the size and cost of the repository. Hence, for example. the higher volume of spent natural uranium CANDU fuel is offset by its much lower decay heat, that allows a higher packing density in the repository and as a corollary smaller the specific disposal costs and repository areas ,compared to spent LWR fuel.

For the electricity utility today operating an existing nuclear power plant, economic optimization means minimizing the costs of producing electricity, based on a high degree of plant reliability, operational flexibility and maximum fuel utilization. This will include the costs of spent fuel management and eventual plant decommissioning.

### **5.1. Burn-up value as a criterion of the economic fuel cycle optimization**

Improvements of fuel utilization in the light water reactors, burn-up increase have led to a necessity to revise strategic approaches of the fuel cycle development. Different trends of the fuel cycle development are necessary to consider in accordance with the type of reactors used, the uranium market and other features that correspond to the nuclear and economic aspects of the fuel cycle.

The economic availability of the further fuel cycle development is determined by:

1) The required enrichment of U235 or fissile Pu contents to achieve higher burn-up.

Fig.9 and Fig.10 present the possible or achievable burnup today for two types of the reactors - light water reactor (LWR, PWR, BWR) and heavy water moderate, water coolant reactor (HWWR). The lower initial contents of fissile materials in the HWWR are required to reach the same the PWR fuel burnup but it depends on the burnup that was achieved during the previous irradiation in the PWR;

2) The MOX fuel fabrication cost (spent fuel regeneration +MOX FA fabrication), spent fuel storage and disposal cost and the cost of natural uranium.

Fig.11 and Fig.12 present the specific fuel cycle cost sensitivity at different costs of fabrication to the cost of natural uranium and initial enrichment of the uranium fuel -3.05% U235 and 4.4% U235;

All evaluations were made for the uranium conversion cost of 8 US\$/kg, uranium enrichment cost of 110 US\$/SWU·kg , storage and disposal fuel cost of US\$610/ kg.U. The effectiveness of the MOX fuel utilization in PWR for high initial enrichment corresponds to the higher cost of natural uranium. For the initial enrichment U235 3.05%(26 MWt.day/kgU) and natural uranium cost of US\$30 /kg the open fuel cycle (direct disposal) cost is equal to the MOX fuel fabrication cost of US\$1100 /kg.U. For the initial enrichment 4.4% (48 MWt.day/kgU) and the MOX fuel fabrication cost of US\$1100 /kg.U. open fuel cycle (direct disposal) cost is equal to the closed fuel cycle cost (MOX fuel utilization) if the natural uranium cost will exceed of US\$/60kg (See Fig.15.);

3) The achieved burn-up in PWR or initial enrichment of the PWR uranium fuel in the case of DUPIC technology.

The initial burn-up increase in PWR impacts on the possible burn-up that may be achieved in HWWR. For initial enrichments more than 3.3 % on U235 the fuel cycle with direct disposal becomes more effective than DUPIC utilization. (See Fig. 13 and Fig.14)

## 6. CONCLUSION

The experience of VVER-1000 FA operation and principal results o the irradiated FAs examination allow to approve a possibility of further of fuel burn-up increase.

The acceptance of the fuel cycle strategy is defined by the cost of natural uranium and the correlation of the cost on disposal services to the costs of fuel regeneration and fabrication. The development of simplified technologies of fuel regeneration and fabrication with utilizing the regenerated fuel in HWWR, is a more achievable strategy today.

The effectiveness of the compound PWR - HWWR fuel utilization is limited by the contents of fissile materials and U236 and other poison elements after the initial irradiation in the PWR. The restriction of the burn-up in PWR by 40-44 MWt.Day /kg.U will allow to ensure a possible burn-up in the HWWR more than 25 MWt.Day /kg.U and to return regenerated U for enrichment in acceptable quantities.

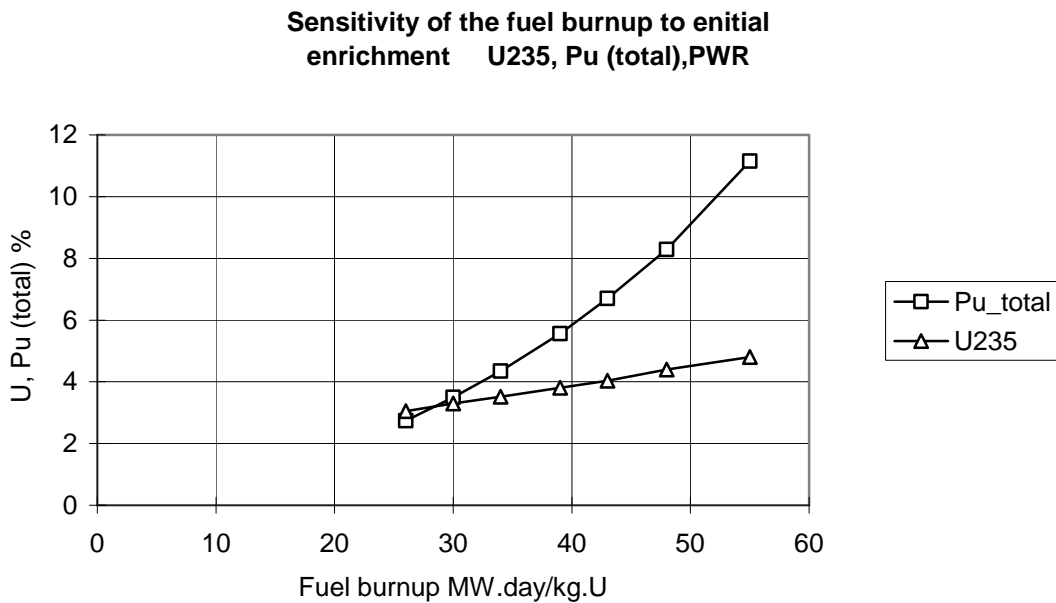
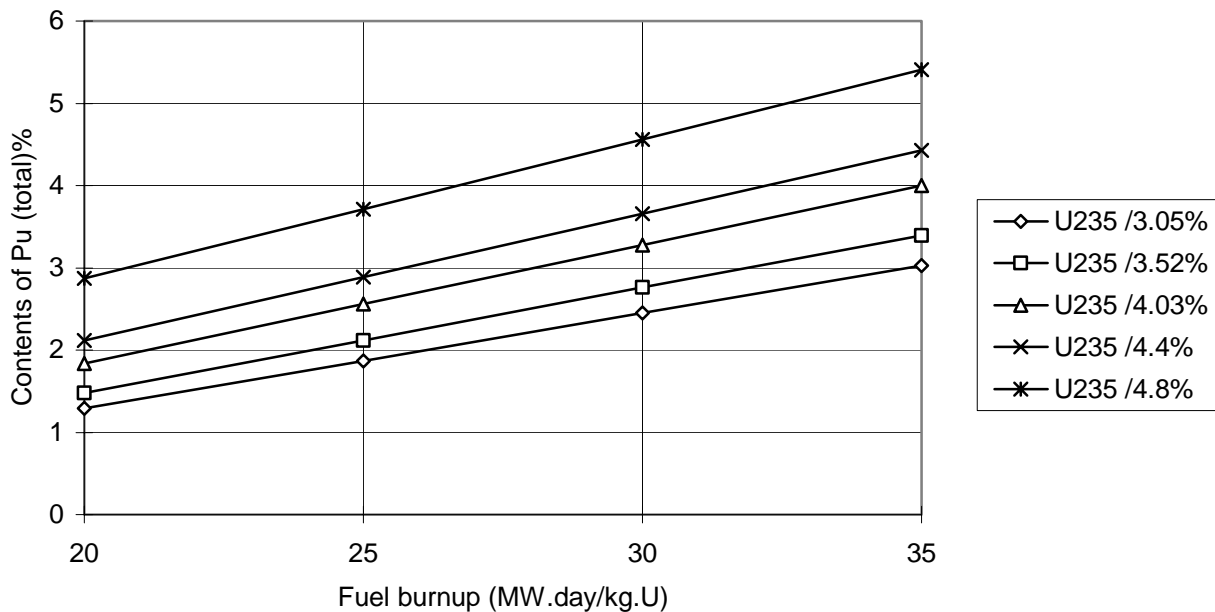


Fig. 9.

**Pu (total) and fuel burnup correlation in HWWR  
for different initial U235 enrichment in LWR**



*Fig. 10.*

**Sensitivity of the kW.h. cost to natural uranium price and MOX fuel fabrication cost (Initial enrichment of U235 - 3.05%)**

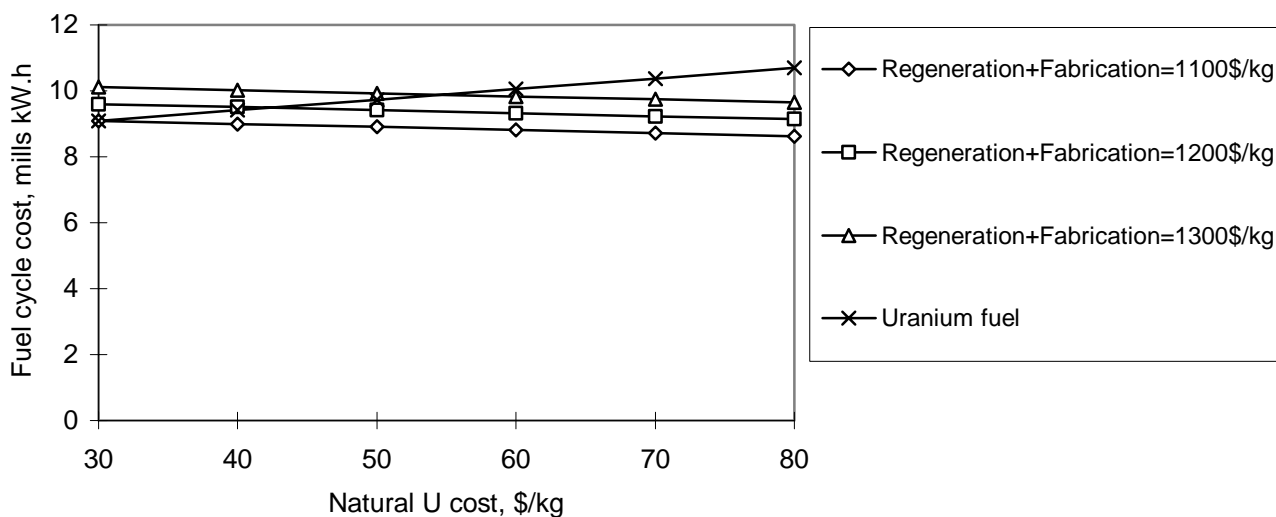


*Fig.11.*

**Sensitivity of the kW.h. price to natural uranium cost and MOX fuel fabrication cost (Initial enrichment of U235 - 4.4%)**

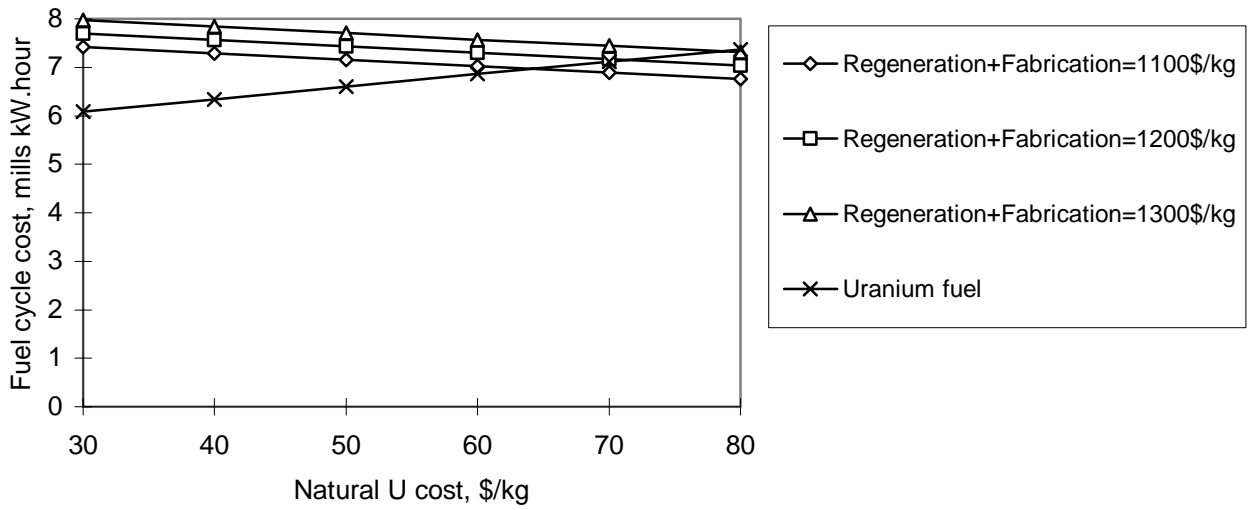


*Fig. 12.*

**DUPIC TECHNOLOGY**  
**Sensitivity of the fuel burnup to the initial enrichment of the loaded fuel into PWR**

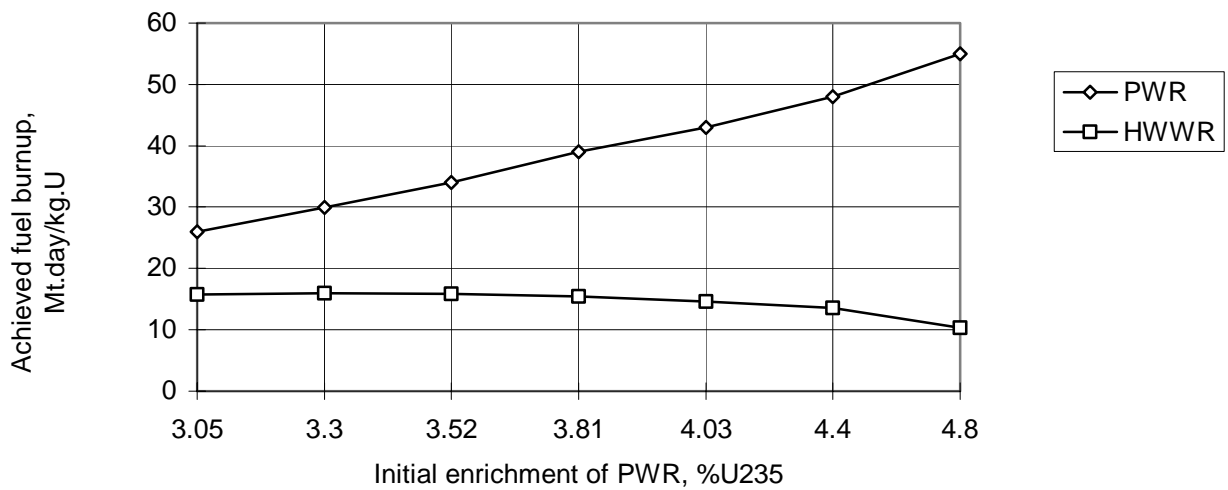


*Fig. 13.*

**Sensitivity of the fuel cycle cost to the initial enrichment of the loaded fuel into PWR**

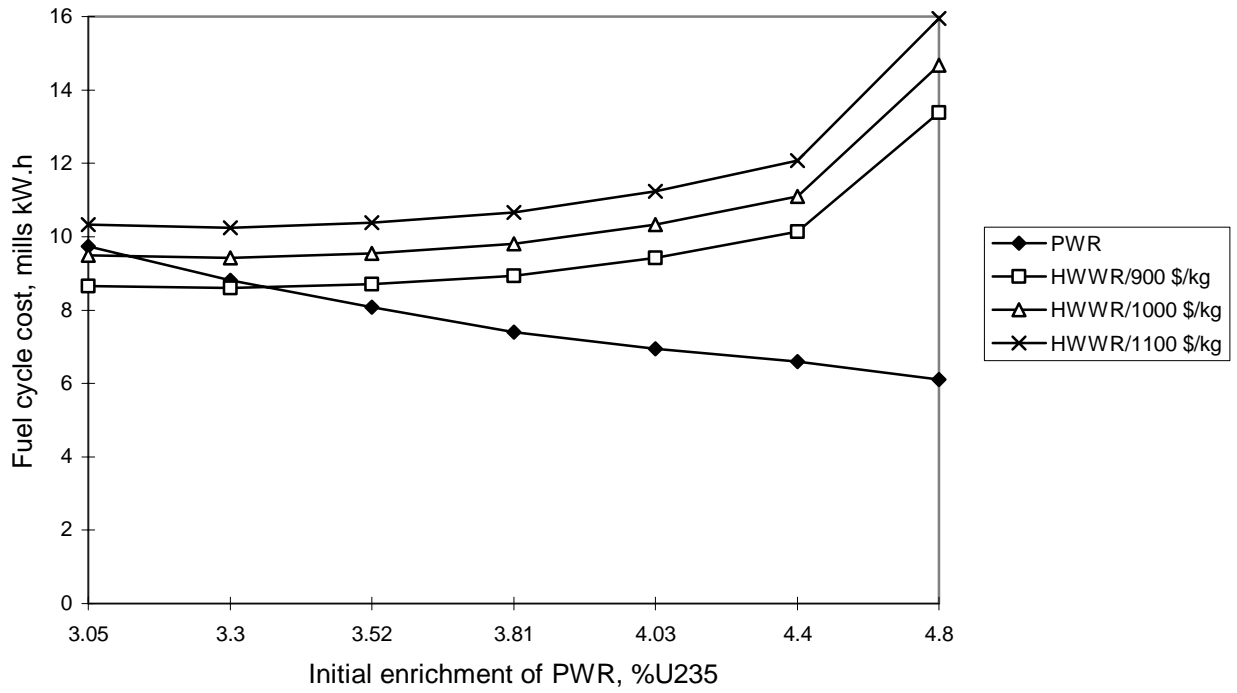


*Fig.14.*

**Sensitivity of the limited burnup (MOX and U fuel cycle costs are equal) to the natural uranium cost, LWR-LWR.**

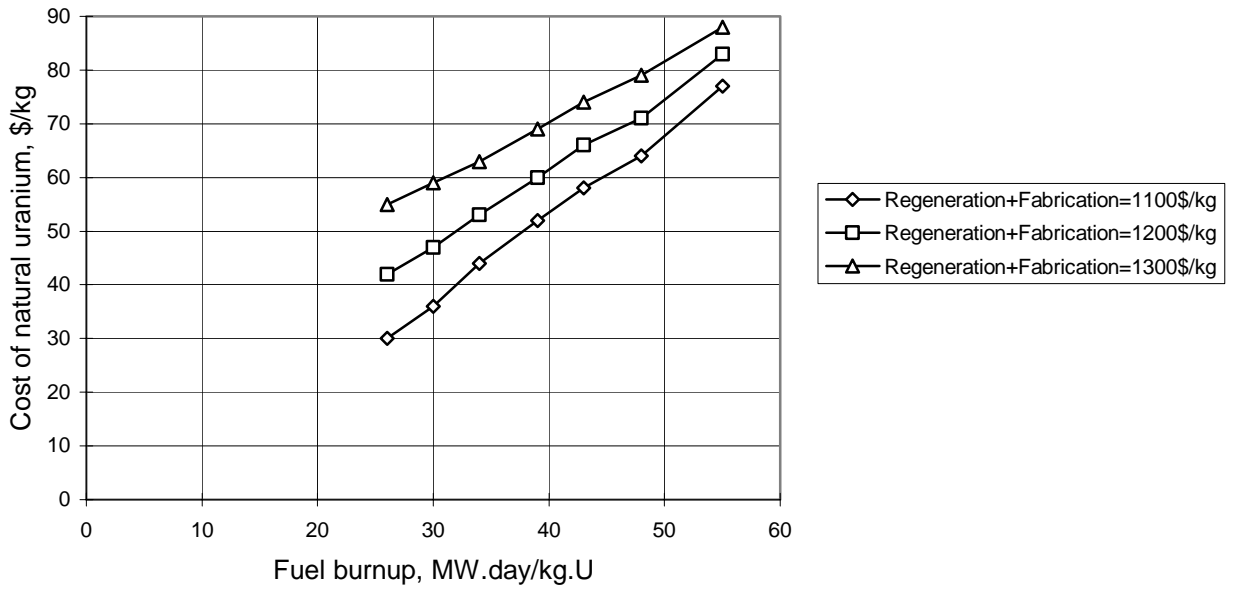


*Fig.15.*

**Sensitivity of the limited (DUPIC and U fuel cycle cost are equal) cost for  
fuel fabrication to the initial enrichment of PWR.  
(uranium cost \$50/kg)**

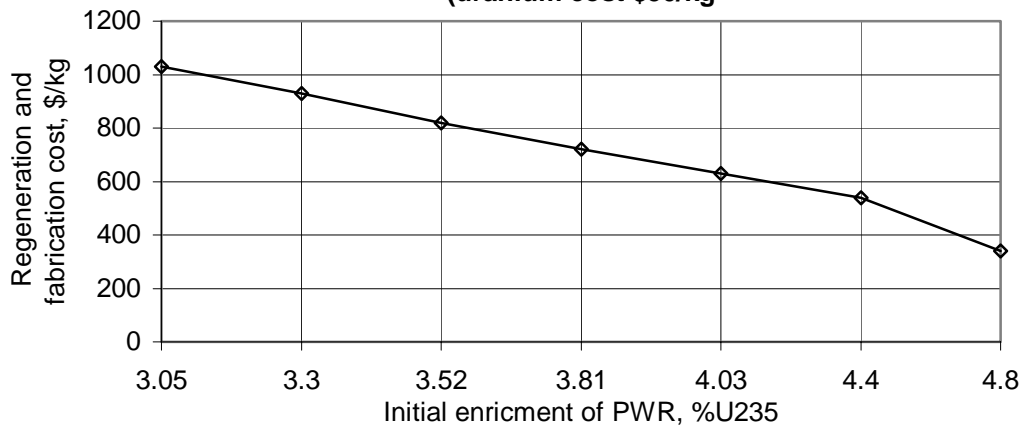


*Fig. 16.*

### REFERENCES

- [1] SMIRNOV et.al., "Investigation of WWER-1000 FA E0328 and E0329, control rod 02.356 and shim rod 15137 after operation at Zaporozhye NPP unit 1", Report about research work, SSCRF RIAR, Dimitrovgrad, Russian Federation (1994).
- [2] VAN SVAM et.al, "BWR and PWR fuel performance at high burnup", Proceedings of the 1997 ANS international topical meeting on LWR fuel performance ,Portland, Oregon March 2-6, 1997 (published by American N.S., INS., La Grand Park, ILL 60526, USA), pp.455-462.
- [3] R. MANZEL, M. COQUERELLE, "Fission gas release and pellet structure at extended burnup" Proceedings of the 1997 ANS international topical meeting on LWR fuel performance ,Portland, Oregon March 2-6, 1997 pp.463-470.
- [4] D.MARKOV, A. SMIRNOV et.al., "Validation of VVER-1000 fuel rod efficiency at operation during for fuel cycles", Third International seminar of WWER fuel performance, modeling and experimental support, Pamporovo, Bulgaria , 4-8 October 1999.
- [5] A. SMIRNOV, B.KANASHOV et.al., "Examination of fission gas release and fuel structure of high burnup under transient condition.", Third International seminar of WWER fuel performance, modeling and experimental support, Pamporovo, Bulgaria , 4-8 October 1999.
- [6] YU. BIBILASHVILI, I. SMIRNOV, B. SMIRNOV, V. ASMOLOV et.al." Experimental and calculation research of WWER high burnup fuel rod behaviour in pulse test on the BGR", Third International seminar of WWER fuel performance, modeling and experimental support, Pamporovo, Bulgaria , 4-8 October 1999.
- [7] Ralph O. MEYER et.al."A regulatory assessment of test data for reactivity accident", Proceedings of the 1997 ANS international topical meeting on LWR fuel performance, Portland, Oregon March 2-6, 1997 pp.729-740.
- [8] J.BANCK," Mechanical systems, components nuclear waste management, marketing &projects", Siemens, (KWU),Proceedings of a Symposium, Storage of spent fuel from power reactors, Vienna, 9-13 Nov. 1998, pp. 207-213.
- [9] Ray DODDS, BNFL/UK " Nuclear Fuel Activities, Evaluation of Option, Economics Summary", The lecture,Paris - Saclay,1994.
- [10] "Spent fuel reprocessing and return of nuclear materials in a fuel cycle", Presentation of Cogema at the fuel reprocessing plant construction problems meeting , Russia, Krasnoyarsk-26 (Zheleznogorsk), February 1996.



## LIST OF PARTICIPANTS

### ARGENTINA

P. Adelfang,  
Nuclear Fuels Department,  
Comisión Nacional de Energía Atómica,  
Avda. del Libertador 8250, 1429 Buenos Aires

L.A. Alvarez,  
Unidad Proyectos Especiales,  
Suministros Nucleares,  
UPESN-IEC / CNEA, Avda. del Libertador 8250,  
1429 Buenos Aires

D. Banchik,  
Materials and Nuclear Fuels Dept.,  
CNEA-CAE, Avda. del Libertador 8250,  
1429 Buenos Aires

R. Cirimello,  
Nuclear Fuel Cycle Project Division,  
CNEA-CAB, Av. Bustillo, Ruta 9, km 500,  
8400 San Carlos de Bariloche, Pcia. Río Negro

H. Daverio,  
Nuclear Fuels Department,  
CNEA-CAC, Avda. del Libertador 8250,  
1429 Buenos Aires

A. Denis,  
Nuclear Fuels Department,  
Comisión Nacional de Energía Atómica,  
(CNEA) - CNEA-CAC, Av. del Libertador 8250,  
1429 Buenos Aires

J. Fink,  
Nucleoeléctrica Argentina S.A.,  
Arribeños 3619, 1429 Buenos Aires

P. Florido,  
Advanced Design and Economical,  
Assessment Dept., CNEA-CAB,  
Av. Bustillo, Ruta 9, km 500,  
8400 San Carlos de Bariloche, Pcia., Río Negro

S.E. Gomez,  
Comisión Nacional de Energía Atómica,  
Av. del Libertador 8250, 1429 Buenos Aires

A. Gonzalez,  
Nuclear Fuels Department, CNEA-CAC,  
Avda. del Libertador 8250, 1429 Buenos Aires

R. Haddad,  
Materials Department, CNEA-CAC,  
Avda. del Libertador 8250, 1429 Buenos Aires

C. Lecot,  
INVAP S.E., CC 961,  
8400 San Carlos de Bariloche, cia. Río Negro

A. Marajofsky,  
Nuclear Fuels Department, CNEA-CAC, vAv. del  
Libertador 8250, 1429 Buenos Aires

A.C. Marino,  
Advanced Design and Econ.,  
Assessment Dept., CNEA-CAB,  
Av. Bustillo, Ruta 9, km 500,  
8400 San Carlos de Bariloche, Pcia. Río Negro

M. Markiewicz,  
Nuclear Engineering Department,  
CNEA-CAB, Av. Bustillo, Ruta 9, km 500,  
8400 San Carlos de Bariloche, Pcia. Río Negro

C. Mazufri,  
INVAP S.E., CC 961,  
8400 San Carlos de Bariloche, Pcia. Río Negro

E. Perez,  
Bariloche Atomic Center,  
CNEA-CAB, Av. Bustillo, Ruta 9, km 500,  
8400 San Carlos de Bariloche, Pcia. Pío Negro

H.F. Reale,  
Conuar S.A., Centro Atómico Ezeiza,  
Camino Borlenghi s/n, 1802 Ezeiza

G. Ruggirello,  
Nuclear Fuels Department,  
CNEA-CAC, Av. del Libertador 8250,  
1429 Buenos Aires

M. Scaffoni,  
Department of Projects Promotion and  
Scientific Coordination, CNEA,  
Av. del Libertador 8250, 1429 Buenos Aires

H. Taboada,  
Nuclear Fuels Department,  
CNEA-CAC, Avda. del Libertador 8250,  
1429 Buenos Aires

D. Yorio,  
Nuclear Fuels Department,  
CNEA-CAC, Avda. del Libertador 8250,  
1429 Buenos Aires

BELGIUM

P. Van Uffelen,  
Reactor Physics Department, SCK-CEN,  
Boeretang 200, B-2400 Mol

BULGARIA

T. Haralampieva,  
Reactor Core Charact. Calculations,  
Dept. of Engineering Support,  
Kozloduy NPP, 3321 Kozloduy

CANADA

P. Boczar,  
Fuel and Fuel Cycle Division,  
AECL Chalk River Laboratories,  
Chalk River, Ontario KOJ 1JO

EUROPEAN COMMISSION

H. Matzke,  
Joint Research Centre of the EC,  
Institute for Transuranium Elements (ITU),  
P.O. Box 2340, D-76125 Karlsruhe, Germany

FRANCE

D. Balestrieri,  
CEA Cadarache, DEC/SESC/LIPA,  
Bât. 315, F-13108 St. Paul Lez Durance

D. Baron,  
EDF, Direction des Etudes et Recherches,  
Département MTC, B.P. 1,  
F-77250 Moret-sur-Loing

L. Desgranges,  
CEA Cadarache, DEC/SFCI/LECMI, Bât. 316,  
F-13108 Saint Paul Lez Durance

GERMANY

W.C. Fenzlein,  
Siemens AG (KWU), P.O. Box 3220,  
D-91050 Erlangen

H.-G. Sonnenburg,  
GRS mbH,  
Forschungsgelände, D-85 748 Garching

INDIA

P.R. Vasudeva Rao,  
Fuel Chemistry Division,  
Indira Gandhi Centre for Atomic Research  
(IGCAR), Kalpakkam 603 102, Tamil Nadu

JAPAN

M. Ichikawa,  
The Japan Atomic Power Company,  
Ohtemachi Bldg. 6-1 Chome,  
Ohtemachi, Chiyoda-Ku, Tokyo 100-0004

I. Ioka,  
Dept. of Nuclear Energy Systems, JAERI,  
2-4 Shirakata-Shirane, Tokai-mura, Naka-gun,  
Ibaraki-ken 319-1195

K. Kiuchi,  
Dept. of Nuclear Energy System, JAERI,  
2-4 Shirakata-Shirane, Tokai-mura, Naka-gun,  
Ibaraki-ken 319-1195

M. Takizawa,  
Mitsubishi Research Institute, Inc.,  
Research Center for Safety Science,  
Nuclear Engineering Systems Department,  
3-6 Otemachi 2-Chome,  
Chiyoda-ku, Tokyo 100-8141

T. Yoshizu,  
Group Leader, Safety Analyzation Group,  
Technical Engineering Department,  
Engineering Development Co., Ltd,  
3-1, Minatomirai 3-chome, Nishi-ku,  
Yokohama 220-8401

LITHUANIA

G. Krivoshein,  
Nuclear Safety Department,  
Ignalina NPP, 4761 Visaginas

NORWAY

T. Tverberg,  
OECD Halden Reactor Project,  
Institutt for Energiteknikk,  
P.O.Box 173, NO-1751 Halden

PAKISTAN

S. Gul,  
Institute for Nuclear Power (INUP),  
INUP P.O. Box 3140, Islamabad

ROMANIA

D. Ohai,  
Institute for Nuclear Research, P.O. Box 78, Pitesti

RUSSIAN FEDERATION

V. Chernyshov,  
JSV TVEL, Minatom, B. Ordynka St. 24/26,  
101 000, Moscow

F.F. Sokolov,  
All-Russian Scientific & Research,  
Institute of Inorganic Materials (ARSRIM),  
St. Rogov 5, Box 369, 123060 Moscow

UKRAINE

A. Afanasyev,  
State Department on Nuclear Energy,  
Ministry of Energy of Ukraine,  
30 Khreshchatik st., 252601 Kiev

I.A.E.A

P. Menut,  
Department of Nuclear Energy,  
Wagramer Srasse 5, P.O. Box 100,  
A-1400 Vienna, Austria

